DEVELOPING PHOTOCHEMICAL PRECURSORS FOR INDEPENDENT GENERATION OF NEUTRAL PURINE RADICALS AND INVESTIGATING THE REACTIVITY OF 2′-DEOXYADENOSIN-N6-YL RADICAL IN DNA

By

Liwei Zheng

A dissertation submitted to Johns Hopkins University in conformity with the requirements for the degree of Doctor of Philosophy

Baltimore, Maryland

December 2018

Abstract

DNA damage is deleterious to cells and can lead to cell death or cancer. The cytotoxicity of DNA damage is exploited by cancer treatments such as radiotherapy. Ionizing radiation damages DNA indirectly by reacting with hydroxyl radicals to generate reactive intermediates, e.g., nucleobase and deoxyribose radicals; or by directly generating nucleobase radicals. Neutral purine radicals (dA•, dG(N1-H)•, and dG(N2-H)•) generated by formal hydrogen atom abstraction of purines are believed to play a prominent role in oxidative DNA damage and DNA hole migration. However, very little is known about their reactivity.

Studying these intermediates via radiolysis is complicated due to the concomitant formation of other reactive species. To overcome the dearth of methods for photochemically generating neutral purine radicals, we developed two general strategies. The first type of precursors utilized photoinduced homolytic cleavage of weak covalent bonds (**3**, **4** and **5**). The second type of precursors (**6** and **7**) underwent a Norrish Type I photocleavage and β-fragmentation cascade to form neutral purine radicals and acetone. These precursors allowed mechanistic studies on the reactivity of neutral purine radicals as monomers in solutions or within DNA.

Herein, we report that dA• initiates tandem lesion formation in 5'-d(GTA) sequences but does not induce DNA hole migration. We propose that the tandem lesion formation is initiated by dA• abstracting the hydrogen atom from the C5-methyl group of the 5'-adjacent thymidine. dA• is converted to dA in this process, and thus the involvement of dA• in the tandem lesion formation is traceless by typical product analysis. Furthermore, we demonstrate, for the first time, that dA• is protonated at neutral pH when flanked by

ii

dA. The formation of dA•+ by this protonation results in DNA damage arising from hole transfer. Finally, we disprove the published mechanism for the formation of strand damage observed during DNA hole migration in poly(dA-T) sequences and provide support for an alternative mechanism, in which the strand damage is tracelessly induced by dA•.

Advisor: Professor Marc. M. Greenberg

Readers: Professor John D. Tovar

Professor Steven E. Rokita

Acknowledgments

I am very thankful to all the people who have helped me through this journey. Thanks to all the members of the Greenberg lab, current and former, for their help. Thanks to Liwei Weng, Josh, Rakesh and Arnab for their help during my early years in graduate school. Special thanks to my best friend Danny who has been by my side through highs and lows. Thanks to Huabing, Shelby, Marco, and Kun for all their help, support, and advice. Thanks to Haozhe and Tingyu for their friendship and tremendous help during my final days in graduate school. I am also very thankful to Dr. Greenberg for his mentorship. I am impressed by his professionalism and enthusiasm for science. I am so grateful for not only the guidance and help in the research but also for his advises for my career path. Without his help, I surely would have never made it this far.

I also would like to thank Dr. Tovar and Dr. Rokita for their valuable suggestions and comments on this thesis. Thanks to Dr. Rokita and Dr. Klausen for their help during my search for a post-doctoral position. Thanks to Dr. Mortimer for his help in the UPLC-MS/MS studies. Thanks to all the collaborators for making this project come into fruition.

Thanks to my parents and parents-in-law who have always been supportive. My deepest appreciation goes to my wife, Yujia, who has always been extremely supportive and understanding. Although I could not be by her side most of the time, her encouragement and unconditional love have always motivated me.

Table of Contents

List of Tables

List of Figures

List of Schemes

List of Abbreviations

ARP   aldehyde reactive probe

BME   2-mercaptoethanol

CV   cyclic voltammetry

dA   2'-deoxyadenosine

dC   2'-deoxycytidine

dG   2'-deoxyguanosine

dHT   dihydrothymidine

dI   2'-deoxyginosine

DIPEA   N,N-diisopropylethylamine

DME   1,2-dimethoxyethane

DMF   dimethylformamide

DNA   deoxyribonucleic acid

dU   2'-deoxyuridine

EDTA   ethylenediaminetetraacetic acid

Endo V   endonuclease V

EPR   electron paramagnetic resonance

ESI   electrospray ionization

FAB   fast atom bombardment

FapydA $N6$-(2-deoxy-α,β-d-erythro-pentofuranosyl)-4,6-diamino-5-
               formamidopyrimidine

FapydG $N6$-(2-deoxy-α,β-d-erythro-pentofuranosyl)-2,6-diamino-4-hydroxy-5-
               formamidopyrimidine

5-fdU   5-formyl-2'-deoxyuridine

Fpg   formamidopyrimidine DNA glycosylase

GC   gas chromatography

HFIP   hexafluoro-2-propanol

HPLC   high pressure liquid chromatography

5-hmdU   5-hydroxymethyl-2'-deoxyuridine

LC-MS   liquid chromatography-mass spectrometry

LFP   laser flash photolysis

MALDI   matrix assisted laser desorption/ionization

MS   mass spectrometry

NMR   nuclear magnetic resonance

•OH   hydroxyl radical

8-oxodA   8-oxo-7,8-dihydro-2′-deoxyadenosine

8-oxodG   8-oxo-7,8-dihydro-2′-deoxyguanosine

PAGE   polyacrylamide gel electrophoresis

ROS   reactive oxygen species

T   thymidine

TEA   triethylamine

TEAA   triethylammonium acetate

Tg   thymidine glycol

THF   tetrahydrofuran

Tris   tris(hydroxymethyl)aminomethane

UPLC   ultra-performance liquid chromatography

UV   ultraviolet

1.   Introduction

Deoxyribonucleic acid (DNA), the storage medium of genetic information, is constantly exposed to potentially damaging reactive species, which are either generated endogenously by normal cellular metabolism or exogenously by, for example, ionizing radiation.[1-3] DNA damage is deleterious to cells and can lead to cell death or cancer. Cancer treatments such as radiotherapy exploit the cytotoxicity of DNA damage.
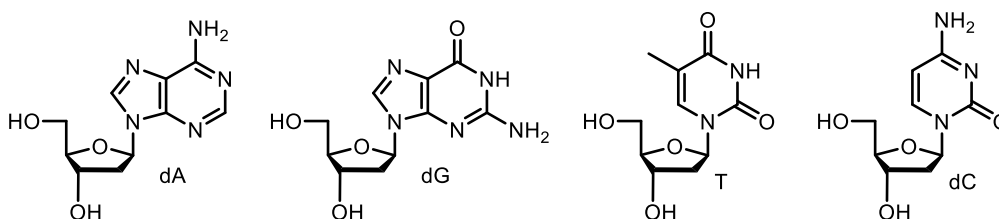
Among the four naturally occurring 2'-deoxyribonucleosides, 2'-deoxyadenosine (dA) and 2'-deoxyguanosine (dG) are more prone to oxidation than 2'-deoxycytidine (dC), and thymidine (T) due to their low oxidation potentials.[4-5] Oxidation of dA and dG by one-electron oxidants and the direct effect of ionizing radiation generates radical cations (dA•+ and dG•+).[6-7] The pKas of these radical cations are lower than their parent molecules.[8] For example, the pK$_a$ of dA•+, although somewhat controversial, is believed to be as low as -0.3.[6] At neutral pH, purine radical cations rapidly deprotonate to generate neutral purine radicals (Scheme 1, dA• and dG•). Moreover, deprotonation of dG•+ can generate two isomeric radicals: dG(N1-H)• and dG(N2-H)•, and the tautomerization between them remains controversial. Neutral purine radicals are also generated by the indirect effect of ionizing radiation via the addition of hydroxyl radical (•OH) at the C4 position of purines to yield **1** and **2**, which eliminate a water molecule to generate neutral purine radicals (Scheme 1). [6, 9-10]

Scheme 1. The formation of neutral purine radicals.
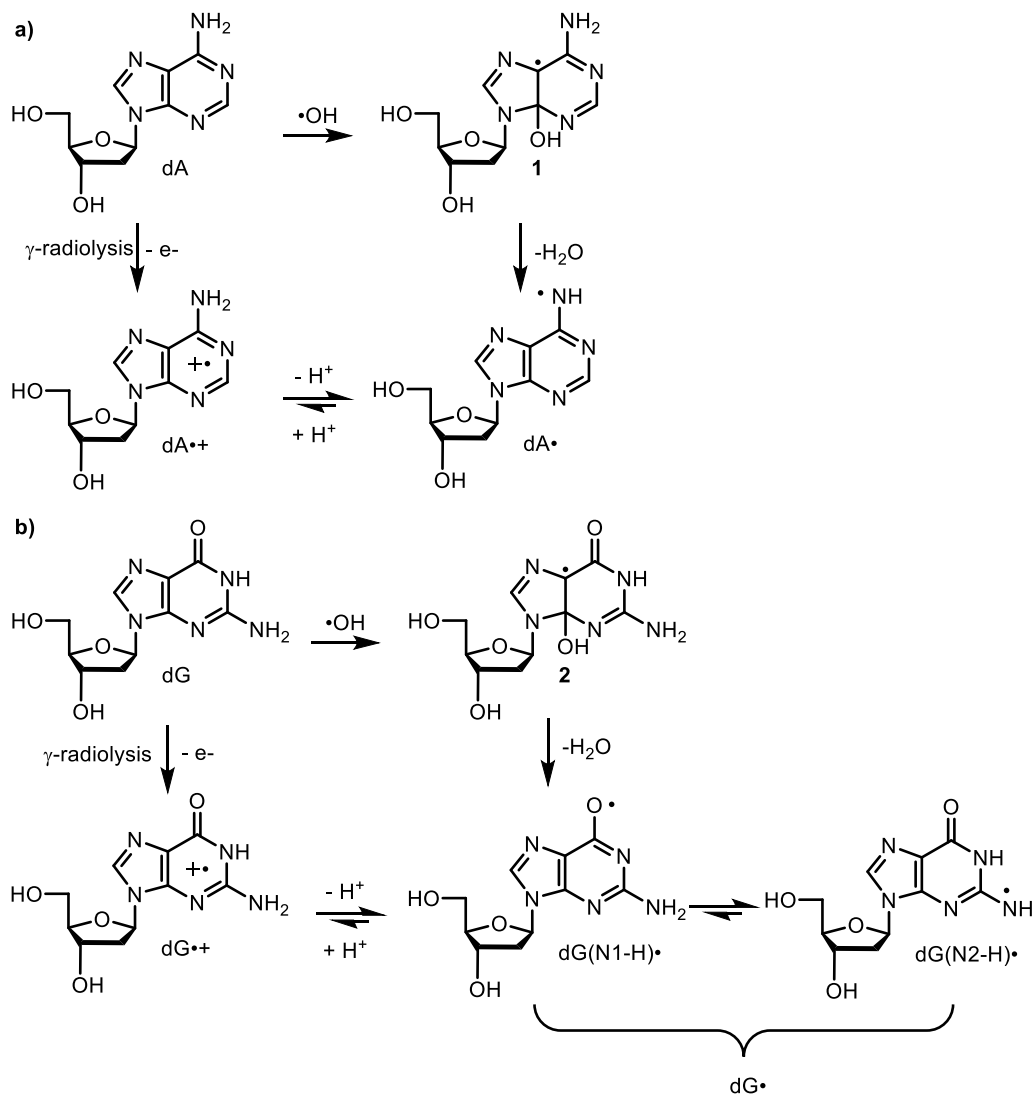
While dG•+ is generally considered to be the major hole carrier in DNA hole migration, the role of dA•+ in hole migration has only gained attention more recently.[11-19] Hole migration can occur in dA-T tracts over long distances, which seemingly contradicts the low pK_a of dA•+ which would lead to spontaneous deprotonation of dA•+ and attenuation of hole migration.[20] To address these two conflicting observations, it has been proposed that a flanking dA increases the pK_a of dA•+ to ~7.[21-23] However, this proposal has only been corroborated by computation and low-temperature electron paramagnetic

2

resonance (EPR) experiments.[21] Furthermore, it is interesting to note that, in the absence of guanine, hole migration in dA-T tracts led to strand damage on T. [24-28] This observation was explained by kinetically favorable irreversible trapping of the radical cation at T, despite the thermodynamically unfavorable electron transfer from T to dA•+.[29] However, the proposed mechanism was not fully consistent with the sequence specificity of the formation of strand damage.

Little is known about the reactivity of neutral purine radicals. Much of the knowledge about the reactivity of purine radicals has been obtained from pulse radiolysis experiments on the nucleoside or dinucleotides. These experiments established that purine radicals react slowly with O_2 and H_2O.[30-31] These studies also lead to the proposal that dA• oxidizes dG to initiate hole migration.[32-34] Additionally, the tautomerization of dG• and the involvement of this tautomerization during DNA oxidation are also controversial.[23, 35-40] Furthermore, the information regarding the downstream products generated from neutral purine radicals, especially dA•, are limited, despite their frequent occurrence during oxidative DNA damage. Therefore, independent, site-specific generation of purine radicals in DNA will greatly advance the understanding of the reactivity of these reactive intermediates.

To overcome the dearth of methods for photochemically generating neutral purine radicals we developed two general strategies. The first approach utilizes photoinduced homolytic cleavage of weak covalent bonds in precursors **3**, **4** and **5**.[41] The second type of precursors (**6** and **7**) undergoes a Norrish Type I photocleavage and β-fragmentation cascade to form neutral purine radicals and acetone.[42] Furthermore, incorporation of **6** into DNA provided significant insight into the reactivity of dA•, including bringing to light the

traceless involvement of dA• in tandem lesion formation.[43] It also enabled us to demonstrate the sequence-dependent protonation of dA• to form dA•+ in an aqueous environment at room temperature and thus validated the results obtained by calculation and EPR in low-temperature matrices.[44] Finally, we disproved the aforementioned proposed mechanism for the formation of strand damage observed during DNA hole migration in poly(dA-T) sequences and provided support for an alternative mechanism, in which the strand damage is induced by dA•.[45]
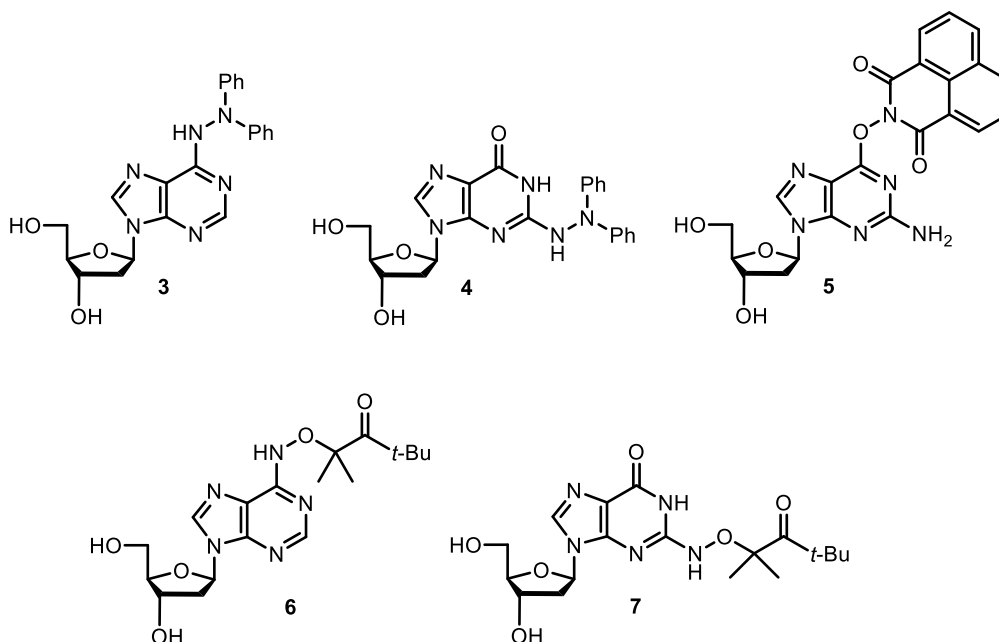
2. Background

2.1 DNA damage induced by ionizing radiation

Ionizing radiation damages DNA via two pathways: the indirect effect and the direct effect. The indirect effect of ionizing radiation refers to DNA damage induced by reactive oxygen species (ROS) generated by radiolysis of water.[2] Ionizing radiation can also directly excite electrons within a nuclei acid molecule. The direct effect results in the

formation of radical cations, particularly in the nucleobases. The components of a mixture absorb the energy of ionizing radiation approximately proportional to their weight.[2] Thus, under low DNA concentration (0.5 μg mL^{-1}), radicals generated by the radiolysis of water are the major contributors to DNA damage, and direct ionization of DNA accounts for a negligible part of the damage events. It is also worth noting that DNA damage induced by the direct effect accounts for $30 - 50$ % of the DNA damage *in vivo*.[46-47] The relative contribution of the direct effect to DNA damage is higher *in vivo* because protein scavenges a significant fraction of the •OH.

The direct effect of ionizing radiation occurs when DNA absorbs the energy from ionizing radiation. The direct effect results in the formation of solvated electrons, electronically excited DNA, and most importantly, radical cations. DNA radical cations can also be accessed via reaction of DNA with one electron oxidants, such as SO_4•-,[31, 48] CO_3•-,[49-51] and Br_2•-.[52] Photosensitization of DNA by irradiating 2-methyl-1,4-naphthoquinone,[53-55] benzophenone,[56] anthraquinone,[24] and riboflavin[57] also generates radical cations.

When a water molecule is excited by ionizing radiation, it can either release an electron to generate a water radical cation or occasionally yield an electronically excited water molecule (eqn. 1 and 2) . The •OH is generated by the deprotonation of the H_2O radical cation, or the homolytic decomposition of the excited water molecule (eqn. 3 and 4).[2] •OH is also generated from the reduction of H_2O_2 by Fe^{2+} or Cu^+, via Fenton chemistry.[58-59]

$$H_2O \xrightarrow{\gamma\text{-radiolysis}} H_2O^{\bullet+} + e^- \qquad \text{eqn. 1}$$

$$H_2O \xrightarrow{\gamma\text{-radiolysis}} H_2O^* \qquad \text{eqn. 2}$$

$$H_2O^{\bullet+} \longrightarrow {}^{\bullet}OH + H^+ \qquad \text{eqn. 3}$$

$$H_2O^* \longrightarrow {}^{\bullet}OH + {}^{\bullet}H \qquad \text{eqn. 4}$$
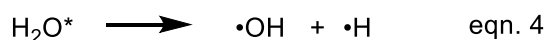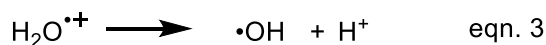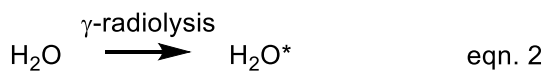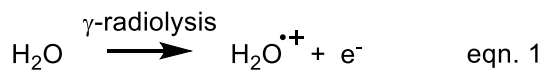
The highly electrophilic $^{\bullet}OH$ readily adds to the C-C and C-N double bonds. Approximately 90% of the pyrimidine nucleoside reactive intermediates generated by $^{\bullet}OH$ result from addition to carbon-carbon double bonds in the nucleobases. $^{\bullet}OH$ undergoes addition to the C-C π-bonds at a nearly diffusion-controlled rate ($k = 3\text{-}10 \times 10^9\,M^{-1}s^{-1}$).[60-61] However, these reactions are regioselective due to the electrophilic nature of $^{\bullet}OH$. For example, the electron-rich C5 of pyrimidines is preferably attacked by $^{\bullet}OH$.[62] The remaining 10% of reactive intermediates arise from the hydrogen atom abstraction from the C5-methyl group of thymine or the deoxyribose.[2]

The susceptibility of nucleobases towards exogenous oxidants, such as ionizing radiation and one-electron oxidants is determined by the reduction potentials of one-electron deficient bases.[4] The reduction potentials of the radical of the four native DNA nucleosides have been measured in aqueous solution by pulse radiolysis (Table 1). Among the four DNA nucleobases, adenine and guanine have relatively low reduction potentials and are preferentially oxidized to their radical cation. The local environment, in which the nucleosides also reside profoundly affects the redox properties of nucleobases. For instance, hydrogen bonding to cytosine reduces the reduction potential of guanine by 100 mV.[63-64] On the other hand, π-stacking in dGGG sequences reduces the reduction potential of

guanine by 77 ± 5 mV, and this reduction makes dGGG triplets the thermodynamic sinks for "holes" (radical cations) in DNA charge transfer (Section 2.3). [65-66]

Table 1. Reduction potentials of nucleoside radical.

Redox couple	E_7 (V)[a]
G• / G	1.29
A• / A	1.42
T• / T	1.7
C• / C	1.6

[a]Versus NHE in H_2O at pH 7.0.

2.1　　Generation of purine radicals

2.1.1　　Generation of adenine radicals

One-electron oxidation of adenosine by the direct effect of ionizing radiation or one-electron oxidants generates adenine radical cations, dA•+ ($pK_a < 4$), which readily deprotonates to yield dA•.[6, 21] This deprotonation is less affected by base pairing than dG•+ in a d(G-C) base pair (see Section 2.1.2) because T is a poor proton acceptor (the pK_a of $T(H)^+$ is -5).[67] However, this equilibrium is significantly affected by π-stacking in poly(dA-T) sequences (Section 2.3.3.2).[21-22] dA• is also generated by the indirect effect of ionizing radiation via the reaction with •OH.[10] Generally, •OH readily adds to double bonds but does not undergo electron transfer. •OH adds to dA at the C8 position (37%), the C4 position (50%) and the C5 position (<5%) (Scheme 2).[10] •OH also abstracts hydrogen atom from the deoxyribose (8%). The C4-OH adduct (**1**) dehydrates to generate dA• with a rate constant of 1.9×10^4 s^{-1}. The C8-OH adduct (**8**) is also generated from the hydration of A•+ at C8 position.

Scheme 2. The generation of adenine radicals.
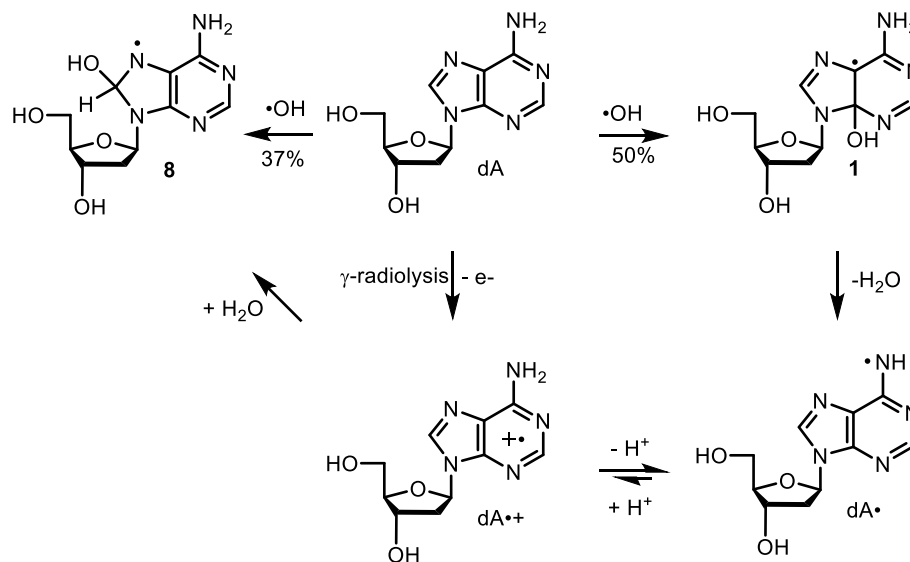
2.1.2 Generation of guanine radicals

Deprotonation of dG•+ (pK$_a$ = 3.9) can generate two isomeric radicals: dG(N1-H)•
resulting from deprotonation from N1 and dG(N2-H)• resulting from deprotonation from
N2 (Scheme 3).[6, 68] dG(N1-H)• is only slightly more stable than dG(N2-H)• because the
radical cations derived from dG and 1-methyl-2'-deoxyguanosine have similar pK$_a$ values
of 3.9 and 4.7, respectively.[7] The B3LYP/6-31G(d) level of theory also suggests that
dG(N1-H)• is 3.26 kcal mol^{-1} more stable than dG(N2-H)• upon hydration by seven water
molecules.[69]

8

Scheme 3. The generation of guanine radicals.
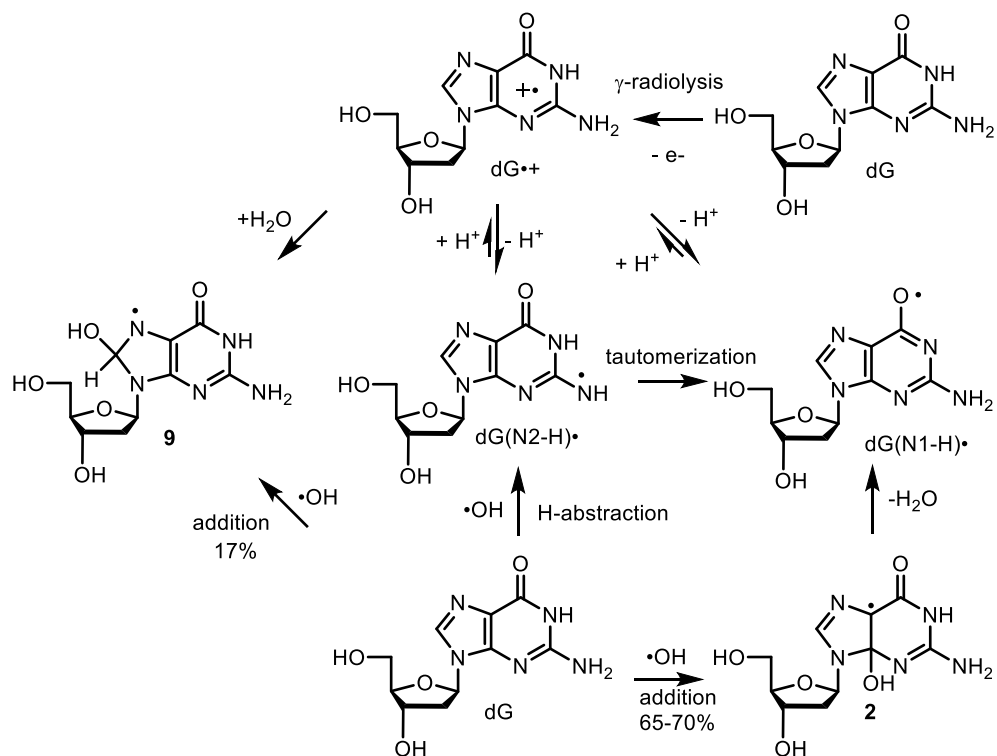
In double-stranded DNA, it is proposed that dG•+ is stabilized by sharing the N1-proton with the N3-site of C in the d[G•+-C] base pair to form d[G(N1-H)•-H+C] (Scheme 4a). Given the pKa values of dG•+ (3.9) and dC (4.3), the ratio between [G•+-C]and [G(N1-H)•-H$^+$C)] is approximately 3:7.[20, 38, 67, 70] The deprotonation from [G(N1-H)•-H$^+$C] base pair to water generates d[G(N2-H)•-C], which is proposed to tautomerize to yield d[G(N1-H)•-C]. However, Anderson et al. proposed an alternative mechanism for deprotonation of d[G•+-C] that did not involve the tautomerization of d[G(N2-H)•-C] (Scheme 4b).[40] They suggested that the oxygen-centered G(N1-H)• abstracts a hydrogen atom from the N4 aminyl group of dC to transiently generate d[G-C•+]. The ensuing deprotonation of the N4 aminyl proton in d[G-C•+] gave rise to d[G-C$_{im}$•], which abstracted the hydrogen atom

from guanine yielding d[G(N1-H)•-C]. The DFT calculations suggested that $dC_{im}\bullet$ is 9.01 kcal mol^{-1} more stable than the aminyl tautomer of dC•.[71-72]

Scheme 4. Deprotonation of dG•+ in the d[G-C] base pair.
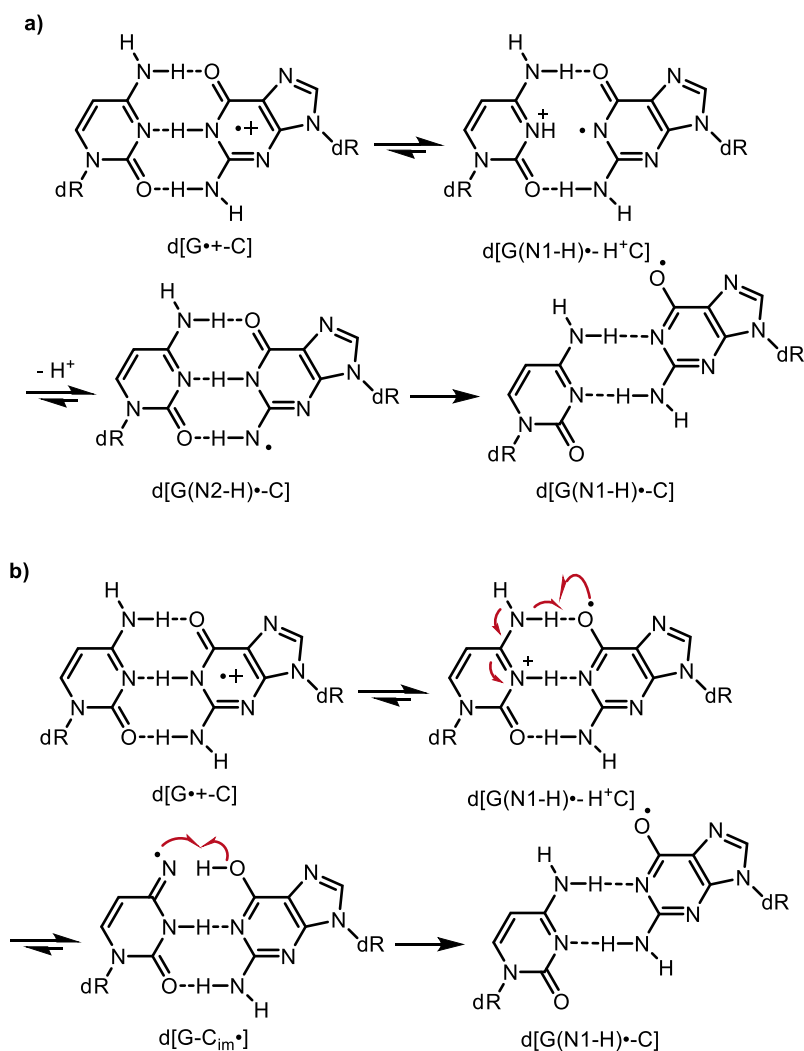
Similar to the reaction between •OH and dA (Scheme 2), •OH adds to dG (Scheme 3) at the C8 position (**9**, 17%) and the C4 position (**2**, 65-70%).[73] It is commonly accepted that dehydration of **2** is the major pathway contributing to the formation of dG(N1-H)•. Recently, however, Chatgilialoglu[35, 37, 74] and co-workers reevaluated the reaction of •OH with dG by pulse radiolysis. They proposed that •OH directly abstracts the hydrogen atom

from the exocyclic NH_2 group of guanine to form of dG(N2-H)•, which undergoes a water-assisted tautomerization to generate dG(N1-H)•. The controversy regarding this proposal will be discussed in Section 2.3.2.1.

2.2 Reactivity of purine radicals

Purine radical cations (dA•+, dG•+) have much lower pK_a values than their parent nucleosides, and readily deprotonate to form neutral purine radicals.[5, 52, 67] Neutral purine radicals, e.g., dA•, dG(N1-H)•, and dG(N2-H)• carry the spin predominantly at oxygen and nitrogen atoms.[75] Carbon-centered radicals react with oxygen at nearly diffusion-controlled rates ($k \sim 10^9$ $M^{-1}s^{-1}$). In contrast, purine radicals have a drastically decreased reactivity towards molecular oxygen ($k \sim (1 - 5) \times 10^2$ $M^{-1}s^{-1}$) due to their reduced electron density on the carbon atoms.[76] In addition, neutral radicals do not undergo hydration like radical cations. According to DFT calculations done on the nucleobases, the reaction of guanine radical cation (Gua•+) with water is exothermic by 75 kcal mol^{-1}, while a corresponding reaction of the guanine radical (Gua•) is endothermic by 29 kcal mol^{-1}.[77] At neutral pH, dG• reacts only slowly with H_2O and lives for ~70 ms in the absence of oxidants, including other radicals.[31]

Gua•+   Gua(N2-H)•   Gua(N1-H)•

Gua•

11
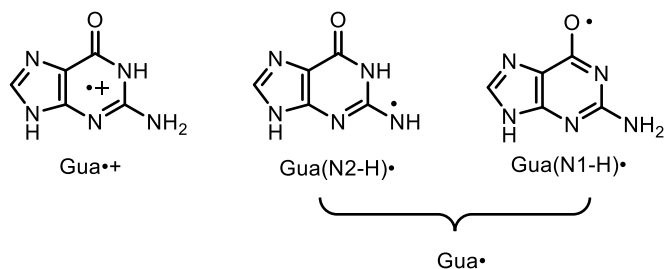
2.2.1 Reactivity of adenine radicals

2.2.1.1 Acid-base equilibria of adenine radicals

The pK_a of nucleobase radical ions affects a variety of biologically significant processes, including DNA hole transfer, and formation of DNA lesions. While the pK_a values of dG•+ (3.9), dC•+ (~4.0), and T•+ (3.6) are generally accepted,[4, 6, 8, 20, 78] the pK_a of dA•+ is still open to question. Steenken and co-workers produced dA•+ from dA in aqueous solution employing 248 nm laser photolysis and estimated the pK_a of dA•+ to be ≤ 1.[6, 20] This pK_a value is significantly lower than that of dA (≥ 14). Sevilla et al. calculated the deprotonation of an adenine radical cation in the presence of a seven water molecule hydration shell (dA•+ + 7 H_2O) and concluded that the pK_a of dA•+ was -0.3.[21] However, in another study, the rates of hole migration in dinucleotide 5'-d(ApG) and 5'-d(GpA) decreased from pH 2.3 to 7, which indicated the population of dA•+ changes within this pH range.[79] This is inconsistent with the aforementioned pK_a of dA•+ (≤ 1). In a more recent transient spectroscopic study, the pK_a of dA•+ is reported to be 4.2.[80] NMR spectral study of one-electron-oxidized adenine produced via laser CIDNP in 5'-AMP suggests that the pK_a of A•+ in aqueous (D_2O) solution is 4 ± 0.2.[81] Furthermore, the recent theoretical calculation by Close predicted the pK_a of A•+ to be 3.9.[8] Additionally, the rate at which dA•+ deprotonates is also controversial. Steenken et al. initially estimated that the deprotonation occurred in less than 1 ps.[6] However, Kobayashi recently reported that dA•+ deprotonated to form dA• in phosphate buffer (20 mM, pH = 7.0) with a rate constant of $2.0 \times 10^7 \ s^{-1}$.[80]

Given the pK_a value of dA•+, the deprotonation rate of dA•+ (< 1 ps) is faster than the rate constants of hole transfer between adjacent adenine ($k = 10^8$ to $10^{10} \ s^{-1}$).[82] This

deprotonation leads to charge-spin separation, which attenuates hole migration.[20] However, this is inconsistent with experiments, which showed that holes efficiently migrate over long dA-T tracts with little distance dependence.[12, 83-86] It has been proposed that the rate of hole transfer in dA-T tracts is faster than the rate of the deprotonation of dA•+. Pulse radiolysis study determined the deprotonation rate of dA•+ to be $0.9-1.1 \times 10^7$ s^{-1} in poly(dA-T) tracts, which is slower than the rate of hole transfer in these sequences.[80] In addition, in the same study, the monomeric dA•+ was reported to deprotonate with a rate constant of $(2.0 \pm 0.2) \times 10^7$ s^{-1}, which is only two times faster than that in poly(dA-T) tracts and significantly slower than that of hole transfer. This result contradicts the previously measured deprotonation rate (< 1 ps) and the observation made in DNA that alternating dA-T sequences serve as insulators in DNA hole migration.[6, 13]
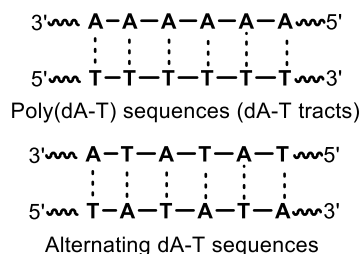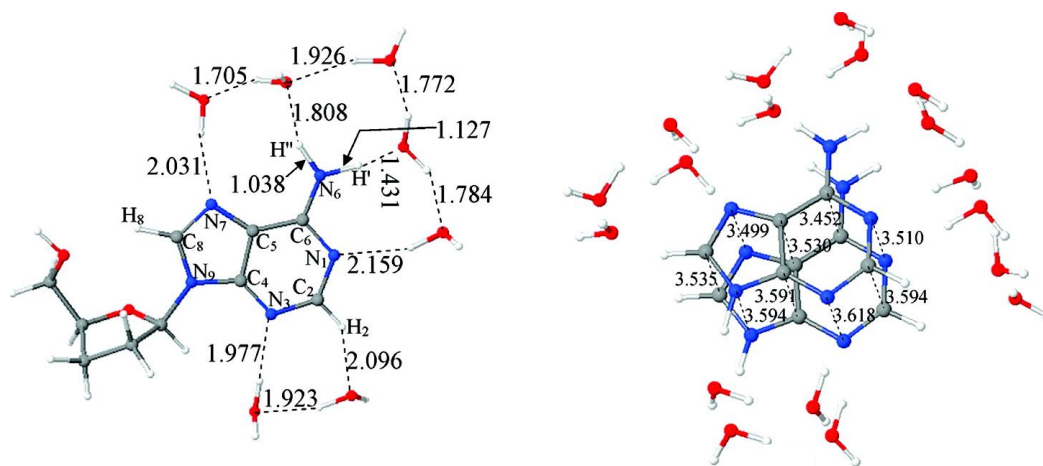
Figure 1. Computationally optimized structures of adenine radical cations. (a) dA•+ + 7 H$_2$O and (b) Ade$_2$•+ + 18 H$_2$O. Reprinted with permission from Adhikary, A.; Kumar, A.; Khanduri, D.; Sevilla, M. D., Effect of Base Stacking on the Acid−Base Properties of the Adenine Cation Radical [A•+] in Solution: ESR and DFT Studies. *J. Am. Chem. Soc.* 2008, *130* (31), 10282-10292.Copyright 2008. American Chemical Society.

13

Another plausible explanation is that the hole within these adenine tracts is delocalized over several stacked adenine bases.[21] Conwell proposed that a hole injected into an extended dA-tract leads to the formation of a polaron delocalized over 3−5 dA-T base pairs.[84] Barton and co-workers suggested that hole delocalization in A-tracts stabilizes the hole towards deprotonation.[85-86] Sevilla and co-workers examined this proposal by DFT calculation and EPR.[21] The geometry of adenine dimer radical cation with an 18 water molecule hydration shell (Ade_2•+ + 18 H_2O) was optimized at the B3LYP/6-31G* level of theory, and the potential energy surface for the stretching of N-H bond was scanned from equilibrium bond length (1.12 Å) to 1.45 Å (Figure 1). Unlike dA•+ + 7 H_2O, which showed no barrier for deprotonation, deprotonation of Ade_2•+ + 18 H_2O was endothermic, and the proton binding energy was calculated to be 12-16 kcal mol^{-1}. The computational studies were validated by generating dA•+ by one-electron oxidation of dA monomer and the oligomer $(dA)_6$ by Cl_2•- in aqueous glass at 150 K. Utilizing EPR, the presence of dA•+ was detected in the pH range of 3-7, and dA• was detected in the pH range of 9-12. These results suggested that the pK_a value of dA•+ was about 8, which was very different from Steenken's estimate (< 1). [6, 20] This contradiction was rationalized by the dimerization of dA in a stacked conformation at millimolar concentration, which stabilized the radical cation.[87-89] Similar behavior of dA•+ was also observed in $(dA)_6$, which is known to adopt a stacked conformation.[88] More recently, dA_n•+ (n > 3) was directly observed in diphenylacetylenedicarboxamide (DPA) capped DNA hairpins using femtosecond transient absorption spectroscopy and dA_n•+ showed a distinct absorbance at 565 nm.[83] The delocalization of dA•+ in stacks of adenines is unique. Similar delocalization of dG•+ in stacks of guanine was not observed. The spin density of d(G•+pG) and d(ApA)•+ were

simulated at the M06-2X/6-31G* level of theory (Figure 2).[90] The calculations suggested

that in d(G•+pG), the spin density was localized at the 5'-guanine. In the d(ApA)•+, the

spin density was equally delocalized on both of the adenines.
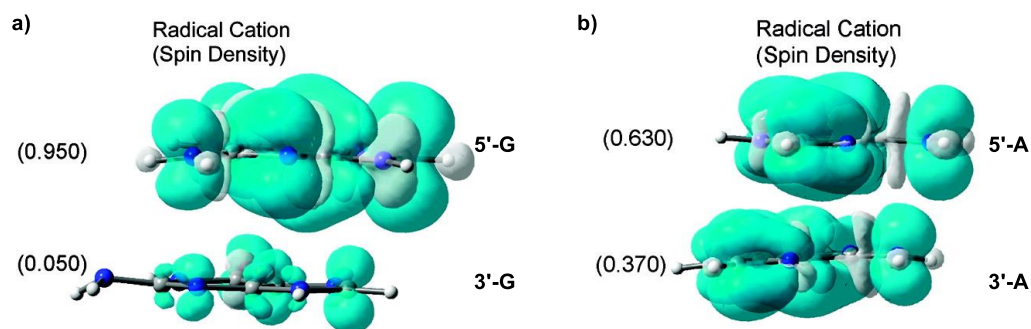
Figure 2. Spin density plots of (a) d(G•+pG) and (b) d(ApA)•+. Reprinted with permission from Kumar, A.; Sevilla, M. D., Density Functional Theory Studies of the Extent of Hole Delocalization in One-Electron Oxidized Adenine and Guanine Base Stacks. *J. Phys. Chem. B* 2011, *115* (17), 4990-5000. Copyright 2011. American Chemical Society.

2.2.1.2   Products formed from adenine radicals

Two major products arise from adenine derived radicals are 8-oxo-7,8-dihydro-2'-

deoxyadenosine (8-oxo-dA, Scheme 5) and *N*6-(2-deoxy-α,β-d-erythro-pentofuranosyl)-

4,6-diamino-5-formamidopyrimidine (FapydA, Scheme 5).[91] Their formation can be

explained by the oxidation and reduction of **8**, which is either generated by hydration of

dA•+ or the addition of •OH at the C8 position of dA (Scheme 2). Another modified

nucleoside that was found to be generated upon one-electron oxidation by photoexcited

riboflavin or menadione is 2'-deoxyinosine (dI), which likely arises from deamination of

dA• (Scheme 5).[92] However, the mechanism for the generation of dI is unclear at this point.

The yields of 8-oxo-dA and FapydA are about eight- to tenfold lower than the yields of 8-

oxo-7,8-dihydro-2'-deoxyadenosine   (8-oxo-dG)   and   *N*6-(2-deoxy-α,β-d-erythro-

pentofuranosyl)-2,6-diamino-4-hydroxy-5-formamidopyrimidine (FapydG).[93] This may

be explained by the lower oxidation potential of guanine, which can result in the transfer of an electron from guanine to radicals in close proximity.[94]

Scheme 5. Products generated from adenine radicals.
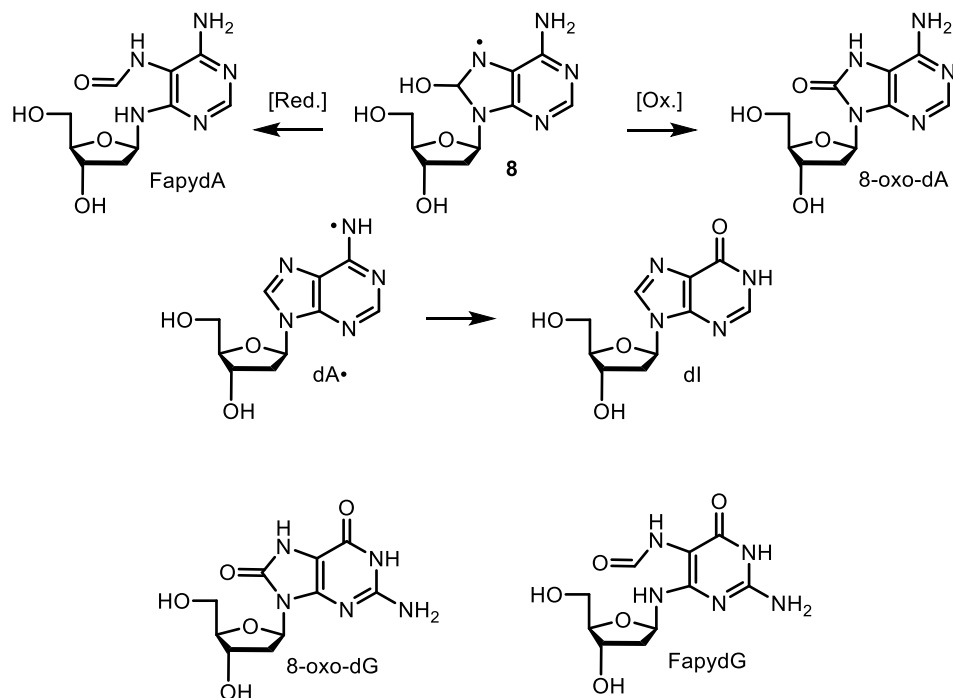
2.2.2 Reactivity of guanine radicals

2.2.2.1 Tautomerization of neutral guanine radical

Recently, Chatgilialoglu and co-workers demonstrated the tautomerization between dG(N2-H)• and dG(N1-H)•. Upon reaction with a solvated electron, 8-bromo-2'-deoxyguanosine (**10**) was converted to its radical anion (**11**), which lost a bromide ion to generate dG(N2-H)• (Scheme 6).[36-37, 95] However, the author did not address the mechanism by which the initially generated vinyl radical (dG(C8-H)•) tautomerized to dG(N2-H)• (Scheme 6). The transient spectrum recorded 2 μs after the pulse had an absorbance at around 600 nm, which was consistent with the DFT simulated spectrum of dG(N2-H)•. The absorbance decayed by a first-order rate constant of $5 \times 10^4\,\text{s}^{-1}$ to generate

dG(N1-H)•, which showed absorbances around 500 nm and 400 nm. The activation energy

of this tautomerization was experimentally measured to be 23.0 ± 2.5 kJ mol^{-1}. DFT

calculations performed in the same study suggested that the energy barrier for direct

tautomerization from dG(N2-H)• to dG(N1-H)• is 183.7 kJ mol^{-1}. The energy barrier was

lowered to 18.8 kJ mol^{-1} by a water-assisted proton transfer, which was consistent with the

experimental measurements.

Scheme 6. Generation of dG(N2-H)• via one-electron reduction of 8-bromo-2'-deoxyguanosine (**10**) and tautomerization between dG(N2-H)• and dG(N1-H)•.
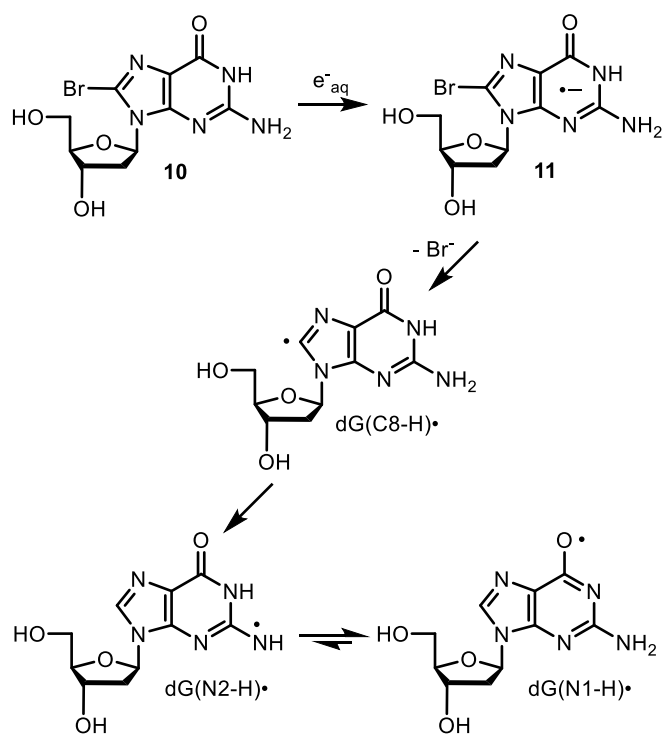
However, the same calculation was performed by Sevilla et al. using the same level

of theory (B3LYP/6-31G*), and the activation energy was found to be 18.9 kcal mol^{-1},

which suggested that units may have been misreported in Chatgilialoglu's original paper

(Figure 3). At 298 K, the rate constant of tautomerization based on Chatgilialoglu's

calculation was $\sim 3.7 \times 10^{10}$ times greater than that derived from Sevilla's calculation. The

calculation performed by Sevilla et al. suggested that the hydrogen atom abstraction, tautomerization pathway was unlikely to be competitive against addition, elimination pathway at room temperature.[69]
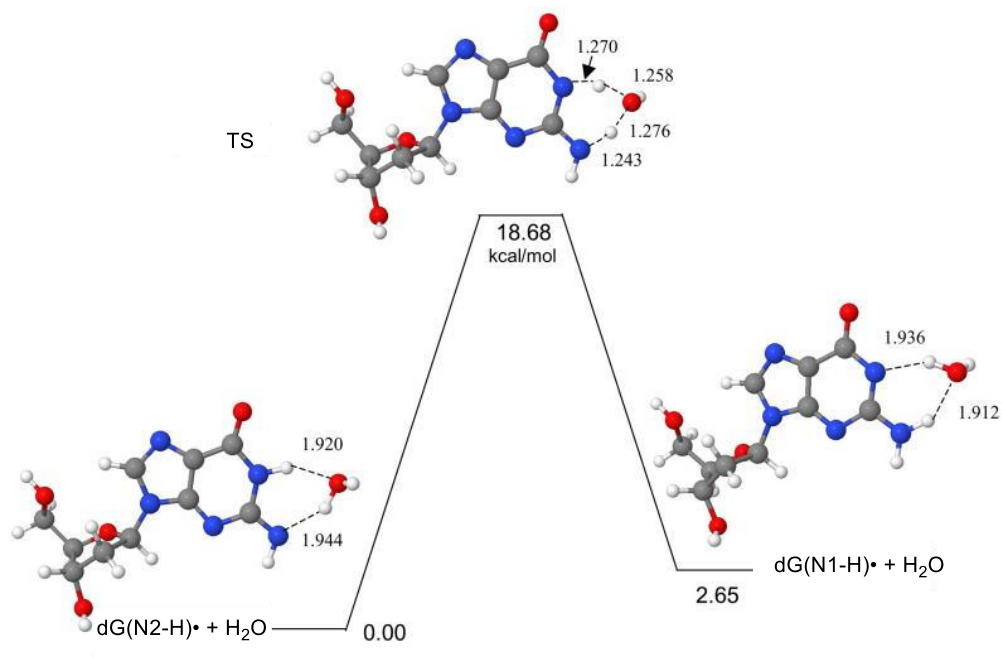
Figure 3. Water-assisted tautomerization between dG(N2-H)• and dG(N1-H)•. Reprinted with permission from Adhikary, A.; Kumar, A.; Becker, D.; Sevilla, M. D., The Guanine Cation Radical: Investigation of Deprotonation States by ESR and DFT. *J. Phys. Chem. B* 2006, *110* , 24171-24180. Copyright 2006. American Chemical Society.

Having assigned the transient spectra of the two tautomers of dG•, Chatgilialoglu et al. reevaluated the reactivity of guanine towards hydroxyl radicals.[35, 74] The transient spectrum obtained from the pulse radiolysis of dG showed an absorbance at around 600 nm, which suggested that the species initially generated by the reaction between hydroxyl radicals and guanine was dG(N2-H)•. This observation led to the proposal that hydroxyl radicals react with guanine via hydrogen atom abstraction from the exocyclic aminyl group. Sevilla et al. also investigated the direct hydrogen abstraction from the exocyclic NH_2 of guanine by •OH and calculated that the activation barrier for hydrogen abstraction was 7

kcal mol^{-1}.[69] Sevilla and co-workers considered an alternative mechanism, the addition elimination mechanism (Scheme 3). They calculated that the initial addition of the •OH at C4-C5 π-bond of guanine is barrier-free, and the C4-OH adduct (Gua(C4-OH)•) has only

Gua(C4-OH)•

a small activation barrier of 1–6 kcal mol^{-1} to form a metastable ion-pair intermediate (Gua•+ --- OH$^-$, Figure 4).[39, 69] The ion-pair deprotonates to form H$_2$O and neutral dG radicals favoring Gua(N1–H)• with an activation barrier of 5 kcal/mol. The overall process from **2** to Gua(N1–H)• and water was found to be exothermic by more than 13 kcal/mol. These results suggested the generation of Gua(N2–H)• is not necessary for the formation of Gua(N1–H)•, and the formation of Gua(N1–H)• more likely goes through the low-energy addition elimination pathway. Interestingly, calculations also suggest that the (Gua•+ --- OH$^-$) ion-pair has a long wavelength absorption peak (λ_{max} = 665 nm) which was previously assigned to absorption of dG(N2-H)•.[69]
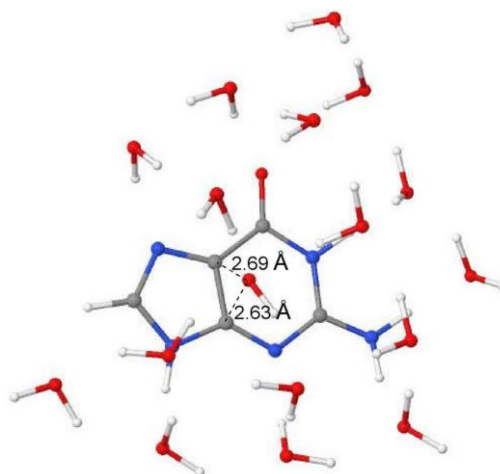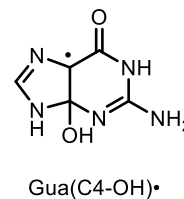
Figure 4. The Metastable ion-pair intermediate (Gua•+ --- OH$^-$) generated by the dehydration of Gua(C4-OH)•. Reprinted with permission from Kumar, A.; Pottiboyina, V.; Sevilla, M. D., Hydroxyl Radical (OH•) Reaction with Guanine in an Aqueous Environment: A DFT Study. *J. Phys. Chem. B* 2011, *115*, 15129-15137. Copyright 2011. American Chemical Society.

2.2.2.2   Products formed from guanine radicals

Guanine is susceptible to one-electron oxidation, which gives rise to dG•+ and the deprotonated neutral radical dG(N1-H)•.[5-7] The two major decomposition pathways involve (i) oxidation of dG• by O_2 (ii) hydration of dG•+ and subsequent oxidation or reduction. The first pathway leads to the formation of 2,2-diamino-4-[(2-deoxy-β-D-erythro-pentofuranosyl)amino]-5(2H)-oxazolone (dOz, Scheme 7) and its precursor 2-amino-5-[(2-deoxy-β-D-erythro-pentofuranosyl)amino]-4H-imidazol-4-one (dIz).[96-99] The formation of these products can be rationalized by dG(N1-H)• which can be generated by deprotonation of dG radical cation or dehydration from the predominant •OH C-4 adduct of the guanine moiety (**2**, Scheme 3).[73] In a subsequent step, dG(N1-H)• reacts with O_2 or more likely O_2•- to form peroxide **12**.[73] The addition of water takes place at the 7,8-double

Scheme 7. The generation of dIz and dOz from dG(N1-H)•.
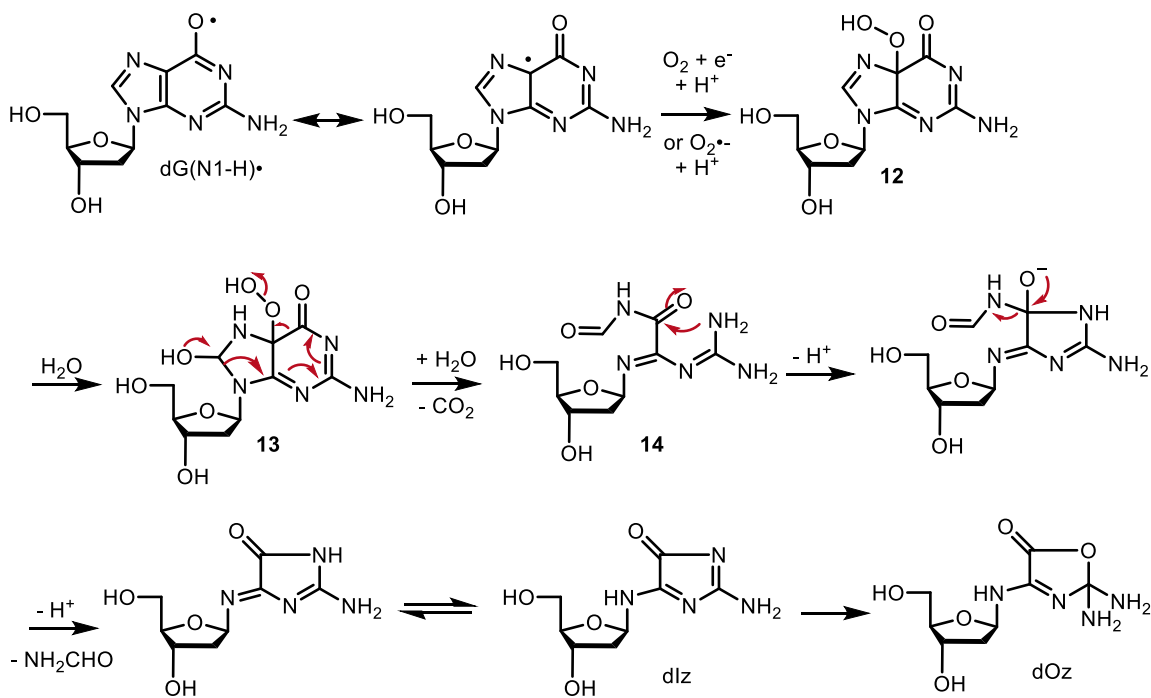
bond of **12** to generate **13**, followed by ring opening of the pyrimidine and loss of CO_2 to generate **14**.[98] The release of formamide leads to the formation of dIz which hydrolyzes to generate dOz (Scheme 7). It is also worth noting regarding that DNA containing dOz or dIz is readily cleaved upon hot piperidine treatment whereas 8-oxo-dG is stable under similar conditions.[96, 100-101]

Scheme 8. Products generated from 8-hydroxy-7,8-dihydroguanyl radical (**9**).
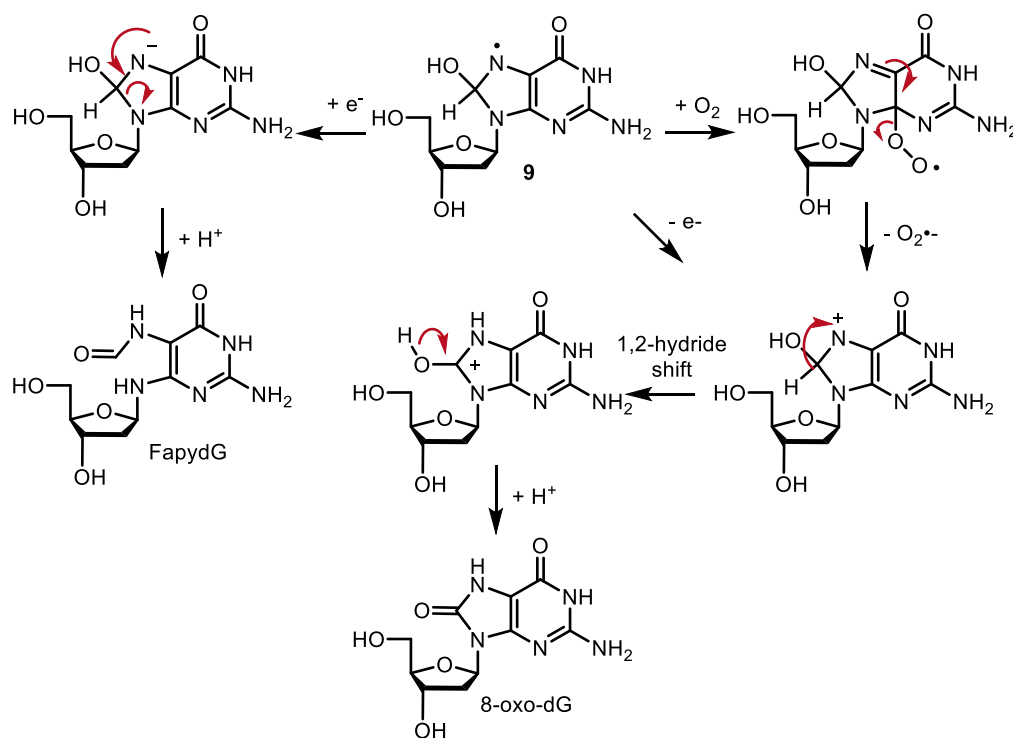
The second major radical-induced decomposition pathway of dG involves 8-hydroxy-7,8-dihydroguanyl radical (**9**) that arises from either the hydration of dG•+ or addition of·•OH at C-8 of dG (Scheme 3).[6] This pathway leads to the predominant formation of 8-oxo-dG together with small amounts of FapydG in aerated aqueous solution (Scheme 8).[73, 102-103] Oxidation of transiently formed **9** leads to the formation of 8-oxo-dG, whereas competitive reduction gives rise to FapydG. However, the formation of 8-oxo-dG

upon exposure of dG and single-stranded DNA to one-electron oxidants is only a minor process. This is caused by the rapid deprotonation of dG•+ at neutral pH since its pK_a is 3.9.[6, 38] In contrast, hydration of dG•+ is more efficient within double-stranded DNA, in which guanine radical cations are likely to be stabilized through base stacking and base pairing. This stabilization leads to higher yields of products resulting from hydration of dG•+.[38, 104]

The two-electron oxidized product of guanine—8-oxo-dG, which has an oxidation potential about 0.5 eV lower than that of dG,[105] is a preferential target for one-electron oxidizing agents.[106-108] For instance, the rate constant describing the reaction of dG• with 8-oxo-dG was found to be 4.6×10^8 M^{-1} s^{-1} at pH 7.0.[109] This fast reaction, together with the slow addition of O_2 to dG• ($k < 10^2$ M^{-1} s^{-1}), could explain the low yield of 8-oxo-dG during γ-radiolysis of an aerated aqueous solution of dG. Instead of 8-oxo-dG, the two diastereomers of spiroiminodihydantoin 2'-deoxynucleosides (dSp, Scheme 9) resulting from two-electron oxidation of 8-oxo-dG were the predominant oxidized products of dG at higher pH (pH > 5.8).[107, 110-112] The formation of dSp containing products was rationalized by the transient generation of 5-hydroxy-8-oxo-7,8-dihydroguanine (**15**) that rearranges via an acyl shift (Scheme 9a). Under slightly acidic conditions (pH < 5.8) or sterically encumbered environments such as double-stranded DNA, **15** undergoes opening of the 5,6-pyrimidine ring followed by a decarboxylation reaction and formation of the two diastereomers of guanidinohydantoin derivatives (dGh, Scheme 9b).[107, 110-113] It is also worth mentioning that **15** is at the same oxidation state as **13** which generates dOz and dIz , (Scheme 9c). However, dOz and dIz are generated in lower yields than dSp and dGh.[108]

22

Scheme 9. Products generated from two-electron oxidation of 8-oxo-dG.
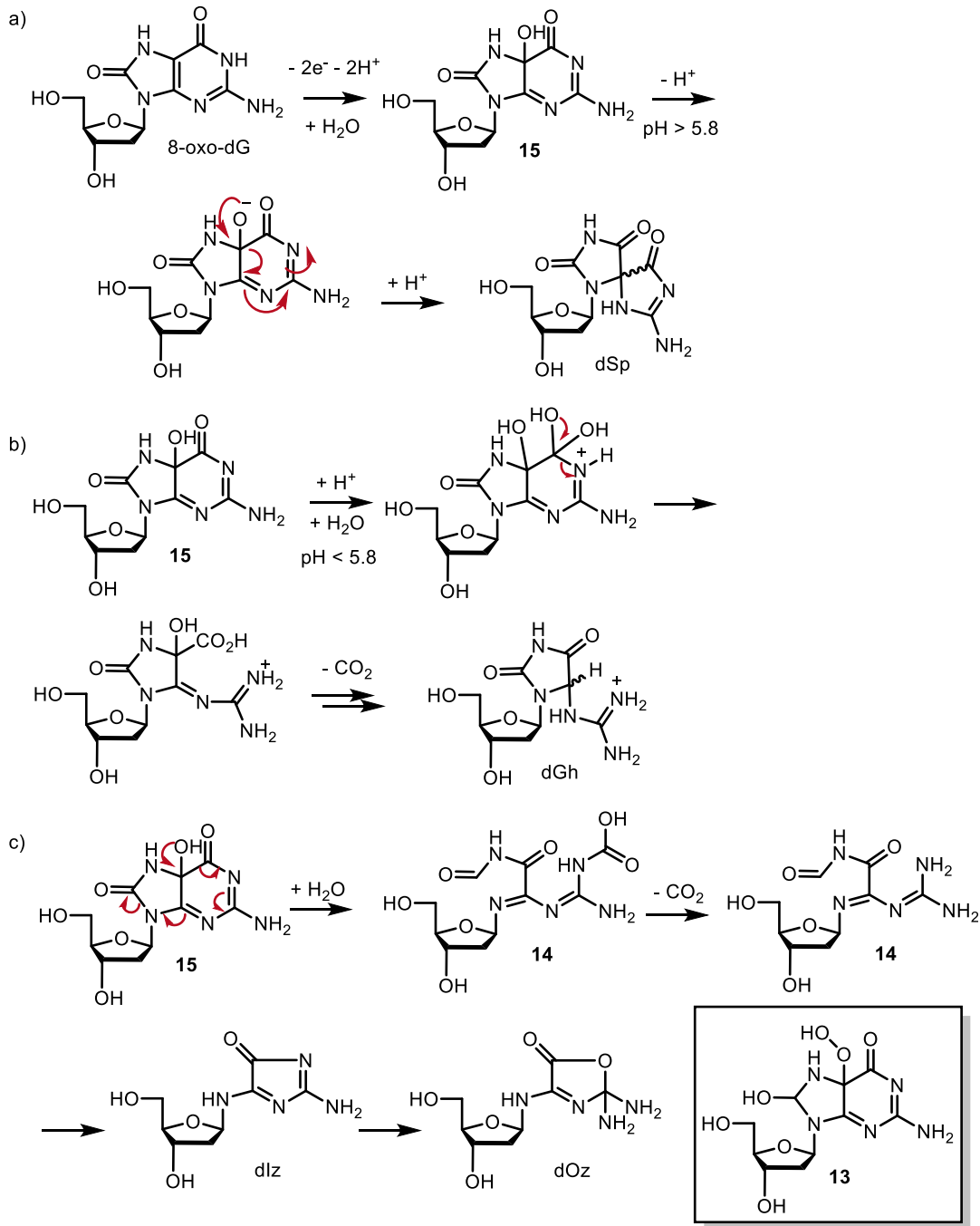
2.2.1 Mechanism of DNA hole migration

2.2.1.1 Hopping mechanism

Over a half century ago, Eley and Spivey demonstrated the semiconductivity of duplex DNA.[114] In 1993, Barton and co-workers reported that holes rapidly migrate through DNA duplexes.[115] DNA hole migration helps to explain how initial oxidation events induce DNA damages at distal positions.[13, 29, 115-117] Furthermore, DNA hole migration chemistry can also be utilized to sense changes in DNA including DNA lesions, mismatches, and protein binding.[118-122] For instance, more recently Barton and co-workers demonstrated that binding of human DNA primase is controlled by the oxidation state of the [4Fe4S] cluster that is modulated by DNA hole migration.[123] As a biologically significant process, the mechanism of DNA hole migration was thoroughly investigated. DNA hole migration was initially proposed to occur via a superexchange mechanism, a process in which the charge transportation is considered as a unistep coherent orbital-mediated tunneling without the oxidation of bridging nucleotides (Figure 5a).[115, 124-125] The superexchange mechanism predicts that the rate of charge transport decreases exponentially as the distance increases (eqn. 5).[126-128]

$$\ln k = -\beta \ln \Delta r \qquad \text{eqn. 5}$$
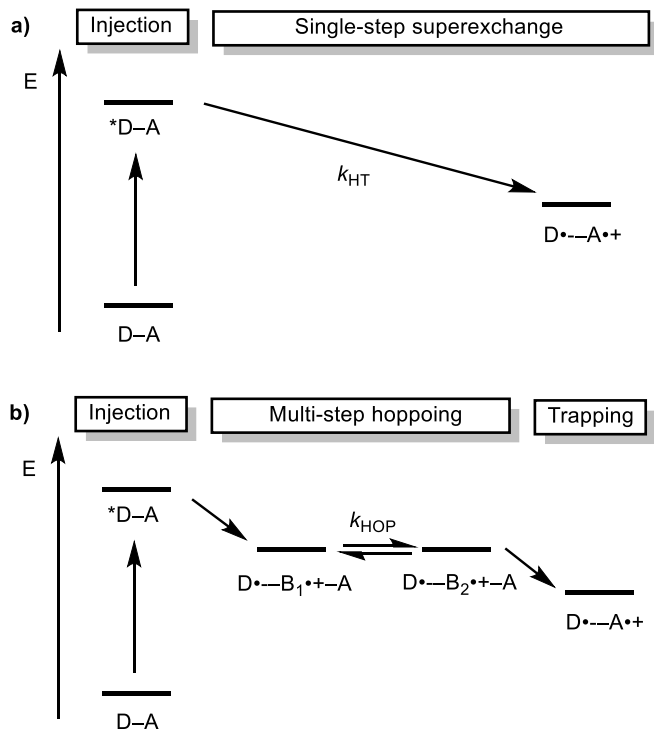
Figure 5. Comparison of photoinduced DNA-mediated hole transfer via (a) the superexchange mechanism and (b) the hopping mechanism (D = donor, A = acceptor, B = base, HT = hole transfer, HOP = hopping).

The β value was independently determined by PAGE analysis of strand-cleavage and femtosecond time-resolved transient-absorption spectroscopy to be 0.7 ± 0.1 Å^{-1}.[13, 126, 129] This strong distance dependence suggests that a single step charge transfer via superexchange over long distance is too slow to compete with trapping reaction of dG•+ by water and deprotonation of dG•+.[11, 130] Alternatively, the hopping mechanism is generally considered as the more plausible mechanism to explain the observed hole migration over long distances (e.g. 50 Å) (Figure 5b).[11, 130] Giese and co-workers demonstrated that the overall hole migration over long distances occurs as a multistep hopping process during which holes reversibly "hop" between hole carriers (dG•+, Figure 2b). Each hopping step can be viewed as a discrete superexchange process and is

25

competitive with hydration and deprotonation.[131-132] The efficiency of hole migration by hopping shows a shallow distance dependence and can be described by eqn. 6, in which E is the efficiency of the hole migration, and N is the number of the equidistant hopping steps.[11, 130, 133-134]

$$\ln E \propto -\ln N \qquad \text{eqn. 6}$$

2.2.1.2 "A-Hopping" and polaron formation in poly(dA) sequences

In the previous section, the discussion was based on the assumption that dG•+ is the hole carrier, and the superexchange between guanines separated by poly(dA-T) tracts does not lead to any oxidation within the poly(dA-T) regions. Based on the distance dependence of the rate of superexchange (eqn. 5), one may mistakenly conclude that hole transfer will collapse when the length of the poly(dA-T) tracts increase, which is not the case.[85, 135-137] Giese and co-workers investigated sequences bearing different lengths of $(dA-T)_n$ tracts between dG•+ and dGGG triplets (Figure 6).[12] For n = 1–3 the alkali-labile lesion yield ratio P_{GGG}/P_G decreased from 250 to 4, which is consistent with the exponential distance dependence of single step superexchange. However, when the number n of $(dA-T)_n$ base pairs increased further, P_{GGG}/P_G only decreased slightly. It was proposed that when the length of $(dA-T)_n$ increases, the rate of superexchange between the dG•+ and the dGGG triplets was so slow that endothermic oxidation of the adjacent adenine by thermally excited dG•+ to generate dA•+ became competitive.[138-140] Once the dA•+ is generated, the hole rapidly migrates through the dA-T base pairs until it reaches the dGGG triplets, the thermodynamic sink for the hole.[65] This nearly distance-independent hole transfer over $(dA-T)_n$ sequences where adenines are charge carriers is named "A-hopping".[117] Giese originally proposed that hole migration occurred in poly(dA-T) tracts via tunneling.[12] As

previously discussed in section 2.2.1.1, this rapid hole migration can also be explained by the delocalization of positive charge over multiple $(dA-T)_n$ base pairs to form polarons, which have been directly observed in DNA hairpins.[83-84] Furthermore, since the calculated polaron size is approximately four adenines, the strong distance dependence that has been found for tracts shorter than this length is consistent with these sequences not supporting polaron formation.[141]
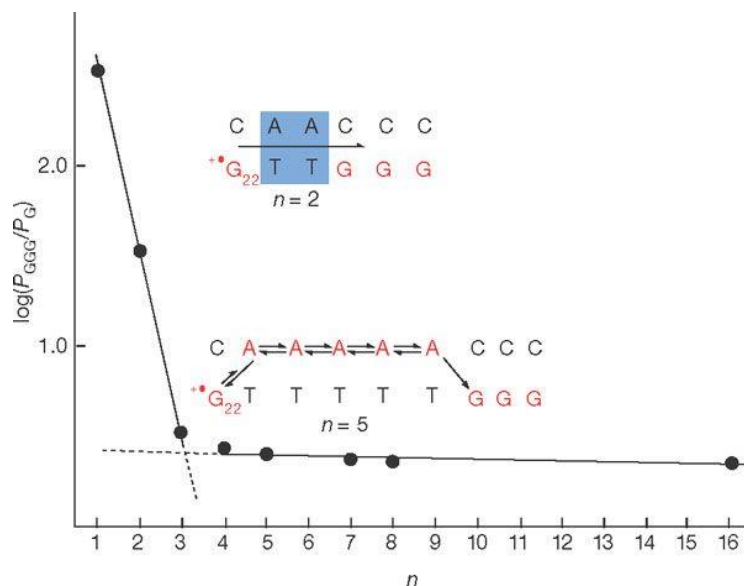
Figure 6. Plot of $\log(P_{GGG}/P_G)$ against the number n of the dA-T base pairs. Reprinted with permission from Giese, B.; Amaudrut, J.; Kohler, A.-K.; Spormann, M.; Wessely, S., Direct observation of hole transfer through DNA by hopping between adenine bases and by tunnelling. *Nature* 2001, *412*, 318-320.Copyright 2001. Springer New York, LLC: Nature.

2.2.2   Strand damage induced by DNA hole migration

2.2.2.1   Hole migration induced strand damage at guanine base stacks

As previously mentioned, dGG and dGGG sites are more easily oxidized than isolated guanine sites and are preferred hot spots for hole localization during hole DNA transfer. Experimental and theoretical studies suggested that there is a distinct preference for hole localization at the 5'-dG in dGG and dGGG sequences.[14] EPR studies suggested

that 60% of holes localize at the 5'-dG of a dGGG triplets at 77 K.[70] However, this localization of holes was not fully consistent with observations made in some strand cleavage assays, in which the central dG was often preferentially damaged. To explain this phenomenon, it has been proposed that the preferential site of strand cleavage is dictated by the stability of neutral radical species.[142] For example, computational studies showed that 5'- d(TG$_1$G$_2$•G$_3$T) was more stable than 5'-d(TG$_1$•G$_2$G$_3$T) by 2.4 kcal mol^{-1}. This was consistent with the strand cleavage assay, in which dG$_2$ of 5'-d(TG$_1$G$_2$G$_3$T) is more reactive than dG$_1$. The same correlation was also found in the 5'-d(CG$_1$G$_2$G$_3$C) sequence. If this proposal is correct, one has to assume that the strand cleavages are induced by alkali-labile lesions generated from the neutral guanine radicals, such as dOz and dIz.[97] However, other reactions at sites where the hole is stabilized, such as nucleophilic addition of H$_2$O at C8 in the guanine moiety, followed by one-electron oxidation leading to the formation of 8-oxo-dG have also been suggested.[143] These proposals raised the question which is yet to be answered. What is/are the structure(s) of hole migration induced guanine lesion(s)?

2.2.2.2   Hole migration induced strand damage in the absence of guanine

Although the majority of literature has focused on hole migration induced strand damage on dG, strand damage induced via hole migration in poly(dA-T) sequences in the absence of guanine has been investigated by Schuster and co-workers.[25-26, 28-29] After holes were introduced by photoexcited anthraquinone (AQ),[144] the alkali-labile lesions detected in duplex **16** were localized at the GG step as one would expect. However, in duplex **17** and **18** which lack guanine, the alkali labile lesions are predominantly generated at the 5'-thymidine in TT steps (in **17**) and the central thymidine in TTT steps (in **18**). These

AQ-5'-d(TTT TAA ATT AAA TTA AAT TAA ACC TAT ATT T)
3'-d(AAA ATT TAA TTT AAT TTA ATT TGG ATA TAA A)-5'-[32]P

16

AQ-5'-d(TTA ATT AAT TTT TAA TTA ATA TA)
3'-d(AAT TAA TTA AAA ATT AAT TAT AT)-5'-[32]P

17

AQ-5'-d(TTT TAA ATT AAA TTA AAT TAA ATA TAT TT)
3'-d(AAA ATT TAA TTT AAT TTA ATT TAT ATA AA)-5'-[32]P

18

AQ-5'-d(TTT TAA TT A ATT AAT TAA TAT ATT T)
3'-d(AAA ATU AAU TAA TUA AUT ATA TAA A)-5'-[32]P

19

AQ
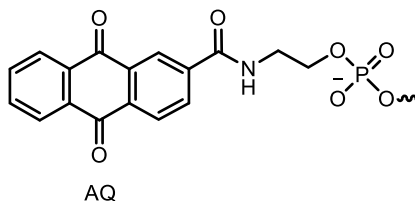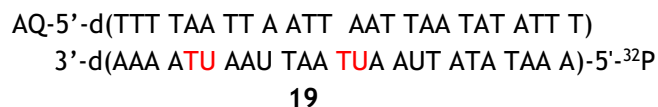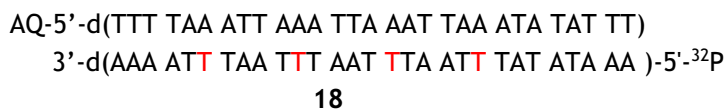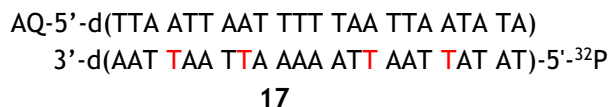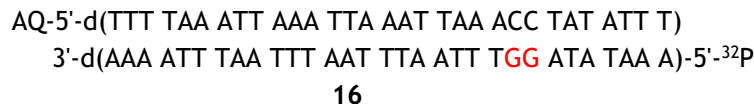
observations are surprising because dAs are more easily oxidized and are the major hole
carriers in these duplexes.[4, 12] The authors proposed that charge transfer from dA•+ on the
opposite strand resulted in the formation of T•+, which was the precursor for the observed
alkali-labile lesions.[25] The Curtin–Hammett principle was invoked to explain the product
formation. Despite the high population of dA•+, T•+ was irreversibly trapped by oxygen
and water, and dA•+ did not generate alkali-labile products. The strand damage in TT steps
was attributed to tandem lesions (Scheme 10). When the T•+ is localized on the 5' end of
a TT step, the hole is trapped by water and oxygen to a give peroxyl radical (Scheme 10a),
which abstracts a hydrogen atom from the C5-methyl hydrogen of the 3'-T. The resulting
carbon-centered radical (T•) is trapped by O_2 and ultimately generates tandem lesion **20**.
Alternatively, 3'-T•+ deprotonates to generate T•, which reacts with oxygen to yield 5-fdU

Scheme 10. The mechanism for tandem lesion generation in 5'-TT steps induced by hole migration.

X = -CHO or -CH₂OH
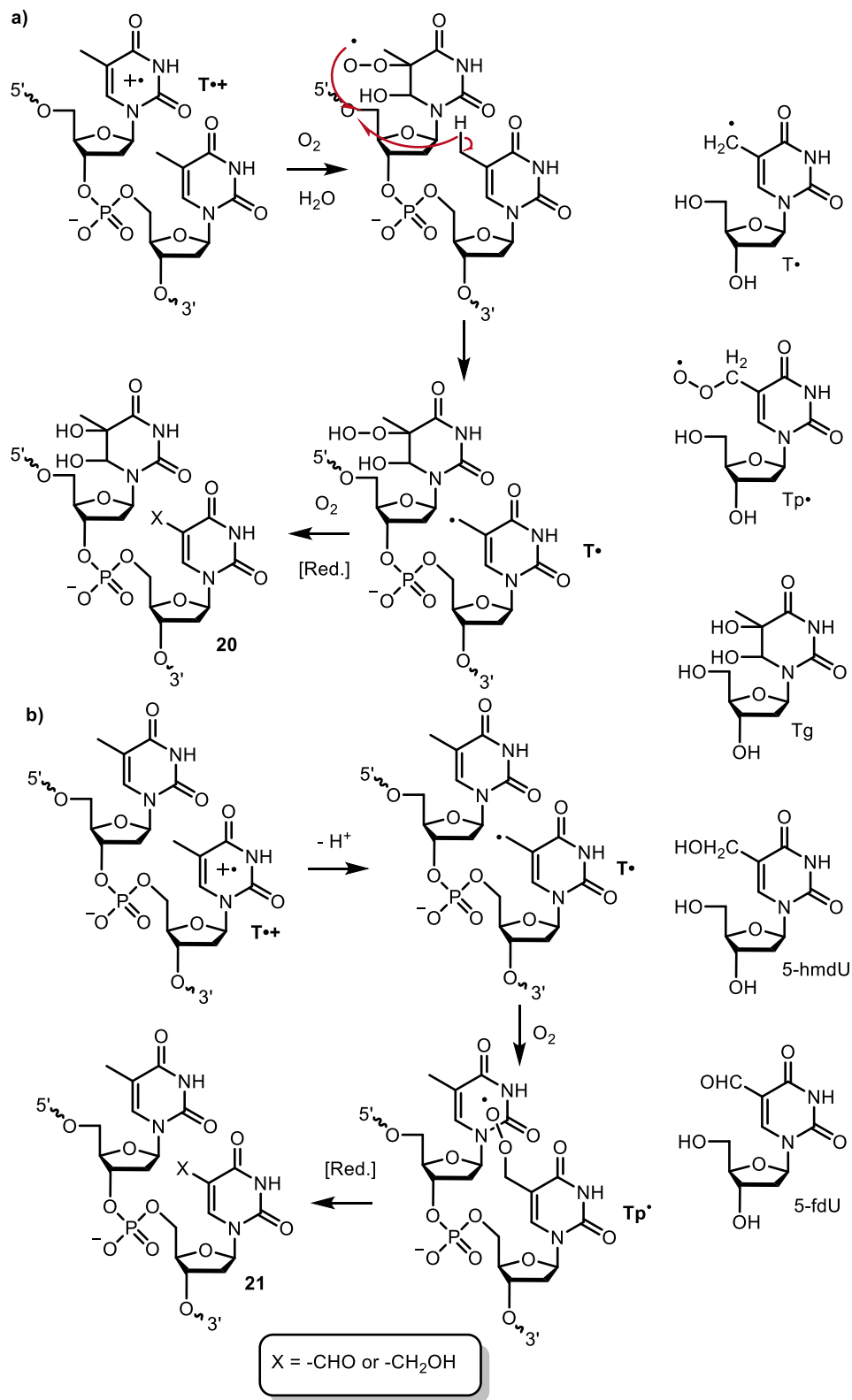
or 5-hmdU single lesions **21** (Scheme 10b). The peroxyl radical (Tp•, Scheme 10b) generated from the 3'-T•+ was proposed to not contribute to the strand damage due to the unfavorable distance for hydrogen atom abstraction from C5-methyl hydrogen of the 5'-T (see Section 3.2.5.1). In addition, alkali-labile lesion formation was sequence specific. For instance, alkali-labile cleavage was observed at TT and 5'-d(UT) steps, but no damage was detected at 5'-d(TU) sequences (**19**). This is consistent with the proposed mechanism that the absence of C5- methyl hydrogen of the 5'-dU inhibits both pathways of strand damage formation (Scheme 10), but the absence of the C5-methyl hydrogen of the 3'-dU does not have such effect. LC-MS analysis of the enzyme digest of the photolyzed oligonucleotides revealed the formation of 5-fdU, 5-hmdU, and Tg, which agreed with the proposed mechanism. The authors also rationalized the preferential damages at the central T in 5'-TTT segments, but the proposal was inconsistent with the observation (see Section 3.2.5.1).

2.3   Tandem lesions

It has been proposed that the cytotoxicity of ionizing radiation largely arises from the formation of clustered lesions.[145-147] A clustered lesion is defined as two or more lesions, such as oxidized bases, abasic sites, or strand breaks formed within 20 bp. Tandem lesions, e.g., **20**, are a subset of cluster lesions in which two adjacent nucleotides on the same strand are damaged.[147] The formation of tandem lesions was first reported by Box and co-workers from X-ray irradiated 5'-d(GpT) in the presence of oxygen.[148] A damaged residue containing an 8-oxo-dG and N-(2-deoxy-d-erythropentofuranosyl)formylamide (**22**, Scheme 11) was isolated. Formation of **22** was proposed to arise from **23**, which resulted from the addition of •OH to the thymidine π-bond (Scheme 10). The resulting carbon-centered radical was trapped by oxygen to form peroxyl radical **24**, which adds to the C8

of 5'-dG. A subsequent breakdown of the peroxide **25** and β-fragmentation of **26** generates the tandem lesion (Scheme 11).[149] Cadet identified and characterized **22** in enzyme-digested (snake venom phosphodiesterase and calf spleen phosphodiesterase) calf thymus DNA that was γ-irradiated utilizing HPLC-ESI-MS/MS.[150] The proposed mechanism for the tandem lesion formation was supported by an isotopic labeling experiment, in which one [18]O atom was incorporated in the tandem lesion.[149]

Scheme 11. The mechanism for tandem lesion generation in 5'-GT.
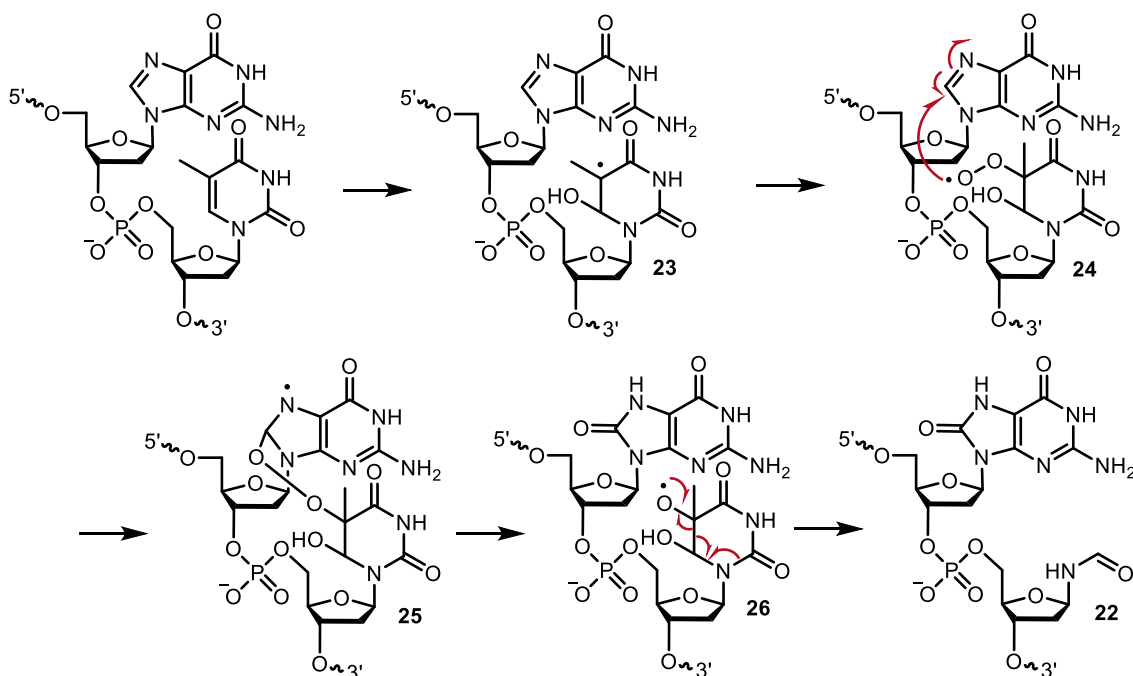
Wang and co-workers identified another tandem lesion (**27**) in calf thymus DNA exposed to Cu(II)/ascorbate/H_2O_2.[151] The oxidized DNA was digested by nuclease P1, which does not hydrolyze the phosphodiester bond 3' to the thymidine glycol (Tg), enabling the detection of the tandem lesion. The tandem lesion with reversed directionality (**28**) was not detected. However, nuclease P1 used to digest the DNA was previously shown to digest

22 that had the same directionality.[149] Hence, the formation of **28** may be masked by the nuclease treatment.
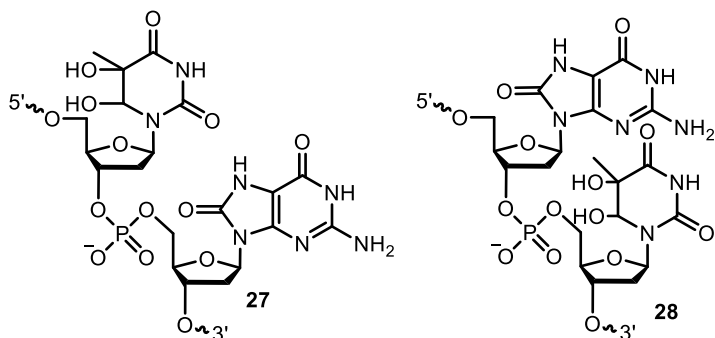
Scheme 12. The mechanism for generation of intrastrand [G-T] cross-links.

dR = 2'-deoxyribose
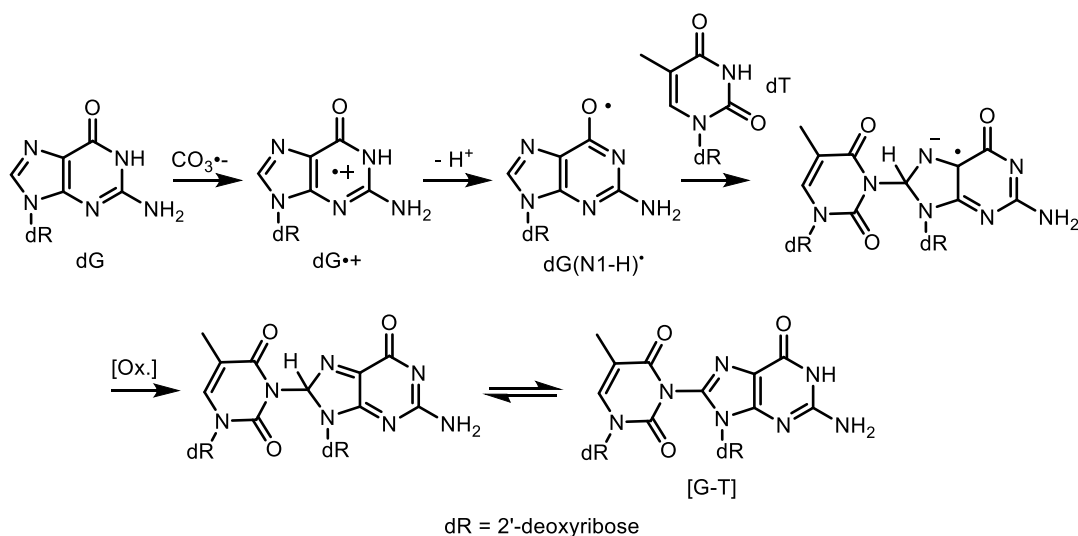
Another example of a tandem lesions is [G-T] (Scheme 12), which has been detected following one-electron oxidation of 5'-d(CCTACGCTACC) by photochemically generated CO$_3$•-.[152-154] The structure of this tandem lesion was characterized by LC-MS/MS following enzymatic digestion, 1D, and 2D NMR studies.[153] The formation of [G-T] cross-links is most efficient in the case of 5'-d(GpCpT). However, the central dC was hydrolyzed by alkaline phosphatase and snake venom phosphodiesterase. Cross-link 5'-

d(GpT) was observed in 5'-d(TTAC**GT**AC**GT**AA) following exposure to $CO_3^{\bullet-}$. The phosphodiester bond in the 5'-d(GpT) crosslink was resistant toward enzymatic treatment. The tandem lesion was proposed to be generated by addition the of thymine N3 atom to guanine radical at the C8 position (Scheme 12). The pH dependence of crosslink yields supported nucleophilic attack by N3. The yields of crosslinks were 22% at pH 10, ~5% at pH 7, and no crosslinks were observed at pH 5. This is consistent with the fact that the pK_a of T is 9.8, and N3-deprotonated thymine is a better nucleophile.[152]

Scheme 13. The mechanism for the generation of intrastrand G[8-5m]T and G[8-5]C cross-links.
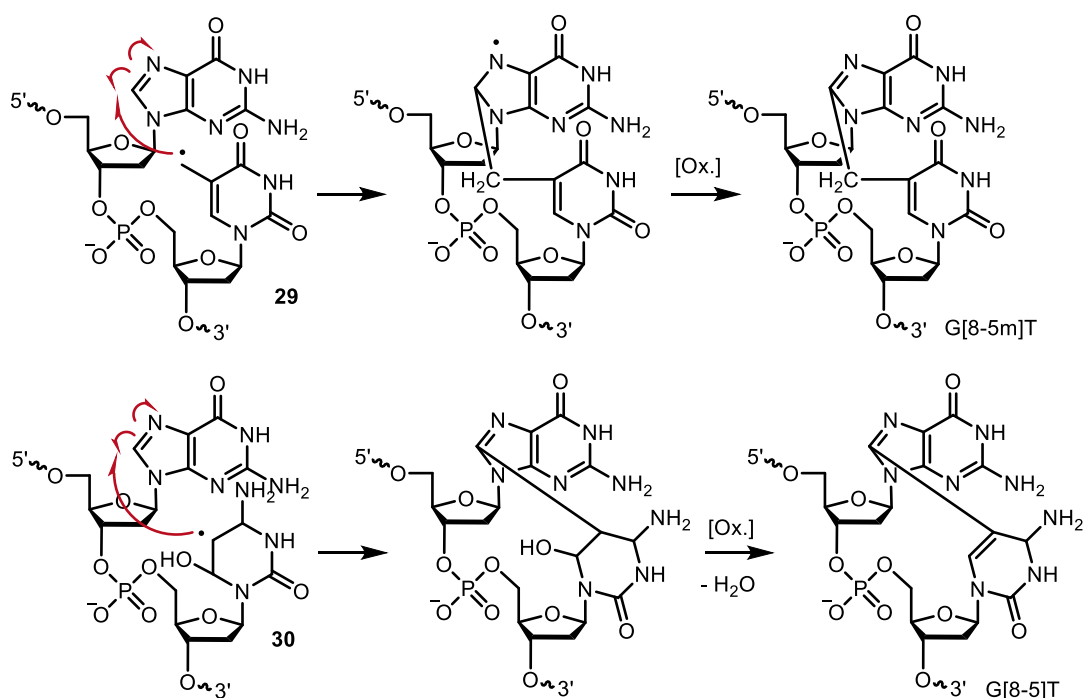
In the absence of O_2, carbon-centered pyrimidine radicals (**29**, **30**, Scheme 13) also react with adjacent bases to generate crosslinks, such as G[8-5m]T and G[8-5]C (Scheme 13).[155-157] These products were quantified using nuclease P1 digestion followed by highly sensitive HPLC-ESI/MS^3 due to their low frequency of generation. In the presence of O_2,

the carbon-centered radicals are efficiently trapped, which significantly limits the formation of these lesions.[157]

Furthermore, it is worth noting that most of the studies on tandem lesion formation rely on enzymatic digestion followed by LC-MS/MS studies, or structural characterization of oxidatively damaged short model oligonucleotides (< 4 nt).[149, 153-154] The enzymatic digestions take advantage of the resistance of the tandem lesion toward hydrolysis.[149, 151] However, evidence for the formation of some tandem lesions is lost during digestion because they are the substrates for the enzyme. Using short model oligonucleotides circumvents the enzymatic digestion, and thus preserves the sequence information of the tandem lesions. However, extra caution should be exercised in extrapolating the results obtained in short oligonucleotides to double-stranded DNA due to the complexity of sequence effects and structural flexibility of long double-stranded DNA.[158]

2.4   Photochemical generation of Heteroatom-centered radicals

2.4.1   Oxygen-centered radicals

O-centered radicals are reactive intermediates that exhibit electrophilic properties in hydrogen atom abstractions and addition reactions to C-C double bonds.[159-160] The main advance in the photochemical generation of O-centered radicals was made by Beckwith, who showed in 1988 that molecules of the general type **31** were sources of alkoxyl radicals (Scheme 14a).[161] However, the synthesis of N-alkoxypyridine-2(1H)-thiones is hampered by poor chemoselectivity between competitive O-substitution and S-substitution.[162] Furthermore, some pyridinethiones decompose at room temperature, and others rearrange to form the thermodynamically more stable 2-(alkylsulfanyl)pyridine N-oxides (**32**), which are not precursors for alkoxy radicals (Scheme 14a).[163] To overcome some of the

35

disadvantages of pyridinethiones, N-alkoxy-2(1H)-pyridone precursors (**33**) were synthesized (Scheme 14b).[164] The synthesis of **33** is simplified because the keto form of N-hydroxy-2(1H)-pyridone (**36**, Scheme 14c) predominates over the enol tautomer (**37**, Scheme 14c).[165] In addition, the 2-pyridyloxyl radical (**34**) generated along with RO• by UV-irradiation, was found to be much less reactive than 2-pyridylthiyl radical (**35**, Scheme 14a).[164] This reduced reactivity is particularly advantageous for using **33** as selective precursors to generate alkoxy radicals for mechanistic studies.

Scheme 14. N-Alkoxypyridine-2(1H)-thione precursors and related precursors for photochemical generation of oxygen-centered radicals.
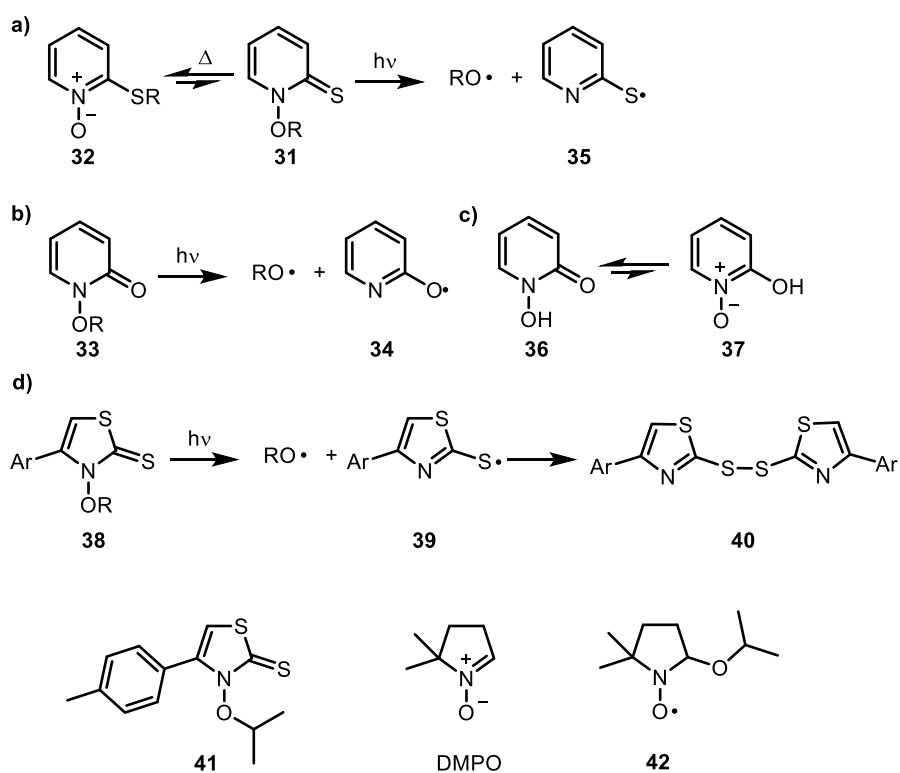
Hartung and co-workers developed another method to access alkoxy radicals via alkoxy-4-arylhioazole-2(3)-thiones (**38**, Scheme 14d).[166] Precursors **38** were synthesized in good yields in two steps because N-(hydroxy)-4-arylthiazole-2(3H)-thiones exhibited higher reactivity for O-substitution against S-substitution. Moreover, N-hydroxy-

thiazolethiones demonstrated improved thermal stability. The effectiveness of these precursors (**38**) was demonstrated by laser flash photolysis and product analysis, in which disulfide **40** resulting from recombination of thiyl radical **39** was identified as the primary product.[167] Upon irradiation (300 nm) of thiazolethione **41** in aqueous media, only isopropoxyl radical was formed, as confirmed by the generation of **42** that resulted from trapping of isopropoxyl radical by 5,5-dimethyl-1-pyrroline N-oxide (DMPO) and EPR spectroscopy.[168]

N-hydroxy-phthalimide derivatives, such as **43**, are another type of photochemical precursors of oxygen-centered radicals (Scheme 15).[169] Although typically activated by one-electron reduction (Scheme 15 a),[170] **43** can also be activated by UV (medium-pressure mercury lamp with Pyrex filter, Scheme 15b).[170] However, the photochemistry is inefficient, possibly because of the low absorbance of the phthalimide chromophore. In order to overcome this shortcoming, N-hydroxy-naphthalimide derivatives have been used as precursors for oxygen-centered radicals via homolytic cleavage of the labile N-O bonds.[171] The extended conjugation shifts the absorbance to around 350 nm, which improves the compatibility with other functional groups. N-hydroxynaphthalimide triflate (**44**, Scheme 15) is used as a photo-acid generator, which is one of the key materials in the field of photoresists for semiconductor fabrication.[172]

Scheme 15. N-hydroxy-phthalimide precursors and related precursors for photochemical generation of oxygen-centered radicals.

a)

43

b)

43

44
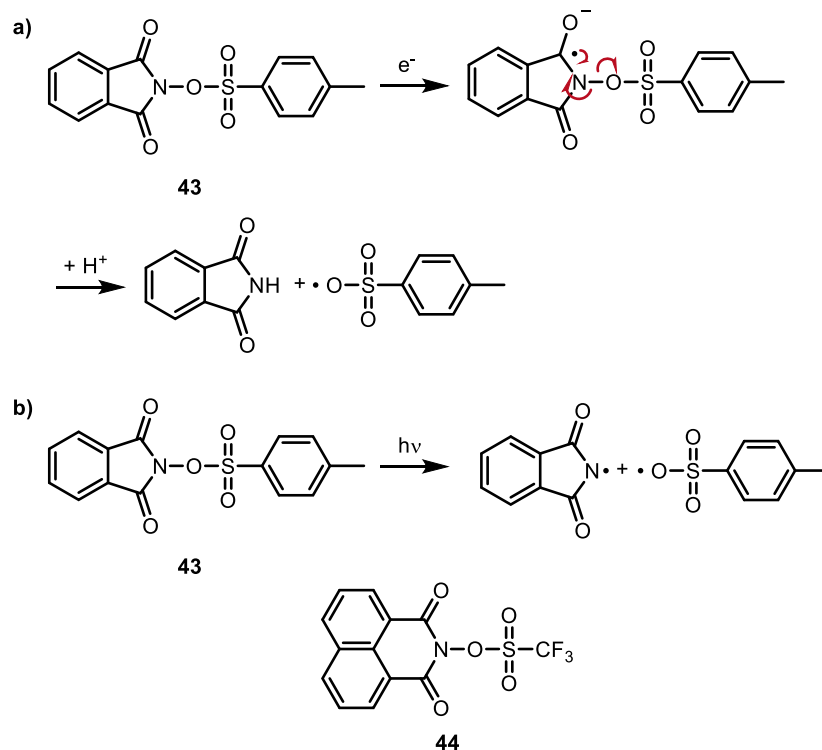
2.4.2 Nitrogen-centered radicals

Compared to carbon-centered radicals, nitrogen-centered radicals are underutilized reactive intermediates in organic synthesis owing to the lack of convenient methods for producing these radical species. Two of the most characteristic reactions of N-centered radicals are hydrogen atom abstraction and amination of unsaturated substrates.[173-175] With the recent development of visible light photoredox catalysis, synthetic methods utilizing nitrogen-centered radicals attracted increasing attention.[176] To independently generate nitrogen-centered radicals in the biopolymers, unimolecular photochemical processes are more feasible. However, the examples of these methods are rather limited.[177]

N-O bonds are generally weaker than N-C and N-N bonds, and their cleavage serves as the basis of several methods to produce nitrogen-centered radicals. Walton et al.

recently studied the photochemistry of oxime carbamates (Scheme 16a).[174] Upon

photolysis, the oxime carbamate **45** underwent homocleavage of the labile N-O bond which

generated an iminyl radical **46**. The subsequent decarboxylation of carbonyloxyl radical **47**

yielded an aminyl radical **48**. Methods based on modified Barton decarboxylation were

also reported. This concept was demonstrated by the photochemical behavior of carbamate

derivative **49** upon irradiation with visible light in the presence of trifluoroacetic acid

(Scheme 16b).[178] Homolysis of the N–O bond is followed by a rapid fragmentation of the

carbonyloxyl radical (**50**) to give a molecule of carbon dioxide and the desired protonated

aminyl radical **51**.

Scheme 16. The generation of nitrogen-centered radical via the cleavage of N-O bonds.
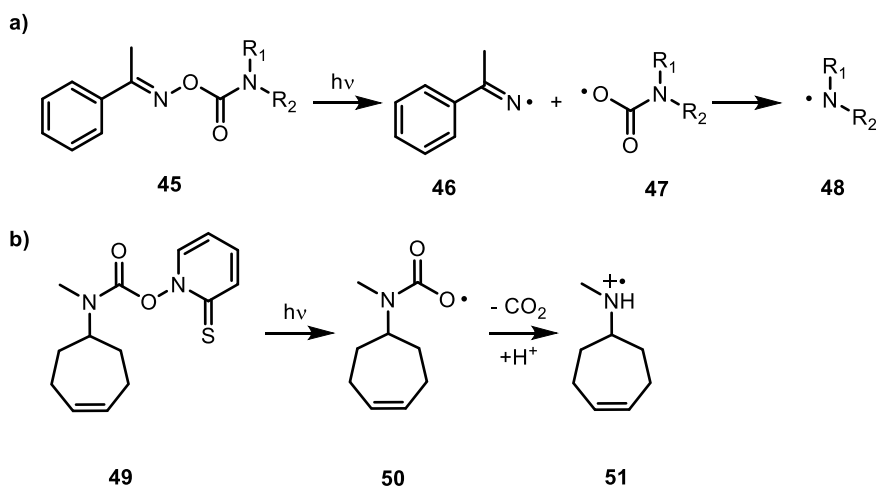
Methods based on a cascade of photocleavage of N-O bond and β-fragmentation

have also been explored. Newcomb and co-workers reported a tandem Barton

decarboxylation, β-fragmentation reaction.[179] The photocleavage of the N-O bond of an

ester of N-hydroxypyridinethione (**52**) resulted in the formation of the carboxyl radical **53**,

which decarboxylated to generate β-(dialkylamino)alkyl radical **54**. The ensuing β-

fragmentation with a rate constant of 10^4 s^{-1} generated the desired aminyl radical (**55**,

Scheme 17a). Similarly, amidyl and iminyl radicals have been generated by β-fragmentation of the N-O bond. Zard and co-workers also applied Barton decarboxylation of N-hydroxypyridinethione ester **56** followed by loss of formaldehyde via β-fragmentation to give the expected iminyl radical **57** (Scheme 17b).[180] Furthermore, an amidyl radical was generated by Begley and co-workers via a similar strategy by the photolysis of hydroxamate **58** (Scheme 17c).[181] The rate constant for β-fragmentation of the N-O bond is measured in compound **61** by the competition between the ring opening of the cyclopropyl group generating radical **62** and the cleavage of the N-O bond generating amidyl radical **59** (Scheme 17d). In the presence of *t*-BuSH, the photolysis of **60** only generated the amide **64**. Product **63** resulting from the opening of the cyclopropyl ring of **61** was not detected. Based on the assumption that the ring-opening rate of radical **61** was 2×10^7 s^{-1}, the author estimated that the rate of β-fragmentation was greater than 2×10^8 s^{-1}.

Scheme 17. Generation of nitrogen-centered radical via tandem Barton decarboxylation, β-fragmentation.

40
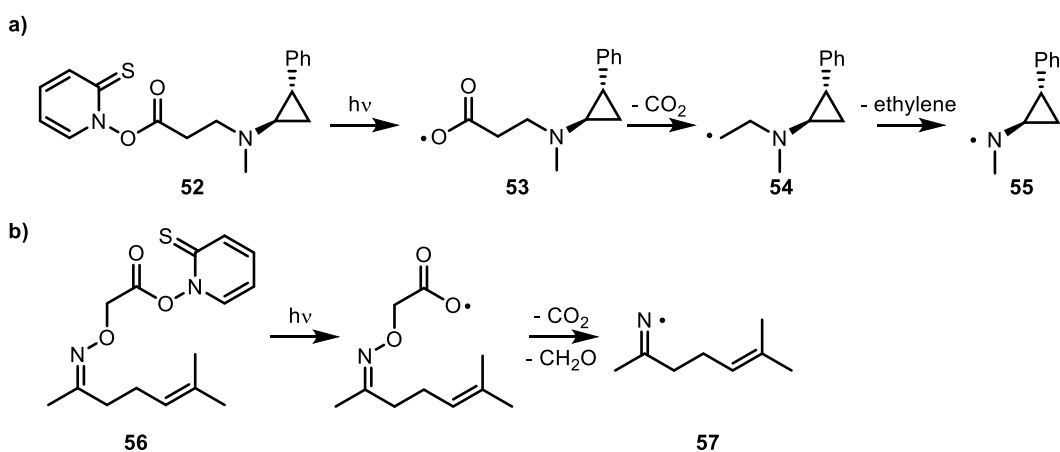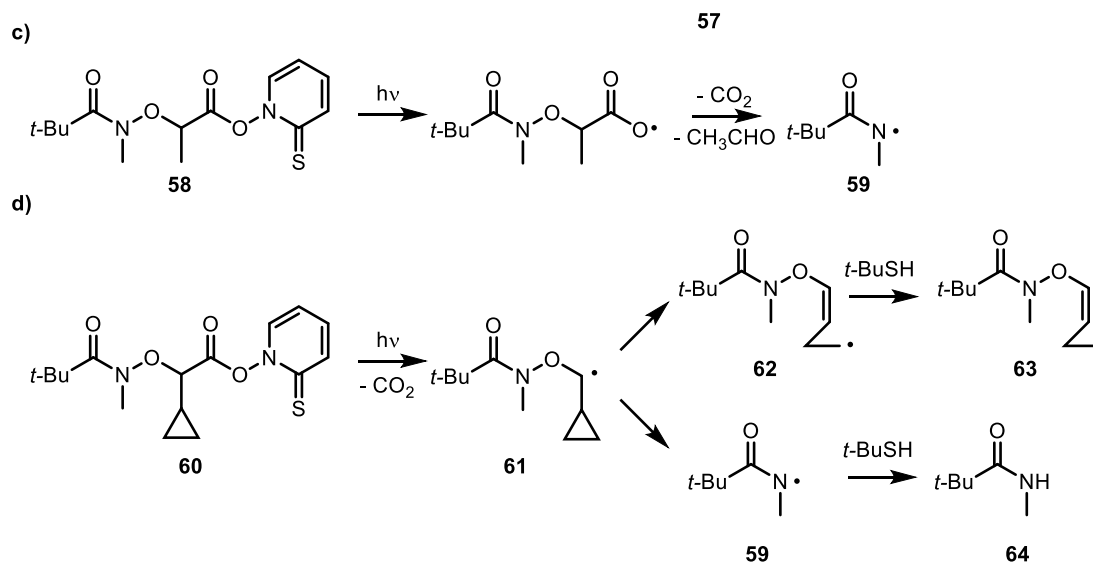
Fewer examples of the photochemical generation of nitrogen-centered radicals via N-N and N-C bond cleavages have been reported because these bonds have higher bond dissociation energies. Steenken et al. demonstrated that upon UV (248 or 308 nm) irradiation in acetonitrile and hexanes, N-(triphenylmethyl)anilines (**65**) exclusively undergo C-N bond homolysis to generate the triphenylmethyl radicals (**67**) and anilinyl radials (**66**, Scheme 18a).[182] Similarly, tetraphenylhydrazine (**68**), which has N-N bond dissociation energy of 30 kcal/mol undergoes homolysis of the N-N bond both thermally and photochemically yielding diphenylaminyl radicals (Scheme 18b), which were detected by EPR.[183] In addition, triphenylhydrazine (**70**) undergoes a similar process upon UV excitation generating an anilinyl radical (**66**) and a diphenylaminyl radical (**69**, Scheme 18c).

Scheme 18. Generation of nitrogen-centered radical via cleavage of N-C and N-N bonds.
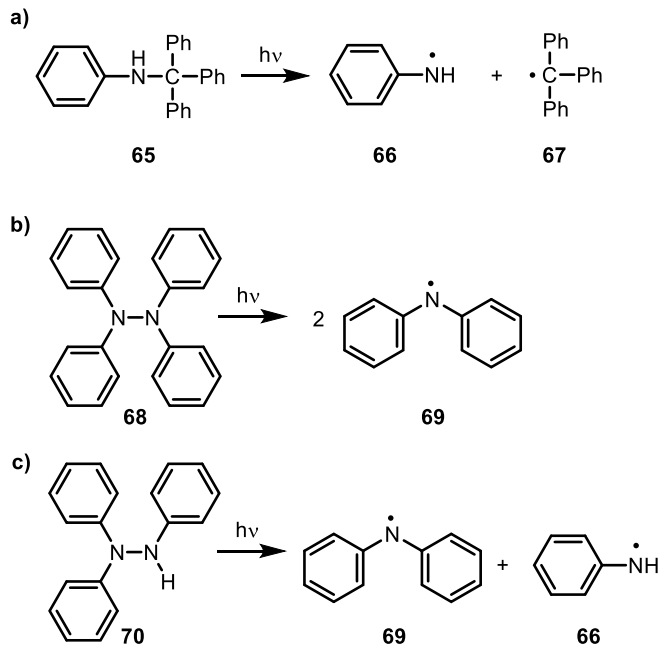
2.5 Independent generation of reactive intermediates in DNA

2.5.1 Investigating reactivity of reactive intermediates via their independent generation

Mechanistic studies of reactive intermediates in biopolymers by non-selective methods, such as pulse radiolysis are hampered by simultaneous generation of multiple reactive intermediates and the lack of site-selectivity. Independent generation of reactive intermediates involved in DNA allows studies of the reactivity of a single reactive intermediate in certain sequence context without producing other reactive intermediates. Unambiguous generation of reactive intermediates at a defined site in a biopolymer can also improve the resolution of complex DNA lesions that would otherwise be masked due to the simultaneous generation of multiple lesions in the same region of DNA. Lastly, in the course of such a mechanistic investigation, it is possible to discover new reaction

processes. In the realm of nucleic acid damage, these processes could have significant relevance to human health.

Our group and Giese's group pioneered independent generation of nucleoside radicals using Norrish Type I photocleavage of ketones **71** and **75**.[184-185] The ketones produced the carbon-centered radicals via α-cleavage and ensuing decarbonylation generating one equivalent of alkyl radical and carbon monoxide.[186] The photolysis of **71** generated the deoxyribose C-4' radical **72** (Scheme 19a), which is one of the key intermediates involved in bleomycin or neocarzinostatin induced DNA damage. The cleavage of the β-C-O bond generates enol ether radical cation **73** which oxidizes dG generating dG•+ and **74**. This chemistry was used as a hole injection method for DNA charge transfer studies.[187] Precursor **75** was synthesized to independently generate 5,6-dihydro-2'-thymidin-6-yl radical **76** (Scheme 19b), which is the formal product of hydrogen atom addition to thymidine.[185]

Scheme 19. Examples for independent generation of reactive intermediates in DNA.
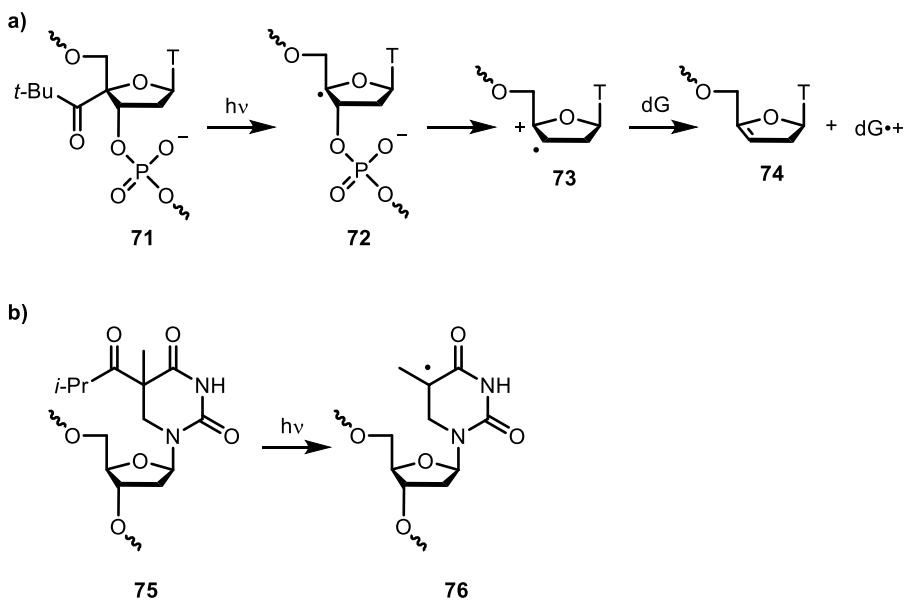
2.5.2 Examples for independent generation of purine radicals

Selective generation of carbon-centered nucleobase and sugar radicals has yielded significant insight into the reactivity of these species. However, the use of photolabile precursors for the site-selective generation of neutral purine radicals has had limited success, owing to the lack of means for the photochemical generation heteroatom-centered radicals.

Photolysis of **77** was designed to produce dG(N1-H)•.[188] However, instead of forming the desired precursor, pyridine-2-thiol 1-oxide **78** was the only observed product. It was proposed that **78** can isomerize to form **77**, which is the photochemical precursor of dG(N1-H)• (Scheme 20a). The generation of dG(N1-H)• was supported by product analysis, in which the presence of H-atom donor increased the yield of dG. However, no transient absorption of dG(N1-H)• was obtained by laser flash photolysis. The author proposed an alternative precursor (**79**) by replacing the pyridinethione moiety with a pyridone.[189] This change not only granted the authors access to the desired precursors but also simplified the analysis of the photochemical processes. The generation of dG(N1-H)• was supported by laser flash photolysis. The author also utilized ring opening of the cyclopropyl group in **80** to support the generation of dG(N1-H)• (Scheme 20b).[189-190] It is worth noting that the authors did not comment on that the ring opening would require the tautomerization of dG(N1-H)• analogue to form **81** (Scheme 20b). No data regarding the effects of hydrogen atom donors was reported, and the authors did not address the formation of dG (38 %) in the absence of hydrogen atom donors. Furthermore, studies on the formation of dG(N1-H)• from **78** and **79** in oligonucleotides have not yet been reported.[188]

Scheme 20. Photochemical generation of dG(N1-H)•.
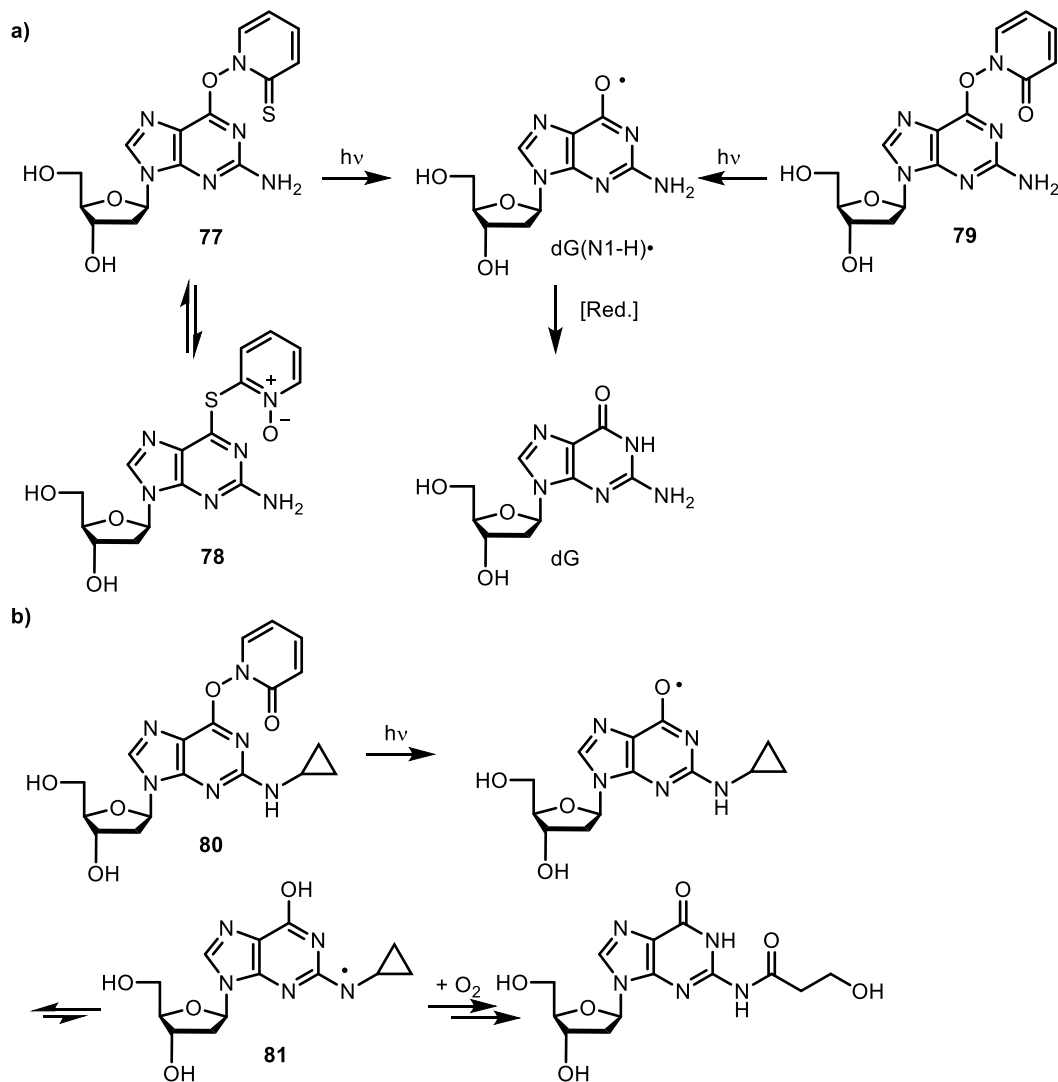
dA• has also been produced from a photochemical precursor (**82**) but not within DNA (Scheme 21).[191] Photolysis (315 nm) of phenylhydrazone **82** in the absence of thiol yielded 32% of dA. In the presence of GSH (50 mM) a 73% yield of dA was observed, as expected. Formation of dI was also observed, which is consistent with the literature.[192]

Scheme 21. Photochemical generation of dA•.
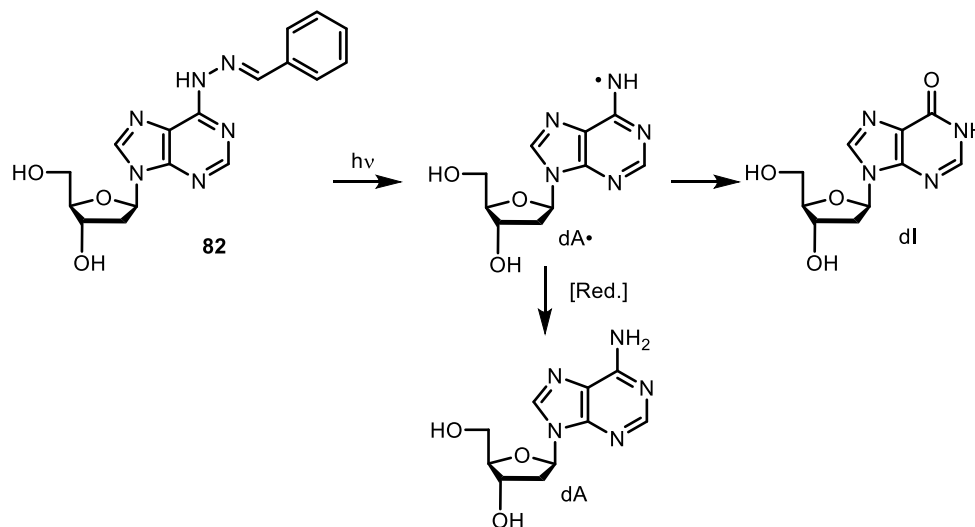
3.   Results and discussion

3.1   Photochemical precursors to generate neutral purine radicals

3.1.1   Generation of neutral purine radicals via homolytic cleavage of N-N and N-C bonds

3.1.1.1   Design and synthesis of precursors

Inspired by the photochemistry of N-(triphenylmethyl)aniline (**65**),[182, 193] we speculated that the

structurally similar tritylated purine nucleosides **83a-c** and **84a-c** may undergo homolytic cleavage of the N-O bonds to yield purine radicals. The tritylated purine nucleosides were synthesized by reacting disilylated dA (**85**) and dG (**86**) with the corresponding trityl chloride **87**-**89** followed by desilylation (Scheme 22).[194-195] However, the syntheses of compounds **83c**, **84b**, and **84c** were unsuccessful because they were moisture sensitive and decomposed during chromatography. Precursor **83b** could be
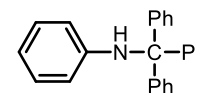
isolated but hydrolyzed in aqueous buffer. In contrast, **83a** and **84a** were stable in phosphate buffer and were used for the subsequent photochemical studies.

Scheme 22. Syntheses of precursors **83a-c** and **84a-c**.

83a R = trityl, 36%
83b R = 4,4'-dimethoxytrityl, 69%
83c R = 4,4',4''-trimethoxytrityl, hydrolyzed on chromatography

84a R = trityl, 19%
84b R = 4,4'-dimethoxytrityl, hydrolyzed on chromatography
84c R = 4,4',4''-trimethoxytrityl, hydrolyzed on chromatography
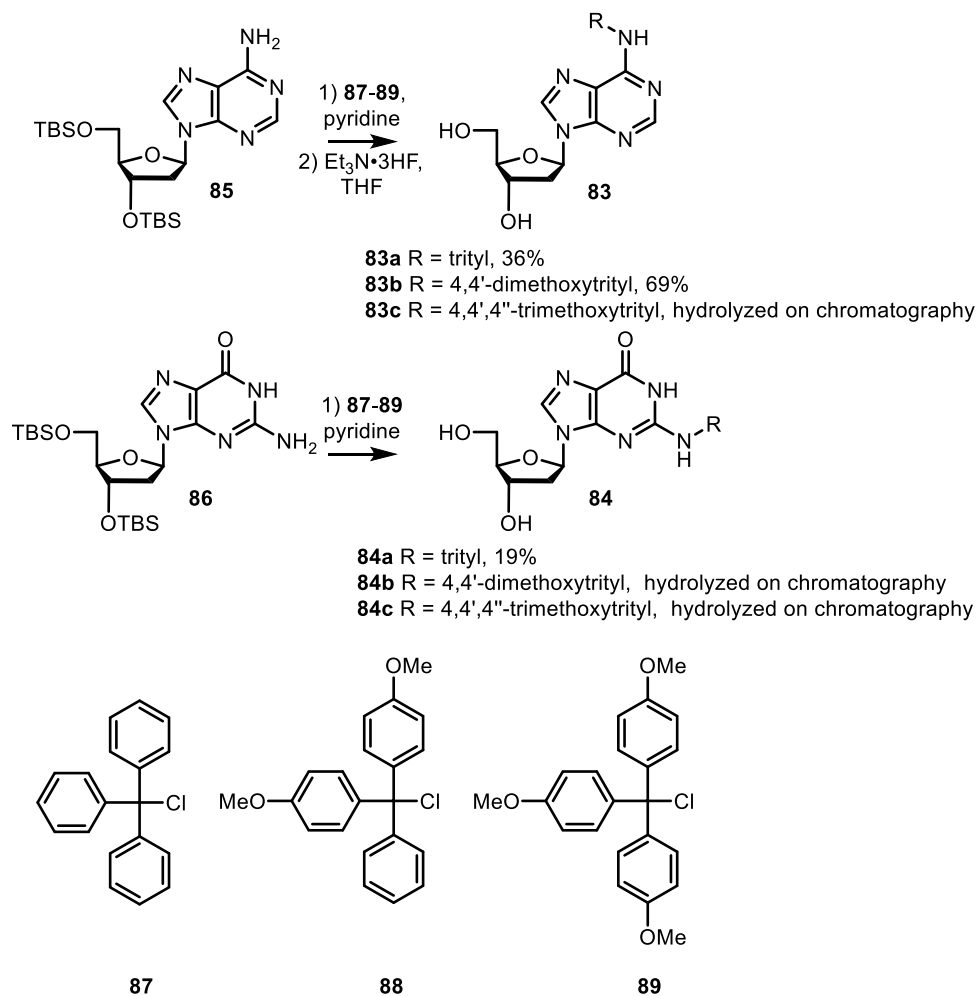
Precursors **83a** and **84a** were photolyzed with 300 nm broadband irradiation. Low yields of dA and dG (~18%) were observed under aerobic or anaerobic conditions, and the generation of dA and dG was independent of the presence of β-mercaptoethanol (BME). These results suggested that the photoinduced dissociation of the C-N bonds were likely to be heterolytic (Scheme 23, pathway a). Alternatively, electron transfer between dA• and Ph₃C• (**67**) following the generation of the radical pair is also consistent with the absence

47

of any effect of BME on the yields of dA and dG (Scheme 23, pathway b). The difference between Steenken's report and our observations may be caused by aqueous solution favoring heterolytic cleavage by stabilizing charged transition states. Furthermore, Steenken et al. pointed out that the electron transfer within the radical pairs is thermodynamically favorable.[182]

Scheme 23. Proposed mechanism for the generation of dA by the photolysis of **83a**.
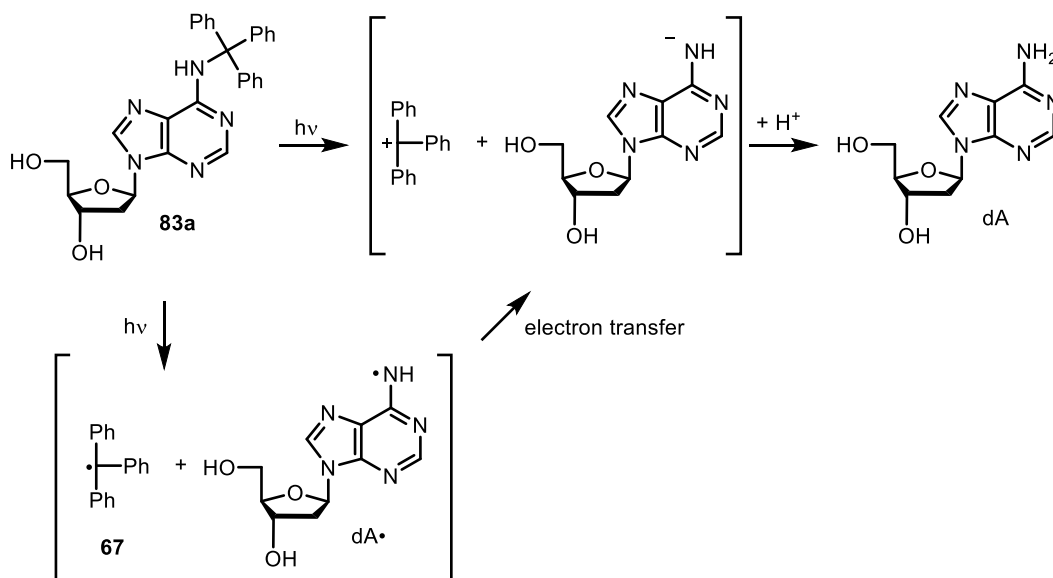
Considering that the polar C-N bonds in **83a** and **84a** favor heterolytic bond cleavage, we designed precursor **90** (Scheme 24), which has a weak non-polar N-N bond (the BDE of N-N bond in 1,2-diphenyl hydrazine is 45.2 kcal mol^{-1}).[196-199] We envisioned that the non-polar N-N bonds would favor homolytic cleavage and suppress electron transfer within the radical pairs.[198] Although there was no report on the photoinduced bond dissociation of a 1,2-diarylhydrazine, *N*6-anilinyl-2'-deoxyadenosine (**90**) was chosen due to its synthetic accessibility. Aromatic nucleophilic substitution on Lakshman's *O6-*

(benzotriazole-1-yl)-2'-deoxyinosine derivatives (**91**) by phenylhydrazine gave **92** quantitatively,[200] and the TBS protecting group was removed to provide **90** (Scheme 24).

Scheme 24. Synthesis of N6-anilinyl-2'-deoxyadenosine (**90**).
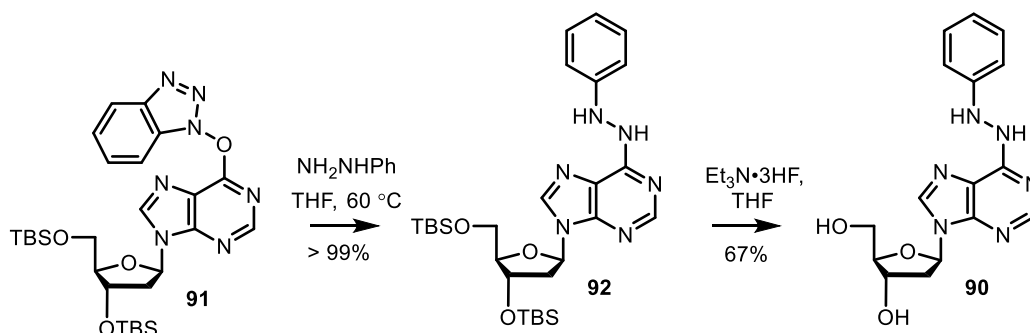
The anaerobic photolysis of **90** (350 nm, 8 h) generated a trace amount of dA, the yield of which was independent of the presence of BME. In the absence of hydrogen atom donor, diazene **93** was detected. While the mechanism involving heterolytic cleavage is plausible, the generation of **93** suggests that **90** can serve as the reducing reagent for dA•. Furthermore, the photochemistry in the presence of O_2 was complicated by the oxidation of **90** to form **93**.
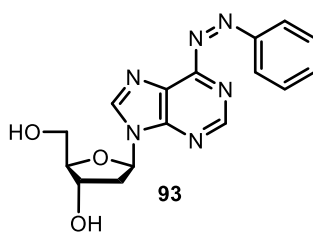
In order to eliminate the possibility for photooxidation, we designed precursor **3** by introducing an additional phenyl group. We also speculated that the introduction of an additional phenyl group would weaken the N-N bond (the BDE of the N-N bond in tetraphenyl hydrazine is 37.3 kcal mol^{-1}).[199] We also were encouraged to pursue the

photolysis of **3** because condensed phase spectroscopy experiments demonstrated that photoexcited tetraphenylhydrazine and triphenylhydrazine underwent N-N homolytic cleavage.[201-204] Another advantage of hydrazine precursors is that the simultaneously produced diphenylaminyl radical (**69**) is less reactive, due to the low BDE of the N-H bond in diphenylamine **94** (<85 kcal/mol).[205-206] Therefore, diphenylaminyl radical (**69**) is less likely to induce side reactions in DNA which would be useful when using these precursors in polymer studies.
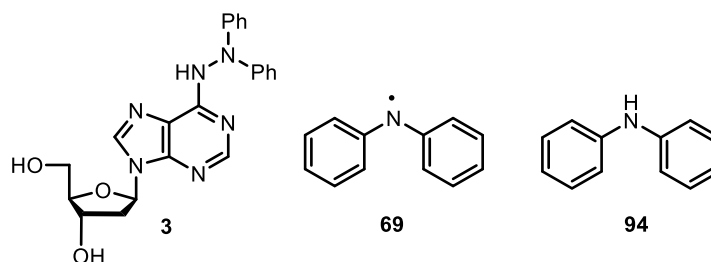
We attempted to synthesize the precursor via nucleophilic aromatic substitution, which was used in the synthesis of **92** and other *N*6-substituted purines.[207-208] Nucleophilic substitution on **91** using the hydrochloride salt of 1,1-diphenylhydrazine (**95**) as nucleophile did not yield any desired product (**96**, Scheme 25a).[200] Additionally, no product was generated when the reaction was carried out at elevated temperature (80 °C) in 1,2-dimethoxyethane (DME). Because the hydrochloride salt of **95** was not soluble in THF or DME, the reaction was also carried out in methanol, which dissolves the salt of **95** (Scheme 25a). However, no desired product was observed. Following these unsuccessful attempts, we turned our attention to other leaving groups. Reacting **95** with disilylated 6-bromopurine-2'-deoxynucleoside (**97**) which readily reacts with a variety of arylamines,[209-210] did not yield **96** (Scheme 25b). Disilylated O^6-mesitylenesulfonate 2'-deoxyinosine (**98**), which undergoes nucleophilic aromatic substitution when activated by DABCO,[211] also

did not react with **95** (Scheme 25c). These results suggested that the nucleophilicity of **95** may be too weak for the nucleophilic aromatic substitution. The poor nucleophilicity might be attributed to the steric hindrance of two phenyl groups.

Scheme 25. Attempts to synthesize **96**.

Condition A: **95**·HCl, Et₃N, THF, 60 °C
Condition B: **95**·HCl, Et₃N, DME, 80 °C
Condition C: **95**·HCl, Et₃N, MeOH, 45 °C
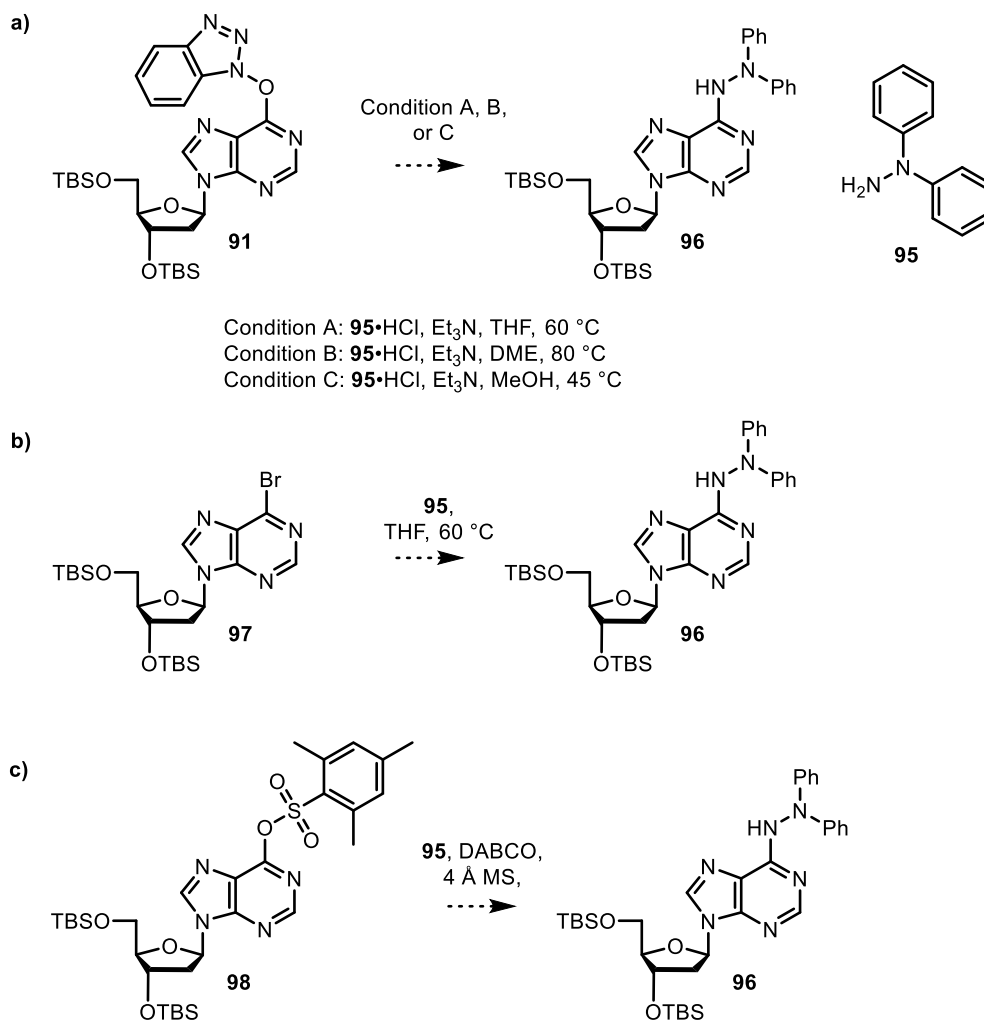
Following the unsuccessful attempts with nucleophilic aromatic substitution , we turned our attention to Buchwald-Hartwig amination.[212-213] A variety of 6-substituted purines and *N*6-amino substituted adenosines have been prepared from **97** using Pd catalysts.[214-215] However, there were few reports on the reactions using hydrazines as the

coupling partner with aryl bromides.[216-217] Use of Pd(OAc)$_2$ and BINAP ligand gave only

trace amounts of the desired product (**96**) (Scheme 26a).[218] It has been proposed that

bidentate phosphine ligands with large bite angles promote reductive elimination, and thus

would improve the yield.[219] Indeed, switching to Xantphos, a phosphine ligand with wide

bite angle and Pd$_2$dba$_3$ as catalyst produced **96** in 48% yield (Scheme 26a). Desilylation

provided the photochemical hydrazine precursor (**3**).

Scheme 26. Synthesis of precursor **3** and **4**.
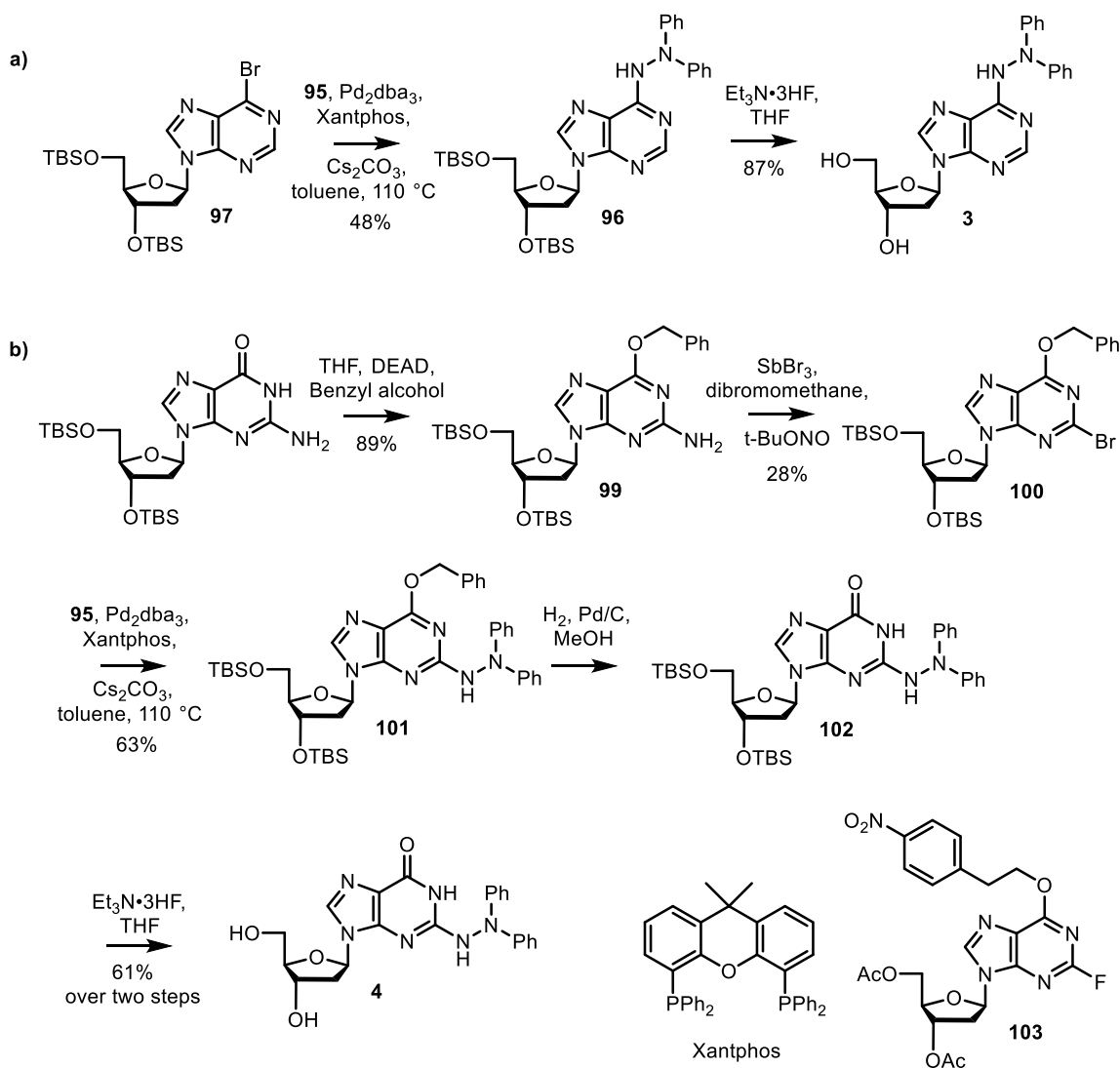
Similarly, the corresponding precursor (**4**) for dG(N2-H)• was also synthesized via cross-coupling (Scheme 26b). This was accomplished by protecting the O6 position of disilylated dG with benzyl alcohol via a Mitsunobu reaction. The *O*6-protected dG (**99**) was brominated according to the method reported by Hopkins et al.[220] Cross-coupling between **100** and 1,1-diphenylhydrazine (**95**) followed by hydrogenolysis and desilylation afforded the desired precursor **4**. It is also worth mentioning that synthesizing **4** via substitution of the 2-fluoro-2'-deoxyinosine derivative (**103**) was unsuccessful, which corroborated the aforementioned poor nucleophilicity of 1,1-diphenylhydrazine (**95**).

3.1.1.2   Photochemical properties of the diphenyl hydrazine type precursors

Hydrazine **3** had a λ_{max} = 267 nm (ε = 1.81 ± 0.01 × 10^4 $M^{-1}cm^{-1}$ in water) and its absorption tailed into the >300 nm region at the concentration (100 µM) at which it was present during photolysis. Hydrazine **3** was completely consumed after photolysis for 4 h. dA was the major product detected under all irradiation conditions (Table 2). The only

Table 2. Product analysis for the photolyses of hydrazine 3.

		%Yield[a]		
[3] (µM)	Reducing agent (mM)	dA	**104**	% Mass balance
100	-	64 ± 2	9 ± 1	73 ± 2
100	Fe^{+2} (10)	65 ± 1	6 ± 1	71± 1
100	BME (10)	57 ± 2	8 ± 1	65 ± 3
100	PhSH (100)	72 ± 1	10 ± 1	81 ± 1
100	PhSH (10)	67 ± 2	11 ± 1	78 ± 2
50	PhSH (10)	72 ± 1	8 ± 1	80 ± 2
25	PhSH (10)	75 ± 1	9 ± 1	84 ± 1

[a]Average ± std. dev. of 3 experiments.

other product detected was formal recombination product **104** (Scheme 27), which was initially identified by UPLC-MS/MS analysis in the photolysates of **3**. It exhibited (Figure 7b) a molecular ion that had identical *m/z* as **3** (Figure 7a). However, in contrast to **3** (Figure 74a), fragmentation of the diphenylamino group was not observed (calculated *m/z* = 168.0808, observed *m/z* = 168.0809). Finally, the yield of **104** was independent of the presence of reducing agents or their concentration, and substrate concentration, suggesting that it could result from a radical pair process.

Scheme 27. Proposed mechanism for the formation of recombination product **104**.
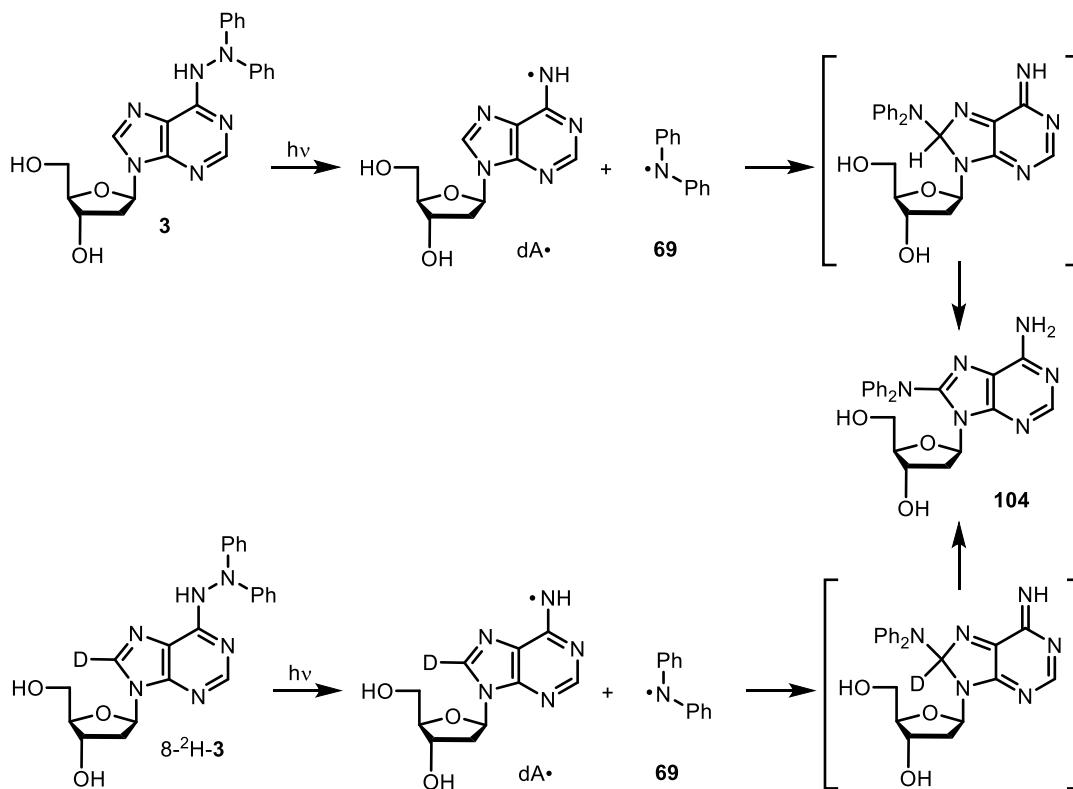
Attempted synthesis of **104** via cross-couplings of the disilylated 8-bromo-2'-deoxyadenosine (**105**) with diphenylamine (**94**) was unsuccessful (Scheme 28a).[221] Consequently, support for the structural assignment of **104** was obtained via UPLC-MS/MS analysis of photolyzed 8-^{2}H-**3** (Figure 4c), which was prepared from **3** via Et$_3$N-

catalyzed deuteron exchange.[222] The recombination product formed from 8-[2]H-**3** (Figure 4d) lacked deuterium, consistent with the proposed structure (**104**, Scheme 27). The formation of this rearranged recombination product is consistent with the homolytic cleavage of the N-N bond (Scheme 27). Structurally similar **106** was synthesized (Scheme 28b), and its extinction coefficient at 260 nm was measured. The extinction coefficient of **106** was compared to that of **3**, whose response factor against thymidine was independently measured to approximate the yield of **104** by HPLC (Table 2).
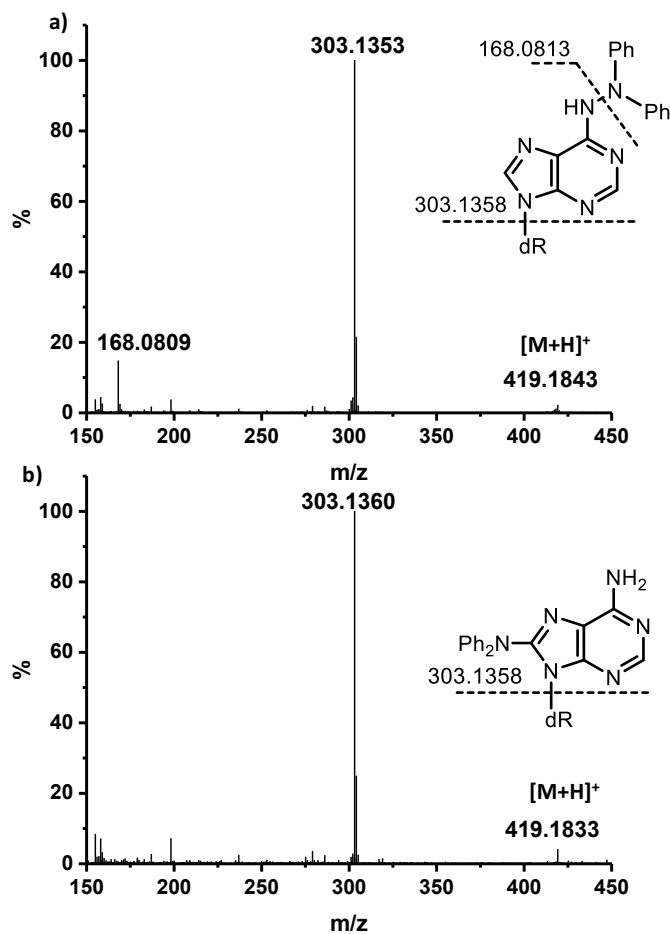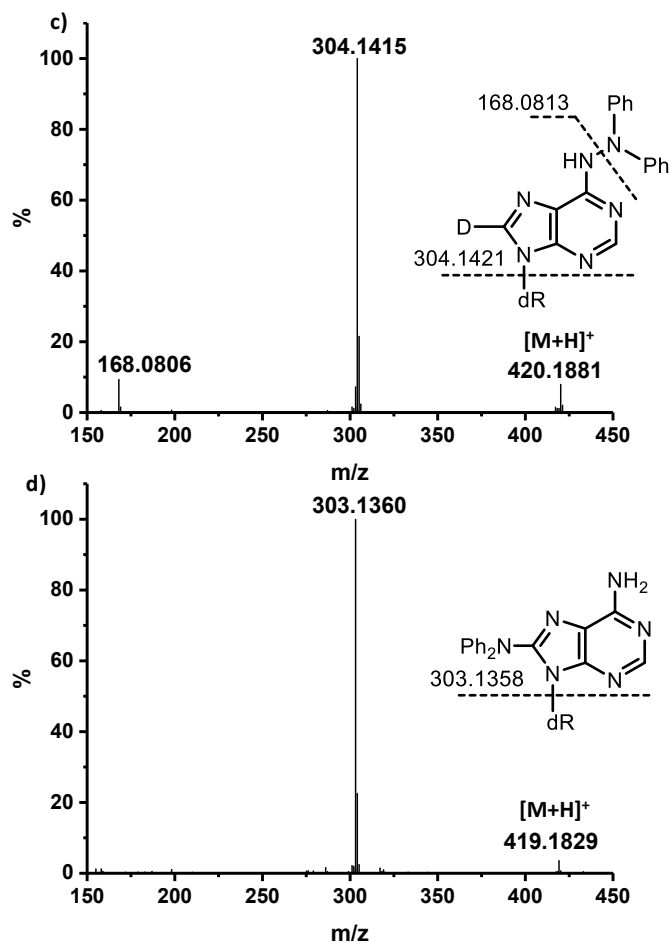
Figure 7. Mass spectrometric characterization of the photolysis of **3**. (a) **3**, (b) recombination product **104** formed from photolysis **3**, (c) 8-^{2}H-**3**, (d) recombination product **104** formed from photolysis 8-^{2}H-**3**. dR = 2'-deoxyribose.

Scheme 28. Synthesis of the recombination product (**104**) and its analogue **106**.
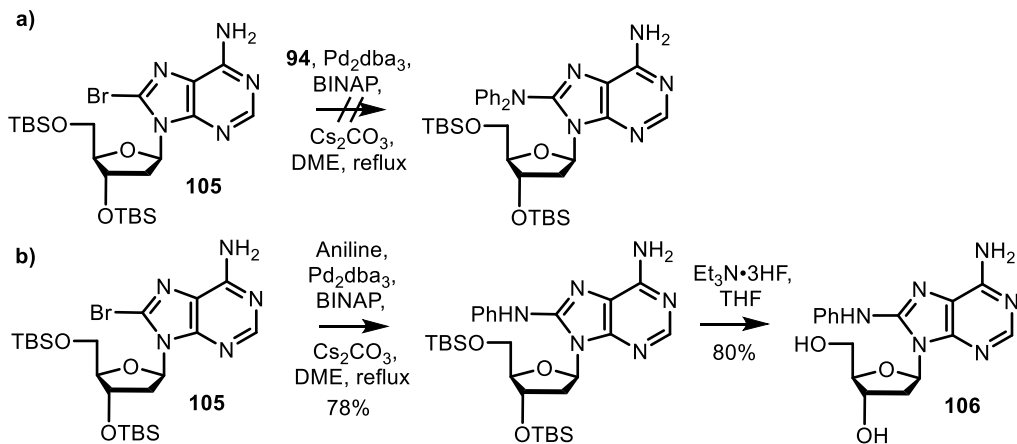
The yield of dA in the absence of reducing agents was 64%, and the presence of BME did not increase the yield of dA (Table 2). Ferrous ion and PhSH only increased the yield of dA by approximately 10%. Furthermore, in the presence of PhSH, there was an inverse relationship between dA yield and concentration of **3**. We proposed that the precursor (**3**) serves as a reducing agent for dA• and effectively competes with other reducing agents, such as PhSH and ferrous ion. Evidence in support of hydrazine **3** serving as a viable reductant for dA• was obtained from cyclic voltammetry (Table 3). The oxidation potential suggests that **3** is more readily oxidized than dG (E(dG•+/dG) = 1.49 V versus NHE in acetonitrile), the most electron rich native nucleotide, and 8-oxo-dG, a DNA lesion that is susceptible to further oxidation (Table 3).[109] However, the yield of dA in the absence of any exogenous reducing agents is >50%, indicating that a species other than **3** also reduces dA•. Given the oxidative nature of dA, it is reasonable to propose that the radical pair also undergoes electron transfer (Scheme 29).

Scheme 29. Proposed mechanism for the generation dA via the photolysis of **3**.
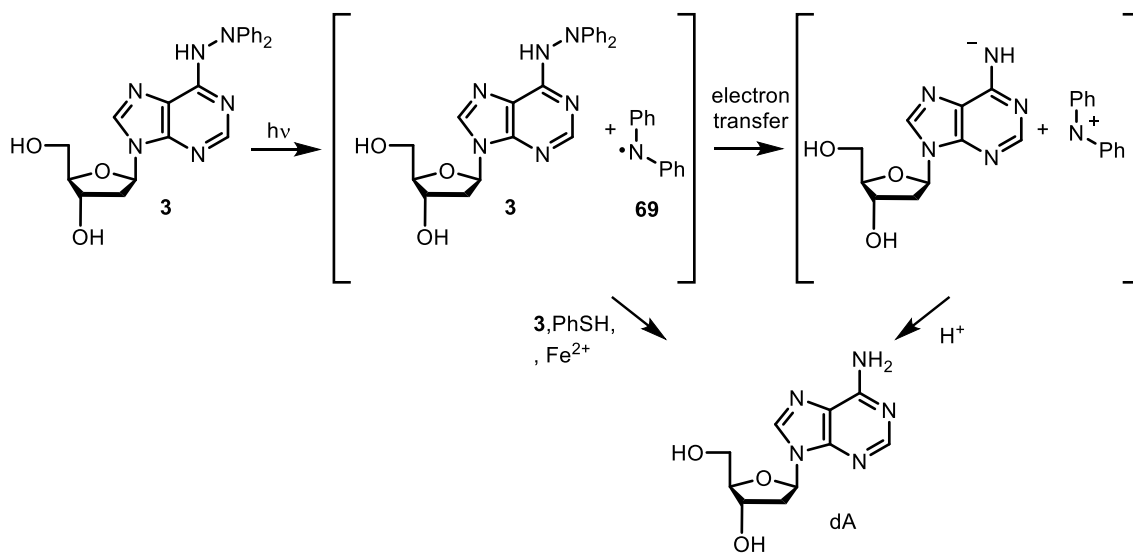
Table 3. Reduction potentials measured by cyclic voltammetry.

Redox couple	E^a (V)
3•+ / 3	0.82
4•+/ 4	0.77
8-oxo-dG•+ / 8-oxo-dG	1.16[41]

a Versus NHE in CH3CN.

Photoconversion of **4** was less efficient than that of **3**, requiring 8 h photolysis for complete conversion compared to 4 h for **3**. dG was the major product from the photolysis of **4** (Table 4). Hydrazine **4** is more readily oxidized than **3**, and cyclic voltammetry indicated that the reduction potential of **4** was 0.77 V vs. NHE (Table 3). Therefore, **4** can also serve as the reducing agent for dG(N2-H)•. However, the yield of dG and mass balance in the absence of exogenous reducing agent were closer to 50%, which would be the maximum yield if **4** is the sole reducing agent of dG(N2-H)•. This could reflect less efficient electron transfer within the radical pair formed upon photodissociation (Scheme 30). This correlates with the smaller thermodynamic driving force for dG(N2-H)• reduction (Table 1). Similar to the photolysis of **3**, the presence of PhSH and ferrous ion moderately increased the yields of dG (Table 4). Interestingly, BME, an inefficient trap for dA•, also increased the yield of dG (Table 4). These observations were attributed to a polarity-matching effect in hydrogen atom transfer reactions (see Section 3.1.2.2).

Scheme 30. Proposed mechanism for the generation dG via the photolysis of **4**.
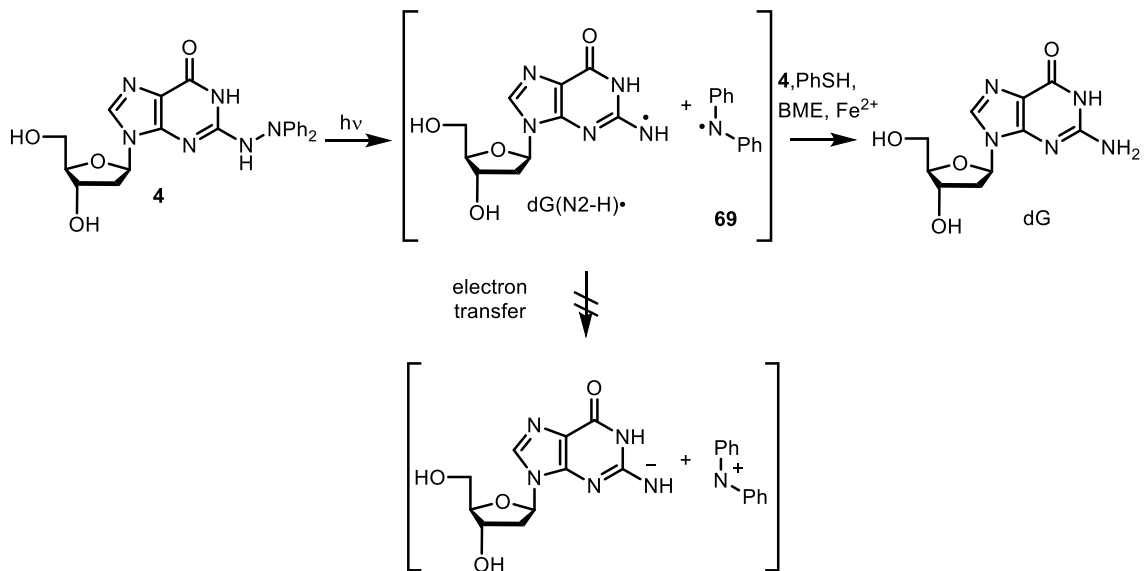
Table 4. Product analysis for the photolyses of hydrazine 4.

[4] (μM)	Reducing agent (mM)	% Yield of dG[a]	% Mass balance[a]
100	-	54 ± 3	54 ± 3
100	Fe^{+2} (10)	67 ± 3	73 ± 1
100	BME (10)	69 ± 1	75 ± 1
100	PhSH (10)	68 ± 2	74 ± 2
50	PhSH (10)	74 ± 3	74 ± 3
25	PhSH (10)	78 ± 1	82 ± 1

[a]Average ± std. dev. of 3 experiments.

3.1.2 Generation of neutral purine radicals via tandem Norrish type I β-fragmentation reactions

3.1.2.1 Design and synthesis of the precursors for independent generation of dA•

Based on Newcomb's original report on the generation of aminyl radicals via tandem Barton decarboxylation, β-fragmentation,[179, 223] we envisioned combining the

59

Norrish Type I photocleavage of a ketone with β-fragmentation to generate dA• (Scheme 31).[42] Aminoketone **107** was an attractive potential precursor due to its stability and the reliability of the Norrish Type I photocleavage of benzyl ketones. The feasibility of β-fragmentation from **108** to yield dA• and isobutylene was uncertain, as there were conflicting reports in the literature. Newcomb reported that the rate constant for generating a dialkylaminyl radical via ethylene elimination was ~4 $\times 10^4$ s^{-1} at 27 °C. However, subsequent experimental and computational experiments argued against aminyl radical formation via alkyl radical β-fragmentation.[224-225] If the rate constant reported by Newcomb was correct, O_2 trapping of the carbon-centered radical ($k[O_2] \sim 10^6$ s^{-1}) would compete with the β-fragmentation. However, it is still possible that **107** would provide a source of dA• under anaerobic conditions.

Scheme 31. Generation of dA• via a tandem Norrish type I reaction, β-fragmentation.
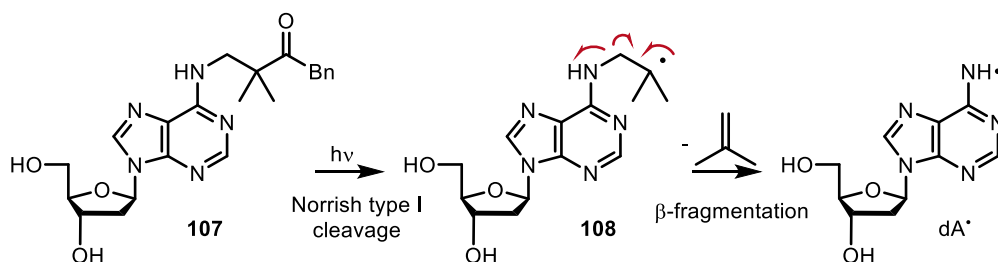
Precursor **107** was readily prepared using the method for synthesizing N6-purine derivatives developed by Lakshman (**91**, Scheme 32).[200] β-Aminylketone (**111**) was synthesized using a reported approach.[226] The α-nitrile ketone **109** was synthesized via nucleophilic addition of ethyl phenylacetate and isobutyronitrile. Both the carbonyl group and nitrile group of **109** was reduced by LiAlH4. The resulting amine was protected with a *t*-butyloxycarbonyl group (Boc) to afford **110**, and the ketone in was restored by oxidation

prior to removing the amine protecting group to generate β-aminoketone (**111**). Displacement of the *O*-benzotriazole group in **91** was carried out at room temperature with **111** to provide the disilylated precursor (**112**), which was deprotected to give **107**.

Scheme 32. Synthesis of precursor **107**.
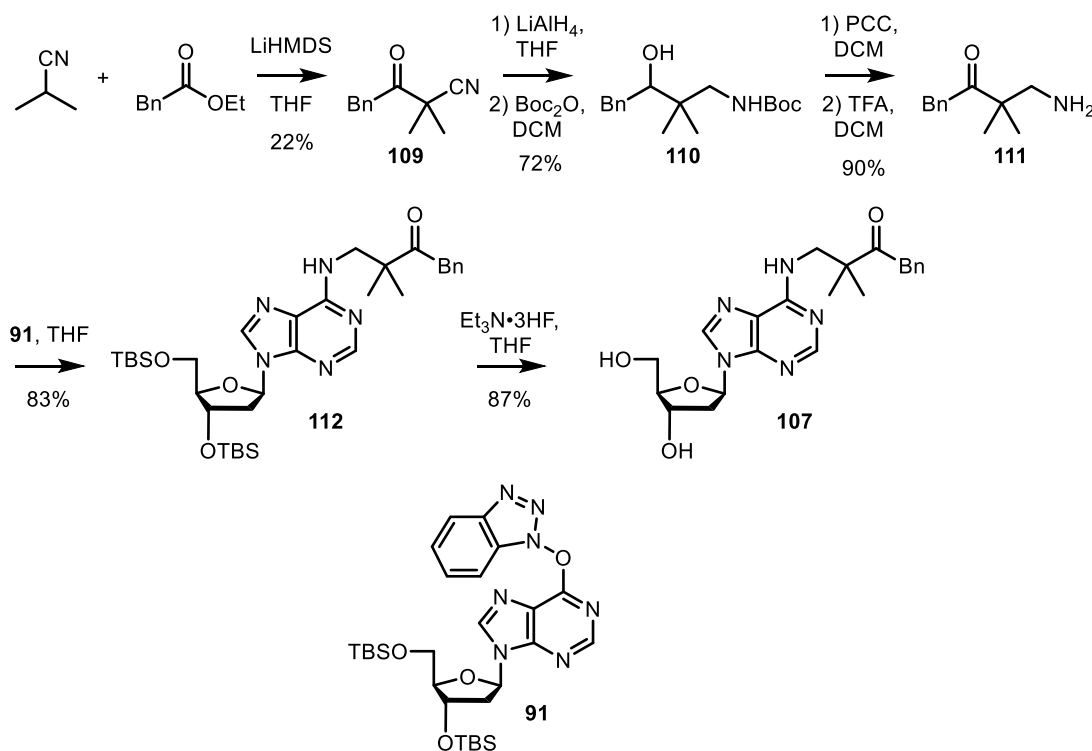
Photolysis of **107** (0.1 mM) by UV irradiation (λ_{max} = 350 nm) did not yield detectable amounts of dA under either aerobic or anaerobic conditions. Low yields of the compound with *m/z* corresponding to **113** and **114** were identified by LC/MS following photolysis under aerobic conditions (Scheme 32). These products may result from O_2 trapping the intermediates (**115**, **108**) produced upon irradiation. The generation of **114** is consistent with the aforementioned competition between O_2 and β-fragmentation. Similarly, **116** was detected by LC/MS following anaerobic photolysis in the presence of

BME (10 mM). These results suggested that β-fragmentation from **108** is too slow to generate dA•.[224-225]

Scheme 33. Products generated from the photolysis of **107**.
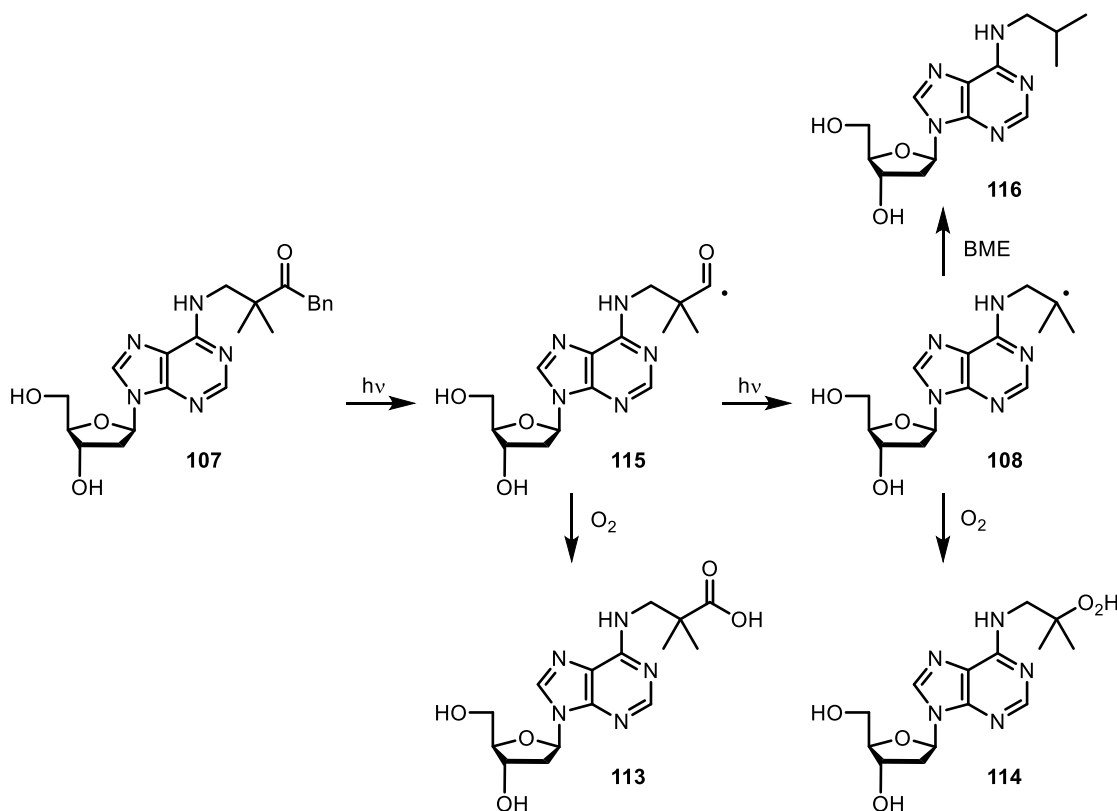
Replacing the methylene group in **108** with oxygen (**118**, Scheme 34) increases the thermodynamic driving force for β-fragmentation to dA• by producing a stronger carbon-oxygen π bond (BDE of $\pi_{C-O} \approx 80$ kcal mol^{-1}, BDE of $\pi_{C-C} \approx 63$ kcal mol^{-1}) and requiring cleavage of a weaker nitrogen-oxygen σ bond (BDE of $\sigma_{C-N} \approx 73$ kcal mol^{-1}, BDE of $\sigma_{N-O} \approx 50$ kcal mol^{-1}).[196] As discussed in Section 2.4.2, methods based on Barton decarboxylation involving carbon-center radical intermediates similar to **105** have been reported.[180-181] Furthermore, Begley estimated that the rate constant for a similar β-fragmentation to form a hydroxamate radical (**61**, Scheme 17) is $> 2 \times 10^8$ s[-1].[181] In addition,

more recently, Baran and co-workers used single electron transfer chemistry to generate a carbon-centered radical intermediate that fragmented to yield aminyl radicals.[227] Due to the ease of synthesis, we designed the acyloin type precursor **117** (Scheme 34), which has been reported to undergo α-cleavage upon UV excitation.[228]

Scheme 34. Generation of dA• via tandem Norrish type I and β-fragmentation reactions.
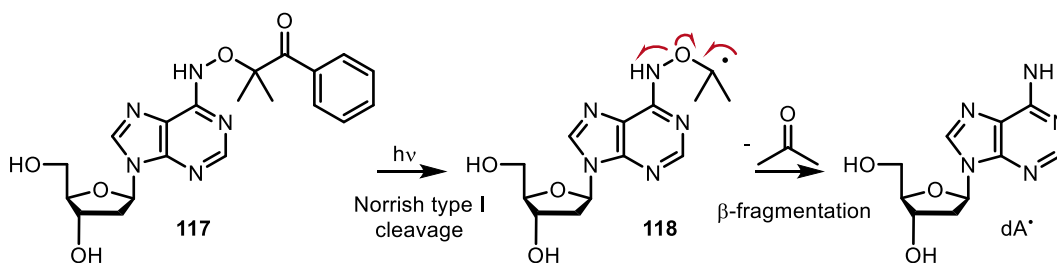
We initially attempted a similar strategy used in the synthesis of **107** by reacting hydroxylamine (**121**) with Lakshman's compound (**91**, Scheme 35a).[200] The α-bromoketone **119** derived from commercially available isopropyl phenyl ketone was substituted by N-Boc-hydroxylamine to yield **120**. After cleavage of the Boc protecting group, **121** was reacted with **91**. However, no desired product **122** was formed (Scheme 35a). Given that the nucleophilic substitution on brominated ketone with N-Boc-hydroxylamine proceeded effectively, we proposed an alternative synthetic route based on the disconnection of oxygen and the α-carbon of the ketone moiety (Scheme 35b). The disilylated *N*6-hydroxy-2'-deoxyadenosine (**123**) was synthesized via the reaction between hydroxylamine hydrochloride and **97.** The purification of **123** required washing with EDTA in MeOH to remove unidentified metals that bound the product, producing an intensely colored complex.[229] The hydroxyl group of **123** was deprotonated by NaH and reacted with **119** to afford desired product **122** in 20% yield.

Scheme 35. Synthesis of precursor **117**.
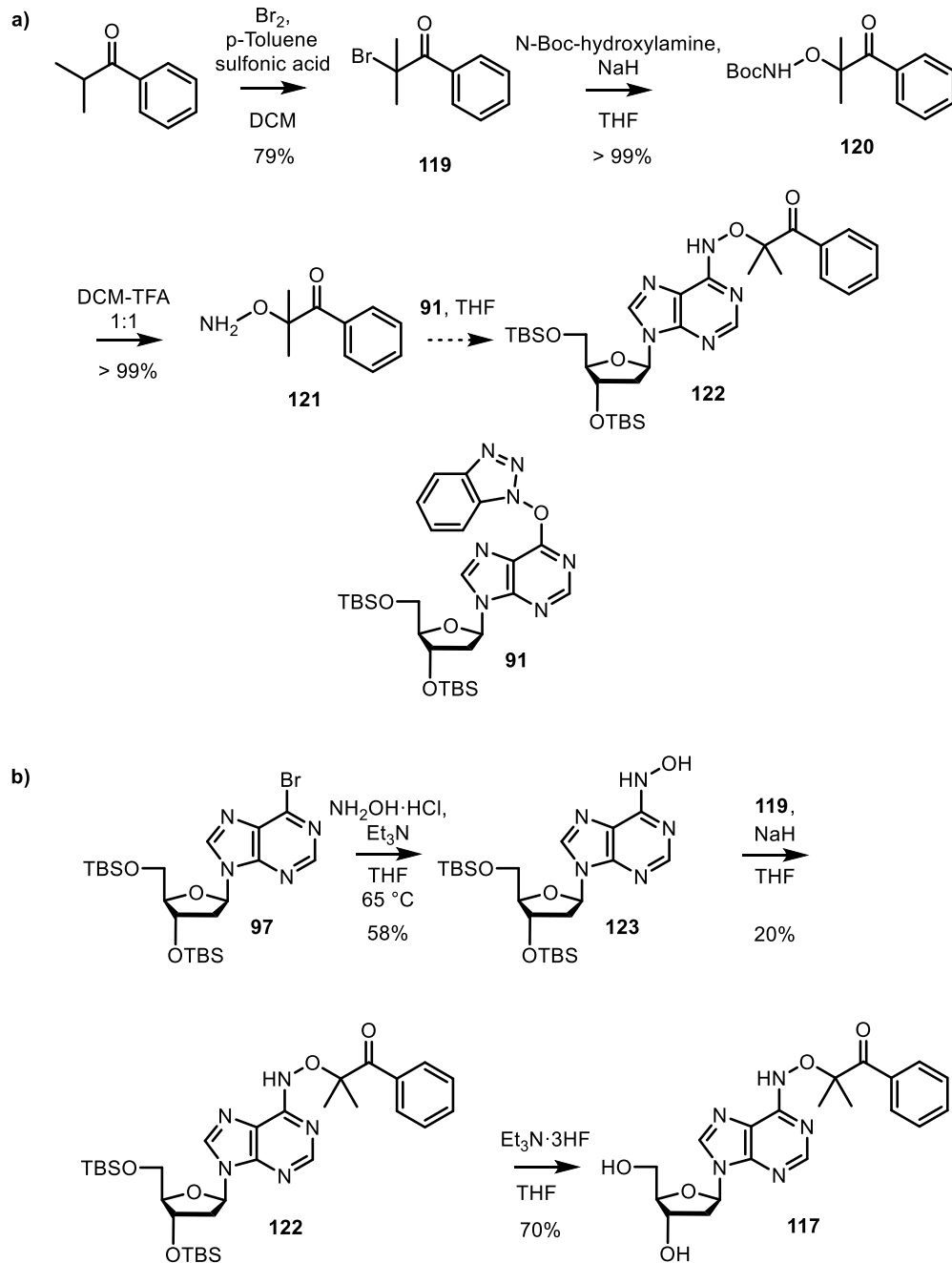
dA was the major product generated by the photolysis of **117** under UV irradiation

(λ_{max} = 350 nm). The yield of dA was 48% under anaerobic condition in the absence of

reducing agents (Table 5). The presence of 10 mM BME did not increase the yield of dA.

This corroborates our hypothesis that BME is an inefficient hydrogen atom donor for dA•.

In contrast, the presence of Et₃N or $(NH_4)_2Fe(SO_4)_2$ as reductant increased the yields of dA to 78% and 71%, respectively. This is consistent with the generation of dA• during photolysis. In addition, a product with *m/z* corresponding to **124** was identified by UPLC-MS. Although we initially attributed the formation of **124** to recombination of radical dA• and **125**, the mechanism involving Norrish type II reaction was also possible (Scheme 36).[230] The excited carbonyl abstracts the hydrogen atom from N6 generating the 1,4-diradical intermediate **126**, which undergoes an intermolecular recombination to form the Yang-type product (**127**).[231] The Yang-type cyclized product (**127**) can then decompose to release acetone and produce **124**.

Scheme 36. Formation of **124** via Norrish type II reaction.
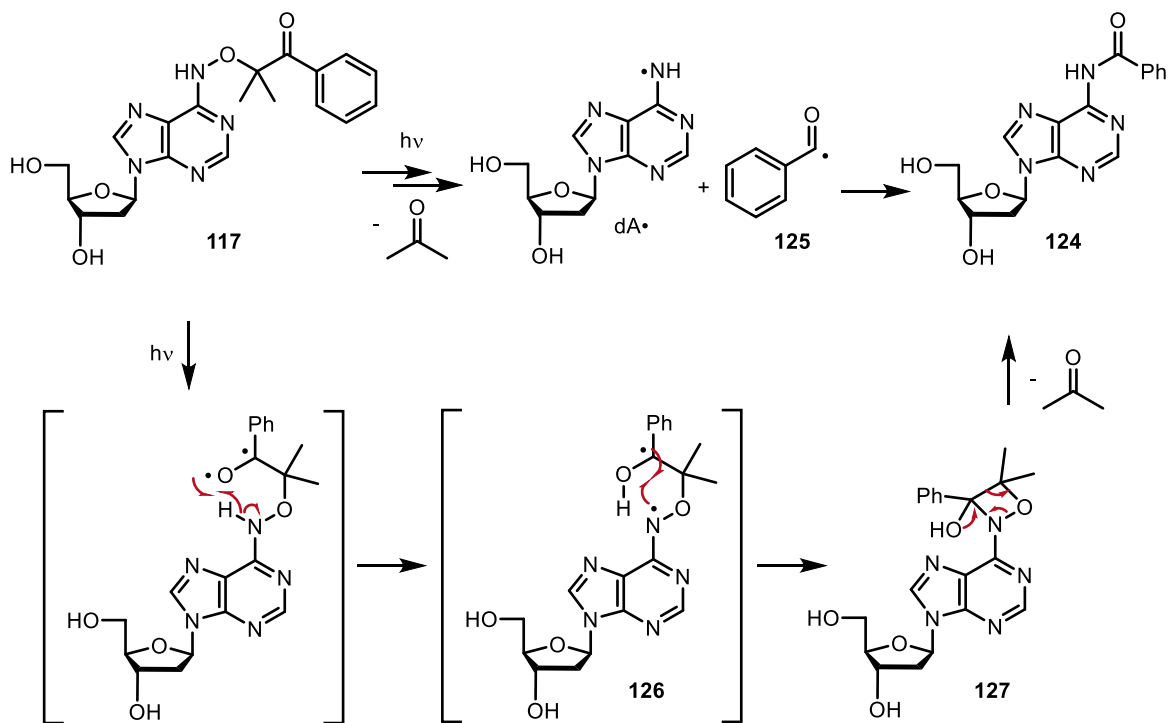
Table 5. Product analysis of the photolysis of 117.

Reducing agent (10 mM)	Yield of dA
-	48%
ascorbic acid	15.6%
dG	52.2%
Fe^{2+}	70.7%
Et_3N	78.0%
isopropanol	38.7%

The photolysis in the presence of Et$_3$N was further investigated by time course experiments. These experiments revealed that the precursor was consumed after 1 h of photolysis, whereas dA grew in over 5 h. We hypothesized two possible causes for this observation: (1) a nonphotochemical reaction of the precursor generates dA; (2) the precursor is converted into other intermediates, which convert to dA photochemically. The possibility of a nonphotochemical reaction was ruled out by an experiment during which the precursor was photolyzed for 1 h and analyzed 4 h after the photolysis. The yield of dA was the same as in the sample analyzed immediately after 1 h photolysis. Furthermore, we were unable to identify any intermediates to support the second hypothesis. Most importantly, the results obtained from the time course experiments cannot be explained by tandem Norrish type I cleavage, β-fragmentation. We believe that the acyloin moiety in **117** may undergo reactions other than Norrish type I reaction, but the process by which this happens is unknown.

Scheme 37. Synthesis of precursor **6**.
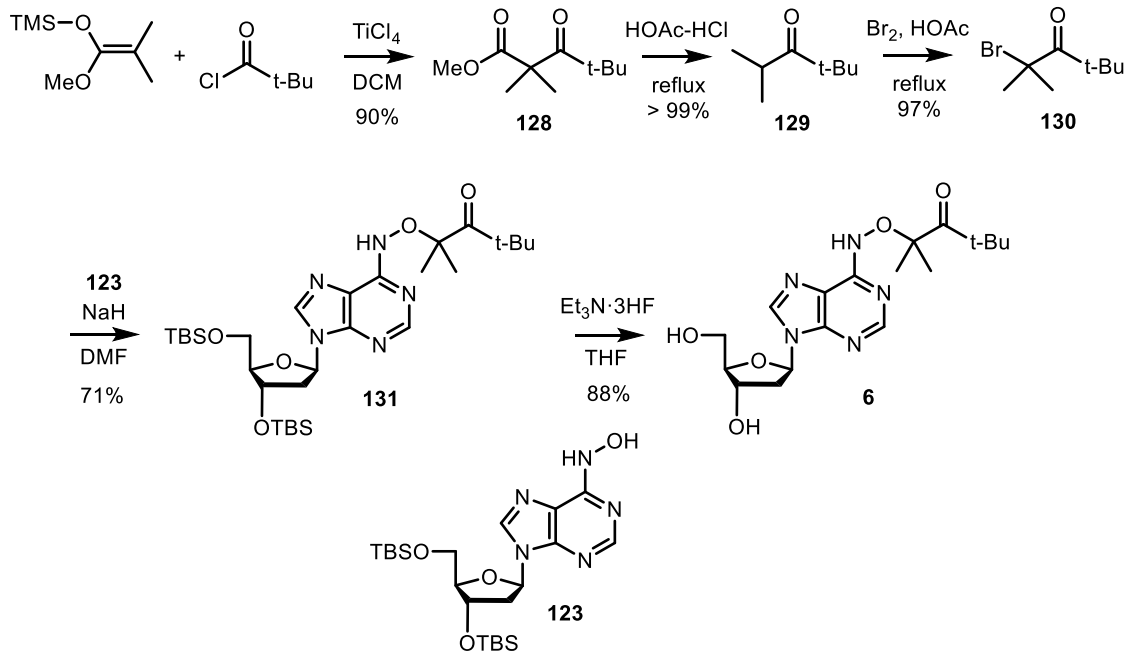
Consequently, we designed precursor **6**, in which the phenyl group was replaced by a *t*-butyl group. The Norrish Type I photochemical cleavage of *t*-butyl ketones has been used successfully to generate a number of DNA and RNA carbon radicals in high yield.[184-185] The same strategy for the synthesis of **117** was used in the synthesis of **6** (Scheme 37). β-Ketoester (**128**) was synthesized via a TiCl₄-catalyzed Claisen-type condensation.[232] The *t*-butyl bromoketone (**130**) was prepared from via decarboxylation and bromination. The yield of **131** via the substitution of **130** by **123** was significantly improved to 71 % by using DMF as the solvent instead of THF. Precursor **6** showed a λ_{max} = 270 nm (ε = 1.20 × 10^4 M^{-1}cm^{-1}) which tails to approximately 350 nm.
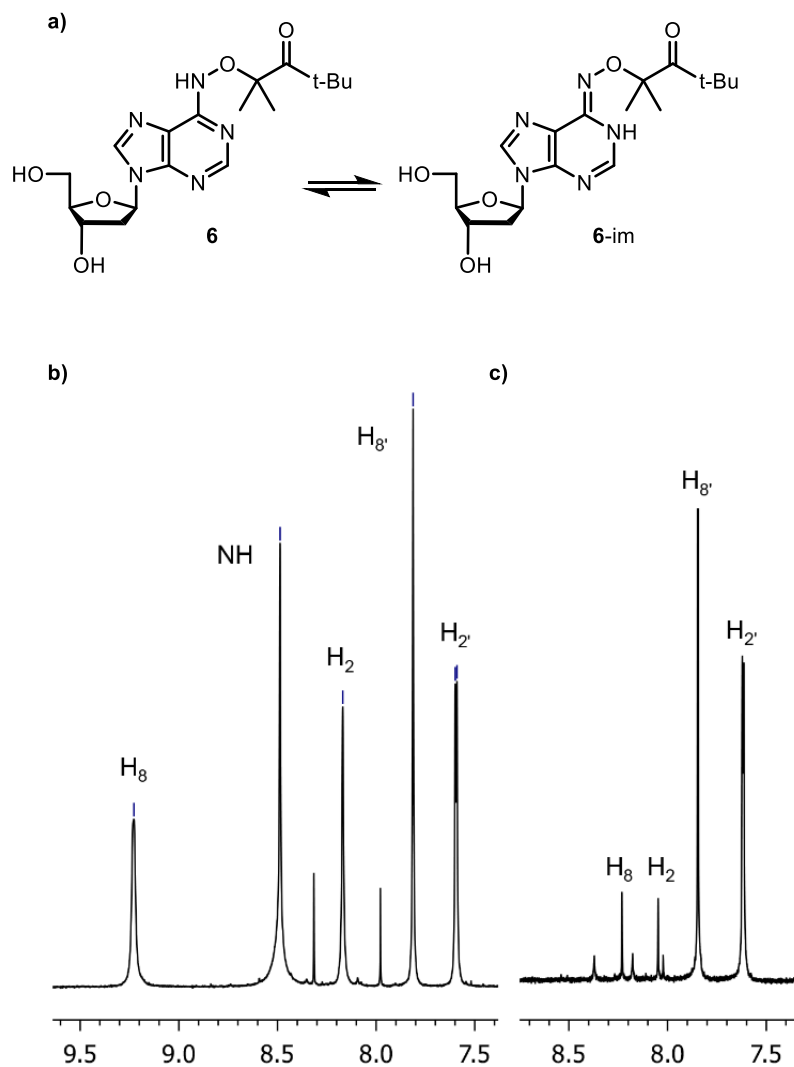
Figure 8. Solvent-dependent tautomerization of **6**. (a) Aminyl (**6**) and iminyl (**6**-im) tautomers. (b) ^{1}H NMR in CDCl$_3$ (c) ^{1}H NMR in CD$_3$CN.

Ketone **6** exists as a mixture of tautomers (Figure 8a). The iminyl tautomer (**6**-im) is slightly favored in CDCl$_3$ (Figure 8b) but dominates in CD$_3$CN (Figure 8c) and protic solvents, such as MeOH-d$_4$. The protons in the aminyl tautomer have higher chemical shifts in the spectrum relative to the corresponding protons in **6**-im, which is consistent with trends reported in the literature.[233] The relevance of the tautomeric equilibrium to the photochemistry of **6** is discussed below.

3.1.2.2 Photochemical properties of 6

Laser flash photolysis of **6** with the 308 nm emission of a
nanosecond-pulsed XeCl excimer laser was carried out to obtain
direct evidence for the transient formation of the aminyl radical dA•.
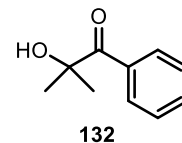
Unfortunately, photolysis (~12 mJ/pulse) in several solvents (e.g.,
acetonitrile, MeOH, aqueous buffer) did not afford any detectable transients. The failure to
detect dA• was consistent with the low quantum yield for **6** disappearance ($\Phi = 0.0015$)
that was determined using 2-hydroxy-2-methylpropiophenone (**132**) as an actinometer,
which led us to explore photosensitization conditions. Addition of low triplet energy
sensitizers (e.g. benzophenone) did not yield detectable transients. However, photolysis in
the presence of acetone (200 mM in acetonitrile) yielded a prominent peak centered around
340 nm and a broader, weaker peak that stretches from 500-600 nm (Figure 9a). These data
are consistent with previously reported spectra of dA•, which also feature a broad
absorbance centered around 590 nm.[32, 234] Since the alkoxyamine **6** is in equilibrium with
the oxime ether (**6**-im), we calculated the UV-vis spectra of both the expected aminyl
radical dA• and that of its iminyl tautomer (dA•-im) (Figure 9b). These calculations
indicate that it is unlikely the observed transient corresponds to the iminyl radical, which
lacks a long wave absorption The calculations, using a N9-methyladenine analog of dA•
(**133**) and dA•-im (**133**-im), indicate that the iminyl radical is 13.0 kcal/mol higher in
energy in the gas phase than the aminyl radical (Figure 10). This result suggests that the
dA•-im will rapidly tautomerize to dA•.
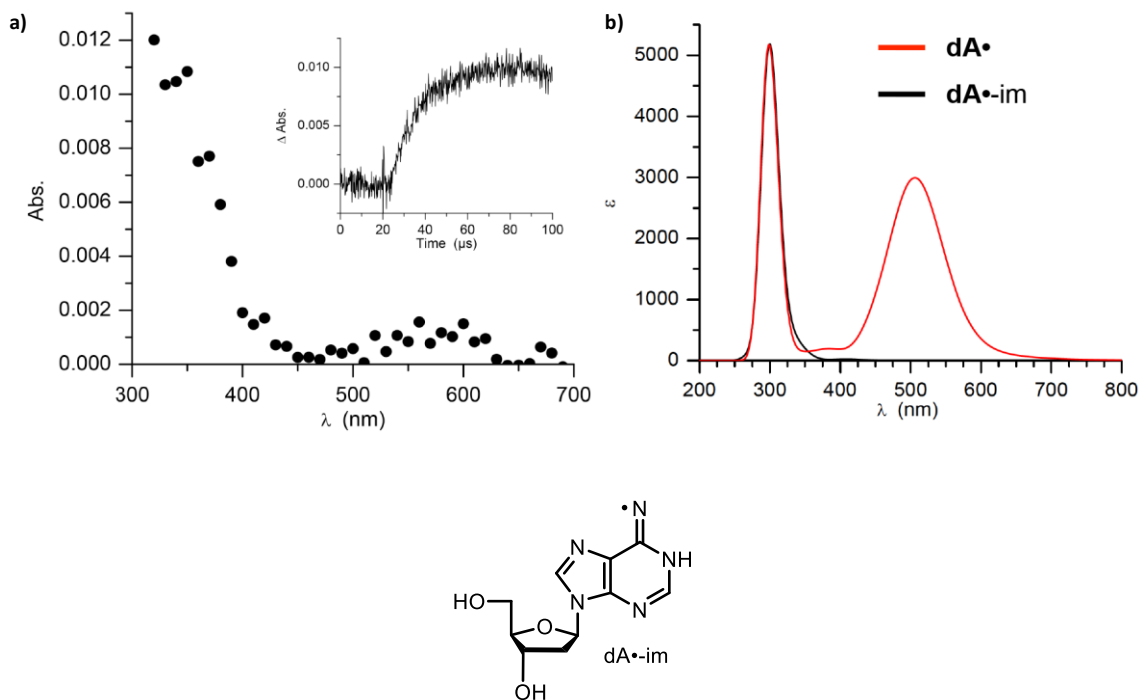
Figure 9. Transient spectroscopic studies of dA•. (a) Transient absorption spectrum obtained 40 µs after photolysis of a solution of (0.2 mM) in acetonitrile containing acetone (200 mM). Inset: the growth of absorption at 340 nm. (b) Calculated absorption spectra for dA• and its iminyl tautomer (dA•-im) (TD-B3LYP/6-311++G(d,p)).
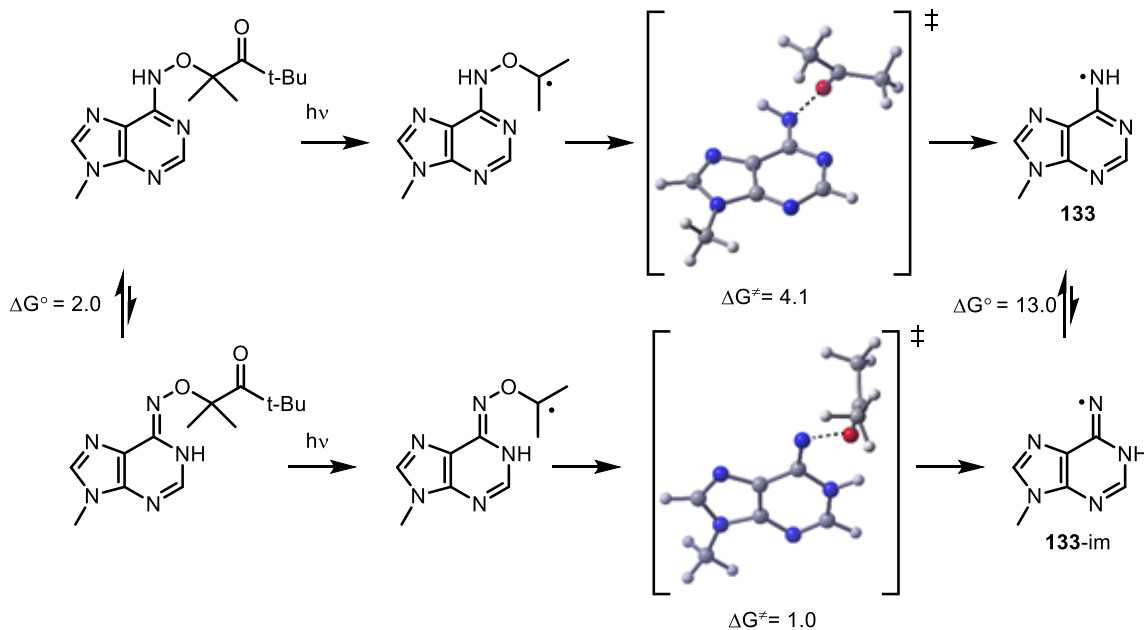
Figure 10. Calculated transition state structures for the fragmentation reactions of **133** and **133**-im (energies given in kcal mol^{-1}).

118
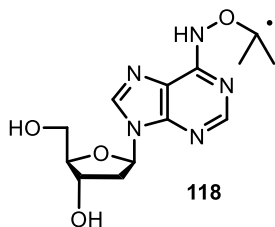
The accumulation of signal at or around 340 nm was attributed to β-fragmentation of the intermediate alkyl radical **118** to produce dA•. Intermediate **118** is not expected to absorb strongly above 300 nm, and its formation is presumably too fast to detect on the μs timescale. The rate constant for formation of dA• was fit to first order growth kinetics, yielding a rate constant of $(2 \pm 2) \times 10^5$ s^{-1} (Figure 9a); more than 10^4- and 10^7-fold slower than the rate of β-fragmentation computed from either **133** or **133**-im, respectively (Figure 10). However, the rate constant derived from the growth rate of dA• is likely underestimated due to the relatively fast concurrent consumption of the radical that suppresses the transient signal. Furthermore, if the rate constant of the β-fragmentation was only $\sim 10^5$ s^{-1}, reaction with O_2 would be competitive ($k[O_2] \sim 10^6$ s^{-1}), which does not appear to be the case (see below). Once the absorption at 340 nm reaches a maximum intensity around 80 μs after photolysis, the transient slowly decays with a half-life of ca. 200 μs (Figure 11). This decay could not be fit to a second-order function, indicating that multiple decay paths are available to the radical under these conditions.

In an attempt to slow the decay of the dA• and possibly obtain cleaner decay kinetics we carried out photolyses of **6** in acetonitrile-buffer mixtures. Unfortunately, this led to a significant reduction in signal intensity (Figure 11). This is consistent with the shorter lifetime of the acetone triplet state in aqueous solution as compared to acetonitrile, rendering photosensitization less efficient and precluding generation of radical **105**.[235] This hypothesis is also consistent with acetone sensitized photochemical conversion of **6** during continuous irradiation in various solvent conditions (Table 6). We found that **6** is converted

71

approximately 3-times more efficiently upon broadband UV-irradiation ($\lambda_{max} = 350$ nm) in acetonitrile than in phosphate buffer in the absence of acetone. Acetone enhances the photoconversion efficiency in both solvents, notably more than 6-fold in acetonitrile, the conditions under which laser flash photolysis experiments were most successful.
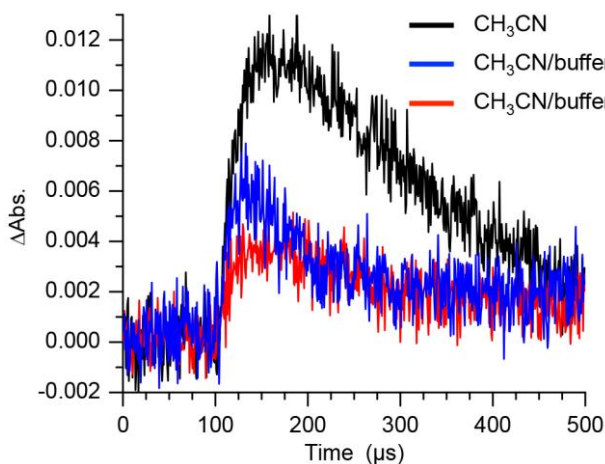
Figure 11. Transient absorption traces of a solution of **6** (0.2 mM) in acetonitrile and different mixtures with buffer (phosphate 10 mM, pH 7.4) in the presence of acetone (200 mM) at 340 nm.

Table 6. Photochemical conversion efficiency of 6 during continuous UV-irradiation.

Solvent	Acetone[a]	Photolysis time (min)	Conversion (%)	Average conversion rate (% min^{-1})
Aq. buffer[b]	-	60	30 ± 1	0.5
Aq. buffer[b]	+	30	51.4 ± 0.2	1.7
CH_3CN	-	30	45.2 ± 0.2	1.5
CH_3CN	+	1	10 ± 1	10

[a][Acetone] = 0.2 M [b]Phosphate (10 mM, pH 7.2)

Although **6** was converted more efficiently in acetonitrile, the product studies involving the photolysis of **6** were carried out in phosphate buffer to mimic t/he conditions under which dA• would be produced in DNA. Inferential support for the intermediacy of

dA• was obtained from the detection of **134** which was formed by DMPO trapping dA•.

Trapping product (**135**) generated by t-butyl radical and DMPO was also observed.[236]

134   135   DMPO
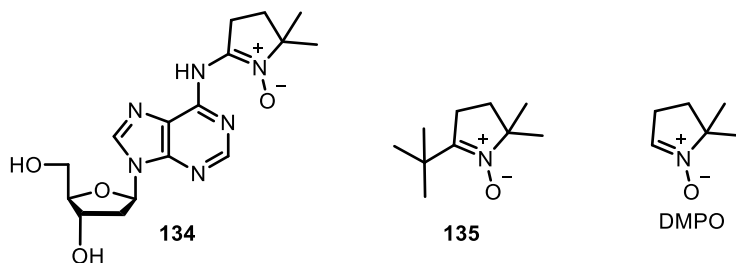
Minor amounts of *t*-butyl amide (**136**) and *N*6-*t*-butyl-2'-deoxyadenosine (**137**) were also detected by LC/MS. The former product was observed under aerobic and anaerobic conditions and was likely to result from a competing Norrish Type II reaction similar to that observed in the photolysis of **117**. Product **137** was only detected under anaerobic conditions and was attributed to the recombination of dA• and *t*-butyl radical.

117   124   136   137
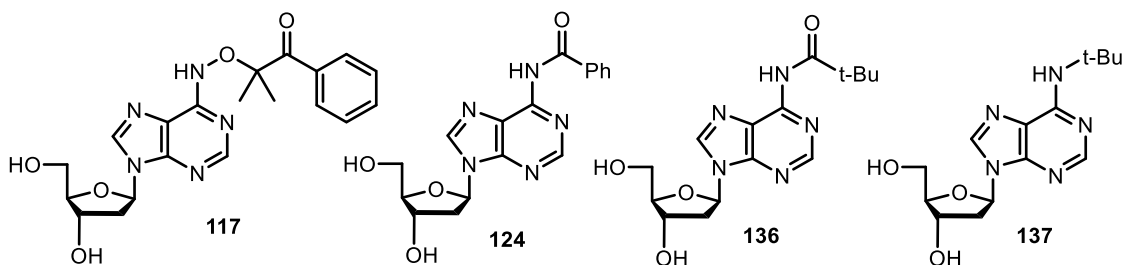
The formation of dA served as the strongest evidence for the formation of dA•. Modest yields of dA were formed following photolysis of **6** in aqueous buffer under aerobic or anaerobic conditions in the absence of exogenous reducing agent (Table 7). The yield almost doubled under anaerobic conditions in the presence of $Fe(NH_4)_2(SO_4)_2$ (10 mM) and increased further when the concentration of **6** was reduced to 25 μM from 100 μM. The reduced dA yield and mass balance in the absence of reductant could be due to a reaction between dA• and **6**. The inverse relationship between the yield of dA and mass

73

balance with the concentration of **6** is consistent with this proposal. Under aerobic conditions, dI was also formed in yields (11.6 ± 0.7 %) comparable to those reported by Wagner upon irradiation of **82**. The yields of dI were not affected by the presence of ferrous ion. The mass balance determined by the amounts of **6**, dA, and dI varied from 73 to 86% in the presence of ferrous ion.

82
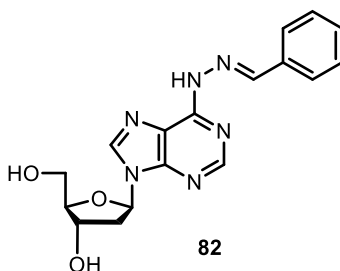
Table 7. Effect of reaction conditions on dA yield from the photolysis of 6 in phosphate buffer (pH = 7.2).

[6] (μM)	O$_2$	Reducing agent (mM)	% Yield of dA[a]	% Mass balance[a]
100	-	Fe^{2+} (10)	64 ± 1	76.9 ± 0.2
50	-	Fe^{2+} (10)	69 ± 6	80 ± 5
25	-	Fe^{2+} (10)	74 ± 2	86 ± 2
100	+	Fe^{2+} (10)	62 ± 1	73 ± 1
100	-	-	34 ± 4	50 ± 3
100	+	-	27 ± 2	59 ± 2
100	-	BME (100)	24 ± 2	51 ± 2
100	-	BME (500)	26 ± 2	51 ± 2
100	-	PhSH (10)	70 ± 2	84 ± 2
100	-	Cys (10)	32 ± 1	63 ± 1
100	-	GSH (10)	48 ± 3	73 ± 2

[a]Average $\pm$ std. dev. of 3 experiments.

The lack of an O_2 effect on the yield of dA from **6** is consistent with the slow reaction of dA• with O_2.[30] However, this also suggests that O_2 does not compete with β-fragmentation in **118**. To further support this, we set out to search for potential products generated by O_2 trapping of **118**. The trapping of **118** is likely to give rise to products such as **138** and **139** (Scheme 38a). Indeed, a product with the *m/z* matching **138** was detected by LC/MS. We independently synthesized **138** (Scheme 38b). However, the aforementioned product observed upon photolysis of **6** had a different reverse phase HPLC retention time than **138**. The absence of detectable levels of **138** is consistent with rapid loss of acetone. We also attempted to trap **118** with hydrogen atom donor, which was expected to react with **118** to generate **141**. However, **141** was not detected by LC/MS in the presence of BME (as high as 0.5 M) under anaerobic conditions. The absence of **141** was further confirmed by independently synthesizing it (Scheme 38c). These experiments enable us to propose that β-fragmentation is significantly greater than 10^6 s^{-1}, and are consistent with the Begley's results for hydroxamate radical formation ($k > 2 \times 10^8$, Scheme 17) and the computational studies described above ($k > 2 \times 10^{10}$ s^{-1}).[181]

Moreover, there is no evidence for BME trapping dA•. Increasing the BME concentration from zero to 0.1 M to 0.5 M does not affect the yield of dA, and a slight decrease in the mass balance is observed (Table 7). In contrast, the presence of cysteine (Cys) and glutathione (GSH) during photolysis of **6** yield modestly higher dA yields and increased mass balances. The greatest dA yield and mass balance are observed when the even more reactive thiophenol (PhSH) is employed. PhSH (10 mM) was even more effective when **6** (0.1 mM) was photolyzed in acetonitrile, where the yield of dA was (90 ± 5 %), and the mass balance was 94 ± 5 % (3 replicates).

Scheme 38. Proposed products generated by trapping of **118** and their independent synthesis
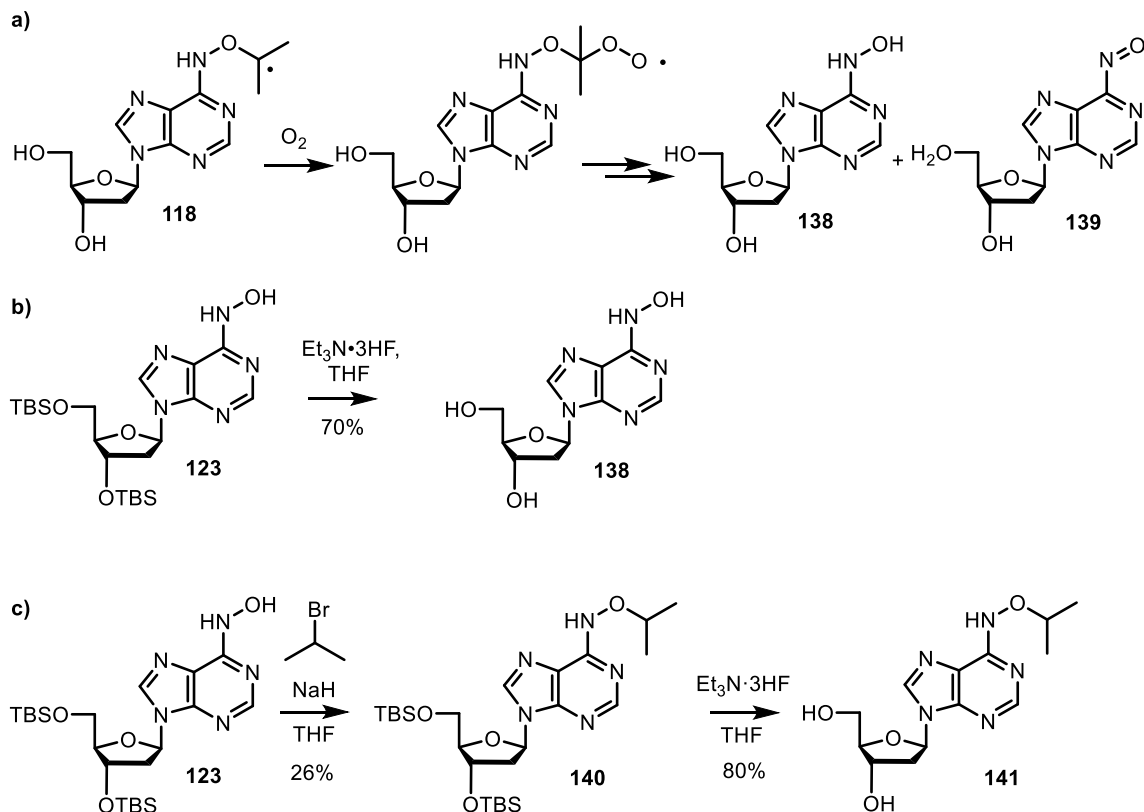
The lower yield of dA in reactions between dA• and thiols other than PhSH cannot be rationalized simply by consideration of the corresponding bond dissociation energies. The thiol bond strength in BME could be as low as 88 kcal/mol, and the BDE of N6-H is greater than 97 kcal/mol in 9-methyladenine.[237-239] Hence, hydrogen atom transfer from BME to dA• is thermodynamically favorable. The slightly more favorable reactivity of dA• with Cys and GSH could be due to a variety of factors, including polarity of the thiol bonds. We suggest that the reactions are kinetically controlled and are a consequence of a polarity mismatch between the electrophilic dA• radical and the polarity of the hydrogen atom donor. Nucleophilic aminyl radicals react readily with alkyl thiols or PhSH.[240] The rate constants for their reaction with thiols are comparable to those of their alkyl radical

counterparts.[240] However, the aminyl radical in dA• is conjugated to the electron withdrawing purine ring, which increases its electrophilic character. The reactivity of dA• is more similar to an amidyl radical than an alkylamine radical. Amidyl radicals react more rapidly with electron-rich donors, such as Bu_3SnH than even PhSH.[241] Hence, dA• reacts slowly with thiols other than PhSH because of polarity mismatching between the electrophilic radical and the relatively electronegative hydrogen atom donor.[240, 242] Unfortunately, testing this hypothesis by examining the reaction of dA• with less electronegative hydrogen atom donors, such as Bu_3SnH is not possible due to the incompatible solubilities of **6** and the tin hydride. Moreover, attempts to measure the rate of reduction of dA• by thiophenol were unsuccessful. The phenylthiyl radical absorbs in the same region as dA• (λ_{max} = 450 nm),[243] which may be produced in this experiment by the desired hydrogen atom transfer, hydrogen atom donation to the acetone triplet, and photolysis of residual diphenyldisulfide in the thiophenol.

Furthermore, with the success in utilizing acetophenone to sensitize precursor **7** (see Section 3.1.2.3), we demonstrated that acetophenone was also able to sensitize the photolysis of **6**. In the presence of 1% (v/v, 86 mM) acetophenone, the photolysis in phosphate buffer containing 10% acetonitrile resulted in 75 ± 2 % conversion of **6** in 5 min. While sensitization by acetone (2% v/v) led to less than 10% conversion of the precursor within 5 min. Compared to the conditions under which the transient spectra of dA• was obtained (200 mM acetone in acetonitrile, Table 6), the consumption of **6** when sensitized by acetophenone in 90% aqueous buffer was 1.5-times faster. In addition, the fidelity of **6** was not affected by acetophenone sensitization, and $82 \pm 3\%$ of dA was generated in the presence of PhSH (10 mM). Hence, we expect that using acetophenone as sensitizer will

enable us to carry out transient spectroscopic studies in buffer-acetonitrile mixtures which are a better approximation of pure aqueous buffer, where DNA naturally exists.

3.1.2.3   Synthesis of the precursors for independent generation of dG(N2-H)•

Based on the same strategy for the generation of dA•, we designed precursor **7** to generate dG(N2-H)• photochemically (Scheme 39). We attempted to synthesize **142** from *O*6-benzyl-2-bromo-2'-deoxyinosine (**100**) under the same conditions for synthesizing *N*6-hydroxy-2'-deoxyadenosine (**123**, Scheme 35). However, the reaction only yielded a trace amount of **142** after 24 h, which was attributed to the low reactivity of electron-rich guanine towards nucleophilic aromatic substitution. Furthermore, carrying out the reaction in DMF under 100 °C led to hydrolysis of the bromide, which may be caused by water residue in DMF. Consequently, we used dioxane as the solvent, which allowed the reaction to be carried out under elevated temperature (100 °C) without hydrolyzing the substrate. The reaction was still inefficient and required 36 h to complete. The ensuing substitution with **130** using NaH as the base was unsuccessful and generated an unidentified side product. By switching the base to Cs_2CO_3, the formation of this side product was avoided, and desired product **143** was obtained with 70% yield. The same reaction condition was also tested for the synthesis of the dA• precursor and gave 72% yield, which was comparable to yield obtained when NaH was used as the base (Scheme 37). The benzyl protecting group was removed by hydrogenolysis while the N-O bond remained intact to generate **144**, and the ensuing desilylation afforded the precursor **7**.

Scheme 39. Synthesis of precursor **7**.
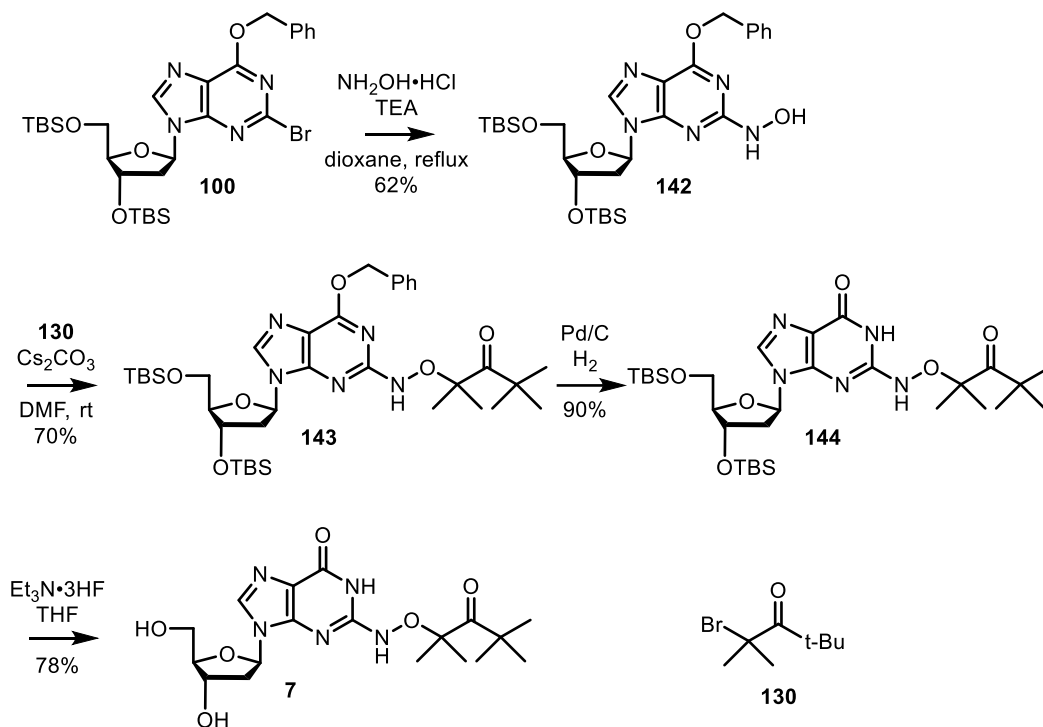
3.1.2.4 Photochemical properties of 7

Precursor **7** shows a λ_{max} = 260 nm (ε = 1.22 × 10^4 M^{-1}cm^{-1} in water), which tails above 300 nm. The photolysis of **7** was less efficient than that of **6**, and the conversion was only 10% even after 8 h photolysis at 350 nm. The quantum yield of the disappearance of **7** (Φ = ~0.0018) was also determined using 2-hydroxy-2-methylpropiophenone (**132**) as an actinometer, and this quantum yield is similar to that of **6**. However, **7** has a lower absorbance than **6** above 300 nm, which exacerbates the inefficient photochemistry. Inspired by the sensitization used during the photolysis of **6**, we used acetone (2% v/v,150 mM) to sensitize the reaction and achieved 63% conversion after 8 h. The yield of dG and mass balance under different conditions are shown in Table 8. When the precursor was photolyzed in the absence of reducing agents or oxygen, the rate of conversion was doubled, and the mass balance was
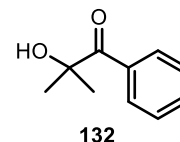
~50%. This is consistent with the proposal that the precursor can serve as a reducing reagent for dG(N2-H)•. In contrast to **6** (Table 7), both BME and PhSH trap dG(N2-H)• and form dG. This can be rationalized by the fact that guanine is more electron-rich than dA, and the corresponding nitrogen radical is less electrophilic, thus has a lower energy barrier to react with electronegative hydrogen atom donors, such as thiols. This observation further corroborates our hypothesis regarding the polarity matching between hydrogen atom donors and neutral purine radicals.

Table 8. Effect of reaction conditions on dG (100 µM) yield from the photolysis of 7 in the presence of acetone (2% v/v) as sensitizer.

O_2	Reducing agent (mM)	% Yield of dG[a]	% Mass balance[a]
-	Fe^{2+} (10 mM)	85 ± 2 %	90 ± 1 %
-	PhSH	89 ± 3 %	93 ± 1 %
-	BME	87 ± 2 %	91 ± 2 %
-	None	53.2%	53.2%
+	None	35 ± 2 %	44 ± 3 %

[a]Average ± std. dev. of 3 experiments.

Despite the success in utilizing acetone to sensitize the photolysis of **7**, the efficiency of the photochemistry was still too low for LFP studies. In order to improve the photolysis efficiency, we investigated photolysis in the presence of other photosensitizers. Acetophenone was a promising candidate due to its efficient intersystem crossing, long triplet lifetime, and relatively high triplet energy.[244-246] Anaerobic photolyses were carried out in the presence of acetophenone (1% v/v, 86 mM), and the consumption of the precursor was significantly accelerated. The sensitization efficiency is proportional to the percentage of acetonitrile in phosphate buffer (Table 9). In the presence of 100 mM BME,

the photolysis of **7** quantitatively yielded dG. This suggested that the fidelity of the photochemistry was not affected by the sensitization.

Table 9. Effect of acetonitrile on the conversion of 7 (1 mM) within 30 min in the presence of acetophenone (1% v/v).

O$_2$	Acetonitrile (% v/v)	% Conversion of **7**[a]
-	20[b]	28 ± 2
-	50[b]	58 ± 1
-	90[c]	95 ± 1

[a]Average ± std. dev. of 3 experiments.
[b]Acetonitirle in phosphate buffer (10 mM, pH = 7.2).
[c]Acetonitirle in water.

3.1.2.5 Attempts to generate dG(N2-H)• via intramolecular sensitization

Encouraged by the success of the intermolecular sensitization of the Norrish type I photocleavage of **6** and **7**, we set out to explore the possibility of sensitizing the Norrish reaction intramolecularly. Intermolecular sensitization is not suitable for polymer studies due to the generation of diffusible excited ketone molecules. It has been reported that acetone and benzophenone damage DNA photochemically.[247-248] Intramolecular sensitization limits the possibility of undesirable photooxidation of DNA and thus is potentially useful for polymer studies. There is precedence to suggest that this could work. Intramolecular energy transfer from ketones have been reported.[249] For instance, Wagner et al. reported intramolecular photosensitization of the pinene–ocimene rearrangement using a tethered *p*-alkoxy acetophenone.[250]
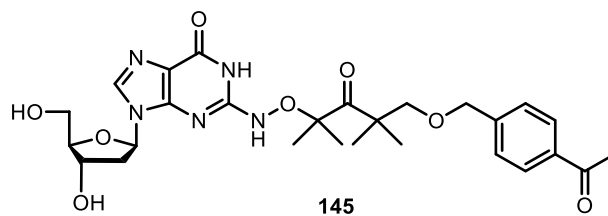
Scheme 40. Attempted synthesis of t-butyl ketone moiety in precursor **145**.
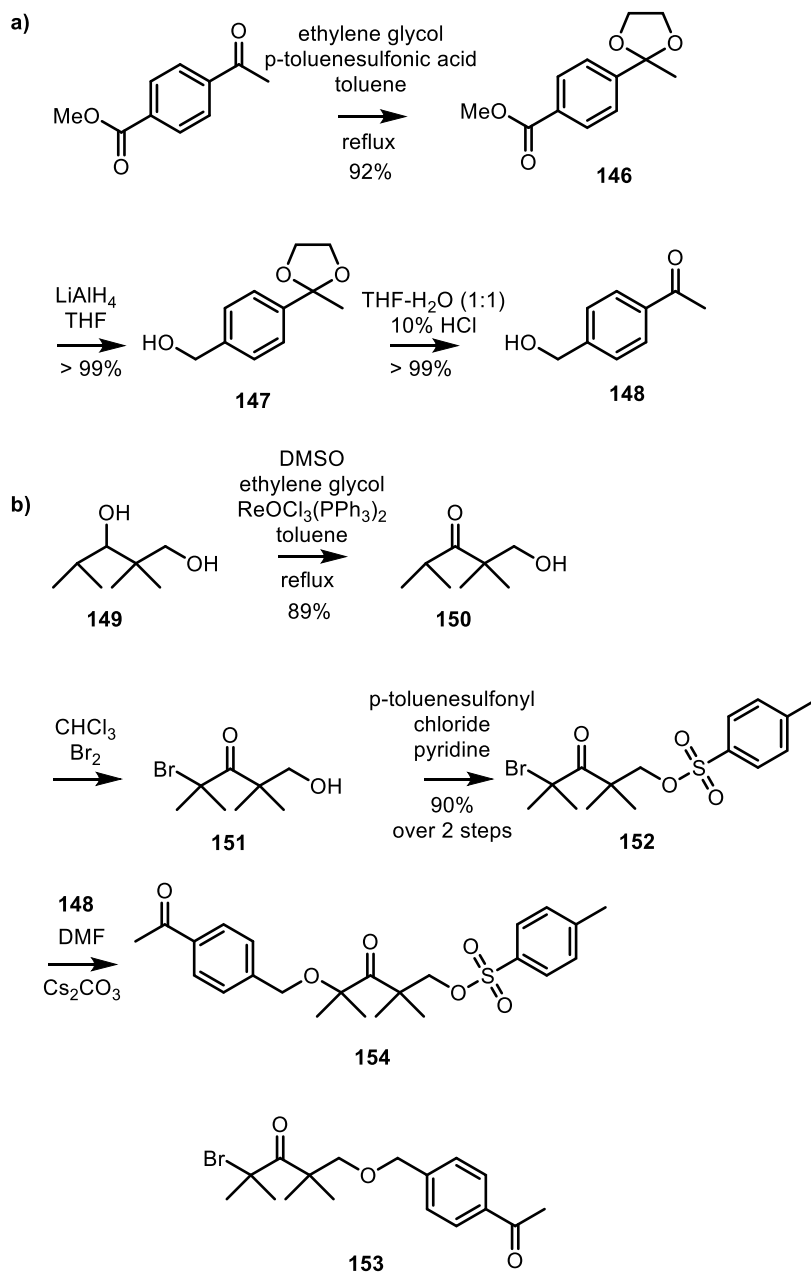
We designed precursor **145**, in which the acetophenone moiety is tethered to the *t*-butyl ketone moiety via an oxymethylene linkage. The *p*-hydroxymethyl acetophenone (**148**) was synthesized according to a report in the literature (Scheme 40a).[251] The *t*-butyl ketone moiety was synthesized from commercially available 2,2,4-trimethyl-1,3-pentanediol (**149**). The secondary alcohol was selectively oxidized via rhenium-catalyzed oxidation using methyl sulfoxide as an oxidant in the presence of ethylene glycol.[252] The β-hydroxy ketone (**150**) was brominated and subsequently converted to the corresponding tosylate **152**. The bromination was carried out at this stage to avoid the undesirable bromination of the acetophenone moiety. The nucleophilic substitution was carried out between **148** and **158** in hopes of forming **153** because the primary carbon is less hindered and may be more reactive. However, the bromine-substituted product (**134**) was the only product isolated (Scheme 40b). This observation suggests that the α-bromo group was more prone to react with nucleophiles.

Consequently, we modified our synthetic strategy to form the O-C bond between the guanine moiety (**155**) and the α-bromo-β-tosylate ketone (**152**) prior to installation of the acetophenone moiety (Scheme 41). Since the desired product **156** only has the tosylate to react with **148**, the possibility of the aforementioned side reaction is eliminated. The hydroxylamine functionalized nucleoside was synthesized via a pathway similar to that used in the synthesis of **142** (Scheme 39). However, β-(trimethylsilyl)ethyl was chosen as the protecting group for O6, because we anticipated that the hydrogenolysis condition would be incompatible with the oxymethylene linkage in **145**. The exocyclic amine group of *O*6-β-(trimethylsilyl)ethyl-2'-deoxyguanosine (**157**) was converted to fluorine via the method reported by Spratt et al.[253] The TBDMS group remained intact during the

fluorination. The 2-fluoro-2'-deoxyinosine derivative **158** was more reactive than the 2-bromo-O6-benzyl-2'-deoxyinosine (**142**, Scheme 39), and the substitution reaction to generate **155** was complete in 12 h. Unfortunately, the reaction between **155** and **152** did not yield the desired product (**156**) but instead provided the cyclized compound **159** (Scheme 41).

Scheme 41. Attempted synthesis of precursor **145**.
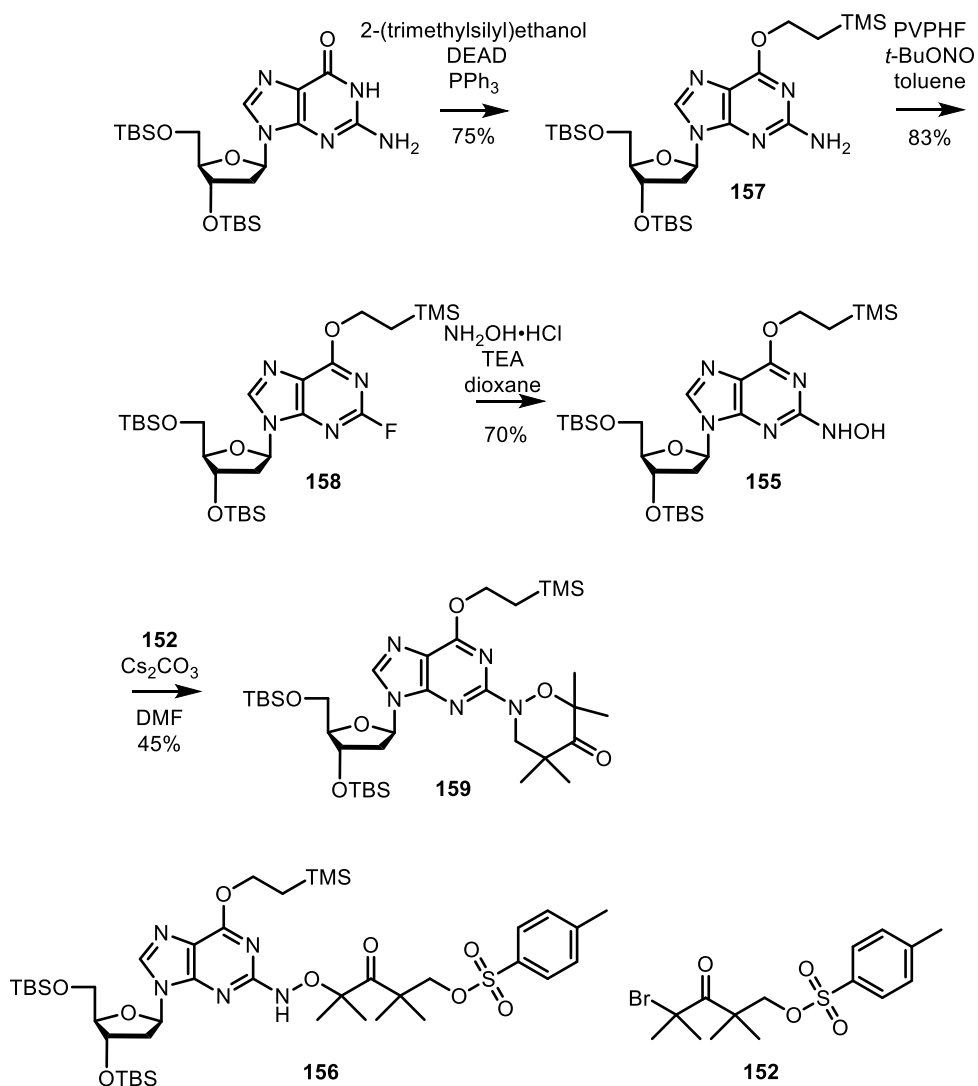
Consequently, we pursued an alternative synthetic strategy, in which the construction of the oxymethylene was achieved by reacting the hydroxy group of **163** with *p*-chloromethyl acetophenone (**164**, Scheme 42). The β-hydroxy ketone (**150**) was brominated following the protection of the hydroxyl group as its benzyl ether. The benzyl protection prevented the hydroxyl group from acting as a nucleophile during the substitution reaction between **161** and **155**. However, the bromination was low-yielding because the benzyl protecting group was labile under oxidative conditions. After the *t*-butyl ketone moiety is coupled to **155**, the hydroxy group was unmasked by hydrogenolysis (**163**). The *p*-chloromethyl acetophenone **164** was prepared by Wacker-type oxidation of *p*-chloromethyl styrene.[254] The reaction between **164** and **163** generated the protected precursor **165**, which was deprotected using TBAF to afford the precursor **145**.

Scheme 42. Synthesis of precursor **145**.
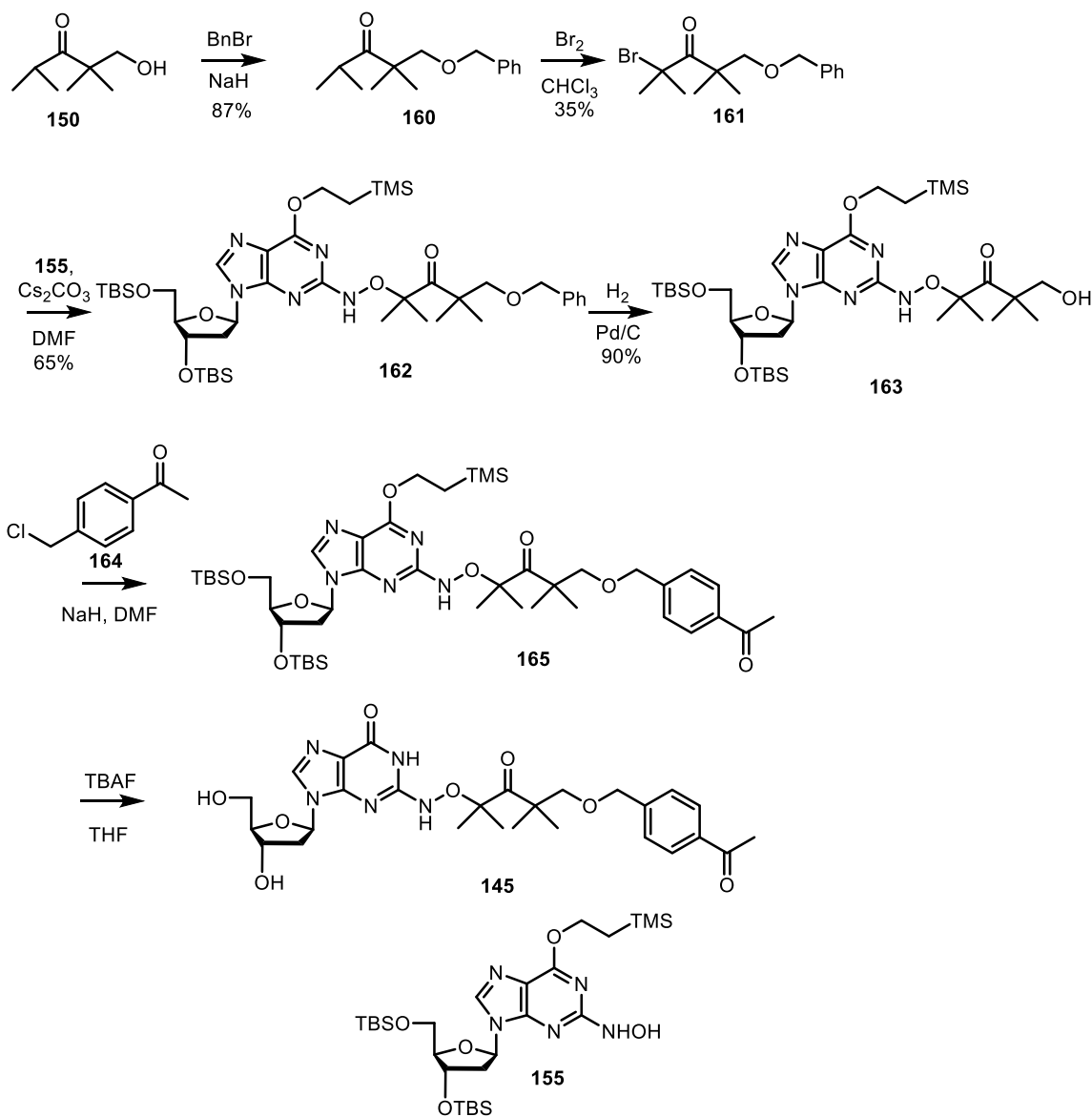
The photolysis of precursor **145** did not generate dG under any conditions, which included the presence or absence of O_2, as well as hydrogen atom donor (BME, 10 mM). UPLC-MS analysis indicated that the major product generated from the anaerobic photolysis was **166**, which was likely to have resulted from the photoinduced hydrolysis of the benzyloxy group. These results suggest that a more chemically robust linkage is

needed in order to test our proposal regarding the intramolecular sensitization of Norrish type I reaction.

166
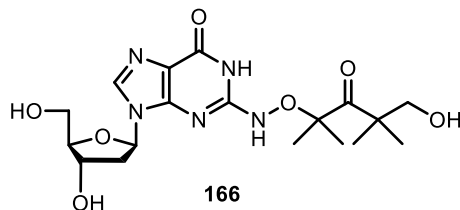
3.1.3 Naphthalimide type precursors for the generation of neutral purine radicals

3.1.3.1 Design and synthesis of precursors for the independent generation of dG(N1-H)•

dG(N1-H)• has two major resonance forms: the oxygen-centered radical **167** and the nitrogen-centered radical **168**. Since reports on installing heteroatom modifications at the N1 position are limited,[255] we focused our efforts on developing precursors in which a cleavable group is bonded to the O6 position of the guanine ring.
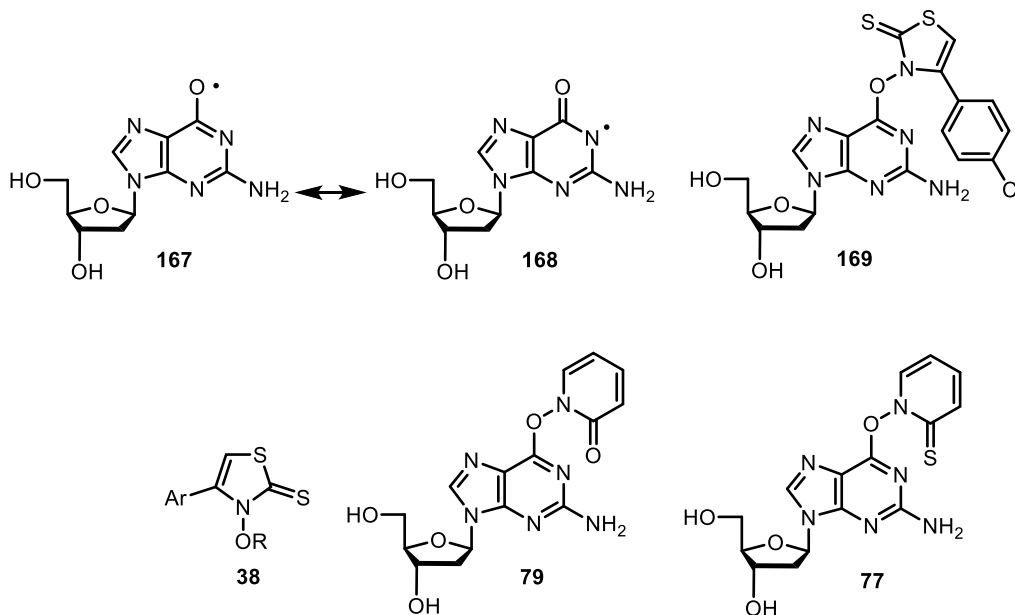
Based on the photochemistry of alkoxy-4-aryllthioazole-2(3)-thiones (**38**) reported by Hartung and co-workers, we designed precursor **169**.[166] The anticipated photochemistry of this precursor is based on the principle utilized by Gimisis (**77** and **79**, Scheme 20).[189] We envisioned that **169** would be more synthetically accessible than **77** because N-hydroxy-thiazolethiones demonstrated better selectivity for O-substitution versus S-substitution compared to N-hydroxypyridine-2(1H)-thione.[162, 166] In addition, it has been reported that alkoxy-4-arylthioazole-2(3)-thiones are cleaner sources for alkoxy radicals.[168] N-hydroxy-4-(*p*-chlorophenyl)thiazole-2(3H)-thione (**172**) was synthesized according to the literature (Scheme 43a).[166] The nucleophilic aromatic substitution was carried out on O6-sulfonylated 2'-deoxyguanosine (**173**) activated by DABCO. However, the desired product was not formed under this condition (Scheme 43b). Interestingly, **173**, which readily reacts with DABCO to yield a polar salt (**175**), is mostly unreacted under this condition. This result suggests that there is a side reaction, possibly **172** reacting with DABCO. To circumvent this side reaction, O6-benzyltriazole-2'-deoxyguanosine (**176**) was used as the substrate to react with **172**. At room temperature, no reaction was observed after 24 h. When the reaction was carried out at 65 °C, a small amount of side product **177** was generated (Scheme 43c). The assignment of the structure was based on the chemical shift of the proton on the thiazole ring. In the desired product (**174**), the chemical shift of this proton was expected to be around 6.5. However, the observed chemical shift of this proton was 7.66, which was consistent with the reported chemical shift for N-oxides.[166] This is surprising given the reported selectivity of the nucleophilic substitution.[166] However, we cannot rule the possibility that elevated temperature reduces the chemoselectivity. It is also possible that the initially formed **174** tautomerizes to **177** at higher temperature.

Scheme 43. Attempted synthesis of precursor **158**.
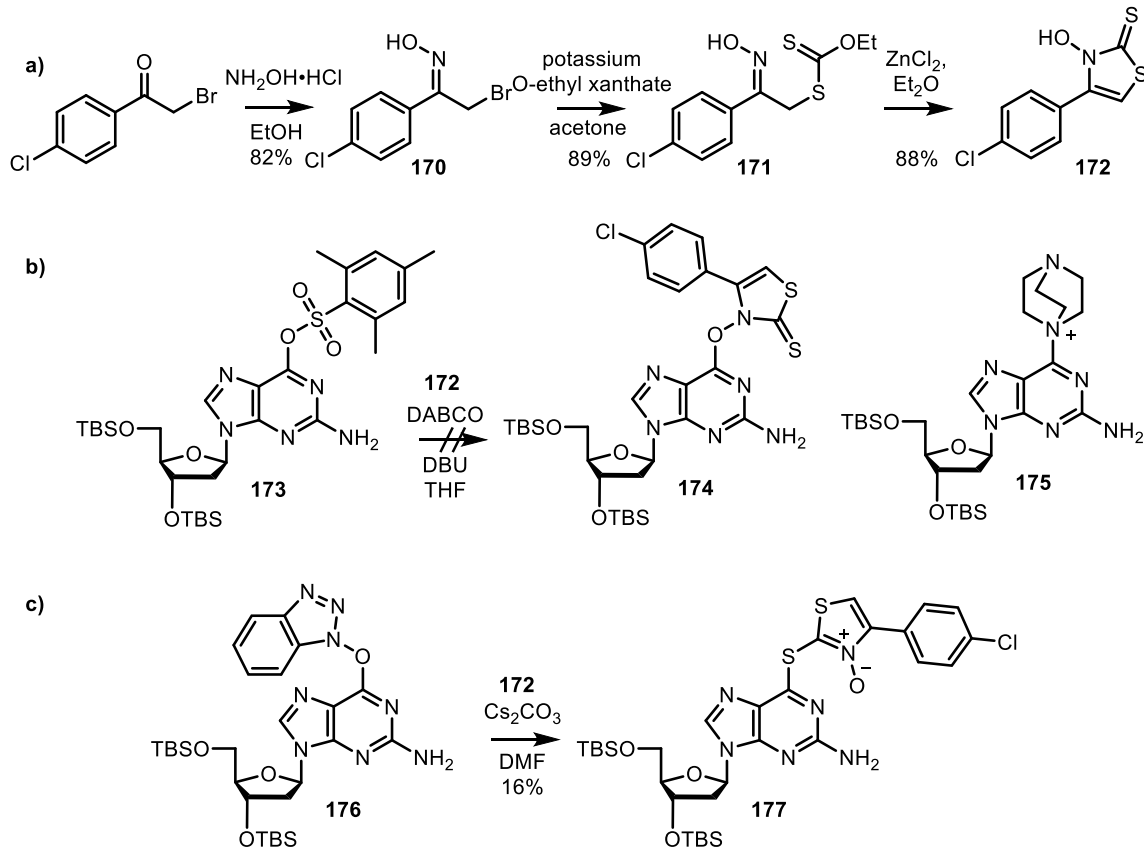
After the unsuccessful attempts to synthesize precursor **169**, we turned our attention to the N-aryloxy-naphthalimide **5** because compounds with similar structure (e.g. **44**, Scheme 44) undergo efficient N-O bond cleavage under UV excitation.[171-172] Precursor **5** was synthesized by reacting N-hydroxy-naphthalimide (**178**) with **173** activated by DABCO (Scheme 44). When the reaction was carried out in DME, no product was observed. This was attributed to poor solubility of **178** in DME. Switching the solvent to DMF, in which **178** was readily soluble, significantly improved the yield. Upon removing the TBMDS protecting group, precursor **5** was obtained. The UV spectrum of **5** shows absorption at 287 nm ($\varepsilon = 1.1 \times 10^4$ M^{-1}cm^{-1}) which arises from the guanine, and another at 346 nm ($\varepsilon = 1.72 \times 10^4$ M^{-1}cm^{-1}) which is attributed to the naphthalimide moiety.

89

Scheme 44. Synthesis of precursor **5**.
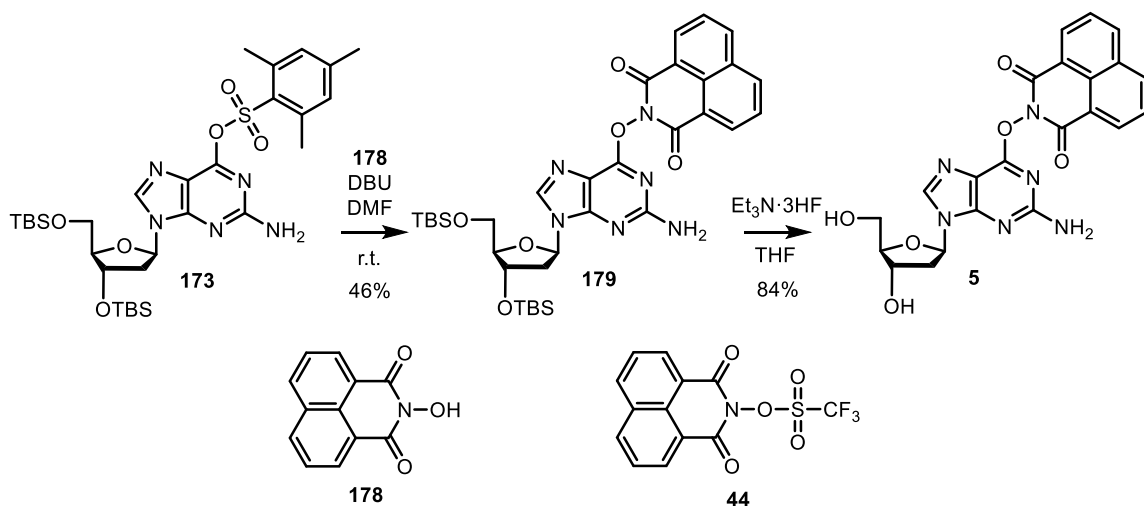
3.1.3.2 Photochemical properties of 5

The photochemistry of **5** was investigated under anaerobic and aerobic conditions. When photolyzed in the absence of O_2, **5** is completely consumed in approximately 2 min. The presence of 10 mM BME increased the yield of dG from $52 \pm 2\%$ (yield of dG in the absence of reducing agents) to nearly quantitative. UPLC-MS/MS analyses suggested that naphthalimide (**180**) was the other major photolysis product. This observation, as well as the lack of formation of **178** are consistent with homolytic N-O bond cleavage and exclude the generation of dG via hydrolysis (Scheme 45). Interestingly, the yield of naphthalimide determined by HPLC was quantitative and independent of the presence of BME. This observation is important to understand the photochemistry of **5** (see below). The quantum yield of the disappearance of **5** ($\Phi = 0.03$) was determined using N-hydroxynaphthalimide triflate as actinometer.[171-172] The quantum yield of **5** is 20 times higher than that of precursors **6** and **7**. This increased quantum yield and the high absorbance around 350 nm ($\lambda_{max} = 346$ nm, $\varepsilon = 1.72 \times 10^4$ $M^{-1}cm^{-1}$) contribute to the rapid conversion of the precursor **5**.

Scheme 45. Proposed mechanism for the generation of dG(N1-H)• from photolysis of **5** and production of dG in the presence of BME.
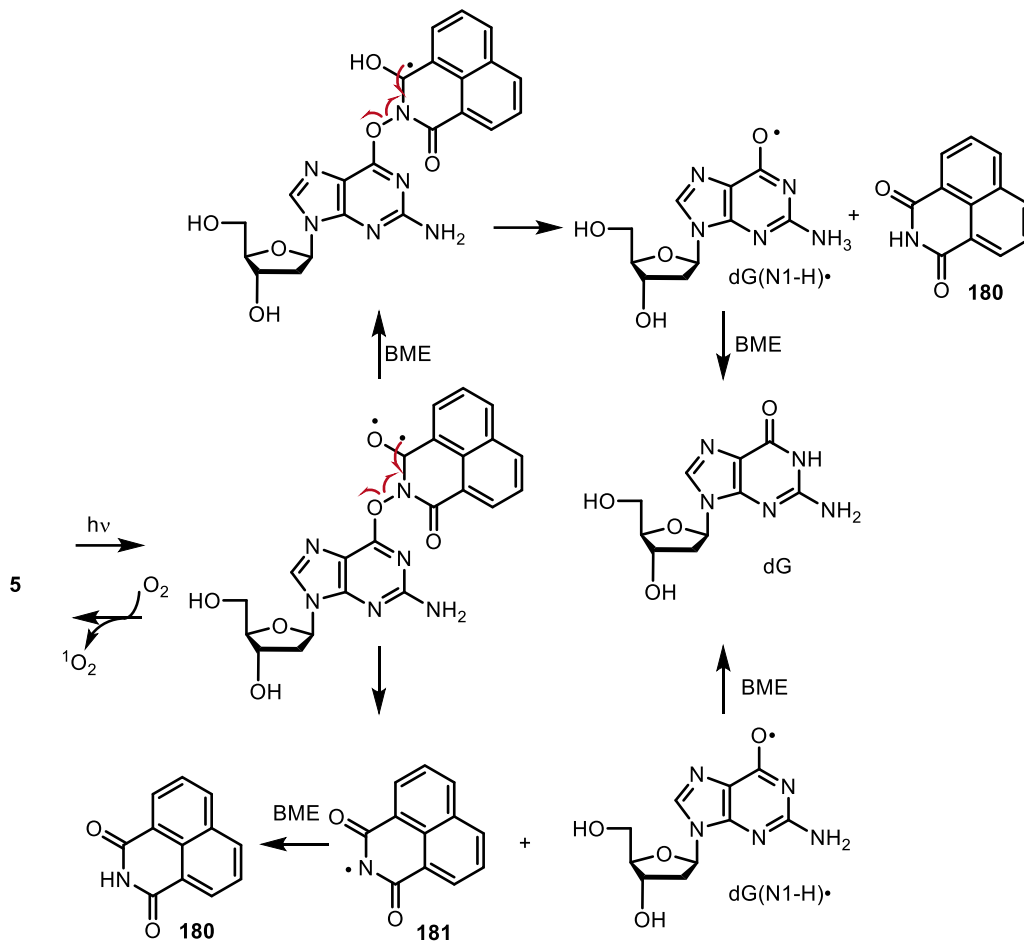
The anaerobic photolyses in the absence of BME generated approximately 50% dG. Naphthalimide (**180**) was formed quantitatively. To explain this result, we propose that the precursor served as the reducing agent of dG(N1-H)• and naphthalimidyl radical (**181**, Scheme 46). Furthermore, to balance the equation, we postulated that the remaining 50% of the guanine would be converted into four-electron oxidized guanines, such as dSp and dGh (Scheme 46). We propose that in the absence of reducing agents, UV-excited **5** initially undergoes homolytic cleavage of the N-O bond to generate dG(N1-H)• and naphthalimidyl radical (**181**). The naphthalimidyl radical can oxidize another molecule of

precursor **5** to generate the radical cation **182** and naphthalimide (Scheme 47). However, we cannot rule out the possibility that dG(N1-H)• oxidizes **5**. The fragmentation of **182** and subsequent hydration result in the formation of 8-oxo-dG and naphthalimidyl radical. Given the low oxidation potential of 8-oxo-dG, both dG(N1-H)• and **181** can be reduced by 8-oxo-dG, and 8-oxo-dG is oxidized to generate product such as dGh and dSp. Admittedly, the proposed reaction between 8-oxo-G•+ with dG(N1-H)• or **181** may not be favorable given the concentration of these species.

Scheme 46. Generation of four-electron oxidized dG during the anaerobic photolysis of **5** in the absence of BME.
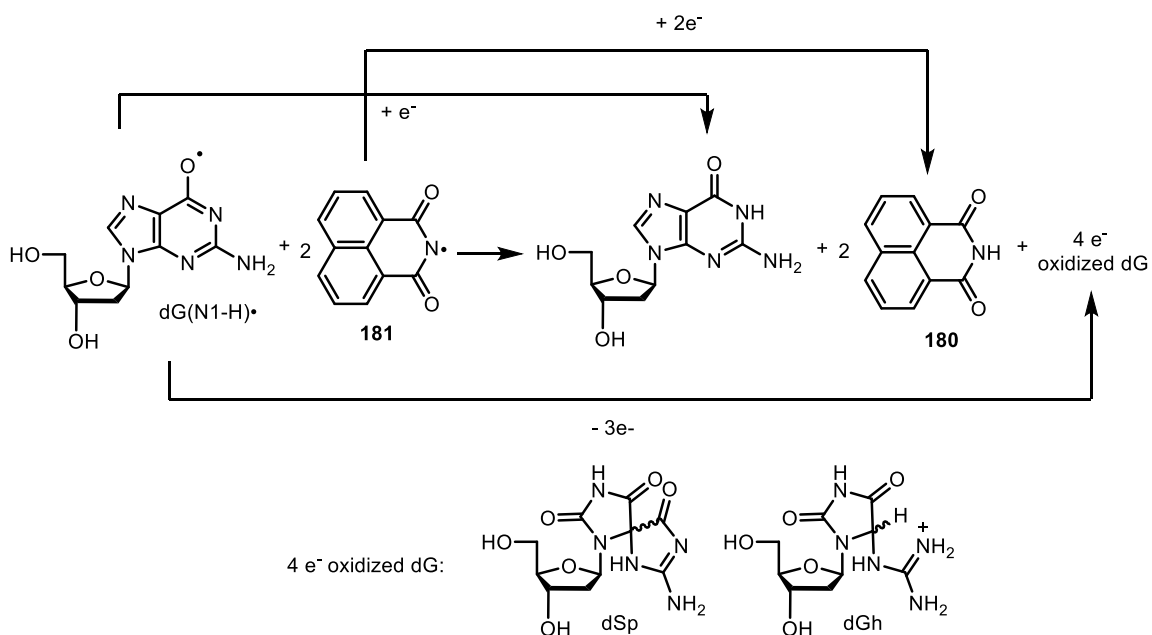
To support the proposed mechanism, the photolysis of **5** was carried out in the presence of two equivalents of 8-oxo-dG. Indeed, the addition of 8-oxo-dG restored the quantitative formation of dG observed under anaerobic conditions, and one equivalent of 8-oxo-dG was consumed. This result supports the proposal that 8-oxo-dG is formed as an intermediate during anaerobic photolysis in the absence of reducing agent (BME).

92

Additional support for the mechanism was obtained by identifying the proposed 4 electron oxidized forms of dG. This was facilitated by Burrow's previous report on the separation

Scheme 47. Proposed mechanism for the generation of dGh and dSp from the anaerobic photolysis of **5** in the absence of BME.
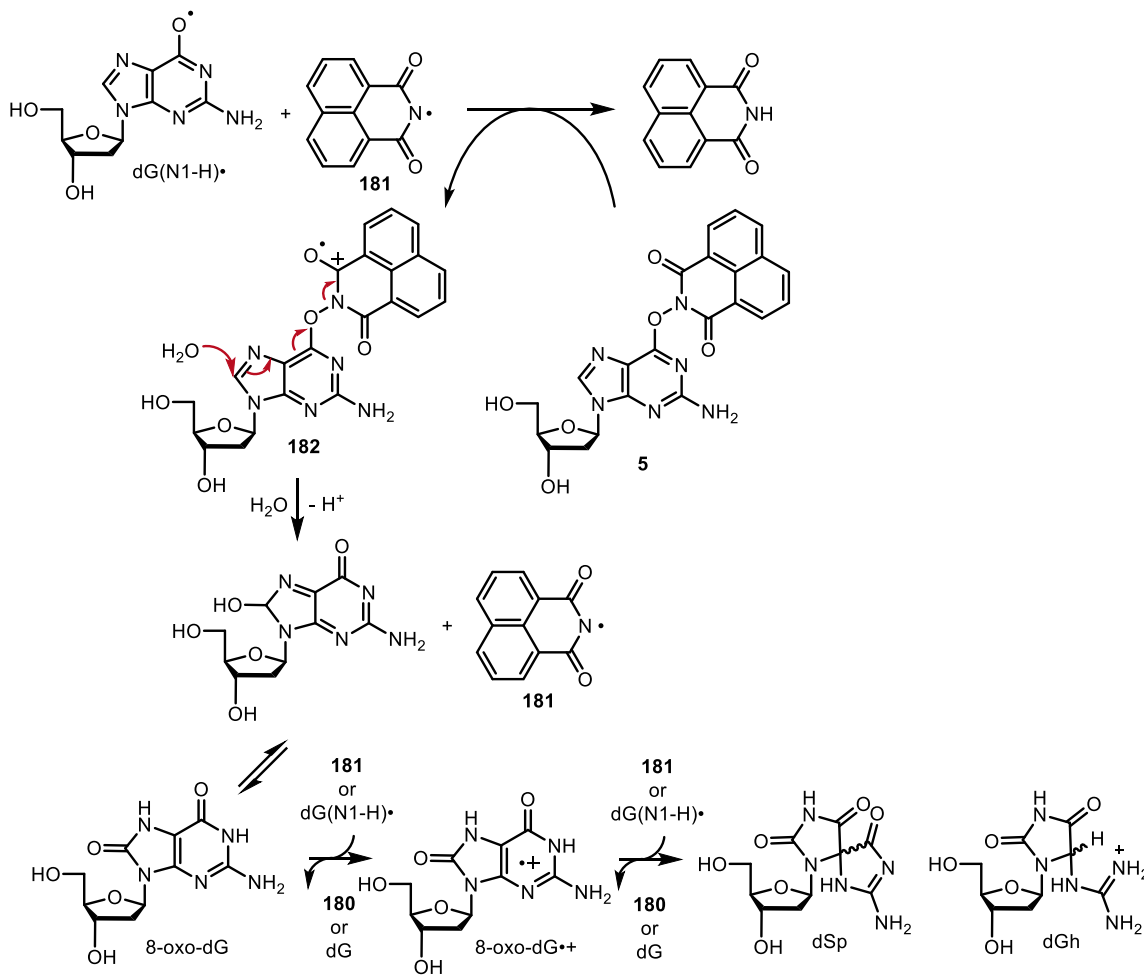
and identification of these products.[256] The photolysates were initially analyzed by C_{18}-reversed phase HPLC, and the void volume containing the polar four-electron oxidized guanines was collected. The void volume was then analyzed by UPLC-MS equipped with a Hypercarb column. The UPLC-MS/MS revealed dSp and dGh, which was consistent with the proposed mechanism (Figure 12, EIC of molecular ion of spiroiminodihydantoin (Sp) was used to improve

93
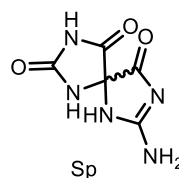
signal to noise ratio). The yields of dSp and dGh were qualitatively higher for the photolyses carried out in the presence of 8-oxo-dG as expected (Figure 12b, 12d).
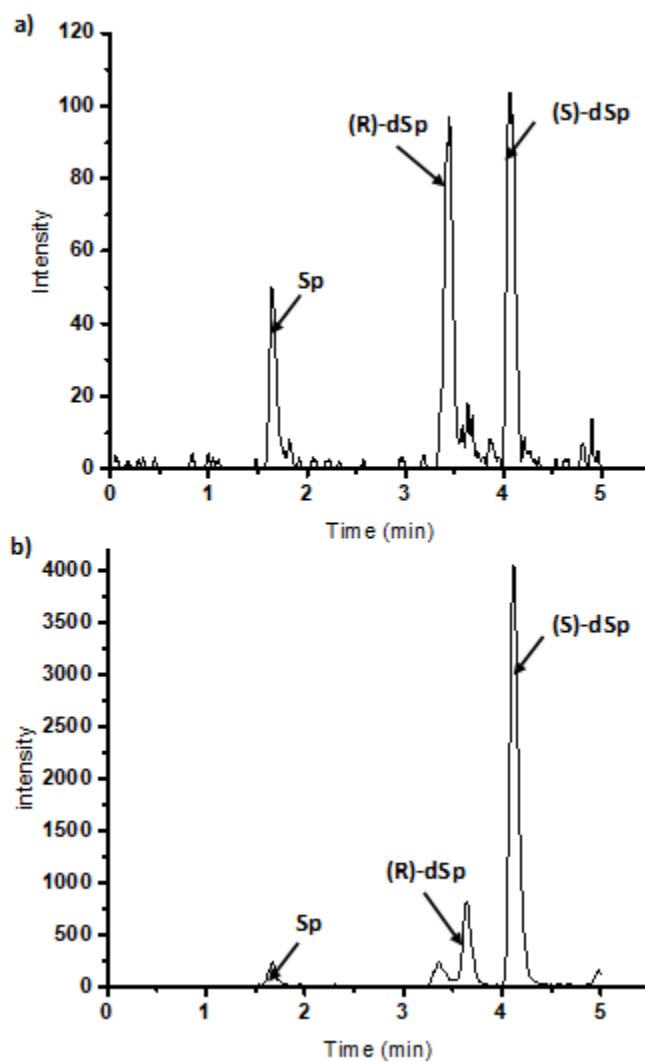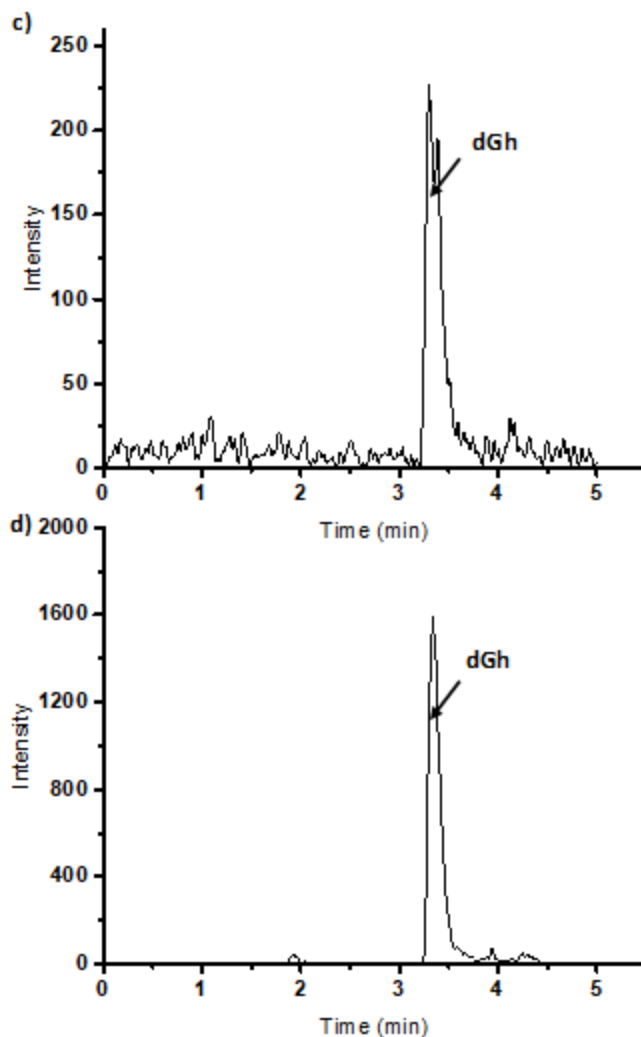
Figure 12. UPLC-MS/MS analysis of the anaerobic photolysis of precursor **5**. (a) Extracted-ion chromatogram (EIC) of Sp (calculated m/z = 184.0465, observed m/z = 184.0468) generated during the photolysis in the absence of 8-oxo-dG (0.2 mM). (b) EIC of Sp (calculated m/z = 184.0465, observed m/z = 184.0468) generated during the photolysis in the presence of 8-oxo-dG (0.2 mM). (c) EIC of dGh (calculated m/z = 274.1146, observed m/z = 274.1143) generated during the photolysis in the absence of 8-oxo-dG (0.2 mM). (d) EIC of dGh (calculated m/z = 274.1146, observed m/z = 274.1143) generated during the photolysis in the presence of 8-oxo-dG (0.2 mM).

When the photolyses were carried out in the presence of O_2, the rate of consumption of precursor was significantly decreased. This is consistent with the report that the triplet excited state of naphthalimide is efficiently quenched by O_2 to yield singlet O_2.[257] In the absence of thiol, the precursor was consumed in 4 h, and only about 10% of dG was

95

generated. We proposed that the low yield of dG was caused by the reaction between singlet oxygen, produced from excitation of the phthalimide, and dG.[258] This proposal was supported by the observation that the yield of dG was 37% based on conversion when **5** was photolyzed for 2 h. In the presence of thiol, the precursor was consumed within 1 h, and the yield of dG was essentially quantitative. Extended photolysis in the presence of O_2 led to the reduction of the yield of dG, possibly due to the singlet oxygen generated reacting with dG. These observations also suggested that BME may reduce photoexcited **5**, which led to faster consumption of the precursor (Scheme 45).

3.1.3.3 Synthesis of the precursors for the independent generation of nitrogen-centered neutral purine radicals

Encouraged by these results, we proposed that **183** and **184** (Scheme 48) may serve as more efficient precursors dA• and dG(N2-H)•,
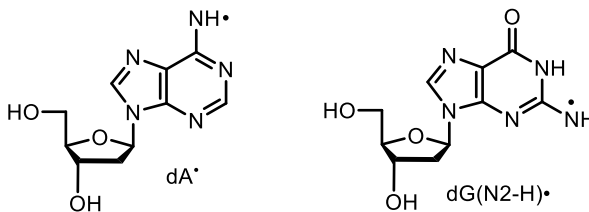
respectively. Precursor **183** was prepared by reacting 1,8-naphthalic anhydride with disilylated *N*6-amino-2'-deoxyadenosine (**185**) in THF at reflux, followed by desilylation (Scheme 48a). Similarly, precursor **184** was prepared by reacting 1,8-naphthalic anhydride with disilylated *N*2-amino-*O*6-*p*-nitrophenylethyl-2'-deoxyadenosine (**187**, Scheme 48b). The *p*-nitrophenylethyl protecting group was removed by treating with DBU, and subsequent desilylation afforded precursor **184**. The UV spectrum of **183** shows UV-absorption maximum at 261 nm ($\varepsilon = 2.04 \times 10^4$ $M^{-1}cm^{-1}$) which arises from the adenine, and a maximum at 346 nm ($\varepsilon = 1.72 \times 10^4$ $M^{-1}cm^{-1}$) which is attributed to the naphthalimide moiety. Similarly, **184** shows absorption maxima at 282 nm ($\varepsilon = 1.08 \times 10^4$ $M^{-1}cm^{-1}$) and

346 nm ($\varepsilon = 1.64 \times 10^4$ M^{-1}cm^{-1}). Unfortunately, anaerobic photolyses of **183** and **184** in the presence of hydrogen atom donor for 4 h did not lead to any consumption of the precursors or the generation of their corresponding 2'-deoxynucleosides.

Scheme 48. Synthesis of precursor **183** and **184**.
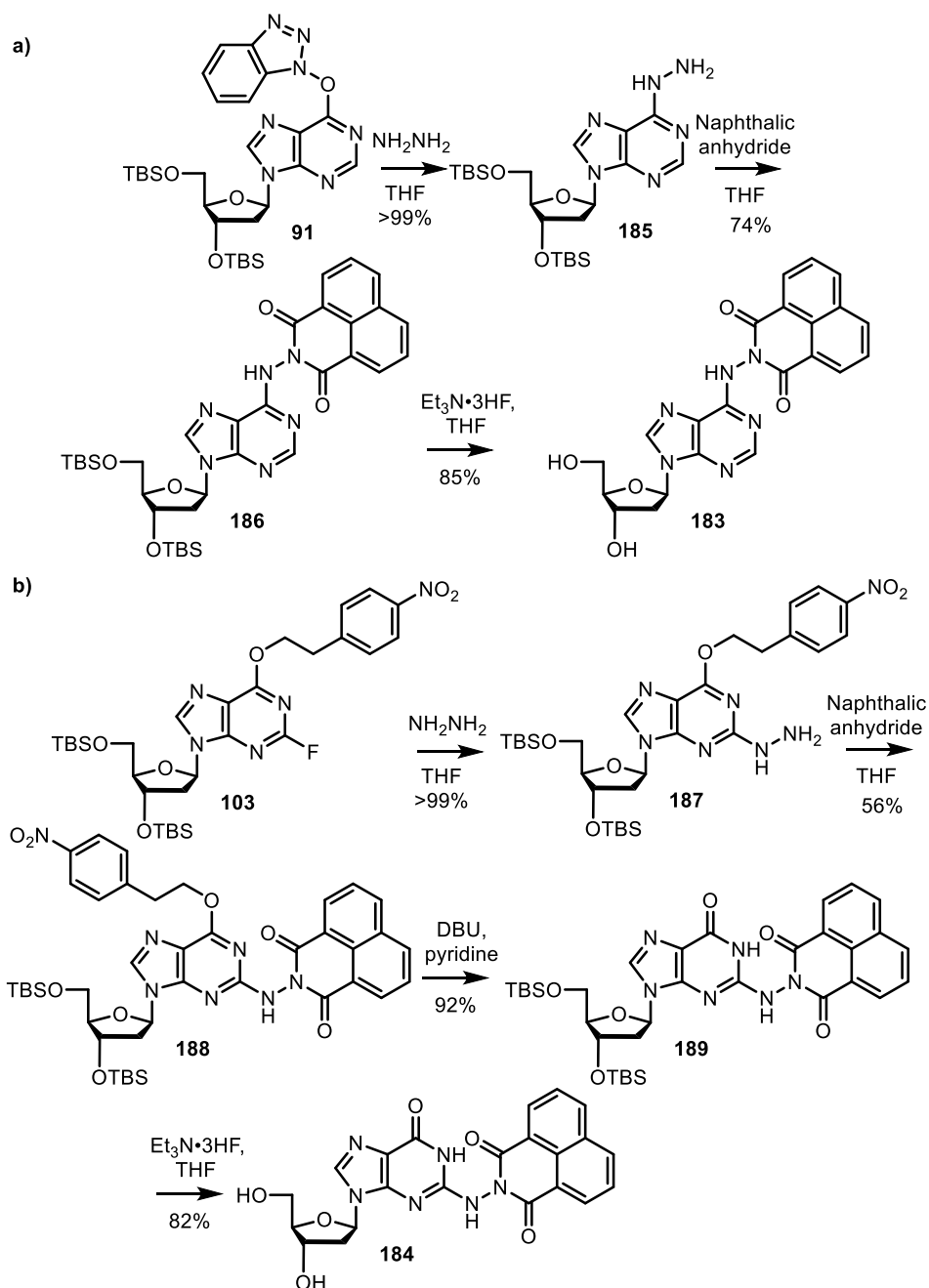
3.2 Reactivity of dA• in DNA

3.2.1 Synthesis of DNA containing precursors 3 and 6

Precursors **3** and **6** are compatible with solid phase oligonucleotide synthesis conditions. Phosphoramidites **191** and **193** were synthesized according to standard procedures and were incorporated in oligonucleotides (Scheme 49). Commercially available fast deprotecting phosphoramidites were used for the synthesis. Deprotection of oligonucleotides containing **6** was performed with concentrated NH_4OH at room temperature for 16 h.

Scheme 49. Synthesis of phosphoramidite **191** and **193**.
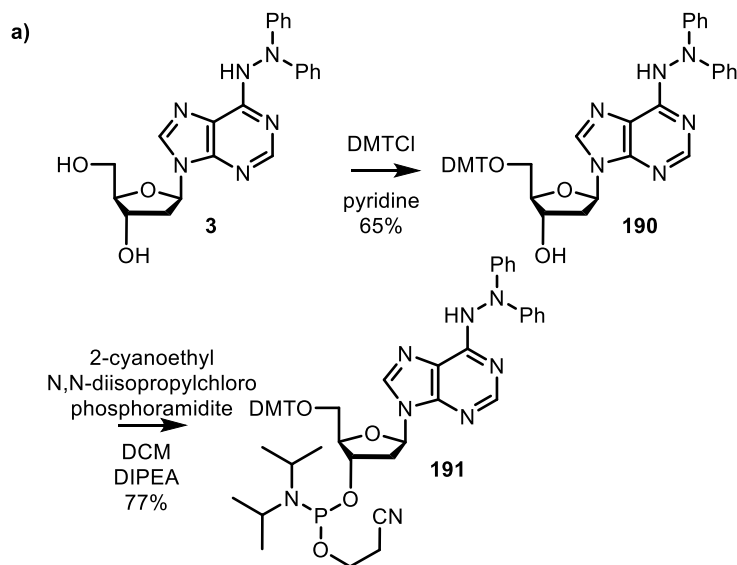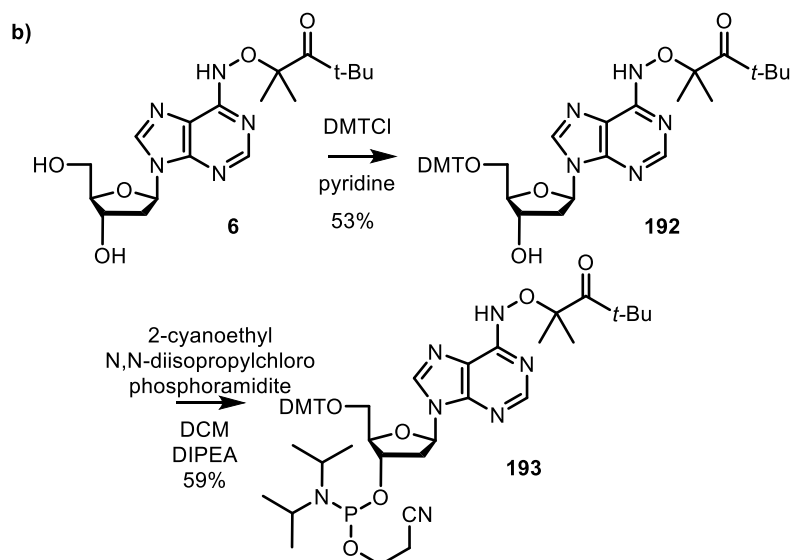
3.2.2 Effects of precursors on the Tm's of duplex DNA

The T_m of a dodecameric duplex containing **3** (**194a**, 29.2 °C) was decreased significantly compared to an otherwise identical one containing dA (**194b**, 49.6 °C) in place of **3**. Similarly, **6** decreases the T_m of the dodecameric duplex from 49.1 °C (**195b**) to 35.8 °C (**195a**). This will not detract from the utility of **3** and **6** as tools for producing dA• in DNA since the lifetime of the radical $(4.0 \pm 1.0$ ms)[259] is long compared to the timescale of conformational changes within the helix.[260]

5'-d(CAG GTX TAC CCG)   5'-d(CGG GTX TAC GTC)
3'-d(GTC CAT ATG GGC)   3'-d(GCC CAT ATG CAG)

194a X = 3; **194b** X = dA   **195a** X = 6; **195b** X = dA

3.2.3 Traceless tandem lesion formation initiated by dA•

3.2.3.1 dA• does not initiate hole migration in DNA

Based on pulse radiolysis experiments on single-stranded oligodeoxynucleotides, O'Neill and co-workers propose that dA• oxidizes dG via electron transfer.[94] This electron transfer is thermodynamically favorable given the redox potential of dA• (1.42 V versus

99

NHE in water at pH 7) and dG• (1.29 V versus NHE in water at pH 7). However, it is also proposed that the deprotonation of $dA^{\bullet+}$ ($pK_a \leq 1$) to dA• attenuates hole transfer.[20] Duplexes **196-200** were designed to probe for hole migration from dA• by incorporating a dGGG sequence proximal to the site of radical generation. Damage at the 5'- and central dG's within a dGGG triplet is characteristic of hole migration. Holes that migrate to dGGG triplets predominantly localize at the 5'- and middle-dG.[142] Approximately 10% of these holes react with water and O_2 to form DNA lesions.[13] These damages are detected by inducing cleavage with reagents known to react at various types of modified nucleotides, followed by denaturing PAGE analysis. Piperidine treatment with or without prior oxidation by Na_2IrCl_6 cleaves DNA at various sugar and nucleobase modifications at different rates.[261-262] To probe the formation of 8-oxo-dG, piperidine treatments are carried out in the presence of BME, which prevents cleavage at 8-oxo-dG by inhibiting further oxidation of 8-oxo-dG to more labile lesions, such as dSp and dGh.[261, 263] The base excision repair enzyme formamidopyrimidine glycosylase (Fpg) cleaves DNA at a variety of modified purines, abasic sites, and some pyrimidines.[264-266]

5'-d(GTC GCA ACG_9 $G_{10}G_{11}T_{12}$ **6**TA CAC GTC GCT G)
3'-d(CAG CGT TGC C C A   TAT GTG CAG CGA C)
196

5'-d(GTC GCA ACT $G_{10}G_{11}G_{12}$ **6**TA CAC GTC GCT G)
3'-d(CAG CGT TGA C C C   TAT GTG CAG CGA C)
197

5'-d(GTC GCA ACG GGT_{12} **6**T_{14}G GGC GTC GCT G)
3'-d(CAG CGT TGC CCA   TA C CCG CAG CGA C)
198

5'-d(GTC GCA CG_8G_9 $G_{10}T_{11}G_{12}$ **6**TA CAC GTC GCT G)
3'-d(CAG CGT TG C C C A   TAT GTG CAG CGA C)
199

5'-d(GTC GCA ACG CAT_{12} **6**$G_{14}G_{15}$ G_{16}AC GTC GCT G)
3'-d(CAG CGT TGC CCA   TC C   C TG CAG CGA C)
200

Applying these diagnostic reactions to photolyzed 5'-^{32}P-**196** (Figure 13a-b) and 5'-^{32}P-**197** (Figure 13c-d), the O_2-dependent formation of modified nucleotides was detected, and the yields in 5'-^{32}P-**196** was 10-fold greater than those in 5'-^{32}P-**197**. (If not mentioned otherwise, the strands containing the modified nucleotides in each duplex were radiolabeled.) For instance, Fpg yielded $28.2 \pm 0.5\%$ strand scission at G_{11} in photolyzed 5'-^{32}P-**196** and $2.9 \pm 0.3\%$ (G_{12}) in 5'-^{32}P-**197**. We initially considered the possibility that the triplet excited state of t-butyl ketone was quenched by DNA in a sequence-dependent manner, and the conversion of **6** in **197** is lower than that in **196**, which led to a lower yield of strand damage. However, UPLC analysis following nuclease digestion showed similar conversions of **6** (~80%, Appendix Figure 1, 2) upon photolysis (8 h) of **196** and **197**. This result suggests that the disparity in strand cleavages was not induced by the difference of conversion of precursor **6** in these two duplexes but is caused by sequence-dependent strand damage formation (see below).

101
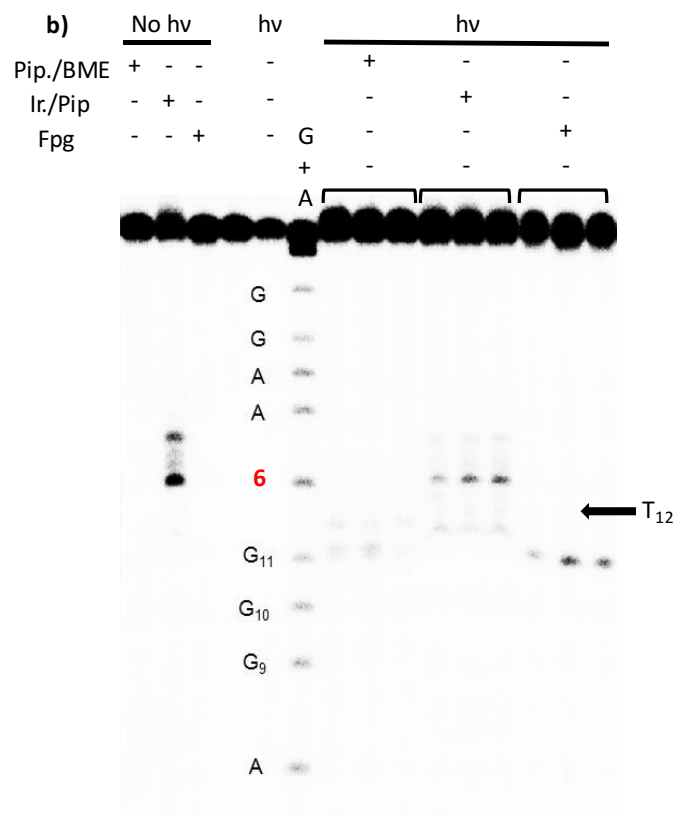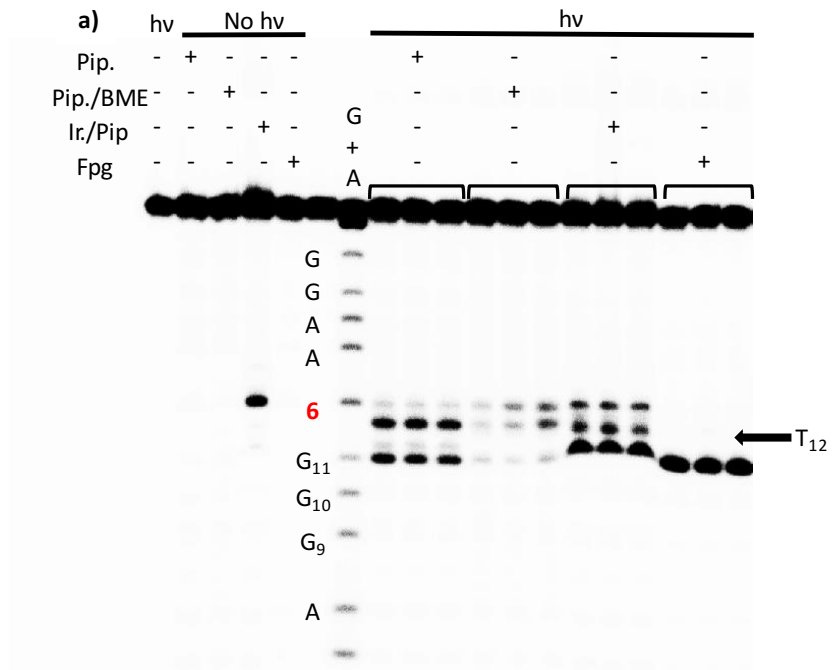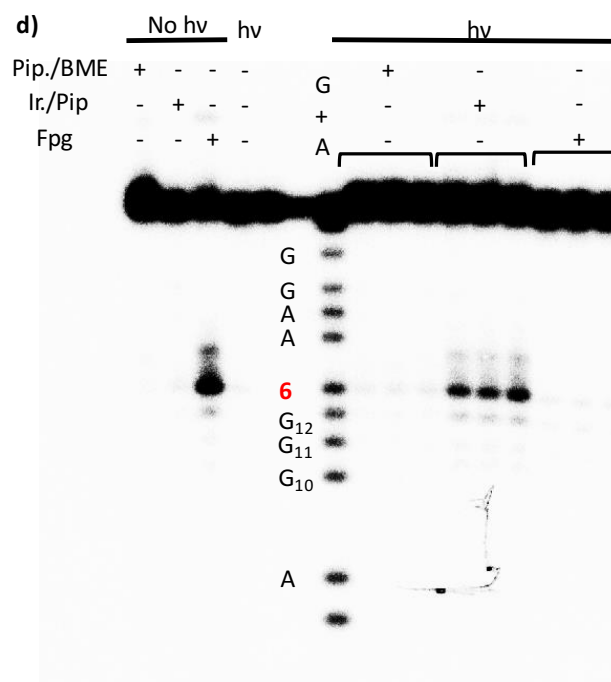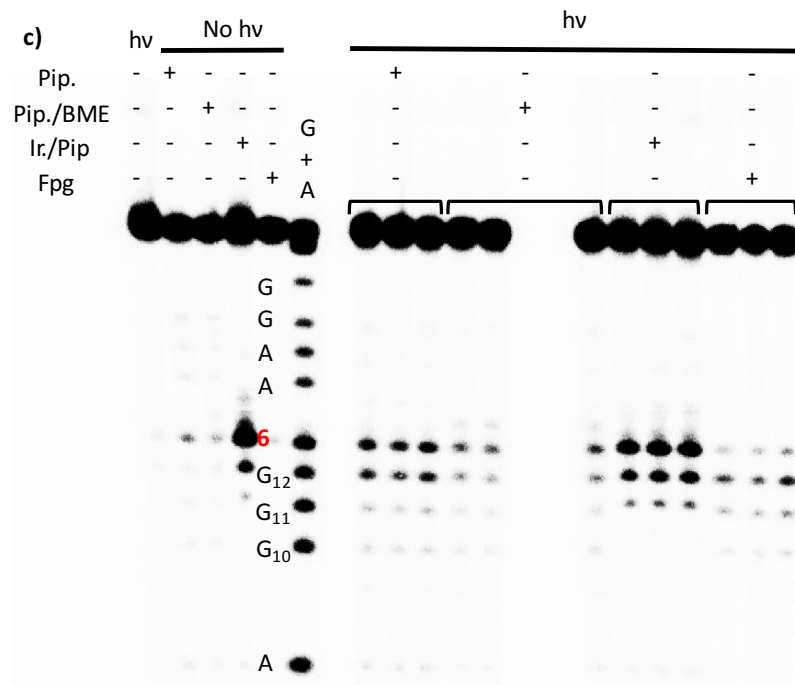
Figure 13. PAGE analysis of oxygen-dependent strand damage in 5'-(GT) sequences. Autoradiogram of (a) aerobic photolysis of 5'-^{32}P-**196**, (b) anaerobic photolysis of 5'-^{32}P-**196**, (c) aerobic photolysis of 5'-^{32}P-**197**, (d) anaerobic photolysis of 5'-^{32}P-**197** followed by chemical and enzymatic treatments.

Neither direct strand scission or damage at the 5'- or central dGs in the dG-triplet was observed in either sequence. These results suggested that hole migration did not occur in these two duplexes. In addition, hole migration was not observed in duplexes **198-200** (Appendix Figure 3-5). Oxidation in irradiated **196** and **197** at the 3'-terminal dG within the respective dGGG-triplets is mechanistically significant and eliminates hole injection from dA•, despite thermodynamically favorable dG oxidation by dA•.[4] In contrast to the proposal by O'Neill, our observations are consistent with computational studies demonstrating that dA• attenuates hole migration.[21, 267]

3.2.3.2   dA• Initiates tandem lesion formation when flanked by a 5'-d(GT) sequence

The major cleavage site at dG_{11} in 5'-[32]P-**196** was accompanied by smaller amounts of piperidine-induced cleavage at T_{12} ($8.2 \pm 0.2\%$). This result suggests that the initially formed purine radical may react with the 5'-adjacent pyrimidine, and ultimately give rise to a tandem lesion involving dG. If the observed damage is caused by two separate oxidative damage events, the observed strand cleavage should be independent of which terminus of an oligonucleotide is labeled with [32]P (Figure 14a).
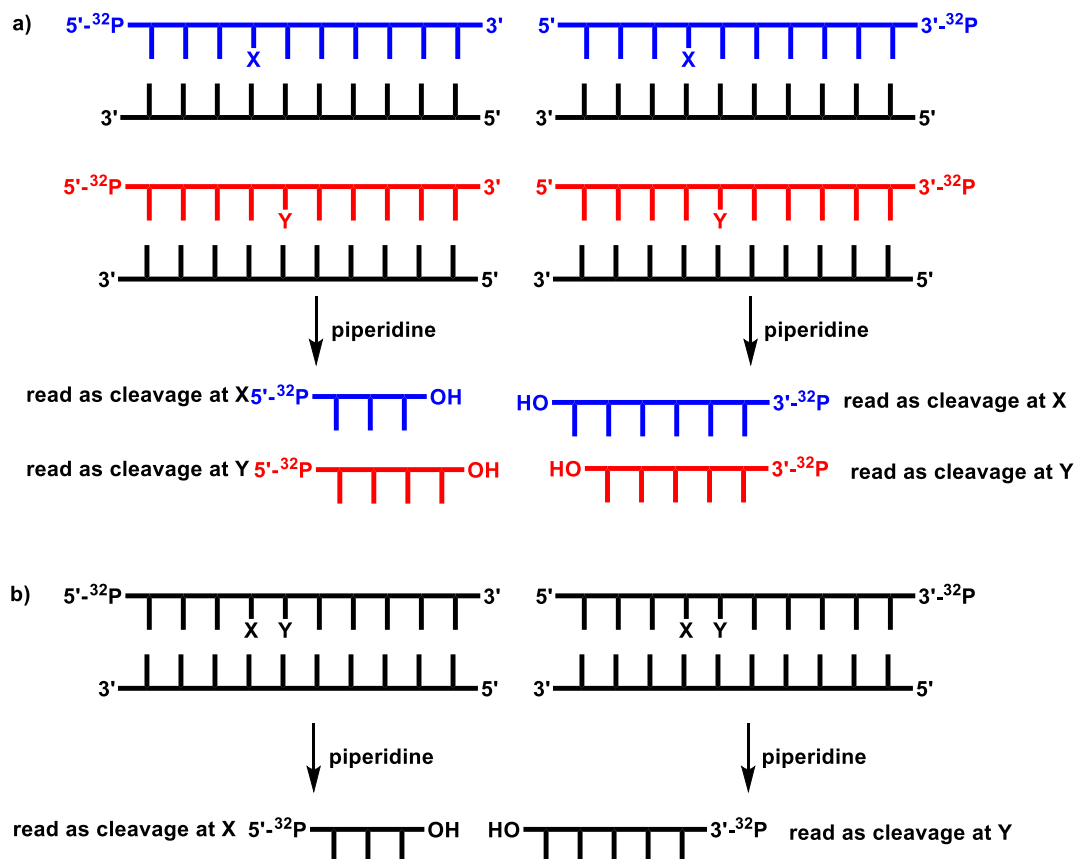
Figure 14. Schematic demonstration of detection of the tandem lesion by labeling the 5'-end or the 3'-end of DNA. (a) Expected cleavage patterns of piperidine (Pip.) treatment if the strand cleavages are caused by two separate damage events. (b) Expected cleavage patterns of tandem lesions induced by piperidine (Pip.) treatment X and Y are alkaline labile and are completely cleaved by piperidine treatment.

If 5'-dGT tandem lesions are formed, greater strand damage at the corresponding thymidine should be observed in 3'-^{32}P-labeled substrates compared to those labeled at their 5'-termini because damage at the 5'-adjacent dG prevents detecting damage at the pyrimidine in 5'-^{32}P substrates (Figure 14b). Indeed, piperidine treatment of photolyzed 5'-^{32}P-**196** yielded $11.9 \pm 0.2\%$ cleavage at dG_{11} and $8.2 \pm 0.2\%$ at T_{12} (Figure 13a, 16), but the preference is reversed in 3'-^{32}P-**196** (dG_{11}, $4.0 \pm 0.2\%$; T_{12}, $14.6 \pm 0.9\%$, Figure 15, 16). These results suggest that the observed strand damage is indeed part of a tandem lesion.
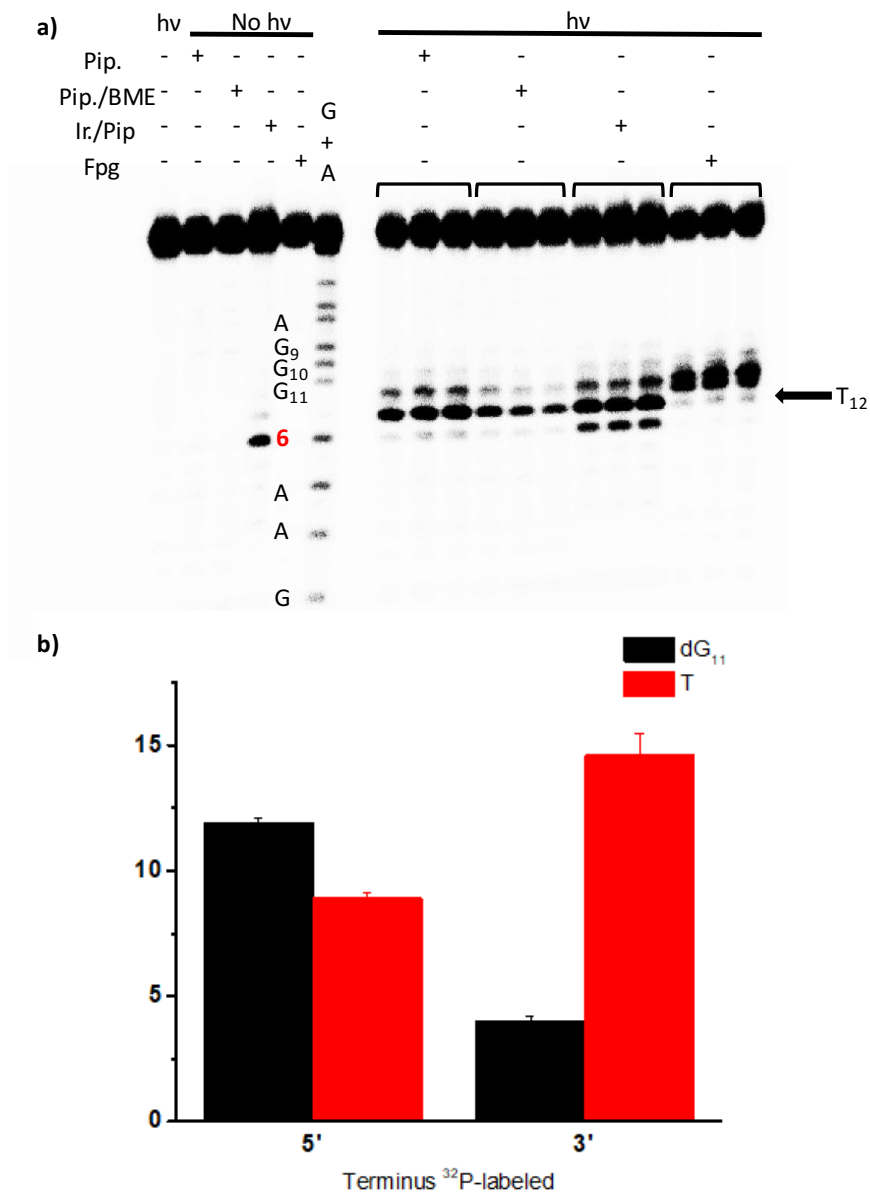
Figure 15. Identification of tandem lesion formation in photolyzed 3'-^{32}P-**196**. (a) Autoradiogram of aerobic photolysis of 3'-^{32}P-**196** followed by chemical and enzymatic treatments. (b) Piperidine-induced cleavage in photolyzed **196**. The values presented are the ave. ± std. dev. of 3 replicates.

The generality of this sequence requirement for tandem lesion formation was examined using several duplexes in which the local sequence was varied. Tandem lesions were observed in duplexes **201-203** (Figure 16, Appendix Figure 6-9). The yields of

tandem lesion formation in **196**, **201**, and **202**, which only differ by a single base at the position most remote from dA• in a 5-nucleotide span (5'-d($XGG_{11}T_{12}$**6**)) correlate with the ionization potential of 5'-d(XGG_{11}) sequences. A plot of the natural logarithm of the strand cleavage against the calculated ionization potentials of the trinucleotide sequence reveals a linear correlation (Figure 17a). Similarly, the amounts of oxidative damages on T_{12} can be plotted against the trinucleotide ionization potentials if we assume that all the damages on G_{11} are transferred via T_{12}, and the overall oxidative damage on T_{12} is the sum of strand cleavage at T_{12} and G_{11} detected by PAGE. The correlation between the ionization potential of flanking sequences and the amounts of oxidative damages on T_{12} is evident (Figure 17b). Overall, these data show that the extended π-system affects the redox properties of DNA.

5'-d(GTC GCA ACC$_9$ G$_{10}$G$_{11}$T$_{12}$ **6**TA CAC GTC GCT G)
3'-d(CAG CGT TGG C   C   A   TAT GTG CAG CGA C)
201

5'-d(GTC GCA ACA$_9$ G$_{10}$G$_{11}$T$_{12}$ **6**TA CAC GTC GCT G)
3'-d(CAG CGT TGT C   C   A   TAT GTG CAG CGA C)
202

5'-d(GTC GCA ACT T   G$_{11}$T$_{12}$ **6**TA CAC GTC GCT G)
3'-d(CAG CGT TGA A   C   A   TAT GTG CAG CGA C)
203
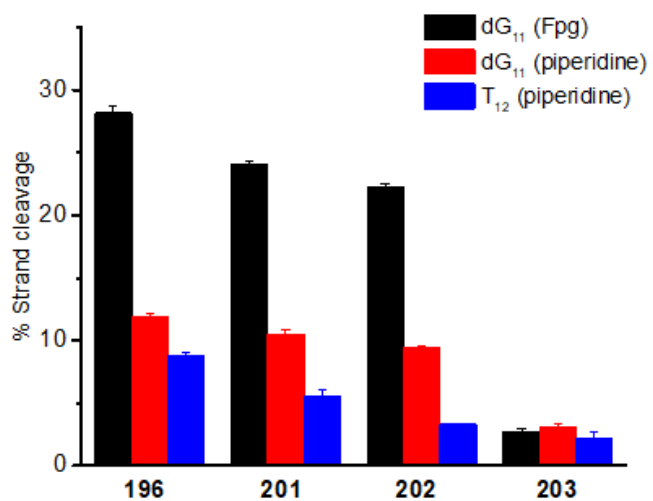
Figure 16. Strand scission at dG_{11} (Fpg) and T_{12} (piperidine) in duplexes 5'-^{32}P-**196**, **201**-**203.** The values presented are the ave. ± std. dev. of 3 replicates.
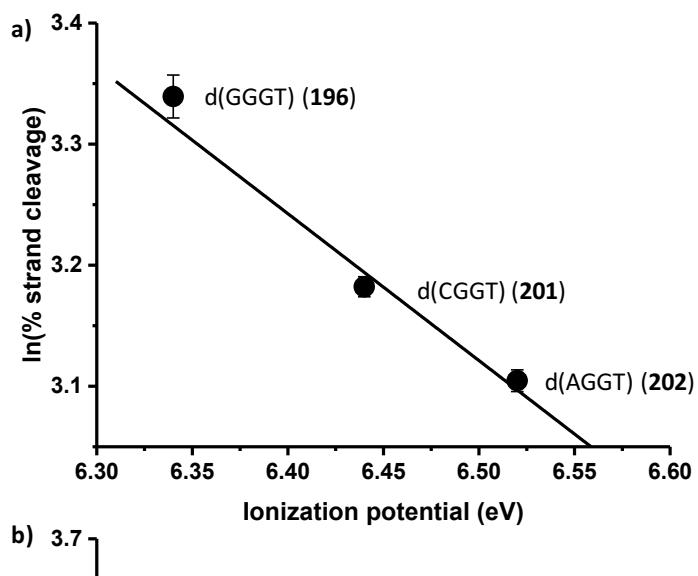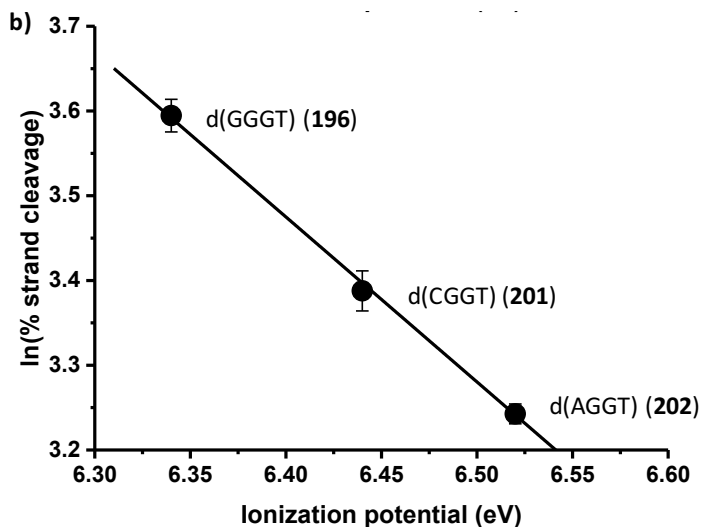
Figure 17. Dependence of strand damage from dA• as a function of the trinucleotide sequence ionization potential. (a) damage at dG_{11} (Fpg); (b) damage at T_{12}. The values presented are the ave. ± std. dev. of 3 replicates.

3.2.3.3   Characterization of the structure of the tandem lesion

3.2.3.3.1   Chemical and enzymatic assays

Insight into the identity of the damaged nucleotides was obtained by a variety of chemical and enzymatic assays. The modification at dG_{11} was labile to Fpg, and the presence of BME prevented piperidine induced cleavage (Figure 13a). These observations suggest that 8-oxo-dG is likely to be the major product at dG_{11} in **196**. The reaction of photolyzed 5'-[32]P-**195a** with aldehyde reactive probe (ARP) produced a product (8.1 ± 0.5 %) that migrated more slowly in a denaturing polyacrylamide gel (Figure 18a). Furthermore, $NaBH_4$ treatment of 5'-[32]P-**196** photolysate prior to piperidine cleavage eliminated strand scission at this position (Figure 18b, 0.4 ± 0.1 %). These observations are consistent with the formation of a piperidine labile carbonyl-containing compound at the thymidine bonded to the 5'-phosphate of dA•, and 5-fdU was a good candidate for this

product. The reduction of 5-fdU by NaBH$_4$ would lead to the formation of 5-hmdU, which is not labile to piperidine and is consistent with observation.[268-269]
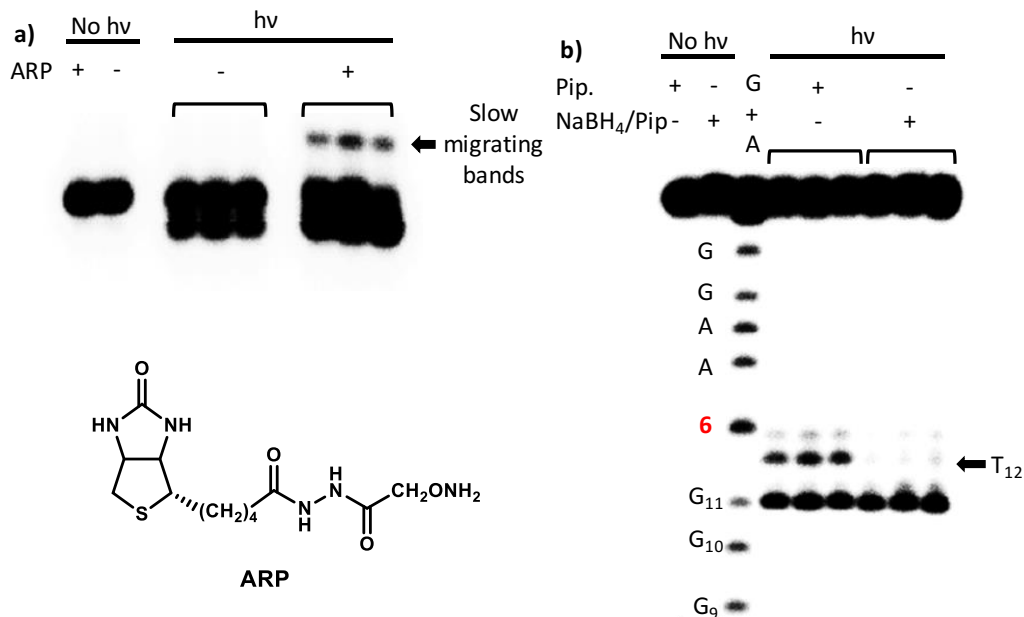
Figure 18. Chemical assays to determine DNA lesion(s) formed at T$_{12}$. (a) aerobic photolysis of 5'-^{32}P-**195a** followed by derivatization using ARP. (b) aerobic photolysis of 5'-^{32}P-**196** followed by piperidine treatment and NaBH$_4$/piperidine treatment.

3.2.3.3.2 Characterization of the structure of the tandem lesion by UPLC-MS/MS

More definitive identification of the tandem lesion was obtained by UPLC-MS/MS analysis of photolyzed **195a**. As discussed in Section 2.4, UPLC-MS/MS is a powerful method for

5'-d(CGG GT**6** TAC GTC)
3'-d(GCC CAT ATG CAG)
195a

identifying nucleic acid modifications.[270] It is most frequently used to identify isolated lesions following enzyme digestion of the DNA.[271] However, DNA lesion location is lost upon enzyme digestion. Tandem lesions have been identified in this manner as well by taking advantage of their resistance to the enzyme digestion conditions and/or covalent bonding between nucleotides.[149, 151-152, 156] Analysis of intact oligonucleotides using

collision-induced dissociation (CID) is a powerful yet underutilized method for DNA lesion detection.[272-274] The commonly used HOAc-TEA (TEAA) ion-pairing system provides excellent separation of oligonucleotides.[275] However, it is not compatible with LC-MS/MS due to the high boiling point of acetic acid, which leads to ion suppression. We took advantage of the HFIP-TEA ion-pairing system.[275] The low boiling point and relatively weak acidity of HFIP provides for rapid evaporation during ionization and improves the signal strength in the mass spectrometer. In addition, utilization of collision-induced dissociation (CID) provides oligonucleotide sequence information. DNA molecules mainly fragment to w-series ions and [a - B]-series ions during CID (Scheme 50).[274] [a - B]-Series ions start from $[a_2 - B_2]$, because $[a_1 - B_1]$ fragment is essentially furfuryl alcohol, which does not contain any DNA sequence information.

Scheme 50. CID induced fragmentation of DNA generating w-series ions and [a - B]-series ions.
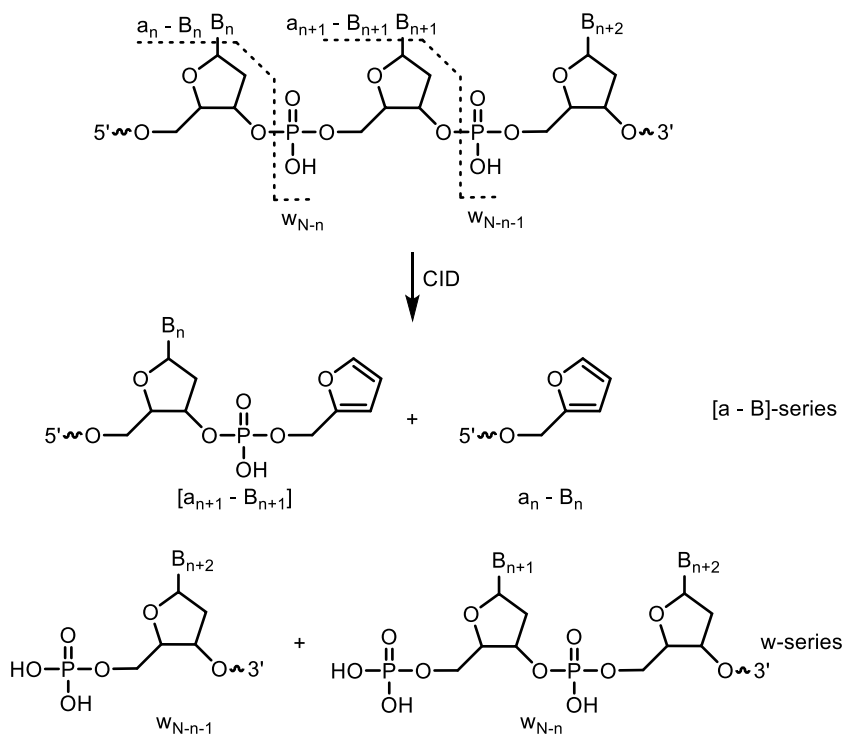
5'-d(CGG GT**6** TAC GTC)
3'-d(GCC CAT ATG CAG)
195a

5'-d(CGG GTA TAC GTC)
204

5'-d(CGG XYA TAC GTC)
205
(X = 8-oxo-dG; Y = 5-fdU)

5'-d(CGG XYA TAC GTC)
206
(X = 8-oxo-dG; Y = 5-hmdU)

8-oxo-dG

5-fdU

5-hmdU

207
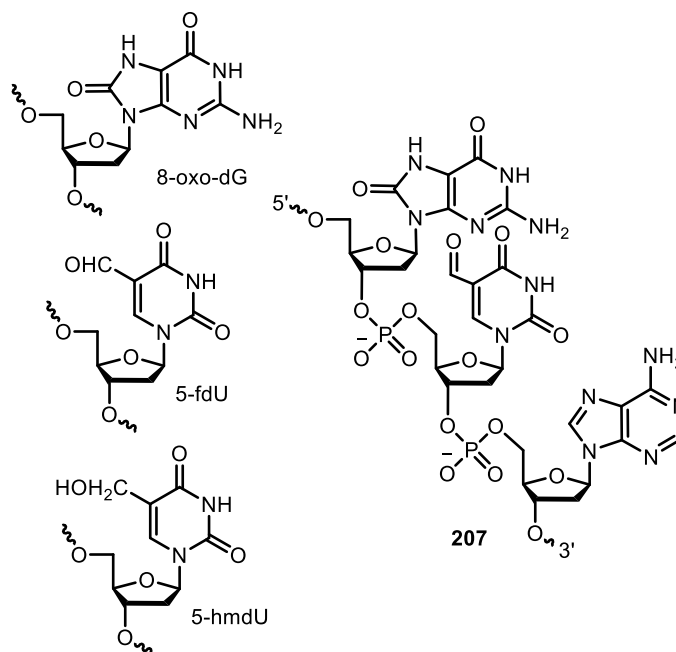
The crude photolysate of **195a** was analyzed by UPLC-MS/MS, and the major product observed was that resulting from the reduction of dA• (**204**). This is consistent with the denaturing PAGE analysis of photolyzed **196**, in which a low yield of strand cleavage was observed where **6** resided. Moreover, we observed a product with m/z =3688.8921 (Figure 19) that is consistent with the expected mass for the tandem lesion containing 5'-d[(8-oxo-dG)-(5-fdU)] and dA at the position where dA• (**207**) is generated (**205**, calculated m/z = 3688.6137).

112
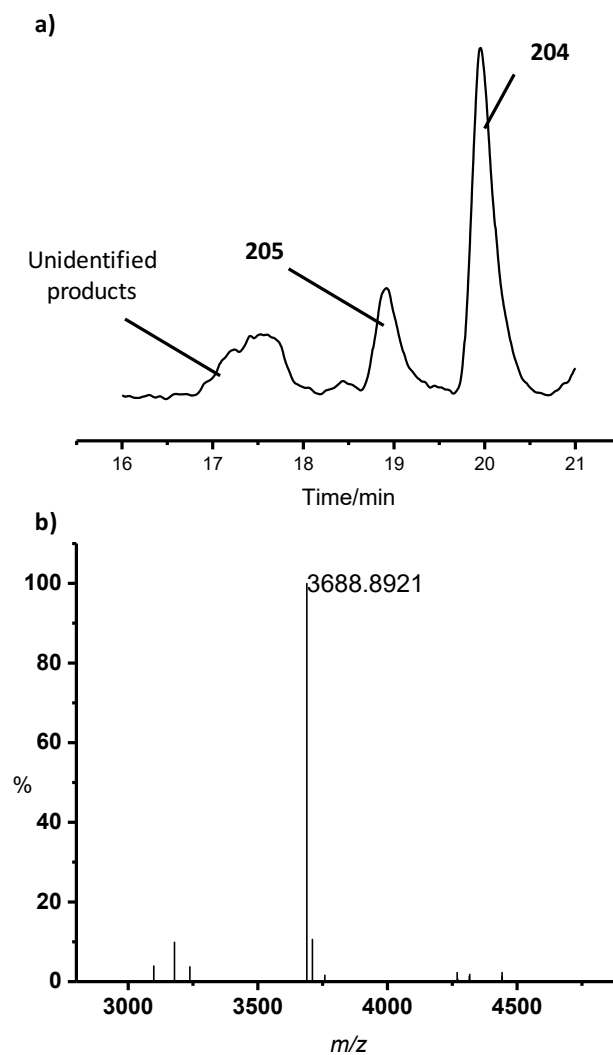
Figure 19. UPLC-MS/MS analysis of the photolysis of **195a**. (a) Total ion chromatogram (TIC) of the photolysate of **195a**. (b) Deconvoluted mass spectrum of **205**.

Furthermore, the treatment of the photolysate with NaBH$_4$ yielded a new product (**206**) that was two mass units higher than **205** (Figure 20, m/z = 3690.9253). This is consistent with the denaturing PAGE analysis (Figure 18b) and further supports the presence of 5-fdU, which is reduced to 5-hmdU by NaBH$_4$. We also tried to derivatize 5-fdU using Girard reagent T,[276] but the attempts were unsuccessful.
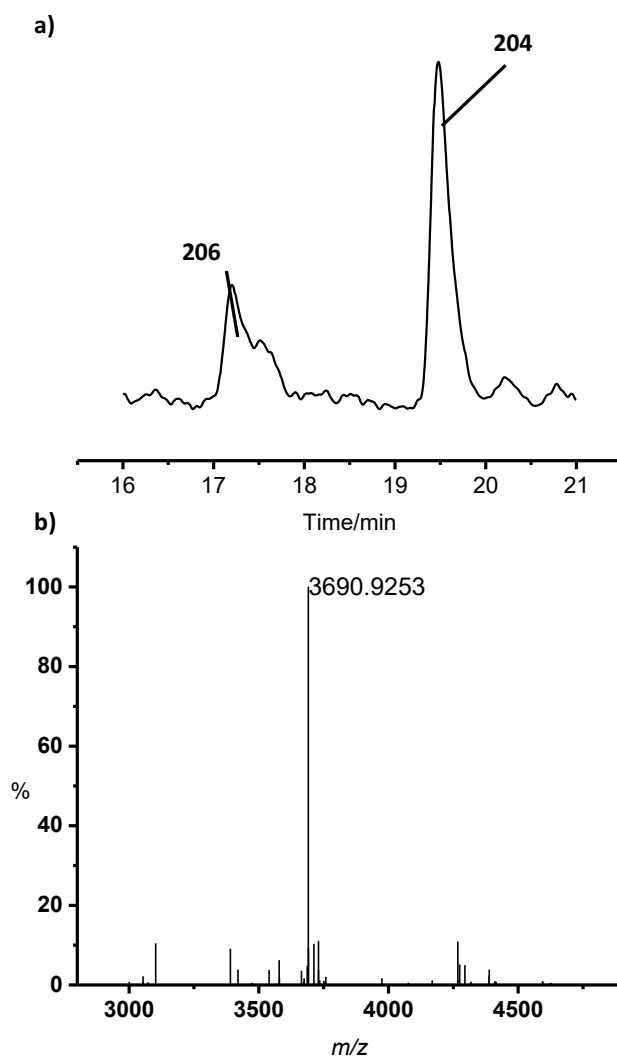
Figure 20. UPLC-MS/MS analysis of the photolysate of **195a** treated with NaBH$_4$. (a) Total ion chromatogram (TIC) of the photolysate. (b) Deconvoluted mass spectrum of **206**.

Finally, the collision-induced dissociation (CID) spectrum of the ion corresponding to $z = 3$ of **205** (Figure 21, Appendix Figure 16) was obtained. The fragment containing 8-oxo-dG ($[a_5 - B_5]^-$) and the intact tandem lesion ($[a_6 - B_6]^-$) was observed. Although the w-series ions containing individual modified DNA lesions were not observed, we detected the fragment containing the entire tandem lesion (w_9^{2-}). The fragmentation is consistent with the proposed structure of the tandem lesion **206** (Table 10).

114
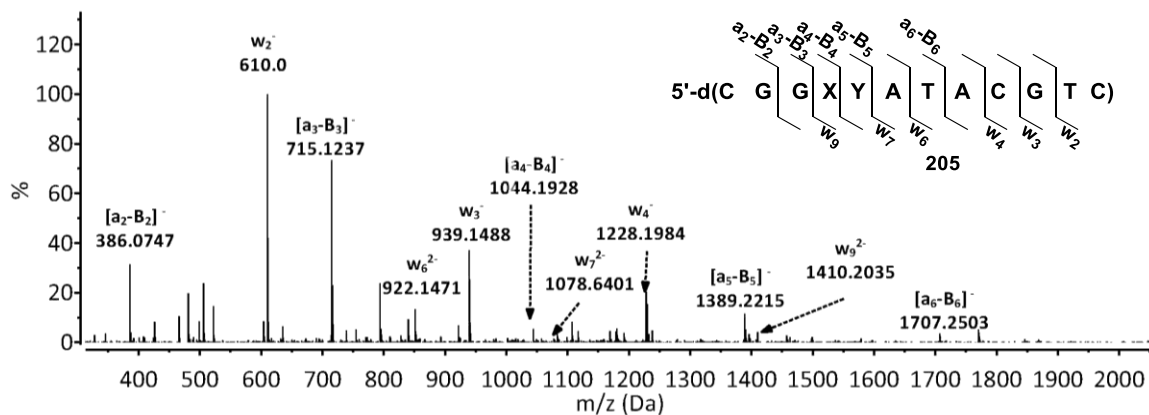
Figure 21. CID mass spectrum of the ion (m/z = 1229.2, z = 3) of oligonucleotide containing tandem lesion **207** (**205**). X = 8-oxo-dG, Y = 5-fdU

Table 10. Observed fragments of 205 from CID and their theoretical *m/z*.

Ion fragments	Theoretical *m/z*	Observed *m/z*	ΔPPM
$a_2\text{-}B_2^-$	386.0761	386.0747	-3.63
w_2^-	610.0972	610.0908	-10.49
$a_3\text{-}B_3^-$	715.1297	715.1237	-8.39
w_3^-	939.1508	939.1488	-2.12
w_4^-	1228.1983	1228.1984	0.08
$a_4\text{-}B_4^-$	1044.1833	1044.1928	9.10
$a_5\text{-}B_5^-$	1389.2322	1389.2215	-7.70
$a_6\text{-}B_6^-$	1707.2576	1707.2503	-4.28
w_6^{2-}	922.1514	922.1471	-4.66
w_7^{2-}	1078.6441	1078.6401	-3.71
w_9^{2-}	1410.2218	1410.2035	-12.98

3.2.3.4 Mechanism of tandem lesion formation

3.2.3.4.1 Hydrogen atom abstraction initiates tandem lesion formation

The strand damage in 5'-[32]P-**197** was inefficient despite the presence of a local

dGGG sequence that has a relatively favorable oxidation potential.[65] Furthermore, the fact

that tandem lesion (**207**) contains 5-fdU suggests that the intervening thymidine was essential for propagating the oxidative damage to the 5'-dG.

5'-d(GTC GCA ACG₉ G₁₀G₁₁X₁₂ **6**TA CAC GTC GCT G)
3'-d(CAG CGT TGC C C A   TAT GTG CAG CGA C)
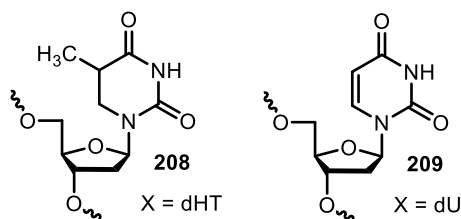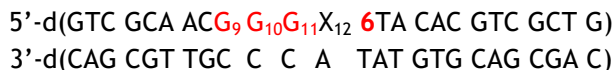
The requirement of the intervening thymidine and the formation of 5-fdU suggested that dA• abstracts the hydrogen atom from the C5-methyl group of the 5'-adjacent thymidine (Scheme 51), and the resulting 5-(2'-deoxyuridinyl)methyl radical (T•) ultimately transfers damage to the 5'-adjacent dG. Based upon the approximate BDEs of the N6-H bond (~97 kcal/mol) in dA and the allylic C5-H bond (BDE ≤ 90 kcal/mol) of thymidine, this process should be exothermic.[238-239] This possibility was explored by examining strand damage in duplexes in which the 5'-adjacent thymidine in **196** was substituted either by 5,6-dihydrothymidine (dHT, **208**) or 2'-deoxyuridine (dU, **209**). The alkyl C-H bond strength of the C5-methyl group in dHT is higher than the that of the allylic C-H bond in dT, and hydrogen atom abstraction from its methyl group by dA• should be less favorable. Since dHT is cleaved by piperidine or Fpg (Appendix Figure 10), photolysates of 5'-^{32}P-**208** and 5'-^{32}P-**196** were treated with hOGG1, followed by NaOH to assay for damage at dG₁₁ (Figure 22a). Strand scission at dG₁₁ was significantly reduced from 26.1 ± 0.2 % in **196** to 2.0 ± 0.6 % in the duplex containing dHT (**208**). The low level of strand damage that is still detected at dG₁₁ in 5'-^{32}P-**208** could be attributed to hydrogen

Scheme 51. dA• abstracts the hydrogen atom from C5-methyl group generating T•.
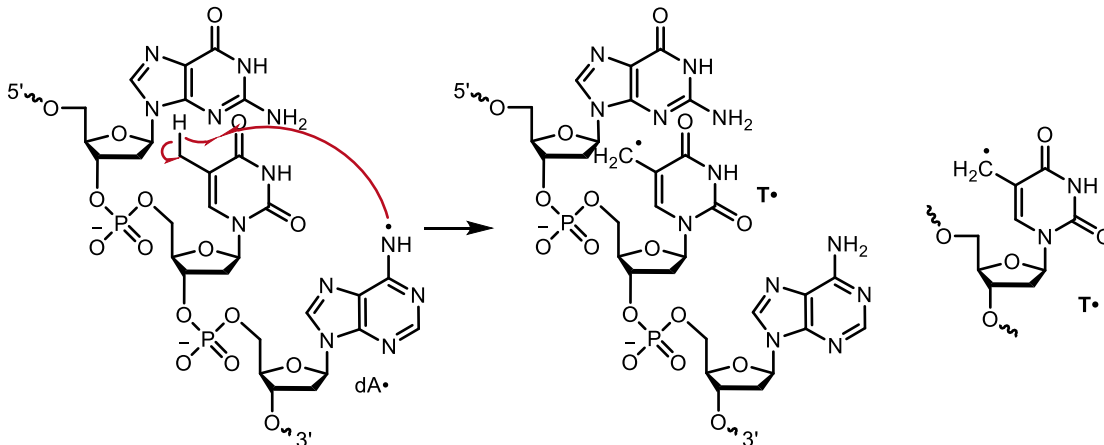
atom abstraction by dA• from the C5-methyl group in dHT, but this is uncertain. Replacement of the 5'-adjacent thymidine by dU (**209**) has an even more definitive effect on tandem lesion formation. Strand damage at dG_{11} in 5'-^{32}P-**209** photolysates is completely eliminated (Figure 22b). Overall, these observations are consistent with the major pathway for tandem lesion formation from dA• involving initial C5-methyl hydrogen atom abstraction from the 5'-adjacent thymidine (Scheme 51). Additionally, the hydrogen atom abstraction also agrees with the observation that dA• is repaired in **207**.
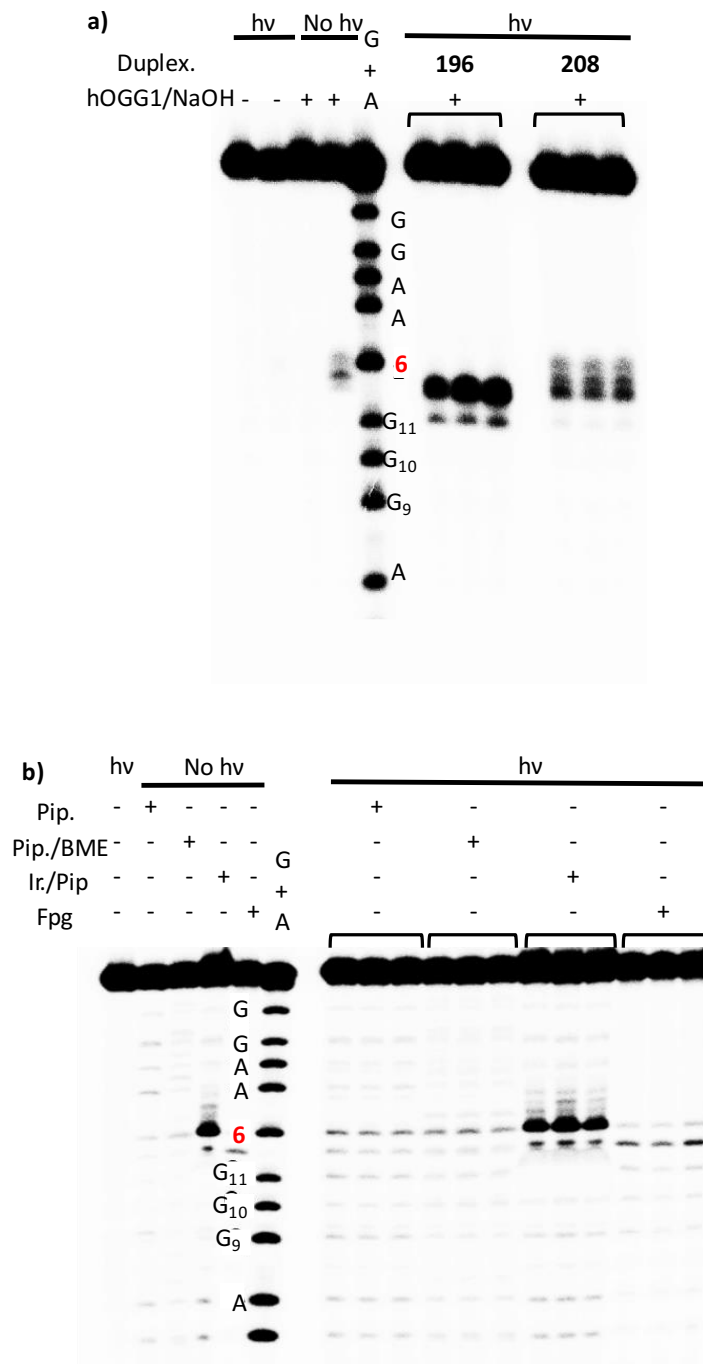
Figure 22. Effect of 5'-allylic C-H bond on tandem lesion formation. Autoradiogram of aerobic photolysis of (a) 5'-^{32}P-**208** (b) 5'-^{32}P-**209** followed by chemical and enzymatic treatments.

The proposed hydrogen atom abstraction also explains the observation that inverting the sequence from 5'-d(GGG$_{11}$T$_{12}$**6**) (**196**) to 5'-d(**6**T$_{14}$G$_{15}$GG) (**198**) results in no

alkali-labile strand damage at T_{14} or dG_{15} upon photolysis of **198**, and only a small amount of piperidine cleavage is observed at T_{12} (1.7 ± 0.1 %). Since the spin density of dA• is mostly localized at N6,[277] the conformational restrictions imposed by the right-handed helix were expected to have a significant effect on tandem lesion formation from dA•. Close inspection of a molecular model revealed that the methyl group of the 5'-adjacent thymidine is approximately 2 Å closer than the corresponding hydrogen in the 3'-adjacent thymidine to the radical at N6 of dA• (Figure 23). Hence, hydrogen atom abstraction from the methyl group of thymidine explains the directional preference for tandem lesion formation.
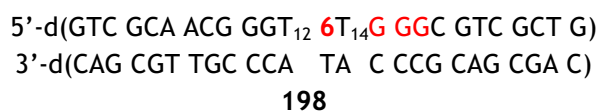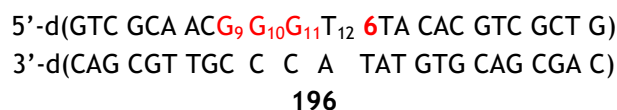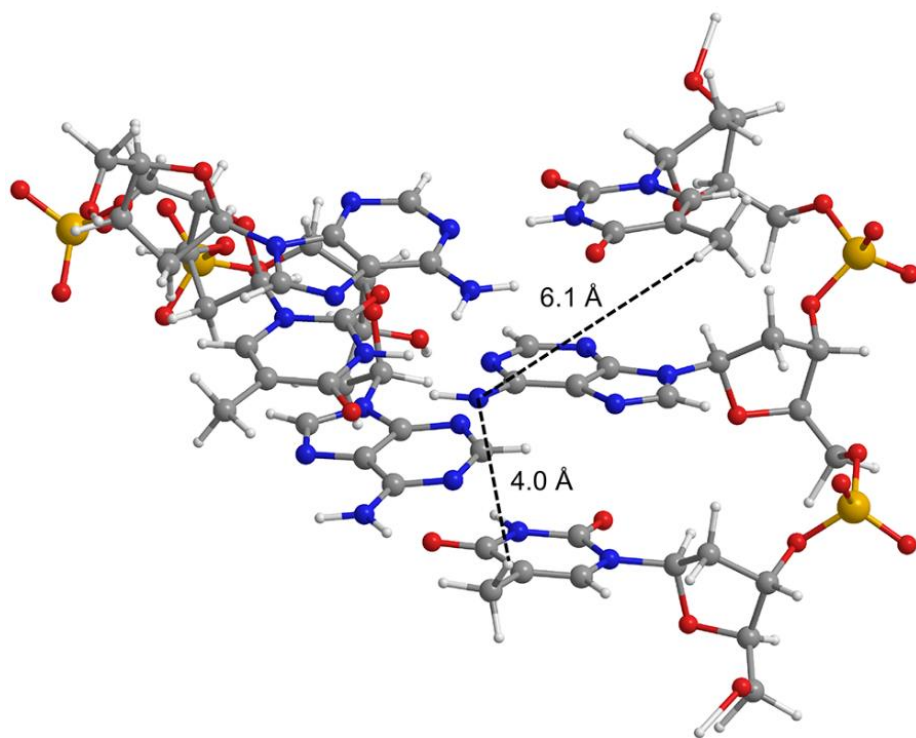
5'-d(GTC GCA ACG_9 $G_{10}G_{11}$$T_{12}$ **6**TA CAC GTC GCT G)
3'-d(CAG CGT TGC C   C   A   TAT GTG CAG CGA C)
196

5'-d(GTC GCA ACG GGT_{12} **6**T_{14}G GGC GTC GCT G)
3'-d(CAG CGT TGC CCA   TA C CCG CAG CGA C)
198

Figure 23. Molecular modeling demonstrating hydrogen atom abstraction by dA• in the trinucleotide sequence 5'-T-dA•-T/3'-dA-T-dA.

3.2.3.4.2 Thymidine peroxyl radical oxidizes 5'-dG

Formation of 5-fdU and the O_2 dependence of tandem lesion formation suggest that the corresponding peroxyl radical of T• (Tp•) is likely formed by oxygen trapping the carbon-centered radical following the generation of T• by hydrogen atom abstraction (Scheme 52). The viability for T• to induce tandem lesion formation was investigated by independently generating T• from **210** (Scheme 53) within DNA (**211,212**).[278-280] These duplexes were designed to replicate the environment in which T• was produced from dA•.

Scheme 52. Oxygen traps T• forming Tp•.

5'-d(GTC GCA ACG$_9$ G$_{10}$G$_{11}$(**210**) ATA CAC GTC GCT G)
3'-d(CAG CGT TGC C   C   A   TAT GTG CAG CGA C)
                              211

5'-d(GTC GCA ACT T G$_{11}$(**210**) ATA CAC GTC GCT G)
3'-d(CAG CGT TGA A   C   A   TAT GTG CAG CGA C)
                              212

Figure 24. T• induced tandem lesion formation in 5'-d(GT) sequences. Autoradiogram of aerobic photolysis of (a) 5'-^{32}P-**211** (b) 5'-^{32}P-**212** followed by enzymatic and chemical treatment.

Scheme 53. Generation of T• and carbocation from **210**.

Indeed, alkali-labile lesions were generated at dG$_{11}$ in photolyzed 5'-^{32}P-**211** and 5'-^{32}P-**212** under aerobic conditions but not under anaerobic conditions (Figure 24, Appendix Figure 11). Yields of alkali-labile lesion products were lower than when dA• was generated from **6** (Figure 24, cleavage at G$_{11}$ = 6.7 ± 0.7 % in **211** and 1.3 ± 0.2 % in **212**). This observation, along with the generation of interstrand cross-links, is consistent with the generation of carbocation from **210** in addition to T• (Scheme 53).[280] The alkali-

labile cleavage yield in the substrate containing the 5'-dGGG sequence (**211**) was considerably higher than that in **212**. This is consistent with the above experiments (Figure 17) in which the oxidation potential of polynucleotide sequences on the 5'-side of dT affected the yield of the tandem lesion. In addition, the lability towards Fpg and the reduction in alkali-induced cleavage at dG_{11} in **211** by piperidine/BME treatment were consistent with the formation of 8-oxo-dG, as was observed when tandem lesion formation was initiated by dA•. Finally, the elimination of alkali-labile lesions at T_{12} following $NaBH_4$ treatment is consistent with 5-fdU formation at this position (Figure 24a). Overall, independent generation of T• at T_{12} (**211**) within the otherwise identical sequence in which dA• is produced (**196**), supports the proposal that T• generated by hydrogen atom abstraction is trapped by oxygen, and that the peroxyl radical (Tp•) oxidizes the 5'-adjacent dG resulting in a tandem lesion (**207**) consisting of 5'-[(8-oxo-dG)-(5-fdU)].

Although peroxyl radicals have been suggested to oxidize dG via an outer sphere process (Scheme 54),[281] studies on related nucleobase peroxyl radicals indicate that addition to the purine ring is more likely.[282] Outer sphere and inner sphere mechanisms are distinguishable by product analysis. The former involves the formation of dG•+ that gives rise to hole migration.[16, 18, 283] The absence of strand damage at dG_9 and dG_{10} in **196** argues against the outer sphere process.[142] Furthermore, the transformation of G•+ into 8-oxo-dG requires incorporation of oxygen from H_2O. However, ^{18}O-incorporation was not detected by LC-MS/MS following photolysis of **195a** in $H_2^{18}O$ (Figure 25), which also agrees with the inner sphere mechanism (Scheme 55).

Scheme 54. Oxidation of dG by Tp• via an outer sphere mechanism.

5'-d(CGG XYA TAC GTC)
205
(X = 8-oxo-dG; Y = 5-fdU)

Figure 25. Mass spectrum of **205** (z = 3) generated by photolysis of **195a** in (a) H_2O, (b) $H_2^{18}O$.

Inspection of molecular models suggested that Tp• was well positioned to add to C8 of the 5'-adjacent dG (Figure 26). The second one-electron oxidation of dG can be achieved by the addition of O_2, followed by superoxide elimination (Scheme 55).[9, 284] We propose that 1,2-hydride migration in **214** generates carbocation **215**, followed by deprotonation from **215** to produce the tandem lesion (**207**).

Scheme 55. Oxidation of dG by Tp• via an inner sphere mechanism.

Figure 26. Molecular modeling demonstrating the addition of peroxyl radical to 5'-dG in the dinucleotide sequence 5'-dG-Tp• /3'-dC-dA.

The rate constant describing Tp• reaction with dG_{11} was determined by measuring the effect of BME on the yield of alkali-labile lesions at the dG_{11} in photolyzed 5'-^{32}P-**196** (Figure 27, Appendix Figure 12, 13). Assuming that the maximum rate constant for trapping T• by BME is 1×10^7 $M^{-1}s^{-1}$, even the highest concentration of BME (0.5 mM) employed should not compete with O_2 (0.2 mM), which reacts with alkyl radicals at $\sim 2 \times 10^9$ $M^{-1}s^{-1}$, for the alkyl radical.[285] In addition, BME reacts inefficiently with dA•.[42] Hence, we are confident that the reduction in cleavage at dG_{11} as a function of BME concentration is a reflection of the competition between the reaction of Tp• with the purine (Scheme 56, $k_{Add.}$) and the thiol (Scheme 56, $k_{Red.}$).

Scheme 56. Competition between the reaction of Tp• with the purine ($k_{Add.}$) and BME ($k_{Red.}$).

The amount of Tp• reduction product was calculated to be the difference in alkali-induced cleavage at dG_{11} in the absence of BME and the presence of a given thiol concentration. The slope of the line (4.8×10^3 M^{-1}, Figure 27) is the ratio of rate constants (k_{Red} / k_{Add}, eqn. 7), and if we assume that $k_{Red} = 2 \times 10^2$ M^{-1}s^{-1}, then $k_{Add} = 4.2 \times 10^{-2}$ s^{-1}.[286] The estimated rate constant for addition of Tp• to the 5'-adjacent dG_{11} is slightly slower than that estimated for other nucleobase peroxyl radicals using competitive kinetics.[282]

$$\frac{[216]}{[207]} = \frac{k_{Red.}}{k_{Add.}}[BME] \qquad\qquad \text{eqn. 7}$$
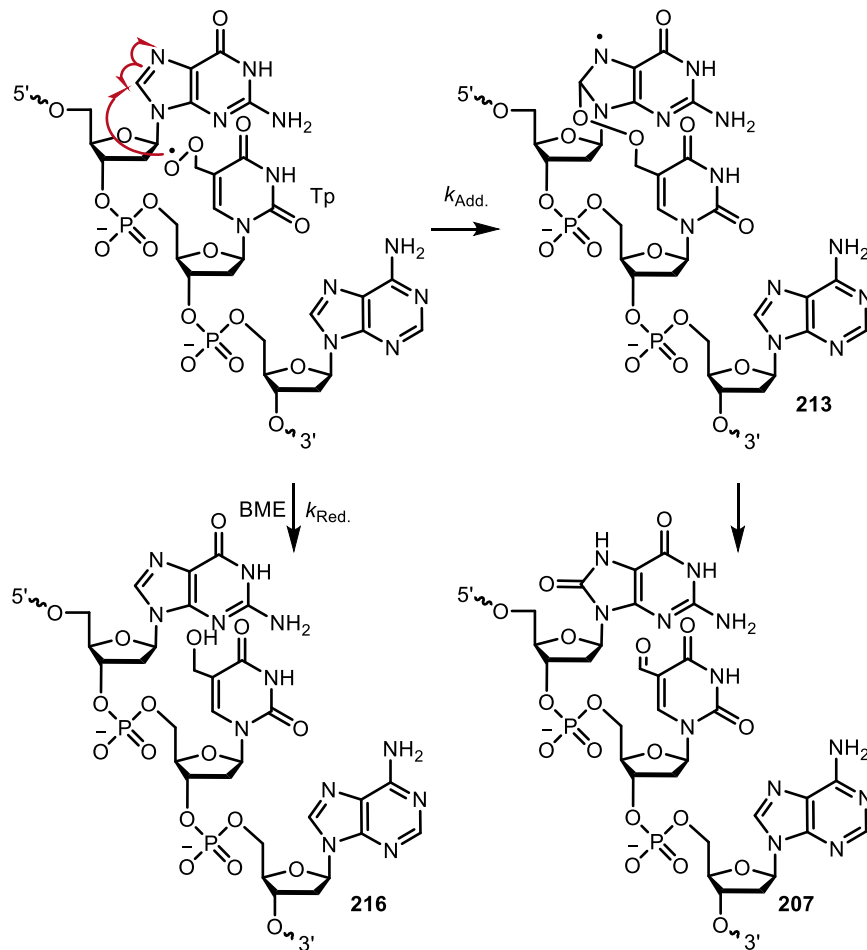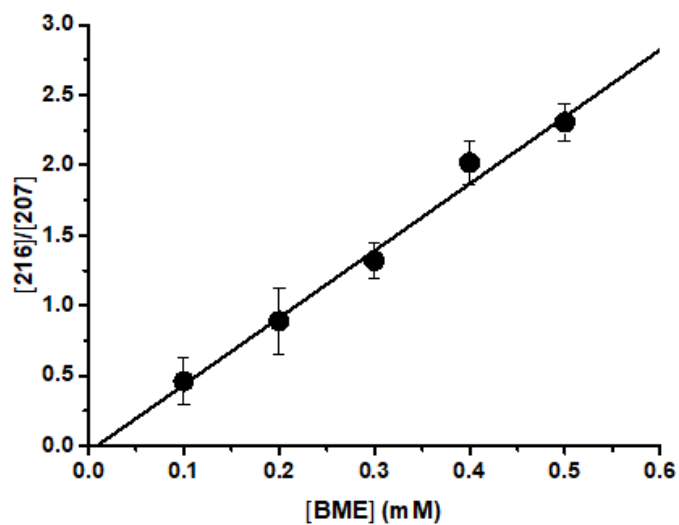
Figure 27. Thiol effect on tandem lesion (**207**) formation in photolyzed 5'-[32]P-**196**. The plot of [**216**] versus tandem lesion formation ([**207**]) as a function of [BME].

The trapping of Tp• by BME is further corroborated by UPLC-MS/MS (Figure 28). When **195a** is photolyzed in the presence of 1 mM BME, the tandem lesion is replaced by a product with $m/z =3674.8979$, which is consistent with the reduction Tp• yielding 5-hydroxymethyl-2'-deoxyuridine (**217**, calculated $m/z = 3674.6344$).

<div align="center">

5'-d(CGG GXA TAC GTC)

217

(X = 5-hmdU)

</div>
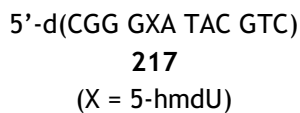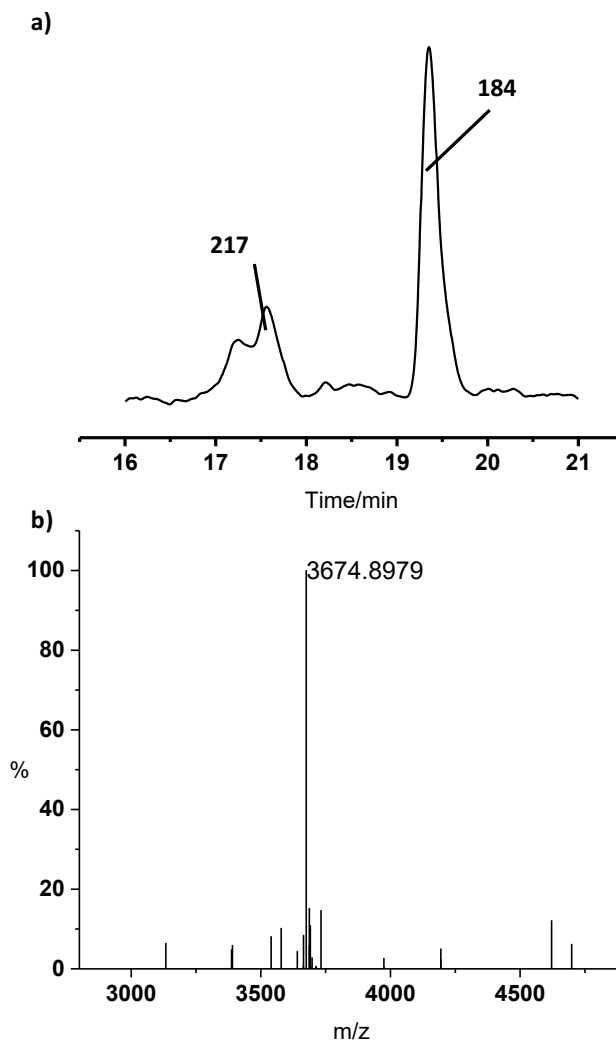
Figure 28. UPLC-MS/MS analysis of photolysis of **195a** in the presence of 1 mM BME. (a) Total ion chromatogram (TIC) of the photolysate of **195a** in the presence of BME. (b) Deconvoluted mass spectrum of **217**.

3.2.3.1   Generation of 2'-deoxyinosine in DNA

During the aerobic photolysis of **6**, 2'-deoxyinosine (dI) was generated. To detect whether dI is also formed in DNA, we treated photolyzed 5'-[32]P-**196** with endonuclease V (Endo V, Figure 29a). Endo V is a 3'-endonuclease involved in DNA repair, which initiates removal of deaminated bases from damaged DNA.[287] The cleavage site generated by Endo V is at the second phosphodiester bond 3' to a lesion (Figure 29b).
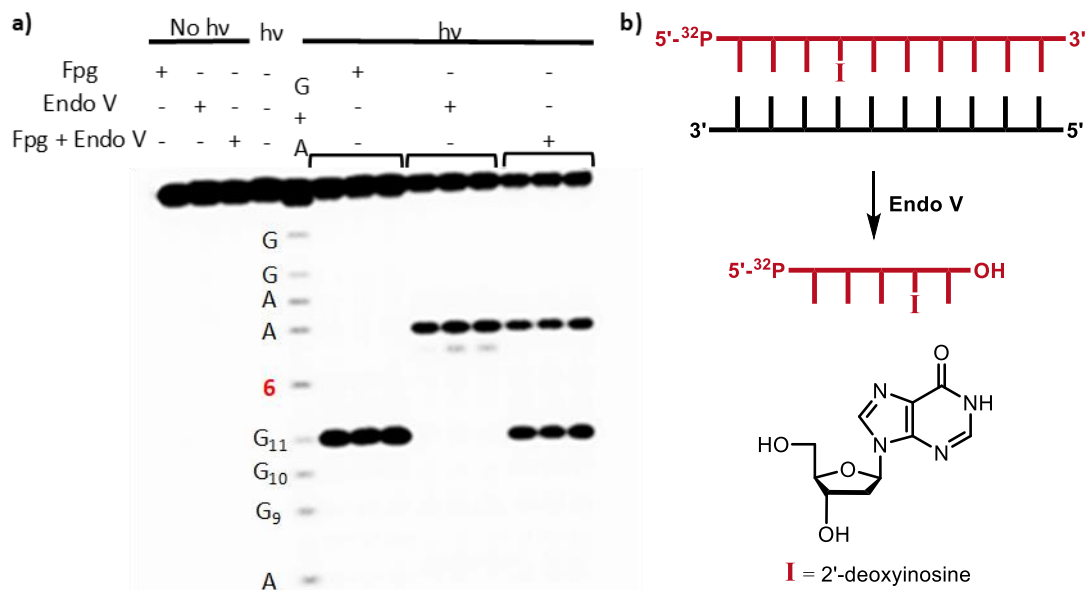
Figure 29. Detection of dI formation by Endo V treatment. (a) Autoradiogram of aerobic photolysis of 5'-^{32}P-**196** followed by Fpg and Endo V treatments. (b) Schematic demonstration of Endo V activity.

Formation of dI was detected in irradiated duplexes **196**, **197** and **203**. The yields of dI were independent of the sequence (14.5 $\pm$ 0.3% in **196**, 12.7 $\pm$ 1.5% in **197**, 13.6 $\pm$ 0.6% in **203,** Appendix Figure 14). Treating photolyzed 5'-^{32}P-**196** with a mixture of Fpg and Endo V does not affect the yield of cleavage induced by either enzyme (Figure 29a). This result suggested the dI formation and tandem lesion formation are two independent pathways. Furthermore, the formation of dI is confirmed by UPLC-MS/MS analysis following nuclease digestion (Figure 30). The yield of dI is determined to be 12.9 $\pm$ 0.1% using the calibration curve,[288] which is consistent with the result obtained by PAGE analysis. However, the mechanism for dI formation is not clear at this point.

5'-d(GTC GCA ACG$_9$ G$_{10}$G$_{11}$T$_{12}$ **6**TA CAC GTC GCT G)
3'-d(CAG CGT TGC C C A   TAT GTG CAG CGA C)
196

5'-d(GTC GCA ACT G$_{10}$G$_{11}$G$_{12}$ **6**TA CAC GTC GCT G)
3'-d(CAG CGT TGA C C C   TAT GTG CAG CGA C)
197

5'-d(GTC GCA ACT T G$_{11}$T$_{12}$ **6**TA CAC GTC GCT G)
3'-d(CAG CGT TGA A C A   TAT GTG CAG CGA C)
203
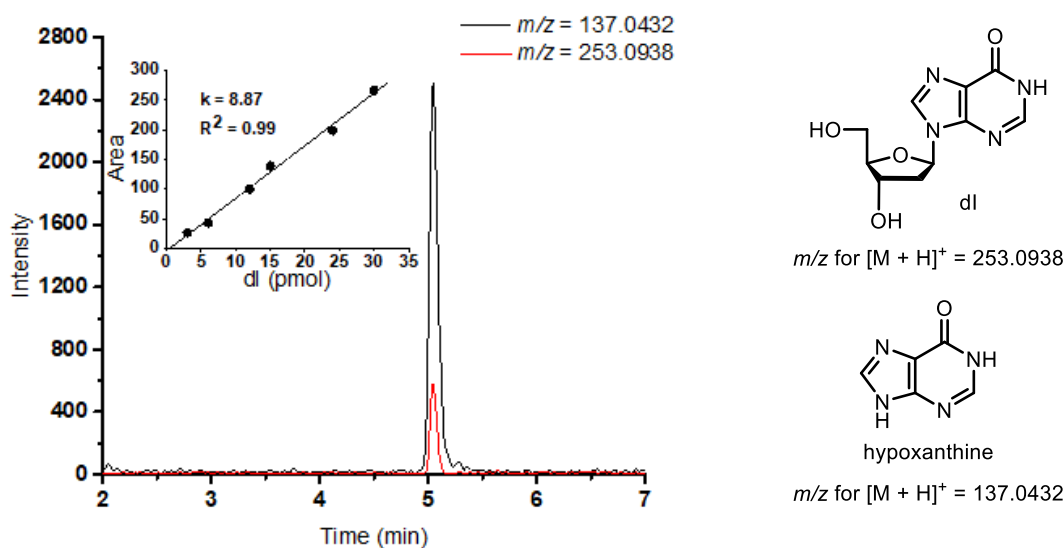
Figure 30. Quantification of dI by UPLC-MS/MS. EIC of dI (m/z = 253.0938, red) and hypoxanthine fragments (m/z = 137.0432, black). Inset, calibration curve plotting the peak area of hypoxanthine fragments against the amount of dI injected.

3.2.3.2 Tandem lesion formation in oligonucleotides containing hydrazine precursor 3

Duplexes containing the hydrazine precursor **3** (**218** and **219**) were synthesized, and **3** was incorporated within sequence contexts that are similar to **196** and **203**, respectively. Tandem lesion was detected in both duplexes after photolysis, consistent with the formation of dA• (Figure 31). The yields of the tandem lesion were lower than those

132

observed in **196** and **203** (4.4 $\pm$ 0.2% Fpg induced cleavage in 5'-^{32}P-**218** at G_{11}, 0.75 $\pm$ 0.02% Fpg induced cleavage in 5'-^{32}P-**219** at G_{11}), but a similar sequence effect was observed. In addition, alkali-labile lesion formation was detected at the position where the precursor was incorporated. Given that the recombination product **104** is the same oxidation state as 8-oxo-dA and 8-oxo-dG, we propose that **104** is alkali-labile, and its formation leads to the observed strand cleavage. Formation of **104** is consistent with the lower yields of the tandem lesion from **3** compared to ketone **6**. Furthermore, piperidine treatment in the presence of BME significantly reduced the observed strand cleavage at the site where precursor **3** resided. This result agrees with **104** behaving similarly to 8-oxo-dG.

5'-d(GTC GCA ACG_9 $G_{10}G_{11}T_{12}$ **3**TA CAC GTC GCT G)
3'-d(CAG CGT TGC   C C A   TAT GTG CTG CGA C)
218

5'-d(GTC GCA ACA C$G_{11}T_{12}$ **3**TA CCC GTC GCT G)
3'-d(CAG CGT TGT GC A   TAT GGG CAG CGA C)
219
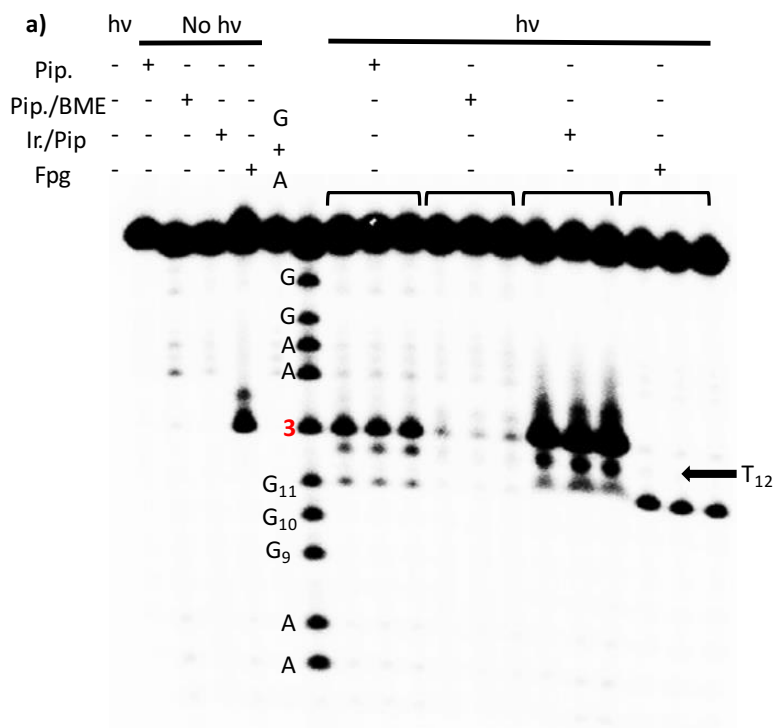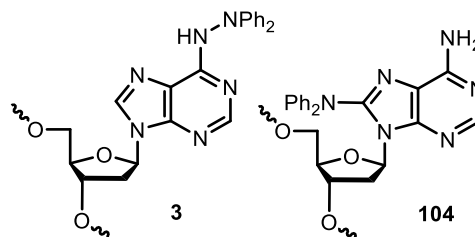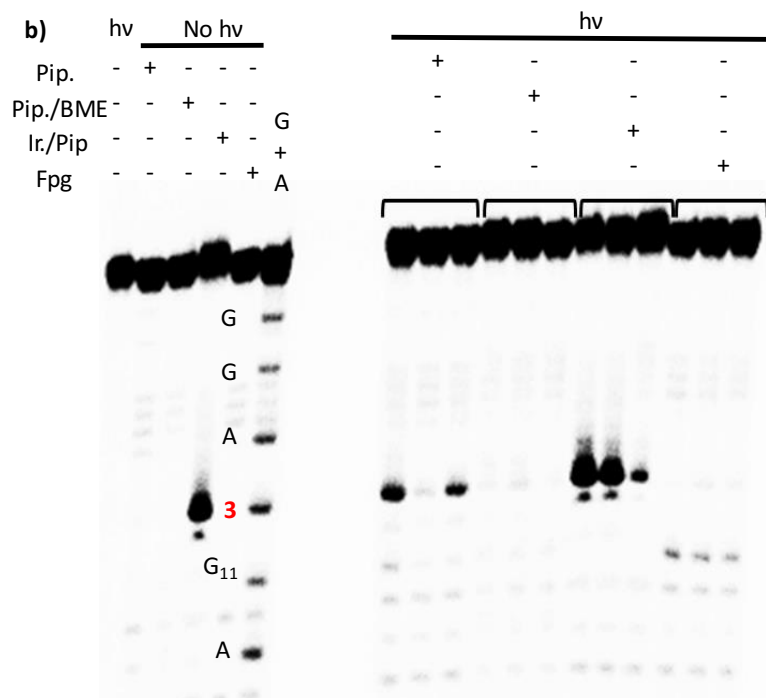
Figure 31. Autoradiogram of aerobic photolysis of DNA containing hydrazine precursor **3** followed chemical and enzymatic treatments. (a) 5'-^{32}P-**218**, (b) 5'-^{32}P-**219**.

3.2.4 Probing π-stacking induced pKa increase of dA radical cation

In Section 3.2.3.1, we established that unlike benzotriazinyl radicals and the neutral radical derived from 2-aminopurine,[64, 289] one-electron oxidation of dG to dG$^{•+}$ by dA• does not compete with other reaction pathways in duplexes **196-200**, despite thermodynamically favorable dG oxidation by dA•. Importantly, dA• is not flanked by dA in these duplexes. The pK$_a$ of dA•+ has been estimated to be as high as 7 at room temperature when it is flanked by dA in DNA.[21] Consequently, we anticipated that when flanked by dA, dA• will be at least partially protonated to form dA•+ and give rise to chemistry in DNA that is attributable to both species. Generation of dA•+ was expected to result in direct one-electron oxidation of dG to dG$^{•+}$. Site-selective, independent dA• generation from **6** in oligonucleotides enables us to probe the effects of the flanking sequence directly.

134

5'-d(GTC GCA ACG_9 $G_{10}G_{11}T_{12}$ **6**TA CAC GTC GCT G)
3'-d(CAG CGT TGC C C A   TAT GTG CAG CGA C)
196

5'-d(GTC GCA ACT $G_{10}G_{11}G_{12}$ **6**TA CAC GTC GCT G)
3'-d(CAG CGT TGA C C C   TAT GTG CAG CGA C)
197

5'-d(GTC GCA ACG GGT_{12} **6**T_{14}G GGC GTC GCT G)
3'-d(CAG CGT TGC CCA   TA C CCG CAG CGA C)
198

5'-d(GTC GCA CG_8G_9 $G_{10}T_{11}G_{12}$ **6**TA CAC GTC GCT G)
3'-d(CAG CGT TG C C C A   TAT GTG CAG CGA C)
199

5'-d(GTC GCA ACG CAT_{12} **6**$G_{14}G_{15}$ G_{16}AC GTC GCT G)
3'-d(CAG CGT TGC CCA   TC C   C TG CAG CGA C)
200

3.2.4.1   Sequence effect on hole migration

We investigated the neutral radical's reactivity when it is flanked by dA (**220-222**). The flanking dA is positioned on the 5' side of dA• to minimize the direct reaction of dA• with 5'-T or dG. In marked contrast to photolyses of **196**, the major sites of strand scission following piperidine or Fpg treatment of 5'-[32]P-**220** photolysates are at the 5'- and middle-dG (dG_9 and dG_{10}) of the dGGG sequence, the characteristic damage pattern for hole transfer (Figure 32). The cleavage pattern indicates that as predicted by Sevilla, π-stacking with the adjacent dA increases the pK_a of dA•+ such that the radical cation is produced from initially formed dA• at pH 7.2. The extent of strand damage increases upon reducing the pH from 7.2 to 6 to 5.1, but the general cleavage pattern is unchanged (Figure 32, 33). More favorable hydration compared to deprotonation of G•+ at lower pH may also contribute to increased strand damage.[187] Furthermore, no hole migration is observed in photolyzed 5'-[32]P-**196** at pH 5.1, and the majority of strand cleavage is localized at G_{11}

135

(Appendix Figure 15). The lack of hole migration is consistent with the pK_a of dA•+ (pK_a ≈ 4), and less than 10% of dA• is protonated at pH 5.1. This observation further underscores the effect of the adjacent dA on the the pK_a of dA•+.

5'-d(GTC CAT ATG$_9$ G$_{10}$G$_{11}$T$_{12}$ A6T ATA CGT GCA G)
3'-d(CAG GTA TAC C C A   TTA TGT GCA CGT C)
220

5'-d(TCC ATA TG$_8$G$_9$ G$_{10}$TG$_{12}$ A6T ATA CGT GCA G)
3'-d(CAG GTC AC C C AC   TTA TAT GCA CGT C)
221

5'-d(GTC GCG CTA TAT 6AG$_{15}$ G$_{16}$G$_{17}$T ATA GCT G)
3'-d(CAG CGC GAT ATA TTC   C C A TAT CGA C)
222
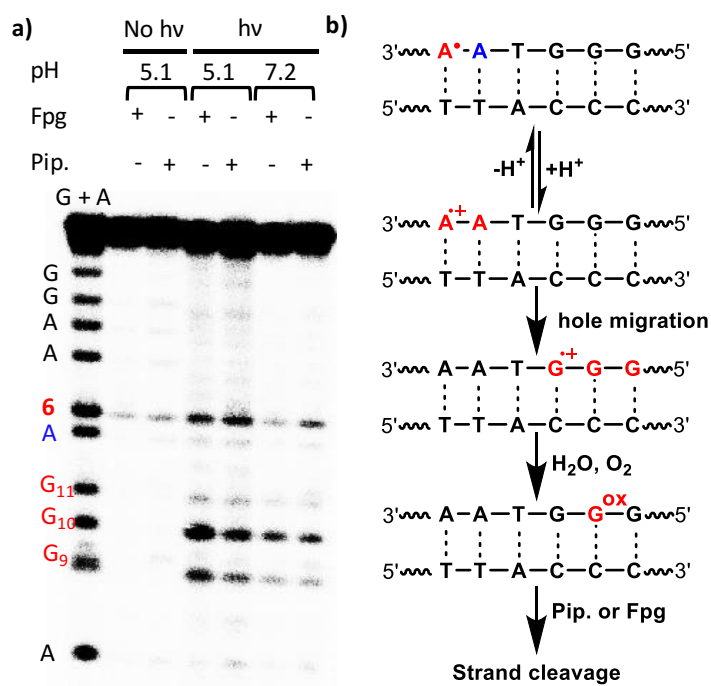
Figure 32. dA•+ induced hole transfer in 5'-^{32}P-**220**. (a) Denaturing PAGE analysis (b) Proposed mechanism for sequence-dependent dA•+ formation, and subsequent hole transfer.

Figure 33. pH Effect on strand damage in duplex 5'-^{32}P-**220**. (a) Fpg treatment (b) Piperidine treatment. $G_{5'}$, G_M, and $G_{3'}$ refer to the dGs in the dGGG triplet. Values are the average ± std. dev. of 3 replicates.

The absolute amount of strand cleavage detected in **220** (9.1 ± 1.2%) corresponds to a high level of hole transfer when one accounts for the ~10% efficiency for G•+ conversion to alkali-labile lesions at pH 5.[13] When combined with the aforementioned UPLC analysis following nuclease digestion (see Section 3.2.3.1), which showed that ~80% of **6** is consumed upon photolysis, these experiments indicate that dA• produced from **6** in **220** results in almost quantitative hole transfer (113.25 ± 15.5%) at pH 5.1. Similar

137

measurements were carried out on all of the duplexes used in the study (Table 11), and the high level of hole migration is observed for all of the substrates at pH 5.1.

Table 11. Estimated efficiency of hole transfer (pH = 5.1)

Duplexes	Total % cleavage on Gs	% Hole transfer[a,b]
220	9.06 ± 1.24	113.25 ± 15.5
221	8.1 ± 0.76	101.25 ± 9.5
222	5.83 ± 0.21	72.88 ± 2.62
223[c]	8.67 ± 0.71	108.38 ± 8.8
224[c]	8.03 ± 0.84	100.38 ± 10.5
225[d]	8.64 ± 0.62	106.75 ± 5.5

[a] The yield of trapping reaction of the hole is ~10%.
[b] The conversion of **6** is 80% after 8 h photolysis.
[c] See Section 3.2.4.2.
[d] See Section 3.2.4.3.

The generality of this sequence-dependent phenomenon was explored using established guidelines governing hole transfer in DNA concerning directionality and sequence/distance effects.[16, 116] For instance, a dGGG triplet is more easily oxidized than a single dG, which provides a driving force for holes to hop short distances from dG•+ to dGGG triplets.[65] Indeed, photolysis (pH 5.1) of 5'-^{32}P-**221** (Figure 34a, 35) produced 7.6-fold greater strand damage at the dGGG triplet than at the single dG adjacent to the site at which dA• was generated (dG$_{12}$). This is consistent with the fact that dGGG triplets have a lower oxidation potential compared to dG.[65] In the corresponding sequence lacking a dA stacked with dA• (**199**), cleavage was detected only at dG$_{12}$, and in much lower yield than in **221** (Figure 34b). In another example, generating dA• in 5'-^{32}P-**222** illustrates the expected ability of hole transfer to proceed in the 3'-direction, unlike tandem lesion

138

formation (Figure 34c). Damage in **222** was detected predominantly at the 5'- and middle

dG's of the dGGG triplet; whereas irradiation of the corresponding sequence lacking a

stacking dA (5'-^{32}P-**200**) produced a small amount of damage at the 5'-T_{12} and none within

the dGGG sequence (Figure 34d). The hole transfer efficiency is slightly lower in the 3'

direction (Table 11, $72.9 \pm 2.6\%$). There have been conflicting reports on the efficiency of

hole migration as a function of migration direction, but it may depend on the nature of the

hole injector and local sequences.[290-294] Overall, these observations are consistent with the

well-established paradigm of hole migration.

5'-d(TCC ATA TG_8G_9 G_{10}TG_{12} A**6**T ATA CGT GCA G)
3'-d(CAG GTC AC C C AC   TTA TAT GCA CGT C)
221

5'-d(GTC GCA CG_8G_9 $G_{10}T_{11}G_{12}$ **6**TA CAC GTC GCT G)
3'-d(CAG CGT TG C C C A   TAT GTG CAG CGA C)
199

5'-d(GTC GCG CTA TAT **6**AG_{15} $G_{16}G_{17}$T ATA GCT G)
3'-d(CAG CGC GAT ATA TTC   C C A TAT CGA C)
222

5'-d(GTC GCA ACG CAT_{12} **6**$G_{14}G_{15}$ G_{16}AC GTC GCT G)
3'-d(CAG CGT TGC CCA   TC C   C TG CAG CGA C)
200
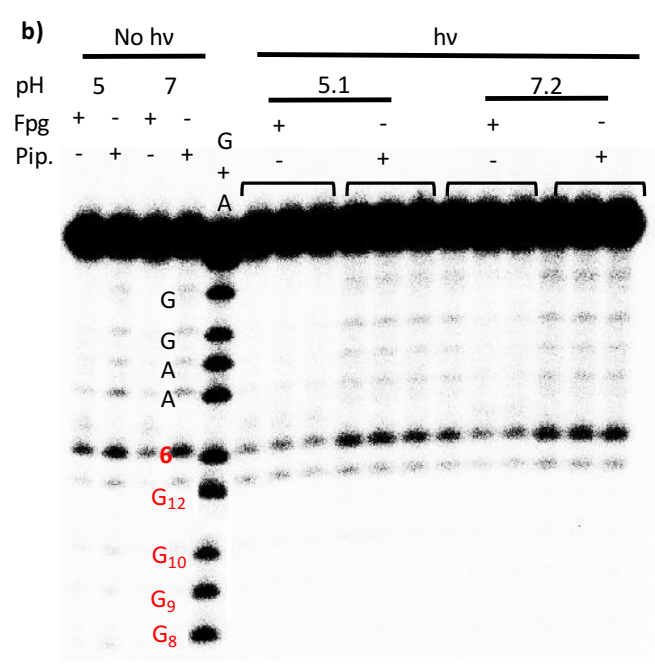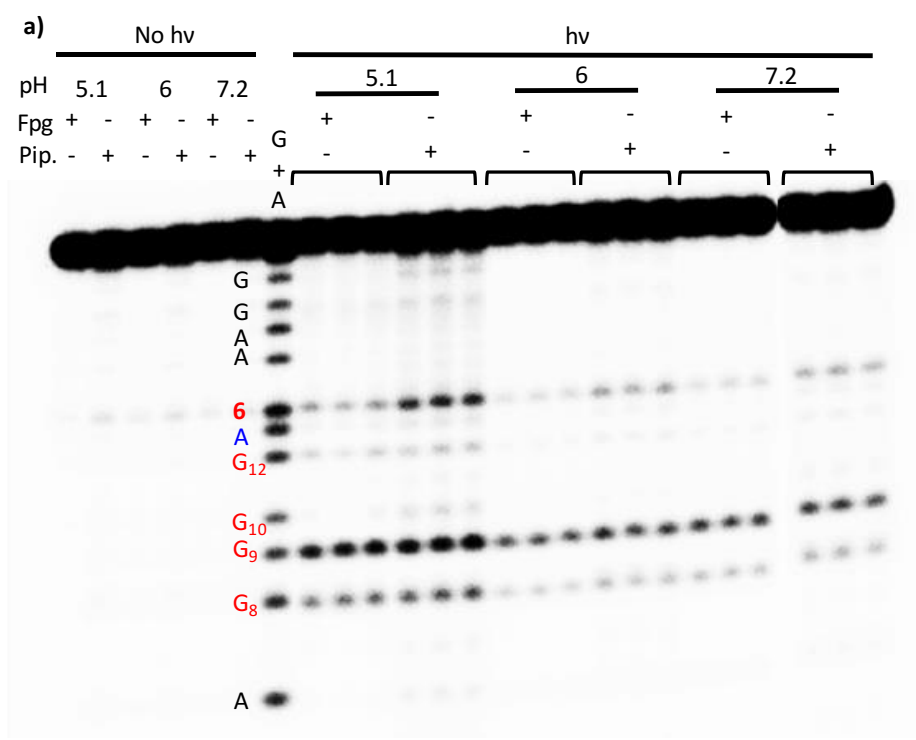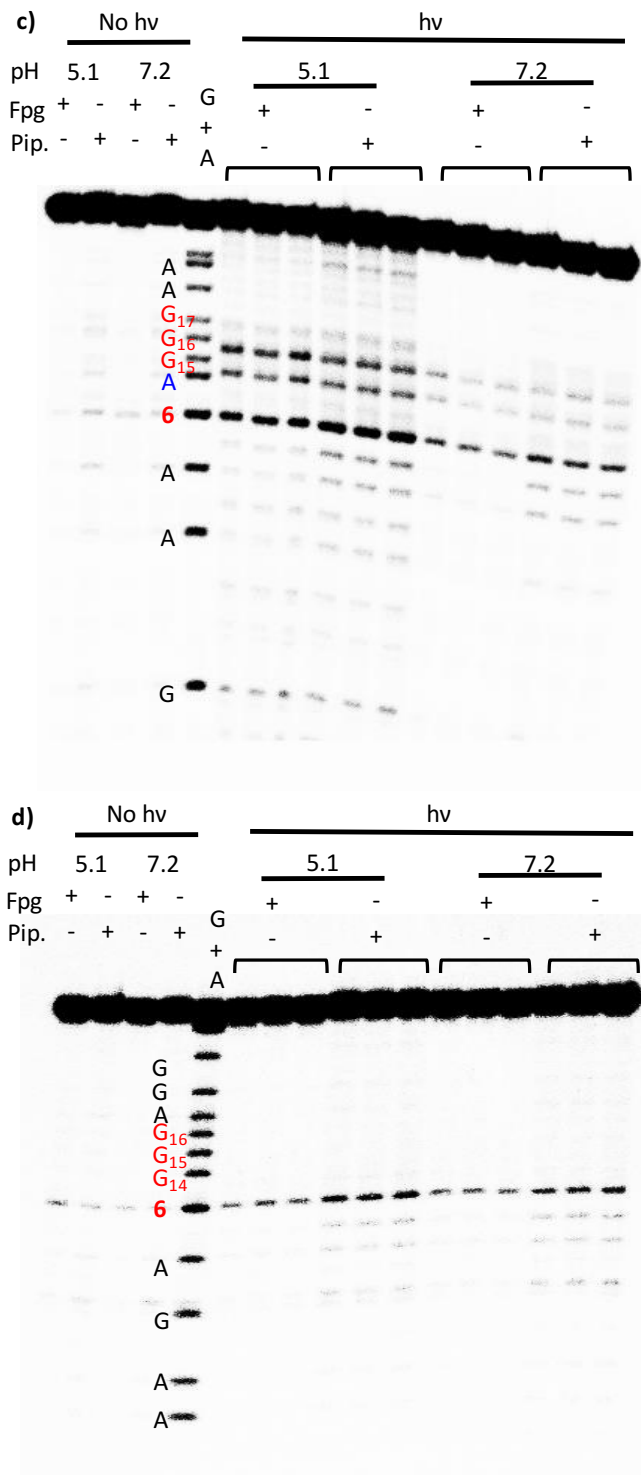
Figure 34. The sequence-dependent hole injection by dA• flanked by dA. Autoradiogram of aerobic photolysis of (a) 5'-^{32}P-**221**, (b) 5'-^{32}P-**199**, (a) 5'-^{32}P-**220**, (a) 5'-^{32}P-**200** followed by piperidine and Fpg treatments.
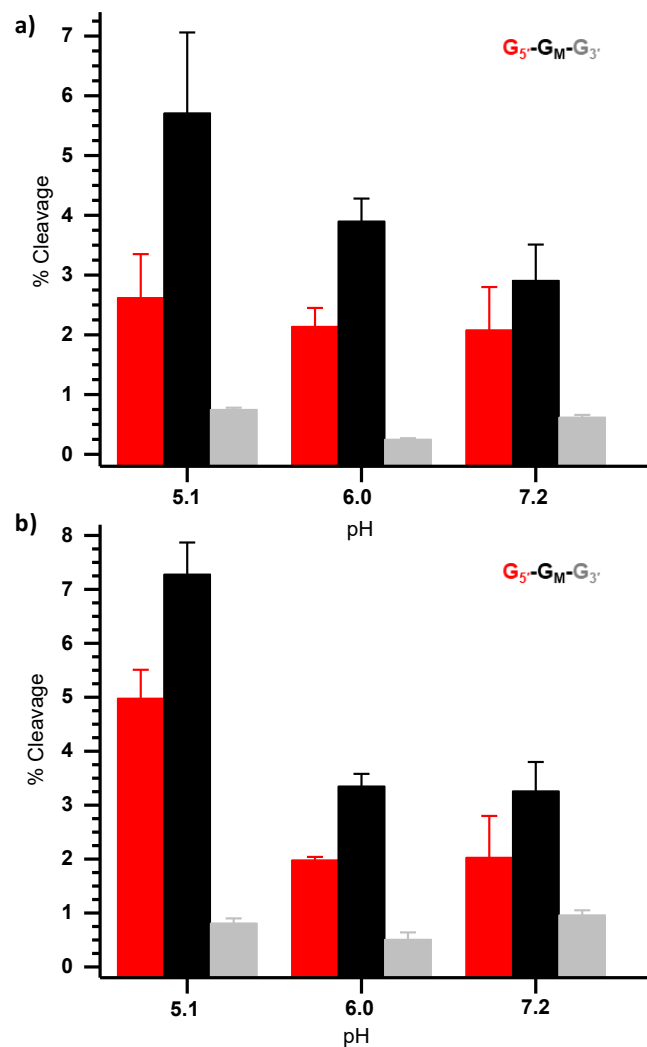
Figure 35. pH Effect on strand damage in duplex 5'-^{32}P-**221**. (a) Fpg treatment (b) Piperidine treatment. $G_{5'}$, G_M, and $G_{3'}$ refer to the dGs in the dGGG triplet. Values are the average ± std. dev. of 3 replicates.

3.2.4.2   dA•+ is the hole carrier

To further support the formation of dA•+, we took advantage of dA•+ delocalization over multiple dAs within poly(dA-T) sequences.[295] The delocalization of positive charge leads to polaron formation and hole transfer with weak distance dependence.[12, 296] Generating dA• within dA$_5$ sequences (**223**, **224**) again yielded strand damage at the 5'- and middle-dGs of the dGGG triplet. The damage detected in dGGG triplets in **223** and

142

224 is the same within experimental error (Figure 36, 37), despite the distances between initial hole injection site and the reporter sequence differing by several angstroms (2 base pairs). This result is consistent with polaron formation in poly(dA-T) sequences, which is unique for dA•+, and supports the intermediacy of dA•+.

5'-d(GTC GAT ATG$_9$ G$_{10}$G$_{11}$T$_{12}$ AAA 6AT ATA GCT G)
3'-d(CAG GTA TAC C C A   TTA TGT GCA CGT C)
223

5'-d(GTC GAT ATG$_9$ G$_{10}$G$_{11}$T$_{12}$ A6A AAT ATA GCT G)
3'-d(CAG GTA TAC C C A   TTA TGT GCA CGT C)
224
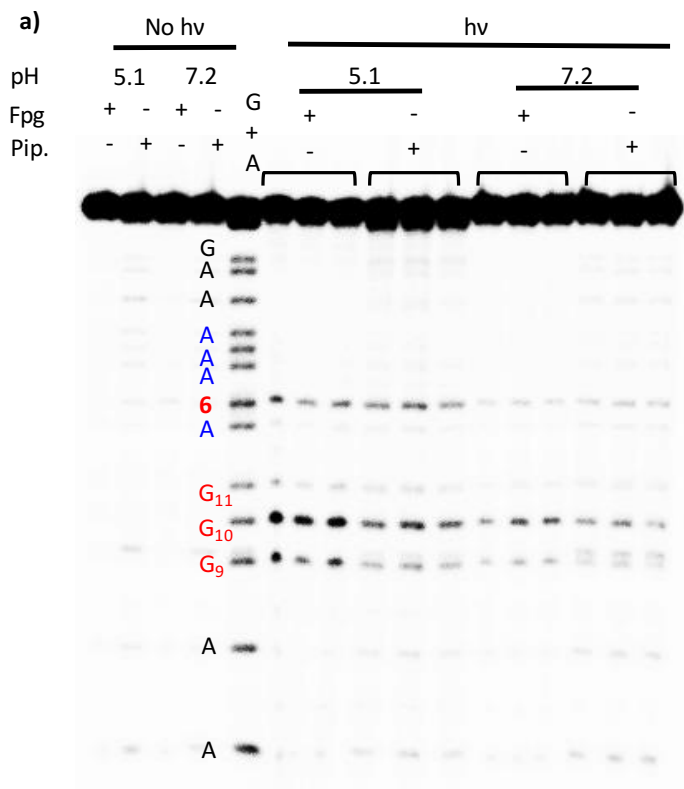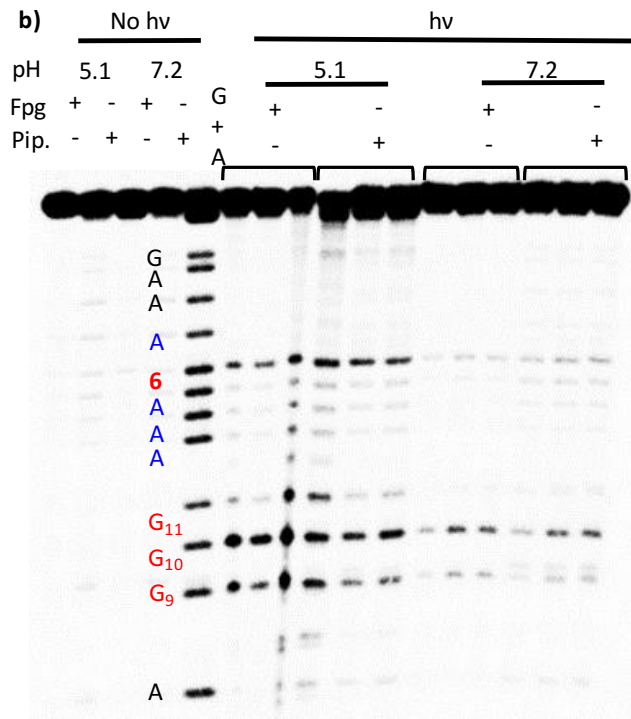
Figure 36. Denaturing PAGE analysis demonstrating the formation of A-polaron. Autoradiogram of aerobic photolysis of (a) 5'-^{32}P-**223**, (b) 5'-^{32}P-**224** followed by piperidine and Fpg treatments.
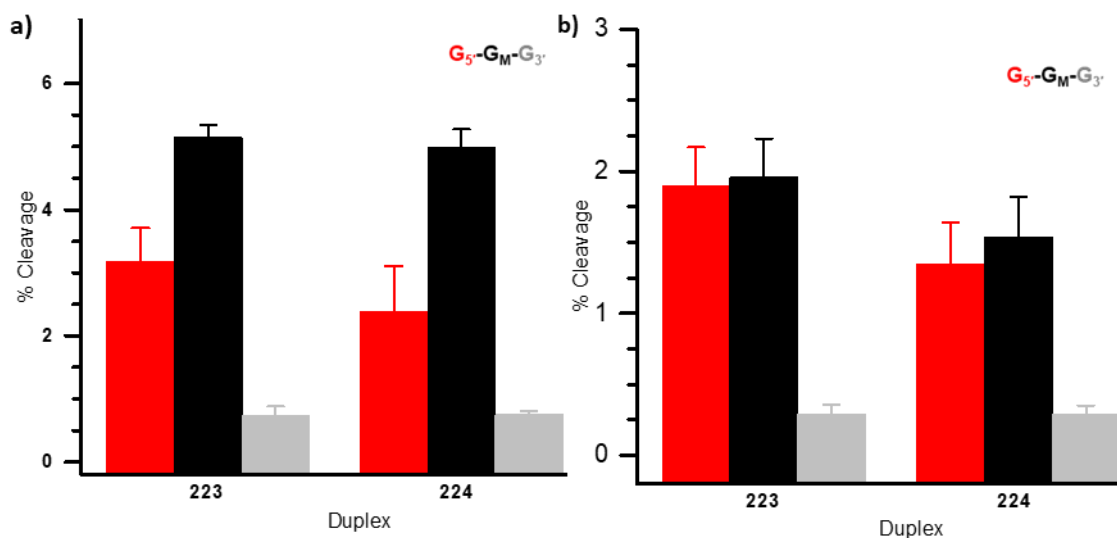
Figure 37. Strand damage in duplex 5'-^{32}P-**223** and 5'-^{32}P-**224**. (a) pH 5.1 (b) pH 7.2. $G_{5'}$, G_M, and $G_{3'}$ refer to the dGs in the dGGG triplet of each respective duplex. Values are the average ± std. dev. of 3 replicates.

3.2.4.3   pH-dependent switching between hole migration and tandem lesion formation

Finally, we examined the strand damage when dA• was generated in a sequence where hole transfer or tandem lesion formation is possible (**225**). dG_{11} was the site of greatest damage (Figure 38a, 40) following photolysis of 5'-^{32}P-**225** at pH 7.2. Also, experiments using 3'-^{32}P-**225** showed strand scission at T_{12}, as expected for tandem lesion formation from dA• (Figure 39). At pH 5.1, the preference switched to G_9 and G_{10}, and the damage pattern was consistent with that of hole transfer. These data suggest that dA• and dA•+ contribute to the observed strand damage in **225** (Figure 38b) in a manner proportional to their relative amounts. Furthermore, the differences observed between **225** and **220** suggest that at pH 7.2 tandem lesion formation from dA• competes with radical cation formation. However, we cannot rule out that dA• is initially formed in a conformation from which tandem lesions are formed more rapidly than dA•+.

5'-d(GTC CAT ATG_9 $G_{10}G_{11}T_{12}$ **6A**T ATA CGT GCA G)
3'-d(CAG GTA TAC C   C   A   TTA TGT GCA CGT C)
225
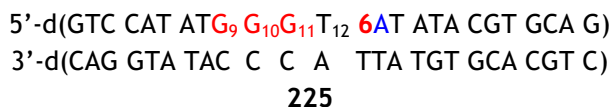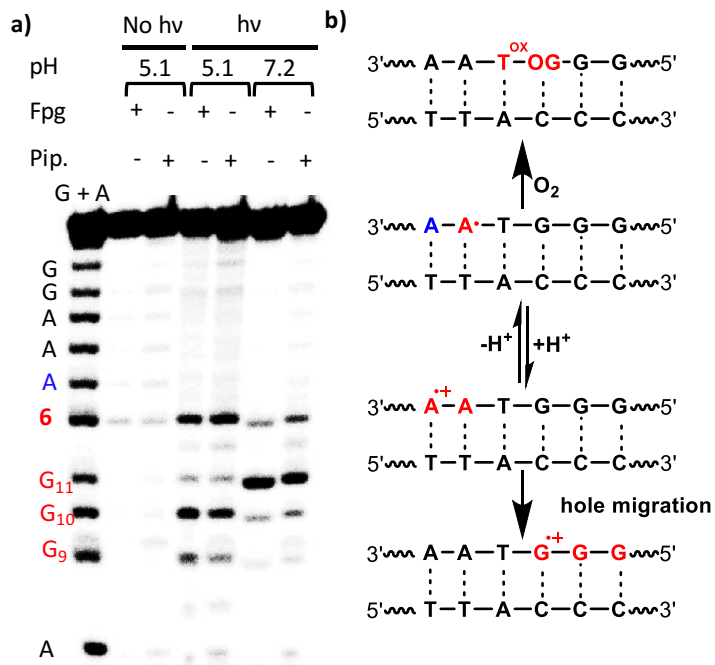
Figure 38. pH-Dependent strand damage in 5'-^{32}P-**225**. (a.) Denaturing PAGE analysis. (b.) The proposed mechanism of pH-dependent switching of strand damage induced by dA• and dA•+.
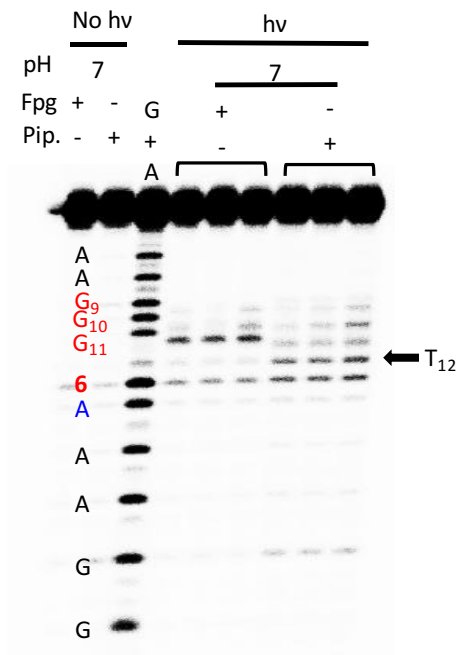
Figure 39. Autoradiogram of aerobic photolysis of 3'-^{32}P-**225** followed by piperidine and Fpg treatments.
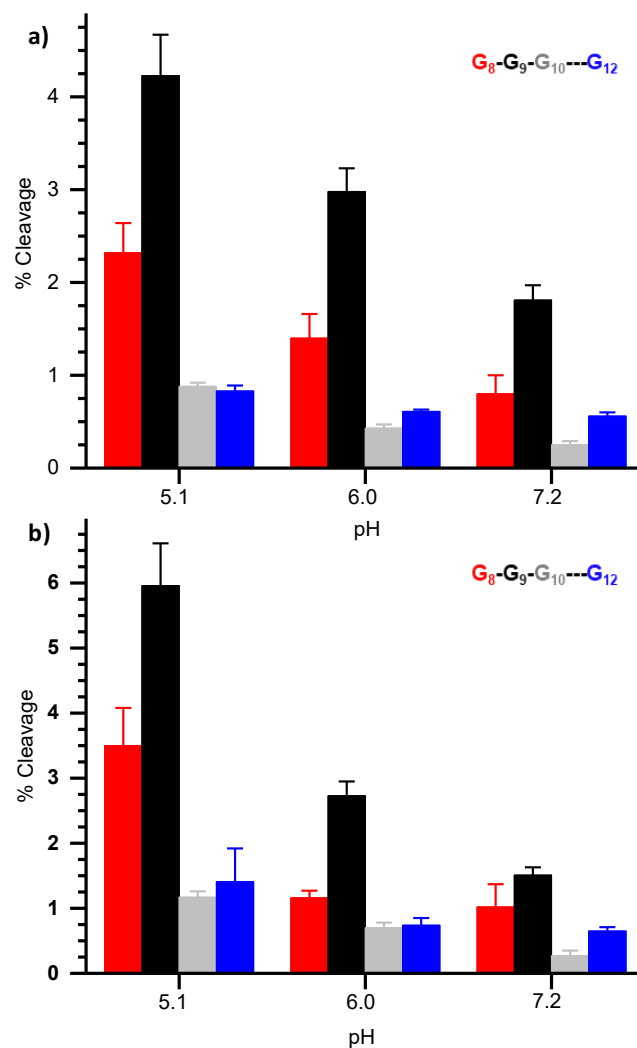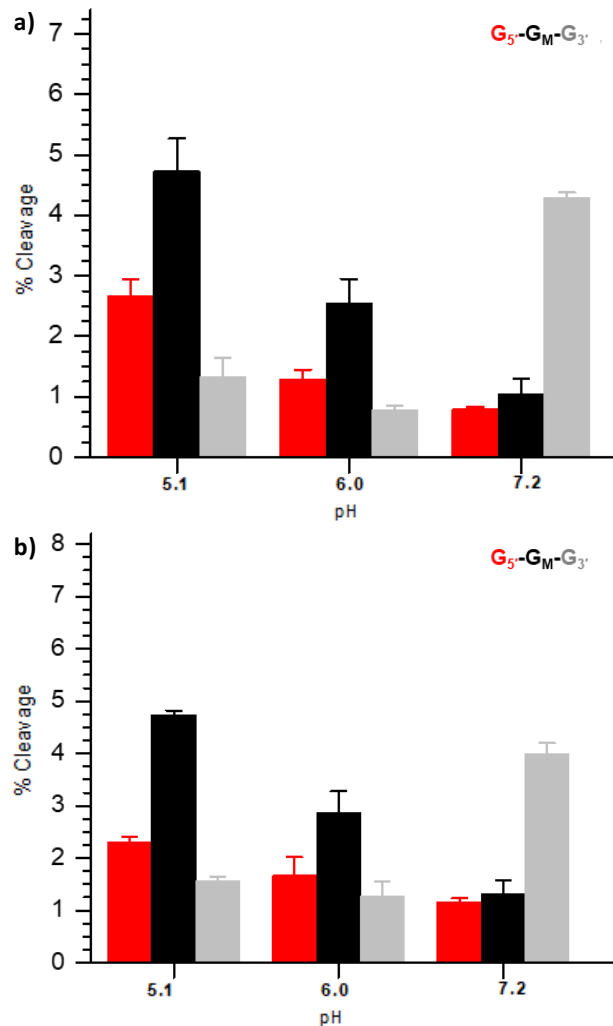
Figure 40. pH Effect on strand damage in duplex 5'-^{32}P-**225**. (a) Fpg treatment (b) Piperidine treatment. $G_{5'}$, G_M, and $G_{3'}$ refer to the dGs in the dGGG triplet. Values are the average ± std. dev. of 3 replicates.

3.2.5   An alternative mechanism for strand damage formed during DNA hole migration within DNA that lacks dG

3.2.5.1   Inconsistency in the proposed mechanism for hole migration induced tandem lesion formation

In Section 2.3.2.2, the strand damages induced by hole migration in poly(dA-T) sequences were discussed. Given the fact that the population of the thymidine radical cation

147

in an A/T base pair will be less than 1% of that at the adenine (ΔE_{ox} ~0.3 V in water), it is surprising that the oxidative reaction occurs at thymidine.[4] The authors proposed that product ratios depend on differences in the energy of the transition states.[297] Thus, the dominant reaction of radical cations at thymidine in DNA suggests a kinetically favorable pathway for a hole to be trapped on this nucleotide.[24, 298] Computational studies and a kinetic isotope effect experiment suggested that a concerted proton-coupled electron transfer (PCET) process avoided the higher-energy intermediates (Scheme 57).[298] The proposed PCET process involves spontaneous deprotonation of the methyl group of the T•+ to form T• (Scheme 57). However, the formation of T• is inconsistent with the formation of Tg which requires trapping of T•+ by O_2 and water when the hole is localized at the 3'-side of TT steps (Scheme 10).
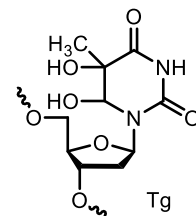
Scheme 57. Generation of T• via PCET from dA•+ in an A/T base pair .
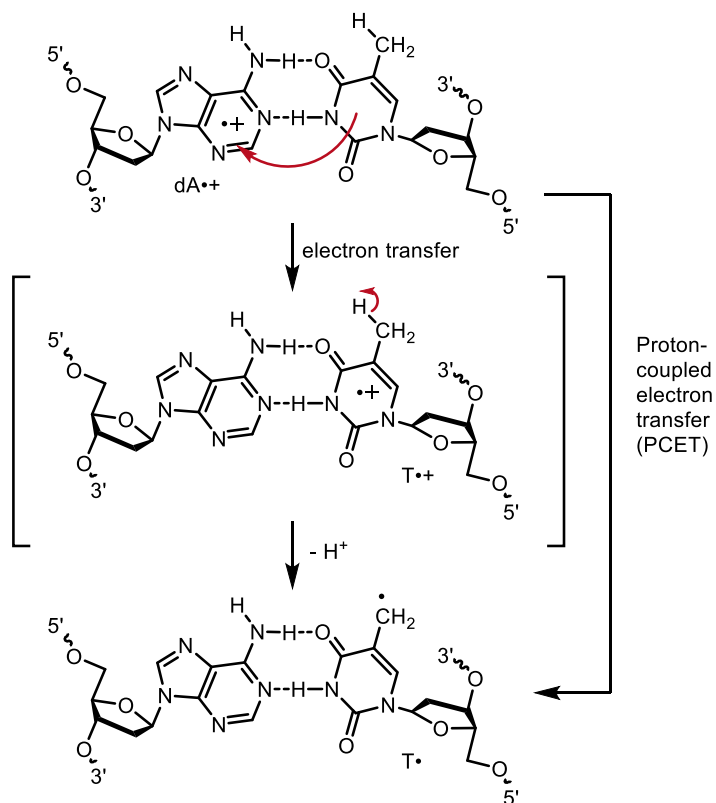
The proposed mechanism does not fully explain the reactivity of T•+ localized at the 5'-side of TT steps. The authors propose that this T•+ deprotonates to generate carbon-centered radical T• rather than reacts with O_2 and H_2O. However, the author does not rationalize this difference of reactivity depending upon which position within a TT step the radical cation is generated. In addition, the authors also proposed that Tp• generated by oxygen trapping of T• does not induce tandem lesion formation because the distance between the terminal oxygen atom of Tp• and the C5-methyl hydrogen atom of the 5'-T is 4.2 Å. The authors conclude that this distance is sufficient to render hydrogen atom abstraction unlikely.[25] However, our molecular modeling (Figure 41) suggests this distance can be as short as 2.6 Å, and the peroxyl radical is well-positioned for the hydrogen atom abstraction. Furthermore, the distances between the Tp• terminal oxygen atom and C5 or C6 are 3.0 Å and 2.5 Å, respectively. These distances are comparable to those measured for the addition of 5,6-dihydro-2'-deoxyuridine C-6 peroxyl radical (Up•) to a 5'-adjacent T, from which tandem lesion formation has been observed.[299] Therefore, we believe that the addition of peroxyl radical to the C5-C6 π bond of the 5'-T is also possible.

149
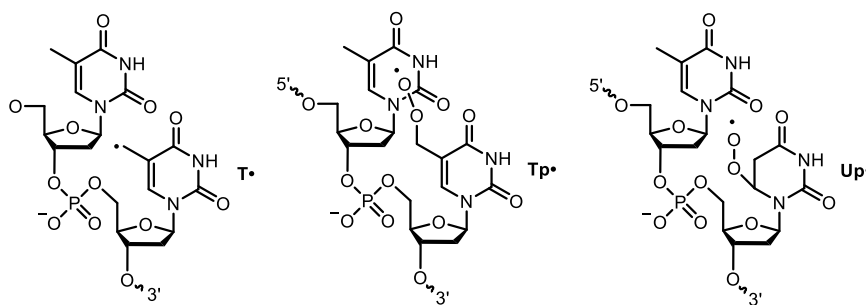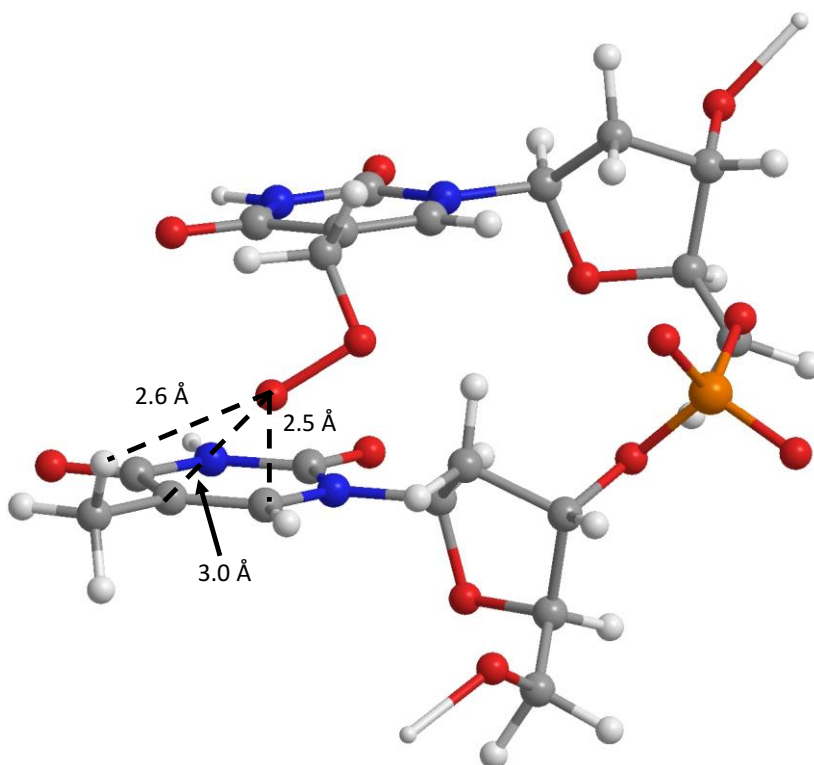
Figure 41. Molecular modeling demonstrating the addition of peroxyl radical Tp• to 5'-T in the dinucleotide sequence 5'-T-Tp•.

Moreover, to explain the predominant damage on the central T of TTT sequences, the authors reasoned that two of three possible products (**226-228**) generated have alkali-labile lesions located where the central T resided, which is consistent with the gel results. However, based on the previous discussion concerning PAGE analysis of tandem lesions (Figure 14), Tg in **226** will be detected when the strand is 5'-labeled, which is inconsistent with the gel results.

X = CH₂OH or CHO
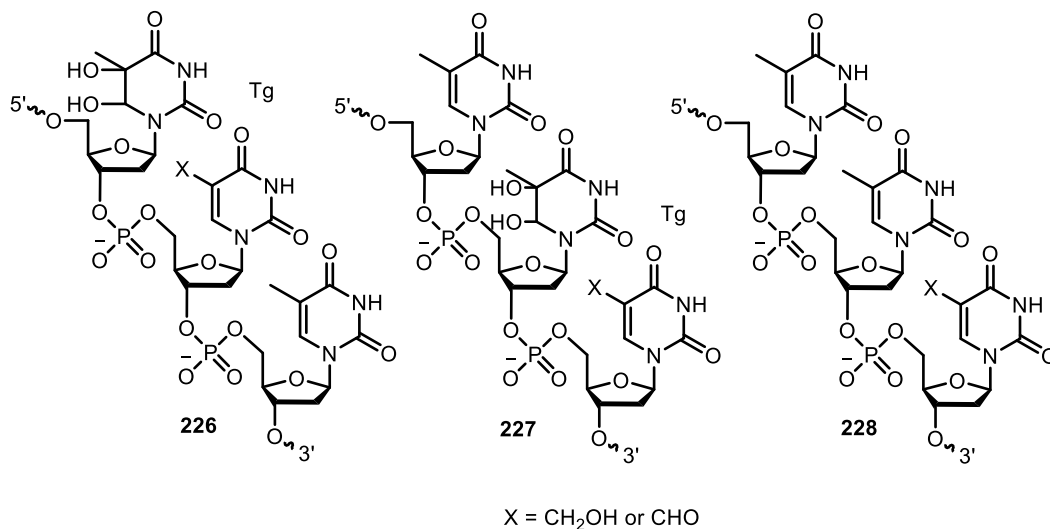
3.2.5.2 Reproducing tandem lesion formation by independently generating dA•

The inconsistency of the previously reported mechanism in explaining the products observed when holes were injected into poly(dA-T) duplexes via photoexcited anthraquinone led us to consider an alternative mechanism. In Section 3.2.3, it was established that dA• abstracts the C5-methyl hydrogen from the 5'-adjacent thymidine which led to the formation of a tandem lesion in 5'-d(GT) sequences. Tandem lesion formation was inhibited by 5'-d(GU) sequences. Interestingly, similar sequence specificity was also observed in photoexcited anthraquinone induced hole migration. For instance, the strand cleavages were preferentially localized at 5'-T in 5'-d(TTA) sequences when the oligonucleotides were 5'-^{32}P labeled. In addition, alkali-labile cleavage was observed at 5'-d(TTA) and 5'-d(UTA) steps, but no damage was detected at 5'-d(TUA) sequences.[25] The requirement for an intervening thymidine is consistent with the tandem lesion formation initiated by hydrogen atom abstraction (see section 3.2.3.4.1).

AQ-5'-d(TTT TAA ATT AAA TTA AAT TAA ACC TAT ATT T)
3'-d(AAA ATT TAA TTT AAT TTA ATT TGG ATA TAA A)-5'-³²P

16

AQ-5'-d(TTA ATT AAT TTT TAA TTA ATA TA)
3'-d(AAT TAA TTA AAA ATT AAT TAT AT)-5'-³²P

17

AQ-5'-d(TTT TAA ATT AAA TTA AAT TAA ATA TAT TT)
3'-d(AAA ATT TAA TTT AAT TTA ATT TAT ATA AA)-5'-³²P

18

AQ-5'-d(TTT TAA TT A ATT AAT TAA TAT ATT T)
3'-d(AAA ATU AAU TAA TUA AUT ATA TAA A)-5'-³²P

19

AQ
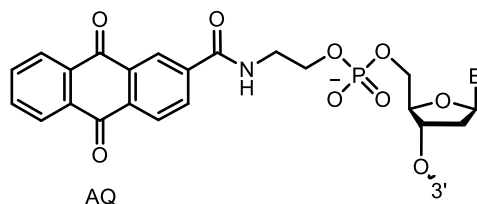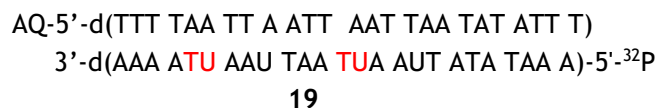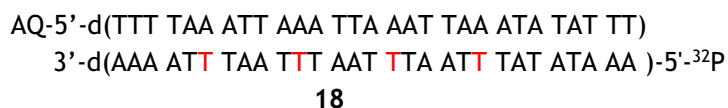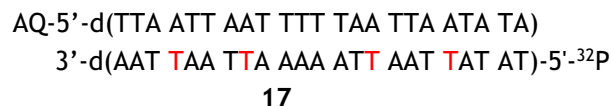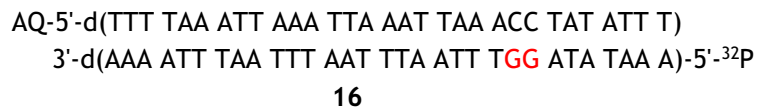
Furthermore, as discussed in Section 3.2.4, dA• and dA•+ equilibrate in duplex DNA in a sequence-dependent manner. In the presence of guanine (**16**), hole transfer outcompetes the deprotonation of dA•+, and the hole is eventually trapped by guanines (Figure 42a).[12-13, 83, 300-301] In the absence of such hole sinks, such as in poly(dA-T) substrates **17-19**, dA•+ randomly migrates over the dA-T tracts and deprotonates to form dA• (Figure 42b). Given the possibility of dA• generation in duplexes **17-19** and the aforementioned sequence specificity of tandem lesion formation, we proposed that the tandem lesion formation may be initiated by dA•.
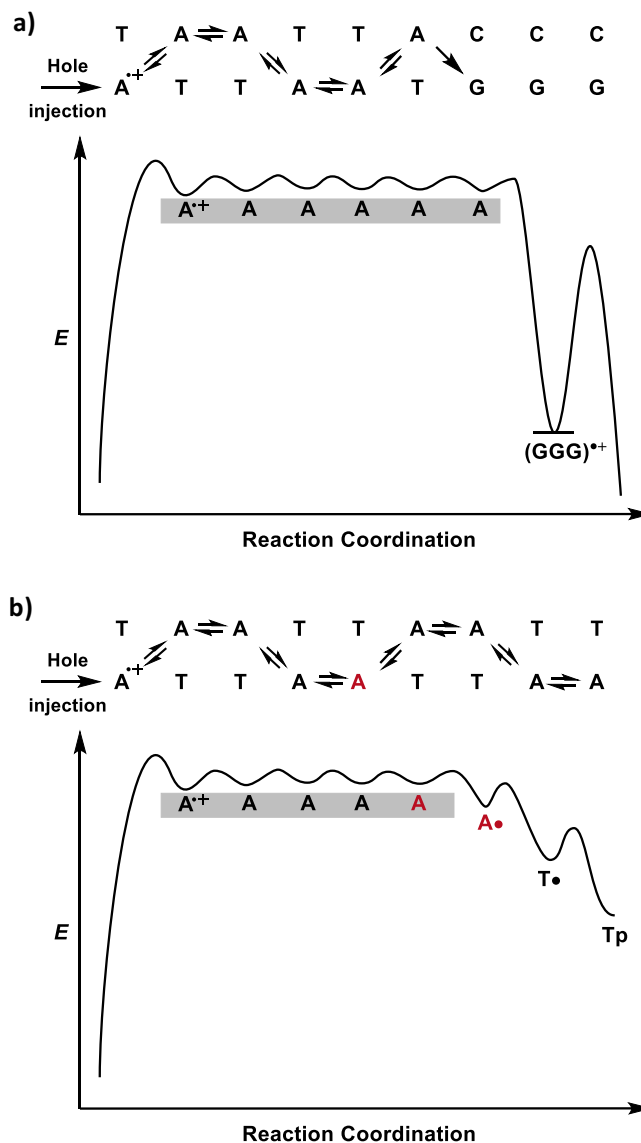
Figure 42. Schematic demonstration of hole migration (a) in the presence of guanine; (b) in the absence of guanine

5'-d(TTT TTT TTT ATA X$_{13}$Y$_{14}$**6** TAT ATT TTT TTT TTT)
3'-d(AAA AAA AAA TAT A A T ATA TAA AAA AAA AAA)
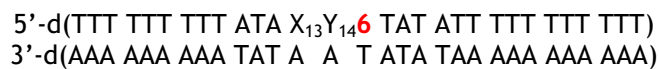
229: X = T Y = T
230: X = T Y = dU
231: X = dU Y = T

Consequently, we tested the possibility that dA• is the species directly responsible

for the products observed following hole migration in poly(dA-T) sequences. Substrates

153

229-231 containing 5'-d(TT), 5'-d(UT), and 5'-d(TU) flanked by a photochemical precursor (**6**) for dA• were prepared. The purpose of these sequences was to reproduce the sequence specificity for tandem lesion formation observed in photoexcited anthraquinone induced hole migration. The dA• precursor was not flanked by dA to minimize dA•+ formation under the reaction conditions. Piperidine treatment of photolyzed 5'-^{32}P-**229-231** produced cleavage patterns that were fully consistent with those reported when duplexes containing the same dinucleotide steps and anthraquinone were irradiated (Figure 43). Specifically, duplex **229**, containing a 5'-T_{13}-T_{14}-dA• sequence results in predominant cleavage at the 5'-thymidine of the dinucleotide sequence. Similarly, strand damage is detected in approximately equal amounts at dU_{13} and T_{14} in 5'-^{32}P-**230**; whereas no damage is detected in the duplex (**231**) containing 5'-T-dU-dA•.
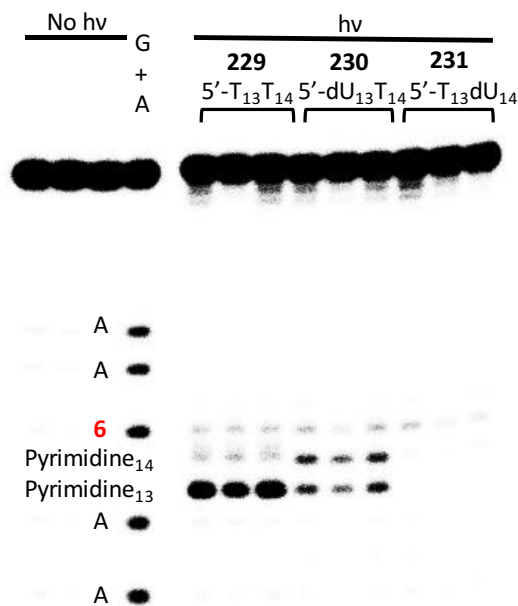
Figure 43. Strand damage in duplexes (5'-^{32}P-**229-231**) containing 5'-pyr$_{13}$-pyr$_{14}$-dA• induced by piperidine. Three replicates are shown for each substrate.

3.2.5.3 Characterization of the structure of the tandem lesion formation

3.2.5.3.1 Chemical assays

Based on the observations made in 5'-d(GTA•) and Schuster's report on the structure of tandem lesions, we proposed that tandem lesion (**232**) containing 5'-d[Tg-(5-fdU)] was formed.

232
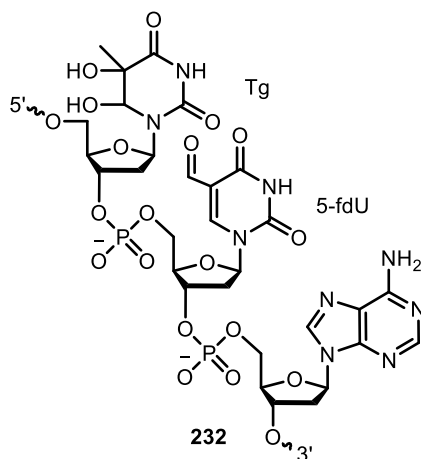
Similar to the 5'-d[(8-oxo-dG)-(5-fdU)], one would expect greater strand damage at 5-fdU to be observed in 3'-^{32}P-**229** substrates compared to 5'-^{32}P-**229** because damage at the 5'-Tg prevents the detection of 5-fdU on the 3' side when the ^{32}P-label is at the 5'-terminus. Indeed, piperidine treatment of photolyzed 5'-^{32}P-**229** yielded $10.5 \pm 0.2\%$ cleavage at T_{13} and $1.4 \pm 0.1\%$ at T_{14} (Figure 44b), but the preference is reversed in 3'-^{32}P-**229** (Figure 44a, T_{13}, $2.8 \pm 0.2\%$; T_{14}, $4.3 \pm 0.1\%$). These results suggest that the observed strand damage is part of a tandem lesion. Cleavage at T_{13} was still observed in 3'-^{32}P-**229**, which is consistent with the report that 5-fdU is not completely cleaved by piperidine treatment.[302] Additionally, NaBH$_4$ treatment of 3'-^{32}P-**229** photolysate before piperidine cleavage resulted in increased strand scission detected at T_{13} (Figure 44a, $5.9 \pm 0.1\ \%$) and

decreased damage at T_{14}. This is consistent with the reduction of 5-fdU to 5-hmdU at T_{14}, which is not labile to piperidine and does not mask the detection of Tg formation at T_{13}.
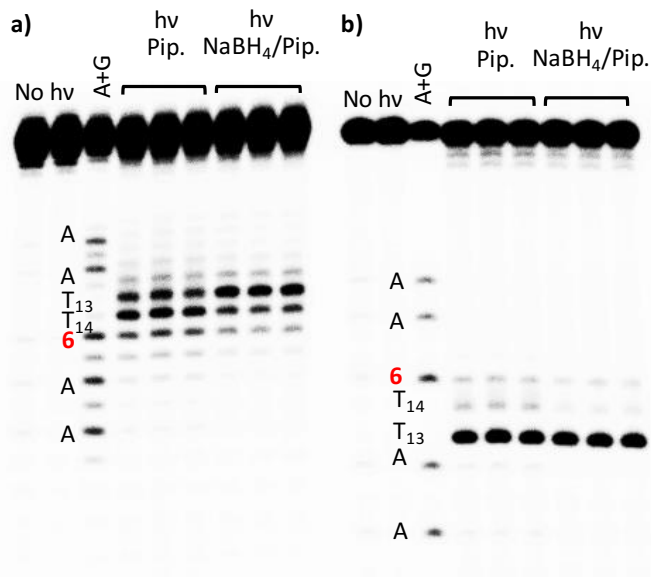
Figure 44. Denaturing PAGE investigation of the structure of the tandem lesion formed in 5'-TT steps using piperidine and NaBH$_4$/piperidine treatments. Autoradiogram of aerobic photolysis of (a) 3'-^{32}P-**229** and (b) 5'-^{32}P-**229** followed by chemical treatments.

3.2.5.3.2 Characterization of the structure of the tandem lesion by UPLC-MS/MS

The structure of the tandem lesion was validated via UPLC-MS/MS analysis of photolysates of **233** using the method mentioned previously (see Section 3.2.3.3.2). The usage of a relatively short duplex is crucial for detection of fragments via CID, which is critical for product assignment.[272-273, 303] The T_m's of dodecameric poly(dA-T) substrates are too low for them to remain hybridized during photolysis. However, since we believe that tandem lesion formation does not involve dA•+, we predicted that sequences containing dGs at distal positions would not affect tandem lesion formation. This was

demonstrated by piperidine treatment following the photolysis of 5'-^{32}P-**234**, which showed

an identical damage pattern compared to 5'-^{32}P-**229**.

5'-d(GCG CGT ATA AGC TT)
3'-d(CGC GCA T**6**T TCG)
233

5'-d(TGA TCG ATC GCT$_{12}$ T$_{13}$**6**T ACG CGC TAG CTA GCT)
3'-d(ACT AGC TAG CGA   A TA TGC GCG ATC GAT CGA)
234
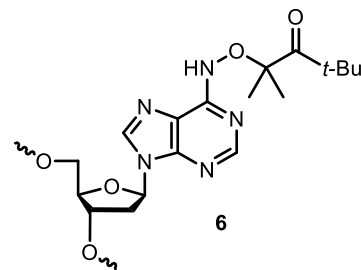
5'-d(GCG CGT ATA AGC)
3'-d(CGC GCA T**6**T TCG)
235

5'-d(GCG CGT ATA AGC)   5'-d(GCG CGT ATA AGC TT)
236   **237**

Figure 45. Autoradiogram of aerobic photolysis of 5-^{32}P-**234** followed by piperidine treatment.

Having established that dGs do not affect the tandem lesion formation, we designed dodecameric substrate **235** for UPLC-MS/MS studies. However, we were unable to separate the products generated by photolysis from the complementary strand **236**. The inclusion of a 3'-TT overhang increased the retention time of the complementary strand (**237**), enabling its separation from the products of interest. Moreover, d(G-C) base pairs stabilized **233** ($T_m = 35.5$ °C) against melting during photolysis.

5'-d(GCT TAT ACG CGC)
238

5'-d(GCX YAT ACG CGC)
239
(X = Tg; Y = 5-fdU)

5'-d(GCT ZAT ACG CGC)
240
(Z = 5-hmdU)

5-hmdU

5-fdU

Tg
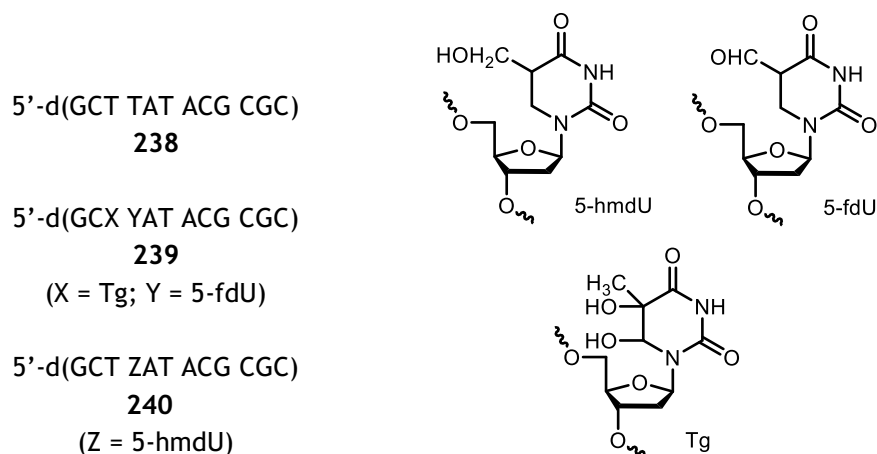
The major product generated by the photolysis of **233** is **238**, which is consistent with the results obtained by UPLC-MS/MS analysis on the photolysate of **195a** (Figure 19). We also observed a product with the expected mass (*m/z* =3666.6240) and fragmentation pattern that is consistent with the oligonucleotide containing tandem lesion **232** (**239**, Figure 46, Appendix Figure 17, Table 12). Oligonucleotide **239** coeluted with another product **240**, the *m/z* of which is consistent with an oligonucleotide containing a single 5-hmdU lesion (Figure 46b). Additionally, a product with m/z = 3648.6965 ([**238** + 30 Da]) was detected, but the structure was not assigned.
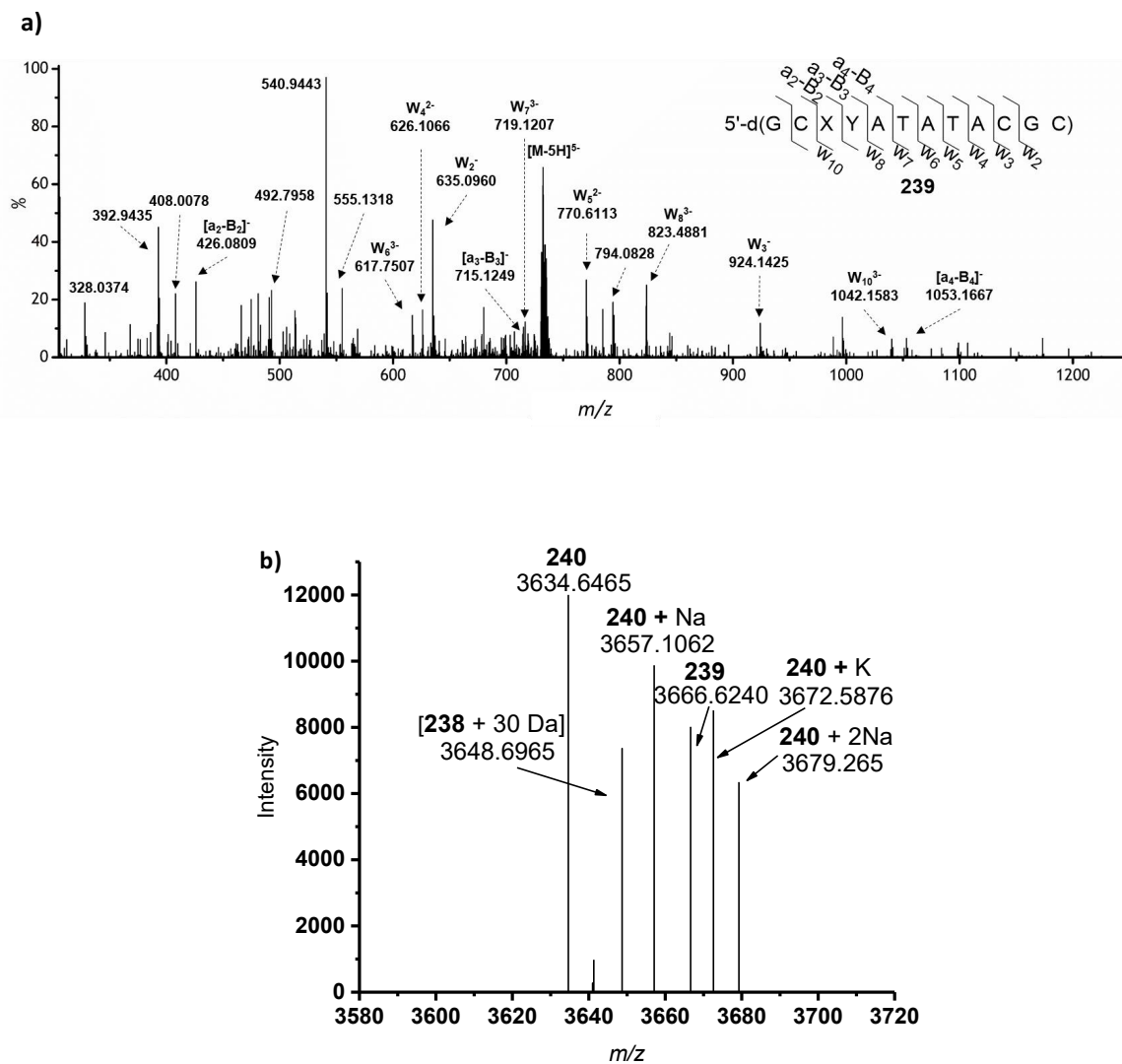
Figure 46. UPLC-MS/MS analysis of photolysis of **233**. (a) CID mass spectrum of the ion (*m/z* = 732.7, z = 5) of the oligonucleotide containing tandem lesion **232** (**239**). X = Tg, Y = 5-fdU. (b) Deconvoluted mass spectrum of oligonucleotide **239** and **240**.

Table 12. Observed fragments of 239 from CID and their theoretical m/z.

Ion fragments	Theoretical m/z	Observed m/z	ΔPPM
$a_2\text{-}B_2^-$	426.0817	426.0809	-1.88
w_2^-	635.1026	635.096	-10.39
$a_3\text{-}B_3^-$	715.1286	715.1249	-5.17
w_3^-	924.1495	924.1425	-7.57
w_4^{2-}	626.1009	626.1066	9.10
$a_4\text{-}B_4^-$	1053.1766	1053.1667	-9.40
w_5^{2-}	770.6208	770.6113	-12.38
w_6^{3-}	617.7639	617.7507	-21.37
w_7^{3-}	719.1128	719.1207	10.99
w_8^{3-}	823.4655	823.4881	27.44
w_{10}^{3-}	1042.1568	1042.1583	1.44

Furthermore, Tg-containing DNA may produce an $[a_n - 143\ \text{Da}]$ fragment instead of $[a_n - \text{Tg}]$ fragments (Scheme 58).[304] However, the expected m/z value for the $[a_3 - 143\ \text{Da}]$ fragment ($m/z = 732.1437$) is very close to the m/z of the precursor ion ($z = 5$) chosen in Figure 29. To unambiguously identify this fragment, we used a different precursor ion ($z = 3$) and acquired the CID spectrum (Figure 47, Appendix Figure 18). The fragmentation of the $z = 3$ ion yielded fewer fragments bearing structural information compared to those obtained from the $z = 5$ ion. However, an ion corresponding to $[a_3 - 143\ \text{Da}]$ ($m/z = 732.1434$) was observed, which was consistent with the presence of Tg lesion.

Scheme 58. CID induced fragmentation of DNA containing Tg generating w-series ions, [a_n – 143 Da] ion and [a - B]-series ions.
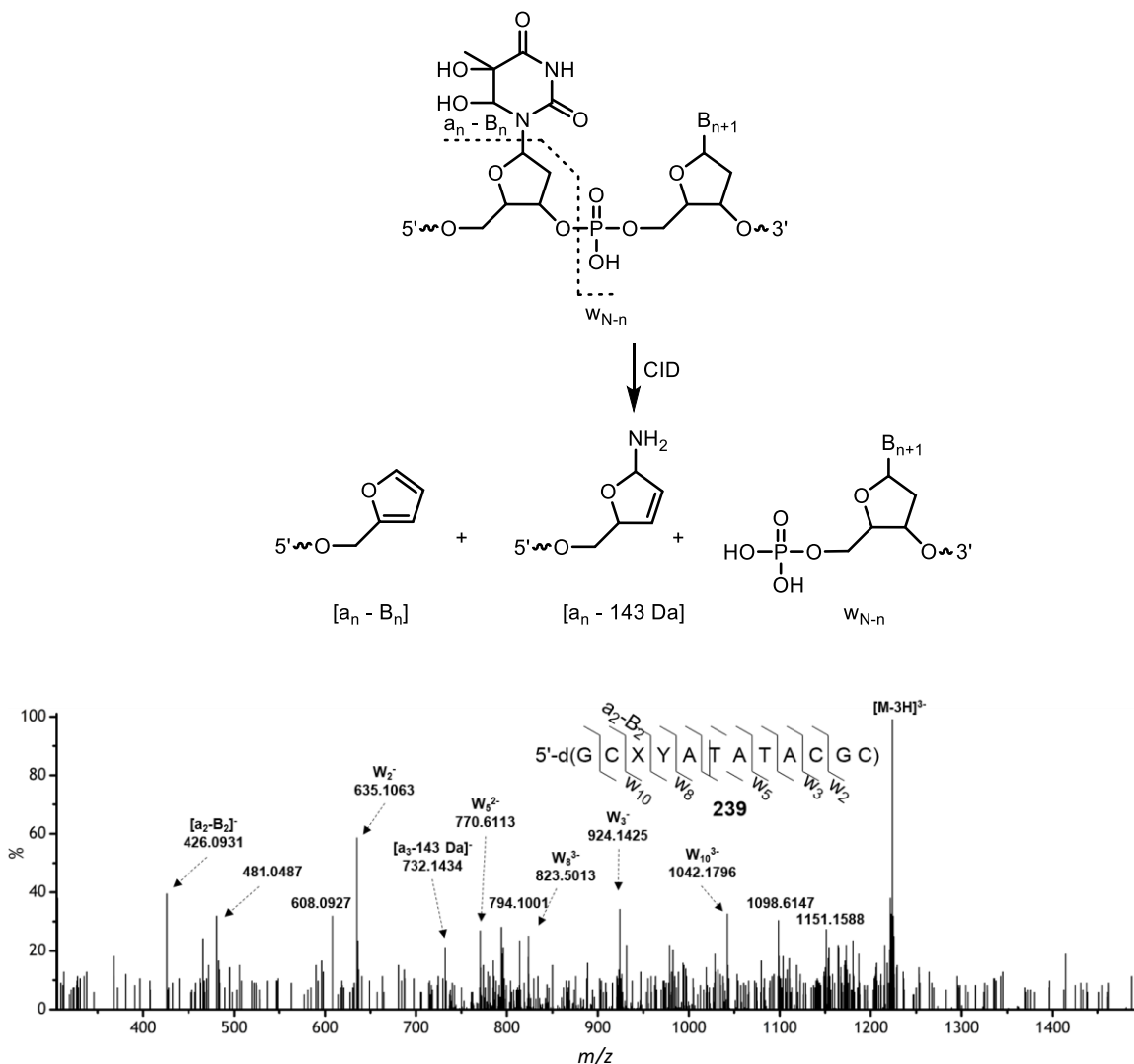
Figure 47. CID mass spectrum of the ion (*m/z* = 1221.6, *z* = 3) of the oligonucleotide containing tandem lesion **232** (**239**). X = Tg, Y = 5-fdU.

3.2.5.4 An alternative mechanism for the tandem lesion formation in poly(dA-T) sequences

3.2.5.4.1 Proposed mechanism for tandem lesion formation

We proposed a mechanism that is consistent with the structure of the tandem lesion (**232**), the sequence specificity of its formation, and previously characterized dA• reactivity.

The mechanism involves initial hydrogen atom abstraction from the C5-methyl group of the thymidine bonded to the 5'-phosphate of the neutral nitrogen radical (Scheme 59·). The initial hydrogen atom abstraction from the thymidine C5-methyl group by dA• explains the lack of tandem lesion formation in 5'-d(TUA) steps. Under aerobic conditions, T• is trapped by O_2 to form Tp•, which reacts with the 5'-adjacent pyrimidine by adding to the pyrimidine double bond. Addition at the C5-position of thymidine is shown in Scheme 59. However, we cannot distinguish between this pathway and addition to the C6-position.[305] Photolysis of **233** in the presence of β-mercaptoethanol (1 mM) eliminates the formation of **232** (within **239**) and is replaced by the product containing 5-hmdU (**240**) (Figure 48). This is consistent with the intermediacy of Tp• in tandem lesion formation. To further validate the addition of Tp• to the 5'-adjacent thymidine, photolysis in $^{18}O_2$ was carried out. Unfortunately, the photolysis (8 h) of samples sparged with $^{18}O_2$ resulted in the formation of a complicated mixture, and thus we were unable to identify the incorporation of ^{18}O by UPLC-MS/MS.

Scheme 59. An alternative mechanism for the formation of tandem lesion **232**.

163
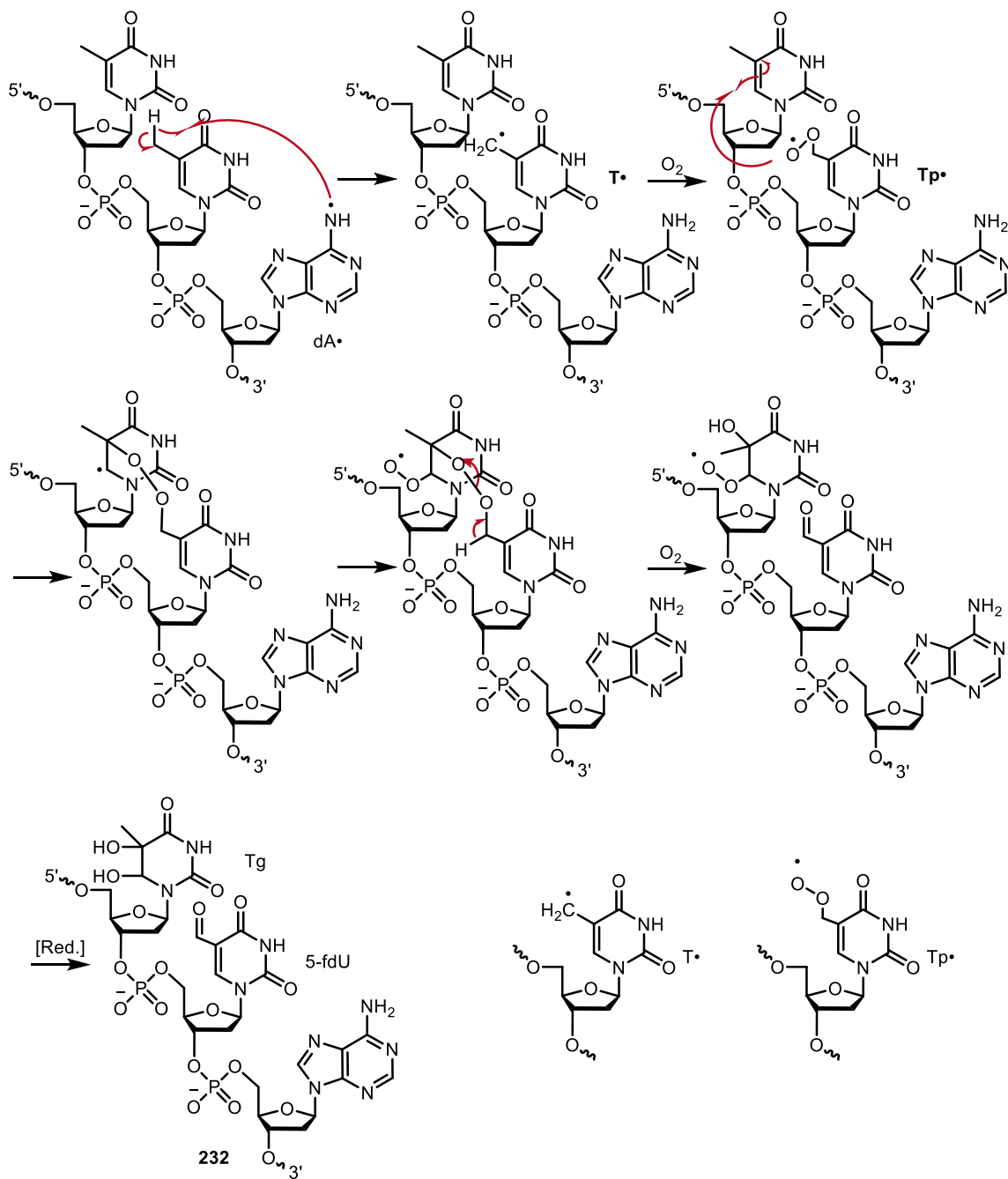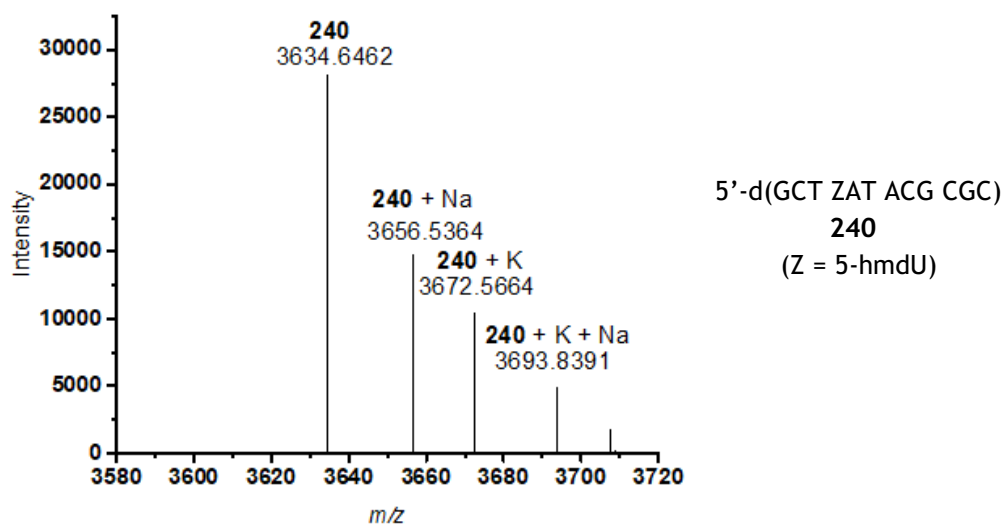
Figure 48. Deconvoluted mass spectrum of oligonucleotide generated after the photolysis of **233** in the presence of 1 mM BME.

Tp• addition to the 5'-adjacent pyrimidine may also explain the damage pattern observed in the the 5'-d(UT) sequence, which yields nearly identical strand cleavage at the two pyrimidine nucleotides. Peroxide **241** generated at dU gives rise to products such as 5-hydroxy-2'-deoxyuridine (Scheme 60 pathway a, 5-HOdU),[306] which does not yield strand scission upon alkali-treatment.[307-309] Furthermore, previous investigations in which pyrimidine peroxyl radicals are independently generated in duplex DNA have shown that alkali-labile lesion formation at a 5'-dU is less efficient than when thymidine is present at this position.[299] Tp• resulted from oxygen trapping the initially formed T• may also ultimately convert to 5-fdU yielding the oligonucleotide containing isolated lesions (Scheme 60 pathway b). [25]

164
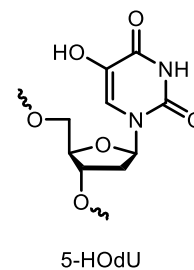
Scheme 60. Formation of the tandem lesion in 5'-d(UT) sequence.
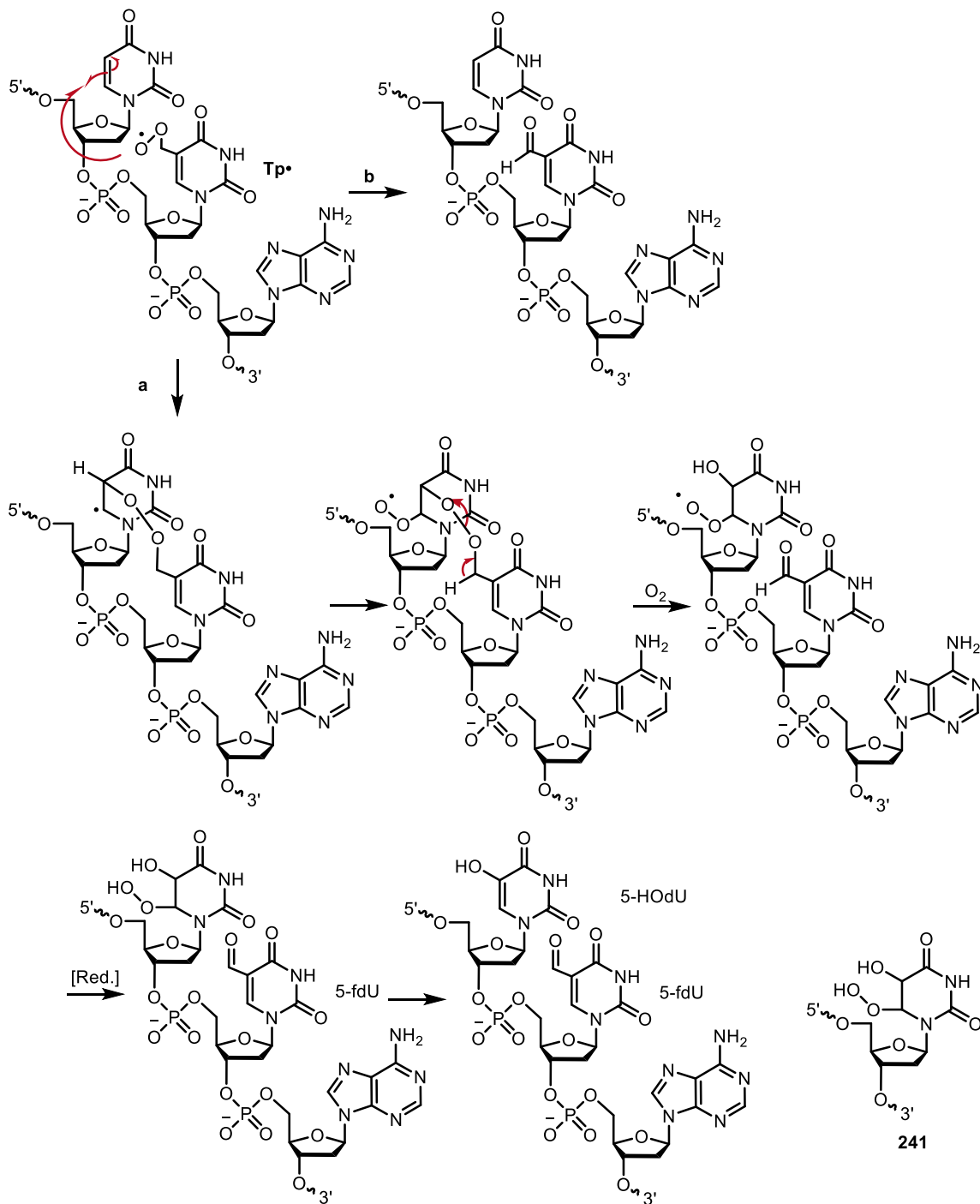
3.2.5.4.2 Distinguishing the alternative mechanism from the published PCET mechanism

Although we successfully reproduced tandem lesion formation in poly(dA-T) via independently generating dA•, these results were not sufficient to disprove the mechanism put forward by Schuster et al.,[25] because our experiments did not rule out the potential contributions of dA•+ and T•+ in tandem lesion formation. To distinguish the mechanism involving interstrand charge transfer from dA•+ to T and that proposed herein involving dA•, we designed anthraquinone tethered duplex **241** similar to duplex **18** designed by Schuster and coworkers,[24] which contains three 5'-d(TTT) steps and one 5'-d(TTU) step. The photoexcited anthraquinone was used to initiate hole migration, and the three 5'-d(TTT) steps acted as positive controls. As mentioned previously 5'-d(TTT) sequences were preferentially damaged at the central thymidine, followed by the 3'-terminal T, during hole migration initiated by anthraquinone excitation.[24-25] If the mechanism involves interstrand charge transfer generating T•+, the TT step in 5'-d(TTU) should give rise to a tandem lesion since the hole transferred from the dA•+ on the opposite strand will not be affected by the presence of dU (Scheme 61a). If the alternative mechanism proposed above is responsible for the products, substituting a single dU for thymidine at the 3'-terminus of a 5'-d(TTT) sequence should eliminate strand damage at that location because the 3'-adjacent dA• radical responsible for initiating tandem lesion formation will not have a C5-methyl hydrogen atom to abstract at the 5'-adjacent pyrimidine (Scheme 61b).

166

Scheme 61. The hypothesized mechanism for tandem lesion formation in a 5'-d(TTU) sequence.

AQ-5'-d(TTT TAA ATT AAA TTA AAT TAA ATA TAT TT)
3'-d(AAA AT**T** TAA T**T**T AAT T**T**A AT**T** TAT ATA AA)-5'-^{32}P
18

AQ-5'-d(TTT TAA A TT AAA TTA AA T TAA A TA TAT TT)
3'-d(AAA ATT T$_1$AA UTT$_2$ AAT TT$_3$A ATT T$_4$AT ATA AA)-5'-^{32}P
242

5'-d(TTT TTT TTA TAT$_{12}$ T$_{13}$X$_{11}$ 6 TAT ATT TTT TTT TTT)
3'-d(AAA AAA AAT ATA   A A   T ATA TAA AAA AAA AAA)
X$_{11}$
243: X$_{11}$ = dU
244: X$_{11}$ = T

AQ
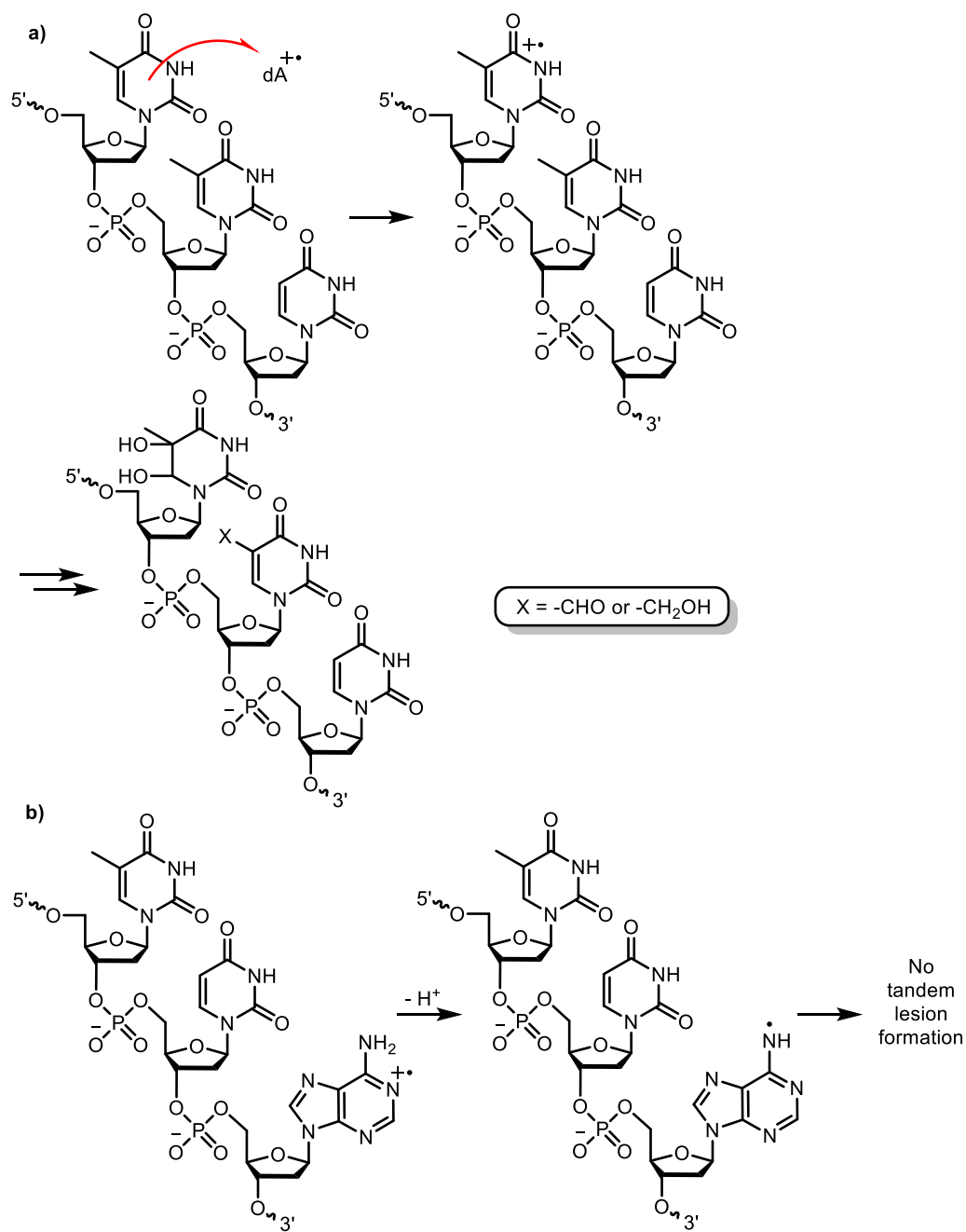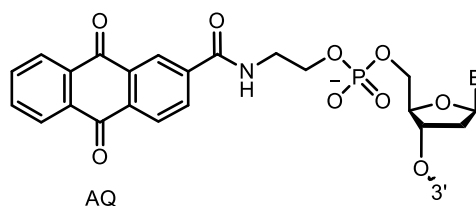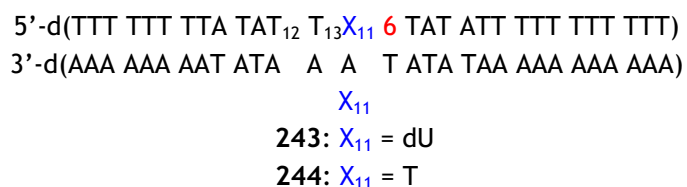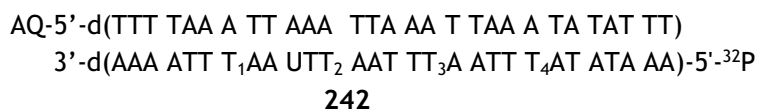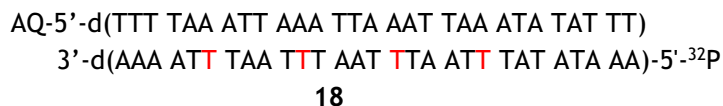
Photolysis of 5'-^{32}P-**242** led to no strand damage at the 5'-d(TTU) sequence (Figure

49a). Furthermore, the strand damages in 5'-d(TTT) steps were predominantly localized at

the central T's (Figure 49a). This observation was consistent with the previous report,[29]

which suggested that hole migration occurred as expected. Finally, the reactivity disparity

between 5'-d(TTT) and 5'-d(TTU) was reproduced by independently generating dA•.

Piperidine treatment of photolyzed 5'-^{32}P-**244** led strand cleavage at T$_{13}$, the central T of

the 5'-d(TTT) sequence. On the other hand, no tandem lesion formation was detected in

photolyzed 5'-^{32}P-**243** (Figure 49b). These observations were consistent with our proposed

mechanism (Scheme 61b). The mechanism proposed by Schuster et al. does not explain

the reactivity of 5'-d(TTU) sequences.[25] Given this result, along with the inconsistency

mentioned in Section 3.2.5.1, we disproved the mechanism (Scheme 10) involving the

formation of T•+. The alternative mechanism proposed (Scheme 59) is consistent with all of these observations, and dA• is the species that initiates the formation of tandem lesion **232**.
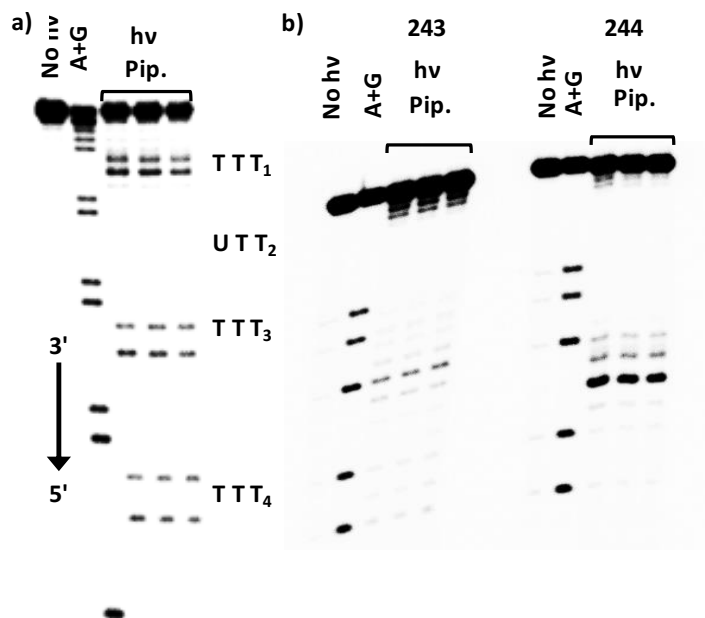
Figure 49. Distinguishing the interstrand charge transfer mechanisms and intrastrand hydrogen atom abstraction mechanism using PAGE analysis. (a) Autoradiogram of photoexcited anthraquinone induced strand damage in 5'-^{32}P-**242**. (b) Autoradiogram of aerobic photolysis of 5'-^{32}P-**243** and 5'-^{32}P-**244**, followed by piperidine treatment.

4.   Conclusions

In summary, in response to a dearth of methods for generating aminyl radicals photochemically, we successfully developed photochemical precursors for dA• (**3**, **6**), dG(N2-H)• (**4**, **7**), and dG(N1-H)• (**5**). Product studies reveal that the photolyses of theses precursors produce their corresponding neutral purine radicals with high fidelity. In addition, dA• is directly observed via laser flash photolysis under photosensitization conditions. Furthermore, **3**, **4**, **6**, and **7** are compatible with solid phase oligonucleotide synthesis conditions, and thus are potentially useful tools for mechanistic studies of neutral

purine radicals. Incorporation of **3** and **6** into DNA enabled us to investigate the reactivity of dA• in DNA, of which little was known prior to our studies.
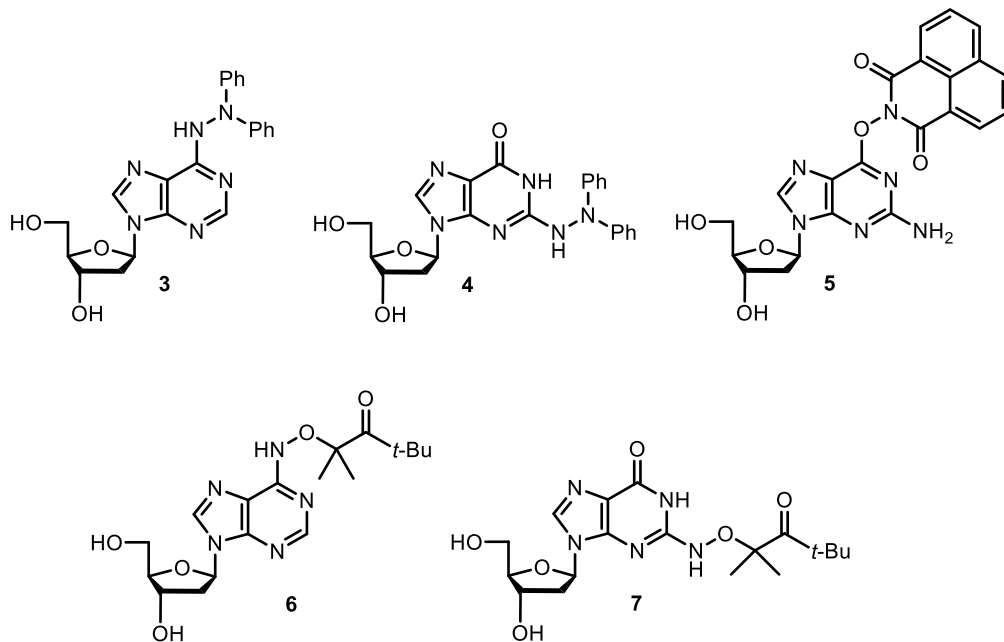
By incorporating **6** in DNA, We examined the proposal based on pulse radiolysis studies that dA• induces hole migration in DNA.[94] Hole migration by dA• was not observed. However, tandem lesion formation was observed in 5'-d(NGGT) sequences. The structure of this tandem lesion was characterized by analyzing intact oligonucleotides using UPLC-MS/MS, a powerful but underutilized method for DNA lesion characterization. Interestingly, dA• is repaired to dA in the final product. Therefore, the involvement of dA• is traceless by typical product analysis. We proposed that dA• initiates the formation of this tandem lesion by abstracting a hydrogen atom from the C5-methyl group of a 5'-adjacent thymidine to form 5-(2'-deoxyuridinyl)methyl radical (T•). The subsequently formed thymidine peroxyl radical (Tp•) adds to the 5'-adjacent dG, ultimately producing a 5'-[(8-oxo-dG)-(5-fdU)] tandem lesion (Scheme 55). The proposed mechanism is supported by UPLC-MS/MS, chemical reactivity experiments, isotopic labeling, as well as the

independent generation of T•. In addition, tandem lesions from dA• are formed relatively efficiently when flanked on the 5'-side by 5'-d(NGGT) sequences, which based upon statistics will appear $>10^6$ times in the human genome. Tandem lesions pose a greater challenge for base excision repair enzymes, and thus this tandem lesion is potentially relevant to human health.

Independent generation of dA• also allowed us to investigate the impact of flanking sequence on the pK_a of dA•+. We demonstrated, for the first time, that a flanking dA dramatically shifts the dA•+/dA• equilibrium and results in the formation of the radical cation (dA•+) that is produced from the direct effect (Figure 32b). Support for dA•+ formation is based on well-precedented DNA hole transfer chemistry. The experiments presented in this dissertation provide the first experimental evidence in DNA that π-stacking increases the pK_a of dA• at room temperature. It is believed that the direct and indirect effects of γ-radiolysis contribute approximately equally to DNA damage.[2, 46, 310] By independently generating dA•, a radical produced by the indirect effect, for the first time in DNA, we demonstrate that when flanked by another dA, dA• generation leads to DNA hole transfer, a process induced by the direct effect of ionizing radiation.[311-312] Results presented in this dissertation suggest that the indirect and direct effects γ-radiolysis are closely intertwined, and converge in a sequence-dependent manner.

The insights into dA• reactivity led us to revisit the tandem lesion(s) observed during hole migration in DNA that lacks dG.[29] Rather than invoking the higher energy T•+, we propose that dA• is responsible for the tandem lesion formation. Holes carried by dA•+ migrate throughout the poly(dA-T) sequences and are fixed at a particular location upon deprotonation. The resulting dA• initiates tandem lesion formation via initial hydrogen

atom abstraction from the C5-methyl group of a 5'-adjacent thymidine, a process also observed in tandem lesion formation in 5'-d(GT) sequences (Scheme 59). [313] Independent generation of dA• reproduced the sequence specificity of tandem lesion formation when holes are injected by photoexcited anthraquinones (Figure 43).[25] The structure of the tandem lesion was determined by UPLC-MS/MS. Furthermore, unlike the previously proposed mechanism, the alternative mechanism also correctly predicted the lack of strand damage in a 5'-d(TTU) sequence using anthraquinone (Figure 49). Finally, in the alternative mechanism proposed by us, dA• is repaired by initial hydrogen atom abstraction, which serves as a second example for the traceless involvement of dA• in the formation of tandem lesions.

The role of nitrogen-centered neutral purine radicals in DNA damage has been overshadowed by other nucleoside reactive intermediates, carbon-centered radicals and radical cations. Unlike radical cations, nitrogen-centered radicals do not react with water.[77] Nitrogen-centered radicals also do not react rapidly with O_2, unlike carbon radicals.[157, 299, 314-315] Consequently, nitrogen-centered radicals may not directly yield DNA lesions, and other reaction pathways of nitrogen-centered radicals may be competitive in DNA. Considering the frequent formation of neutral purine radicals, their heretofore minor role in DNA damage is surprising.[316] With the capability of site-specific independent generation dA•, we demonstrated tandem lesion formation initiated hydrogen atom abstraction by dA•, and sequence-dependent protonic equilibrium of dA•/dA•+. These results raise the possibility that nitrogen-centered neutral purine radicals and other heteroatom-centered radicals may play important, general roles in DNA damage.

5.   Future directions

The results presented here suggest several potential future experiments. The acetophenone sensitized photolyses of **6** and **7**, and direct photolysis of **5** is very efficient. We expect to be able to observe the transient spectra of dA•, dG(N2-H)•, and dG(N1-H)• with sufficient signal strength in aqueous buffer or buffer-acetonitrile mixtures. This will allow us to determine the reactivity of these radicals towards H_2O, O_2, and other species, such as thiols. Furthermore, with the capability of unequivocally generating dG(N2-H)• and dG(N1-H)•, the two tautomers of dG•, we will be able to investigate the tautomerization between these two species.[36-37, 69, 95] We expect to determine whether this tautomerization happens, and measure the rate of tautomerization.

There is no precursor for dG(N1-H)• or dG(N2-H)• that can be used in DNA polymer studies at this point. Precursor **7** requires sensitization to achieve photocleavage efficiency that is useful for mechanistic studies. On the other hand, photolysis of precursor **5** in the presence of O_2 leads to the generation of singlet O_2,[257] which will hamper studies on the reactivity of dG(N1-H)• in DNA in the presence of O_2 by generating unwanted damage. Furthermore, the reactivity of naphthalimidyl radical (**181**) towards DNA is also unclear. In addition, incorporation of **5** into oligonucleotides might be challenging, considering N-hydroxy-naphthalimide (**178**) is a reasonable leaving group and may not be compatible with common solid-phase synthesis deprotection conditions. For these reasons, precursors based on intramolecular sensitization (e.g. **145**) are particularly attractive. Intramolecular sensitization reduces the possibility of undesirable photooxidation of DNA, and thus is potentially useful for polymer studies.

181 **145**
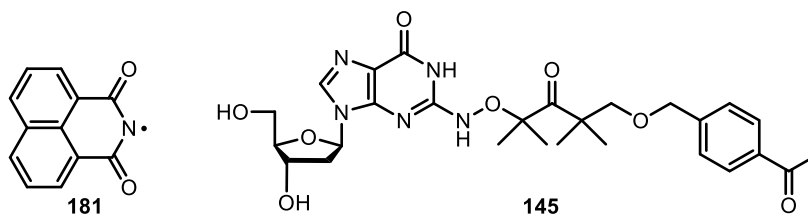
Lastly, the reactivity of $dC_{im}\bullet$ is unclear.[40, 71, 75] We propose that the reactivity of $dC_{im}\bullet$ may be similar to that of $dA\bullet$, because the spin density of $dC_{im}\bullet$ also resides in the major groove of B-form DNA, and the BDE of N-H bond is ~100 kcal mol^{-1}.[317] We envision that $dC_{im}\bullet$ can be accessed by photolyzing precursor **245**. It is also worth noting that imino tautomer is favored in **245**, which grants us direct access to $dC_{im}\bullet$ without generating the amino tautomer $dC\bullet$.[318]

245 $dC_{im}\bullet$ $dC\bullet$
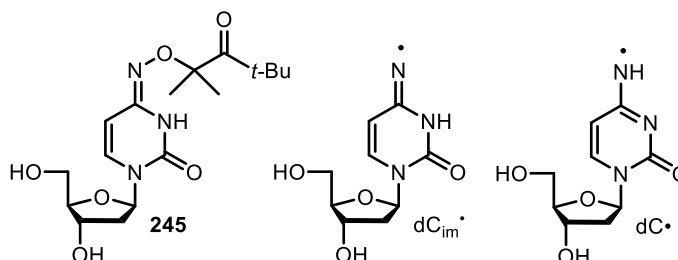
6.   Experimental

Materials and methods. Dichloromethane, DIPEA, DME, DMF, toluene, and pyridine were distilled from CaH_2. THF and dioxane were distilled from sodium. All other reagents were purchased from commercial sources and were used without further purification unless noted otherwise. T4 polynucleotide kinase (T4 PNK), human 8-oxoguanine DNA N-glycosylase 1 (hOGG1), endonuclease V (Endo V), and terminal transferase were obtained from New England Biolabs. DNA Degradase Plus was obtained from Zymo Research. γ-^{32}P-ATP and α-^{32}P-cordycepin 5'-triphosphate were purchased from Perkin Elmer. C18-Sep-Pak cartridges were obtained from Waters. PBS buffer (0.1

M NaCl, 10 mM sodium phosphate, pH 7.2) and water were treated with Chelex® 100 resin (BioRad). All reactions were carried out under a positive pressure of argon atmosphere and monitored by TLC on Silica Gel G-25 UV254 (0.25 mm) plates unless stated otherwise. Spots were detected under UV light and/or by ethanolic solution p-anisaldehyde, or aqueous solution of ammonium molybdate. Column flash chromatography was performed with Silicycle® grade 70−230 mesh, 60−200 μm, 60 Å silica. UV absorbance was measured with a Thermo Scientific NanoDrop® 2000c spectrometer. UV-melting was measured with a Beckman DU® 640 spectrometer. HPLC was performed on a Phenomenex Luna C-18 column (250 × 4.6 mm). ESI-MS was carried out on a Thermoquest LCQDeca. UPLC-MS/MS analyses were carried out on Waters Acquity/ Xevo-G2 UPLC-MS system equipped with an ACQUITY UPLC HSS T3 Column (100 Å, 1.8 μm, 2.1 mm × 100 mm), Oligonucleotide BEH C18 Column (130 Å, 1.7 μm, 2.1 mm × 100 mm), or Thermo Scientific Hypercarb column (130 Å, 5 μm, 2.1 × 100 mm,). Oligonucleotide masses were obtained via deconvolution using MassLynx 4.1 software. CID fragmentation patterns were processed using Microsoft Excel. MALDI-TOF analyses were carried out on a Bruker AutoFlex III Maldi-TOF MS. Quantification of radiolabeled oligonucleotides was carried out using a Molecular Dynamics Phosphorimager 860 equipped with ImageQuant Version TL software.

Procedure for the photolysis of precursors and subsequent HPLC analysis. Photolyses were carried out in Pyrex tubes using a Rayonet photochemical reactor (Southern New England Ultraviolet) equipped with a merry-go-round apparatus and 16 lamps having a maximum output at 350 nm. Photolyses were carried out at 25 °C. This temperature was maintained by using the fan at the bottom of the unit provided by the

manufacturer and a Dayton® 239 CFM AC axial fan at the top facing such that air flowing through the unit is drawn out through the top. Reaction mixtures (50 μL each) containing precursor (100 μM), internal standard (thymidine, 100 μM), and additives (reducing agents, organic solvent, sensitizers) in buffer (10 mM phosphate, pH 7.2) were photolyzed at room temperature under aerobic or anaerobic conditions. Samples for anaerobic reactions were degassed by three freeze-pump-thaw cycles at 2 mTorr and flame sealed under vacuum. Samples containing acetone or a high percentage of acetonitrile (> 30%) were evaporated to dryness and resuspended in water. Samples using thiophenol as reducing agent were washed with hexanes (3 × 50 μL), evaporated to dryness and resuspended in water before HPLC analysis.

The reaction mixtures (including unphotolyzed controls) were analyzed by reversed-phase HPLC while being monitored at 260 nm and 284 nm. HPLC was performed on a Phenomenex Luna C-18 column (A, water; B, ACN; 3% B from t = 0 to t = 1 min; 3-28% B linearly over 9 min; 28-97% B linearly over 5 min; 97% B from t = 25 to t = 20 min; 97-3% B linearly over 2 min; 3% B from t = 22 to t = 42 min; flow rate, 1 mL/min). The retention times of the internal standard, precursors, and products generated by photolysis are listed in Table 13. The peaks were integrated and quantified against the internal standard (thymidine), and the response factors are reported in Table 13.

Table 13. Retention times and response factors for HPLC analysis.

Compound	Retention time (min)	Response factor (260 nm)
T	8.2	
dA	8.9	0.66

dG	7.4	0.84
dI	5.4	1.12
3	16.1	1.13
4	15.4	0.71
5	15.5	2.2
6	15.4	0.75
7	15.1	0.78
180	16.0	9.1

Cyclic voltammetry.[a] A solution of the nucleoside (e.g. **3**) was prepared in acetonitrile containing 0.1 M tetrabutylammonium perchlorate (TBAP). Subsequently, the solution was saturated with nitrogen. A three-electrode system was utilized to carry out cyclic voltammetric studies of these N_2-saturated solutions: glassy carbon as the working electrode, Pt wire as the counter electrode, and Ag wire as the reference electrode. The scan rate was 100 mV/s. The conditioning potential was set at 0 V. The cyclic voltammetric scan was started along with the anodic pathway, followed by the cathodic pathway. This was done to avoid the probable interference from the reduction process. All potentials were calibrated based on Fc^+/Fc (Fc=ferrocene) toward the normal hydrogen electrode (NHE). The redox potentials of dG and 8-oxo-dG were determined by employing 10 mM of each nucleoside. The redox potentials of **3** and **4** were obtained at 0.15 mM.

Determination of the quantum yield for photoconversion of 6 and 7 in acetonitrile under continuous photolysis. The light flux of the photoreactor was determined by using 2-hydroxy-2-methylpropiophenone actinometry in acetonitrile. 2-Hydroxy-2-

---

[a] The cyclic voltammetry studies were carried out in collaboration with Lu Lin, Ke Qu, Amitava Adhikary , Michael D. Sevilla in the Department of Chemistry at Oakland University.

methylpropiophenone has a 0.38 quantum yield for Norrish type I cleavage.[319] Solutions containing the actinometer (50 μL, 320 mM) were degassed using 3 freeze–pump–thaw cycles and sealed under high vacuum prior to photolysis. The extent of reaction of the actinometer was measured using an Agilent 6890N GC equipped with an Agilent HP-5 column (30 m × 0.320 mm, 0.5 micron film)) from t = 0 to 1 min holding 80 °C, from t = 1 to 10 min, from 80 °C - 240 °C linearly, from t = 10 to 16 min, from 200 °C - 310 °C linearly over 5 min. The conversion of 2-hydroxy-2-methylpropiophenone (retention time = 4.09 min) was determined after 30 min of photolysis using dodecane (retention time = 3.62 min) as internal standard. The conversion of the actinometer was 30.0 ± 0.7%. The optical density at 350 nm (OD_{350}) changed from 3.2 to 2.4. Therefore, the change of transmittance was negligible during photolysis. Using eqn. 8, the light flux was calculated to be $(4.2 \pm 0.1) \times 10^{-7}$ Einstein·min^{-1}. Solutions containing **6** (50 μL, 100 μM) had an OD_{350} at 0.016. The OD_{350} of solution containing **7** (50 μL, 100 μM) was estimated using a 10 mM solution of **7** to be 0.0009 samples containing were degassed and photolyzed for 60 min using the calibrated photoreactor. The extent of reaction of **6** was determined by HPLC using thymidine as internal standard. The conversion of **6** was 30 ± 1%. The quantum yield for conversion of precursor **6** was calculated using eqn. 9, and determined to be $(1.5 \pm 0.1) \times 10^{-3}$. Similarly, 6 h photolysis of samples containing **7** resulted in 12.4 ± 0.5% conversion, and the quantum yield of conversion of precursor **7** was determined to be $(1.8 \pm 0.1) \times 10^{-3}$.

$$\text{Light flux} = \frac{n_{actinometer\ conversion}}{\Phi_{actinometer}\ t_{photolysis}} \qquad \text{eqn. 8}$$

$$\Phi_x = \frac{n_{x\ conversion}}{\left(1 - \frac{\%T}{100}\right)(Light\ flux) \times t_{photolysis}} \qquad \text{eqn. 9}$$

Determination of the quantum yield for photoconversion of 5 in acetonitrile under continuous photolysis. The light flux of the photoreactor was determined by N-hydroxynaphthalimide triflate actinometry in acetonitrile. N-Hydroxynaphthalimide triflate has a 0.23 quantum yield for N-O bond cleavage.[171-172] Solutions containing the actinometer (50 μL, 50 mM) were degassed using 3 freeze–pump–thaw cycles and sealed under high vacuum prior to photolysis. The extent of reaction of the actinometer was measured by UV absorbance at 360 nm. The conversion of the actinometer was 12.4% in 30 s. the % transmittance of actinometer solution was less than 0.1% during the photolysis. Therefore, the change of transmittance was negligible during photolysis. Using eqn. 8, the light flux was calculated to be $(2.5 \pm 0.1) \times 10^{-7}$ Einstein·min^{-1}. Solutions containing **5** (50 μL, 100 μM) had an OD_{350} at 1.72. The samples were degassed and photolyzed for 1 min using the calibrated photoreactor. The extent of reaction of **5** was determined by HPLC using thymidine as internal standard. The conversion of **5** was 30.7 ± 0.9 %. The quantum yield for conversion of precursor **5** was calculated using eqn. 9, and determined to be 0.03.

Nanosecond transient absorption.[b] Experiments were performed on an LFP-112 spectrometer (Luzchem, Canada) employing an EX10 (GAM Laser, USA) XeCl Excimer laser (308 nm, ca. 12 mJ/pulse, ca. 12 ns pulse width) for excitation. The transient absorption spectra were recorded in acetonitrile or buffer mixtures (phosphate 10 mM, pH 7.4) in a quartz cuvette (1 x 1 cm²) equipped with a septum under a nitrogen atmosphere (bubbled for 10 minutes before measurement).

---

[b] The nanosecond transient absorption was measured in collaboration with Markus Griesser and Derek A. Pratt in the Department of Chemistry & Biomolecular Sciences at University of Ottawa.

Oligonucleotide synthesis. Oligonucleotides were synthesized on an Applied Biosystems Incorporated 394 oligonucleotide synthesizer. Oligonucleotide synthesis reagents were purchased from Glen Research (Sterling, VA). Commercially available CE phosphoramidites were used for synthesizing unmodified oligonucleotides. Deprotection of unmodified oligonucleotides was performed with concentrated aqueous ammonia-methylamine (v/v = 1:1, 1 mL) at 65 °C for 1 h, followed by concentration under reduced pressure.

Commercially available CE phosphoramidites were used for DNA synthesis of oligonucleotides containing **3** or anthraquinone (AQ). A 5 min coupling time was used for the modified phosphoramidites. Deprotection of synthesized oligonucleotides was performed with concentrated aqueous ammonia-methylamine (v/v = 1:1, 1 mL) at 65 °C for 1 h, followed by concentration under reduced pressure.[144]

Commercially available UltraMILD CE phosphoramidites were used for DNA synthesis of oligonucleotides containing **6**. A 5 min coupling time was used for the modified phosphoramidite **193**. Deprotection of synthesized oligonucleotides containing **6** was performed with concentrated aqueous ammonia at room temperature for 16 h, followed by concentration under reduced pressure.

Commercially available UltraMILD CE phosphoramidites and UltraMild Cap Mix A (5% phenoxyacetic anhydride in THF/pyridine) were used for DNA synthesis of oligonucleotides containing 5,6-dihydrothymidine (dHT). A 5 min coupling time was used for the dHT phosphoramidite. Deprotection of synthesized oligonucleotides

containing dHT was performed with concentrated aqueous ammonia at room temperature for 2 h, followed by concentration under reduced pressure.[320]

Commercially available UltraMILD CE phosphoramidites were used for DNA synthesis of oligonucleotides containing **210**. A 5 min coupling time was used for the modified phosphoramidite. Pivaloyl anhydride/2,6-lutidine/THF (1:1:8) was used as capping reagent and 1 M t-butyl-hydroperoxide in toluene was used as oxidizing reagent. The oxidation time is 40 s, and the capping time is 25 s. Deprotection of synthesized oligonucleotides containing **210** was performed with concentrated aqueous ammonia at room temperature for 5 h, followed by concentration under reduced pressure.[279, 321]

The oligonucleotides were purified using 20% denaturing PAGE. Oligonucleotides were eluted from polyacrylamide gel with elution buffer (10 mL, 200 mM NaCl, 1 mM EDTA) at room temperature for 12 h and desalted using C18-Sep-Pak cartridges. Oligonucleotides containing **210** were subjected to additional purification HPLC on a Phenomenex Luna C-18 column (A: 0.05 M TEAA (pH 7.0)/MeCN 95:5; B: 0.05 M TEAA (pH 7.0)/MeCN 50:50; 0% B from t = 0 to t = 5 min; 0-15% B linearly over 15 min; 15-22% B linearly over 35 min; 22-80% B linearly over 5 min; 80-0% B linearly over 5 min; 0% B from t = 65 to t = 75 min; flow rate, 1 mL/min).[322] The extinction coefficients at 260 nm of modified oligonucleotide were calculated using IDT OligoAnalyzer® program based on nearest neighbor method,[323] and the modified nucleotide were treated as their unmodified counterparts. The concentrations of oligonucleotides were determined using their absorbance at 260 nm. Anthraquinone (AQ)-modified oligonucleotide solution concentrations were determined using the absorbance of the anthraquinone at 333 nm (5.5×10^3 M^{-1} cm^{-1}).[144]

UV melting experiments. Solutions containing a single-stranded oligonucleotide (1 μM) and their corresponding complementary oligonucleotide (1 μM) were prepared in hybridization buffer (200 μL, 100 mM NaCl, 10 mM sodium phosphate, pH 7.2) and were hybridized by heating the samples to 90 °C and slowly cooled to 17 °C. Melting studies were carried out in 1 cm path length quartz cells. Absorbance at 260 nm was monitored while the temperature was ramped at a rate of 1.0 °C/min from 20 °C to 70 °C. Experiments were carried out in duplicate.

Photolysis of oligonucleotides. The strand (1 μM) containing the radical precursor was labeled at the 5'-terminus with γ-^{32}P-ATP using T4 PNK (30 units) in T4 PNK buffer (70 mM Tris-HCl, pH 7.6, 10 mM MgCl$_2$, 5 mM DTT, 1 h, 37 °C). Alternatively, the strand (1 μM) containing the radical precursor was labeled at the 3'-terminus with α-^{32}P-cordycepin triphosphate using terminal transferase (40 units) in CoCl$_2$ (250 μM) and TdT buffer (20 mM Tris-HOAc, pH 7.9, 50 mM KOAc, 10 mM Mg(OAc)$_2$, 1 h, 37 °C). The labeled strand was hybridized to the complementary strand (1.5 eq.) in PBS by heating at 90°C for 1 min and slowly cooling to room temperature. The hybridized duplexes were diluted to 0.1 μM in PBS before photolysis. All photolyses were carried out in Pyrex tubes using a Rayonet photoreactor equipped with 16 lamps having a maximum output at 350 nm. All anaerobic photolyses were carried out in sealed Pyrex tubes, which were degassed by freeze-pump-thaw degassing (3 cycles). Samples were sealed while under vacuum at 77 K. Photolyses of DNA containing **3** and **6** were carried out for 4 h and 8 h respectively.

Post-photolysis treatments. Aliquots from photolyzed solutions or unphotolyzed controls were treated with piperidine (1 M, 30 min, 90 °C), Fpg (1.25

µM, 1 µL, 10 mM Bis Tris-Propane HCl (pH 7), 10 mM $MgCl_2$, 1 mM DTT, 100 µg/mL BSA, 1 h, 37 ℃), ARP (1 mM, 1 h, 37 °C), Endo V (10 units, 1 µL, 50 mM KOAc, 20 mM Tris-acetate, 10 mM $Mg(OAc)_2$, 1 mM DTT, 1 h, 37 °C) or Ir^{4+} (0.1 mM of $Na_2IrCl_6•6H_2O$) for 1 h at 25 °C, quenched (2 mM Hepes, 10 mM EDTA, pH 7), followed by treatment with piperidine (1 M, 30 min, 90 ℃). Alternatively, photolysates were treated with piperidine (1 M, 30 min, 90 ℃) in the presence of 0.25 M BME. In addition, the photolysates were treated with $NaBH_4$ (100 mM, 1 h, 4 °C), prior to piperidine treatment (1 M, 30 min, 90 ℃), or hOGG1 (8 units, 50 mM NaCl, 10 mM Tris-HCl (pH 7.9), 10 mM $MgCl_2$, 1 mM DTT, 100 µg/mL BSA) for 1 h at 37 °C, followed by NaOH (1 M, 30 min, 37 ℃). NaOH treated samples were neutralized with HCl (1 equiv.). All samples treated with enzymes were precipitated (0.3 M NaOAc, pH 5.2, 0.1 g/mL calf thymus DNA) with ethanol. Piperidine treated samples were evaporated to dryness under vacuum and washed with 2 × 10 µL water, which was also removed under vacuum. Samples were analyzed by dissolving in formamide loading buffer prior to analyzing by 20% denaturing PAGE. BME, piperidine, $NaBH_4$, and Ir^{4+} solutions were prepared fresh on the day of the experiment.

Enzymatic digestion of oligonucleotides to 2'-deoxynucleosides for UPLC analysis. Duplexes **179**, **180**, and the corresponding photolysates (10 µL, 2 µM) in 1 × PBS buffer, 5 µL water, 10 × DNA Degradase Plus® buffer (2.5 µL) and dU (2.5 µL, 100 µM) as internal standard were incubated with DNA Degradase Plus® (5 µL, 5 U/µL) for 4 h at 37 °C. The reaction mixture was filtered through a nanosep® 3K filter by centrifuging the mixture for 5-10 min at 16000 × g. The filter was washed once with H_2O (25 µL) and the combined filtrate (50 µL) was analyzed using an Agilent

1290 infinity UPLC equipped with the ACQUITY UPLC HSS T3 Column (A, 10 mM ammonium formate; B, acetonitrile; 5% B from t = 0 to t = 2 min; 5-80% B linearly over 7.5 min; 80% B from t = 9.5 to t = 12.5 min; 80-5% B linearly over 1 min; 5% B from t = 13 to t = 16 min; flow rate, 0.3 mL/min.)

UPLC and UPLC-MS/MS analysis of oligonucleotides. Photolysates (8 μL) containing 5 μM of duplex dodecamer were analyzed by UPLC-MS/MS using the Oligonucleotide BEH C18 Column (A, 100 mM HFIP and 8.6 mM TEA; B, Methanol; 2% B from t = 0 to t = 5 min; 2-9% B linearly over 3 min; 9% B from t = 8 to t = 20 min; 9-30% B linearly over 5 min; 30% B from t = 25 to t = 30 min; 30-2% B linearly over 5 min; 2% B from t = 35 to t = 40 min; flow rate, 0.2 mL/min.). The column temperature was 60 °C. The collision energy was set to ramp from 10 to 45 V. MS Conditions: capillary, 2 kV; sample cone, 40 V; extraction cone 4 V; source temperature, 130 °C; desolvation temperature, 500 °C; gas flow, 0.3 mL min^{-1}.

Photolysis of oligonucleotides in the presence of H$_2$^{18}O and ^{18}O$_2$. For photolyses carried out in H$_2$^{18}O, 100 μL of the double-stranded oligonucleotide in 1x PBS buffer was concentrated using the SpeedVac and redissolved in 100 μL H$_2$^{18}O. For photolyses carried out using ^{18}O$_2$, the sample was sparged with ^{18}O$_2$ while on ice for 15 min, and the tube was subsequently sealed with a torch. The subsequent photolysis was carried out according to the typical procedures.
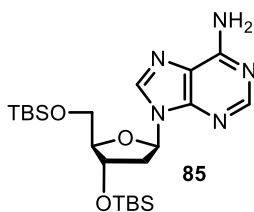
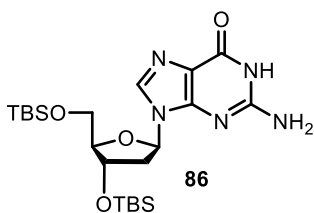**Preparation of 85.** 2'-Deoxyadenosine monohydrate (673 mg, 2.5 mmol) and imidazole (1.02 g, 15 mmol) were dissolved in anhydrous DMF (10 mL). *t*-Butyldimethylsilyl chloride (1.126 g, 7.5 mmol) was slowly added, and the reaction was stirred at room temperature overnight. The resulting mixture was washed with water and saturated NaHCO$_3$, extracted with DCM (3 × 50 mL), and dired over Na$_2$SO$_4$. Na$_2$SO$_4$ was removed via filtration. The organic phase was concentrated under vacuum and purified by flash chromatography on a silica column. Elution with 3% MeOH in DCM gave **85** as a white solid (948 mg, 80%). ^{1}H NMR (400 MHz, CDCl$_3$) δ 8.35 (s, 1H), 8.13 (s, 1H), 6.45 (t, *J* = 6.4 Hz, 1H), 5.62 (s, 2H), 4.61 (dt, *J* = 5.7, 3.3 Hz, 1H), 4.01 (dd, *J* = 7.3, 3.3 Hz, 1H), 3.87 (dd, *J* = 11.2, 4.2 Hz, 1H), 3.77 (dd, *J* = 11.2, 3.2 Hz, 1H), 2.70 – 2.57 (m, 1H), 2.43 (ddd, *J* = 13.1, 6.2, 3.9 Hz, 1H), 0.91 (s, 9H), 0.91 (s, 9H), 0.10 (s, 6H), 0.09 (s, 3H), 0.09 (s, 3H).
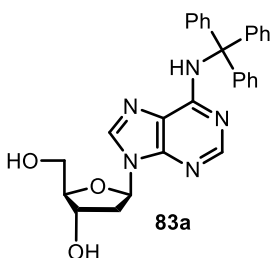
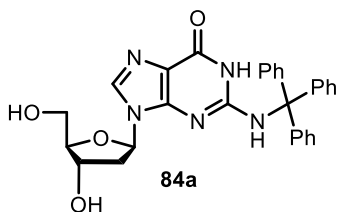**Preparation of 83a.** Compound **85** (47.5 mg, 0.1 mmol) was azeotropically dried 3 times using pyridine (2 mL × 3) and disolved in pyridine (2 mL). Triphenylmethyl chloride **75** (45 mg, 0.16 mmol) was added to the solution. The reaction was stirred at 100 ºC for 12 h, while a water-cooled condenser was attached to the round bottom flask. The reaction mixture was concentrated under vacuum and dissolved using THF (2 mL). Et$_3$N•3HF (161 mg, 1.0 mmol) was slowly added to the solution. The reaction was stirred overnight at room temperature. The reaction mixture was concentrated under vacuum and purified by flash chromatography on a silica column. Elution with 3% MeOH in DCM gave

83a as a white solid (17.8 mg, 36%). ^{1}H NMR (MeOH-d$_4$) δ 8.34 (s, 1H), 7.84 (s, 1H), 7.42 – 7.11 (m, 15H), 6.40 (dd, J = 7.9, 6.0 Hz, 1H), 4.61 – 4.48 (m, 1H), 4.05 (d, J = 2.6 Hz, 1H), 3.82 (dd, J = 12.3, 2.9 Hz, 1H), 3.71 (dd, J = 12.3, 3.4 Hz, 1H), 2.79 (ddd, J = 13.6, 8.0, 5.8 Hz, 1H), 2.39 (ddd, J = 13.6, 6.0, 2.7 Hz, 1H).

Preparation of 86. 2'-Deoxyguanosine monohydrate (1.425 g, 5 mmol) and imidazole (2.04 g, 30 mmol) were dissolved in anhydrous DMF (20 mL). t-Butyldimethylsilyl chloride (2.25 g, 15 mmol) was slowly added, and the reaction was stirred at room temperature overnight. The resulting mixture was washed with water and saturated NaHCO$_3$, extracted with DCM (3 × 200 mL), and dried over Na$_2$SO$_4$. Na$_2$SO$_4$ was removed via filtration. The organic phase was concentrated under vacuum, and purified by flash chromatography on a silica column. Elution with 5% MeOH in DCM gave **86** as a white solid (1.83 g, 75%). ^{1}H NMR (400 MHz, CDCl$_3$) δ 7.80 (s, 1H), 6.24 (t, J = 6.4 Hz, 1H), 5.90 (s, 2H), 4.63 – 4.48 (m, 1H), 3.97 (dd, J = 7.2, 3.6 Hz, 1H), 3.80 (dd, J = 11.2, 4.1 Hz, 1H), 3.75 (dd, J = 11.2, 3.2 Hz, 1H), 2.56 – 2.46 (m, 1H), 2.41 – 2.29 (m, 1H), 0.91 (s, 18H), 0.10 (s, 6H), 0.08 (s, 3H), 0.08 (s, 3H).

Preparation of 84a. Compound **86** (49.4 mg, 0.1 mmol) was azeotropically dried 3 times using pyridine (2 mL × 3) and dissolved in pyridine (2 mL). Triphenylmethyl chloride **75** (45 mg, 0.16 mmol) was added to the solution. The reaction was stirred at 100 ºC for 12 h, while a water-cooled condenser was attached to the round bottom flask. The reaction mixture was concentrated under vacuum and

186

dissolved using THF (2 mL). Et₃N•3HF (161 mg, 1.0 mmol) was slowly added to the solution. The reaction was stirred overnight at room temperature. The reaction mixture was concentrated under vacuum and purified by flash chromatography on a silica column. Elution with 3% MeOH in DCM gave **84a** as a white solid (37.8 mg, 74%). ^{1}H NMR (400 MHz, MeOH-d₄) δ 7.90 (s, 1H), 7.45 – 7.07 (m, 17H), 5.61 (t, J = 6.5 Hz, 1H), 4.18 (dt, J = 7.0, 3.7 Hz, 1H), 3.80 (q, J = 3.7 Hz, 1H), 3.55 (d, J = 1.4 Hz, 1H), 3.54 (d, J = 1.4 Hz, 1H), 2.02 (dt, J = 13.2, 6.4 Hz, 1H), 1.85 (ddd, J = 13.2, 6.2, 3.9 Hz, 1H).
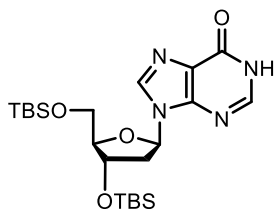
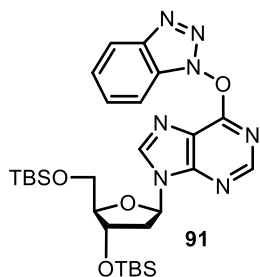3',5'-bis-O-(*t*-butyldimethylsilyl)-2'-deoxyinosine

Preparation of 3′,5′-bis-O-(*t*-butyldimethylsilyl)-2′-deoxyinosine. 2'-Deoxyinosine (630 mg, 2.5 mmol) and imidazole (1.02 g, 15 mmol) were dissolved in anhydrous DMF (10 mL). *t*-Butyldimethylsilyl chloride (1.126 g, 7.5 mmol) was slowly added, and the reaction was stirred at room temperature overnight. The resulting mixture was washed with water and saturated NaHCO₃, extracted with DCM (3 × 50 mL), and dried over Na₂SO₄. Na₂SO₄ was removed via filtration. The organic phase was concentrated under vacuum, and purified by flash chromatography on a silica column. Elution with 5% MeOH in DCM gave 3′,5′-bis-O-(*t*-butyldimethylsilyl)-2′-deoxyinosine as a white solid (1.07 g, 89%). ^{1}H NMR (400 MHz, CDCl₃) δ 8.18 (s, 1H), 8.16 (s, 1H), 6.44 (t, J = 6.4 Hz, 1H), 4.63 (dt, J = 5.6, 3.7 Hz, 1H), 4.04 (dd, J = 7.2, 3.7 Hz, 1H), 3.87 (dd, J = 11.2, 4.1 Hz, 1H), 3.80 (dd, J = 11.2, 3.1 Hz, 1H), 2.65 – 2.51 (m, 1H), 2.51 – 2.36 (m, 1H), 0.94 (s, 9H), 0.94 (s, 9H), 0.13 (s, 6H), 0.11 (s, 3H), 0.11 (s, 3H).

Preparation of 91.[200] 3′,5′-Bis-O-(*t*-butyldimethylsilyl)-2′-deoxyinosine (481 mg, 1 mmol) and (benzotriazol-1-yloxy)tris(dimethylamino)phosphonium hexafluorophosphate (BOP reagent, 900 mg, 2.03 mmol) were dissolved in THF (10 mL). DIPEA (194 mg, 262 μL, 1.5 mmol) were added, and the mixture was allowed to stir at room temperature for 24 h. The mixture was washed with water, extracted with DCM (3 × 30 mL), and dried over Na_2SO_4. Na_2SO_4 was removed via filtration. The organic phase was concentrated under vacuum, and purified by flash chromatography on a silica column. Elution with 20% EtOAc in hexanes gave **91** as a white solid (467 mg, 78% yield). ^{1}H NMR (400 MHz, CDCl$_3$) δ 8.56 (s, 1H), 8.43 (s, 1H), 8.16 (d, *J* = 8.1 Hz, 1H), 7.53 (dd, *J* = 18.1, 6.0 Hz, 3H), 6.58 (d, *J* = 5.5 Hz, 1H), 4.67 (s, 1H), 4.09 (s, 1H), 3.94 (d, *J* = 11.2 Hz, 1H), 3.83 (d, *J* = 11.2 Hz, 1H), 2.80 – 2.61 (m, 1H), 2.55 (s, 1H), 0.95 (s, 18H), 0.13 (s, 12H).
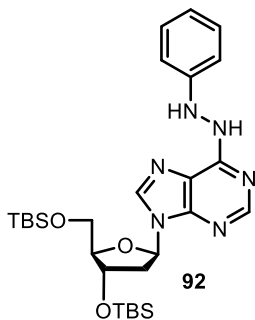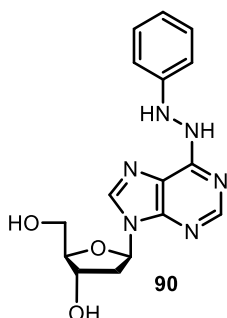
Preparation of 92. Compound **91** (59.8 mg, 0.1 mmol) was dissolved in THF (2 mL), and phenylhydrazine (108 mg, 1 mmol) was added. The reaction was stirred at 65 ºC for 3 h. The resulting mixture was washed with 10% citric acid solution, extracted with EtOAc (3 × 10 mL)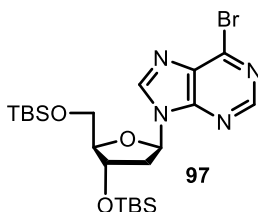, and dried over Na_2SO_4. Na_2SO_4 was removed via filtration. The combined organic phase was concentrated under vacuum, and purified by flash chromatography on a silica column. Elution with 30% EtOAc in hexanes gave **92** as an orange foam (57.0 mg, > 99%). ^{1}H NMR (400 MHz, MeOH-d$_4$) δ 8.31 (s, 1H), 8.23 (s, 1H), 7.24 – 7.05 (m, 2H), 6.93 – 6.71 (m, 3H), 6.44 (dd, *J* = 7.8, 6.1 Hz, 1H), 4.58 (dt, *J* = 5.5, 2.5 Hz, 1H), 4.07 (q, *J* = 3.1 Hz, 1H), 3.84 (dd, *J* = 12.3, 3.1 Hz, 1H), 3.78 – 3.69

188

(m, 1H), 2.79 (td, J = 7.8, 3.9 Hz, 1H), 2.41 (ddd, J = 13.4, 6.1, 2.8 Hz, 1H), 0.92 (s, 9H), 0.87 (s, 9H), 0.12 (s, 6H), 0.07 (s, 3H), 0.06 (s, 3H). ^{13}C NMR (101 MHz, CDCl$_3$) δ 159.0, 153.6, 151.4, 143.6, 143.5, 128.7, 124.8, 120.6, 119.9, 108.7, 88.2, 85.1, 71.7, 62.6, 41.7, 26.0, 25.7, 18.4, 18.0, -4.7, -4.8, -5.4, -5.5. HRMS (ESI-TOF) *m/z* calcd for (C$_{28}$H$_{47}$N$_6$O$_3$Si$_2$)$^+$ (M + H)$^+$ = 571.3248, found *m/z* = 571.3239.

Preparation of 90. Compound **92** (57.0 mg, 0.1 mmol) was dissolved in THF (2 mL), and Et$_3$N•3HF (1.0 mmol, 161 mg) was slowly added to the solution, and the mixture is allowed to react at room temperature overnight. The reaction was concentrated under vacuum and purified by flash chromatography on a silica column. Elution with 3% MeOH in DCM gave **78** as a brown solid (22.9 mg, 67%). ^{1}H NMR (MeOH-d$_4$) δ 8.31 (s, 1H), 8.23 (s, 1H), 7.24 – 7.05 (m, 2H), 6.93 – 6.71 (m, 3H), 6.44 (dd, J = 7.8, 6.1 Hz, 1H), 4.58 (dt, J = 5.5, 2.5 Hz, 1H), 4.07 (q, J = 3.1 Hz, 1H), 3.84 (dd, J = 12.3, 3.1 Hz, 1H), 3.78 – 3.69 (m, 1H), 2.79 (td, J = 7.8, 3.9 Hz, 1H), 2.41 (ddd, J = 13.4, 6.1, 2.8 Hz, 1H).

Preparation of 97.[324] 3',5'-Bis-O-TBDMS-2'-deoxyadenosine (**85**, 475 mg, 1 mmol) was dissolved in bromoform (6 mL). The reaction mixture was heated to 40 ºC. tBuONO (2.4 mL) was slowly added to the solution, and the reaction was reacted at 40 ºC for 45 min. The reaction was concentrated under vacuum and purified by flash chromatography on a silica column. Elution with 20% EtOAc in hexanes gave **97** as a white solid (288.3 mg, 53%). ^{1}H NMR (CDCl$_3$) δ 8.54 (s, 1H), 8.38 (s, 1H), 6.40 (t, J = 6.4 Hz, 1H), 4.52 (dt, J = 5.7, 3.7 Hz, 1H), 3.93 (q, J = 3.3 Hz, 1H), 3.77 (dd, J = 11.3, 3.9 Hz, 1H), 3.67 (dd, J =

11.3, 2.9 Hz, 1H), 2.65 – 2.48 (m, 1H), 2.38 (ddd, J = 13.1, 6.1, 3.9 Hz, 1H), 0.79 (s, 9H), 0.77 (s, 9H), - 0.01 (s, 6H), - 0.03 (s, 3H), - 0.04 (s, 3H).
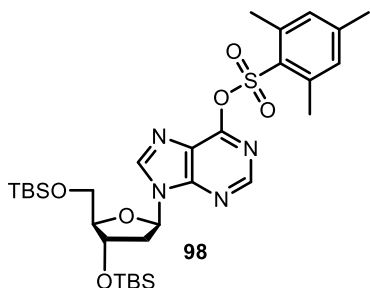
Preparation of 98.[211] 3′,5′-Bis-O-(t-butyldimethylsilyl)-2′-deoxyinosine (48 mg, 0.1 mmol) was dissolved in DCM (2 mL). HMPA (0.2 mL), DMAP (0.02 mmol, 2.5 mg), and TEA (200 mg, 0.28 mL ,0.2 mmol) were added. 2-Mesitylenesulfonyl chloride (43.8 mg, 0.2 mmol) was slowly added while stirring, and the mixture was allowed to stir at room temperature overnight. The mixture was washed with water, extracted with DCM (3 × 10 mL), and dried over Na_2SO_4. Na_2SO_4 was removed via filtration. The organic phase was concentrated under vacuum, and purified by flash chromatography on a silica column. Elution with 25% EtOAc in hexanes gave **98** as a white solid (20 mg, 30% yield). ^{1}H NMR (400 MHz, $CDCl_3$) δ 8.54 (s, 1H), 8.38 (s, 1H), 6.99 (s, 2H), 6.48 (t, J = 6.4 Hz, 1H), 4.61 (dt, J = 5.9, 3.5 Hz, 1H), 4.03 (dd, J = 6.9, 3.5 Hz, 1H), 3.86 (dd, J = 11.3, 3.9 Hz, 1H), 3.76 (dd, J = 11.3, 3.0 Hz, 1H), 2.76 (s, 6H), 2.62 (dt, J = 12.7, 6.2 Hz, 1H), 2.45 (ddd, J = 12.7, 6.2, 3.9 Hz, 1H), 2.31 (s, 3H), 0.91 (s, 9H), 0.89 (s, 9H), 0.10 (s, 6H), 0.08 (s, 3H), 0.07 (s, 3H).
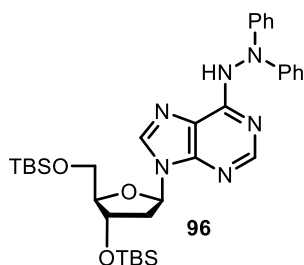
Preparation of 96. Compound **97** (288.3 mg, 0.53 mmol), Pd_2dba_3 (48.5 mg, 0.053 mmol), N,N-diphenylhydrazine (196 mg, 1.06 mmol), Xantphos (47 mg 0.080 mmol), and Cs_2CO_3 (260 mg, 0.8 mmol) was added to a dry Schlenk flask. The flask was purged with argon for three times, and toluene (10 mL) was added. The reaction was stirred at 80 ºC for 3 h. The reaction was concentrated under vacuum and purified by flash chromatography on a silica column. Elution with 20% EtOAc

in hexanes gave **96** as a red foam (164 mg, 48%). ^{1}H NMR (400 MHz, CDCl$_3$) δ 10.29 (s, 1H), 8.46 (s, 1H), 7.60 (s, 1H), 7.33 (d, J = 8.0 Hz, 5H), 7.29 – 7.19 (m, 5H), 7.06 – 6.92 (m, 2H), 6.33 (t, J = 5.9 Hz, 1H), 4.71 – 4.47 (m, 1H), 4.00 (dd, J = 7.5, 4.7 Hz, 1H), 3.73 (dd, J = 11.0, 4.8 Hz, 1H), 3.68 (dd, J = 11.0, 4.8 Hz, 1H), 2.78 – 2.49 (m, 1H), 2.35 (ddd, J = 13.1, 6.0, 3.5 Hz, 1H), 0.93 (s, 9H), 0.89 (s, 9H), 0.12 (s, 6H), 0.06 (s, 3H), 0.04 (s, 3H). ^{13}C NMR (101 MHz, CDCl$_3$) δ 153.6, 146.3, 139.6, 129.2, 122.8, 119.3, 87.9, 84.5, 72.2, 62.9, 40.4, 25.9, 25.8, 18.4, 18.0, -4.7, -4.8, -5.4. HRMS (ESI-TOF) m/z calcd for (C$_{34}$H$_{51}$N$_6$O$_3$Si$_2$)$^+$ (M + H)$^+$ = 647.3561, found m/z = 647.3567.


3
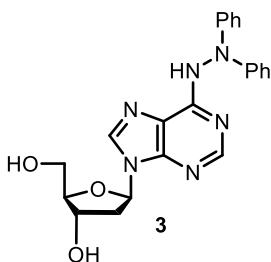
Preparation of 3. Compound **96** (164 mg, 0.26 mmol) was dissolved in THF (7 mL). While stirring, Et$_3$N•3HF (2.6 mmol, 419 mg) was slowly added. The reaction was stirred at 25 °C overnight. The reaction was concentrated under vacuum and purified by flash chromatography on a silica column. Elution with 1% to 3% MeOH in DCM gave **3** as a light yellow oil (95 mg, 87%). ^{1}H NMR (400 MHz, MeOH-d$_4$) δ 8.24 (s, 2H), 7.23 (s, 8H), 6.96 (s, 2H), 6.42 (s, 1H), 4.56 (s, 1H), 4.05 (s, 1H), 3.81 (d, J = 11.9 Hz, 1H), 3.72 (d, J = 11.9 Hz, 1H), 2.78 (br, 1H), 2.40 (br, 1H). ^{13}C NMR (101 MHz, MeOH-d$_4$) δ 150.6, 147.3, 145.0, 139.4, 127.2, 121.0, 117.7, 117.3, 86.9, 84.1, 70.0, 60.7, 38.6. HRMS (ESI-TOF) m/z calcd for (C$_{22}$H$_{23}$N$_6$O$_3$)$^+$ (M + H)$^+$ = 419.1832, found m/z = 419.1843. UV/Vis $λ_{max}$ (H$_2$O) = 267 nm, ε = 1.88 × 10^4 dm^3 mol^{-1} cm^{-1}.


99
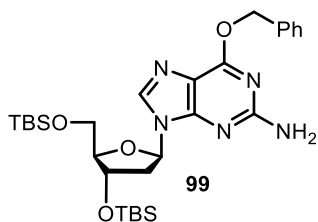
Preparation of 99.[220] 3',5'-Bis-O-TBDMS-2'-deoxyguanosine (**86**, 306 mg, 0.61 mmol), benzyl alcohol (141 mg, 1.3 mmol), and PPh$_3$ (340 mg, 1.3 mmol) was dissolved in dioxane (10 mL). DEAD (226 mg, 1.3 mmol) and

were slowly added. The reaction was stirred at 25 ºC overnight. The reaction was concentrated under vacuum, and purified by flash chromatography on a silica column. Elution with 20% EtOAc in hexanes gave **99** as a light yellow oil (319 mg, 89%). ^{1}H NMR (400 MHz, CDCl$_3$) δ 7.90 (s, 1H), 7.54 – 7.43 (m, 2H), 7.37 – 7.17 (m, 5H), 6.30 (t, J = 6.5 Hz, 1H), 5.63 – 5.46 (m, 2H), 4.94 (s, 2H), 4.69 (s, 2H), 4.62 – 4.49 (m, 1H), 3.96 (dd, J = 7.3, 3.3 Hz, 1H), 3.81 (dd, J = 11.2, 4.2 Hz, 1H), 3.75 (dd, J = 11.2, 4.2 Hz, 1H), 2.55 (ddd, J = 12.9, 8.4, 4.9 Hz, 1H), 2.34 (ddd, J = 12.9, 6.1, 3.8 Hz, 1H), 0.91 (s, 9H), 0.90 (s, 9H), 0.44 – -0.19 (m, 12H).
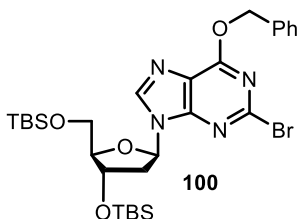
Preparation of 100.[220] Compound **99** (319 mg, 0.54 mmol), SbBr$_3$ (320 mg, 0.87 mmol) was dissolved in methylene bromide (7 mL). The reaction mixture was cooled to -10 ºC. tBuONO (260 µL, 268 mg, 2.17 mmol) was slowly added to the solution, and the reaction was stirred at -10 ºC for 1 h. The reaction mixture was poured into saturated NaHCO$_3$ and extracted with DCM (3 × 20 mL). The resulting mixture was dried using Na$_2$SO$_4$. Na$_2$SO$_4$ was removed via filtration, and the solution was concentrated under vacuum. The reaction was purified by flash chromatography on a silica column. Elution with 20% EtOAc in hexanes gave **100** as a light yellow oil (158 mg, 45%). ^{1}H NMR (400 MHz, CDCl$_3$) δ 8.16 (s, 1H), 7.50 (dd, J = 8.0, 1.4 Hz, 2H), 7.31 (m, 3H), 6.37 (t, J = 6.3 Hz, 1H), 5.69 – 5.45 (m, 2H), 4.64 (dt, J = 5.7, 4.0 Hz, 1H), 3.98 (dd, J = 7.4, 3.5 Hz, 1H), 3.88 (dd, J = 11.2, 4.3 Hz, 1H), 3.76 (dd, J = 11.2, 4.3 Hz, 1H), 2.63 (ddd, J = 13.1, 6.1, 3,8 Hz, 1H), 2.40 (ddd, J = 13.1, 6.3, 4.3 Hz, 1H), 0.91 (s, 9H), 0.90 (s, 9H), 0.11 (s, 6H), 0.08 (s, 3H), 0.08 (s, 3H).
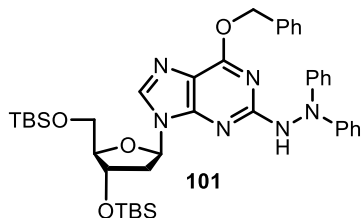
Preparation of 101. Compound **100** (91.5 mg, 0.14 mmol), Pd₂dba₃ (13.8 mg, 0.014 mmol), N,N-diphenylhydrazine (36.8 mg, 0.28 mmol), Xantphos (13 mg, 0.021 mmol), and Cs₂CO₃ (75 mg, 0.21 mmol) were added to a dry Schlenk flask .The flask was purged with argon three times, and toluene (10 mL) was added. The reaction reacted at 80 °C for 3 h. The reaction was concentrated under vacuum and purified by flash chromatography on a silica column. Elution with 20% EtOAc in hexanes gave **101** as an orange foam (66.4 mg, 63%). ^{1}H NMR (400 MHz, CDCl₃) δ 7.94 (s, 1H), 7.38 (s, 2H), 7.33 (s, 1H), 7.31 – 7.21 (m, 12H), 7.05 – 6.95 (m, 2H), 6.30 (s, 1H), 5.45 (s, 2H), 4.53 (s, 1H), 3.97 (d, J = 3.6 Hz, 1H), 3.86 – 3.60 (m, 2H), 2.51 (br, 1H), 2.28 (br, 1H), 0.94 (s, 9H), 0.93 (s, 9H), 0.12 (s, 3H), 0.11 (s, 3H), 0.09 (s, 3H), 0.08 (s, 3H). ^{13}C NMR (101 MHz, CDCl₃) δ 161.0, 153.5, 146.4, 138.2, 136.3, 129.0, 128.8, 128.3, 127.9, 122.2, 119.1, 117.0, 87.8, 72.0, 68.1, 62.8, 26.0, 25.8, 25.7, 18.4, 18.0, -3.5, -4.6, -4.8, -5.37, -5.41. HRMS (ESI-TOF) m/z calcd for $(C_{41}H_{57}N_6O_4Si_2)^+$ $(M + H)^+$ = 753.3980, found m/z = 753.3983.
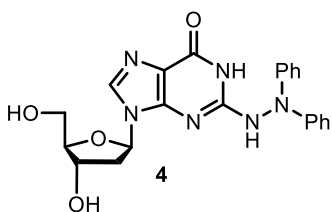
**Preparation of 4.** Compound **101** (66.4 mg, 0.09 mmol) was dissolved in THF (2 mL). Et₃N•3HF (161 mg, 1.0 mmol) was slowly added, and the reaction was stirred at 25 °C overnight. The reaction was concentrated under vacuum, and directly carried on to the next step without purification. The residue was dissolved in MeOH (6 mL), and 20 mg 10% Pd/C was added to the solution. The flask was bubbled with hydrogen using a balloon. The reaction was monitored by TLC and was completed after 30 min. The Pd/C was removed by passing the reaction through a silica plug. The

reaction was concentrated under vacuum and purified by flash chromatography on a silica column. Elution with 1% to 3% MeOH in DCM gave **4** as a white foam (24 mg, 61.4%). ^{1}H NMR (400 MHz, MeOH-d$_4$) δ 8.02 (s, 1H), 7.34 (dd, J = 8.6, 7.3 Hz, 4H), 7.24 (dd, J = 8.6, 1.0 Hz, 4H), 7.10 (t, J = 7.3 Hz, 2H), 6.28 (t, J = 6.8 Hz, 1H), 4.50 (s, 1H), 3.97 (d, J = 3.3 Hz, 1H), 3.72 (dd, J = 23.3, 11.5 Hz, 2H), 2.68 (dt, J = 13.5, 6.7 Hz, 1H), 2.33 (s, 1H). ^{13}C NMR (101 MHz, MeOH-d$_4$) δ 156.1, 152.0, 149.2, 145.2, 135.8, 127.4, 122.1, 118.4, 86.4, 82.8, 69.7, 60.4, 38.3. HRMS (ESI-TOF) m/z calcd for $(C_{22}H_{23}N_6O_4)^+$ (M + H)$^+$ = 435.1781, found m/z = 435.1788. UV/Vis λ_{max} (H$_2$O) = 264 nm, ε = 1.74 × 10^4 dm^3 mol^{-1} cm^{-1}.
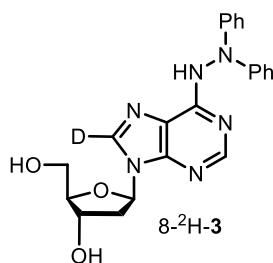
Preparation of 8-^{2}H-3. Compound **3** (42.1 mg, 0.1 mmol) is dissolved in d$_3$-acetonitrile-D$_2$O (3 mL, 1:1). TEA (11 mg, 0.1 mmol) was added to the mixture, and the reaction was stirred at 65 ºC for 48 h. The reaction was concentrated and dried under vacuum overnight to provide 8-^{2}H-**3** (42 mg, 99%). ^{1}H NMR (400 MHz, MeOH-d$_4$) δ 8.25 (s, 1H), 7.23 (t, J = 6.7 Hz, 8H), 6.98 (dt, J = 8.6, 4.1 Hz, 2H), 6.44 (t, J = 6.7 Hz, 1H), 4.67 – 4.46 (m, 1H), 4.06 (d, J = 2.7 Hz, 1H), 3.82 (dd, J = 12.2, 3.0 Hz, 1H), 3.73 (dd, J = 12.2, 3.0 Hz, 1H), 2.79 (dd, J = 13.0, 6.3 Hz, 1H), 2.40 (d, J = 8.9 Hz, 1H). HRMS (ESI-TOF) m/z calcd for $(C_{22}H_{22}DN_6O_3)^+$ (M + H)$^+$ = 420.1894, found m/z = 420.1881.
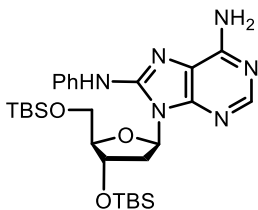
Preparation of disilylated 106.[325] Racemic 2,2'-bis(diphenylphosphino)-1,1'-binaphthyl (rac-BINAP, 37.4 mg, 0.06 mmol) and Pd$_2$(dba)$_3$, 18.3 mg, 0.02 mmol) were suspended in anhydrous DME (2 mL). Bis-TBDMS 8-bromo-2'-deoxyadenosine[326] (**105**, 111 mg, 0.2 mmol), aniline (47 mg, 0.5 mmol), and Cs$_2$CO$_3$ (98

mg, 0.3 mmol) were added and the mixture was stirred under reflux for 48 h. The reaction mixture was allowed to cool to room temperature and quenched with saturated $NaHCO_3$ solution. The mixture was extracted with ethyl acetate (3 × 5 mL). The organic layer was dried with Na_2SO_4. Na_2SO_4 was removed via filtration, and concentrated under vacuum. Purification of the residue by flash chromatography on silica gel (5 to 35% ethyl acetate in hexanes) gave disilylated **106** as a light yellow oil (89 mg, 78%). ^{1}H NMR (400 MHz, CDCl$_3$) δ 8.19 (s, 1H), 7.79 (s, 1H), 7.56 (dd, J = 8.6, 1.1 Hz, 2H), 7.35 – 7.27 (m, 2H), 7.08 – 6.98 (m, 1H), 6.43 (dd, J = 7.9, 5.8 Hz, 1H), 4.58 (dt, J = 6.2, 3.1 Hz, 1H), 4.04 (q, J = 3.4 Hz, 1H), 3.95 (dd, J = 11.4, 3.4 Hz, 1H), 3.83 (dd, J = 11.4, 3.5 Hz, 1H), 2.89 (ddd, J = 13.2, 7.9, 6.3 Hz, 1H), 2.31 (ddd, J = 13.0, 5.8, 3.1 Hz, 1H), 0.92 (s, 9H), 0.82 (s, 9H), 0.11 (s, 3H), 0.11 (s, 3H), 0.01 (s, 3H), -0.01 (s, 3H).
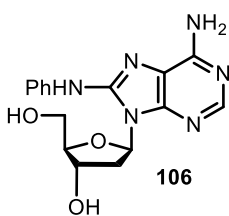

Preparation of 106. Disilylated **106** (89 mg, 0.16 mmol) was dissolved in THF (2 mL). While stirring, Et$_3$N•3HF (1.6 mmol, 258 mg) was slowly added. The reaction was stirred at 25 ºC overnight. The reaction was concentrated under vacuum and purified by flash chromatography on a silica column. Elution with 1% to 7% MeOH in DCM gave **106** as a colorless foam (44 mg, 80%). ^{1}H NMR (400 MHz, MeOH-d$_4$) δ 8.05 (s, 1H), 7.59 (d, J = 7.9 Hz, 2H), 7.32 (t, J = 7.9 Hz, 2H), 7.05 (t, J = 7.4 Hz, 1H), 6.61 (dd, J = 9.3, 5.9 Hz, 1H), 4.60 (d, J = 6.0 Hz, 1H), 4.09 (s, 1H), 3.93 (d, J = 11.8 Hz, 1H), 3.87 (d, J = 11.8 Hz, 1H), 2.87 – 2.68 (m, 1H), 2.24 (dd, J = 13.4, 5.9 Hz, 1H). ^{13}C NMR (101 MHz, MeOH-d$_4$) δ 151.2, 147.8, 147.2, 146.9, 137.8, 127.1, 121.3, 118.6, 86.3, 82.4, 70.4, 60.0, 37.0. HRMS (ESI-TOF) m/z calcd for $(C_{16}H_{19}N_6O_3)^+$ (M + H)$^+$ = 343.1519, found m/z = 343.1510. UV/Vis λ_{max} (ACN) = 292 nm, ε = 1.17 × 10^4 dm^3 mol^{-1} cm^{-1}.
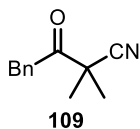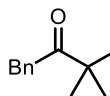
Preparation of 109. HMDS (3.2 mL, 15.0 mmol) was added to a solution of n-butyl lithium (14.5 mmol, 11 mL) at -78 °C in THF (7 mL), and the mixture was stirred at this temperature for 1 h. Isobutyronitrile (966 mg, 14.0 mmol) in THF (5 mL) was slowly added to the solution. The solution was stirred for 1 h at which time ethyl phenylacetate (2.228 g, 14.0 mmol) in THF (10 mL) was added. The mixture was allowed to warm to room temperature and stirred overnight. The reaction was quenched with MeOH at room temperature, concentrated under vacuum, and purified by flash chromatography. Elution with 20% ethyl acetate in hexanes gave **109** as a colorless oil (597 mg, 22%). ^{1}H NMR (300 MHz, CDCl$_3$) δ 7.45 – 7.18 (m, 5H), 4.10 (s, 2H), 1.52 (s, 6H). ^{13}C NMR (75 MHz, CDCl$_3$) δ 201.7, 132.8, 129.7, 128.7, 127.4, 121.9, 45.2, 43.9, 23.9. IR (KBr plate) 2998, 2902, 2856, 2344, 1721, 792, 713 cm^{-1}. HRMS (FAB) C$_{12}$H$_{14}$NO$^+$ (M + H)$^+$ calcd. 188.1075, found 188.1072.
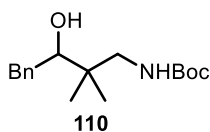
Preparation of 110. A solution of **109** (168 mg, 0.9 mmol) in THF (1 mL) was added dropwise to a suspension of LiAlH$_4$ (36 mg, 0.95 mmol) in THF (1 mL) over 2 min at 0 °C. The ice bath was removed, and the reaction was stirred at room temperature for 4 h. The reaction mixture was poured into THF/H$_2$O (1:1, 1 mL) at 0 °C and stirred at 80 °C for 10 min, and then filtered through celite. The filtrate was extracted with DCM (3 × 10 mL). The organic layers were combined and dried over Na$_2$SO$_4$. Na$_2$SO$_4$ was removed via filtration, and the solution was concentrated under vacuum to give 4-amino-3,3-dimethyl-1-phenylbutan-2-ol. 4-Amino-3,3-dimethyl-1-phenylbutan-2-ol was used without further purification. A solution of di-tert-butyl dicarbonate (207 mg, 0.95 mmol) in DCM (2 mL) was added to a solution of 4-amino-3,3-dimethyl-1-phenylbutan-2-ol in DCM (2 mL) at 0 °C and stirred

at room temperature overnight. The reaction mixture was poured into water and extracted with DCM (3 × 10 mL), dried over Na_2SO_4. Na_2SO_4 was removed via filtration, and the solution was concentrated under vacuum. The residue was chromatographed on silica gel and eluted with 25% ethyl acetate in hexanes to give **110** as colorless oil (188.7 mg, 72% over two steps). ^{1}H NMR (400 MHz, CDCl$_3$) δ 7.27 (m, 5H), 5.26 (t, J = 6.2 Hz, 1H), 3.53 (d, J = 9.2 Hz, 1H), 3.39 (dd, J = 14.1, 7.2 Hz, 1H), 3.26 (s, 1H), 2.81 (dd, J = 21.6, 9.1 Hz, 2H), 2.56 (dd, J = 13.8, 10.5 Hz, 1H), 1.44 (s, 9H), 0.97 (d, J = 7.5 Hz, 6H).^{13}C NMR (75 MHz, CDCl$_3$) δ 146.3, 139.6, 129.1, 122.8, 119.4, 87.9, 84.5, 72.1, 62.9, 40.6, 25.9, 25.8, 18.4, 18.0. IR (KBr plate) 3457, 3398, 2970, 2934, 2859, 1719, 1685, 792, 743, 729 cm^{-1}. HRMS (FAB) $C_{17}H_{28}NO_3^+$ (M + H)$^+$ calcd. 294.2069, found 294.2065.

Preparation of t-Boc-protected 111. A solution of **110** (153 mg, 0.52 mmol) in DCM (2 mL) was added to a solution of pyridine (60 mg, 0.75 mmol), PCC (162 mg, 0.75 mmol) and celite (1.3 g) in DCM (2.5 mL). The reaction mixture was refluxed for 6.5 h. After quenching excess PCC with isopropanol (5 mL), diethyl ether (20 mL) was added to the solution. The reaction mixture was filtered through celite and concentrated under vacuum. The residue was chromatographed on silica gel and eluted with 25% ethyl acetate in hexanes to give t-Boc-protected **111** as a light yellow oil (137.6 mg, 90%). ^{1}H NMR (400 MHz, CDCl$_3$) δ 7.34 − 7.27 (m, 2H), 7.27 − 7.20 (m, 1H), 7.15 (dd, J = 7.7, 0.9 Hz, 2H), 4.95 (s, 1H), 3.78 (s, 2H), 3.25 (d, J = 6.6 Hz, 2H), 1.41 (s, 9H), 1.22 (s, 6H). ^{13}C NMR (75 MHz, CDCl$_3$): δ 212.7, 156.3, 134.4, 129.7, 128.5, 126.9, 79.1, 49.4, 48.0, 43.7, 28.4, 22.5. IR (KBr plate) 3387, 2975, 2935, 2849, 1760, 1697, 749, 735 cm^{-1}. HRMS (FAB) $C_{17}H_{26}NO_3^+$ (M + H)$^+$ calcd. 292.1913, found 292.1905.
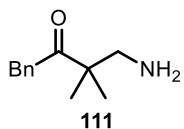
**Preparation of 111.** t-Boc-protected **111** (137.6 mg, 0.47 mmol) was treated with DCM-TFA (1:1, 2 mL) for 1 h at 25 °C. The reaction mixture was then poured into saturated NaHCO$_3$ solution, extracted with DCM (3 × 10 mL), dried over Na$_2$SO$_4$. Na$_2$SO$_4$ was removed via filtration, and the solution was concentrated under vacuum. The residue was chromatographed on silica gel and eluted with 40% ethyl acetate in hexanes to give **111** as a colorless oil (91 mg, > 99%). ^{1}H NMR (300 MHz, CDCl$_3$) δ 7.25 (m, 5H), 3.80 (s, 2H), 2.81 (s, 2H), 1.47 (s, 2H), 1.19 (s, 6H). ^{13}C NMR (75 MHz, CDCl$_3$) δ 212.5, 134.6, 129.6, 128.4, 126.7, 53.5, 50.8, 49.9, 44.1, 22.4. IR (KBr plate) 3391 (broad), 2963, 2925, 2854, 1700, 1043, 725, 696, 667 cm^{-1}. HRMS (FAB) C$_{12}$H$_{18}$NO$^+$ (M + H)$^+$ calcd. 192.1388, found 192.1391.
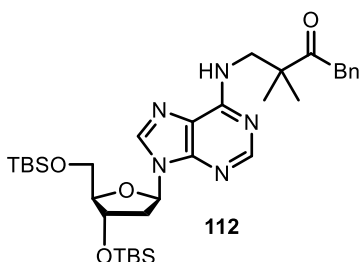
Preparation of 112. Compound **91** (59.8 mg, 0.1 mmol) and **111** (46 mg, 0.24 mmol) were stirred in THF (1 mL) at room temperature overnight. The reaction was concentrated under vacuum and purified by flash chromatography on a silica column. Elution with 3% MeOH in DCM gave **112** as a white solid (53.9 mg, 83%). ^{1}H NMR (400 MHz, CDCl$_3$) δ 8.33 (s, 1H), 8.04 (s, 1H), 7.34 – 7.26 (m, 2H), 7.24 (dd, J = 5.1, 3.7 Hz, 1H), 7.18 – 7.12 (m, 2H), 6.42 (t, J = 6.5 Hz, 1H), 4.65 – 4.57 (m, 1H), 4.00 (dd, J = 7.5, 3.3 Hz, 1H), 3.90 – 3.67 (m, 6H), 2.69 – 2.54 (m, 1H), 2.41 (ddd, J = 13.0, 6.1, 3.8 Hz, 1H), 1.32 (s, 6H), 0.91 (s, 9H), 0.91 (s, 9H), 0.09 (s, 6H), 0.08 (s, 3H), 0.08 (s, 3H). ^{13}C NMR (75 MHz, CDCl$_3$) δ 212.2, 155.1, 152.8, 150.6, 138.2, 134.3, 129.6, 128.4, 126.8, 87.8, 84.2, 71.9, 62.8, 49.6, 43.7, 41.2, 26.0, 25.8, 22.6, 18.4, 18.0, -4.7, -4.8, -5.4, -5.5. IR (KBr plate) 2953, 2928, 2855, 1708, 1613, 1471, 1252, 835,

777, 724 cm^{-1}; HRMS (ESI-TOF) C$_{34}$H$_{56}$N$_5$O$_4$Si$_2{}^+$ (M + H)$^+$ calcd. 654.3871, found 654.3871.
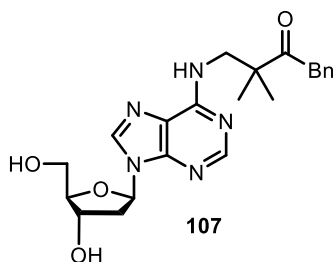
Preparation of 107. Et$_3$N•3HF (161 mg, 1.0 mmol) was slowly added to **112** (65 mg, 0.1 mmol) in THF (1 mL). The reaction was stirred at 25 ºC overnight. The reaction was concentrated under vacuum and purified by flash chromatography on a silica column. Elution with 5% MeOH in DCM gave **107** as a white solid (37.0 mg, 87%). ^{1}H NMR (400 MHz, MeOH-d$_4$) δ 8.29 (s, 1H), 8.23 (s, 1H), 7.34 – 7.03 (m, 5H), 6.43 (dd, J = 7.8, 6.0 Hz, 1H), 4.65 – 4.56 (m, 1H), 4.09 (dd, J = 5.5, 2.9 Hz, 1H), 3.97 (s, 2H), 3.86 (dd, J = 12.3, 2.9 Hz, 2H), 3.75 (dd, J = 12.3, 3.3 Hz, 1H), 3.43 – 3.10 (m, 2H), 2.81 (ddd, J = 13.6, 8.0, 5.8 Hz, 1H), 2.41 (ddd, J = 13.6, 6.0, 2.6 Hz, 1H), 1.32 (s, 6H). ^{13}C NMR (101 MHz, MeOH-d$_4$) δ 211.1, 153.6, 150.5, 138.2, 133.3, 129.5, 127.9, 126.9, 126.3, 124.6, 87.0, 84.3, 70.2, 60.8, 48.0, 41.9, 38.7, 27.8, 20.0. IR (KBr plate) 3279 (broad), 2928, 1610, 1580, 1473, 1228, 1111, 1071, 836, 774, 728 cm^{-1}. HRMS (ESI-TOF) C$_{22}$H$_{28}$N$_5$O$_4{}^+$ (M + H)$^+$ calcd. 426.2141, found 426.2136.
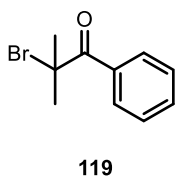
Preparation of 119. p-Toluenesulfonic acid (19 mg, 0.1 mmol), isobutyrophenone (148 mg, 1 mmol) was dissolved in DCM (2 mL). Br$_2$ (168 mg, 1.05 mmol) was slowly added while stirring. The reaction was stirred at room temperature for 1 h. The reaction was poured into water and extracted with EtOAc (5 mL × 3). The organic phase was dried over Na$_2$SO$_4$, passed through a silica plug, concentrated under vacuum gave **119** as a yellow oil (178.6 mg, 79%). ^{1}H NMR (300 MHz, CDCl$_3$) δ 8.14 (ddd, J = 7.0, 2.4, 1.2 Hz, 2H), 7.62 – 7.48 (m, 1H), 7.48 – 7.37 (m, 2H), 2.03 (s, 6H).
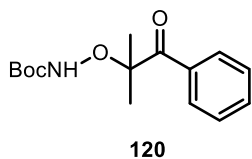
Preparation of 120. N-Boc-hydroxylamine (27 mg, 0.2 mmol) was dissolved in DMF (1 mL). NaH (60% in mineral oil, 8 mg, 0.2 mmol) was slowly added while stirring. The reaction was stirred at 0 °C for 30 min, and **119** (17 mg, 0.075 mmol) was then added at 0 °C. The reaction was stirred at room temperature overnight. The reaction was concentrated under vacuum and purified by flash chromatography on a silica column. Elution with 10% EtOAc in hexanes gave **120** as a yellow oil (23.9 mg, > 99%). ^{1}H NMR (300 MHz, CDCl$_3$) δ 8.54 – 7.92 (m, 2H), 7.62 – 7.52 (m, 1H), 7.47 (ddt, J = 8.3, 6.9, 1.4 Hz, 2H), 6.71 (s, 1H), 1.63 (s, 6H), 1.44 (s, 9H).
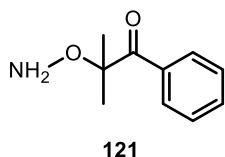
Preparation of 121. DCM-TFA (1:1, 1 mL) was added to a dry round bottom flask containing **120** (21 mg, 0.075 mmol). The reaction was stirred at room temperature for 1 h. The reaction was quenched by saturated NaHCO$_3$ solution and extracted with DCM (5 mL × 3). The combined organic phases were dried over Na$_2$SO$_4$. Na$_2$SO$_4$ was removed via filtration. The organic phase was concentrated under vacuum and purified by flash chromatography on a silica column. Elution with 10% EtOAc in hexanes gave **121** as a white solid (12.5 mg, > 99%). ^{1}H NMR (400 MHz, CDCl$_3$) δ 8.61 – 7.97 (m, 2H), 7.49 (m, 3H), 1.55 (s, 6H).
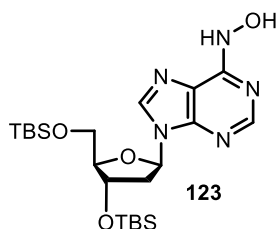
Preparation of 123. TEA (1.01 g, 10 mmol) was added to hydroxylamine hydrochloride (345 mg, 5 mmol) in THF (10 mL). After stirring at room temperature for 30 min **97** (270 mg, 0.5 mmol) was added, and the reaction was refluxed at 65 °C overnight. The reaction was concentrated under vacuum and purified by flash chromatography on a silica column. Elution with 5% MeOH and 1% Et$_3$N in DCM gave **123** as a light purple

foam. The sample was dissolved in MeOH (10 mL) and Na$_2$-EDTA (1.7 g, 5 mmol) was added to the solution and the reaction was stirred at 50 ℃ until the purple color faded. The mixture was cooled to room temperature and filtered to remove Na$_2$-EDTA. The organic phase was then concentrated under vacuum to give **123** as a white foam (143 mg, 58%).^{1}H NMR (300 MHz, MeOH-d$_4$) δ 8.20 (s, 1H), 8.05 (s, 1H), 6.37 (t, J = 6.4 Hz, 1H), 4.69 (dt, J = 5.6, 4.0 Hz, 1H), 3.97 (dd, J = 7.8, 3.6 Hz, 1H), 3.86 (dd, J = 11.2, 4.5 Hz, 1H), 3.76 (dd, J = 11.2, 3.6 Hz, 1H), 2.75 (dt, J = 13.0, 6.1 Hz, 1H), 2.43 (ddd, J = 13.0, 6.2, 4.2 Hz, 1H), 0.93 (s, 9H), 0.87 (s, 9H), 0.17 – 0.00 (m, 12H). ^{13}C NMR (75 MHz, MeOH-d$_4$) δ 149.7, 147.2, 145.9, 140.3, 139.5, 119.8, 89.2, 85.7, 73.4, 64.0, 41.6, 26.6, 26.5, 19.3, 19.0, 9.7, -4.2, -4.3, -5.1. IR (KBr plate) 3408 (broad), 2954, 2929, 2896, 2857, 1691, 1680, 1254, 1110, 837, 778 cm^{-1}. HRMS (ESI-TOF) C$_{22}$H$_{42}$N$_5$O$_4$Si$_2$$^+$ (M + H)$^+$ calcd. 496.2775, found 496.2768.

122
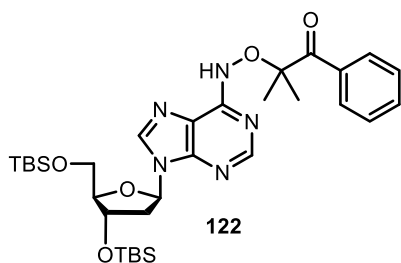
Preparation of 122. NaH (60% in mineral oil, 20 mg, 0.5 mmol) was slowly added while stirring to **123** (241 mg, 0.5 mmol) in DMF (3 mL) at 0 °C. The reaction was stirred at 0 ℃ for 30 min at which time **119** (227 mg, 0.55 mmol) was added. The reaction was stirred at room temperature for 4 h, concentrated under vacuum, and purified by flash chromatography on a silica column. Elution with 50% EtOAc in hexanes gave **122** as a red oil (209 mg, 64%). ^{1}H NMR (400 MHz, MeOH-d$_4$) δ 8.17-8.13 (m, 2H), 7.86 (s, 1H), 7.62 (s, 1H), 7.45-7.38 (m, 1H), 7.38-7.31 (m, 2H), 6.22 (t, J = 6.2 Hz, 1H), 4.63 (dd, J = 8.9, 3.9 Hz, 1H), 3.92 (dd, J = 7.8, 3.7 Hz, 1H), 3.80 (dd, J = 11.2, 4.6 Hz, 1H), 3.72 (dd, J = 11.2, 3.6 Hz, 1H), 2.69 – 2.55 (m, 1H), 2.35 (ddd, J = 13.1, 6.2, 4.3 Hz, 1H), 1.63 (s, 6H), 0.91 (s, 9H), 0.85 (s, 9H), 0.11 (s, 6H), 0.03 (s, 3H),

0.01 (s, 3H). ^{13}C NMR (101 MHz, MeOH-d$_4$) δ 203.0 , 151.5, 145.3, 143.9, 141.1, 140.5, 136.3, 135.4, 131.8, 129.3, 127.6, 118.6, 87.9, 87.8, 86.1, 85.2, 84.1, 71.9, 62.4, 40.2, 25.1, 25.0, 24.9, 24.0, 17.9, 17.5, -5.8, -5.93, -6.65, -6.66. IR (KBr plate): 2934, 1610, 1592, 1494, 1475, 1320, 834, 760, 743, 695 cm^{-1}. HRMS (ESI-TOF) C$_{32}$H$_{52}$N$_5$O$_5$Si$_2^+$ (M + H)$^+$ calcd. 642.3507, found 642.3503.
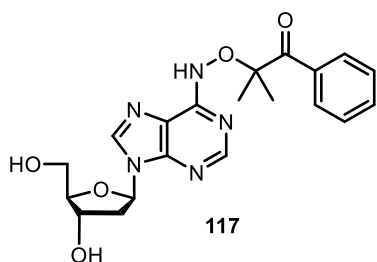
Preparation of 117 Et$_3$N•3HF (530 mg, 3.3 mmol) was added to **123** (209 mg, 0.33 mmol) in THF (5 mL). The reaction was stirred at 25 °C overnight, concentrated under vacuum, and purified by flash chromatography on a silica column. Elution with 5% MeOH in DCM gave **117** as a yellow foam (101 mg, 75%). ^{1}H NMR (300 MHz, MeOH-d$_4$) δ 8.23 – 8.06 (m, 2H), 7.91 (s, 1H), 7.63 (s, 1H), 7.45-7.38 (m, 1H), 7.38-7.30 (m, 2H), 6.30 – 6.21 (m, 1H), 4.49 (dt, J = 5.5, 2.7 Hz, 1H), 3.99 (dd, J = 6.2, 3.3 Hz, 1H), 3.77 (dd, J = 12.2, 3.3 Hz, 1H), 3.68 (dd, J = 12.2, 3.7 Hz, 1H), 2.63 (ddd, J = 13.6, 7.7, 6.0 Hz, 1H), 2.34 (ddd, J = 13.6, 6.0, 2.9 Hz, 1H), 1.65 (s, 6H). ^{13}C NMR (101 MHz, MeOH-d$_4$) δ 203.1, 144.0, 141.0, 140.2, 137.0, 135.3, 131.9, 129.2, 127.9, 127.7, 118.9, 88.2, 86.2, 85.2, 71.4, 62.1, 40.5, 24.0. IR (KBr plate): 3273 (broad), 2928, 1606, 1590, 1494, 1471, 1328, 1252, 1105, 835, 777, 747, 692 cm^{-1}. HRMS (ESI-TOF) C$_{20}$H$_{24}$N$_5$O$_5^+$ (M + H)$^+$ calcd. 414.1777, found 414.1770.
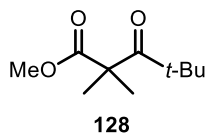
Preparation of 128.[232] Methyl trimethylsilyl dimethylketene acetal (2.61 g, 15 mmol) and pivaloyl chloride (1.44 g, 12 mmol) was dissolved in DCM (30 mL). TiCl$_4$ (2.845 g, 15 mmol) was slowly added to the reaction at 0 °C. The reaction was stirred at room temperature overnight. The reaction was quenched with water, extracted with DCM (30 mL × 3). The organic phase was dried
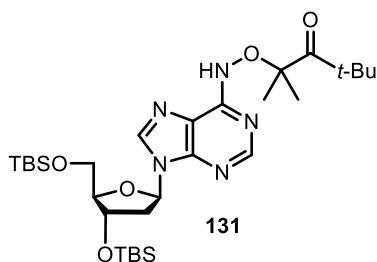
over Na_2SO_4, and Na_2SO_4 was removed via filtration. The mixture was concentrated under vacuum, and purified by flash chromatography on a silica column. Elution with 10% EtOAc in hexanes gave **128** as a colorless oil (2 g, 90%). ^1H NMR (400 MHz, $CDCl_3$) δ 3.66 (s, 3H), 1.32 (s, 6H), 1.12 (s, 9H).
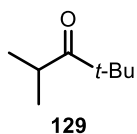
Preparation of 129. Acetic acid-conc. HCl (1:1, 30 mL) was added to **128** (2.0 g, 10 mmol). The reaction was refluxed at 110 ºC for 8 h. The cooled reaction was quenched by saturated $NaHCO_3$ solution and extracted with DCM (30 mL × 3). The organic phase was dried over Na_2SO_4. The organic phase was concentrated under vacuum to give **129** as an orange oil (1.75 g, > 99%). ^1H NMR (300 MHz, $CDCl_3$) δ 3.12 (hept, J = 6.7 Hz, 1H), 1.14 (s, 9H), 1.03 (d, J = 6.7 Hz, 6H). ^{13}C NMR (75 MHz, $CDCl_3$) δ 220.1, 44.6, 33.8, 26.0, 20.1. IR (KBr plate) 2973, 2936, 2874, 1732 cm^{-1}.
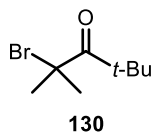
Preparation of 130. Br_2 (176 mg, 1.1 mmol) was slowly added to **129** (128 mg, 1 mmol) in HOAc (2 mL). The reaction was heated at 70 ºC for 5 h, poured into water, and extracted with EtOAc (5 mL × 3). The organic phase was passed through a silica plug and then concentrated under vacuum to yield **130** as a yellow oil (200 mg, 97%). ^1H NMR (400 MHz, $CDCl_3$) δ 1.91 (s, 6H), 1.36 (s, 9H). ^{13}C NMR (75 MHz, $CDCl_3$) δ 209.2, 62.3, 45.5, 31.9, 29.3. IR (KBr plate) 2981, 2876, 1733, 1699, 1263, 1194, 1145 cm^{-1}.

Preparation of 131. NaH (60% in mineral oil, 28 mg, 0.7 mmol) was slowly added to **123** (335 mg, 0.7 mmol) in DMF (7 mL). The reaction was stirred at 0 ºC for 1 h, at which time **130** (290 mg, 1.4 mmol) was added at 0 ºC. The reaction was stirred at room temperature for 4 h, and quenched with MeOH. The
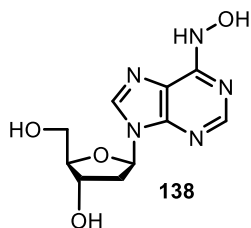
mixture was concentrated under vacuum and purified by flash chromatography on a silica column. Elution with 50% EtOAc in hexanes gave bis-silylated **131** as a yellow foam (320 mg, 74%). ^{1}H NMR (400 MHz, MeOH-d$_4$) δ 7.94 (s, 1H), 7.62 (s, 1H), 6.28 (t, J = 6.4 Hz, 1H), 4.69 (dd, J = 9.2, 3.9 Hz, 1H), 3.95 (dd, J = 7.7, 3.7 Hz, 1H), 3.84 (dd, J = 11.2, 4.5 Hz, 1H), 3.76 (dd, J = 11.2, 3.6 Hz, 1H), 2.73 (dt, J = 13.1, 6.1 Hz, 1H), 2.40 (ddd, J = 13.1, 6.3, 4.3 Hz, 1H), 1.48 (s, 6H), 1.25 (s, 9H), 0.93 (s, 9H), 0.88 (s, 9H), 0.14 (s, 6H), 0.07 (s, 3H), 0.04 (s, 3H). ^{13}C NMR (101 MHz, MeOH-d$_4$) δ 218.4, 144.1, 140.5, 136.5, 118.8, 87.9, 87.2, 84.2, 71.9, 62.4, 43.8, 40.2, 27.9, 25.1, 24.91, 23.8, 17.9, 17.5, -5.9, -6.0, -6.8. IR (KBr plate) 2927, 1672, 1609, 1474, 1254, 1112, 832, 782, 662 cm^{-1}. HRMS (ESI-TOF) $C_{30}H_{56}N_5O_5Si_2^+$ (M + H)$^+$ calcd. 622.3820, found 622.3820.
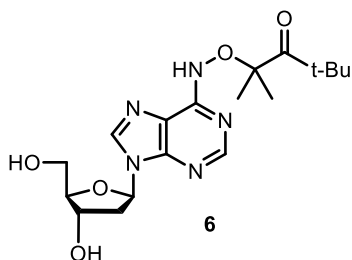
Preparation of 6. Et$_3$N•3HF (0.83 g, 5.2 mmol) was slowly added to **131** (320 mg, 0.52 mmol) and the reaction was stirred at 25 ºC overnight. The reaction was concentrated under vacuum and purified by flash chromatography on a silica column. Elution with 5% MeOH in DCM gave **6** as a yellow foam (163 mg, 59%). ^{1}H NMR (400 MHz, MeOH-d$_4$) δ 8.01 (s, 1H), 7.64 (s, 1H), 6.45 – 6.17 (m, 1H), 4.60 – 4.40 (m, 1H), 4.02 (dd, J = 6.1, 3.2 Hz, 1H), 3.80 (dd, J = 12.2, 3.2 Hz, 1H), 3.75 – 3.67 (m, 1H), 2.77 – 2.62 (m, 1H), 2.39 (ddd, J = 13.4, 6.0, 2.9 Hz, 1H), 1.48 (s, 6H), 1.24 (s, 9H). ^{13}C NMR (101 MHz, MeOH-d$_4$) δ 218.4, 144.2, 140.5, 140.3, 137.1, 119.2, 88.3, 87.3, 85.3, 71.4, 62.1, 43.8, 40.6, 27.9, 23.8. IR (KBr plate) 3278 (broad), 2932, 1669, 1610, 1471, 1254, 1110, 837, 778, 665 cm^{-1}. HRMS (ESI-TOF) $C_{18}H_{28}N_5O_5^+$ (M + H)$^+$ calcd. 394.2090, found 394.2085.
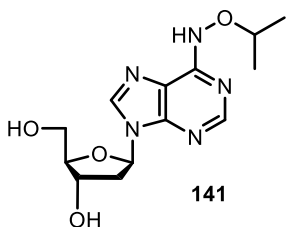
Preparation of 138. Et₃N•3HF (323 mg, 2.0 mmol) was slowly added to **123** (99 mg, 0.2 mmol) in THF (2 mL). The reaction was stirred at 25 °C overnight, concentrated under vacuum, and purified by flash chromatography on a silica column. Elution with 10% MeOH in DCM gave **138** as a light purple foam. The sample was dissolved in MeOH (2 mL) and Na₂-EDTA (770 mg, 2 mmol) was added to the solution and the reaction was stirred at 50 °C until the purple color faded. The mixture was cooled to room temperature and filtered to remove Na₂-EDTA. The organic phase was then concentrated under vacuum give **138** as a white foam (37.5 mg, 70%). ^{1}H NMR (400 MHz, MeOH-d₄) δ 8.36 (s, 1H), 8.20 (s, 1H), 6.44 (dd, J = 7.9, 6.0 Hz, 1H), 4.58 (dt, J = 5.6, 2.7 Hz, 1H), 4.07 (dd, J = 5.8, 3.1 Hz, 1H), 3.84 (dd, J = 12.3, 3.0 Hz, 1H), 3.74 (dd, J = 12.3, 3.4 Hz, 1H), 2.80 (ddd, J = 13.6, 7.9, 5.8 Hz, 1H), 2.42 (ddd, J = 13.6, 6.0, 2.8 Hz, 1H). The spectral data matches the literature.[327]
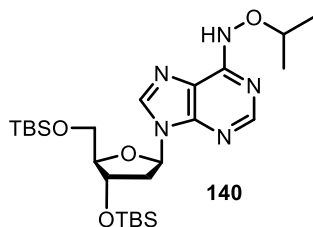
Preparation of 140. NaH (60% in mineral oil, 20 mg, 0.5 mmol) was slowly to **123** (241 mg, 0.5 mmol) in THF (3 mL). The reaction was stirred at 0 °C for 30 min, at which time 2-bromopropane (68 mg, 0.55 mmol) was added at 0 °C. The reaction was stirred at room temperature for 2 h and quenched with MeOH. The reaction was concentrated under vacuum and purified by flash chromatography on a silica column. Elution with 50% EtOAc in hexanes gave **140** as a red oil (70 mg, 26%). ^{1}H NMR (400 MHz, MeOH-d₄) δ 8.03 (s, 1H), 7.69 (s, 1H), 6.31 (s, 1H), 5.50 (d, J = 10.6 Hz, 1H), 4.76 – 4.59 (m, 1H), 4.27 (hept, J = 6.3 Hz, 1H), 3.95 (dd, J = 8.0, 3.7 Hz, 1H), 3.85 (dd, J = 11.2, 4.6 Hz, 1H), 3.76 (dd, J = 11.2, 3.7 Hz, 1H), 2.80 – 2.67 (m, 1H), 2.40 (ddd, J = 13.1,

6.2, 4.2 Hz, 1H), 1.29 (d, J = 6.2 Hz, 6H), 0.93 (s, 9H), 0.89 (s, 9H), 0.14 (s, 6H), 0.07 (s, 3H), 0.05 (s, 3H). ^{13}C NMR (101 MHz, CDCl$_3$) δ 156.1, 152.9, 149.8, 142.4, 140.7, 140.1, 139.6, 136.0, 120.1, 118.8, 87.9, 84.4, 83.9, 78.0, 75.1, 71.8, 62.8, 41.5, 41.2, 26.0, 25.8, 21.8, 20.6, 18.4, 18.0, -4.6, -4.8, -5.4, -5.5. IR (KBr plate) 2975, 2920, 1670, 1581, 1412, 1223, 889, 748, 659 cm^{-1}. HRMS (ESI-TOF) C$_{25}$H$_{48}$N$_5$O$_4$Si$_2^+$ (M + H)$^+$ calcd. 538.3245, found 538.3240.

Preparation of 141. Et$_3$N•3HF (122 mg, 0.76 mmol) was added to **140** (40.5 mg, 0.076 mmol) in THF (1 mL). The reaction was stirred at 25 °C overnight. The reaction was concentrated under vacuum and purified by flash chromatography on a silica column. Elution with 5% MeOH in DCM gave **141** as a yellow foam (19 mg, 80%). ^{1}H NMR (400 MHz, MeOH-d$_4$) δ 8.06 (s, 1H), 7.64 (s, 1H), 6.34 (s, 1H), 4.61 – 4.41 (m, 1H), 4.27 (hept, J = 6.1 Hz, 1H), 4.04 (d, J = 2.8 Hz, 1H), 3.81 (dd, J = 12.2, 3.1 Hz, 1H), 3.72 (dd, J = 12.2, 3.6 Hz, 1H), 2.72 (m, 1H), 2.39 (ddd, J = 13.4, 6.0, 2.8 Hz, 1H), 1.29 (d, J = 6.2 Hz, 6H). ^{13}C NMR (101 MHz, MeOH-d$_4$) δ 153.6, 145.5, 142.6, 138.6, 121.1, 89.73, 86.8, 76.1, 73.6, 63.6, 41.9, 21.9. IR (KBr plate) 3274 (broad), 2973, 2924, 1659, 1589, 1416, 1393, 1327, 1217, 1095, 1058, 967, 942, 893, 753, 653 cm^{-1}. HRMS (ESI-TOF) C$_{13}$H$_{20}$N$_5$O$_4^+$ (M + H)$^+$ calcd. 310.1515, found 310.1513.
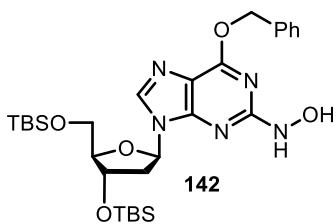
Preparation of 142. Hydroxylamine hydrochloride (345 mg, 5 mmol) was treated with TEA (1.01 g, 10 mmol) in dioxane (10 mL) for 30 min before **100** (324 mg, 0.5 mmol) was added. The reaction was refluxed at 110 °C overnight. The reaction was cooled to room temperature, concentrated under vacuum, and purified by

flash chromatography on a silica column. Elution with 5% MeOH and 1% Et$_3$N in DCM gave **142** as a white foam (186 mg, 62%). ^{1}H NMR (400 MHz, CDCl$_3$) δ 9.70 (s, 1H), 8.09 (s, 1H), 7.58 (s, 1H), 7.41 (d, J = 6.6 Hz, 2H), 7.33 – 7.07 (m, 3H), 6.60 (t, J = 6.2 Hz, 1H), 5.48 (q, J = 12.3 Hz, 2H), 4.57 (dt, J = 7.4, 3.9 Hz, 1H), 4.00 (d, J = 3.1 Hz, 1H), 3.83 (dd, J = 11.3, 3.1 Hz, 1H), 3.79 (dd, J = 11.3, 3.1 Hz, 1H), 2.60 – 2.45 (m, 1H), 2.36 (dt, J = 12.7, 6.2 Hz, 1H), 0.91 (s, 9H), 0.90 (s, 9H), 0.11 (s, 6H), 0.08 (s, 6H). ^{13}C NMR (101 MHz, CDCl$_3$) δ 162.3, 160.7, 152.4, 138.0, 136.0, 128.4, 128.3, 128.3, 128.27, 128.25, 128.23, 128.23, 128.22, 128.0, 117.0, 87.6, 84.0, 71.8, 68.4, 62.7, 42.2, 26.0, 25.8, 18.4, 18.0, -4.6, -4.8, -5.4, -5.5. HRMS (ESI-TOF) m/z calcd for (C$_{29}$H$_{47}$N$_5$O$_5$Si$_2$)$^+$ (M + H)$^+$ = 602.3194, found m/z = 602.3197.

143
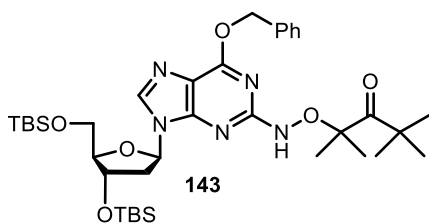
Preparation of 143. Compound **142** (186 mg, 0.31 mmol) was dissolved in DMF (3 mL). Cs$_2$CO$_3$ (101 mg, 0.31 mmol) was slowly added while stirring. The reaction was stirred at 0 ℃ for 30 min before **130** (81 mg, 0.39 mmol) was added at 0 ℃. The reaction was stirred at room temperature overnight. The reaction was quenched by water and extracted with DCM (3 × 10 mL). The organic phase was dried over Na$_2$SO$_4$. Na$_2$SO$_4$ was removed by filtration, and the mixture was concentrated under vacuum. The residue was purified by flash chromatography on a silica column. Elution with 50% EtOAc in hexanes gave **143** as a yellow foam (158 mg, 70%). ^{1}H NMR (400 MHz, CDCl$_3$) δ 8.03 (s, 1H), 7.60 (s, 1H), 7.38 (d, J = 6.7 Hz, 2H), 7.22 (ddd, J = 8.5, 7.7, 2.3 Hz, 3H), 6.33 (t, J = 6.5 Hz, 1H), 5.57 – 5.40 (m, 2H), 4.60 – 4.41 (m, 1H), 3.95 (dd, J = 6.3, 3.1 Hz, 1H), 3.75 (qd, J = 11.2, 3.5 Hz, 2H), 2.48 – 2.36 (m, 1H), 2.30 (ddd, J = 12.9, 5.8, 3.5 Hz, 1H), 1.48 (s, 7H), 1.32 (s, 10H), 0.86 (s, 18H),

0.04 (d, $J = 2.3$ Hz, 12H). ^{13}C NMR (101 MHz, CDCl$_3$) δ 215.6, 161.1, 160.6, 153.0, 138.4, 136.1, 128.3, 128.0, 127.9, 117.4, 91.2, 87.8, 84.1, 72.0, 68.1, 62.9, 45.2, 41.7, 26.8, 26.0, 25.9, 25.7, 24.4, 24.3, 18.4, 17.9, -4.7, -4.8, -5.4, -5.5. HRMS (ESI-TOF) m/z calcd for (C$_{37}$H$_{62}$N$_5$O$_6$Si$_2$)$^+$ (M + H)$^+$ = 728.4239, found m/z = 728.4245.
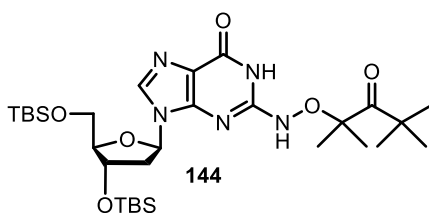
Preparation of 144. Compound **143** (158 mg, 0.22 mmol) was dissolved in MeOH (4 mL), and 20 mg 10% Pd/C was added to the solution. The flask was sparged with hydrogen using a balloon. The reaction was monitored by TLC (3% MeOH in DCM) and was complete after 30 min. The Pd/C was removed by passing the reaction through a silica plug. The reaction was concentrated under vacuum and purified by flash chromatography on a silica column. Elution with 1% to 3% MeOH in DCM gave **144** as a white solid (126 mg, 90%). ^{1}H NMR (400 MHz, CDCl$_3$) δ 7.84 (s, 1H), 6.23 (t, $J = 6.5$ Hz, 1H), 4.51 (br, 1H), 3.96 (br, 1H), 3.72 (d, $J = 12.1$ Hz, 2H), 2.55 – 2.21 (m, 2H), 1.54 (s, 3H), 1.52 (s, 3H), 1.33 (s, 9H), 0.89 (s, 9H), 0.88 (s, 9H), 0.08 (s, 6H), 0.06 (s, 3H), 0.05 (s, 3H). ^{13}C NMR (101 MHz, CDCl$_3$) δ 214.9, 157.7, 154.7, 149.6, 136.0, 119.4, 90.9, 87.9, 83.9, 72.2, 62.9, 44.9, 41.4, 27.2, 25.9, 25.7, 24.1, 18.4, 18.0, -4.7, -4.8, -5.4, -5.5. HRMS (ESI-TOF) m/z calcd for (C$_{30}$H$_{56}$N$_5$O$_6$Si$_2$)$^+$ (M + H)$^+$ = 638.3769, found m/z = 638.3742.
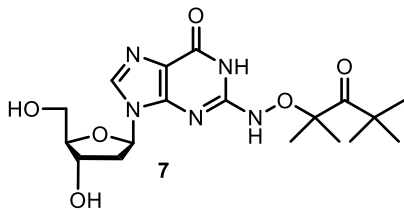
Preparation of 7. Compound **144** (126 mg, 0.2 mmol) was dissolved in THF (2 mL). Et$_3$N•3HF (322 mg, 2.0 mmol) was slowly added while stirring. The reaction was stirred at 25 °C overnight. The reaction was concentrated under vacuum and purified by flash chromatography on a silica column. Elution with 7% MeOH in DCM gave **7** as a

208

light pink foam (63.8 mg, 78%). ^{1}H NMR (400 MHz, MeOH-d4) δ 8.14 (s, 1H), 6.31 (t, J = 6.7 Hz, 1H), 4.56 – 4.42 (m, 1H), 3.98 (dd, J = 7.3, 3.8 Hz, 1H), 3.75 (dd, J = 7.3, 4.0 Hz, 1H), 2.64 (ddd, J = 13.4, 7.1, 6.2 Hz, 1H), 2.39 (ddd, J = 13.4, 6.2, 3.6 Hz, 1H), 1.57 (d, J = 1.1 Hz, 6H), 1.31 (s, 9H). ^{13}C NMR (101 MHz, MeOH-d4) δ 215.5, 157.2, 155.3, 149.8, 137.4, 118.4, 90.3, 87.8, 84.2, 71.1, 61.7, 44.4, 40.3, 26.4, 23.3. HRMS (ESI-TOF) m/z calcd for $(C_{18}H_{28}N_5O_6)^+$ $(M + H)^+$ = 410.2040, found m/z = 410.2038.
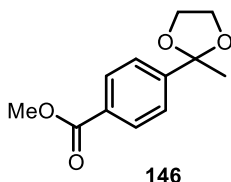
Preparation of 146. Methyl 4-acetylbenzoate (2.67 g, 15 mmol), ethylene glycol (1.24 g, 1.1 mL, 20 mmol), and p-toluenesulfonic acid (26 mg, 0. 15 mmol) were dissolved in toluene (15 mL) was added. A Dean-Stark trap was attached, and the solution was refluxed for 24 h. The solution was washed with saturated NaHCO$_3$ (50 mL) and extracted with DCM (3 × 50 mL). The combined organic phase was dried over Na$_2$SO$_4$. Na$_2$SO$_4$ was removed by filtration, and the mixture was concentrated under vacuum. The product was purified by flash chromatography on a silica column. Elution with 20% EtOAc in hexanes gave **146** as white solid (3.1g, 92%). ^{1}H NMR (400 MHz, CDCl$_3$) δ 8.01 (d, J = 8.6 Hz, 2H), 7.55 (d, J = 8.6 Hz, 2H), 4.05 (td, J = 6.2, 4.2 Hz, 2H), 3.91 (s, 3H), 3.76 (td, J = 6.2, 4.2 Hz, 2H), 1.65 (s, 3H).
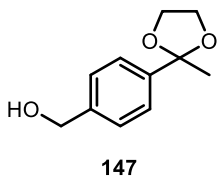
Preparation of 147. A solution of **146** (3.1 g, 14 mmol) in THF (20 mL) was added dropwise to a suspension of LiAlH$_4$ (1.33 g, 35 mmol) in THF (25 mL) over 10 min at 0 °C. The ice bath was removed, and the reaction was stirred at room temperature for 12 h. The reaction mixture quenched by 10% NaOH and extracted with DCM (3 × 50 mL). The combined organic phase was dried over Na$_2$SO$_4$. Na$_2$SO$_4$ was removed by filtration, and the mixture was concentrated

under vacuum to give **147** as a white solid (3.14 g, 99%). ^{1}H NMR (400 MHz, CDCl$_3$) δ 7.43 (d, J = 8.3 Hz, 2H), 7.29 (d, J = 8.3 Hz, 2H), 4.59 (s, 2H), 3.98 (td, J = 6.1, 4.2 Hz, 2H), 3.72 (td, J = 6.1, 4.2 Hz, 2H), 3.40 (s, 1H), 1.62 (s, 3H).
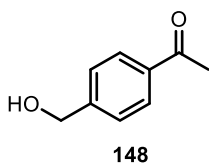

Preparation of 148. A mixture of THF (2.5 mL), H$_2$O (1.5 mL) and concentrated HCl (1 mL) was added to **147** (1 g, 5 mmol). The reaction was stirred at room temperature for 30 min. The reaction mixture was extracted with DCM (3 × 30 mL), dried over Na$_2$SO$_4$. Na$_2$SO$_4$ was removed by filtration, and the mixture was concentrated under vacuum. The residue was chromatographed on silica gel and eluted with 30% ethyl acetate in hexanes to give **148** as white solid (744 mg, 99%). ^{1}H NMR (400 MHz, CDCl$_3$) δ 7.90 (d, J = 8.6 Hz, 2H), 7.42 (d, J = 8.6 Hz, 2H), 4.74 (s, 2H), 3.01 (s, 1H), 2.57 (s, 3H).
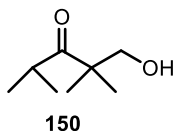
Preparation of 150. To a mixture of 2,2,4-trimethyl-1,3-pentanediol (730 mg, 5 mmol), ethylene glycol (1.24 g, 1.1 mL, 20 mmol), dimethyl sulfoxide (470 mg, 425 µL, 6 mmol), and Re(O)Cl$_3$(PPh$_3$)$_2$ (210 mg, 0.25 mmol), toluene (25 mL) was added. A Dean-Stark trap was attached, and the solution was heated to reflux. An additional portion of ethylene glycol (2.5 g, 2.2 mL, 40 mmol) was added after 1 h. The reaction was removed from the heat after a total of 3 h. The solution was washed with saturated NaHCO$_3$ (50 mL) and extracted with DCM (3 × 50 mL). The combined organic phase was dried over Na$_2$SO$_4$. Na$_2$SO$_4$ was removed by filtration, and the mixture was concentrated under vacuum. The product was purified by flash chromatography on a silica column. Elution with 10% EtOAc in hexanes gave **150** as a colorless oil (635 mg, 88%). ^{1}H NMR (400 MHz, CDCl$_3$) δ 3.57 (s, 2H), 2.49 (s, 1H),

1.92 (s, 6H), 1.42 (s, 6H). ^{13}C NMR (101 MHz, CDCl$_3$) δ 209.8, 71.8, 62.4, 50.7, 31.6, 23.75, 23.73.


152
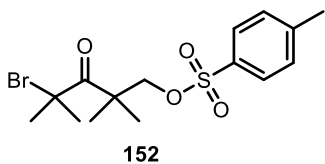
Preparation of 152. Br$_2$ (635 mg, 4.5 mmol) was added to a solution of **150** (635 mg, 4.4 mmol) in chloroform (15 mL). The solution was refluxed for 1 h and stirred at room temperature overnight. The reaction was concentrated under vacuum, and the product (**151**) was used for the next step without further purification. *p*-Toluenesulfonyl chloride (1.72 g, 9 mmol) was added to a solution of crude **151** (1 g, 4.5 mmol) in pyridine (10 mL). The reaction was stirred overnight. The solution was washed with saturated NaHCO$_3$ (20 mL) and extracted with DCM (3 × 10 mL). The combined organic phase was dried over Na$_2$SO$_4$. Na$_2$SO$_4$ was removed by filtration, and the mixture was concentrated under vacuum. The product was purified by flash chromatography on a silica column. Elution with 20% EtOAc in hexanes gave **152** as a yellow oil (1.5 g, 90%). ^{1}H NMR (400 MHz, CDCl$_3$) δ 7.73 (d, *J* = 8.0 Hz, 2H), 7.33 (d, *J* = 8.0 Hz, 2H), 4.04 (s, 2H), 2.43 (s, 3H), 1.85 (s, 6H), 1.44 (s, 6H). ^{13}C NMR (101 MHz, CDCl$_3$) δ 205.76, 144.9, 132.7, 129.9, 127.9, 62.1, 49.1, 31.3, 24.0, 21.7.

154
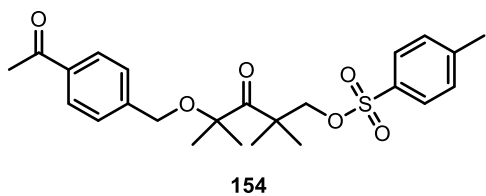
Preparation of 154. A mixture of **152** (32.7 mg, 0.1 mmol) and *p*-hydroxymethyl acetophenone (**148**, 15 mg, 0.1 mmol), was dissolved in DMF (1 mL), and Cs$_2$CO$_3$ (32.5 mg, 0.1 mmol) was added. The reaction was stirred overnight. The reaction was concentrated under vacuum and purified by flash chromatography on a silica column. Elution with 10% EtOAc in hexanes gave **154** as a colorless oil (35 mg, 88%). ^{1}H NMR (400 MHz, CDCl$_3$) δ 7.94 – 7.87 (m, 2H), 7.83 – 7.76

(m, 2H), 7.34 (dd, J = 8.6, 0.7 Hz, 2H), 7.27 (dd, J = 8.1, 0.5 Hz, 2H), 4.58 (d, J = 13.4 Hz, 1H), 4.51 (d, J = 13.4 Hz, 1H), 4.14 (d, J = 9.0 Hz, 1H), 3.96 (d, J = 9.0 Hz, 1H), 2.62 (s, 3H), 2.46 (s, 3H), 1.50 (s, 3H), 1.27 (s, 4H), 1.11 (s, 3H), 1.10 (s, 3H).
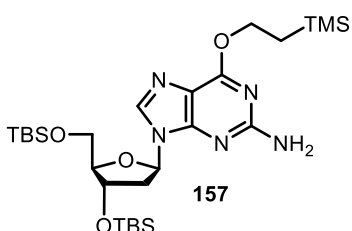
Preparation of 157.[253] 3',5'-Bis-O-TBDMS-2'-deoxyguanosine (**86**, 980 mg, 2 mmol), 2-(trimethylsilyl)ethanol (472 mg, 4 mmol), and PPh₃ (1.05 g, 4 mmol) was dissolved in THF (25 mL). DEAD (696 mg, 4 mmol) was slowly added. The reaction was stirred at 25 °C overnight. The reaction mixture quenched with water and extracted with DCM (3 × 20 mL). The combined organic phase was dried over Na₂SO₄. Na₂SO₄ was removed by filtration, and the mixture was concentrated under vacuum. The product was purified by flash chromatography on a silica column. Elution with 20% EtOAc in hexanes gave **157** as a light yellow oil (610 mg, 49%). ¹H NMR (400 MHz, CDCl₃) δ 7.85 (s, 1H), 6.30 (t, J = 6.8, 1H), 4.92 (s, 2H), 4.59 – 4.39 (m, 3H), 3.95 (dd, J = 7.4, 3.3 Hz, 1H), 3.78 (dd, J = 11.1, 4.3 Hz, 1H), 3.73 (dd, J = 11.1, 3.3 Hz, 1H), 2.54 (ddd, J = 13.0, 7.1, 5.8 Hz, 1H), 2.33 (ddd, J = 13.0, 6.1, 3.7 Hz, 1H), 1.24 – 1.17 (m, 2H), 0.89 (s, 9H), 0.89 (s, 9H), 0.08 (s, 6H), 0.06 (s, 9H), 0.05 (s, 3H), 0.05 (s, 3H).
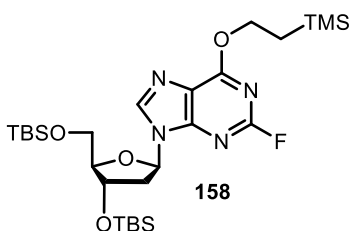
Preparation of 158.[253] Compound **157** (610 g, 1.02 mmol) was dissolved in 28 mL anhydrous toluene and cooled to -10 °C. Polyvinylpyridine-HF (3.7 g) and tert-butyl nitrite (850 mg, 0.88 mL, 7.4 mmol) were added. After 1 h, the reaction was poured into cold saturated NaHCO₃ (100 mL). The resulting solid was removed by filtration, and the organic phase product extracted with EtOAc (3 ×30 mL).

The organic phase was dried using Na$_2$SO$_4$. Na$_2$SO$_4$ was removed by filtration, and the mixture was concentrated under vacuum. The reaction was purified by flash chromatography on a silica column. Elution with 10% EtOAc in hexanes gave **158** as a colorless oil (402.5 mg, 67%). ^{1}H NMR (400 MHz, CDCl$_3$) δ 8.13 (s, 1H), 6.32 (t, J = 6.4 Hz, 1H), 4.66 – 4.51 (m, 3H), 3.94 (dd, J = 7.0, 3.3 Hz, 1H), 3.82 (dd, J = 11.2, 4.2 Hz, 1H), 3.71 (dd, J = 11.2, 3.1 Hz, 1H), 2.56 (dt, J = 13.1, 4.7 Hz, 1H), 2.36 (ddd, J = 13.1, 6.1, 3.9 Hz, 1H), 1.30 – 1.14 (m, 2H), 0.84 (s, 9H), 0.84 (s, 9H), 0.04 (s, 6H), 0.03 (s, 9H), 0.02 (s, 3H), 0.01 (s, 3H).
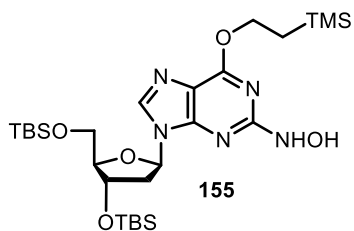
Preparation of 155. A mixture of **158** (402.5 mg, 0.67 mmol), hydroxylamine hydrochloride (467 mg, 6.7 mmol), and triethylamine (1.35 g, 1.9 mL, 13.4 mmol) was dissolved in anhydrous dioxane (7 mL). The reaction was refluxed overnight. The reaction mixture quenched with water and extracted with DCM (3 × 20 mL). The combined organic phase was dried over Na$_2$SO$_4$. Na$_2$SO$_4$ was removed by filtration, and the mixture was concentrated under vacuum. The product was purified by flash chromatography on a silica column. Elution with 30% EtOAc in hexanes gave **155** as a light yellow foam (307.5 mg, 75%). ^{1}H NMR (400 MHz, CDCl$_3$) δ 9.61 (s, 1H), 8.04 (s, 1H), 7.40 (s, 1H), 6.58 (t, J = 6.3 Hz, 1H), 4.67 – 4.38 (m, 3H), 3.99 (dd, J = 6.4, 3.2 Hz, 1H), 3.83 (dd, J = 11.2, 3.6 Hz, 1H), 3.77 (dd, J = 11.2, 2.8 Hz, 1H), 2.51 (ddd, J = 12.9, 5.9, 4.0 Hz, 1H), 2.40 – 2.26 (m, 1H), 1.24 – 1.11 (m, 2H), 0.90 (s, 9H), 0.89 (s, 9H), 0.09 (s, 6H), 0.07 (s, 6H), 0.03 (s, 9H). ^{13}C NMR (101 MHz, CDCl$_3$) δ 162.4, 161.1, 152.0, 137.8, 117.1, 87.6, 84.0, 71.8, 65.4, 62.7, 42.2, 25.9, 25.8, 25.8, 25.7, 18.43, 18.42, 18.04, 18.03, 17.5, -1.4, -1.4, -1.4, -4.5, -4.8, -5.3, -5.5.
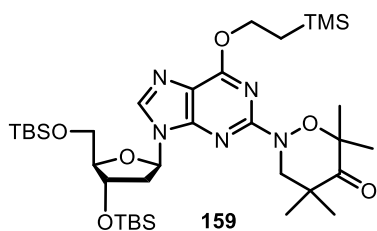
Preparation of 159. A mixture of **155** (61.5 mg, 0.1 mmol), **152** (32.7 mg, 0.1 mmol), and Cs_2CO_3 (32.5 mg, 0.1 mmol) was dissolved in anhydrous DMF (1 mL). The reaction wa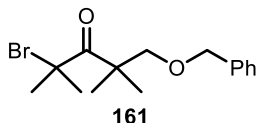s stirred at room temperature overnight. The reaction was quenched with water and extracted with EtOAC (3 × 10 mL). The combined organic phase was dried over Na_2SO_4. Na_2SO_4 was removed by filtration, and the mixture was concentrated under vacuum. The product was purified by flash chromatography on a silica column. Elution with 20% EtOAc in hexanes gave **159** as a light yellow oil (307.5 mg, 75%). ^{1}H NMR (400 MHz, CDCl$_3$) δ 8.01 (s, 1H), 6.43 (t, J = 6.6 Hz, 1H), 4.70 – 4.63 (m, 2H), 4.61 – 4.51 (m, 1H), 4.06 – 3.97 (m, 3H), 3.84 (dd, J = 11.2, 4.3 Hz, 1H), 3.79 (dd, J = 11.2, 3.5 Hz, 1H), 2.58 (ddd, J = 13.0, 7.0, 5.8 Hz, 1H), 2.42 (ddd, J = 13.0, 6.1, 3.7 Hz, 1H), 1.53 (s, 3H), 1.51 (s, 3H), 1.34 (s, 6H), 1.30 – 1.26 (m, 2H), 0.94 (s, 9H), 0.93 (s, 9H), 0.12 (s, 6H), 0.11 (s, 9H), 0.10 (s, 2H), 0.10 (s, 3H).
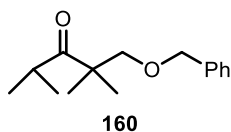
Preparation of 160. NaH (60% in mineral oil, 168 mg, 4.2 mmol) was slowly added to **150** (576 mg, 4 mmol) in DMF (20 mL). The reaction was stirred at 0 ℃ for 30 min, at which time benzyl bromide (718.2 mg, 4.2 mmol) was added at 0 ℃. The reaction was stirred at room temperature for 4 h. The reaction was quenched with MeOH, washed with water, and extracted with DCM (30 mL × 3). The combined organic phase was dried over Na_2SO_4. Na_2SO_4 was removed by filtration, and the mixture was concentrated under vacuum. The product was purified by flash chromatography on a silica column. Elution with 10% EtOAc in hexanes gave **160** as a colorless oil (814 mg, 87%). ^{1}H NMR (400 MHz, CDCl$_3$) δ 7.40 – 7.28 (m, 5H), 4.53 (s, 2H), 3.52 (s, 2H), 3.15 (hept, J = 6.7 Hz, 1H), 1.21 (s, 6H), 1.08

(d, $J = 6.7$ Hz, 6H). ^{13}C NMR (101 MHz, CDCl$_3$) δ 218.8, 138.3, 128.3, 127.5, 127.4, 73.3, 49.0, 34.3, 21.7, 19.9.
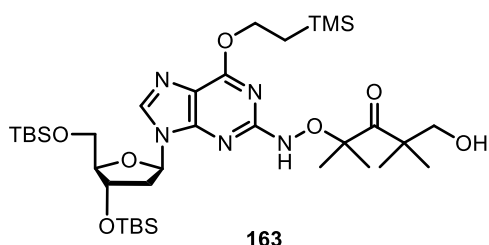
Preparation of 161. Br$_2$ (160 mg, 1 mmol) was added to a solution of **160** (230 mg, 1 mmol) in chloroform (3 mL). The solution was refluxed for 1 h and stirred at room temperature overnight. The reaction was washed with water, extracted with DCM (10 mL × 3). The combined organic phase was dried over Na$_2$SO$_4$. Na$_2$SO$_4$ was removed by filtration, and the mixture was concentrated under vacuum. The product was purified by flash chromatography on a silica column. Elution with 10% EtOAc in hexanes gave **161** as a colorless oil (104 mg, 35%). ^{1}H NMR (400 MHz, CDCl$_3$) δ 7.43 – 7.25 (m, 5H), 4.50 (s, 2H), 3.59 (s, 2H), 1.96 (s, 6H), 1.51 (s, 6H).
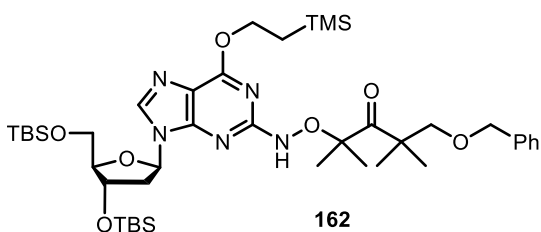
Preparation of 162. Compound **155** (61 mg, 0.1 mmol) was dissolved in. DMF (3 mL). Cs$_2$CO$_3$ (33 mg, 0.1 mmol) was slowly added while stirring. The reaction was stirred at room temperature for 30 min. The solution was cooled to 0 °C and **161** (32 mg, 0.1 mmol) was added. The reaction was warmed to room temperature and stirred overnight. The reaction was washed with water, extracted with DCM (10 mL × 3). The combined organic phase was dried over Na$_2$SO$_4$. Na$_2$SO$_4$ was removed by filtration, and the mixture was concentrated under vacuum. The product was purified by flash chromatography on a silica column. Elution with 50% EtOAc in hexanes gave **162** as a yellow foam (50.2 mg, 59.5%). ^{1}H NMR (400 MHz, CDCl$_3$) δ 8.01 (s, 1H), 7.53 (s, 1H), 7.32 – 7.19 (m, 6H), 6.36 (t, $J = 6.5$ Hz, 1H), 4.61 – 4.46 (m, 5H), 3.96 (d, $J = 3.3$ Hz, 1H), 3.80 (dd, $J = 11.2, 4.0$ Hz, 1H),

3.76 (dd, J = 11.2, 3.1 Hz, 1H), 3.72 – 3.60 (m, 2H), 2.50 – 2.38 (m, 1H), 2.33 (ddd, J = 12.9, 5.9, 3.4 Hz, 1H), 1.53 (s, 6H), 1.39 (s, 6H), 1.23 (dt, J = 6.7, 4.5 Hz, 2H), 0.91 (s, 9H), 0.89 (s, 9H), 0.10 – 0.07 (m, 12H), 0.05 (s, 9H). ^{13}C NMR (101 MHz, CDCl$_3$) δ 214.2, 161.0, 152.7, 138.3, 138.1, 128.2, 127.7, 127.5, 117.4, 91.0, 87.8, 83.9, 72.0, 65.1, 62.9, 49.8, 41.7, 26.0, 25.8, 24.01, 23.98, 23.2, 23.1, 18.4, 18.0, 17.5, -1.4, -4.6 -4.8, -5.3, -5.5.


163

Preparation of 163. Compound **162** (50.2 mg, 0.06 mmol) was dissolved in MeOH (1 mL), and 13 mg 10% Pd/C was added to the solution. The flask was sparged with hydrogen using a balloon. The reaction was monitored by TLC and was complete after 3 h. The Pd/C was removed by passing the reaction through a silica plug. The combined organic phase was dried over Na$_2$SO$_4$. Na$_2$SO$_4$ was removed by filtration, and the mixture was concentrated under vacuum. The product was purified by flash chromatography on a silica column. Elution with 1% to 3% MeOH in DCM gave **163** as a white solid (11 mg, 25%). ^{1}H NMR (400 MHz, CDCl$_3$) δ 8.13 (s, 1H), 7.40 (s, 1H), 6.43 (t, J = 6.1 Hz, 1H), 4.65 – 4.58 (m, 2H), 4.56 (dd, J = 9.9, 4.7 Hz, 1H), 3.99 (dd, J = 6.6, 3.4 Hz, 1H), 3.88 (dd, J = 11.3, 3.6 Hz, 1H), 3.80 (dd, J = 11.3, 2.9 Hz, 3H), 2.47 (ddd, J = 13.0, 6.2, 4.7 Hz, 1H), 2.41 – 2.26 (m, 1H), 1.56 (d, J = 3.7 Hz, 6H), 1.33 (s, 6H), 1.30 – 1.24 (m, 3H), 0.94 (s, 9H), 0.92 (s, 9H), 0.12 (s, 3H), 0.12 (s, 3H), 0.11 (s, 9H), 0.10 (s, 3H), 0.10 (s, 3H).

164
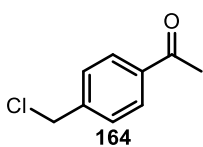
Preparation of 164.[254] To the solution of 4-vinylbenzyl chloride (304 mg, 2 mmol) in CH$_3$CN (10 mL), Pd/C (5 wt%, 420 mg, 0.1 mmol) and H$_2$SO$_4$ (70 wt%, 25 μL) were added. The mixture was stirred for about 15 min at room temperature. Then H$_2$O$_2$ (30 wt%, 1.36 g, 12 mmol) was added

dropwise, and the mixture was heated to 65 °C for 12 h. The Pd/C was removed by passing the reaction through a silica plug. The reaction was concentrated, washed with water, and extracted with DCM (3 × 20 mL). The combined organic phase was dried over Na_2SO_4. Na_2SO_4 was removed by filtration, and the mixture was concentrated under vacuum. The product was purified by flash chromatography on a silica column. Elution with 5% EtOAc in hexanes gave **164** as a light yellow solid (320 mg, 95%). ^{1}H NMR (400 MHz, CDCl3) δ 10.03 (s, 1H), 7.89 (d, $J = 7.8$ Hz, 2H), 7.57 (d, $J = 7.6$ Hz, 2H), 4.65 (s, 2H).
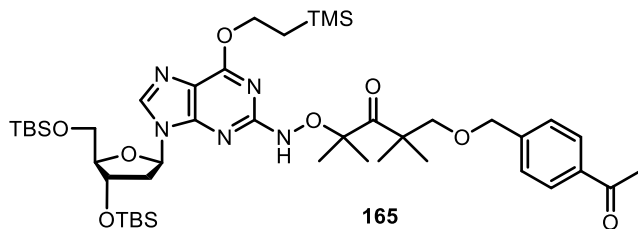
Preparation of 165. NaH (60% in mineral oil, 0.6 mg, 0.015 mmol) was slowly added to **163** (11 mg, 0.015 mmol) in DMF (0.5 mL). The reaction was stirred at 0 °C for 30 min, at which time *p*-chloromethyl-acetophenone (**164**, 5.1 mg, 0.03 mmol) was added at 0 °C. The reaction was stirred at room temperature for 2 h. The reaction was concentrated under vacuum and purified by flash chromatography on a silica column. Elution with 50% EtOAc in hexanes gave **165** as a yellow solid (11.5 mg, 87%). ^{1}H NMR (400 MHz, CDCl3) δ 8.20 (s, 1H), 7.91 – 7.82 (m, 2H), 7.35 (s, 2H), 6.45 (s, 1H), 5.62 (s, 1H), 5.00 (s, 1H), 4.85 (s, 1H), 4.50 (d, $J = 7.1$ Hz, 3H), 4.07 (s, 1H), 3.99 – 3.94 (m, 1H), 3.88 (s, 1H), 3.80 (dd, $J = 11.3, 2.4$ Hz, 1H), 2.58 (s, 3H), 2.49 (br, 1H), 2.25 (br, 1H), 1.53 (d, $J = 18.4$ Hz, 6H), 1.21 – 1.09 (m, 8H), 0.94 (s, 9H), 0.91 (s, 9H), 0.12 (d, $J = 1.9$ Hz, 6H), 0.10 (dd, $J = 7.1, 3.6$ Hz, 6H), 0.02 (s, 9H).
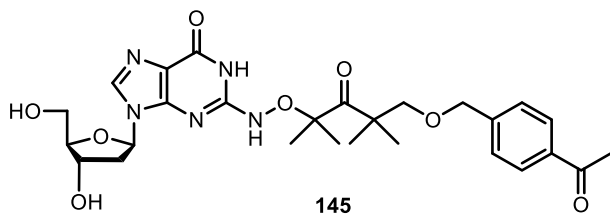
Preparation of 145. A solution of TBAF trihydrate (95 mg, 0.3 mmol) in THF (0.3 mL) was added to **165** (11.5 mg, 0.013 mmol). The reaction was stirred at room temperature for 1 h. The reaction was concentrated under vacuum and purified by flash chromatography on a silica column. Elution with 6% MeOH in methanol gave **145** as a white solid (5.6 mg, 82%) ^{1}H NMR (400 MHz, MeOH-d$_4$) δ 8.36 (s, 1H), 7.98 – 7.81 (m, 2H), 7.42 (d, J = 8.4 Hz, 2H), 6.44 (t, J = 6.5 Hz, 1H), 4.49 (m, 3H), 3.97 (q, J = 3.8 Hz, 1H), 3.92 – 3.64 (m, 4H), 2.55 (m, 4H), 2.41 (ddd, J = 13.5, 6.2, 4.1 Hz, 1H), 1.56 (s, 6H), 1.26 (s, 6H).

Preparation of 170.[166] ω-Bromo-p-chloroacetophenone (2.3 g, 10 mmol) is dissolved in ethanol (10 mL), and treated with a solution of hydroxylamine hydrochloride (695 mg, 10 mmol) in water (2 mL) at 20°C. The reaction was stirred for 24 h at 20°C and poured into a mixture of ice and water. The precipitate is washed with water (5 mL) and dried under vacuum to afford of **170** as a colorless powder (2.01 g, 82%, as a mixture of E/Z isomers). ^{1}H NMR (400 MHz, CDCl$_3$) δ 9.24 (s, 1H), 7.65 (d, J = 8.8 Hz, 1H), 7.42 (d, J = 8.8 Hz, 1H), 4.62 (s, 1.4H), 4.43 (s, 0.6H).
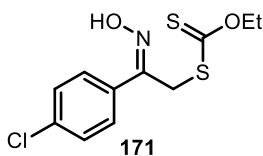
Preparation of 171.[166] Potassium O-ethyl xanthate (1.42 g, 8.8 mmol) is dissolved in acetone (6 mL). A solution of **170** (2.01 g, 8 mmol) in acetone (6 mL) is added dropwise at room temperature. The mixture is stirred for 3 h at 20°C. Solids are removed by filtration using celite plug to afford a clear orange solution. The combined washings and filtrate are

concentrated under vacuum to dryness. The yellow residue is dissolved in diethyl ether (30 mL). This solution was washed with water (10 mL), dried with NaSO$_4$, and evaporated to dryness to afford of **171** as a yellow amorphous solid (2.06 g, 89%, as a mixture of E/Z isomers). ^{1}H NMR (400 MHz, CDCl$_3$) δ 8.94 (s, 0.6H), 8.68 (s, 0.4H), 7.63 – 7.54 (m, 1.2H), 7.50 – 7.45 (m, 0.8H), 7.43 – 7.38 (m, 1.2H), 7.38 – 7.32 (m, 0.8H), 4.71 – 4.57 (m, 2H), 4.51 (s, 1.2H), 4.30 (s, 0.8H), 1.40 (m, 3H).
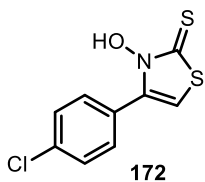
Preparation of 172.[166] Compound **171** (2.06 g, 7.1 mmol) is dissolved in diethyl ether (5 mL), and the slurry is treated at 0°C in small portions with solid anhydrous ZnCl$_2$ (2.93 g, 22 mmol) at such a rate that the solvent does not boil constantly. After the addition is complete, the flask is stoppered with a drying tube (CaCl$_2$) and stirring is continued for 48 h at 20°C. ZnCl$_2$ is fully dissolved toward the end of the reaction, and resulted in a brown, clear slurry. The flask is immersed in an ice bath and treated dropwise with 5.5 M hydrochloric acid (7 mL). Stirring is continued for 30 min at 0°C, a tan-colored solid separates. This material is collected by filtration. It is washed with small portions of diethyl ether (5 mL) and dried to afford 1.7 g (87.8%) of **172**. The crude material was recrystallized from 2-propanol (25 mL). Precipitation of **172** is completed by immersing the flask for 30 min in an acetone-dry ice bath (-78°C). The product is collected by filtration and dried to afford **172** as yellow crystals (1.2 g, 62%). ^{1}H NMR (400 MHz, CDCl$_3$) δ 10.06 (s, 1H), 7.71 – 7.56 (m, 3H), 7.52 – 7.40 (m, 3H), 6.69 (s, 1H).
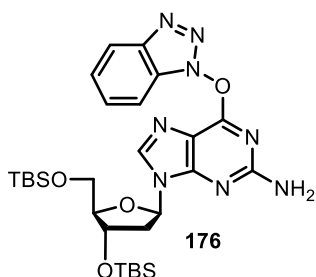
Preparation of 176.[200] Compound **86** (248 mg, 0.5 mmol) and BOP reagent (442 mg, 1 mmol) were dissolved in THF (5 mL). DIPEA (97 mg, 131 μL, 0.75 mmol) were added, and the mixture was allowed to stir at room temperature for 24 h. The mixture was washed with water, extracted with DCM (3 × 20 mL). The combined organic phase was dried over Na_2SO_4. Na_2SO_4 was removed by filtration, and the mixture was concentrated under vacuum. The product was purified by flash chromatography on a silica column. Elution with 50% EtOAc in hexanes gave **176** as a white foam (230 mg, 75% yield). ^{1}H NMR (300 MHz, CDCl₃) δ 8.18 – 8.08 (m, 2H), 7.65 – 7.39 (m, 3H), 6.37 (t, J = 6.3 Hz, 1H), 4.77 (s, 1H), 4.64 (s, 1H), 4.03 (s, 1H), 3.87 (dd, J = 11.0, 4.0 Hz, 1H), 3.79 (dd, J = 11.0, 3.0 Hz, 1H), 2.60 (dt, J = 12.5, 6.1 Hz, 1H), 2.51 – 2.36 (m, 1H), 0.95 (s, 18H), 0.13 (s, 6H), 0.12 (s, 6H).
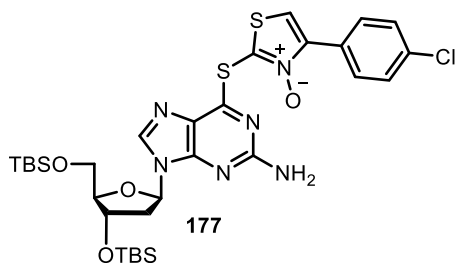
Preparation of 177. Compound **176** (61.2 mg, 0.1 mmol) is dissolved in THF (1 mL). Cs_2CO_3 (65 mg, 0.2 mmol) and **172** (48 mg, 0.2mmol) were added to the solution, and the reaction was stirred at 65 ºC overnight. The reaction was washed with water, extracted with DCM (10 mL × 3). The combined organic phase was dried over Na_2SO_4. Na_2SO_4 was removed by filtration, and the mixture was concentrated under vacuum. The product was purified by flash chromatography on a silica column. Elution with 50% EtOAc in hexanes gave **177** as a brown oil (12 mg, 16%). ^{1}H NMR (400 MHz, CDCl₃) δ 8.04 (s, 1H), 7.91 (d, J = 8.4 Hz, 2H), 7.66 (s, 1H), 7.42 (d, J = 8.4 Hz, 2H), 6.36 (t, J = 6.5 Hz, 1H), 4.99 (s, 2H), 4.62 (d, J = 2.6 Hz, 1H), 4.02 (d, J = 2.6 Hz, 1H), 3.84 (dd, J = 11.1, 3.0 Hz, 1H), 3.78 (dd, J =

11.1, 3.0 Hz, 1H), 2.61 (dt, $J = 12.9$, 6.3 Hz, 1H), 2.45 – 2.35 (m, 1H), 0.95 (s, 9H), 0.93 (s, 9H), 0.14 (s, 6H), 0.11 (s, 3H), 0.10 (s, 3H).
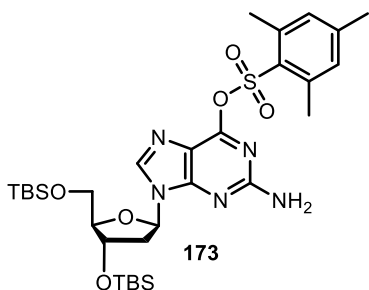
Preparation of 173.[211] Compound **86** (500 mg, 1 mmol), and DMAP (30 mg, 0.25 mmol) were dissolved in DCM (16 mL), and stirred for 30 min. Et$_3$N (202 mg, 280 µL, 0.2 mmol) was added. 2-Mesitylenesulfonyl chloride (436 mg, 2 mmol) was slowly added while stirring, and the mixture was allowed to stir at room temperature overnight. The reaction was quenched by saturated NaHCO$_3$ and extracted by DCM (3 × 20 mL). The combined organic phase was dried over Na$_2$SO$_4$. Na$_2$SO$_4$ was removed by filtration, and the mixture was concentrated under vacuum. The product was purified by flash chromatography on a silica column. Elution with 50% EtOAc in hexanes gave **173** as a white solid (562 mg, 83%). ^{1}H NMR (400 MHz, CDCl$_3$) δ 7.98 (s, 1H), 6.97 (s, 2H), 6.28 (t, $J = 6.6$ Hz, 1H), 4.84 (s, 2H), 4.57 (dt, $J = 6.3$, 3.3 Hz, 1H), 3.97 (dd, $J = 7.2$, 3.3 Hz, 1H), 3.79 (dd, $J = 11.2$, 4.2 Hz, 1H), 3.73 (dd, $J = 11.2$, 3.2 Hz, 1H), 2.74 (s, 6H), 2.54 (ddd, $J = 12.9$, 7.0, 5.8 Hz, 1H), 2.37 – 2.26 (m, 4H), 0.91 (s, 9H), 0.89 (s, 9H), 0.09 (s, 6H), 0.07 (s, 3H), 0.06 (s, 3H).
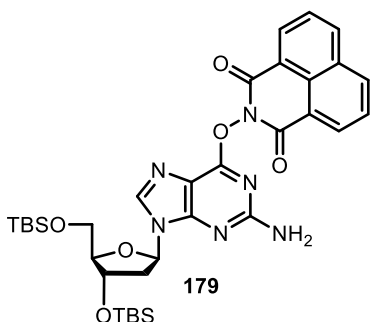
Preparation of 179. Compound **173** (135.4 mg, 0.2 mmol), and DABCO (22.4 mg, 0.4 mmol) were dissolved in DMF (2 mL), and stirred for 30 min. DBU (45 mg, 0.3 mmol) and N-hydroxynaphthalimide (**178**, 213 mg, 1 mmol) were added, and the reaction was kept at room temperature overnight. The reaction was quenched by water and extracted by DCM (3 × 10 mL). The combined organic phase was dried over Na$_2$SO$_4$. Na$_2$SO$_4$ was removed by filtration, and

the mixture was concentrated under vacuum. The product was purified by flash chromatography on a silica column. Elution with 50% EtOAc in hexanes gave **179** as a yellow solid (64 mg, 46%). ^{1}H NMR (400 MHz, CDCl$_3$) δ 8.63 (d, J = 7.3 Hz, 2H), 8.27 (d, J = 8.2 Hz, 2H), 7.95 (s, 1H), 7.78 (t, J = 7.8 Hz, 2H), 6.26 (t, J = 6.2 Hz, 1H), 4.55 (dd, J = 9.2, 4.3 Hz, 1H), 3.99 – 3.89 (m, 1H), 3.80 (dd, J = 11.2, 3.0 Hz, 1H), 3.73 (dd, J = 11.2, 3.0 Hz, 1H), 2.50 (dt, J = 12.4, 6.1 Hz, 1H), 2.41 – 2.25 (m, 1H), 0.89 (s, 9H), 0.85 (s, 9H), 0.08 (s, 6H), 0.04 (s,3H), 0.03 (s, 3H). ^{13}C NMR (101 MHz, CDCl$_3$) δ 159.9, 158.7 155.18, 139.2, 134.7, 131.9, 131.8, 127.7, 127.0, 122.7, 113.8, 87.5, 83.8, 71.4, 62.5, 41.1, 25.9, 25.7, 18.3, 17.9, -4.6, -4.8, -5.4, -5.5. HRMS (ESI-TOF) m/z calcd for $(C_{34}H_{47}N_6O_6Si_2)^+$ (M + H)$^+$ = 691.3096, found m/z = 691.3097.
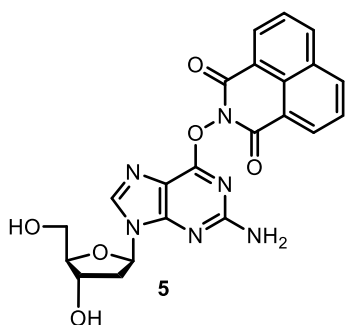
Preparation of 5. Compound **179** (64 mg, 0.092 mmol) was dissolved in THF (1 mL). While stirring, Et$_3$N•3HF (161 mg, 1 mmol) was slowly added. The reaction was stirred at 25 ºC overnight. The reaction was concentrated under vacuum and purified by flash chromatography on a silica column. Elution with 5% MeOH in DCM gave **5** as a yellow foam (35.7 mg, 84%). ^{1}H NMR (400 MHz, MeOH-d$_4$) δ 8.64 (d, J = 6.8 Hz, 2H), 8.48 (d, J = 7.8 Hz, 2H), 8.20 (s, 1H), 7.90 (s, 2H), 6.37 (s, 1H), 4.57 (s, 1H), 4.03 (s, 1H), 3.83 (d, J = 10.1 Hz, 1H), 3.74 (d, J = 10.1 Hz, 1H), 2.80 (s, 1H), 2.41 (s, 1H). ^{13}C NMR (101 MHz, DMSO) δ 160.1, 159.8, 140.1, 135.9, 132.1, 132.0, 127.9, 127.4, 122.5, 112.0, 88.1, 83.3, 71.1, 62.0. HRMS (ESI-TOF) m/z calcd for $(C_{22}H_{19}N_6O_6)^+$ (M + H)$^+$ = 463.1366, found m/z = 463.1369.
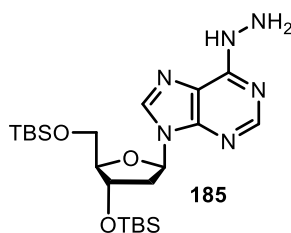
Preparation of 185. Compound **91** (598 mg, 1 mmol) was dissolved in THF (10 mL). Hydrazine (3.2 g, 100 mmol) was slowly added while stirring. The reaction was stirred at 25 ºC for 1 h. The reaction was washed with water and extracted by DCM (3 × 30 mL). The combined organic phase was dried over Na_2SO_4. Na_2SO_4 was removed by filtration, and the mixture was concentrated under vacuum. The product was purified by flash chromatography on a silica column. Elution with 5% MeOH in DCM gave **185** as a yellow foam (467 mg, 94%). ^{1}H NMR (CDCl3) δ 8.42 (s, 1H), 8.13 (s, 1H), 7.96 (s, 1H), 6.44 (t, *J* = 6.5 Hz, 1H), 4.73 – 4.49 (m, 1H), 4.24 (s, 2H), 4.00 (dd, *J* = 7.5, 3.3 Hz, 1H), 3.84 (dd, *J* = 11.2, 4.4 Hz, 1H), 3.75 (dd, *J* = 11.2, 3.3 Hz, 1H), 2.70 – 2.59 (m, 1H), 2.41 (ddd, *J* = 13.0, 6.1, 3.7 Hz, 1H), 0.90 (s, 9H), 0.89 (s, 9H),0.08 (s, 6H), 0.06 (s, 3H) 0.08 (s, 3H).
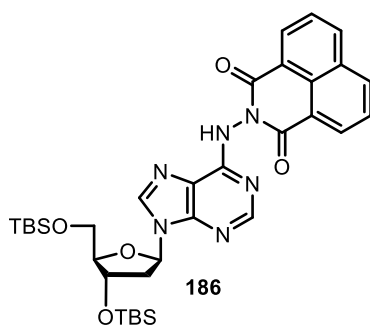
Preparation of 186. THF (2 mL) was added to **185** (98 mg, 0.2 mmol). Naphthalic anhydride (44 mg, 0.22 mmol) was added to the mixture, and the reaction was stirred at 65 ºC for 24 h. The reaction was quenched by saturated $NaHCO_3$ and extracted by DCM (3 × 20 mL). The combined organic phase was dried over Na_2SO_4. Na_2SO_4 was removed by filtration, and the mixture was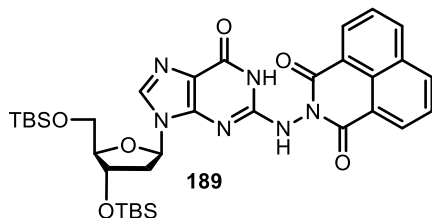 concentrated under vacuum. The product was purified by flash chromatography on a silica column. Elution with 3% MeOH in DCM gave **186** as a yellow solid (99.7 mg, 74%). ^{1}H NMR (400 MHz, CDCl3) δ 9.74 (s, 1H), 8.58 (d, *J* = 7.2 Hz, 2H), 8.38 (s, 1H), 8.21 (dd, *J* = 8.4, 1.1 Hz, 2H), 8.12 (s, 1H), 7.71 (dd, *J* = 8.1, 7.4 Hz, 2H),

6.38 (s, 1H), 4.54 (s, 1H), 3.95 (s, 1H), 3.78 (s, 1H), 3.74 – 3.61 (m, 1H), 2.72-2.52 (m, 1H), 2.47 – 2.27 (m, 1H), 0.86 (s, 9H), 0.76 (s, 9H), 0.05 (s, 6H), -0.03 (s, 6H).
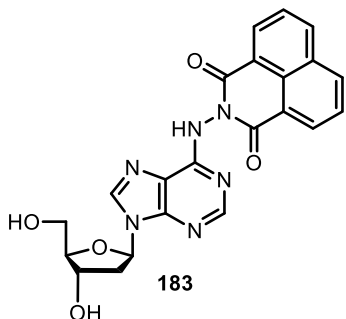
Preparation of 183. Compound **169** (99.7 mg, 0.14 mmol) was dissolved in THF (2 mL). While stirring, Et$_3$N•3HF (225 mg, 1.4 mmol) was slowly added. The reaction was stirred at 25 ºC overnight. The reaction was concentrated under vacuum and purified by flash chromatography on a silica column. Elution with 7% MeOH in DCM gave **183** as a yellow foam (53.1 mg, 85%, as a mixture of imino and amino tautomers). ^{1}H NMR (400 MHz, MeOH-d$_4$) δ 8.63 (d, J = 7.3 Hz, 2H), 8.45 (d, J = 8.2 Hz, 3H), 8.24 (s, 1H), 7.88 (s, 2H), 6.44 (d, J = 52.8 Hz, 1H), 4.60 (s, 1H), 4.10 (d, J = 9.0 Hz, 1H), 3.81 (d, J = 36.1 Hz, 2H), 2.84 (s, 1H), 2.45 (s, 1H).
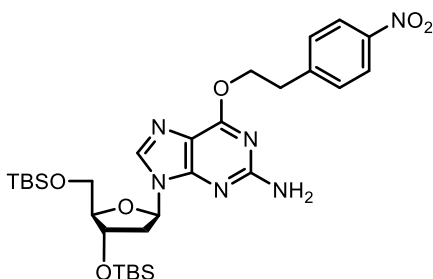
Preparation of 3',5'-bis-O-TBDMS-O6-2-(*p*-nitrophenyl)ethyl 2'-deoxyguanosine.[253] 3',5'-Bis-O-TBDMS-2'-deoxyguanosine (**86**, 498 mg, 1 mmol), 2-(*p*-nitrophenyl)ethanol (334 mg, 2 mmol), and PPh$_3$ (525.mg, 2 mmol) was dissolved in THF (10 mL). DEAD (348 mg, 2 mmol) was slowly added. The reaction was stirred at 25 ºC overnight. The reaction mixture quenched with water and extracted with DCM (3 × 20 mL). The combined organic phase was dried over Na$_2$SO$_4$. Na$_2$SO$_4$ was removed by filtration, and the mixture was concentrated under vacuum. The product was purified by flash chromatography on a silica column. Elution with 20% EtOAc in hexanes gave 3',5'-bis-O-TBDMS-O6-2-(*p*-nitrophenyl)ethyl 2'-deoxyguanosine as a light yellow oil (391 mg, 60%). ^{1}H NMR (400 MHz, CDCl$_3$) δ 8.12

(d, J = 8.6 Hz, 3H), 7.88 (s, 1H), 7.45 (d, J = 8.6 Hz, 2H), 6.28 (t, J = 6.7 Hz, 1H), 4.99 (s, 2H), 4.70 (t, J = 6.8 Hz, 2H), 4.59 – 4.51 (m, 1H), 3.95 (d, J = 3.3 Hz, 1H), 3.78 (dd, J = 11.2, 4.1 Hz, 1H), 3.72 (dd, J = 11.1, 3.1 Hz, 1H), 3.24 (t, J = 6.8 Hz, 2H), 2.51 (dt, J = 13.0, 6.4 Hz, 1H), 2.32 (ddd, J = 13.0, 6.0, 3.6 Hz, 1H), 0.88 (s, 18H), 0.07 (s, 6H), 0.05 (s, 3H), 0.05 (s, 3H).
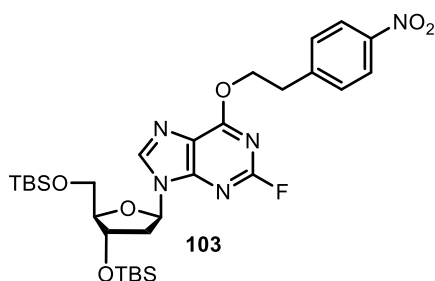
Preparation of 103.[253] 3',5'-Bis-O-TBDMS-O6-2-(*p*-nitrophenyl)ethyl 2'-deoxyguanosine (391 g, 0.6 mmol) was dissolved in 9 mL anhydrous toluene and cooled to -10 °C. Polyvinylpyridine-HF (1.2 g) and tert-butyl nitrite (275 mg, 0.29 mL, 2.4 mmol) were added. After 1h, the reaction was poured into cold saturated NaHCO$_3$ (40 mL). The resulting solid was removed by filtration, and the organic phase product extracted with EtOAc (3 ×20 mL). The organic phase was dried using Na$_2$SO$_4$, concentrated under vacuum and purified by flash chromatography on a silica column. Elution with 10% EtOAc in hexanes gave **103** as a yellow foam (163 mg, 42%).^{1}H NMR (400 MHz, CDCl$_3$) δ 8.20 (s, 1H), 8.11 (d, J = 8.8 Hz, 2H), 7.46 (d, J = 8.8 Hz, 2H), 6.35 (t, J = 6.4 Hz, 1H), 4.79 (t, J = 6.8 Hz, 2H), 4.58 (dt, J = 5.7, 3.3 Hz, 1H), 3.97 (dd, J = 7.0, 3.3 Hz, 1H), 3.84 (dd, J = 11.3, 4.1 Hz, 1H), 3.73 (dd, J = 11.3, 3.1 Hz, 1H), 3.28 (t, J = 6.8 Hz, 2H), 2.63 – 2.50 (m, 1H), 2.39 (ddd, J = 13.1, 6.2, 3.9 Hz, 1H), 0.87 (s, 9H), 0.86 (s, 9H), 0.06 (s, 6H), 0.05 (s, 3H), 0.04 (s, 3H).

187
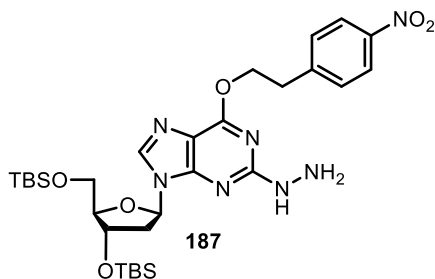
Preparation of 187. To a solution of **103** (96 mg, 0.15 mmol) in THF (2 mL), hydrazine (48 mg, 15 mmol) was added to the mixture, and the reaction was stirred at 50 °C overnight. The reaction was concentrated under vacuum and purified by flash chromatography on a silica column. Elution with 3% MeOH in DCM gave **187** as a yellow solid (98 mg, 99%). ^{1}H NMR (400 MHz, CDCl$_3$) δ 8.13 (d, $J = 8.7$ Hz, 2H), 7.94 (s, 1H), 7.47 (d, $J = 8.7$ Hz, 2H), 6.39 (t, $J = 6.6$ Hz, 1H), 6.25 (s, 1H), 4.73 (t, $J = 6.8$ Hz, 2H), 4.64 – 4.55 (br, 2H), 3.99 (dd, $J = 7.0, 3.3$ Hz, 1H), 3.84 (t, $J = 6.3$ Hz, 1H), 3.82 (dd, $J = 11.1, 4.2$ Hz, 1H), 3.77 (dd, $J = 11.1, 3.3$ Hz, 1H), 3.27 (t, $J = 6.8$ Hz, 2H), 2.57 (ddd, $J = 13.0, 7.1, 5.9$ Hz, 1H), 2.37 (ddd, $J = 13.0, 6.0, 3.5$ Hz, 1H), 0.92 (s, 9H), 0.91 (s, 9H), 0.10 (d, $J = 3.0$ Hz, 6H), 0.09 (s, 3H), 0.08 (s, 3H).

188
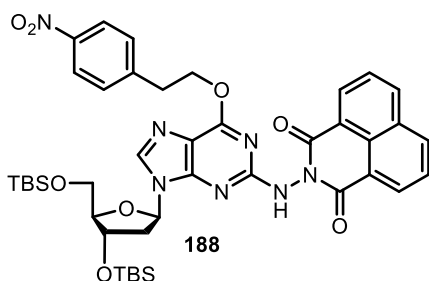
Preparation of 188. To a solution of **187** (98 mg, 0.15 mmol) in THF (2 mL), naphthalic anhydride (45 mg, 0.225 mmol) was added, and the reaction was refluxed for 24 h. The reaction mixture was poured into saturated NaHCO$_3$ and extracted with DCM (3 × 10 mL). The combined organic phase was dried over Na$_2$SO$_4$. Na$_2$SO$_4$ was removed by filtration, and the mixture was concentrated under vacuum. The product was purified by flash chromatography on a silica column. Elution with 30% EtOAc in hexanes gave **188** as a yellow solid (116 mg, 92%). ^{1}H NMR (400 MHz, CDCl$_3$) δ 8.63 (d, $J = 7.1$ Hz, 2H), 8.27 (d, $J = 8.1$ Hz, 2H), 8.01 (s, 1H), 7.91 (s, 2H), 7.77 (t, $J = 7.7$ Hz, 2H), 7.43 (s, 1H), 7.10 (s, 2H), 6.21 (s, 1H), 4.54 (s, 2H), 4.42 (s, 1H), 4.10 (dd, $J = 14.2, 7.1$ Hz, 1H), 3.88 (s,

1H), 3.72 (s, 2H), 3.08 (s, 2H), 2.37 (s, 1H), 2.25 (s, 1H), 2.02 (s, 1H), 0.88 (s, 9H), 0.77 (s, 9H), 0.06 (s, 6H), -0.01 (s, 3H), -0.07 (s, 3H).

Preparation of 189. Compound **188** (86 mg, 0.1 mmol) was dissolved in pyridine (1 mL). While stirring, DBU (76 mg, 0.5 mmol) was slowly added. The reaction was stirred at 25 °C for 24 h. The reaction mixture was poured into saturated NaHCO₃ and extracted with DCM (3 × 20 mL). The combined organic phase was dried over Na₂SO₄. Na₂SO₄ was removed by filtration, and the mixture was concentrated under vacuum. The reaction was purified by flash chromatography on a silica column. Elution with 50% EtOAc in hexanes gave **189** as a yellow foam (55.3 mg, 82%). ^{1}H NMR (400 MHz, CDCl₃) δ 8.68 (d, J = 6.9 Hz, 2H), 8.26 (d, J = 8.1 Hz, 2H), 7.77 (t, J = 7.4 Hz, 2H), 7.57 (s, 1H), 5.84 (t, J = 6.5 Hz, 1H), 4.12 (s, 1H), 3.74 – 3.60 (m, 1H), 3.53 (dd, J = 11.1, 3.3 Hz, 1H), 3.47 (dd, J = 11.1, 4.5 Hz, 1H), 2.20 – 2.05 (m, 1H), 2.03 – 1.88 (m, 1H), 0.67 (s, 9H), 0.57 (s, 9H), -0.15 (s, 3H), -0.18 (s, 6H), -0.32 (s, 3H).
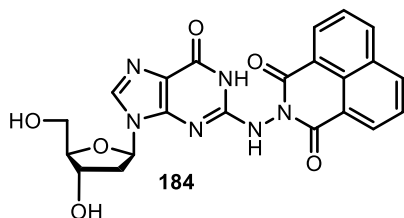
Preparation of 184. Compound **189** (55.3 mg, 0.08 mmol) was dissolved in THF (1 mL). While stirring, Et₃N•3HF (160 mg, 1.0 mmol) was slowly added. The reaction was stirred at 25 °C overnight. The reaction was concentrated under vacuum and purified by flash chromatography on a silica column. Elution with 10% MeOH in DCM gave **184** as a yellow oil (32 mg, 90%). ^{1}H NMR (400 MHz, MeOH-d₄) δ 8.57 (d, J = 7.3 Hz, 2H), 8.46 (d, J = 7.5 Hz, 2H), 8.04 (s, 1H), 7.93 –

7.76 (m, 2H), 6.03 (t, J = 6.9 Hz, 1H), 4.02 (s, 1H), 3.70 (d, J = 3.4 Hz, 1H), 2.52 (dt, J = 13.4, 6.7 Hz, 1H), 2.15 – 2.00 (m, 1H).
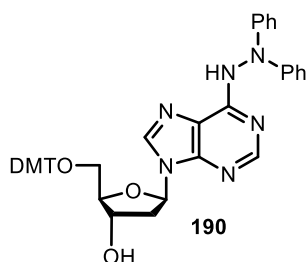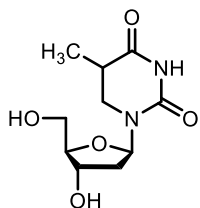
Preparation of 190. Compound **3** (54.3 mg, 0.13 mmol), was azeotropically dried with pyridine (1 mL) three times. Pyridine (1 mL) and DMTCl (53 mg, 0.16 mmol) were added. The reaction was stirred at room temperature overnight. The reaction was concentrated under vacuum, and purified by flash chromatography (50% ethyl acetate in DCM) on a silica column to give **190** as a light yellow foam (62.5 mg, 65%). ^{1}H NMR (400 MHz, CDCl$_3$) δ 9.53 (s, 1H), 8.38 (s, 1H), 7.57 (s, 1H), 7.39 (d, J = 7.3 Hz, 2H), 7.33 – 7.13 (m, 15H), 6.99 (t, J = 7.1 Hz, 2H), 6.80 (d, J = 8.8 Hz, 4H), 6.35 (t, J = 6.2 Hz, 1H), 4.61 (s, 1H), 4.12 (d, J = 4.0 Hz, 1H), 3.76 (s, 6H), 3.41 (dd, J = 9.9, 4.7 Hz, 1H), 3.33 (dd, J = 9.9, 5.7 Hz, 1H), 2.77 – 2.65 (m, 1H), 2.51 – 2.38 (m, 1H).^{13}C NMR (101 MHz, CDCl$_3$) δ 159.0, 158.6, 153.8, 147.5, 146.1, 145.8, 139.6, 137.8, 131.0, 129.7, 129.2, 127.85, 127.82, 127.7, 119.7, 113.0, 88.2, 84.9, 82.0, 81.5, 71.8, 62.7, 55.3, 55.2. HRMS (ESI-TOF) m/z calcd for (C$_{43}$H$_{41}$N$_6$O$_5$)$^+$ (M + H)$^+$ = 721.3138, found m/z = 721.3134.
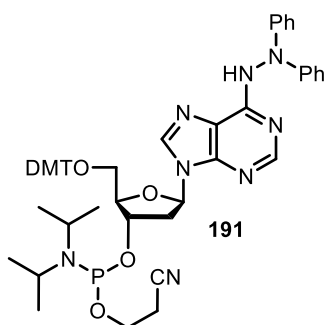
Preparation of 191. DIPEA (51.6 mg, 0.36 mmol) and DCM (2 mL) were added to **190** (96 mg, 0.14 mmol). The reaction was stirred at 0 °C for 30 min, while 2-cyanoethyl-N,N-diisopropylchlorophosphoramidite (28.4 mg, 0.12 mmol) was added dropwise. The reaction was stirred at room temperature for 30 min. The reaction was concentrated under vacuum, and purified by flash chromatography (50% ethyl acetate in hexanes) on a silica column to give **191** as a white

foam (62.5 mg, 77%). ^{1}H NMR (300 MHz, CDCl$_3$) δ 9.33 (s, 1H), 8.37 (s, 1H), 7.66 (s,

1H), 7.40 (d, J = 8.1 Hz, 2H), 7.35 – 7.13 (m, 15H), 7.00 (t, J = 7.0 Hz, 2H), 6.80 (dd, J =

8.8, 3.8 Hz, 4H), 6.37 (dd, J = 11.4, 6.8 Hz, 1H), 4.73 (s, 1H), 4.29 (s, 1H), 3.75– 3.55 (m,

10H), 3.42 – 3.29 (m, 2H), 2.83 (dd, J = 12.2, 6.0 Hz, 1H), 2.62 (t, J = 6.3 Hz, 1H), 2.59 –

2.52 (m, 1H), 2.48 (t, J = 6.4 Hz, 1H), 1.24 – 1.11 (m, 12H). ^{31}P NMR (121 MHz, CDCl$_3$)

δ 148.84 (s), 148.70 (s). HRMS (ESI-TOF) m/z calcd for (C$_{52}$H$_{58}$N$_8$O$_6$P)$^+$ (M + H)$^+$ =

921.4217, found m/z = 921.4211.
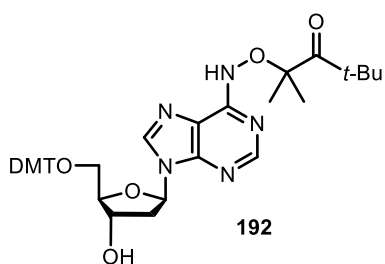
Preparation of 192. Radical precursor **6** (104 mg, 0.26 mmol), was azeotropically dried with pyridine (2 mL) three times. Pyridine (2 mL) and DMTCl (106 mg, 0.32 mmol) were added. The reaction was stirred at room

temperature overnight. The reaction was concentrated under vacuum, and purified by flash

chromatography (50% ethyl acetate in DCM) on a silica column to give **192** as a light

yellow foam (96 mg, 53%). ^{1}H NMR (400 MHz, MeOH-d$_4$) δ 7.87 (s, 1H), 7.55 (s, 1H),

7.38 – 7.31 (m, 2H), 7.30 – 7.20 (m, 4H), 7.16 (t, J = 7.4 Hz, 2H), 7.12 – 7.07 (m, 1H),

6.74 (dd, J = 8.9, 1.4 Hz, 4H), 6.29 (t, J = 6.3 Hz, 1H), 4.56 (dd, J = 9.4, 4.0 Hz, 1H), 4.10

(q, J = 4.3 Hz, 1H), 3.32 – 3.28 (m, 2H), 2.83 – 2.70 (m, 1H), 2.43 (ddd, J = 13.5, 6.4, 4.3

Hz, 1H), 1.47 (s, 6H), 1.22 (s, 9H). ^{13}C NMR (101 MHz, MeOH-d$_4$) δ 160.0, 146.3, 145.4,

142.1, 137.9, 137.2, 137.0, 131.3, 131.2, 129.3, 128.7, 127.8, 120.4, 114.0, 88.6, 88.0, 87.5,

85.9, 72.7, 65.1, 61.5, 55.7, 45.2, 40.9, 29.3, 25.2, 20.9, 14.5. IR (neat) 3273 (broad), 2932,

1691, 1659, 1592, 1463, 1301, 1250, 1176, 1035, 954, 887, 829, 754, 700, 660 cm^{-1}. HRMS

(ESI-TOF) m/z calcd for (C$_{39}$H$_{46}$N$_5$O$_7$)$^+$ (M + H)$^+$ = 696.3397, found m/z = 696.3392.
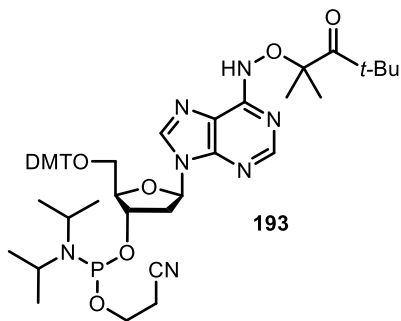
Preparation of 193. DIPEA (66.3 mg, 89.3 μL, 0.54 mmol) and DCM (3.5 mL) were added to **192** (96 mg, 0.14 mmol). The reaction was stirred at 0 °C, and 2-cyanoethyl N,N-diisopropylchloro-phosphoramidite (40.5 mg, 0.17 mmol) was added dropwise. The reaction was stirred at room temperature for 30 min. The reaction was concentrated under vacuum, 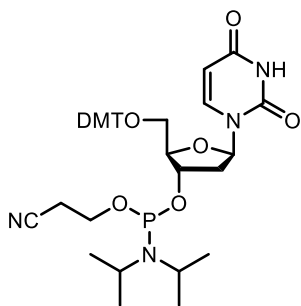and purified by flash chromatography (50% ethyl acetate in hexanes) on a silica column to give **193** as a white foam (74 mg, 59%). ^{1}H NMR (400 MHz, MeOH-d$_4$) δ 7.88 (d, J = 2.1 Hz, 1H), 7.53 (d, J = 2.1 Hz, 1H), 7.44 – 7.33 (m, 2H), 7.31 – 7.23 (m, 4H), 7.23 – 7.06 (m, 3H), 6.88 – 6.62 (m, 5H), 6.29 (td, J = 6.4, 3.1 Hz, 1H), 4.85 (s, 1H), 4.83 – 4.73 (m, 1H), 4.29 – 4.14 (m, 1H), 3.88 – 3.52 (m, 12H), 3.42 – 3.35 (m, 1H), 3.02 – 2.83 (m, 1H), 2.69 – 2.40 (m, 4H), 1.47 (s, 6H), 1.23 (s, 9H), 1.15 (m, 14H). ^{31}P NMR (162 MHz, MeOH-d$_4$) δ 148.4, 148.3. HRMS (ESI-TOF) m/z calcd for $(C_{48}H_{63}N_7O_8P)^+$ $(M + H)^+$ = 896.4476, found m/z = 896.4471.

Preparation of 5,6-dihydrothymidine (dHT).[320] Rhodium on alumina (5%, 24 mg) was added to a solution of thymidine (1.2 g, 5 mmol) in a mixture of MeOH and water (1:1, 9mL) in a sealed tube. The mixture was stirred under 50 psi of H$_2$ for 48 h. The catalyst was removed by filtration through of a silica plug, and the filtrate was lyophilized to dryness. The reaction was purified by flash chromatography (3% MeOH in DCM) on a silica column to give **dHT** as a white foam (1.08 g, 90%). ^{1}H NMR (400 MHz, MeOH-d$_4$) δ 6.28 (dd, J = 8.0, 6.4 Hz, 1H), 4.28 (dtd, J = 3.8, 3.3, 0.4 Hz, 1H), 3.77 (dd, J = 7.8, 4.3 Hz, 1H), 3.67 (dd, J = 11.8, 4.0 Hz, 1H), 3.62 (dd, J = 11.8, 4.7 Hz, 1H), 3.51 (dd, J = 12.8, 5.5 Hz,

1H), 3.22 (dd, J = 12.8, 9.7 Hz, 1H), 2.73 – 2.59 (m, 1H), 2.22 (ddd, J = 13.6, 8.1, 6.6 Hz, 1H), 1.99 (ddd, J = 13.6, 6.4, 3.3 Hz, 1H), 1.21 (d, J = 7.0 Hz, 3H).
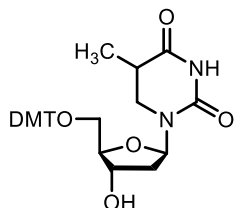
5'-O-dimethoxytrityl-5,6-dihydrothymidine

Preparation of 5'-O-dimethoxytrityl-5,6-dihydrothimidine (5'-O-DMT-dHT).[320] dHT (122 mg, 0.5 mmol), was azeotropically dried with pyridine (2 mL) three times. Pyridine (2 mL) and DMTCl (180 mg, 0.53 mmol) were added. The reaction was stirred at room temperature overnight. The reaction was concentrated under vacuum, and purified by flash chromatography (50% ethyl acetate in DCM) on a silica column to give **5'-O-DMT-dHT** as a white foam (220 mg, 80%). ^{1}H NMR (400 MHz, MeOH-d$_4$) δ 7.44 (d, J = 7.2 Hz, 2H), 7.32 (d, J = 7.7 Hz, 4H), 7.25 – 7.17 (m, 3H), 6.81 (d, J = 9.0 Hz, 4H), 6.35 (dd, J = 7.5, 6.6 Hz, 1H), 4.43 (dt, J = 6.6, 3.4 Hz, 1H), 3.94 (q, J = 3.8 Hz, 1H), 3.69 (s, 6H), 3.43 (dd, J = 12.8, 5.6 Hz, 1H), 3.29 (d, J = 3.8 Hz, 2H), 3.08 (dd, J = 12.8, 9.9 Hz, 1H), 2.62 – 2.41 (m, 1H), 2.37 – 2.16 (m, 4H), 2.08 (ddd, J = 13.4, 6.4, 3.4 Hz, 1H), 0.98 (d, J = 7.0 Hz, 3H).

5,6-dihydrothymidine phosphoramidite

Preparation of 5,6-dihydrothimidine phosphoramidite (dHT phosphoramidite).[320] DIPEA (193.5 mg, 1.5 mmol), DCM (10 mL) was added to **5'-O-DMT-dHT** (220 mg, 0.4 mmol). The reaction was stirred at 0 °C, and 2-cyanoethyl N,N-diisopropylchloro-phosphoramidite (118.5 mg, 0.5 mmol) was added dropwise. The reaction was stirred at room temperature for 30 min. The reaction was concentrated under vacuum, and purified by flash chromatography (50% ethyl

acetate in hexanes) on a silica column to give **dHT phosphoramidite** as white foam (245

mg, 83%). ^{1}H NMR (400 MHz, MeOH-d$_4$) δ 7.43 (m, 2H), 7.35 – 7.28 (m, 4H), 7.27 –

7.11 (m, 3H), 6.82 (m, J = 4H), 6.30 (t, J = 6.8 Hz, 1H), 4.69 – 4.56 (m, 1H), 3.97 (m, 1H),

3.84 – 3.65 (m, 8H), 3.64 – 3.45 (m, 4H), 3.30 (m, 2H), 3.19 – 3.07 (m, 1H), 2.64 (m, 1H),

2.61 – 2.51 (m, 1H), 2.51 – 2.44 (m, 1H), 2.34 (m 1H), 2.28 – 2.09 (m, 1H), 1.16 (t, J =

7.4 Hz, 9H), 1.05 (d, J = 6.7 Hz, 3H), 1.00 (dd, J = 7.0, 2.7 Hz, 3H). ^{31}P NMR (162 MHz,

MeOH-d$_4$) δ 148.08, 147.86.
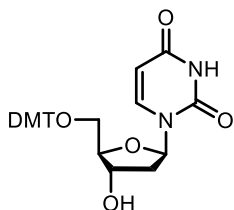
5'-O-dimethoxytrityl-2'-deoxyuridine

Preparation of 5'-O-dimethoxytrityl-2'-deoxyuridine (5'-O-DMT-dU). 2'-Deoxyuridine (2.3 g, 10 mmol), was azeotropically dried with pyridine (10 mL) three times. Pyridine (10 mL) and DMTCl (4.1 g, 12 mmol)

were added. The reaction was stirred at room temperature overnight. The reaction was

concentrated under vacuum, and purified by flash chromatography (50% ethyl acetate in

DCM) on a silica column to give **5'-O-DMT-dU** as a white foam (5.71 g, > 99% with

minor impurities). ^{1}H NMR (400 MHz, CDCl$_3$) δ 8.59 (s, 1H), 7.80 (d, J = 8.2 Hz, 1H),

7.40 (d, J = 7.7 Hz, 2H), 7.35 – 7.27 (m, 7H), 6.86 (d, J = 8.8 Hz, 4H), 6.33 (t, J = 6.3 Hz,

1H), 5.42 (dd, J = 8.2, 1.8 Hz, 1H), 4.57 (dd, J = 10.2, 4.4 Hz, 1H), 4.04 (q, J = 3.5 Hz,

1H), 3.82 (s, 6H), 3.51 (dd, J = 10.6, 3.2 Hz, 1H), 3.46 (dd, J = 10.6, 3.1 Hz, 1H), 2.51 –

2.42 (m, 1H), 2.32 – 2.24 (m, 1H).

2'-deoxyuridine phosphoramidite

Preparation of 2'-deoxyuridine phosphoramidite (dU phosphoramidite). DIPEA (4.18 g, 32.4 mmol), DCM (20 mL) was added to **5'-O-DMT-dU** (5.714, 10.8 mmol). The reaction was stirred at 0 °C, and 2- cyanoethyl N,N-diisopropylchloro-phosphoramidite (3.1 g, 13 mmol) was added dropwise. The reaction was stirred at room temperature for 30 min. The reaction was concentrated under vacuum, and purified by flash chromatography (50% ethyl acetate in hexanes) on a silica column to give **dU phosphoramidite** as white foam (6.2 g, 78%). ^{1}H NMR (400 MHz, MeOH-d$_4$) δ 7.90 (dd, J = 10.1, 8.1 Hz, 1H), 7.53 – 7.37 (m, 3H), 7.27 (ddd, J = 11.0, 10.6, 6.2 Hz, 10H), 6.87 (dd, J = 8.6, 6.1 Hz, 5H), 6.22 (s, 1H), 5.38 – 5.22 (m, 1H), 4.75 – 4.66 (m, 1H), 4.10 (m, 1H), 3.90 – 3.53 (m, 14H), 3.52 – 3.38 (m, 3H), 2.72 (t, J = 5.8 Hz, 1H), 2.61 – 2.32 (m, 4H), 1.19 (m, 13H), 1.09 (d, J = 6.8 Hz, 6H). ^{31}P NMR (162 MHz, MeOH-d$_4$) δ 147.06, 174.03.

7.   Appendix
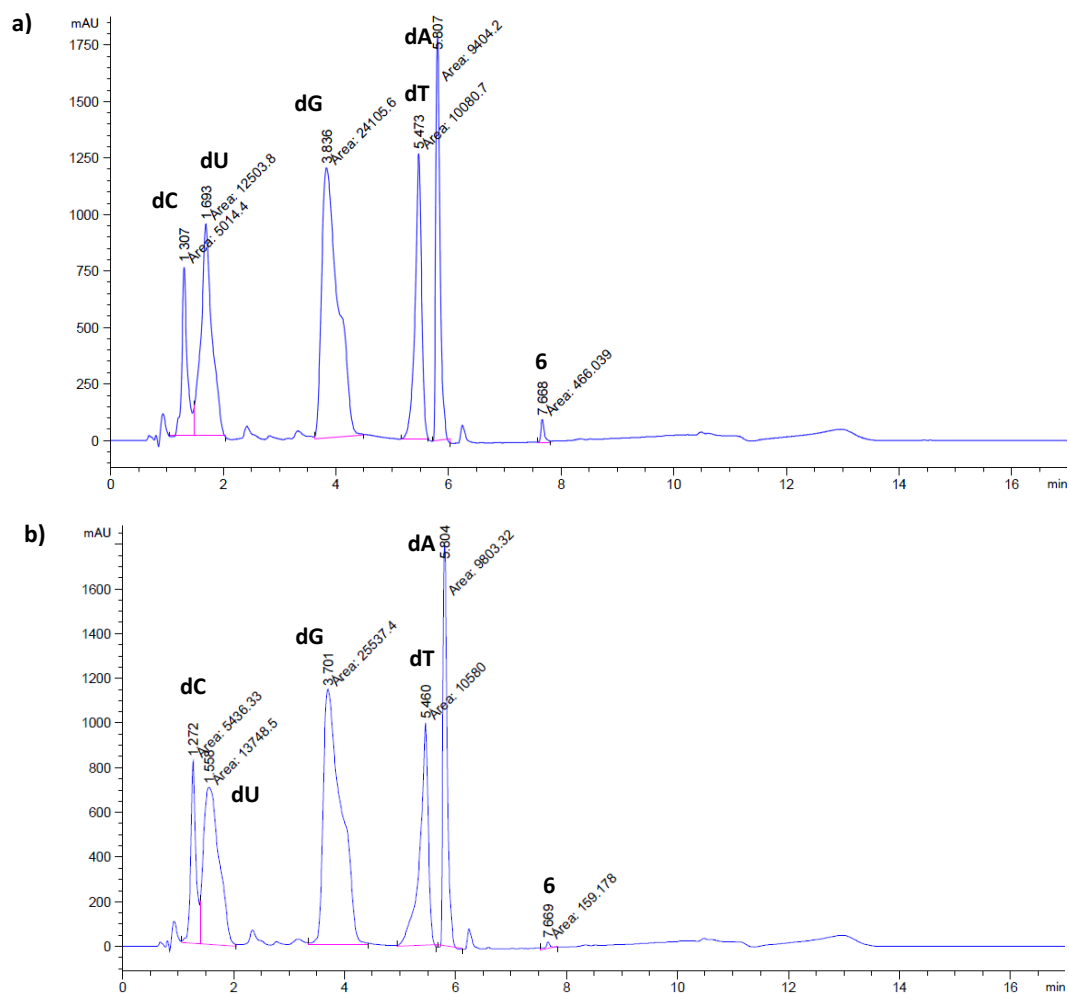
Appendix Figure 1. UPLC quantification of the conversion of precursor **6** in during photolysis. (a) Chromatogram of duplex **196** after enzyme digestion. (b) Chromatogram of photolysate of **196** after enzyme digestion.
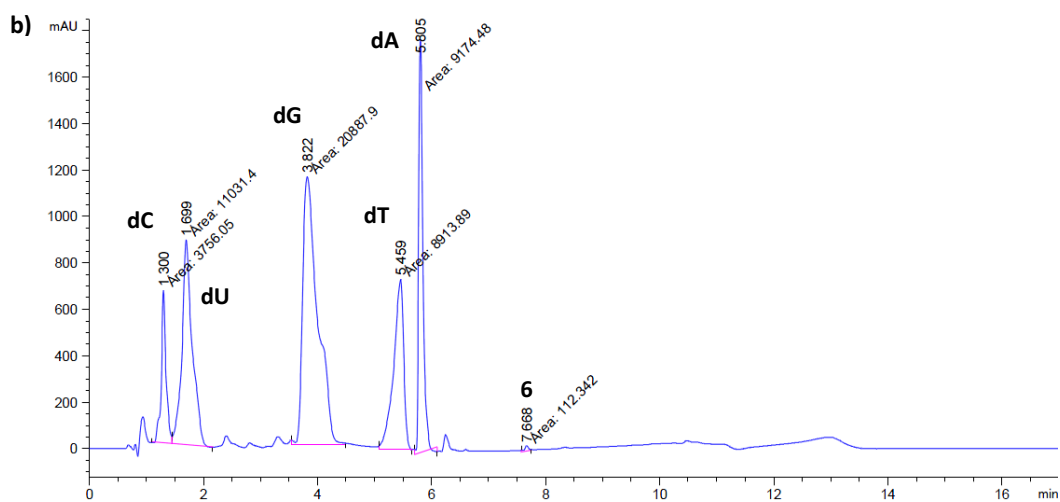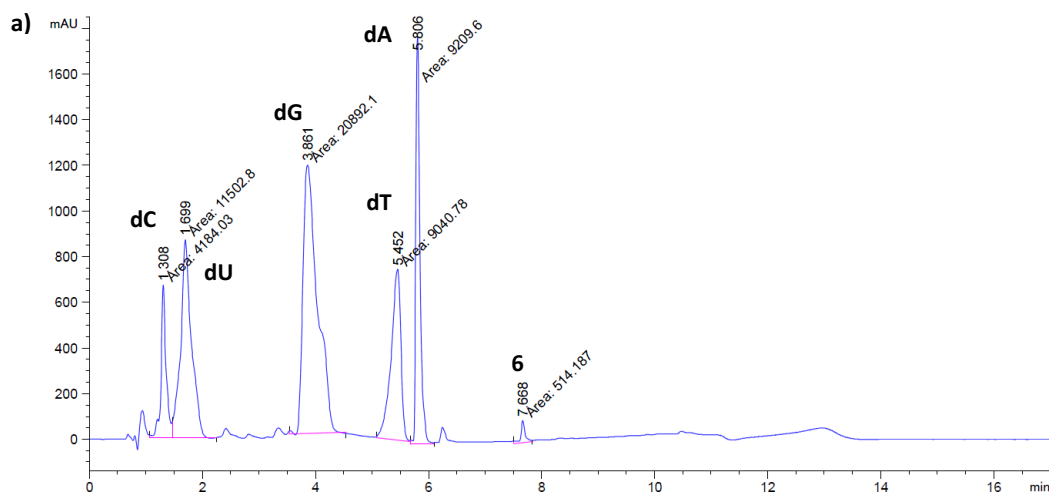
Appendix Figure 2. UPLC quantification of the conversion of precursor **6** in during photolysis. (a) Chromatogram of duplex **197** after enzyme digestion. (b) Chromatogram of photolysate of **197** after enzyme digestion.
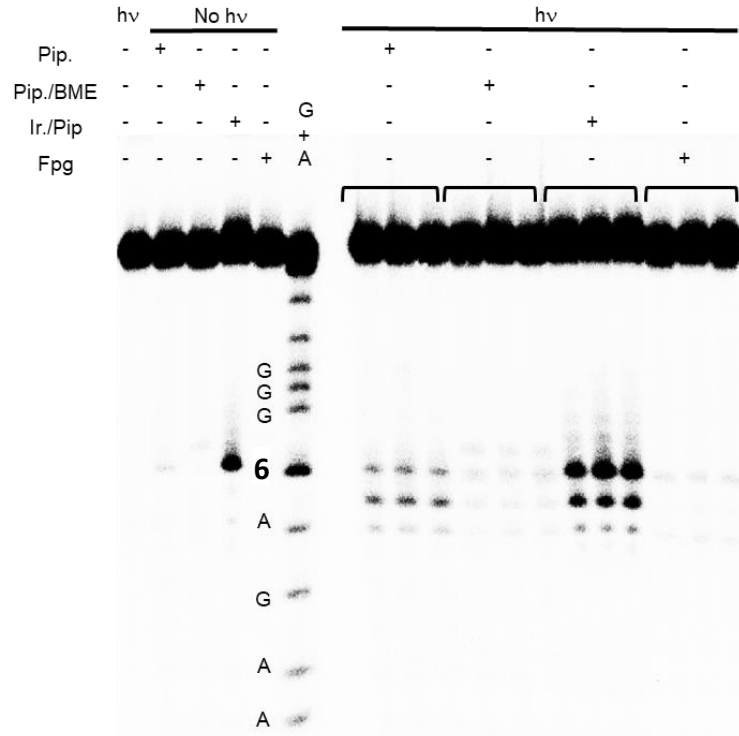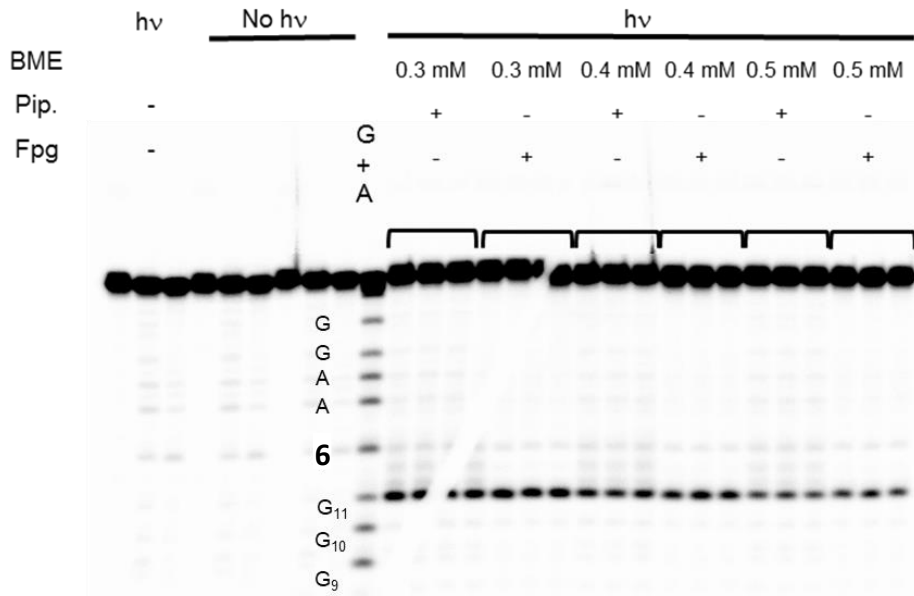
Appendix Figure 3. Autoradiogram of aerobic photolysis of 5'-^{32}P-**198**, followed by chemical and enzymatic treatments.
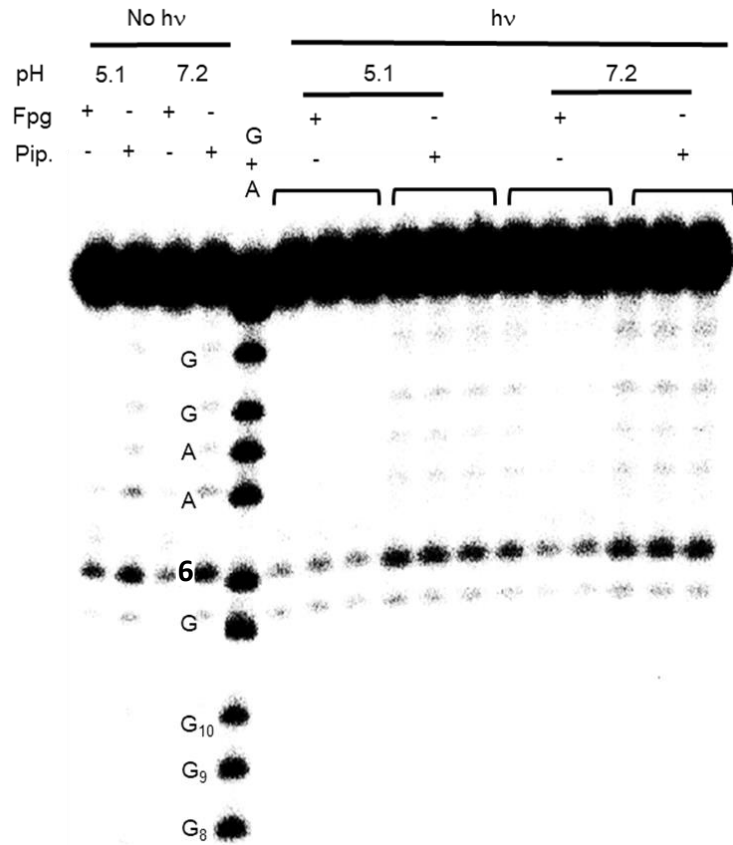
Appendix Figure 4. Autoradiogram of aerobic photolysis of 5'-^{32}P-**199**, followed by chemical and enzymatic treatments.
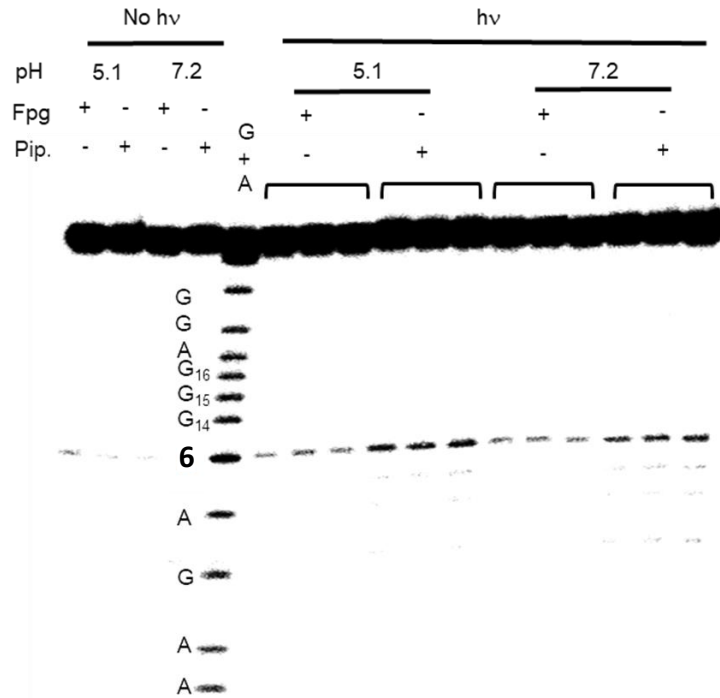
Appendix Figure 5. Autoradiogram of aerobic photolysis of 5'-^{32}P-**200**, followed by chemical and enzymatic treatments.
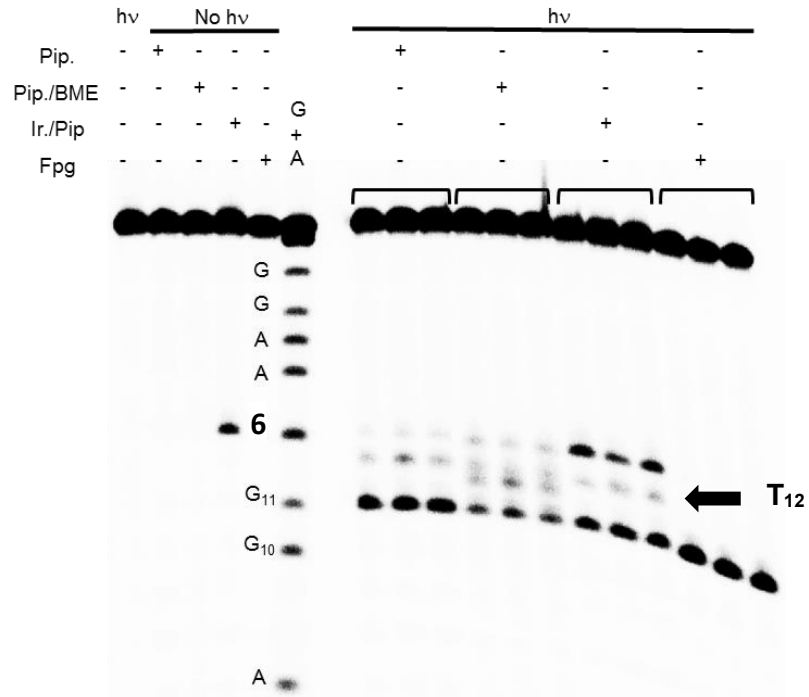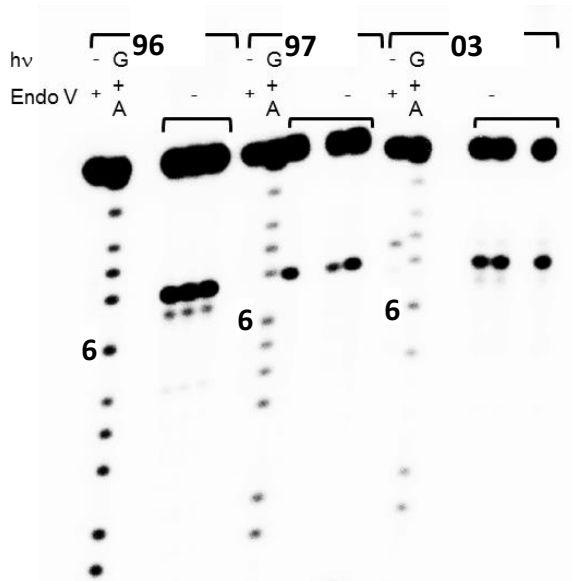

Appendix Figure 6. Autoradiogram of aerobic photolysis of 5'-^{32}P-**201**, followed by chemical and enzymatic treatments.
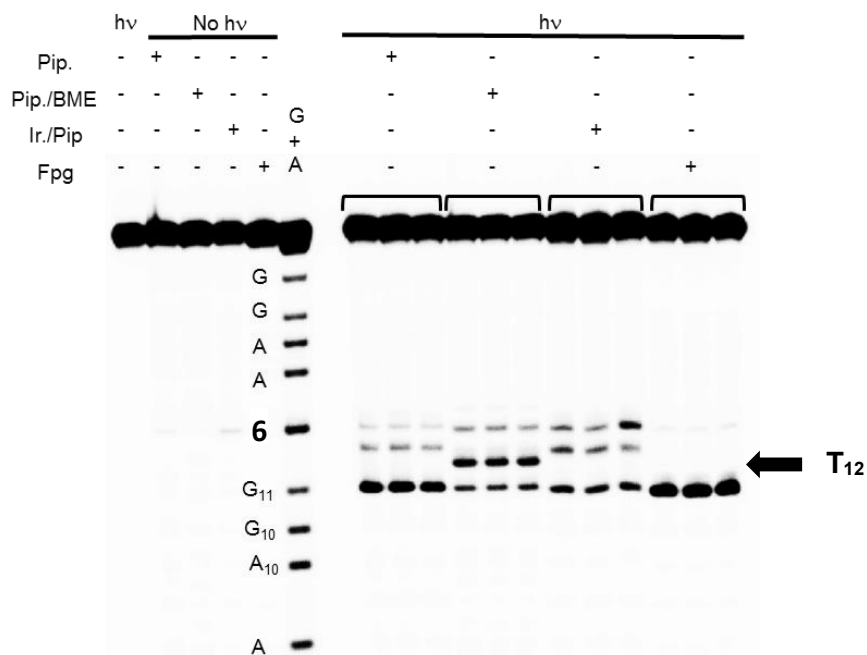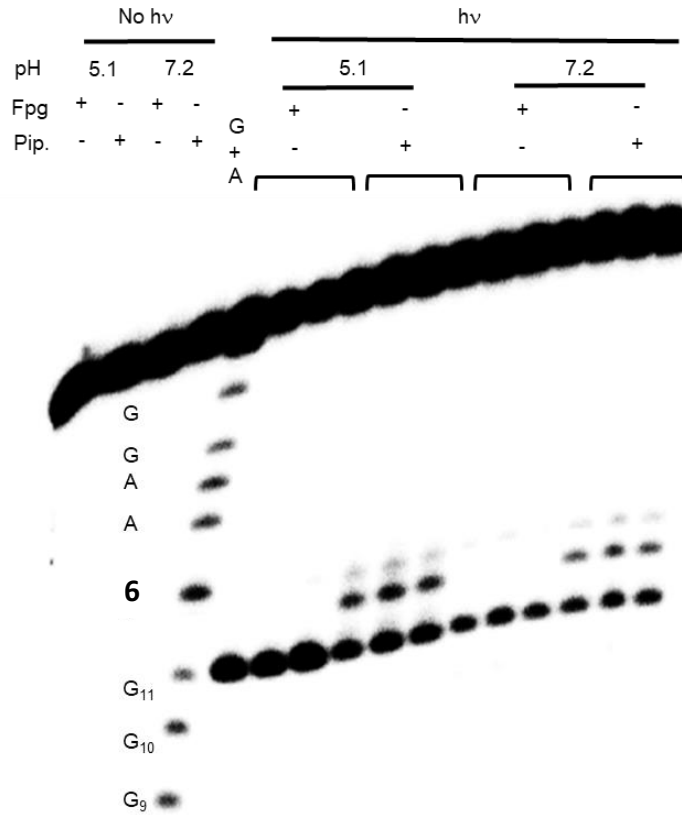
Appendix Figure 7. Autoradiogram of aerobic photolysis of 5'-^{32}P-**202**, followed by chemical and enzymatic treatments.
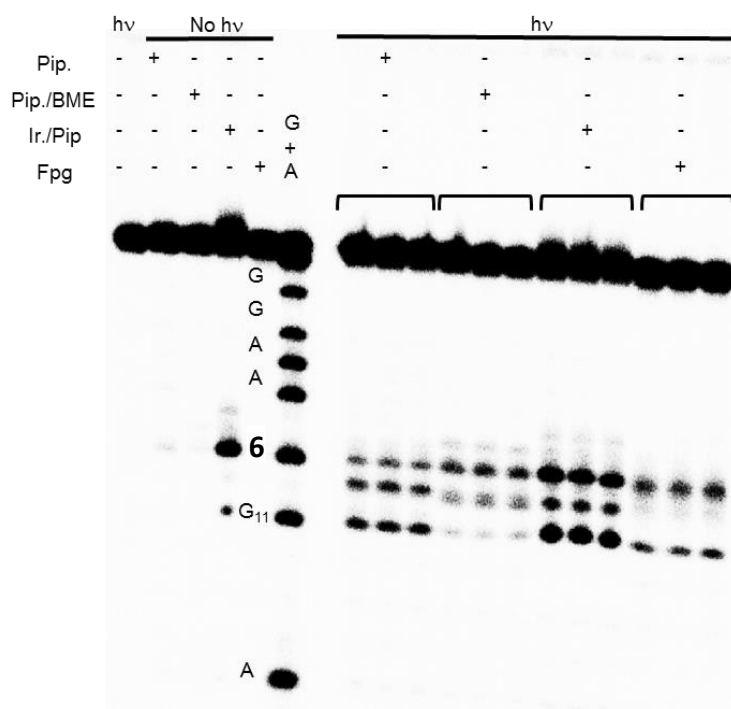
Appendix Figure 8. Autoradiogram of aerobic photolysis of 5'-^{32}P-**203**, followed by chemical and enzymatic treatments.
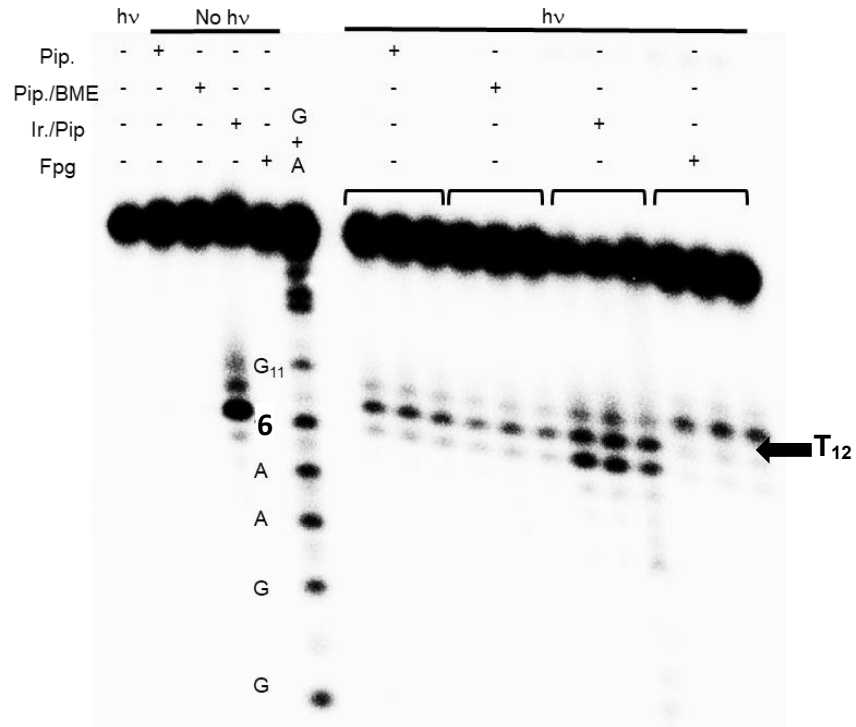
Appendix Figure 9. Autoradiogram of aerobic photolysis of 3'-^{32}P-**203**, followed by chemical and enzymatic treatments.
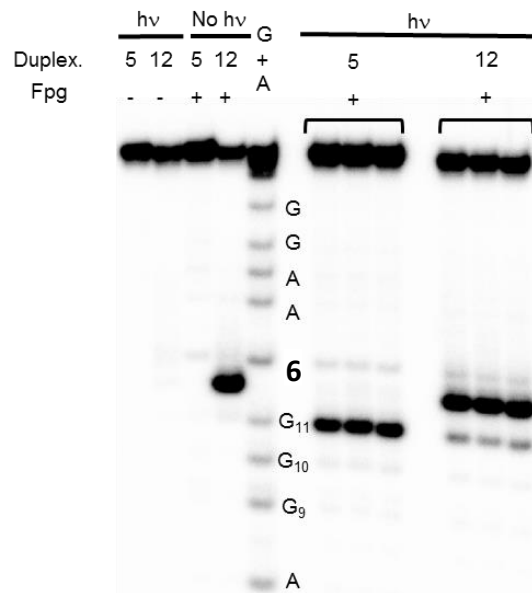
Appendix Figure 10. Autoradiogram of aerobic photolysis of 5'-^{32}P-**208**, followed by chemical and enzymatic treatments.
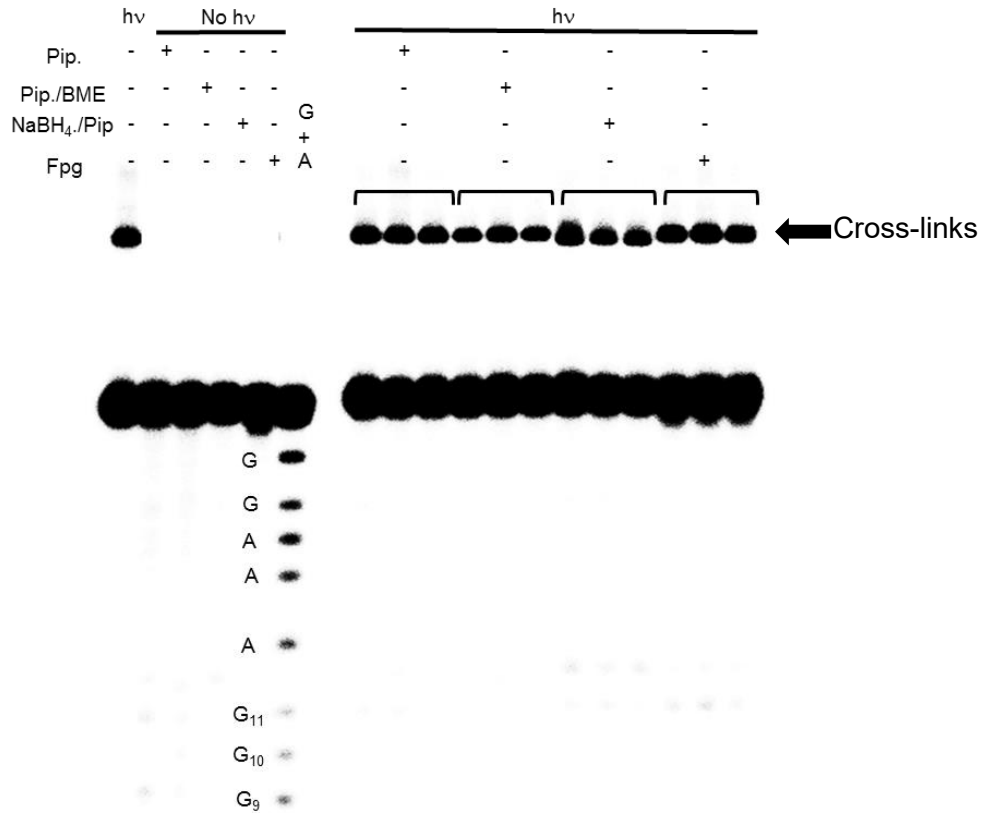
Appendix Figure 11. Autoradiogram of anaerobic photolysis of 5'-^{32}P-**211**, followed by followed by chemical and enzymatic treatments.
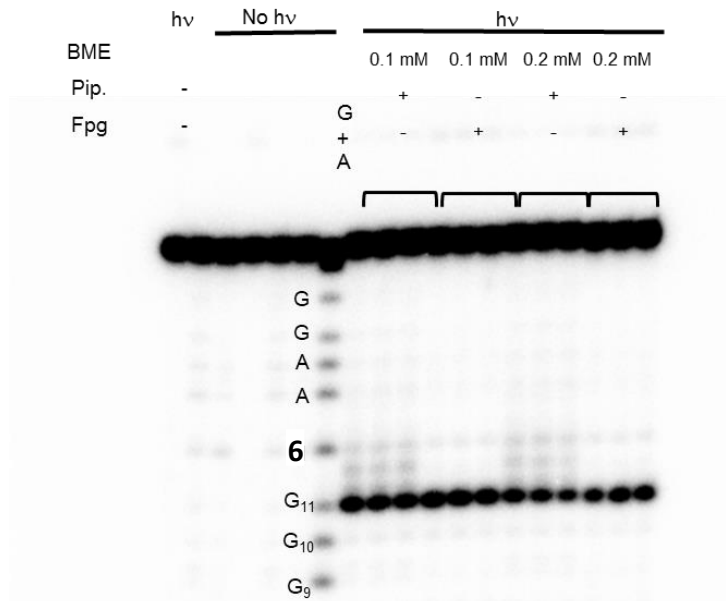
Appendix Figure 12. Autoradiogram of aerobic photolysis of 5'-^{32}P-**196** in the presence of BME, followed by chemical and enzymatic treatments.

Appendix Figure 13. Autoradiogram of aerobic photolysis of 5'-^{32}P-**196** in the presence of BME, followed by chemical and enzymatic treatments.

Appendix Figure 14. Autoradiogram of aerobic photolysis of 5'-^{32}P-**196,** 5'-^{32}P-**197,** and 5'-^{32}P-**203**, followed by Endo V treatments.

**Appendix Figure 15.** Autoradiogram of aerobic photolysis of 5'-^{32}P-**196**, followed by chemical and enzymatic treatments.
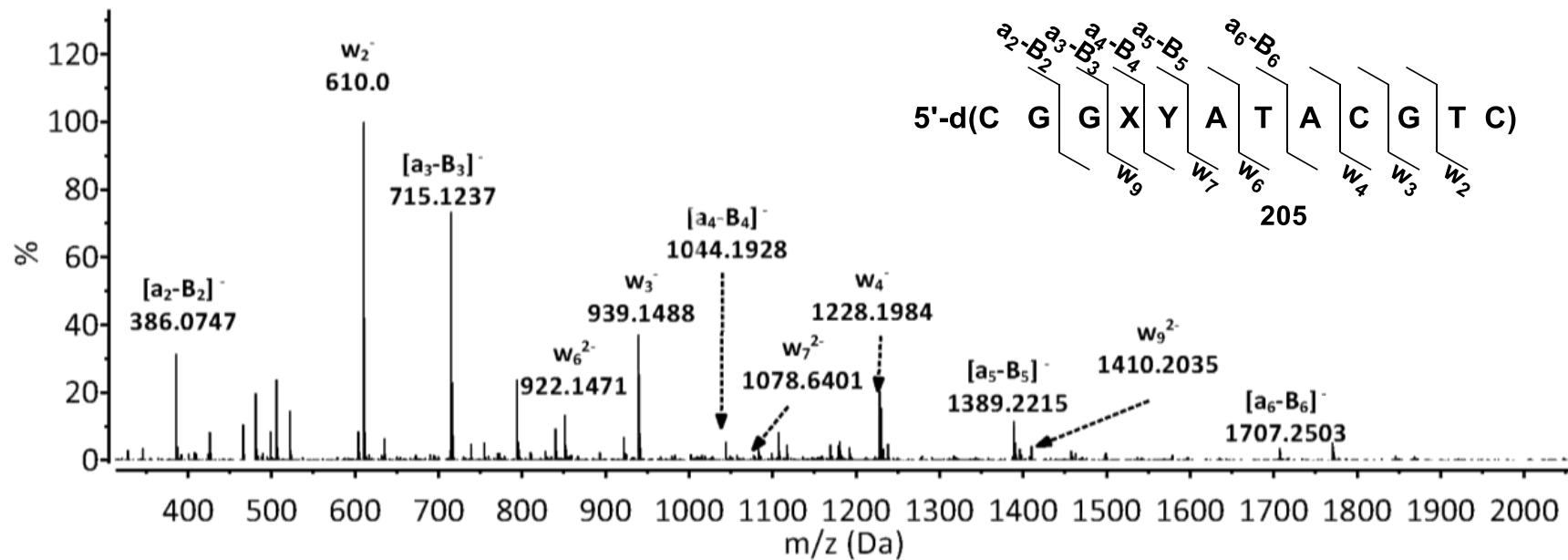
Appendix Figure 16. CID mass spectrum of the ion (m/z = 1229.2, z = 3) of oligonucleotide containing tandem lesion **207** (**205**). X = 8-oxo-dG, Y = 5-fdU
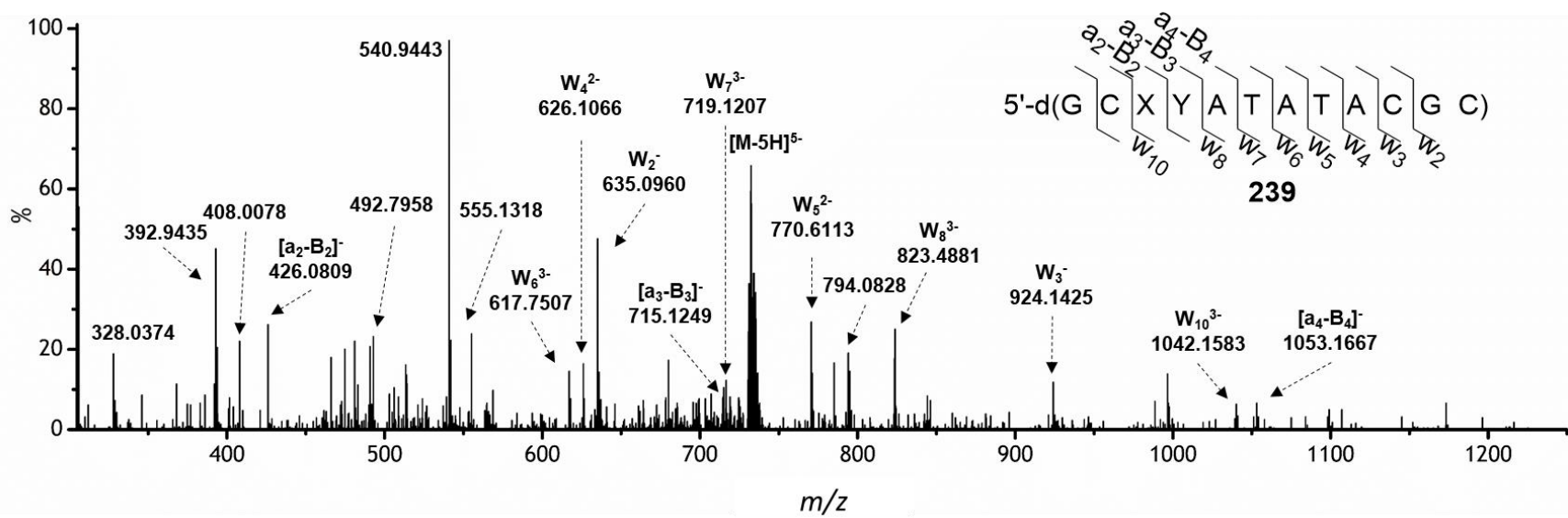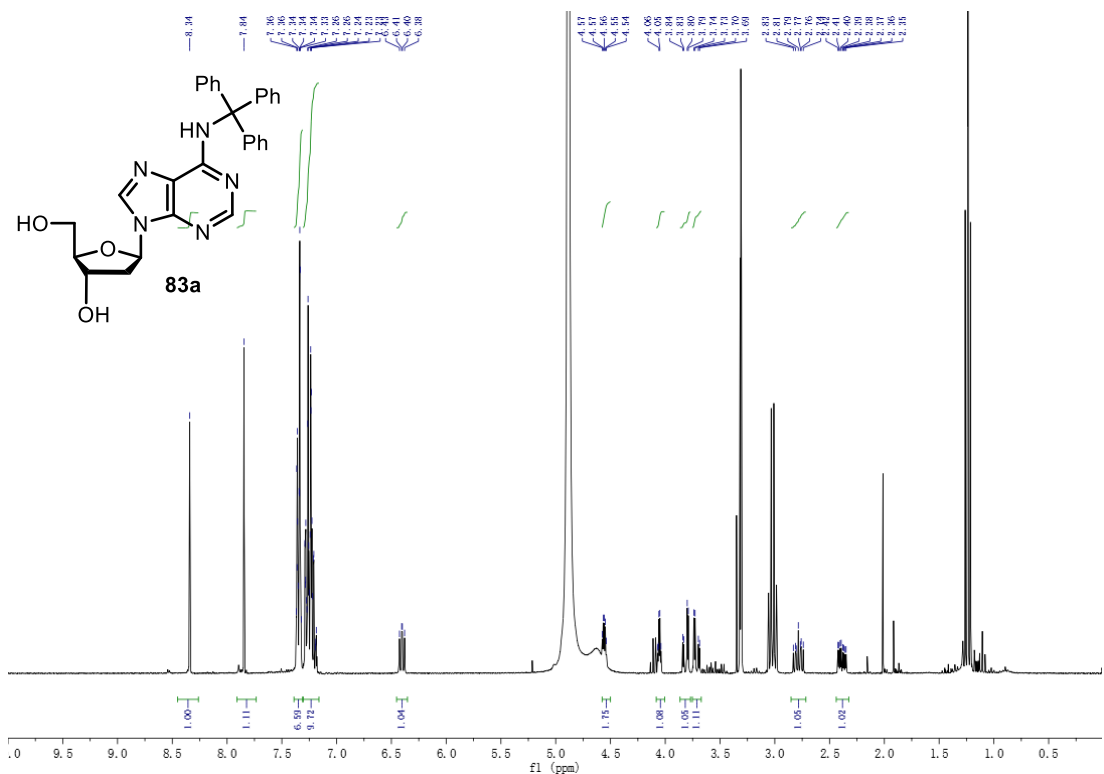
Appendix Figure 17. CID mass spectrum of the ion (m/z = 732.7, z = 5) of the oligonucleotide containing tandem lesion **232** (**239**). X = Tg, Y = 5-fdU.
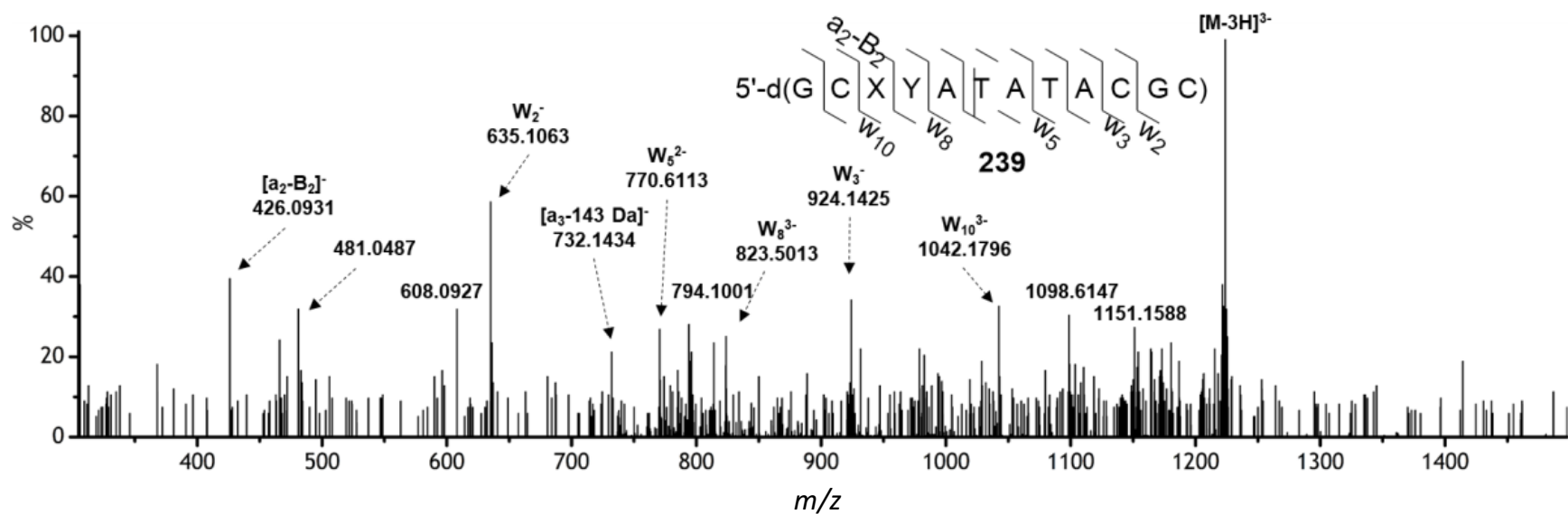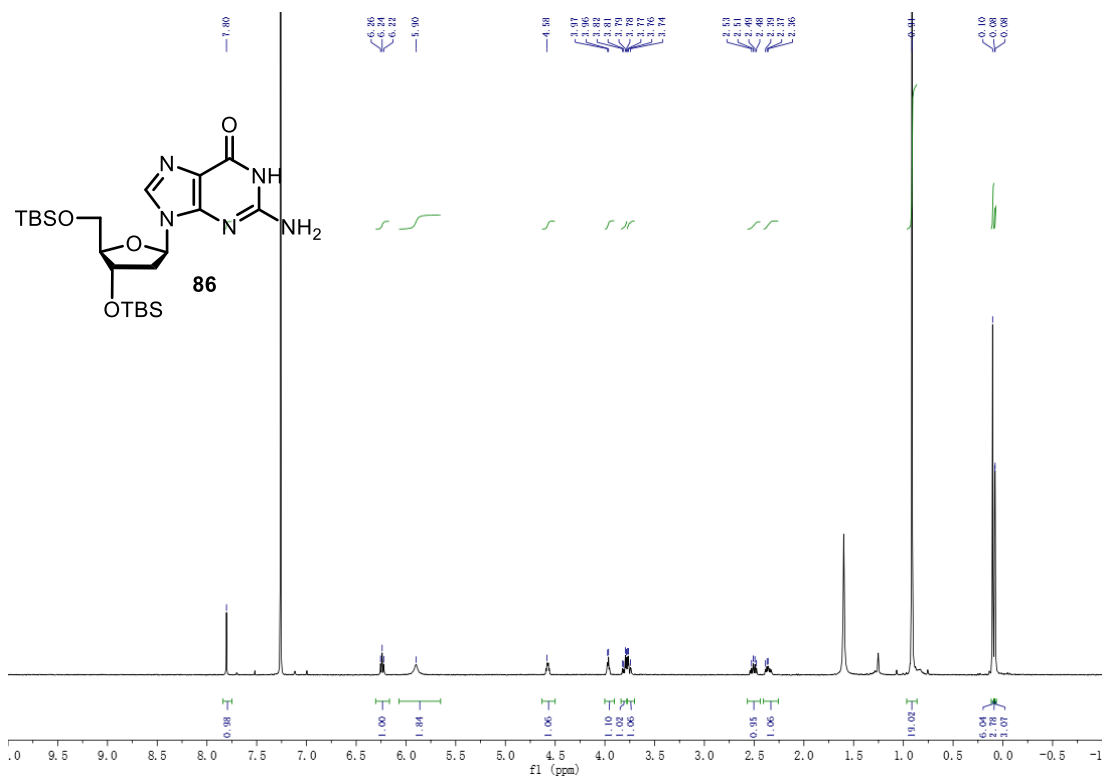
Appendix Figure 18. CID mass spectrum of the ion (m/z = 1221.6, z = 3) of the oligonucleotide containing tandem lesion **232** (**239**). X = Tg, Y = 5-fdU.
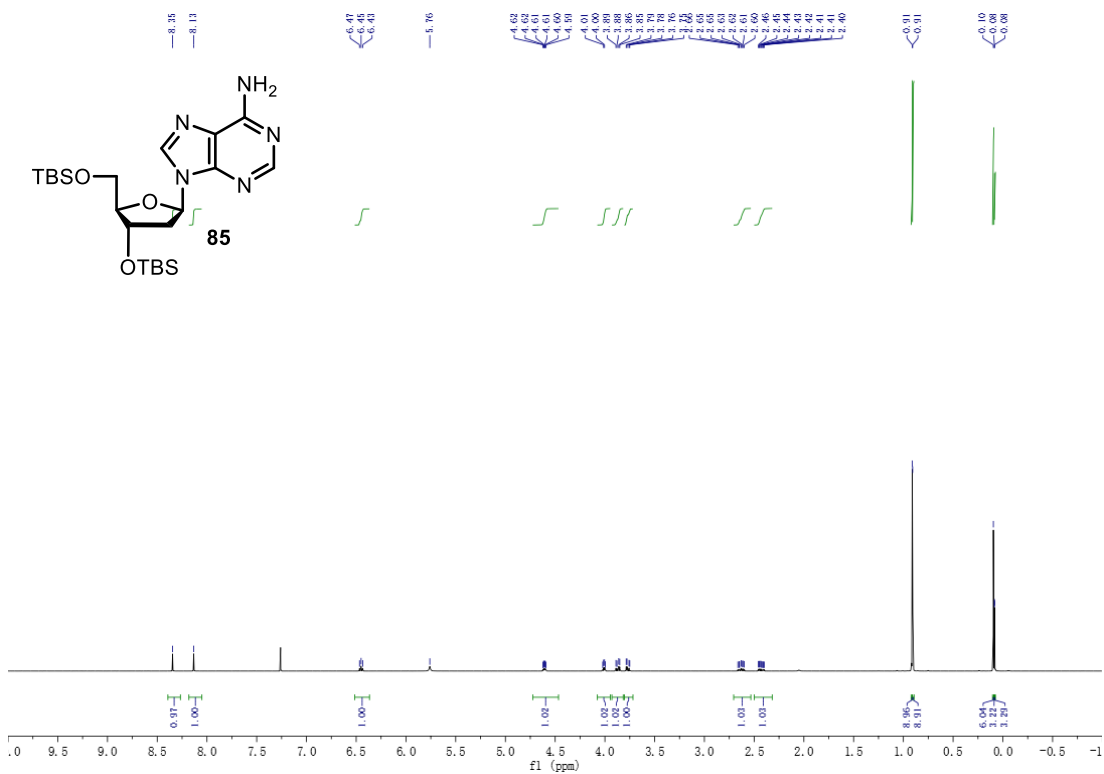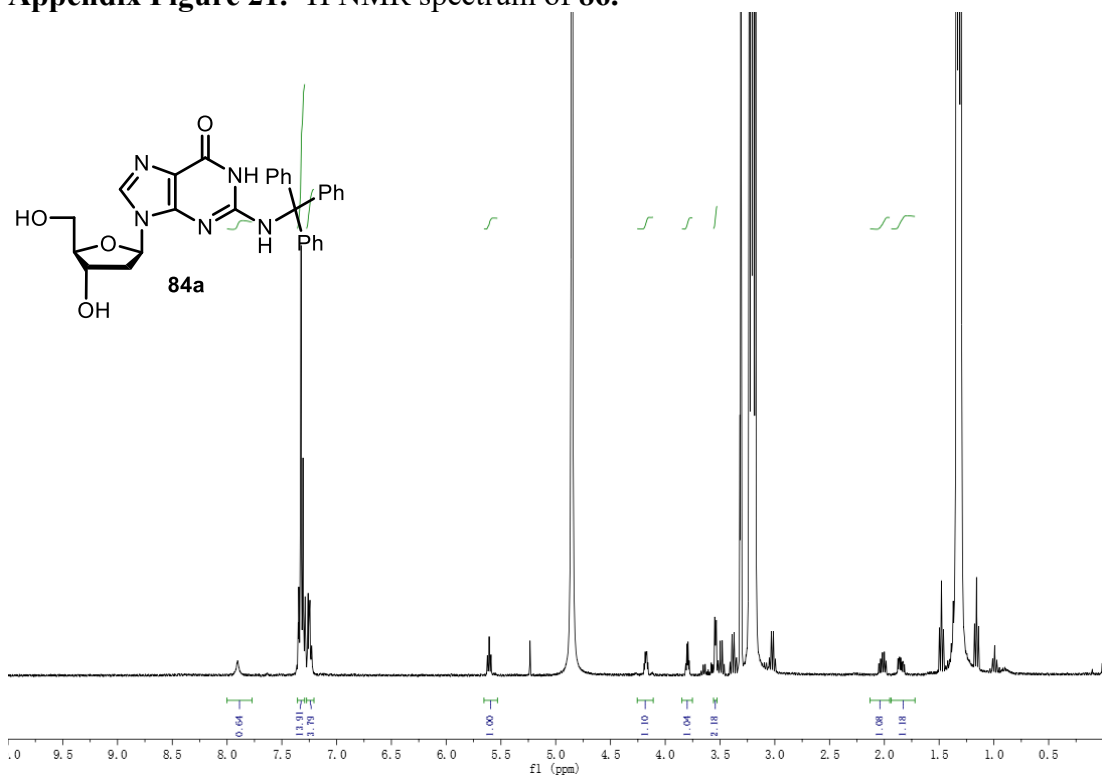
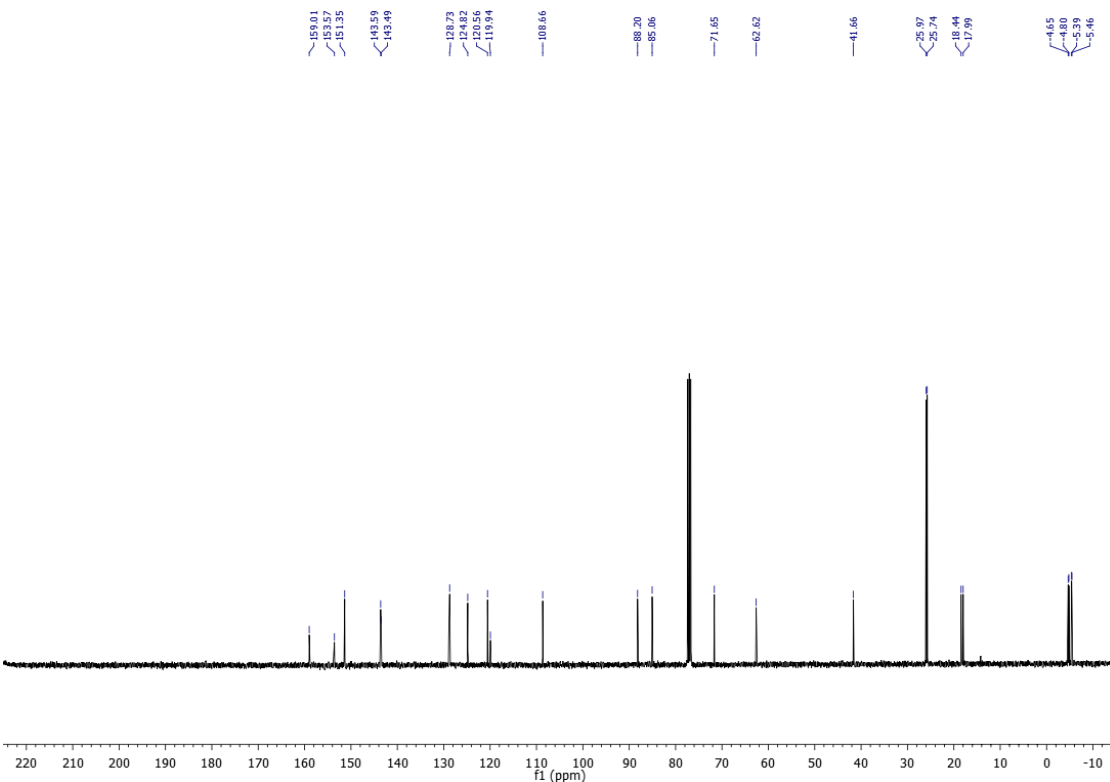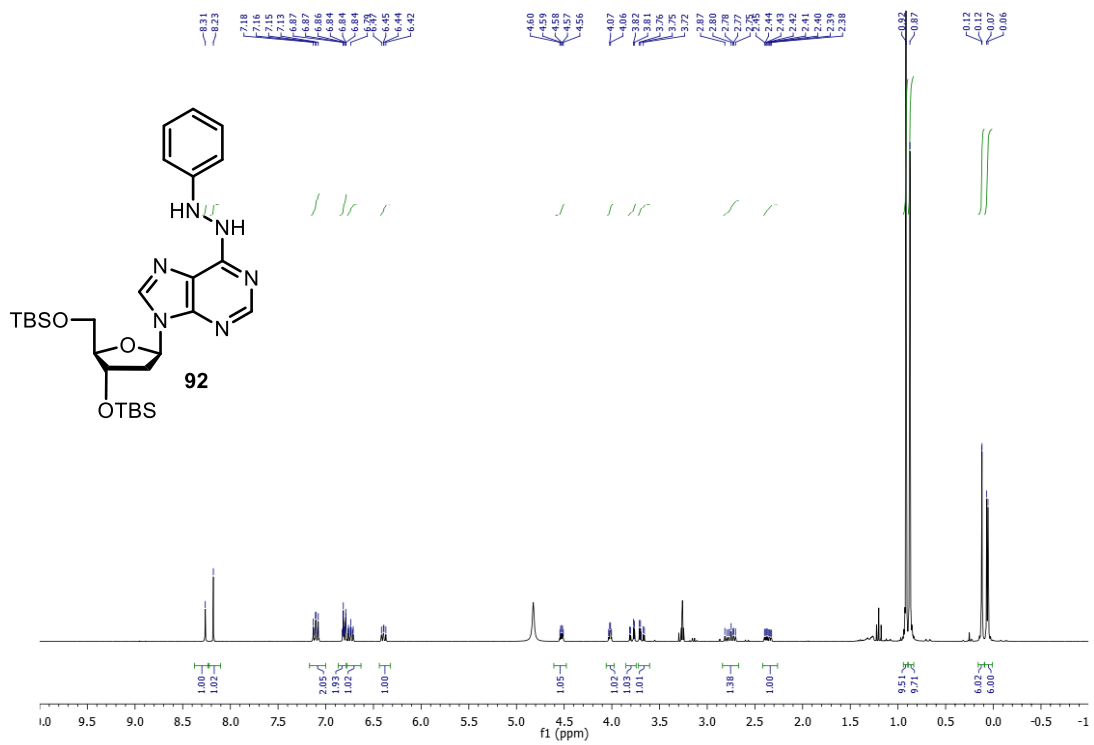**Appendix Figure 19.** ^{1}H NMR spectrum of **85**.

Appendix Figure 20. ^{1}H NMR spectrum of **83a**.

Appendix Figure 21. ^{1}H NMR spectrum of **86.**

Appendix Figure 22. ^{1}H NMR spectrum of **84a.**

Appendix Figure 23. ^{1}H NMR spectrum of 3',5'-bis-O-(t-butyldimethylsilyl)-2'-deoxyinosine.

Appendix Figure 24. ^{1}H NMR spectrum of **91**.

Appendix Figure 25. ^{1}H NMR and ^{13}C NMR spectra of **92**.
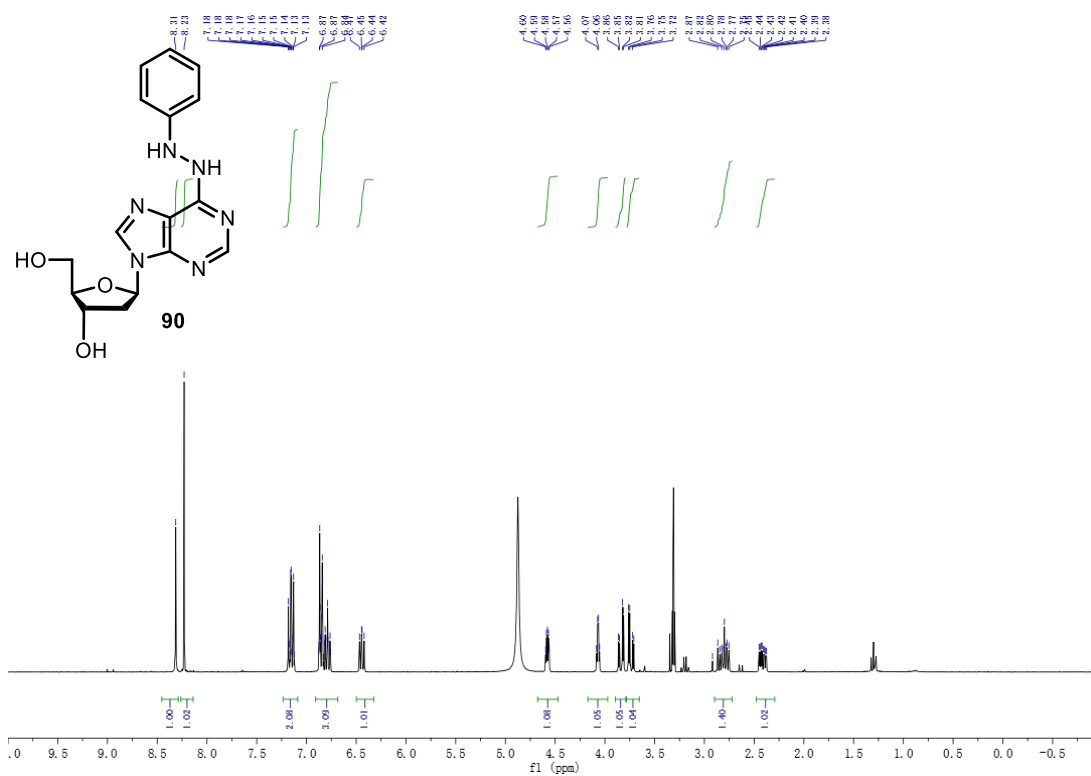
Appendix Figure 26. ^{1}H NMR spectrum of **90**.
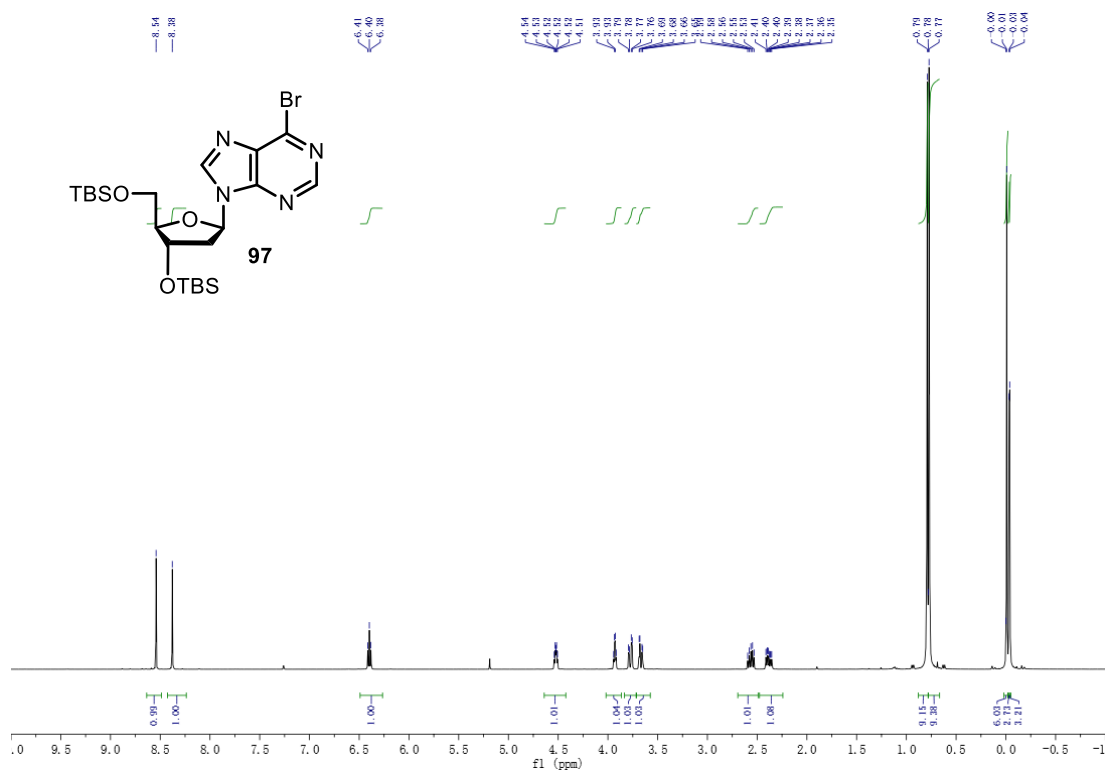
Appendix Figure 27. ^{1}H NMR spectrum of **97**.

251

Appendix Figure 28. ^{1}H NMR spectrum of **98**.
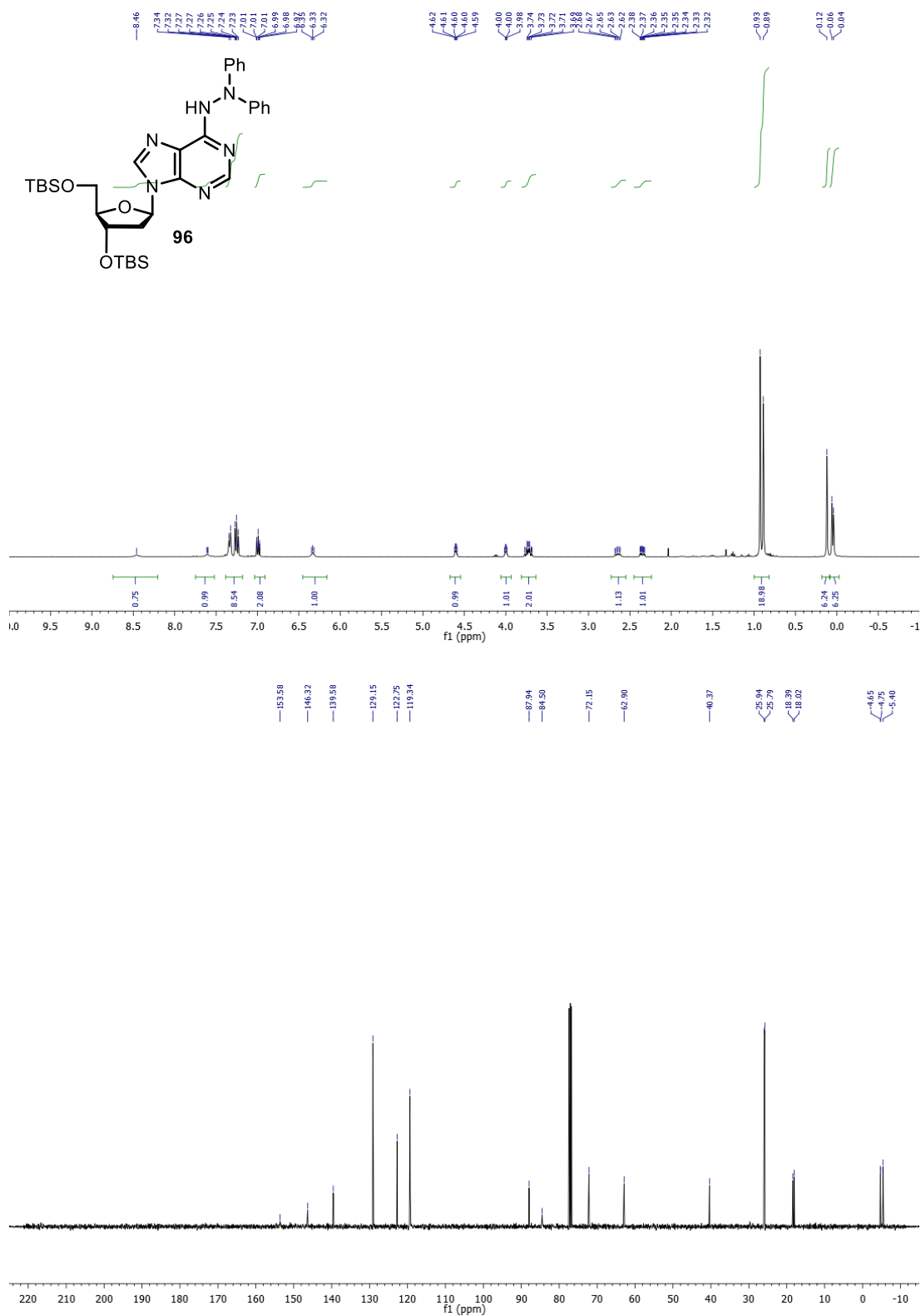
Appendix Figure 29. ^{1}H NMR and ^{13}C NMR spectra of **96**.
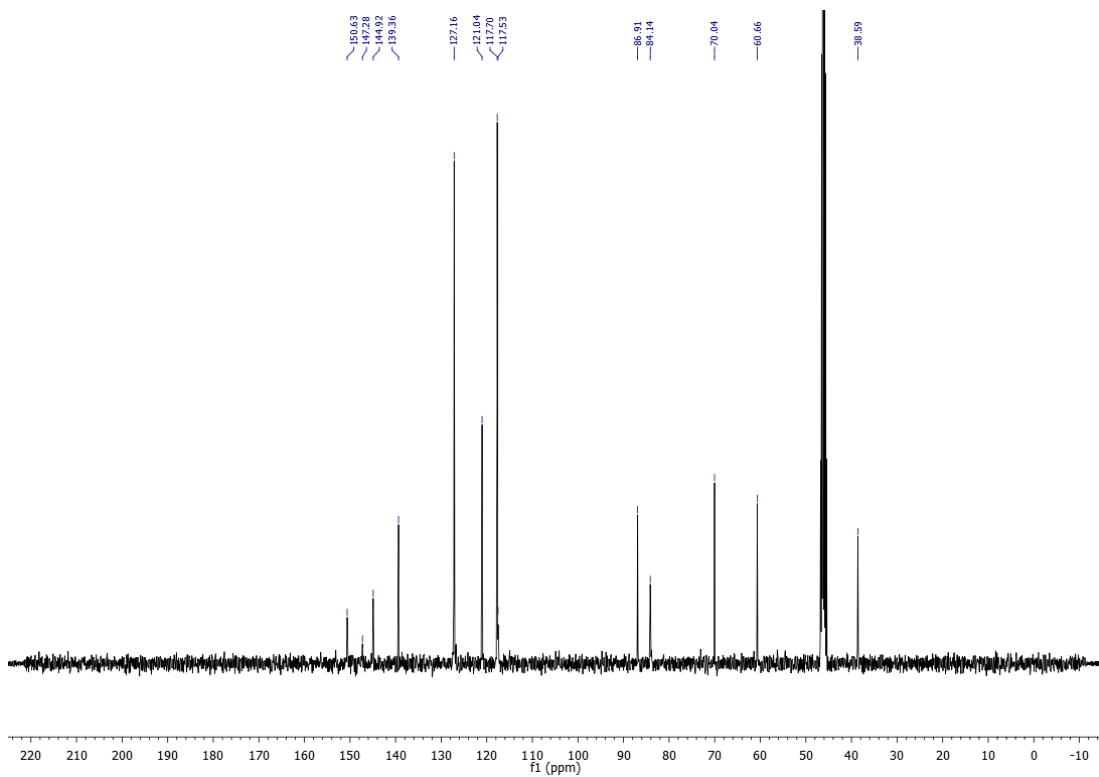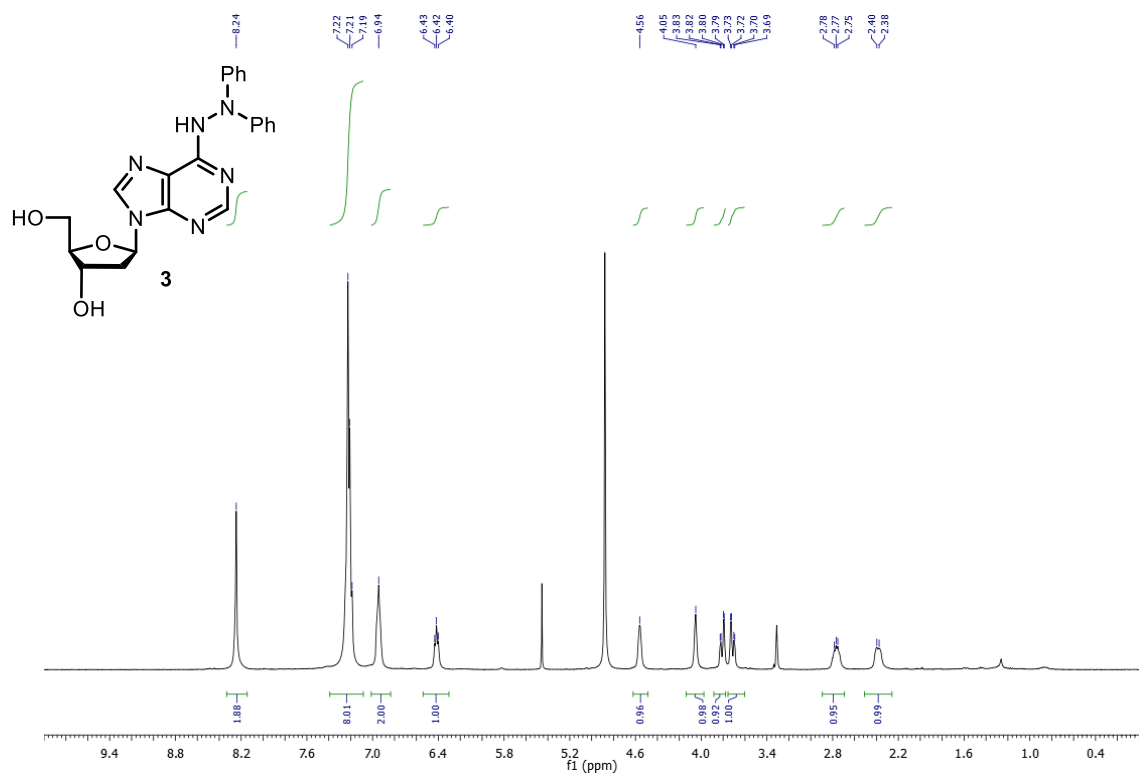
Appendix Figure 30. ^{1}H NMR and ^{13}C NMR spectra of **3**.
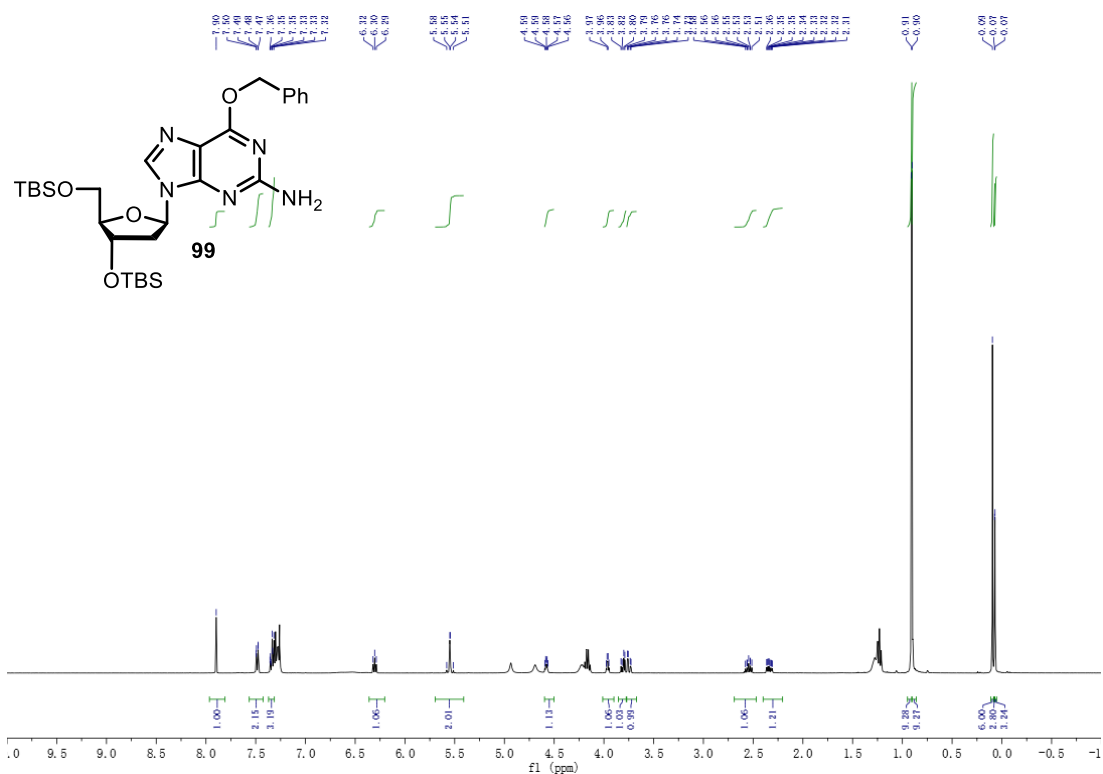
Appendix Figure 31. ^{1}H NMR spectrum of **99**.
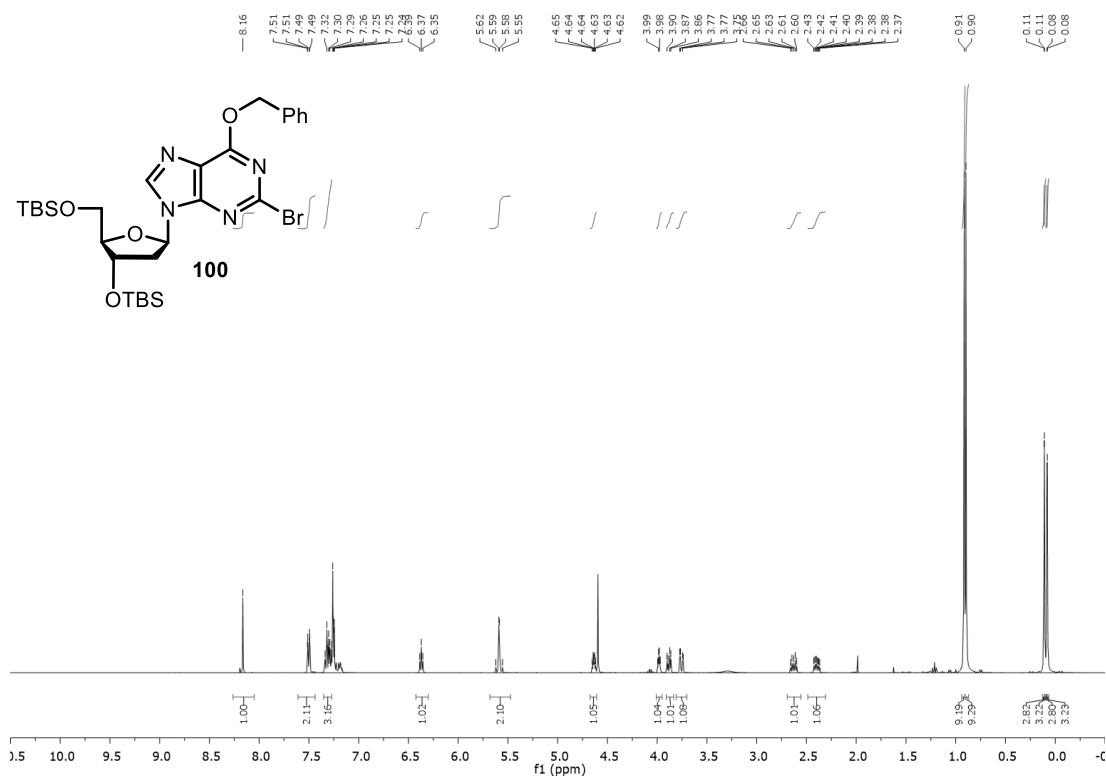
Appendix Figure 32. ^{1}H NMR spectrum of **100**.
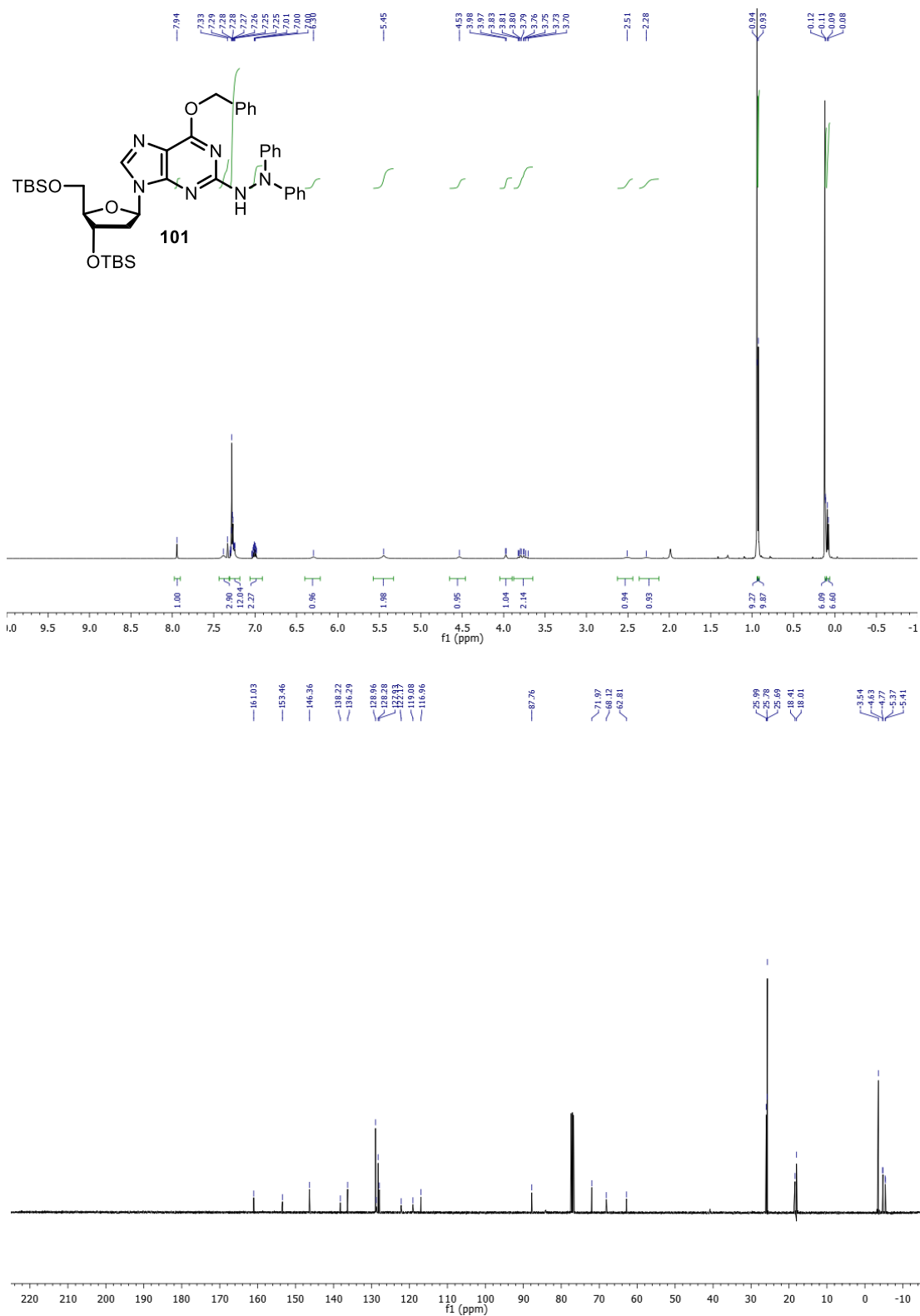
Appendix Figure 33. ^{1}H NMR and ^{13}C NMR spectra of **101**.
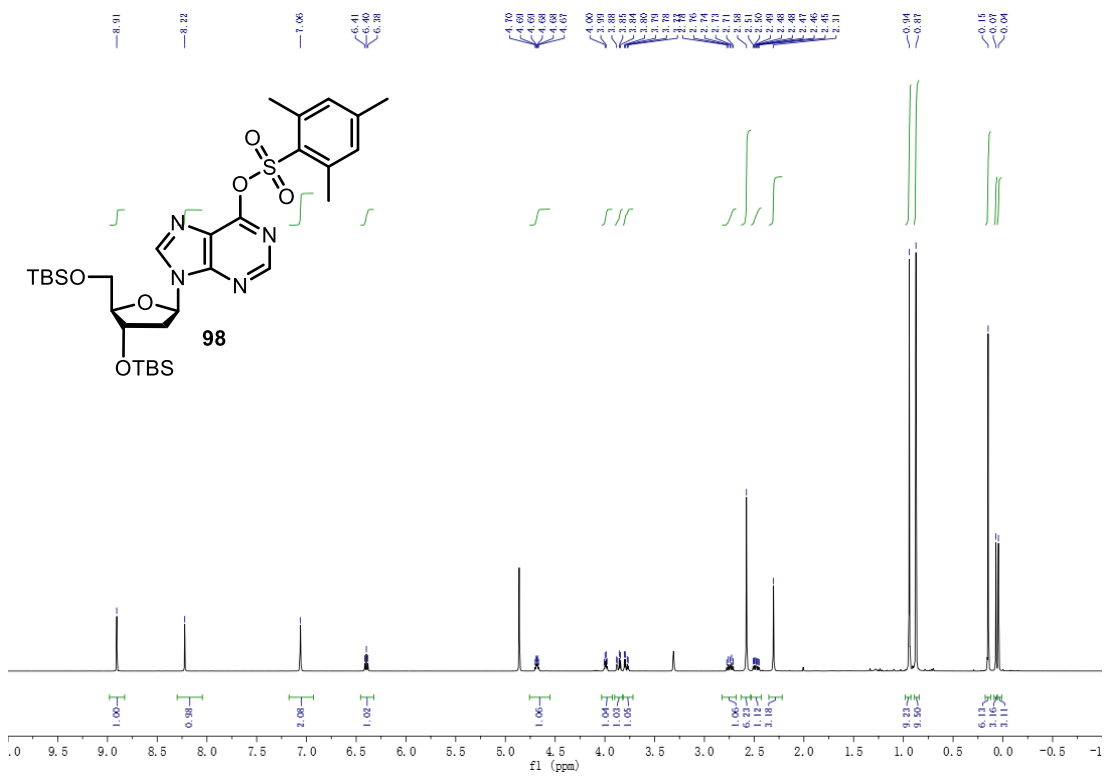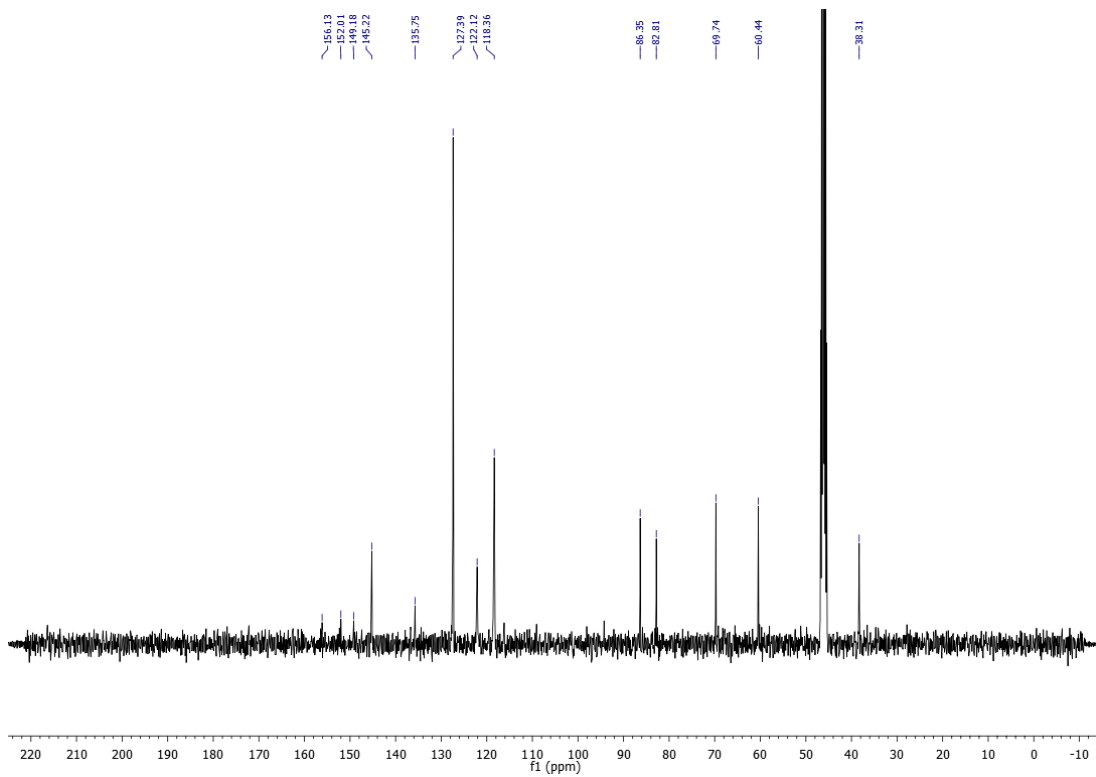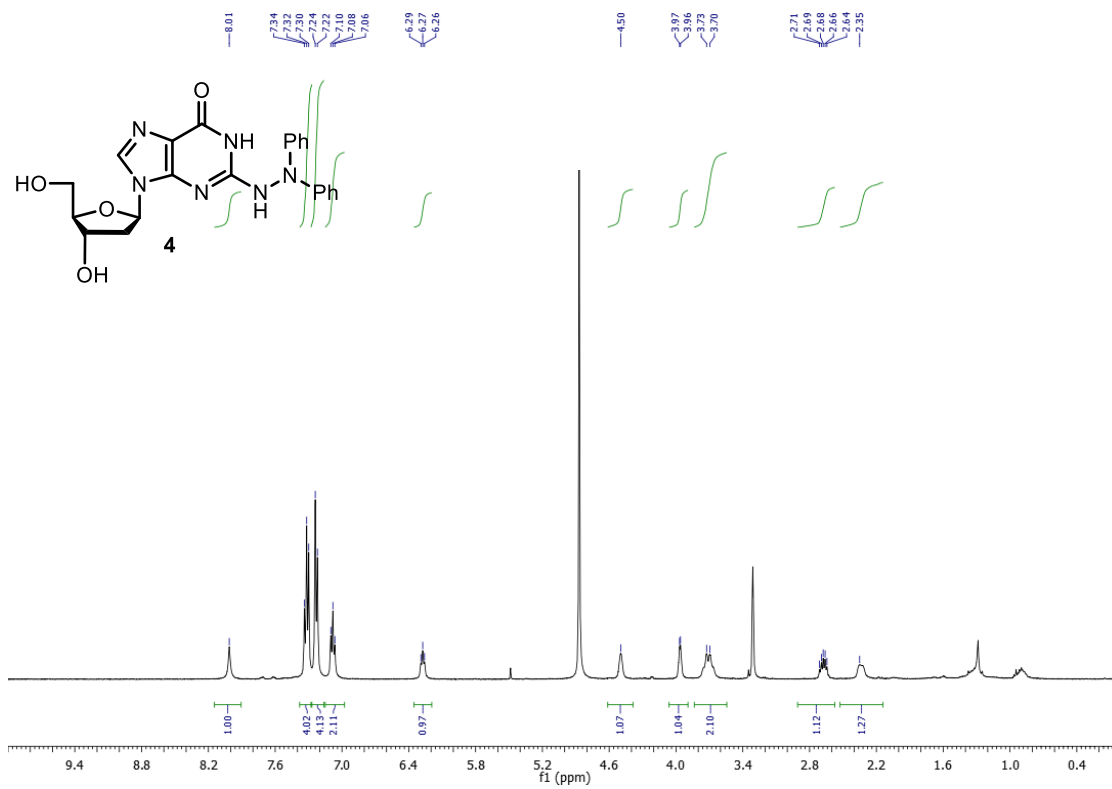
Appendix Figure 34. ¹H NMR and ¹³C NMR spectra of **4**.
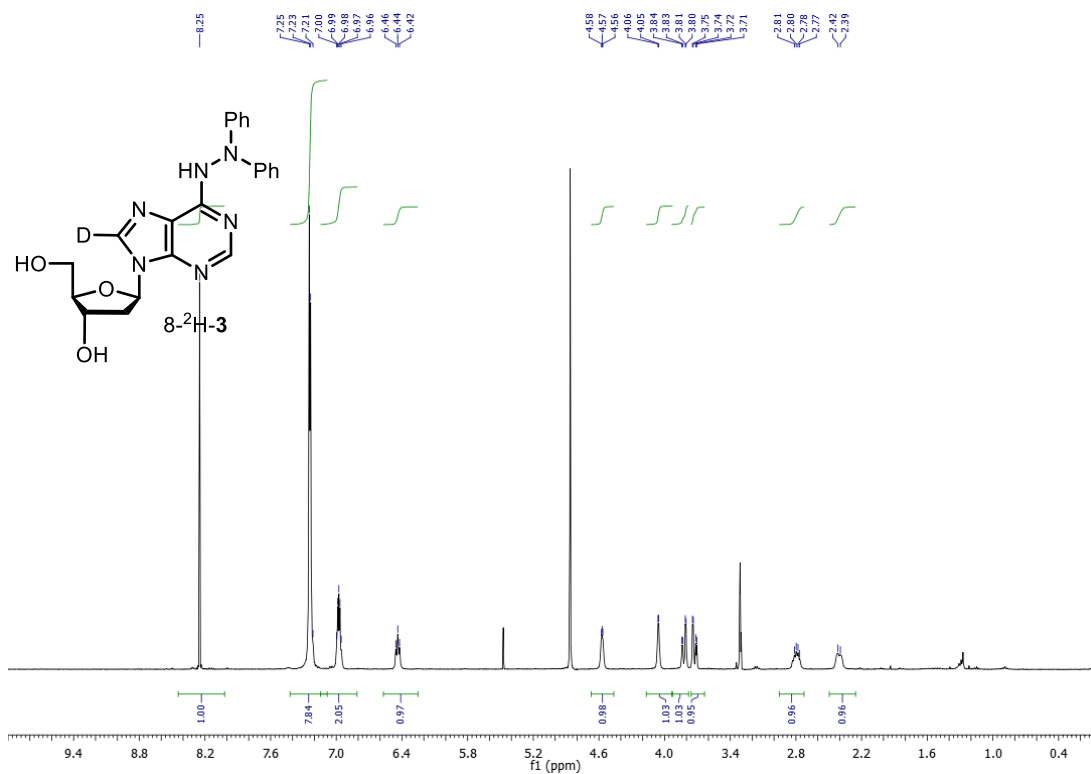
Appendix Figure 35. ^{1}H NMR spectrum of 8-^{2}H-**3**.
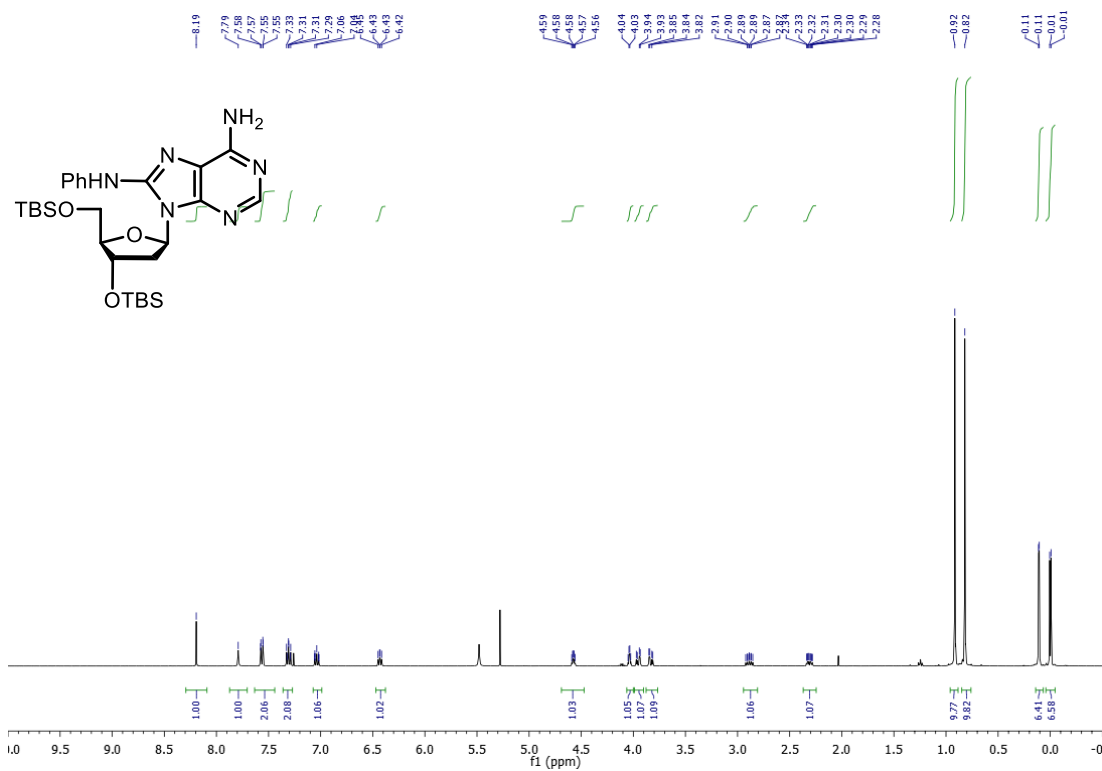
Appendix Figure 36. ^{1}H NMR spectrum of disilylated **106**.
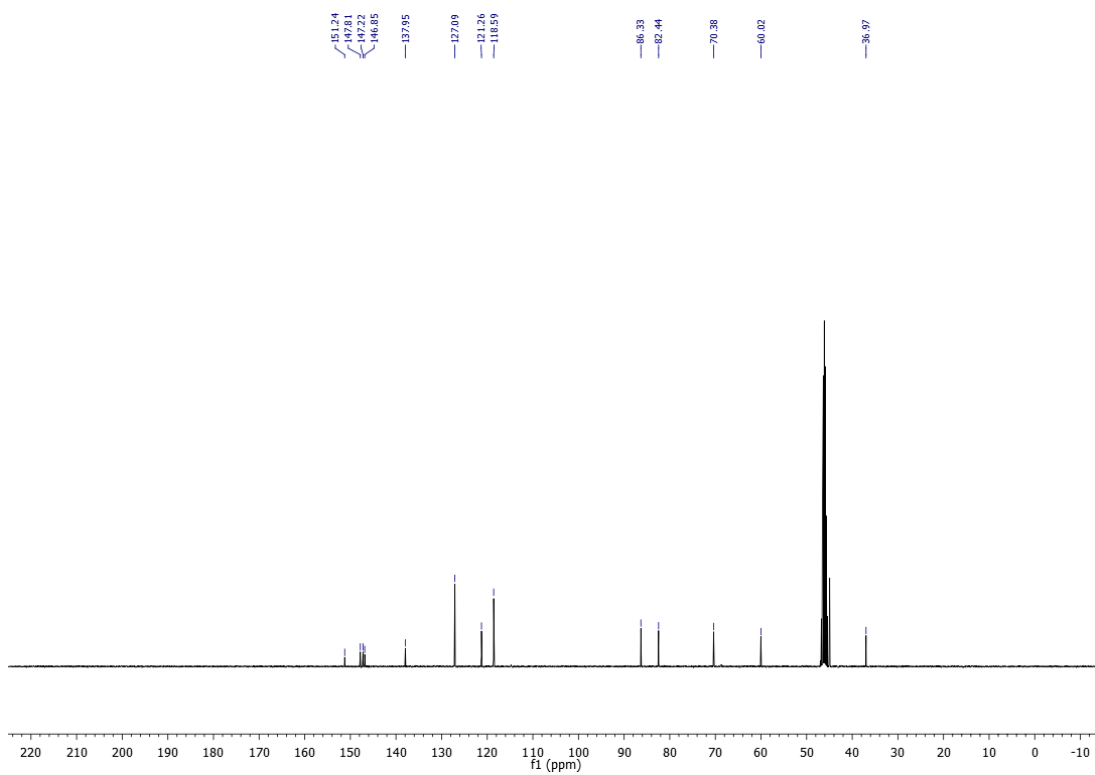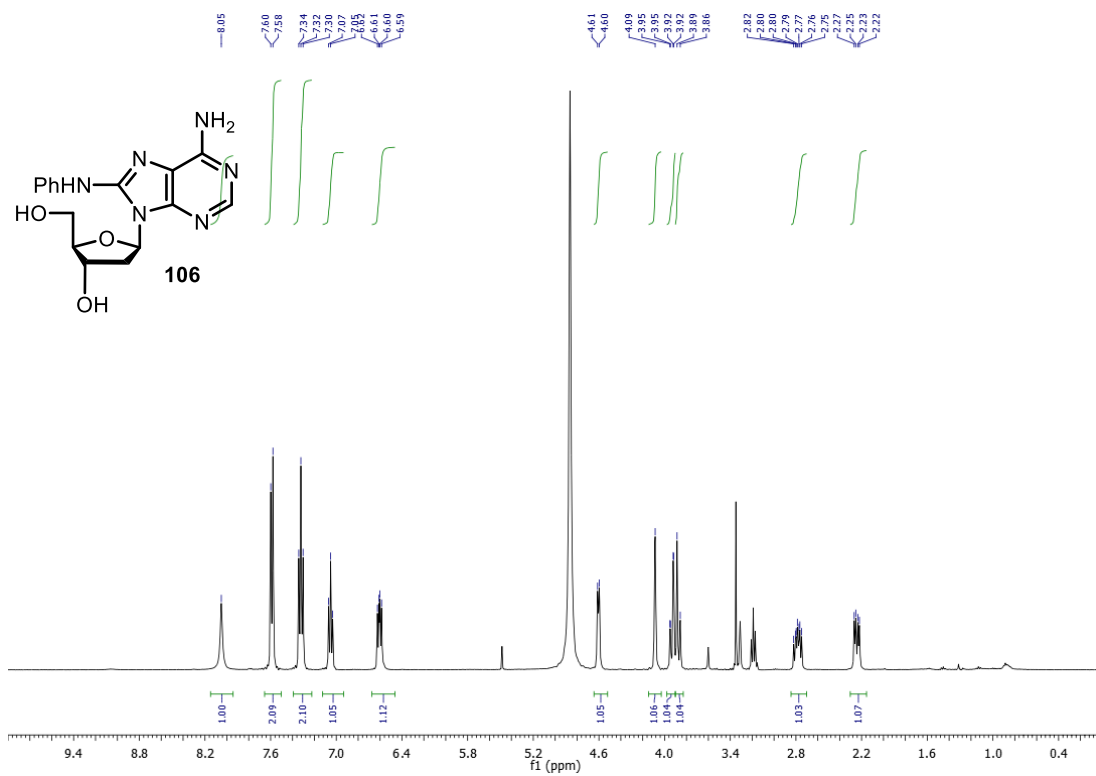
Appendix Figure 37. ^{1}H NMR and ^{13}C NMR spectra of **106**.
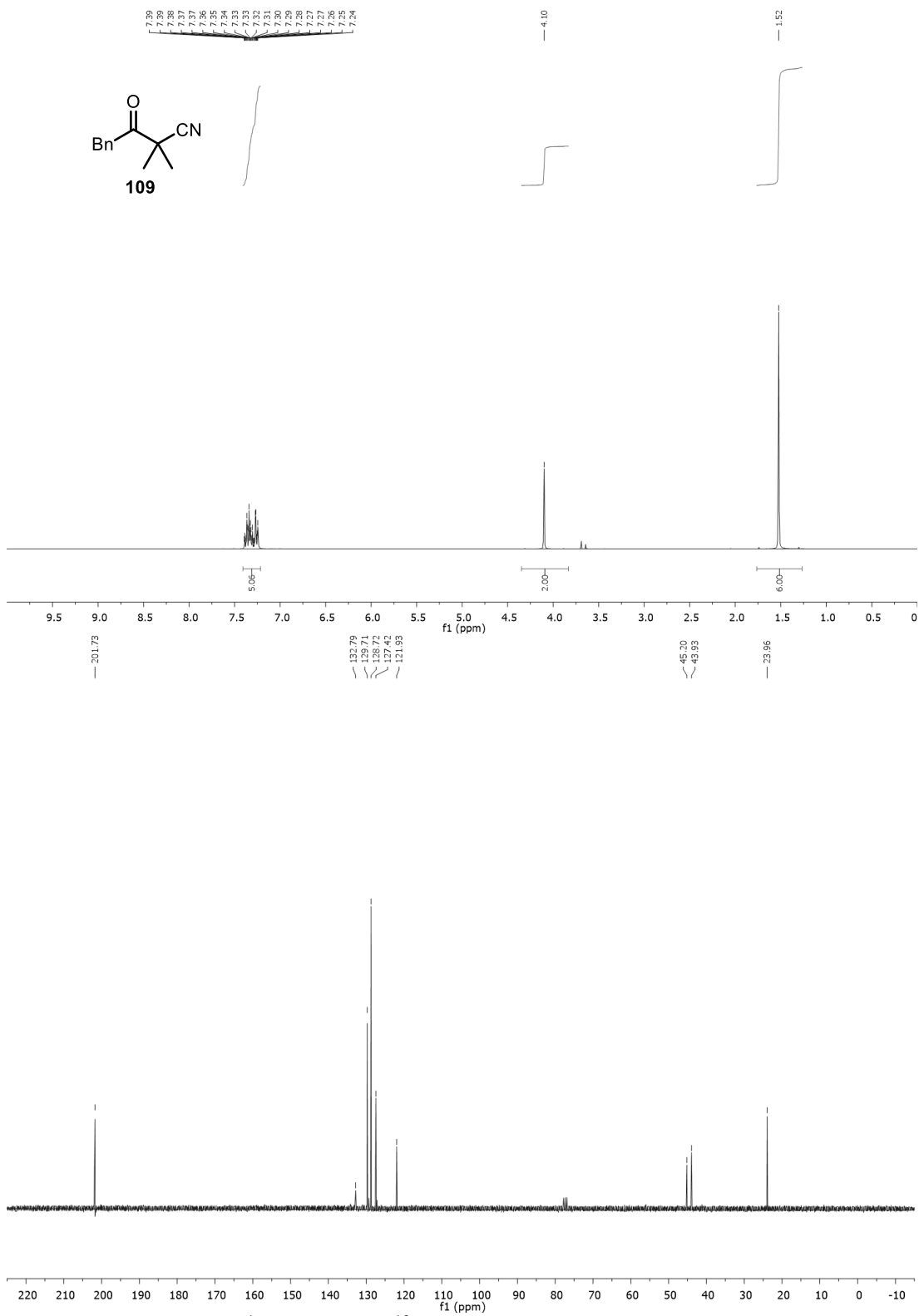
Appendix Figure 38. ^{1}H NMR and ^{13}C NMR spectra of **109**.
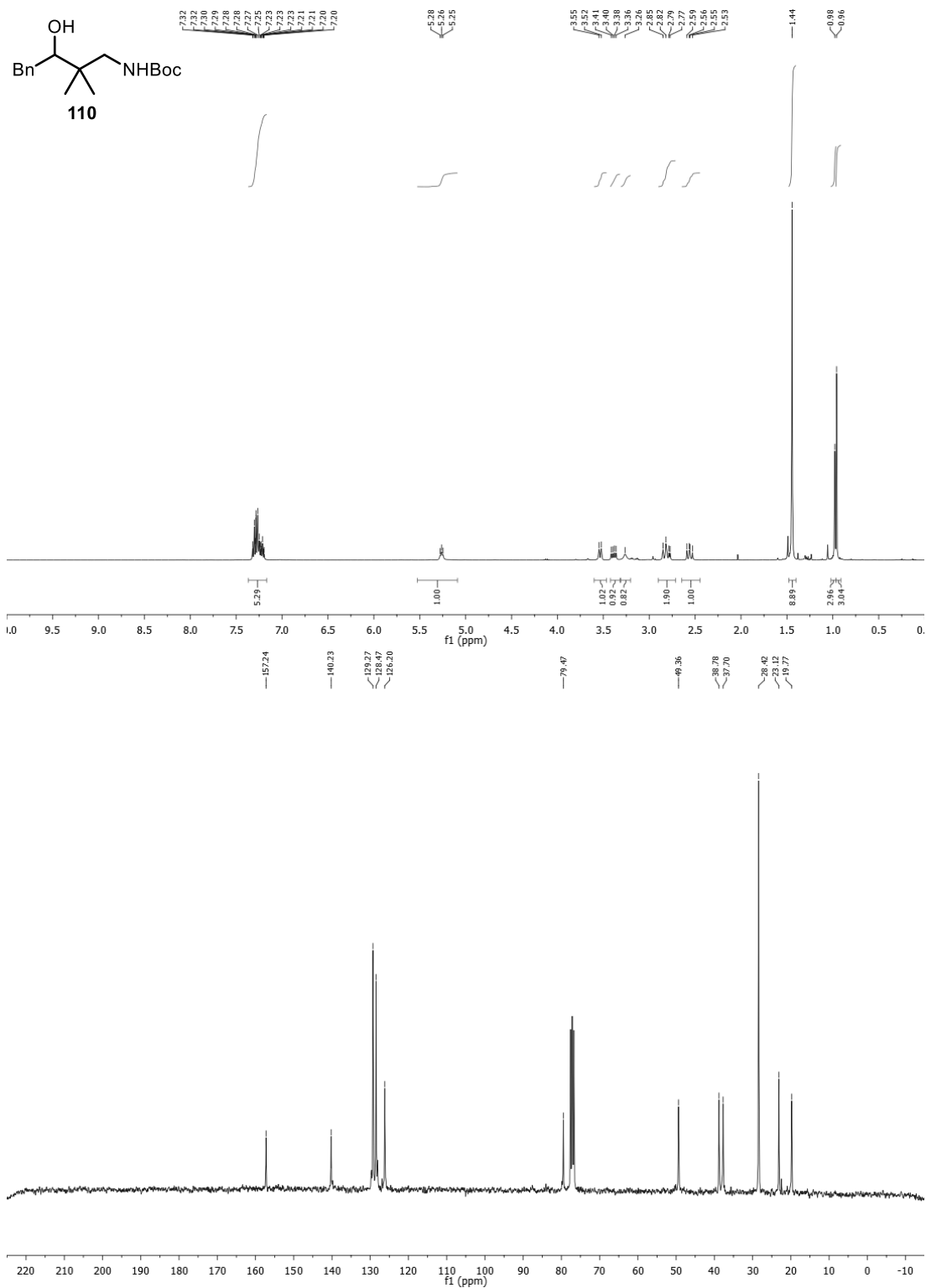
Appendix Figure 39. ^{1}H NMR and ^{13}C NMR spectra of **110**.
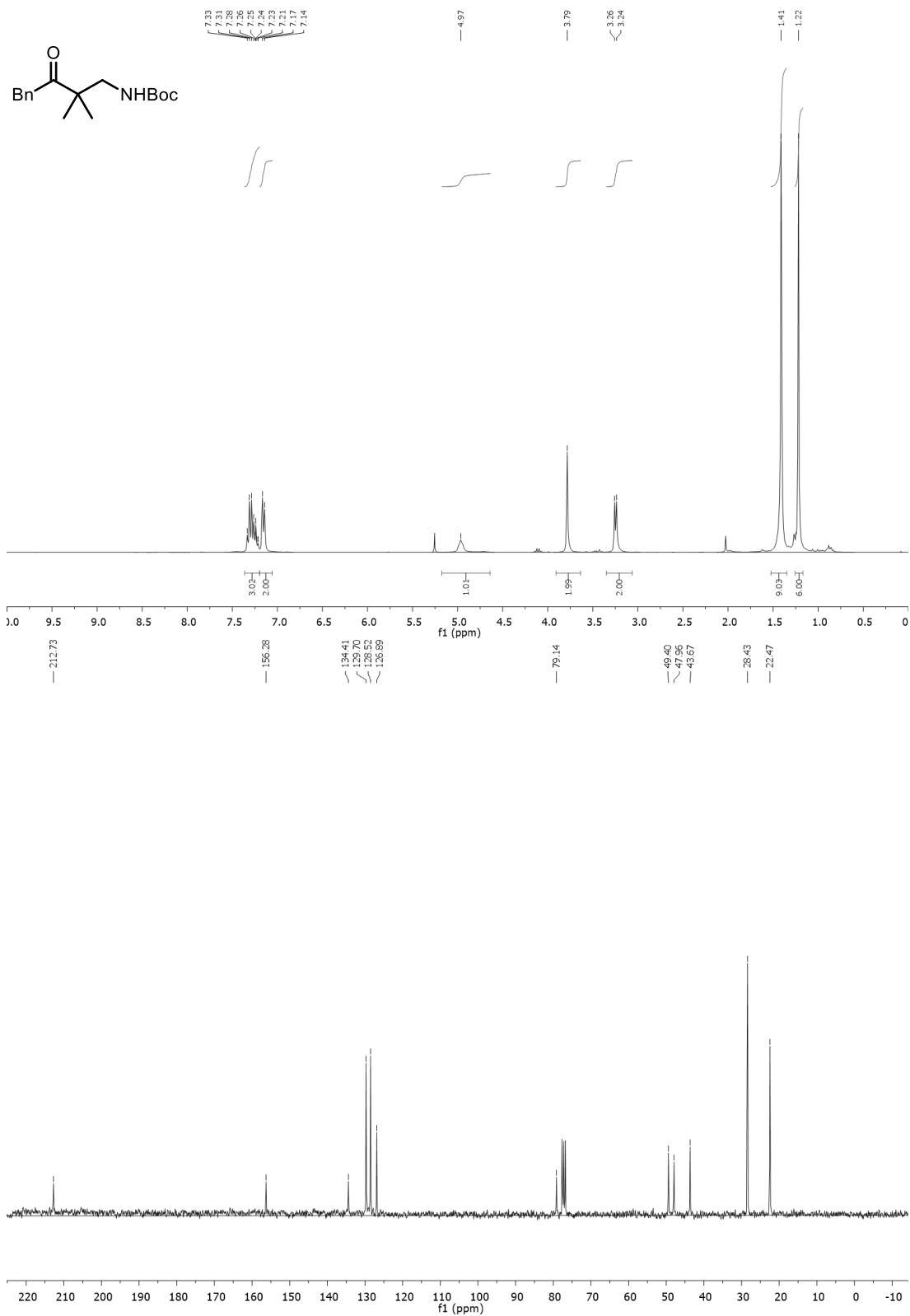
Appendix Figure 40. ^{1}H NMR and ^{13}C NMR spectra of t-Boc-protected **111**.
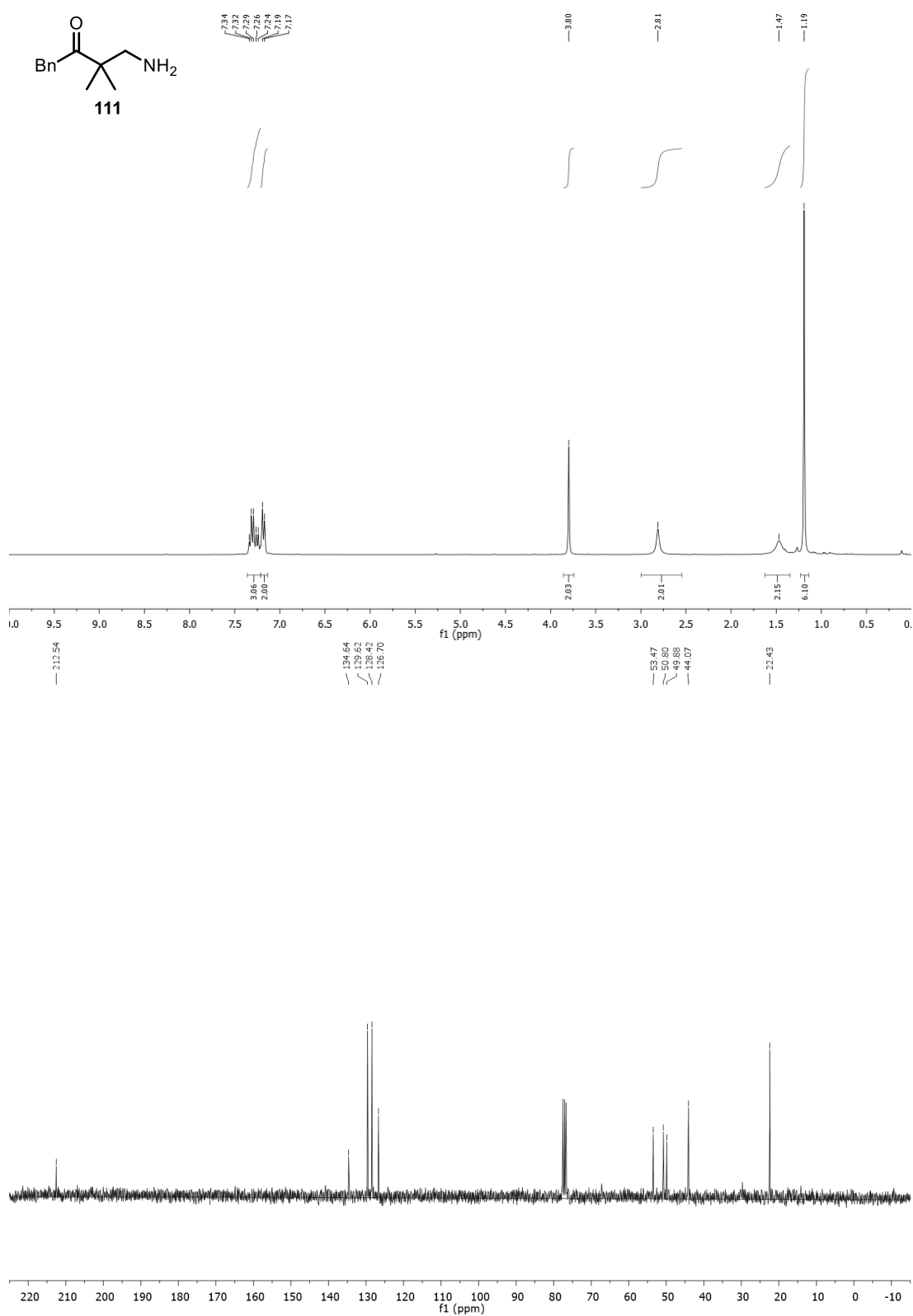
Appendix Figure 41. ^{1}H NMR and ^{13}C NMR spectra of **111**.
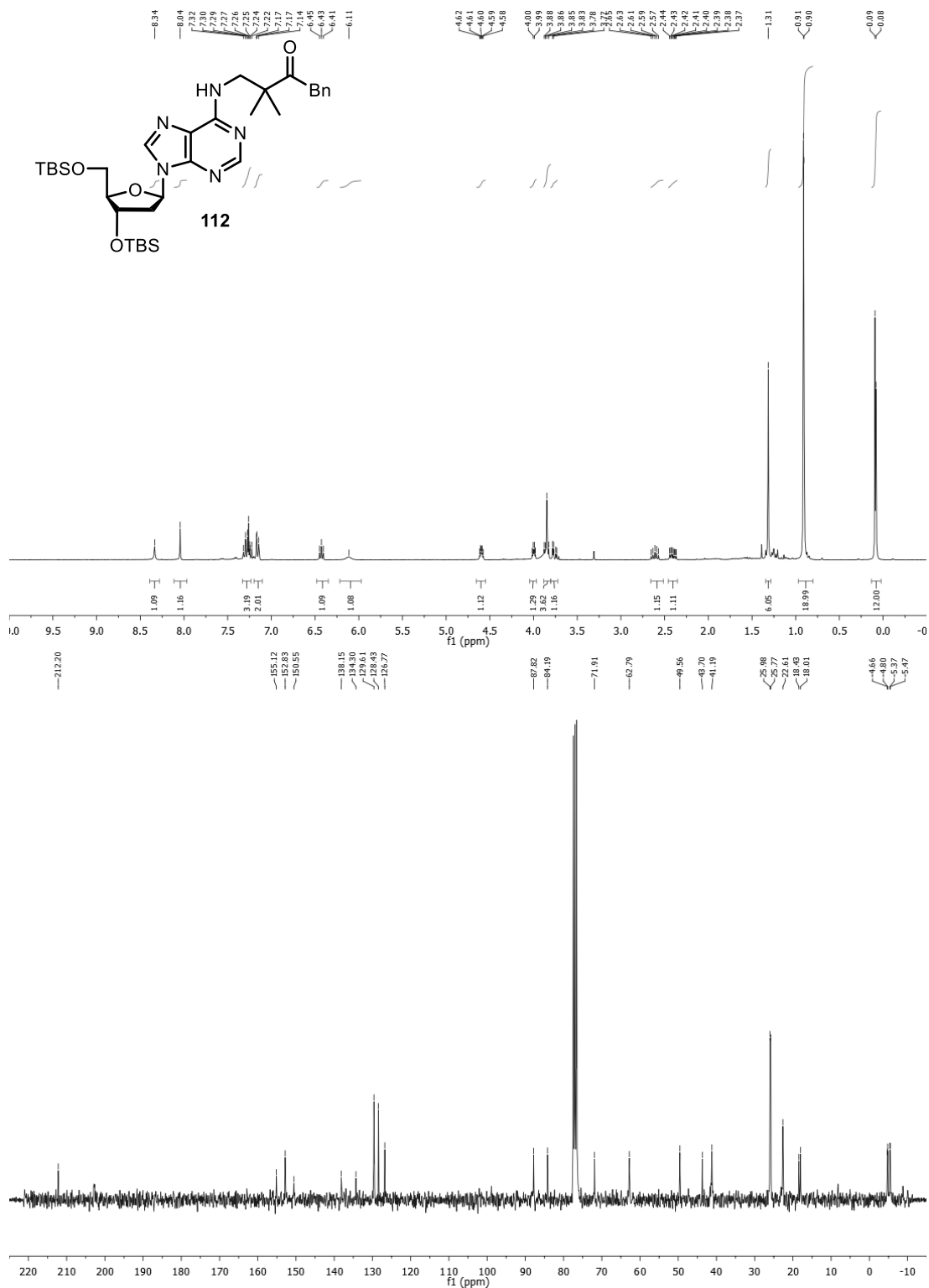
Appendix Figure 42. ^{1}H NMR and ^{13}C NMR spectra of **112**.
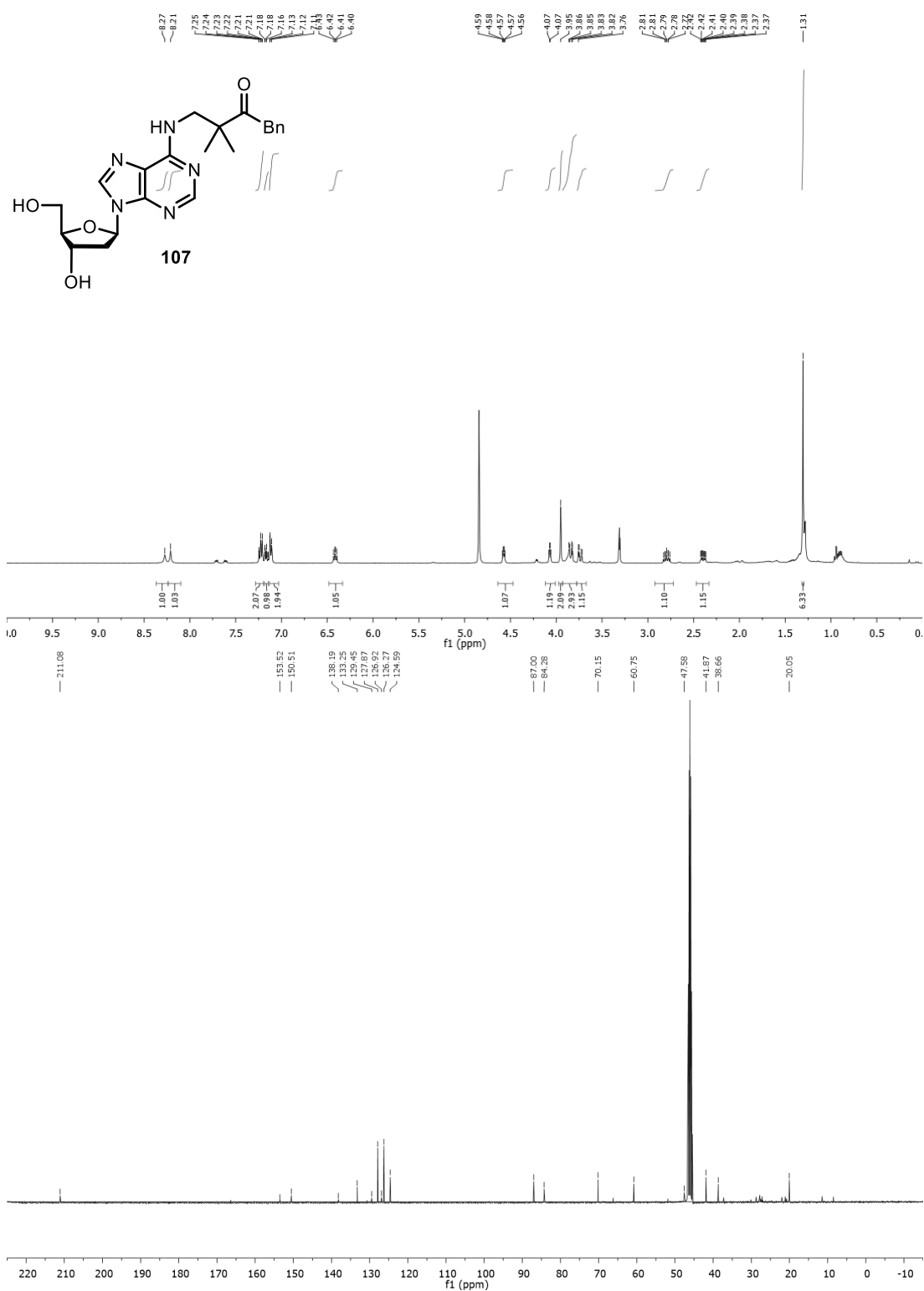
Appendix Figure 43. ^{1}H NMR and ^{13}C NMR spectra of **107**.
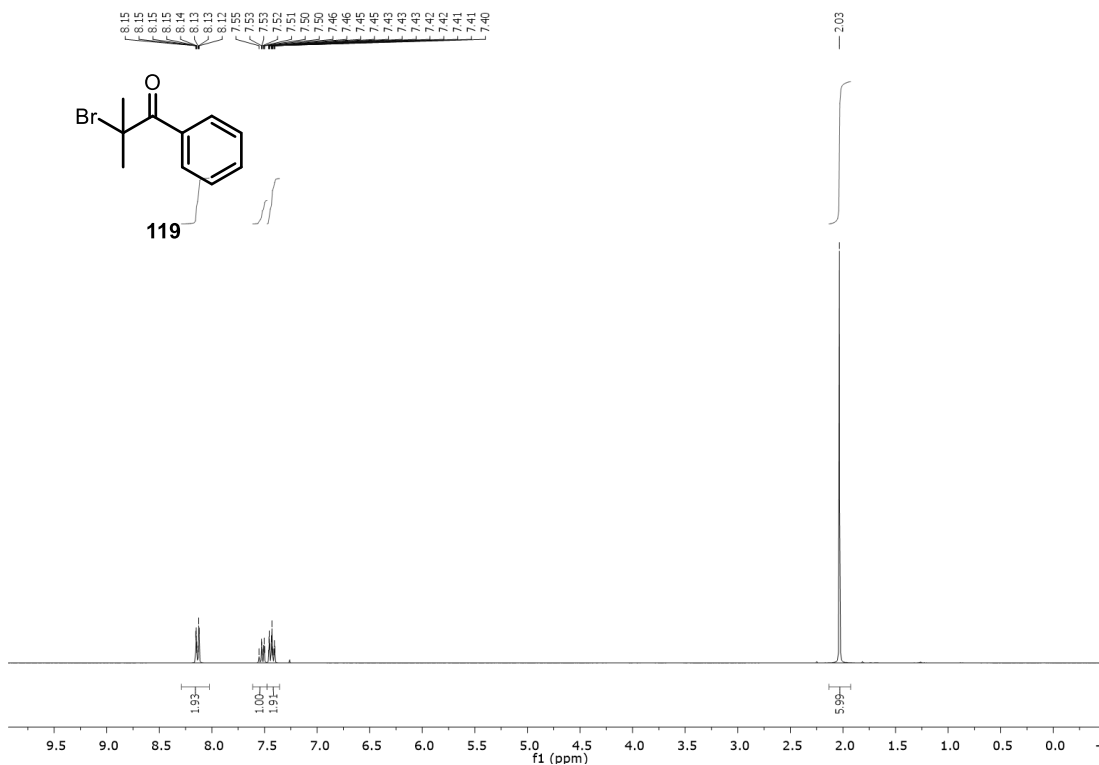
Appendix Figure 44. ^{1}H NMR spectrum of **119**.
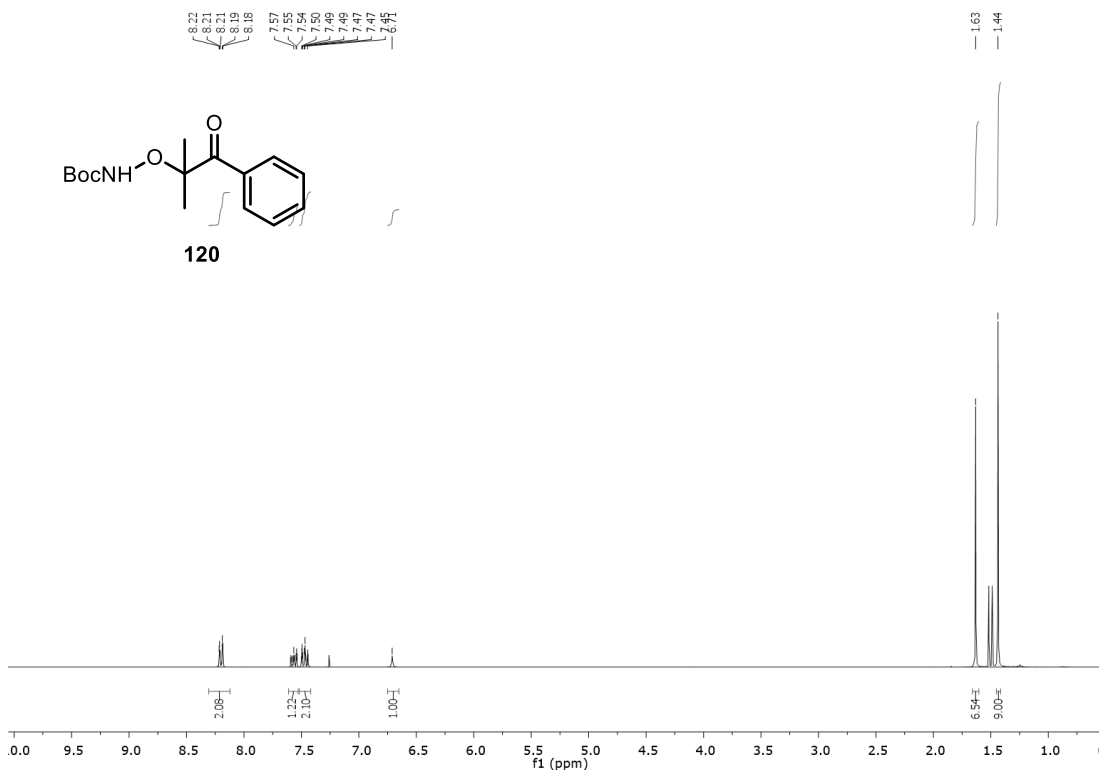
Appendix Figure 45. ^{1}H NMR spectrum of **120**.

266
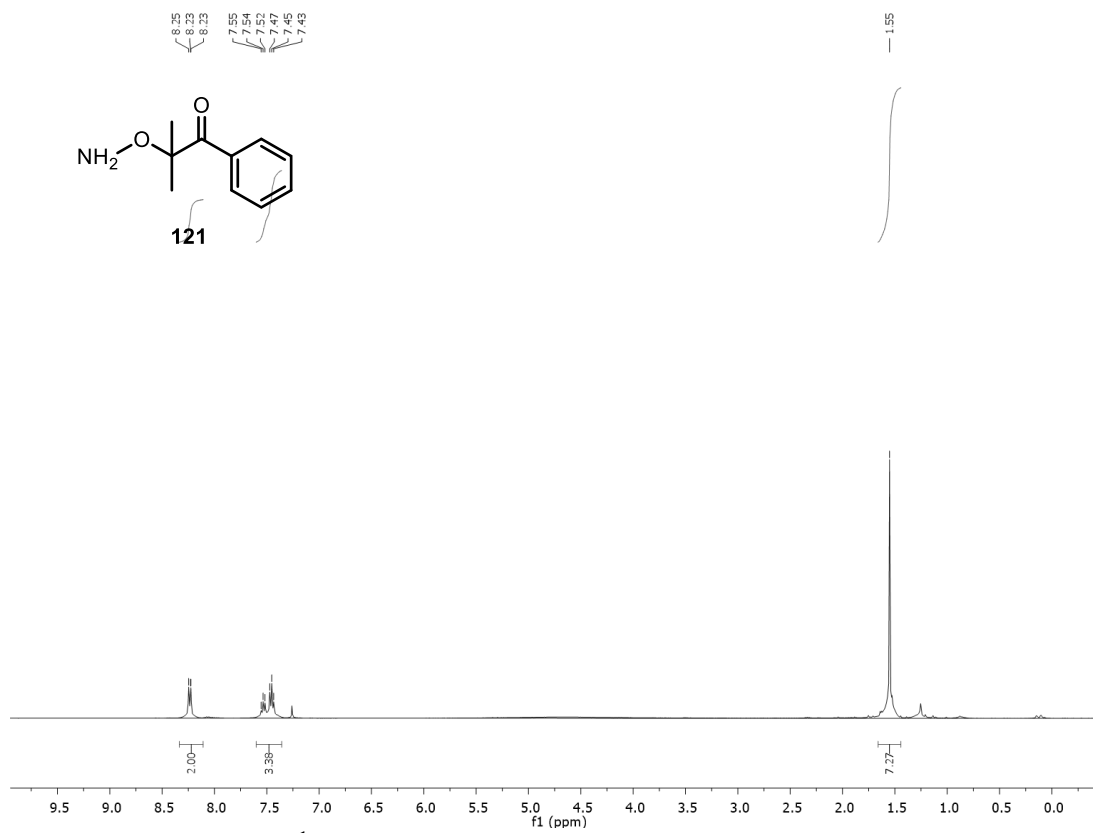
Appendix Figure 46. ^{1}H NMR spectrum of **121**.
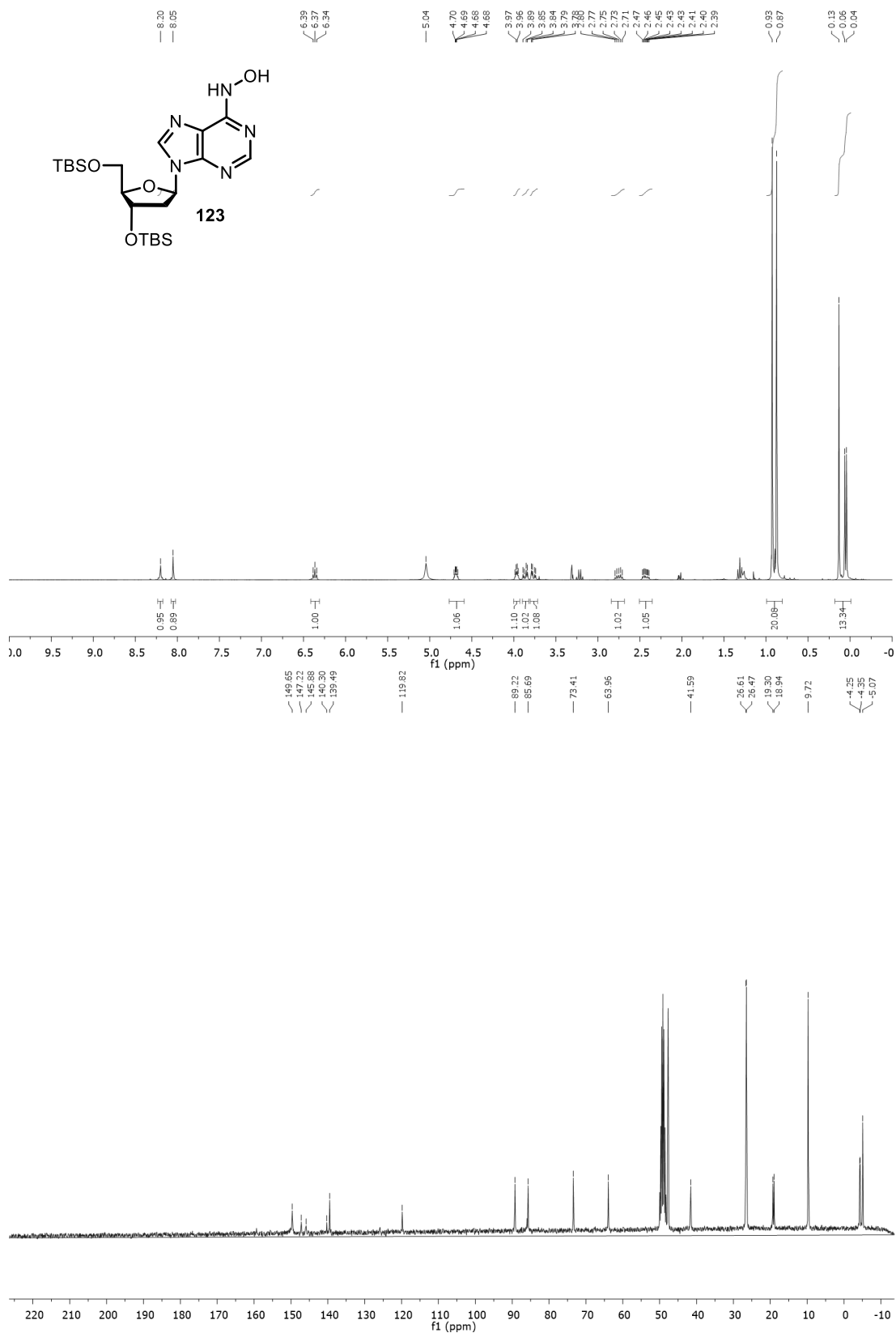
Appendix Figure 47. ^{1}H NMR and ^{13}C NMR spectra of **123**.
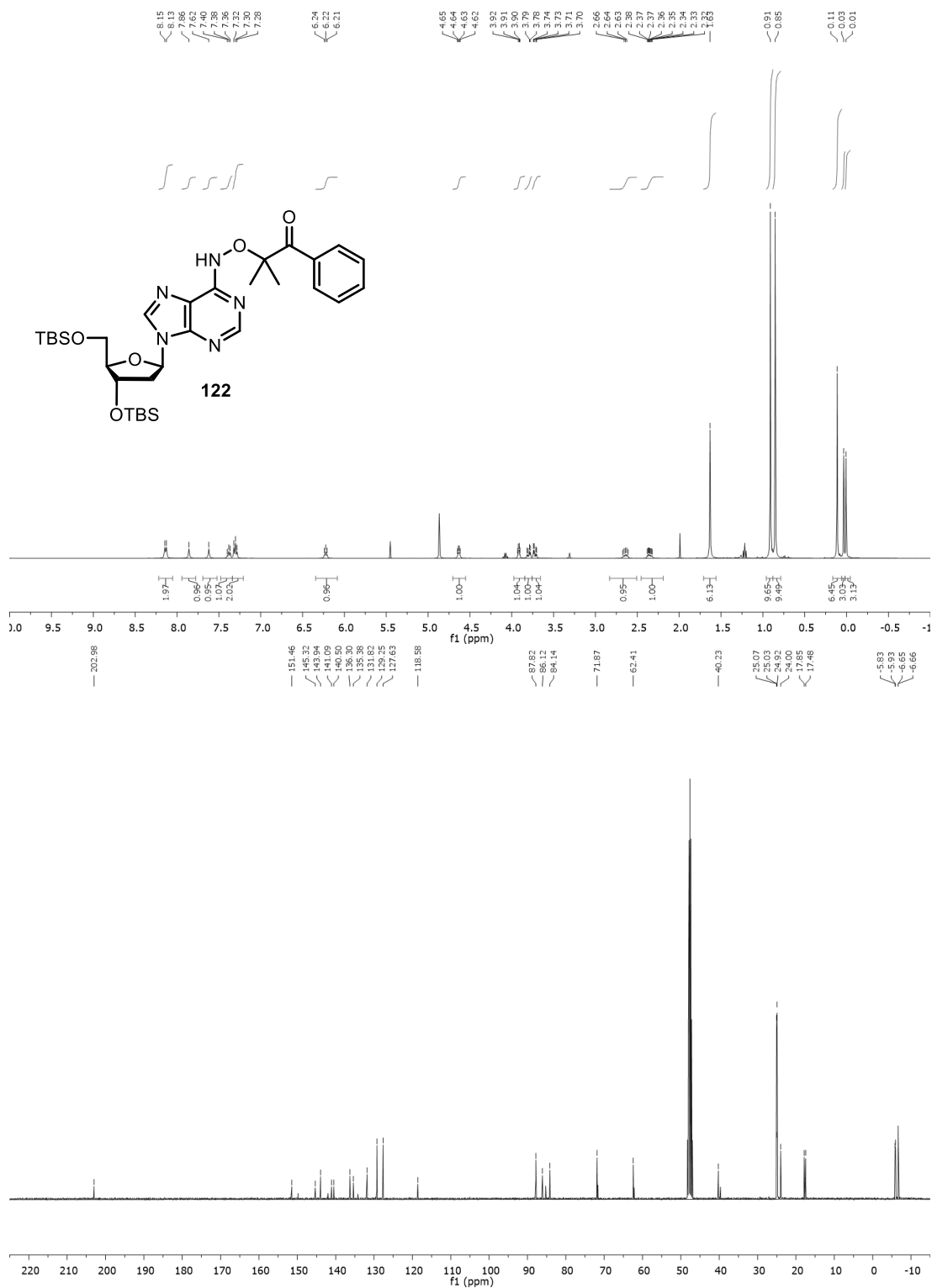
Appendix Figure 48. ^{1}H NMR and ^{13}C NMR spectra of **122**.
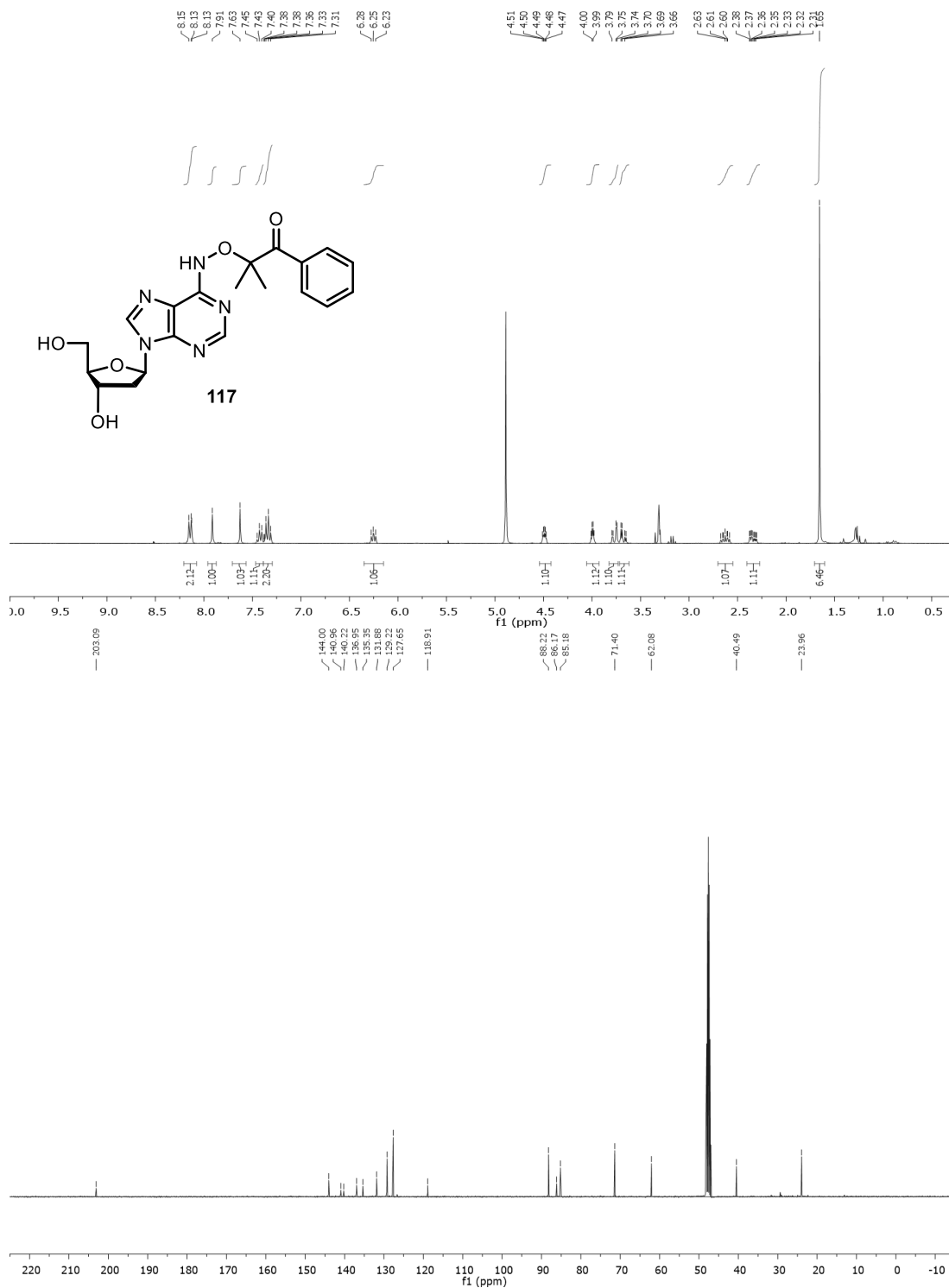
Appendix Figure 49. ^{1}H NMR and ^{13}C NMR spectra of **117**.

Appendix Figure 50. ^{1}H NMR spectrum of **128**.
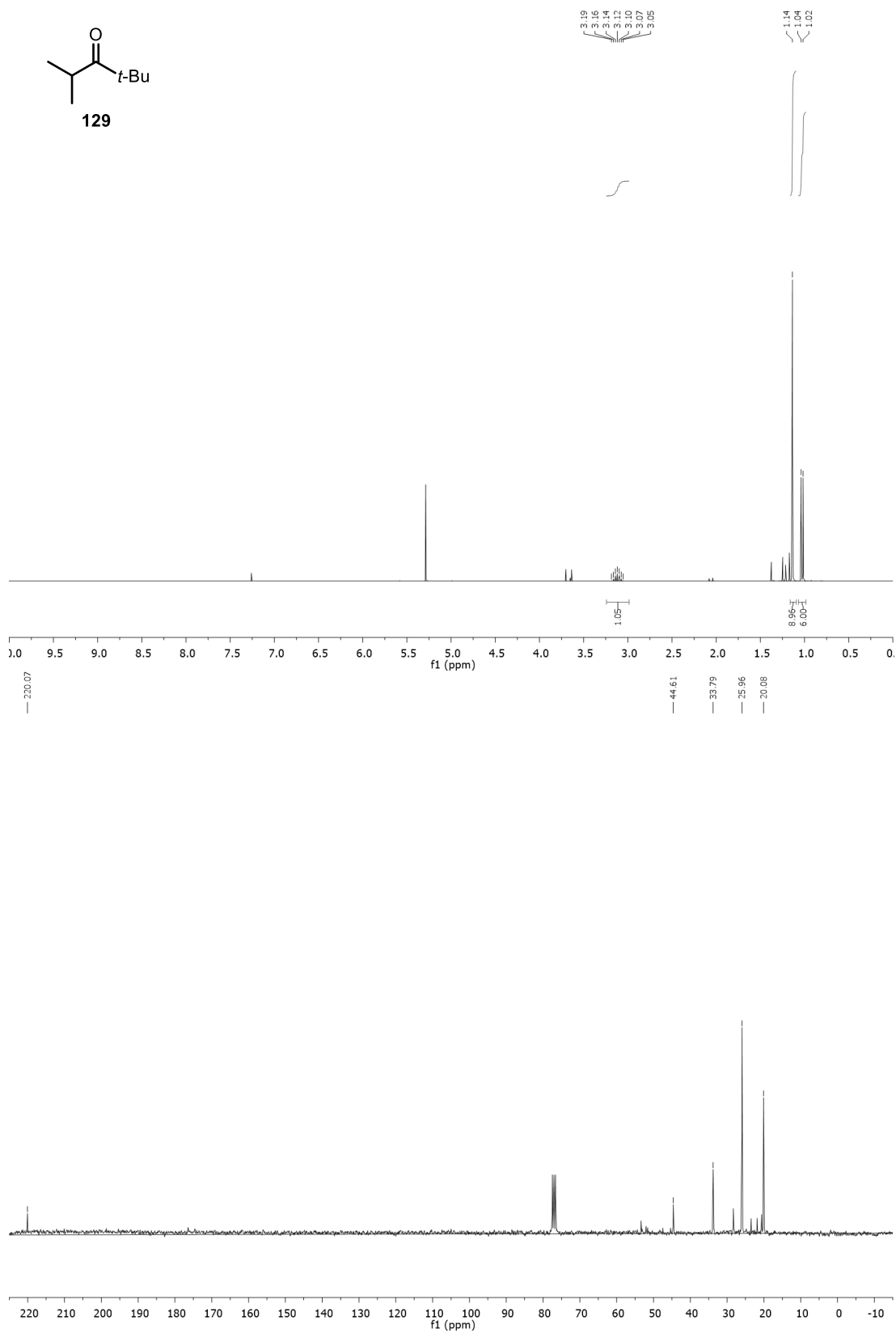
Appendix Figure 51. ^{1}H NMR and ^{13}C NMR spectra of **129**.
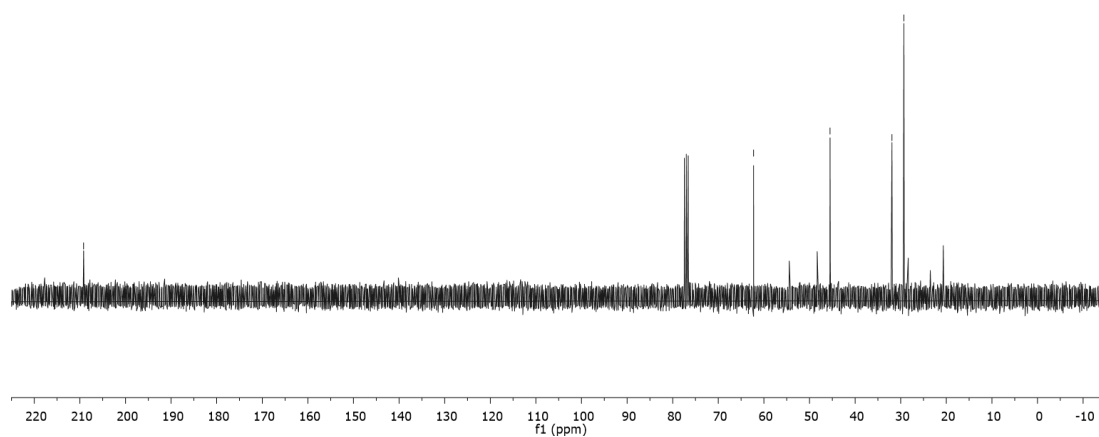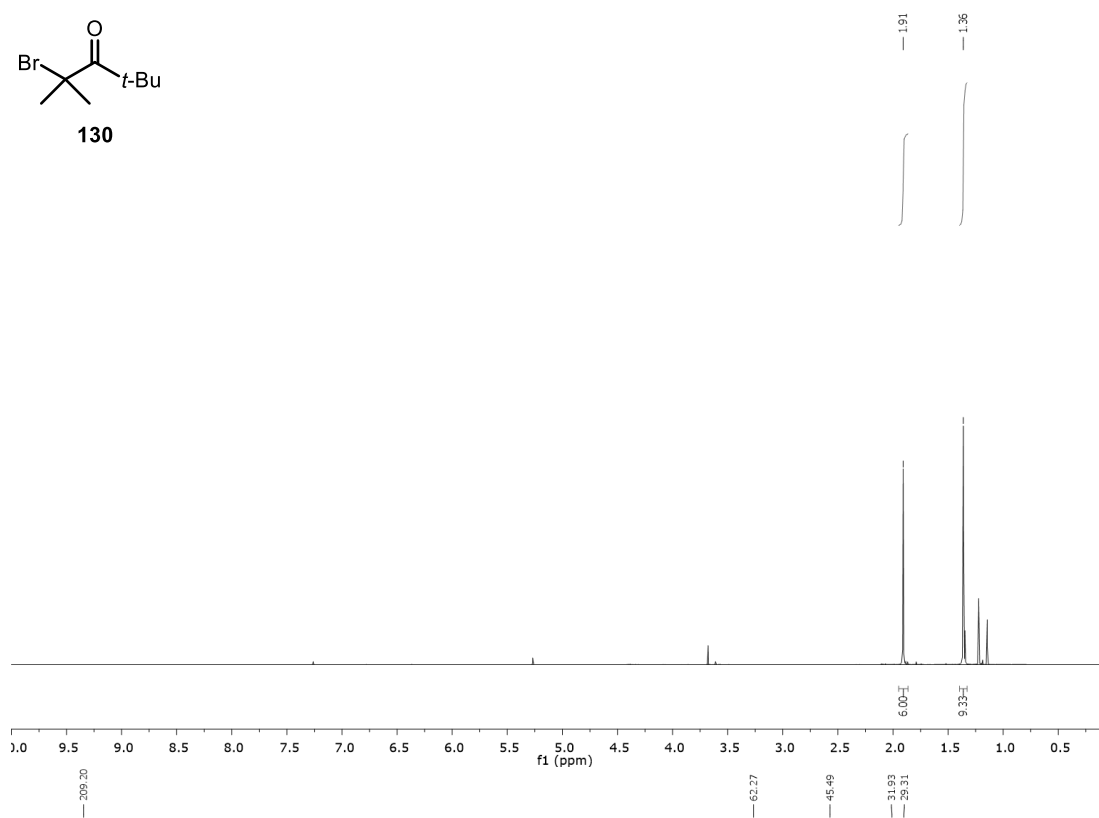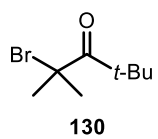
Appendix Figure 52. ^{1}H NMR and ^{13}C NMR spectra of **130**.
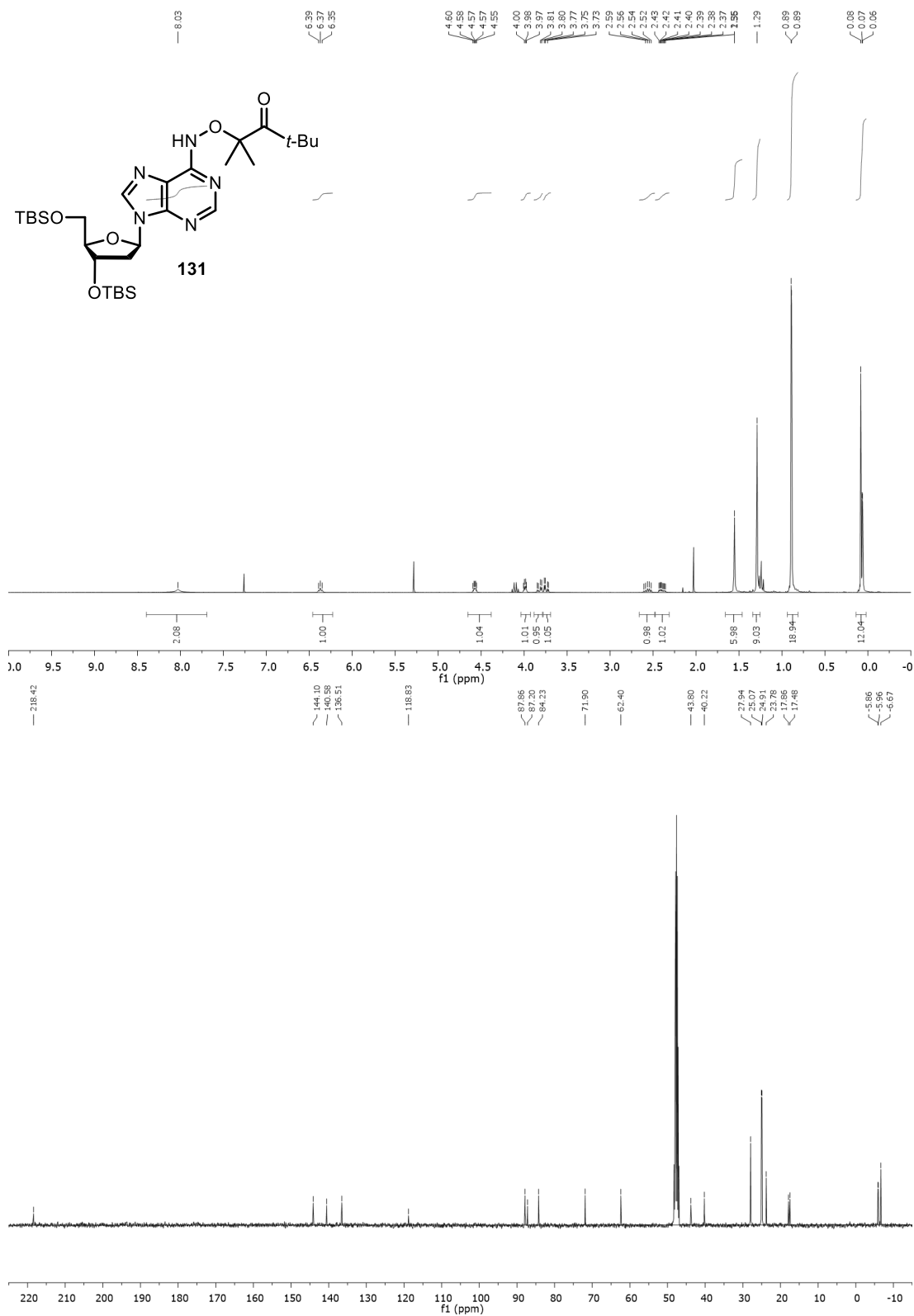
Appendix Figure 53. ^{1}H NMR and ^{13}C NMR spectra of **131**.
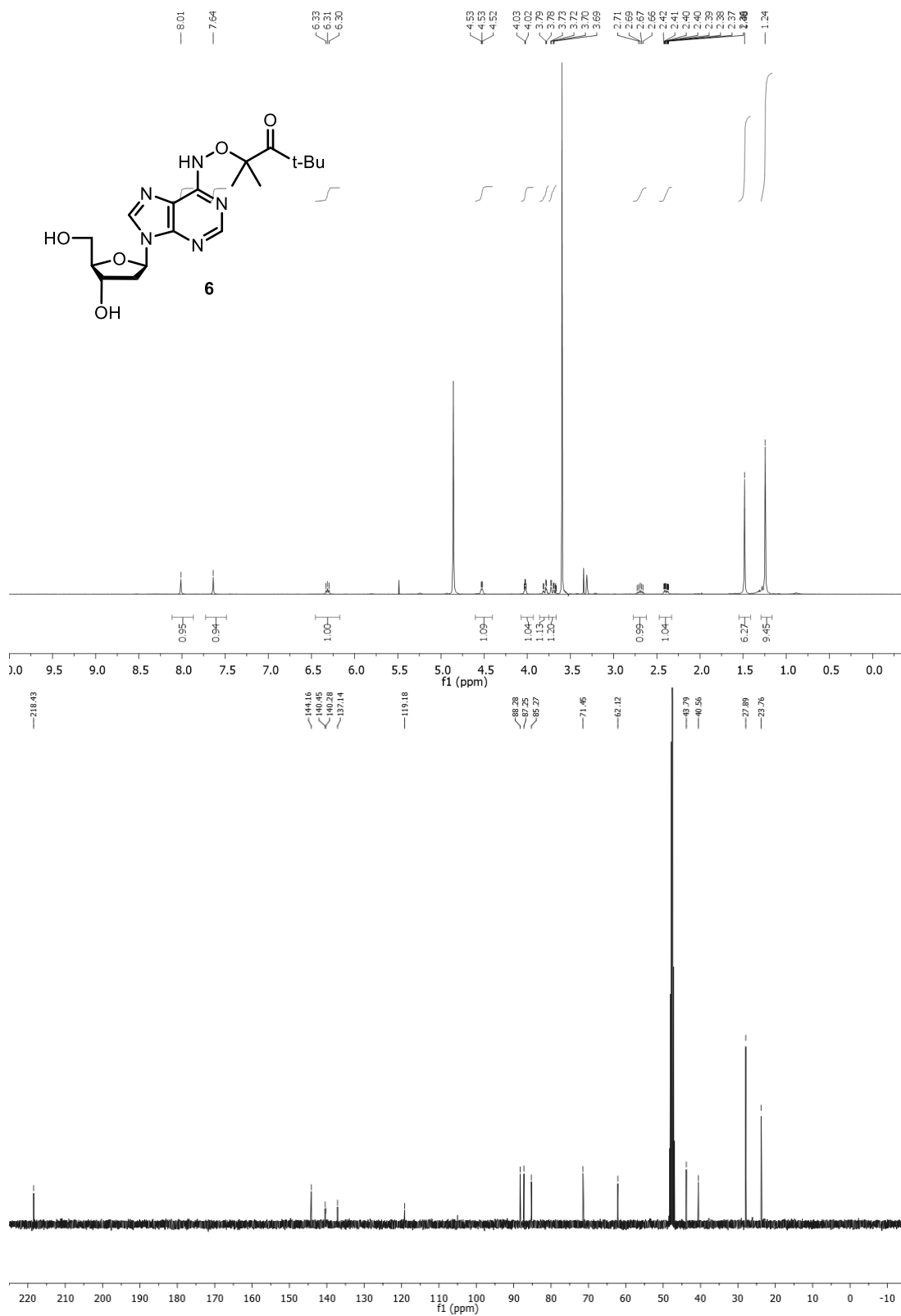
Appendix Figure 54. ^{1}H NMR and ^{13}C NMR spectra of **6**.
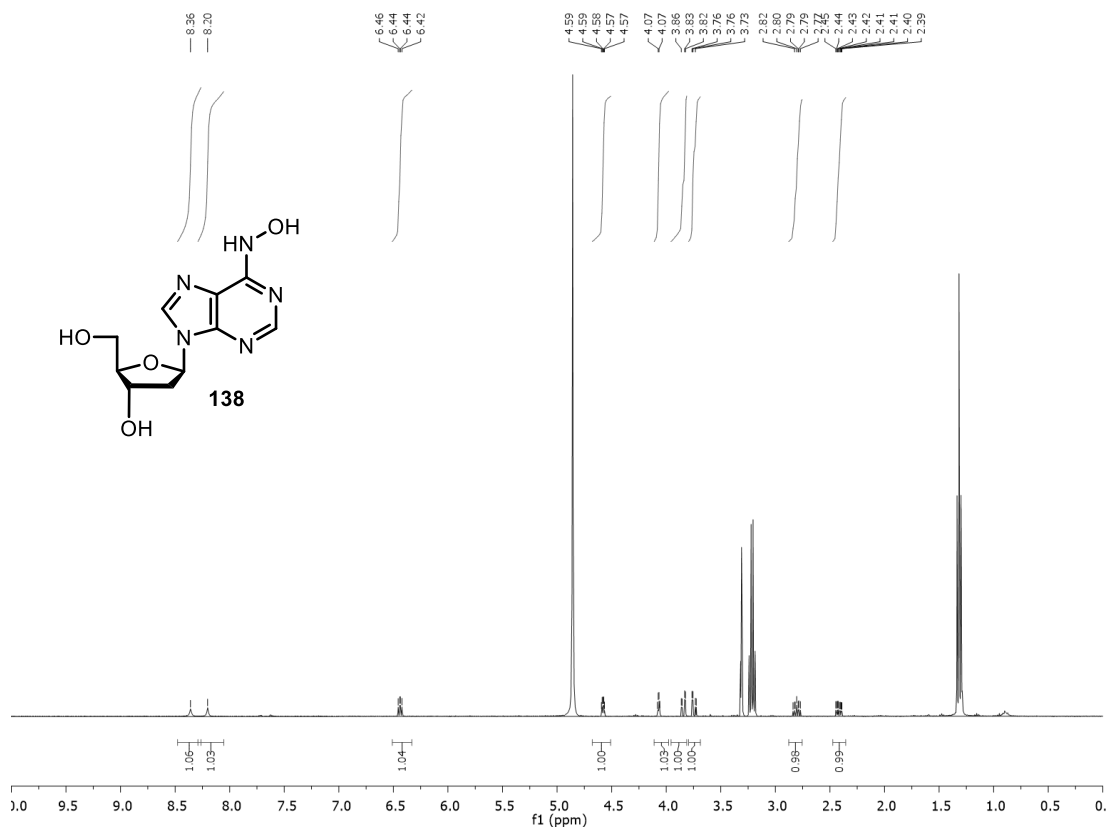
Appendix Figure 55. ^{1}H NMR spectrum of **138**.
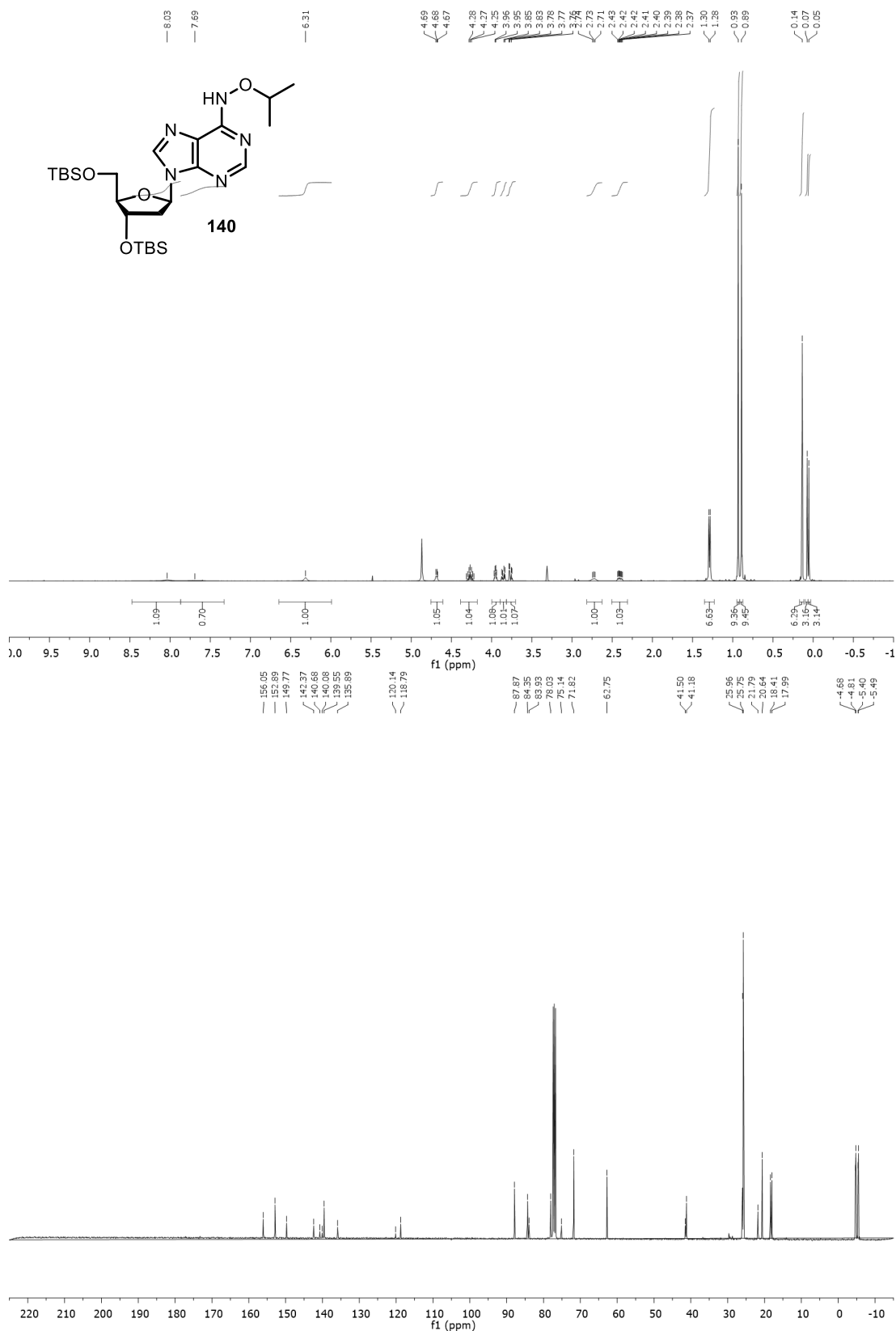
Appendix Figure 56. ^{1}H NMR and ^{13}C NMR spectra of **140**.
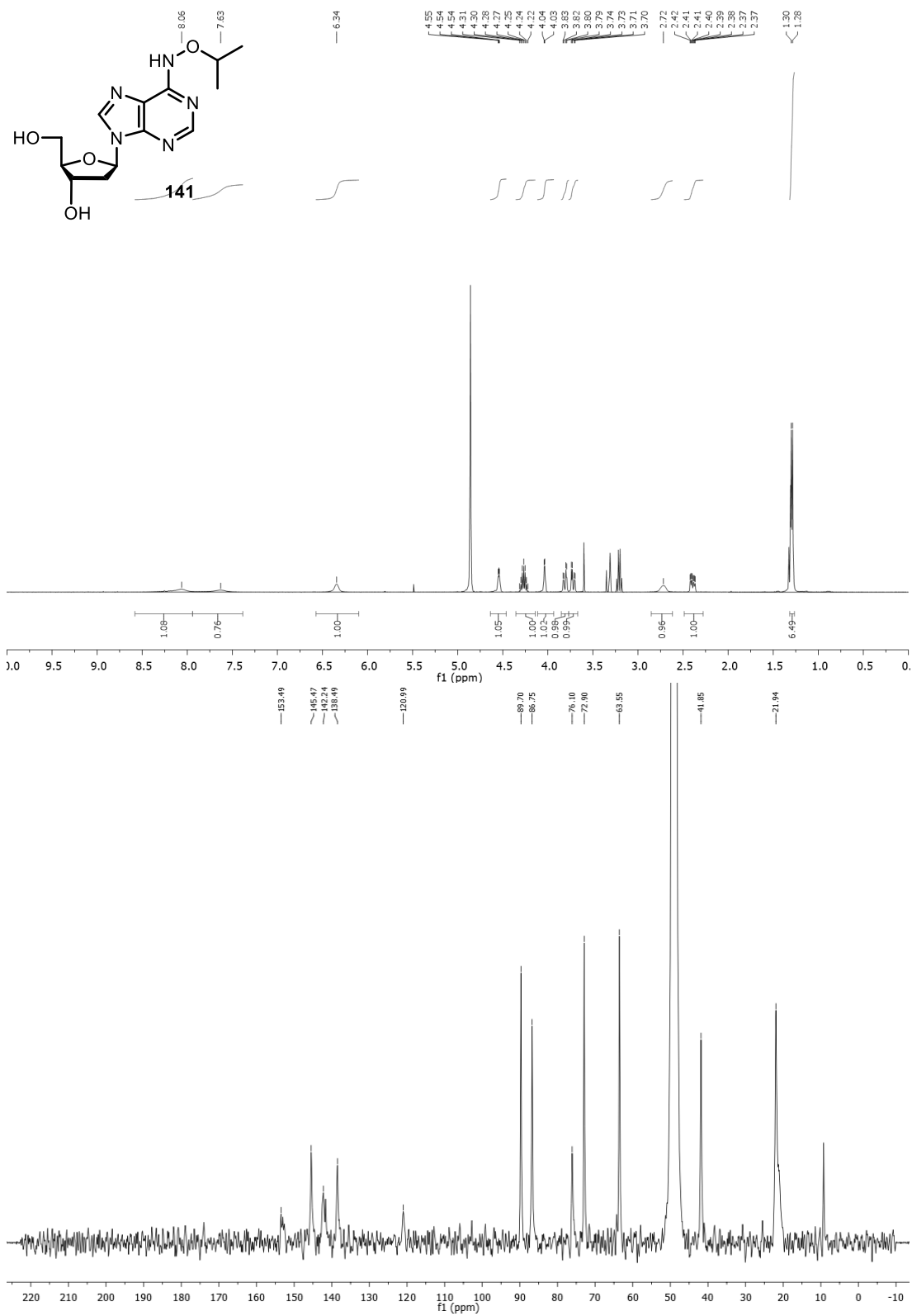
Appendix Figure 57. ^{1}H NMR and ^{13}C NMR spectra of **141**.
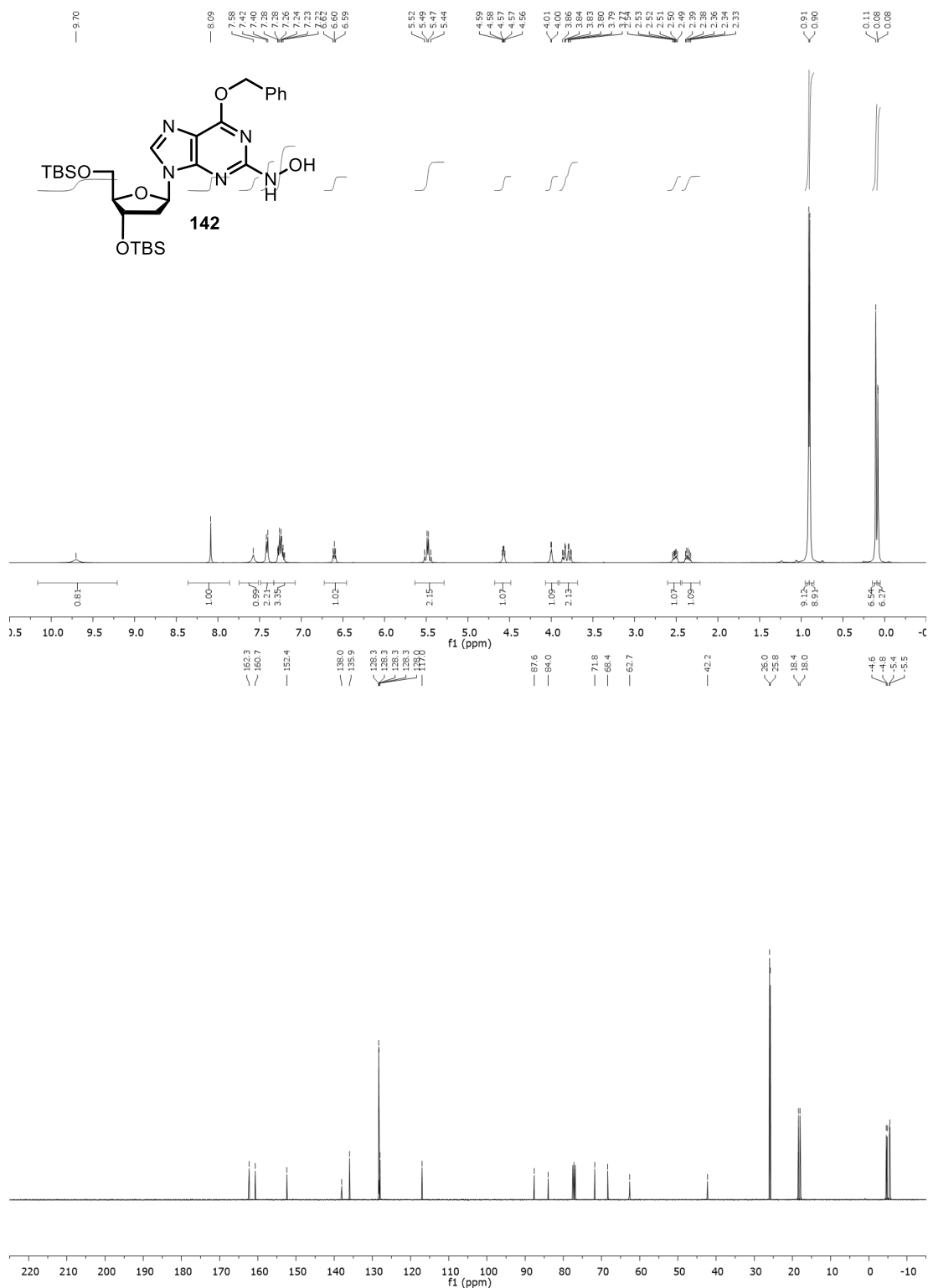
Appendix Figure 58. ^{1}H NMR and ^{13}C NMR spectra of **142**.
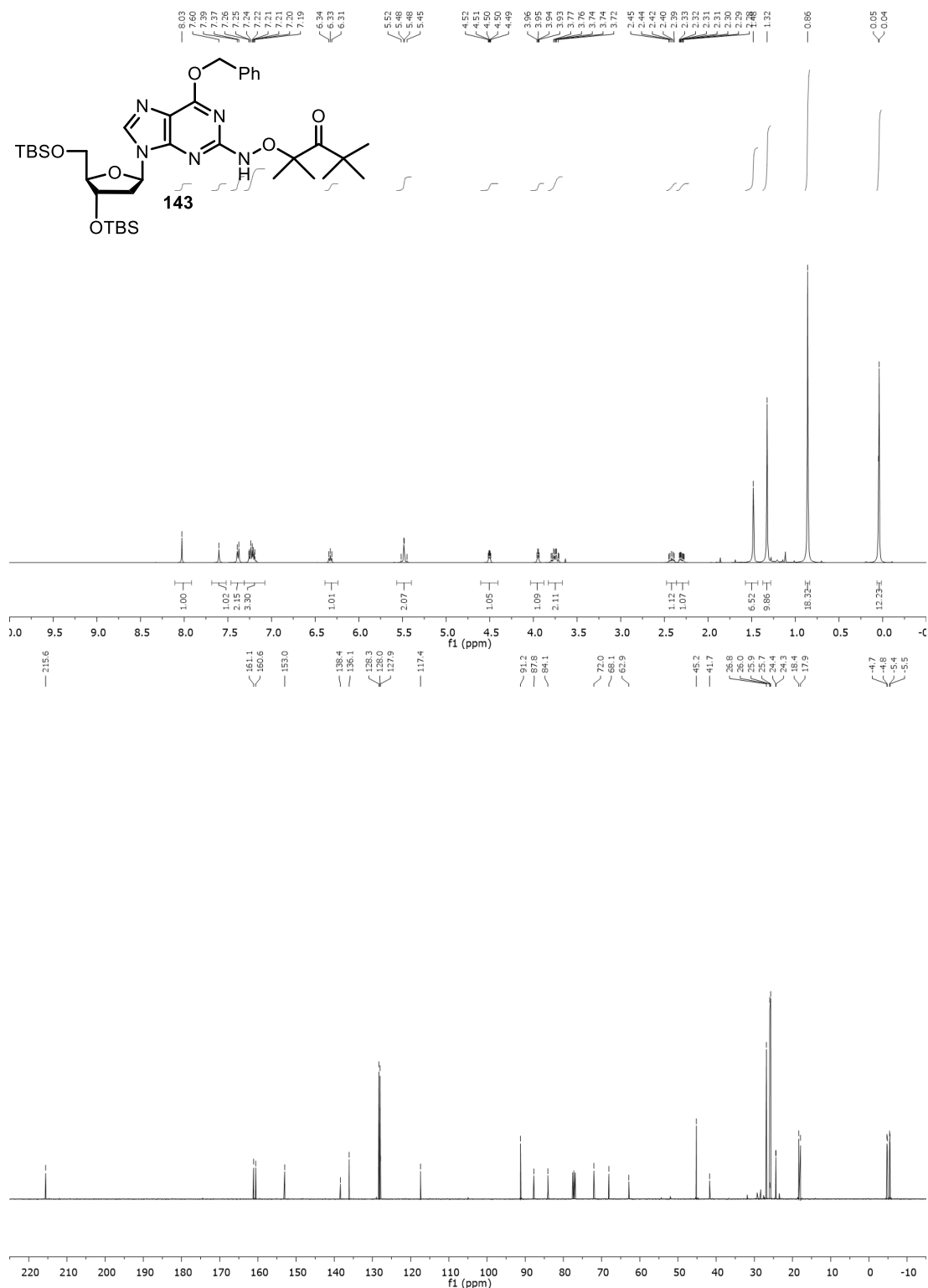
Appendix Figure 59. ^{1}H NMR and ^{13}C NMR spectra of **143**.
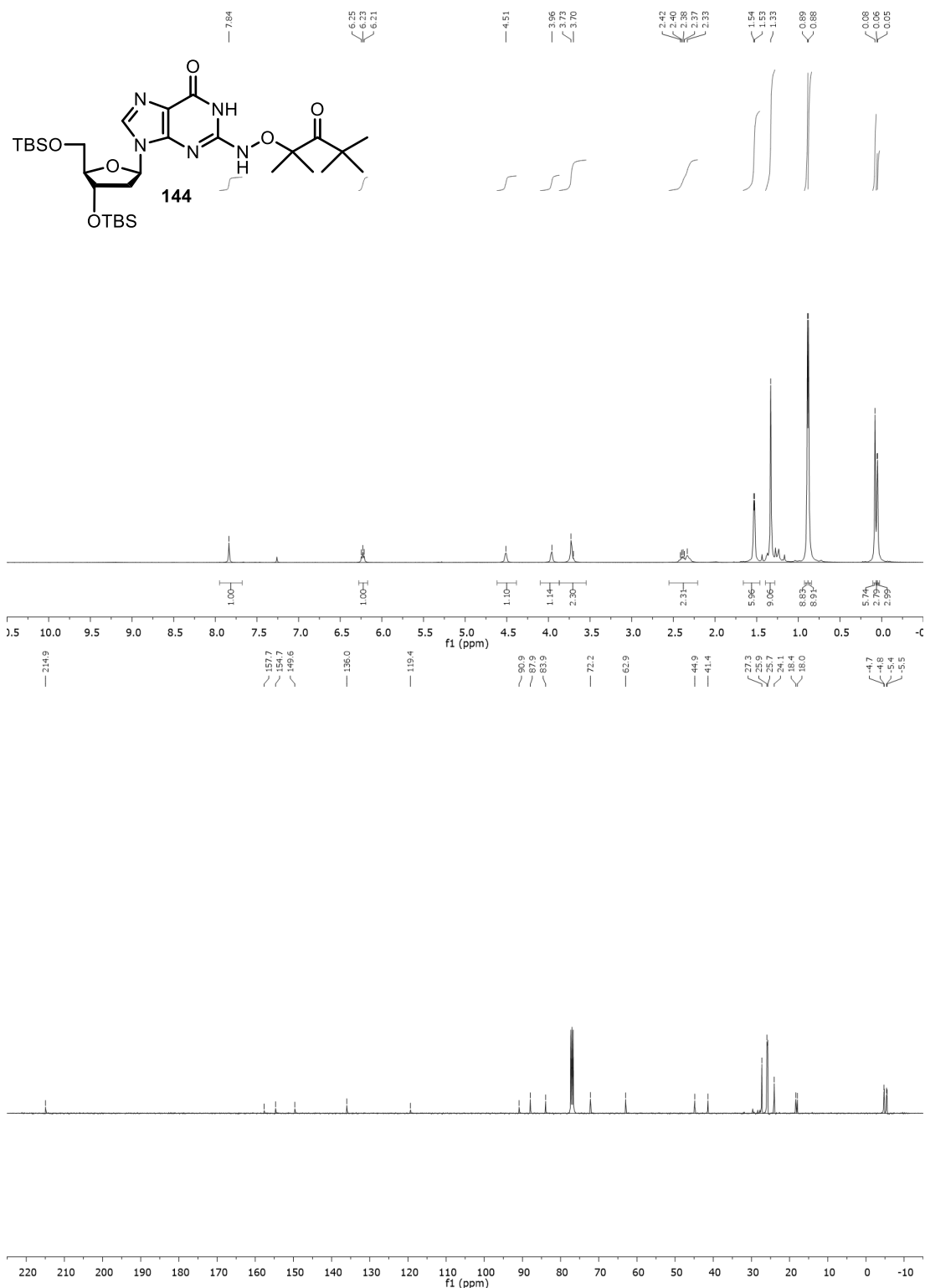
Appendix Figure 60. ^{1}H NMR and ^{13}C NMR spectra of **144**.
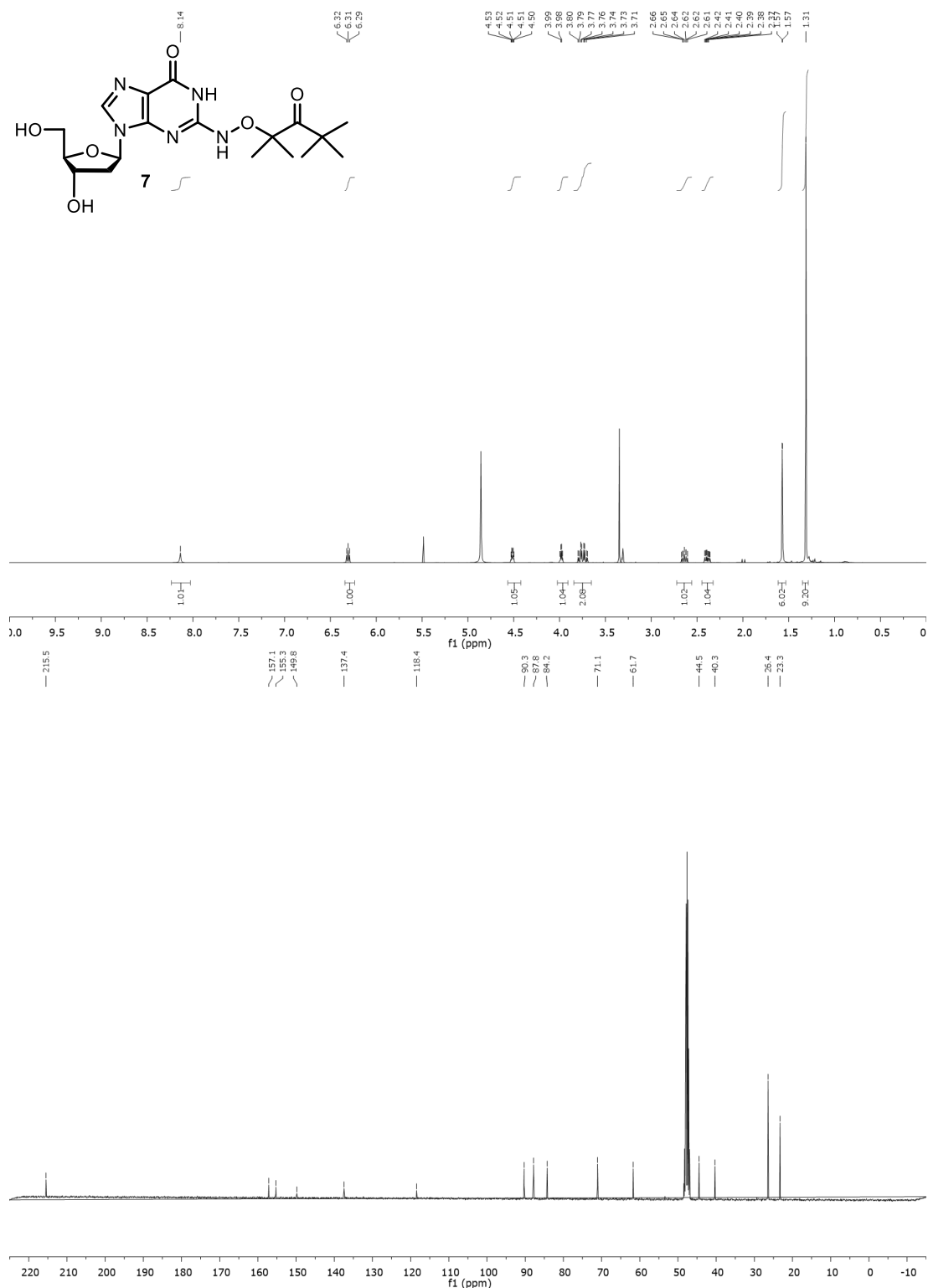
Appendix Figure 61. ^{1}H NMR and ^{13}C NMR spectra of **7**.
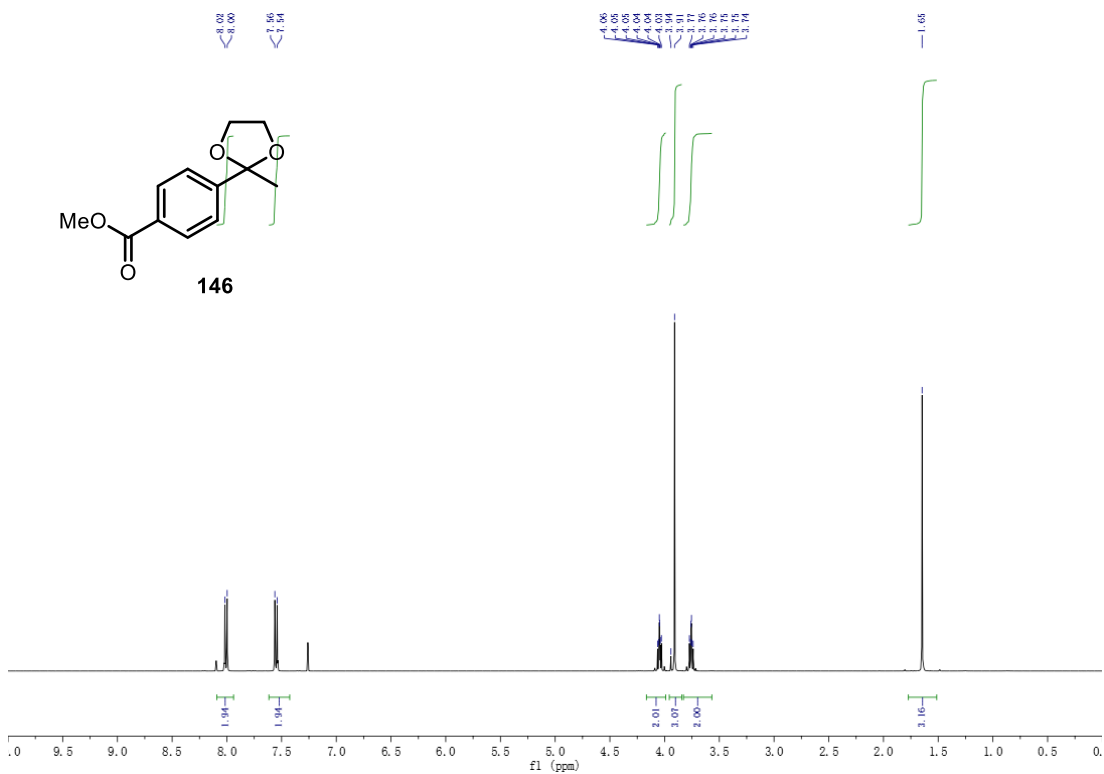
Appendix Figure 62. ^{1}H NMR spectrum of **146**.
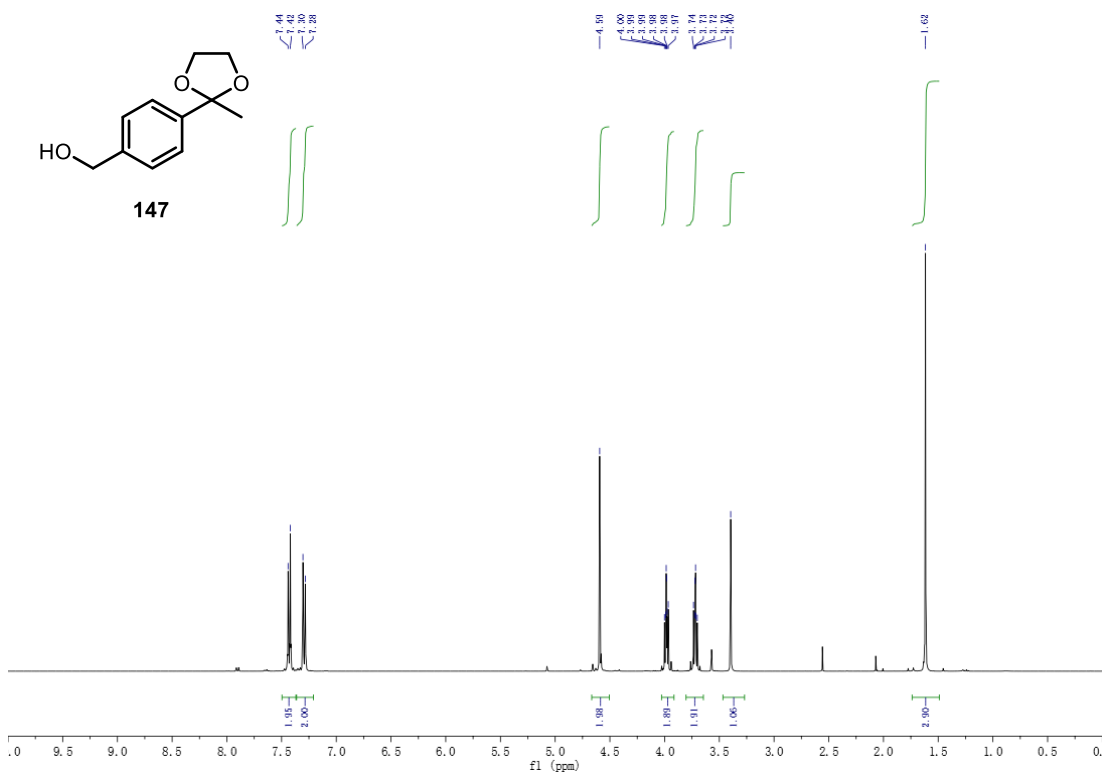
Appendix Figure 63. ^{1}H NMR spectrum of **147**.
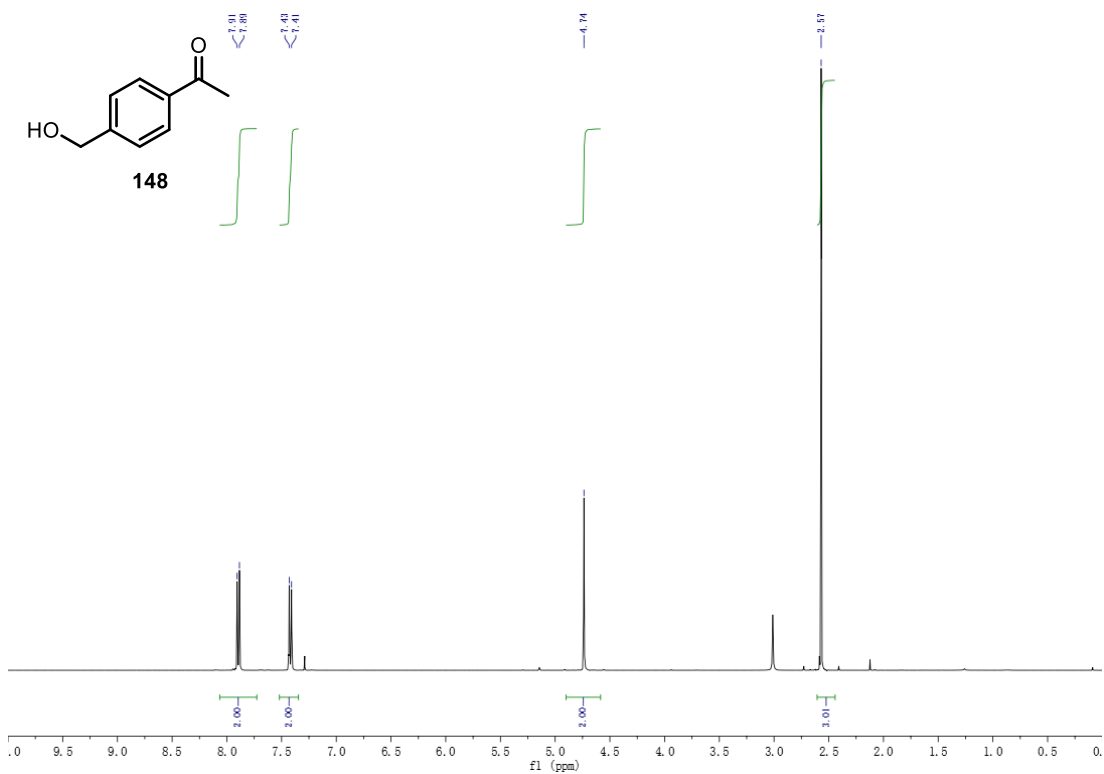
Appendix Figure 64. ^{1}H NMR spectrum of **148**.
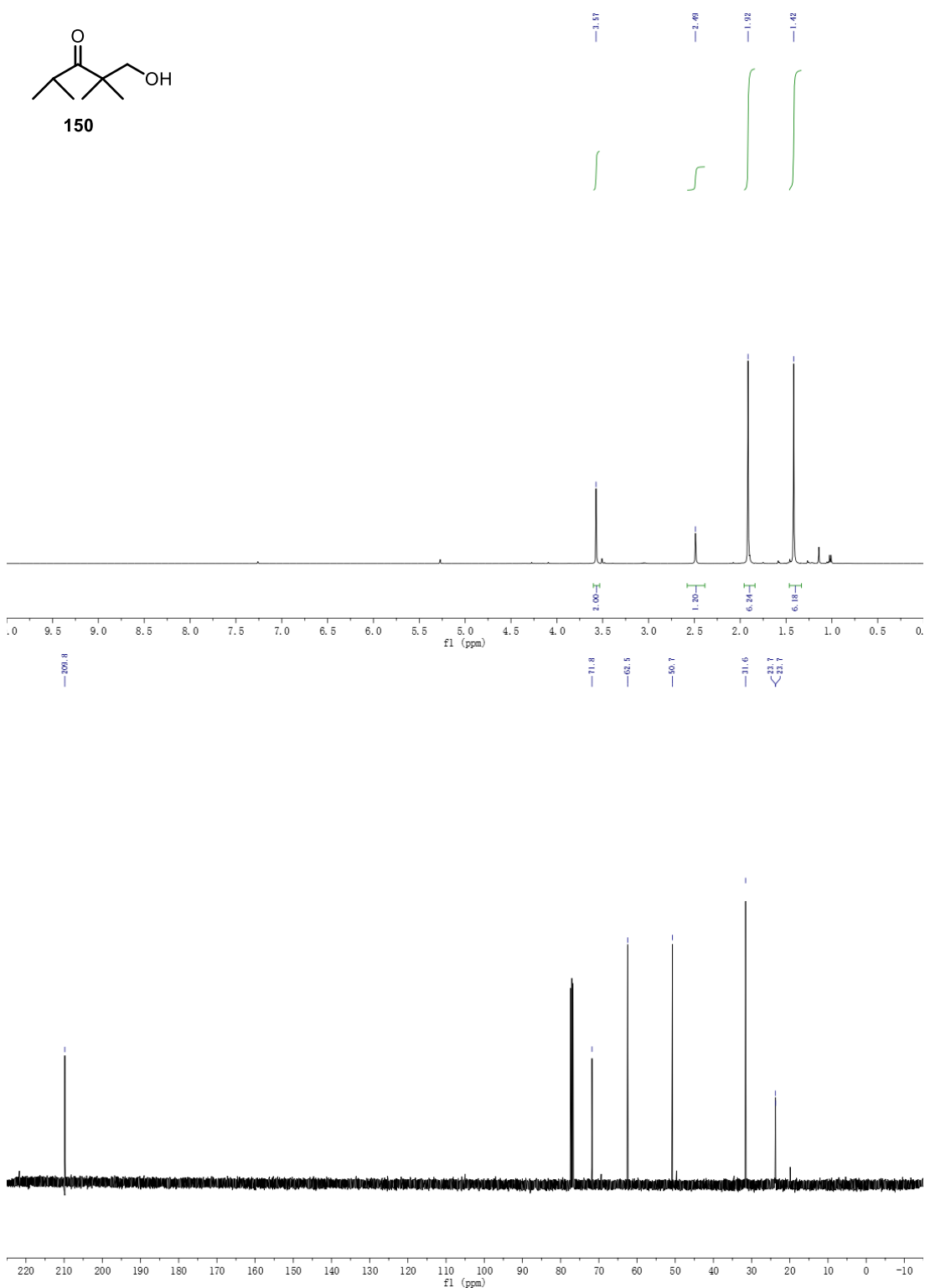
Appendix Figure 65. ^{1}H NMR and ^{13}C NMR spectra of **150**.
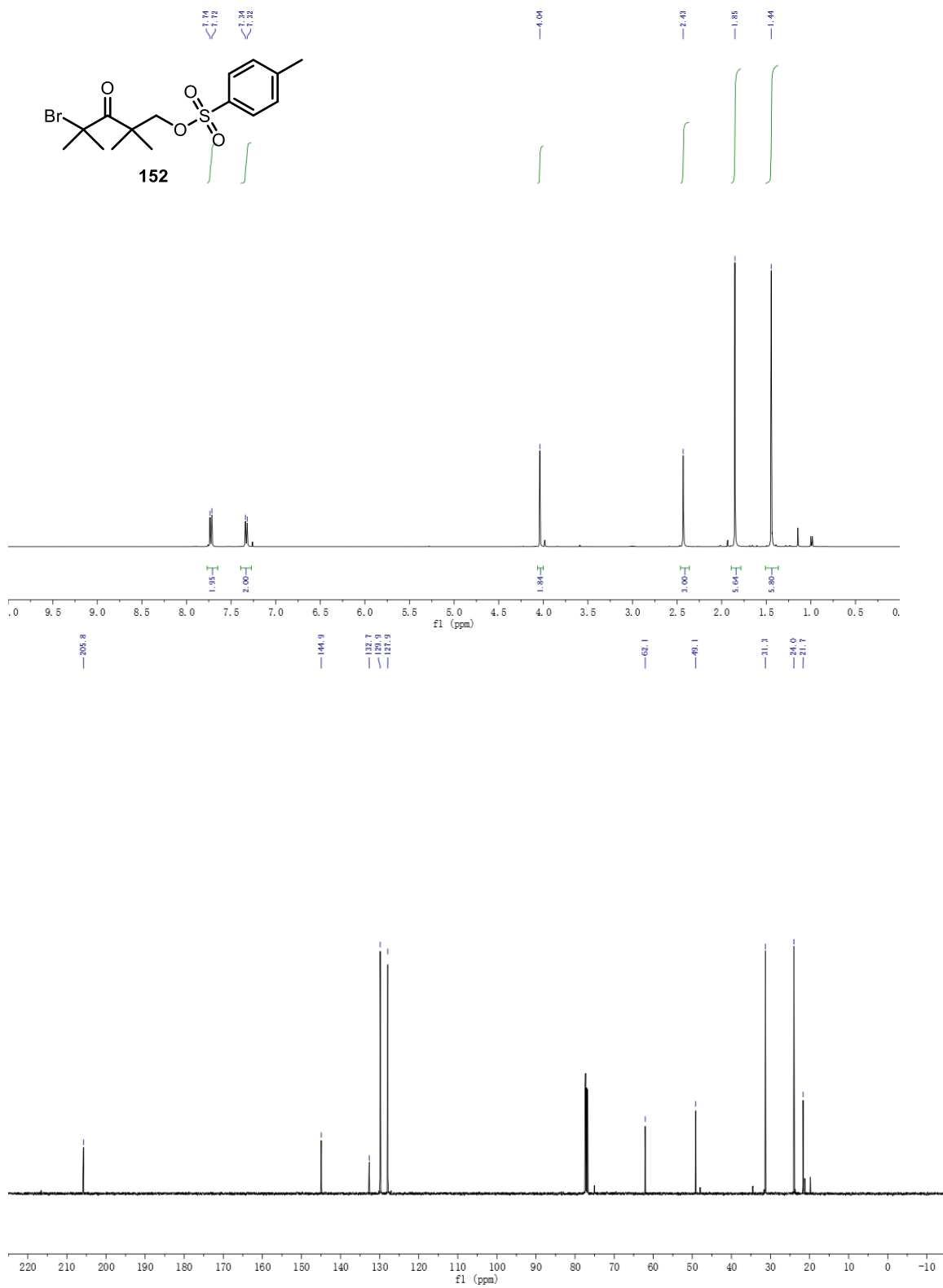
Appendix Figure 66. ^{1}H NMR and ^{13}C NMR spectra of **152**.
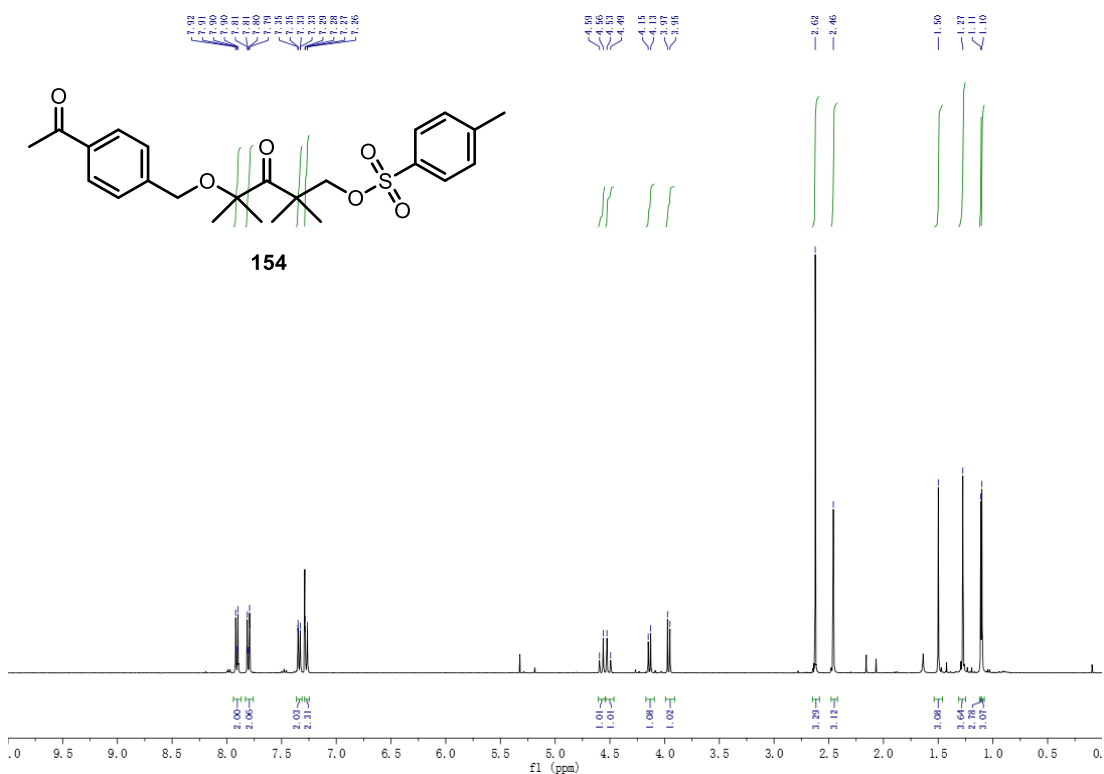
Appendix Figure 67. ^{1}H NMR spectrum of **154**.
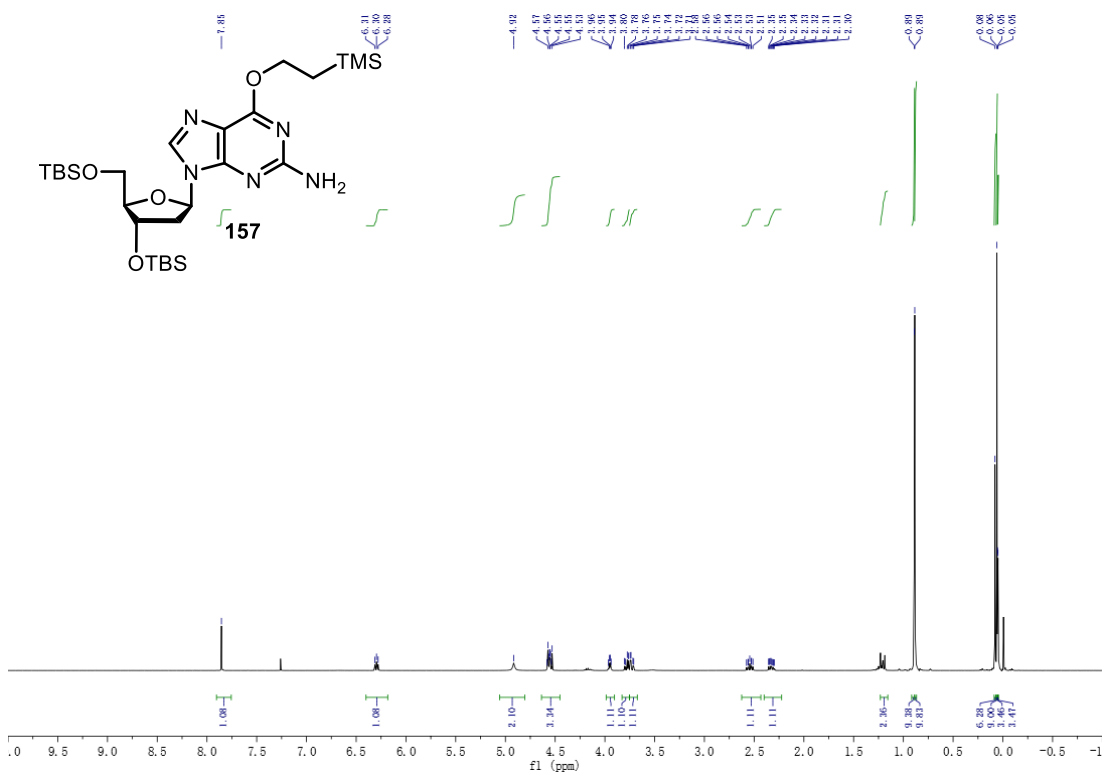
Appendix Figure 68. ^{1}H NMR spectrum of **157**.
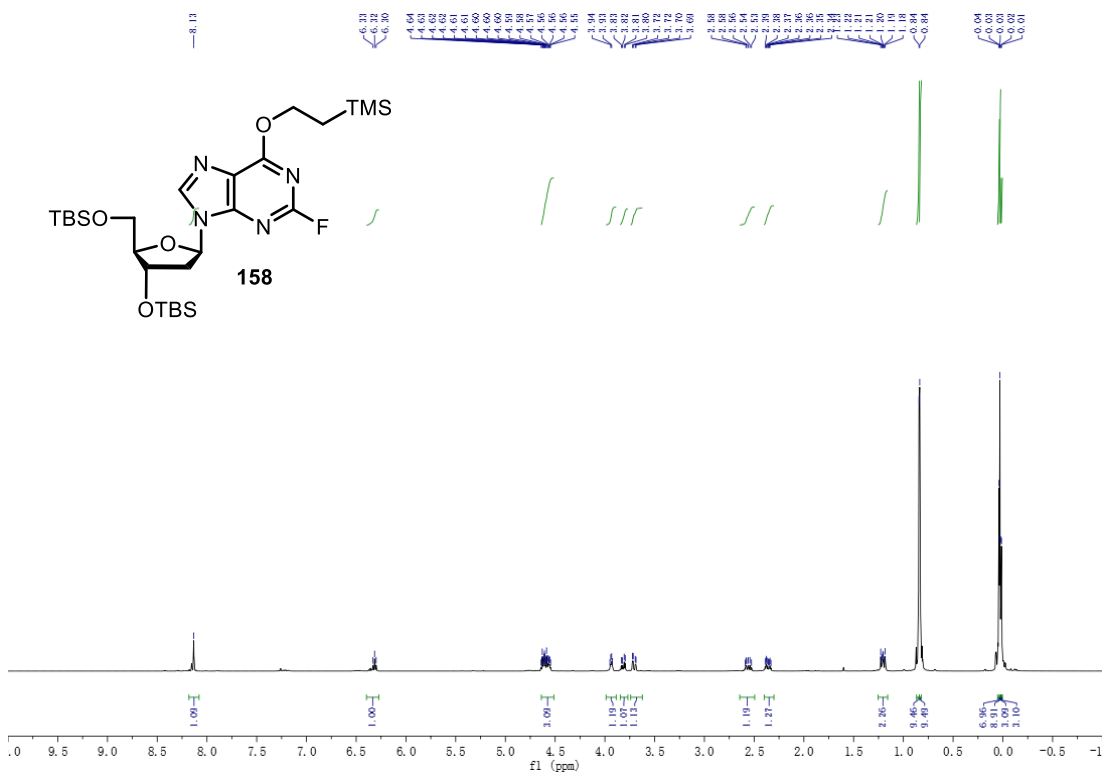
Appendix Figure 69. ^{1}H NMR spectrum of **158**.
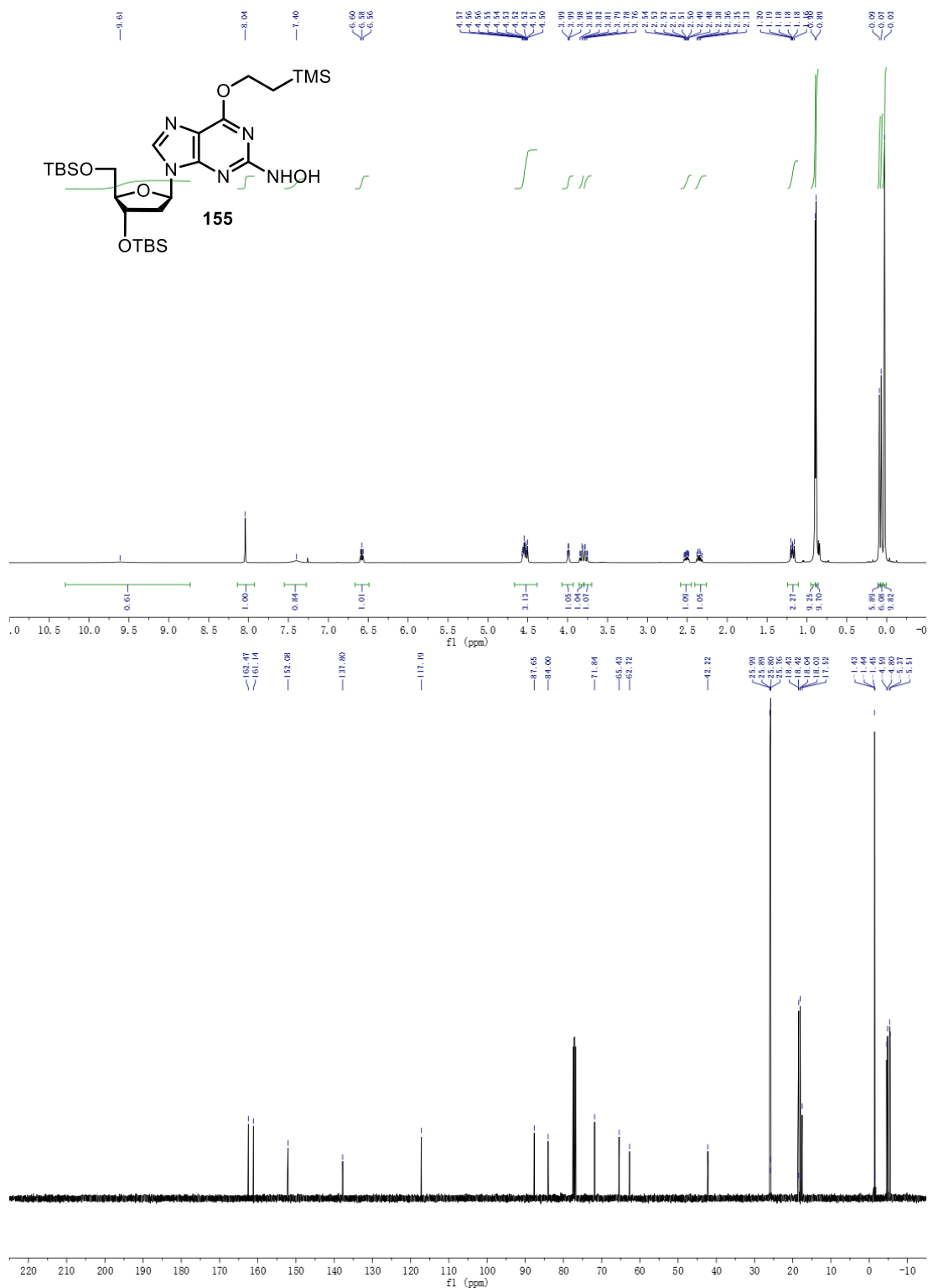
Appendix Figure 70. ^{1}H NMR and ^{13}C NMR spectra of **155**.
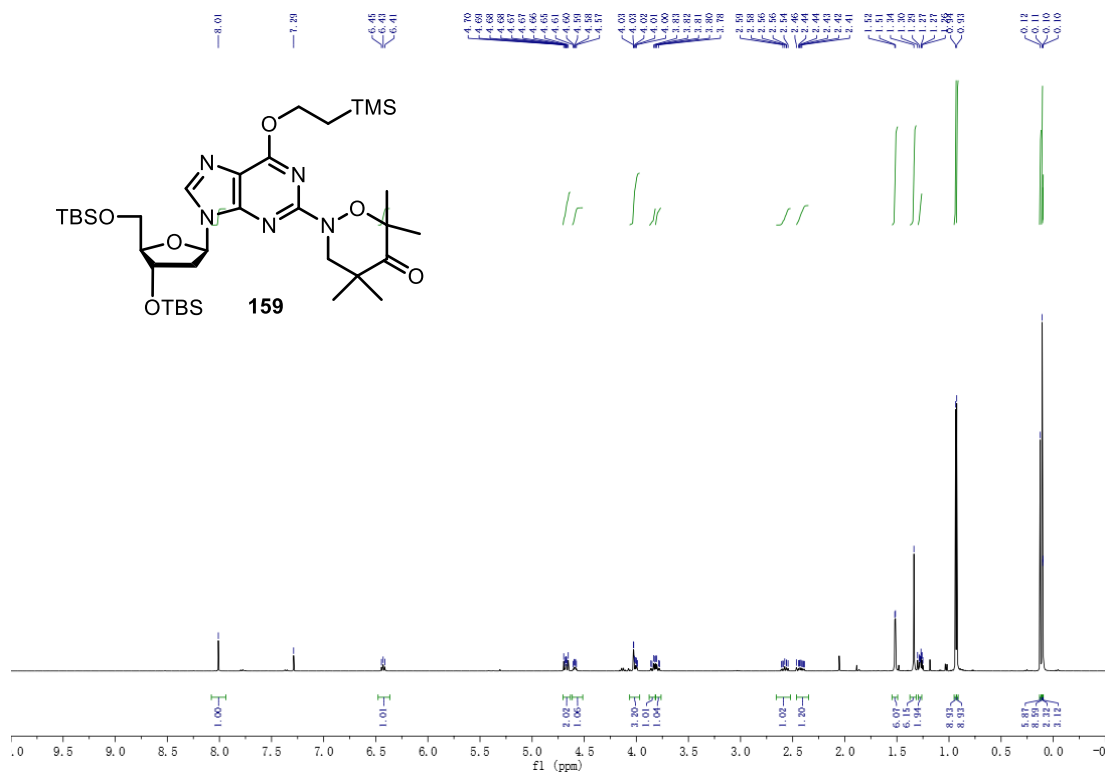
Appendix Figure 71. ^{1}H NMR spectrum of **159**.
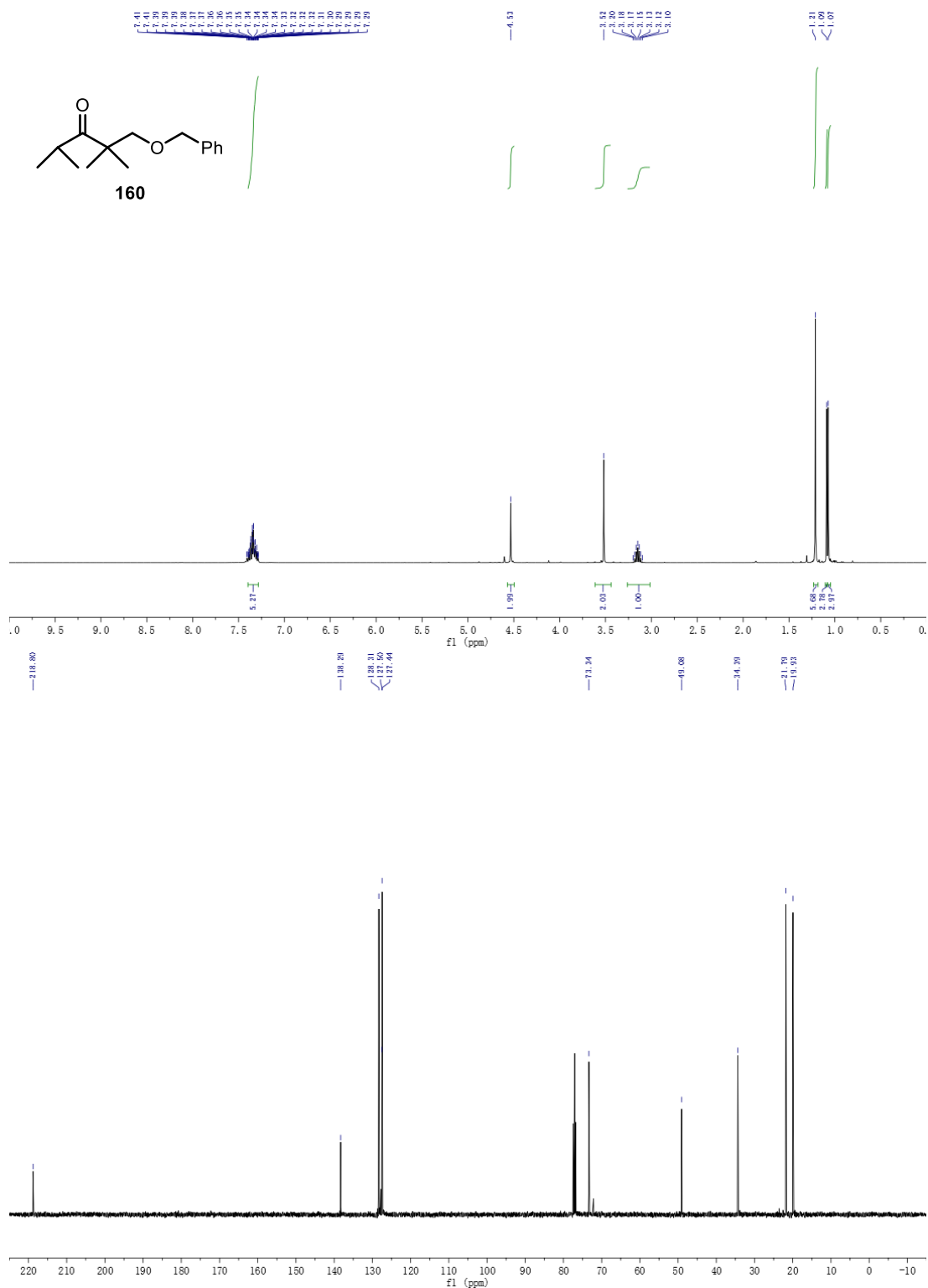
Appendix Figure 72. ^{1}H NMR and ^{13}C NMR spectra of **160**.
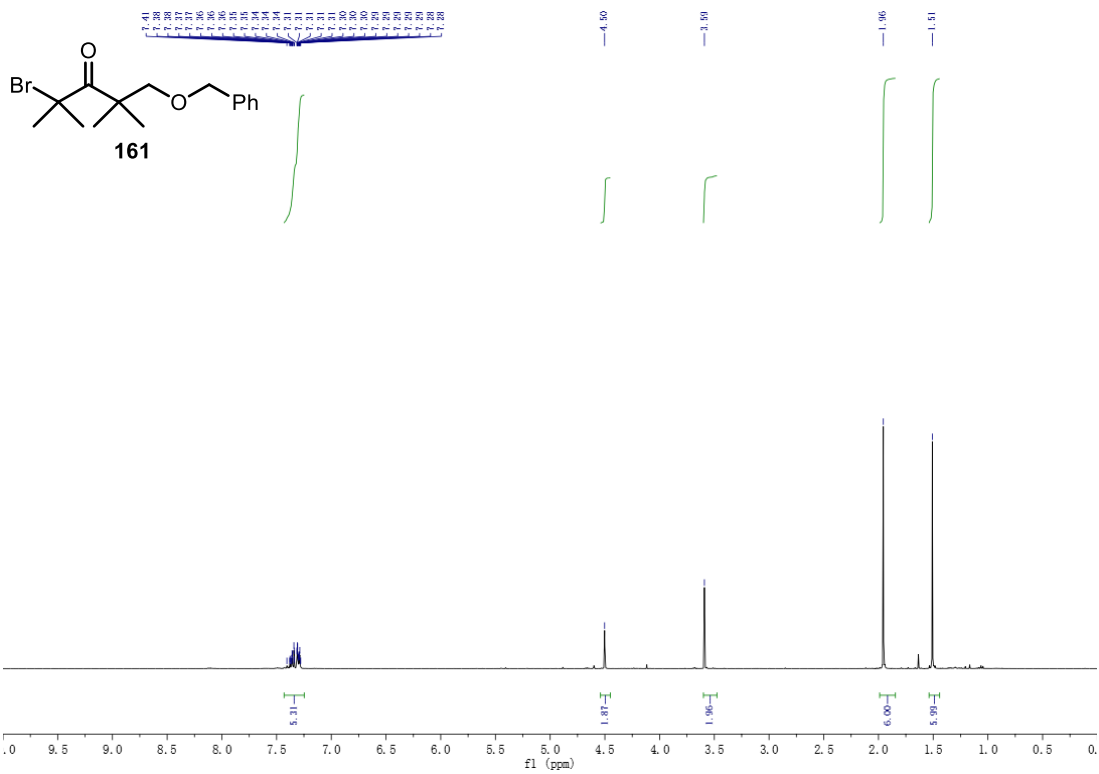
Appendix Figure 73. ^{1}H NMR spectrum of **161**.
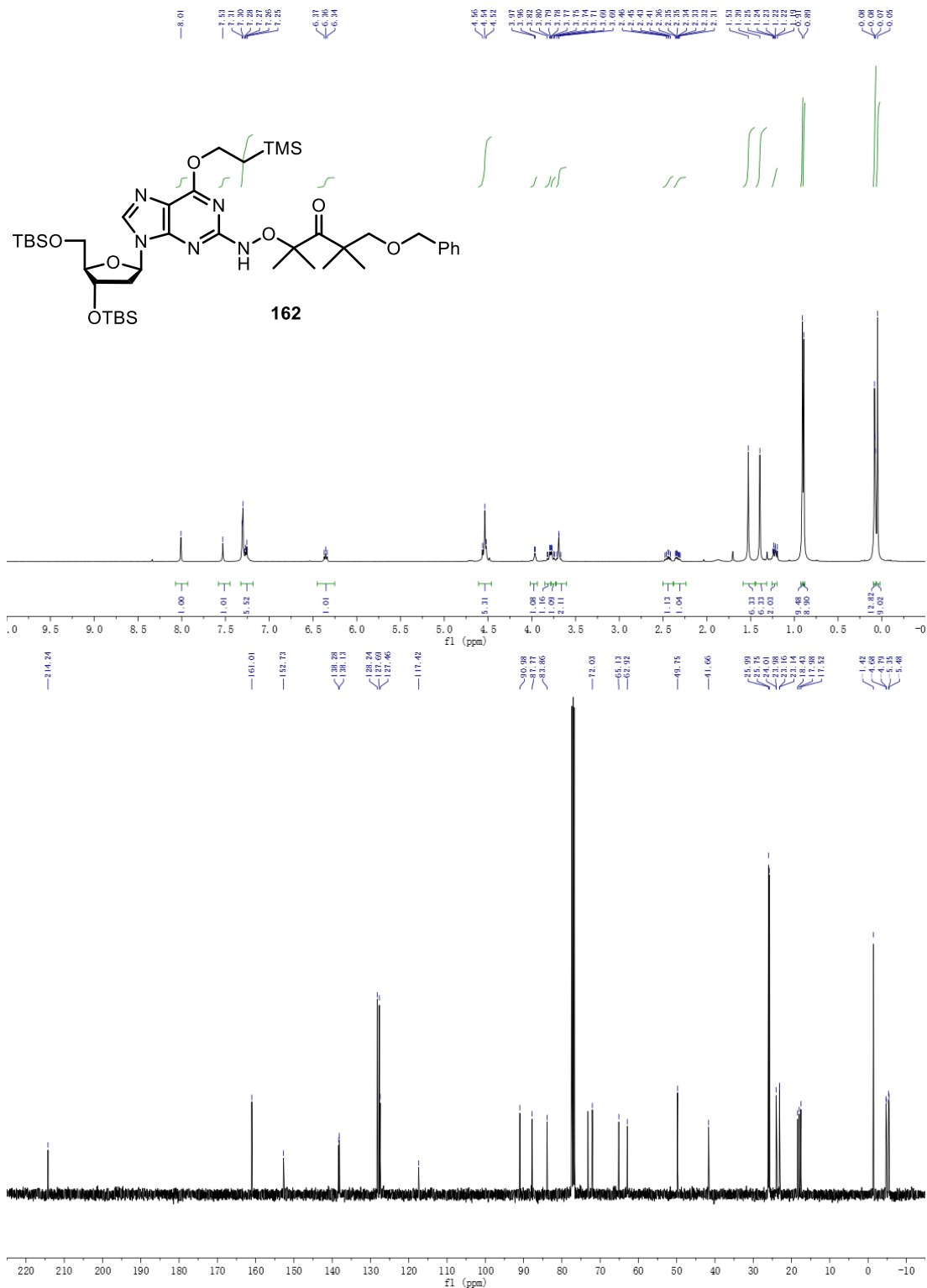
Appendix Figure 74. ^{1}H NMR and ^{13}C NMR spectra of **162**.
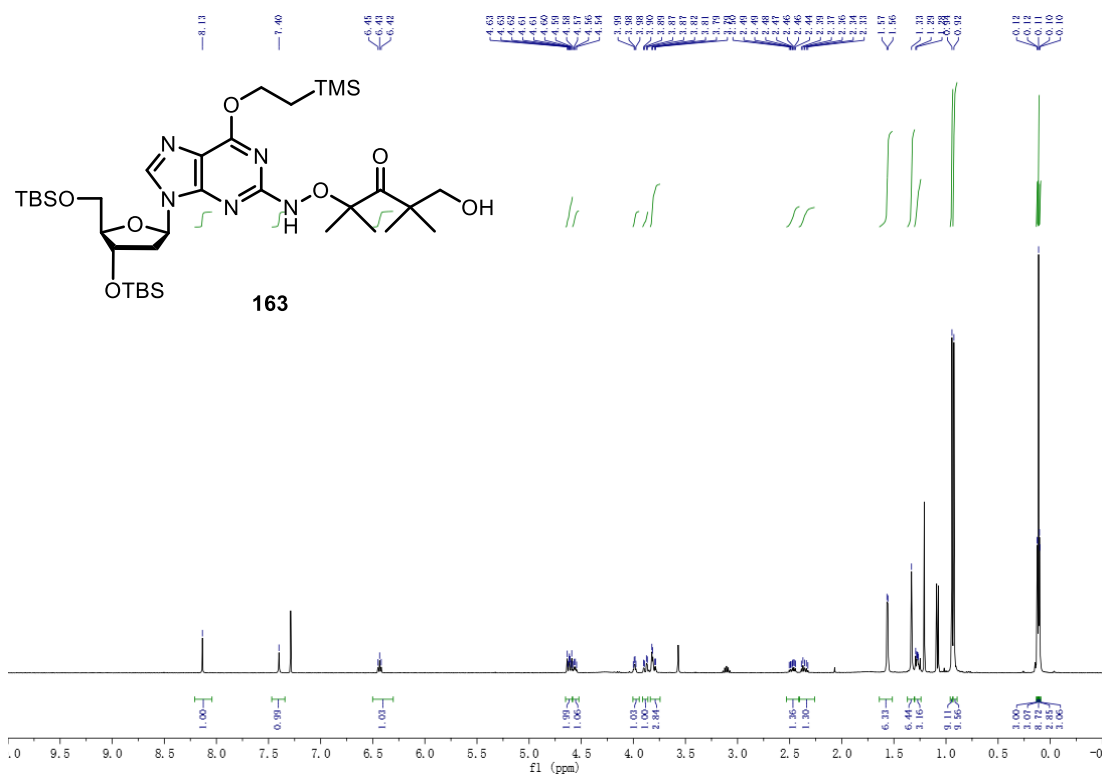
Appendix Figure 75. ^{1}H NMR spectrum of **163**.
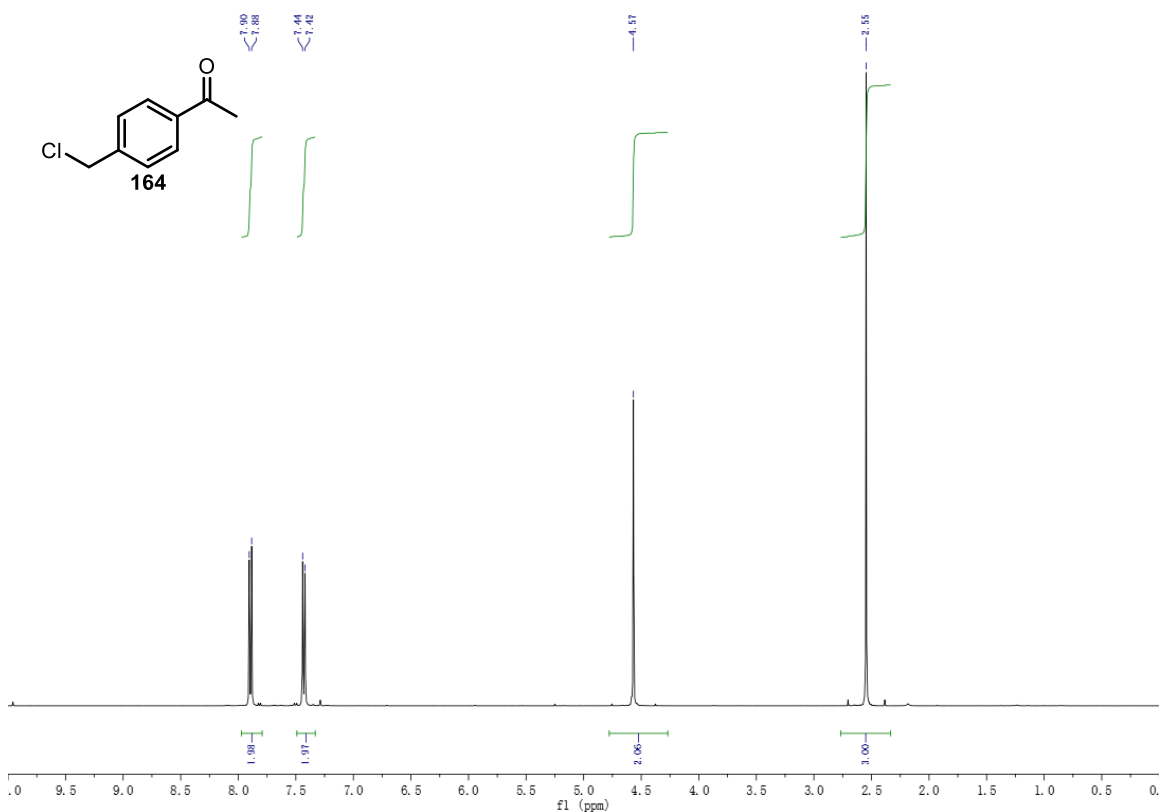
Appendix Figure 76. ^{1}H NMR spectrum of **164**.
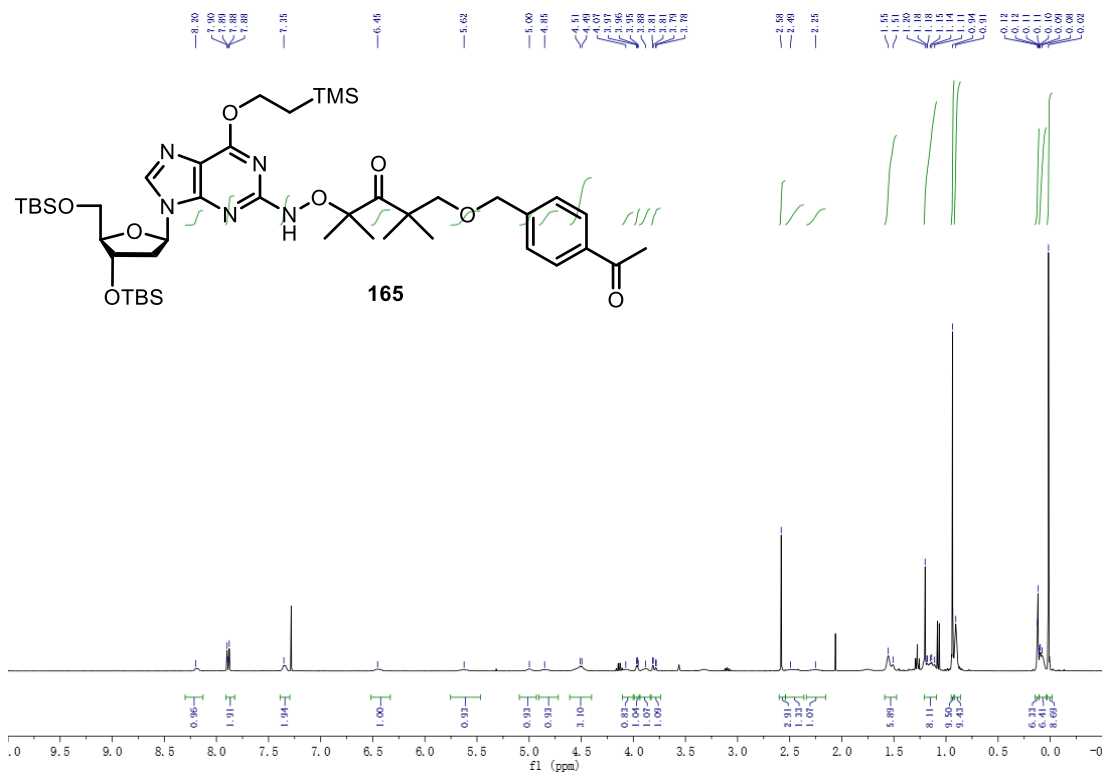
Appendix Figure 77. ^{1}H NMR spectrum of **165**.
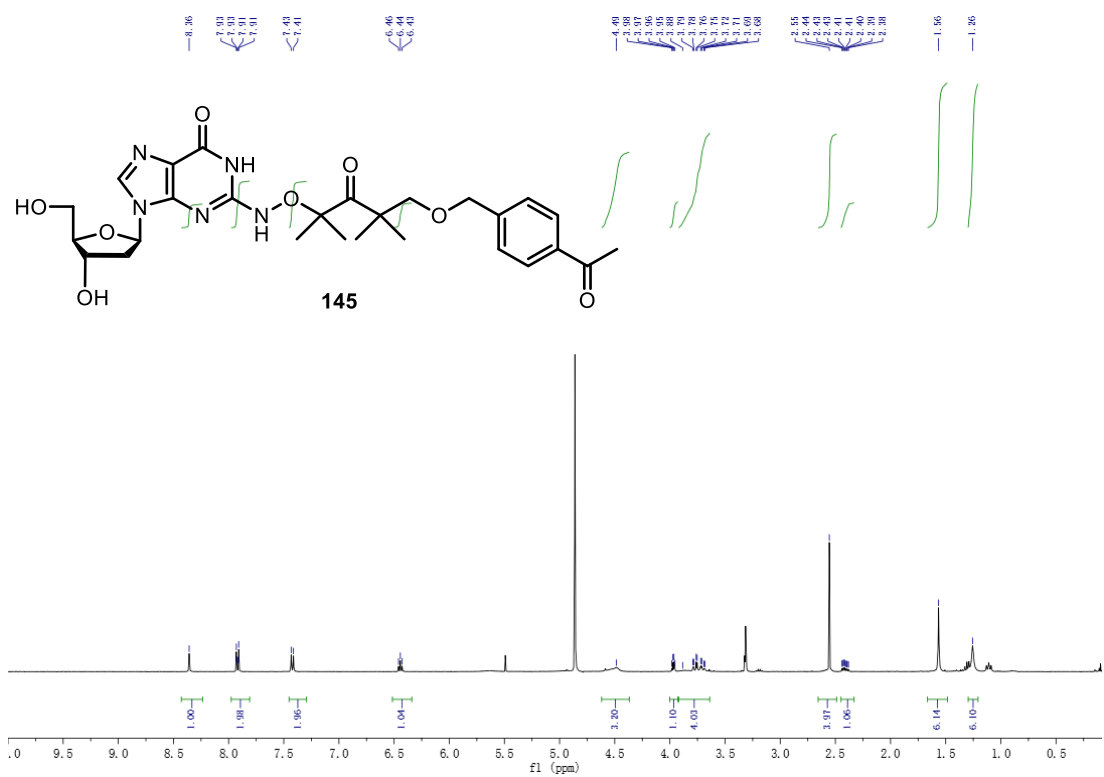
Appendix Figure 78. ^{1}H NMR spectrum of **145**.
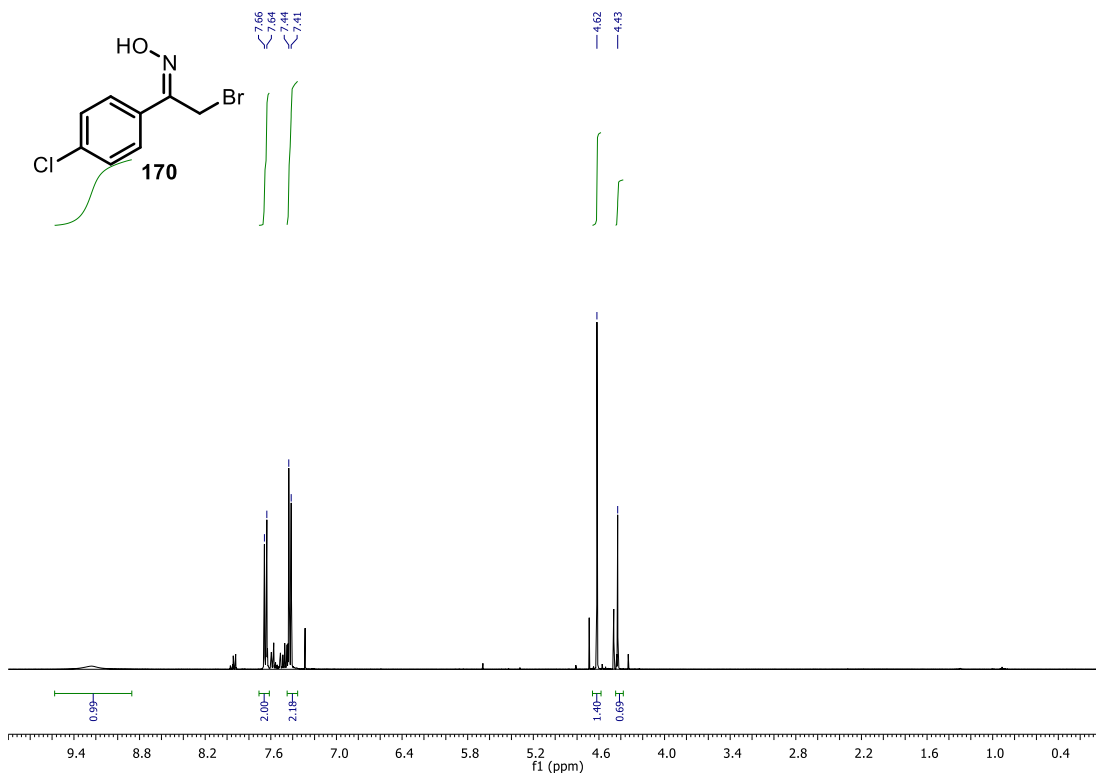
Appendix Figure 79. ¹H NMR spectrum of **170**.
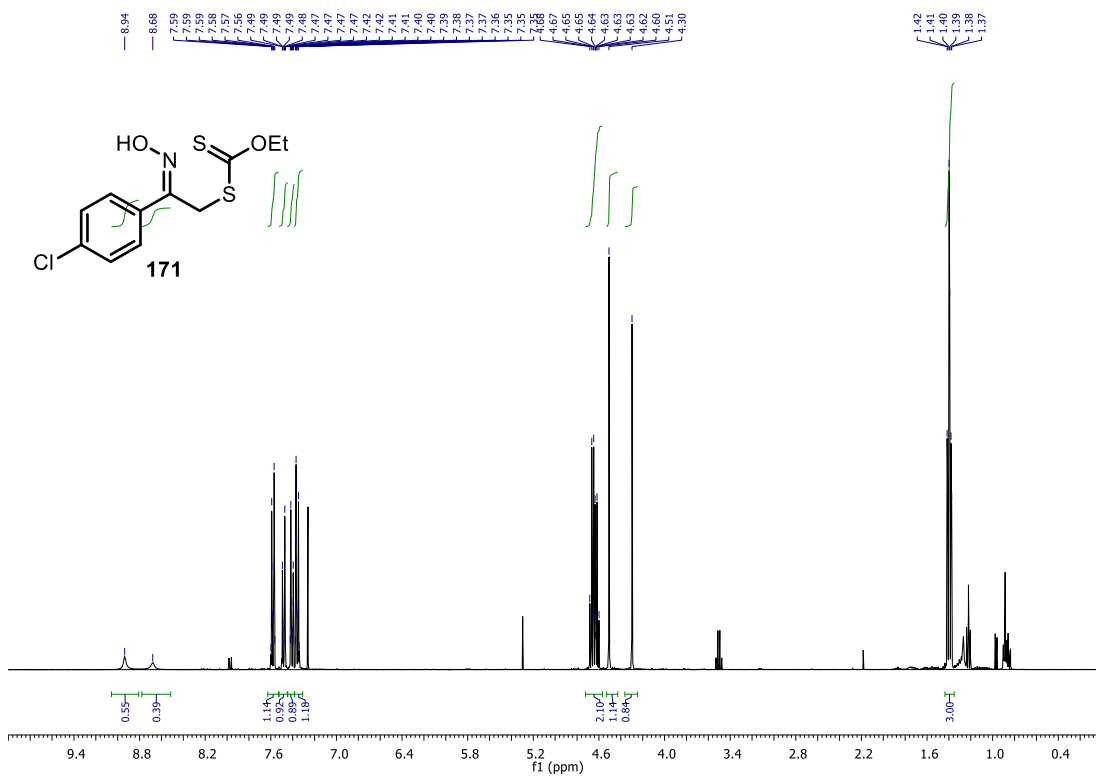
Appendix Figure 80. ¹H NMR spectrum of **171**.
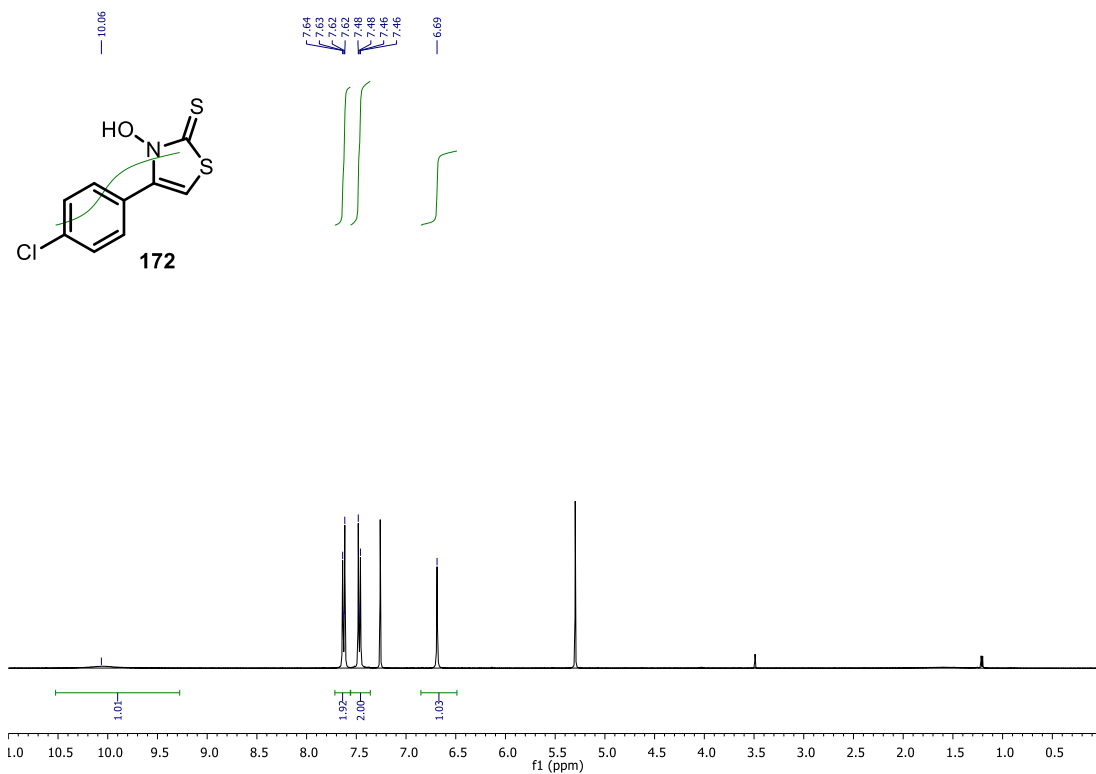
Appendix Figure 81. ^{1}H NMR spectrum of **172**.
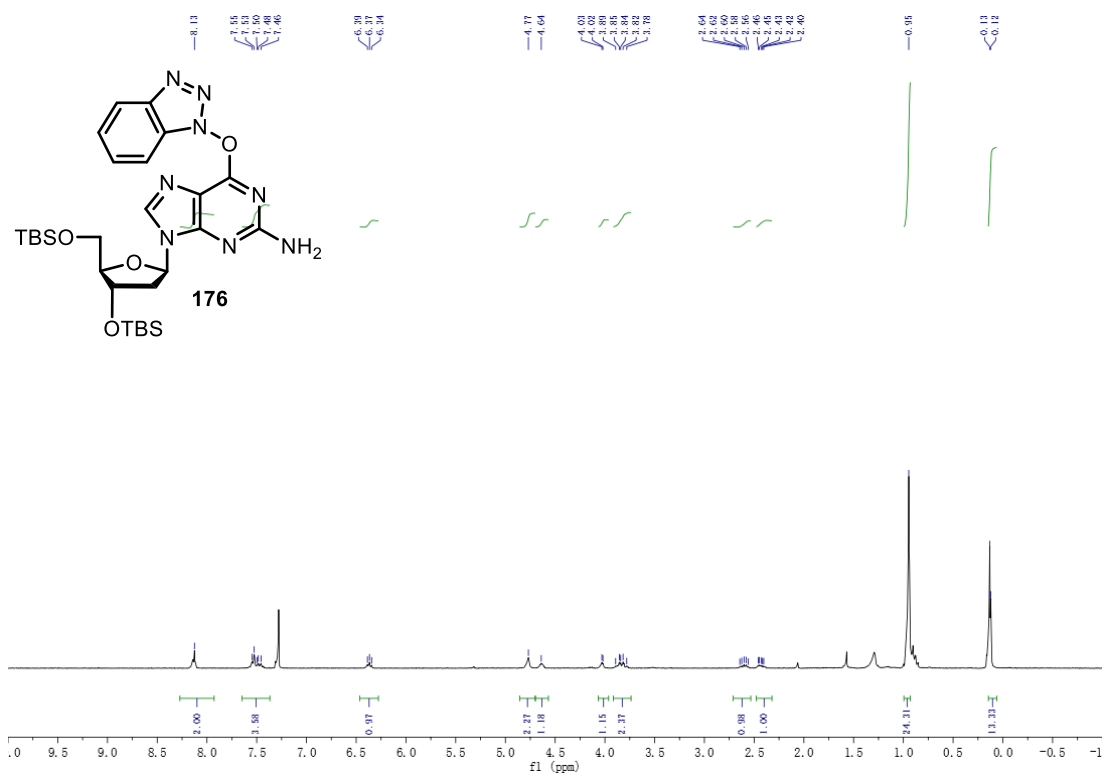
Appendix Figure 82. ^{1}H NMR spectrum of **176**.
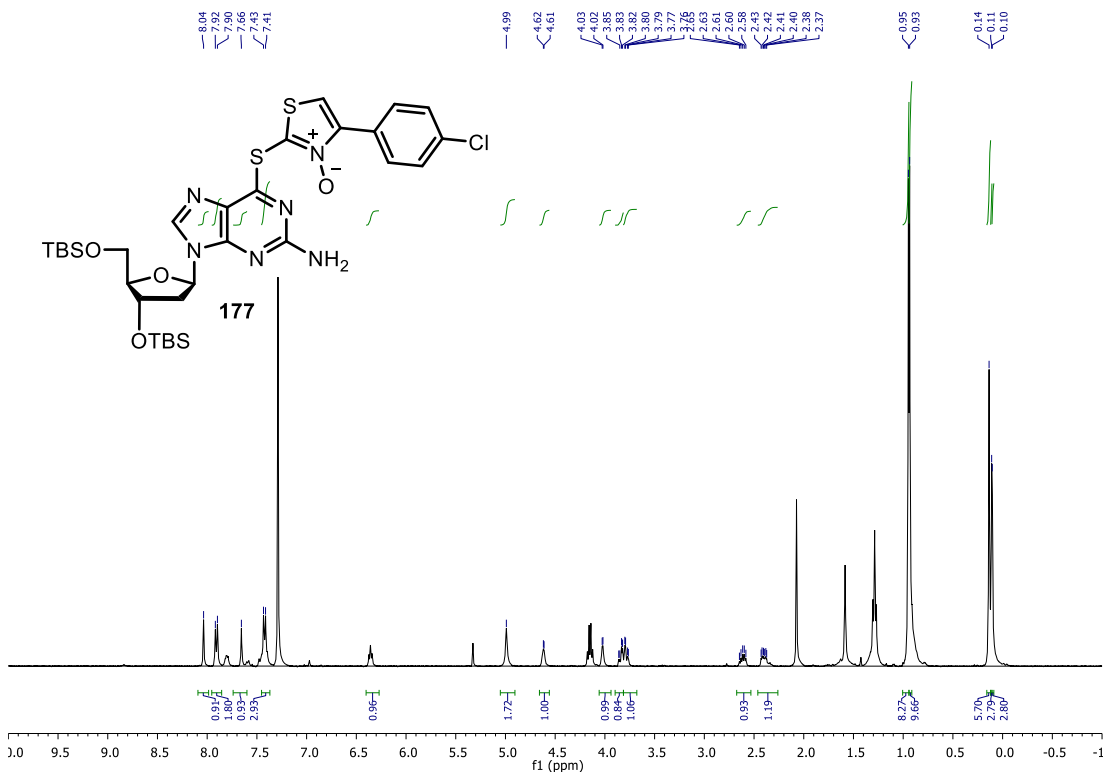
Appendix Figure 83. ^{1}H NMR spectrum of **177**.
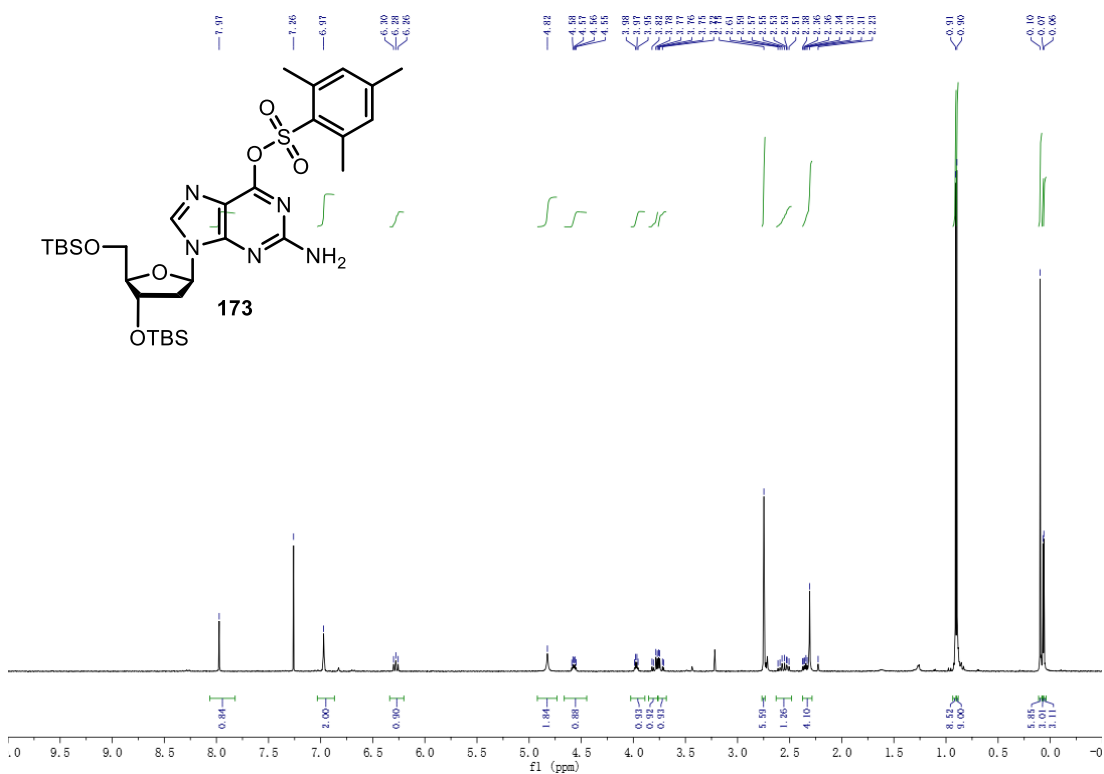
Appendix Figure 84. ^{1}H NMR spectrum of **173**.
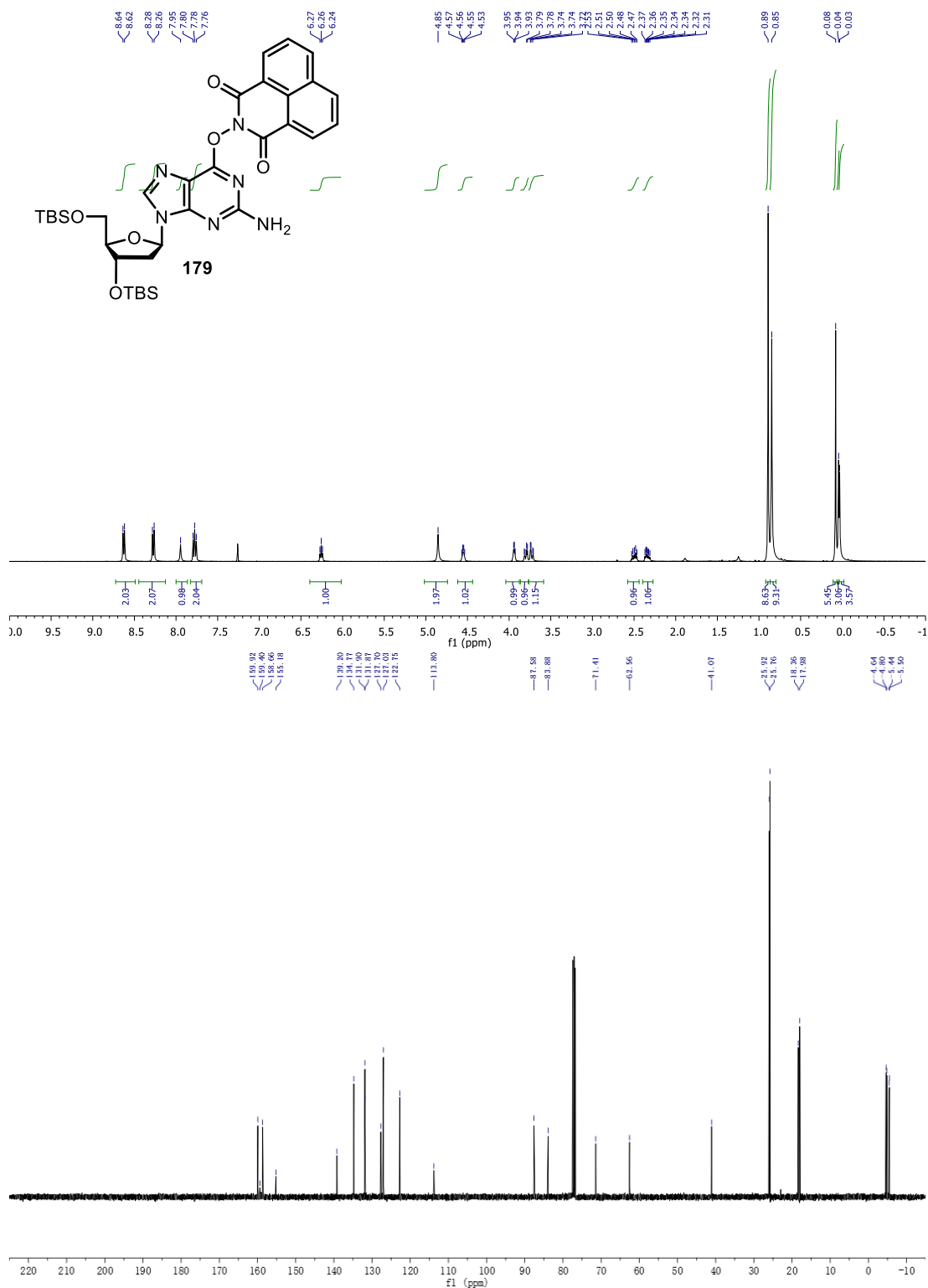
Appendix Figure 85. ^{1}H NMR and ^{13}C NMR spectra of **179**.
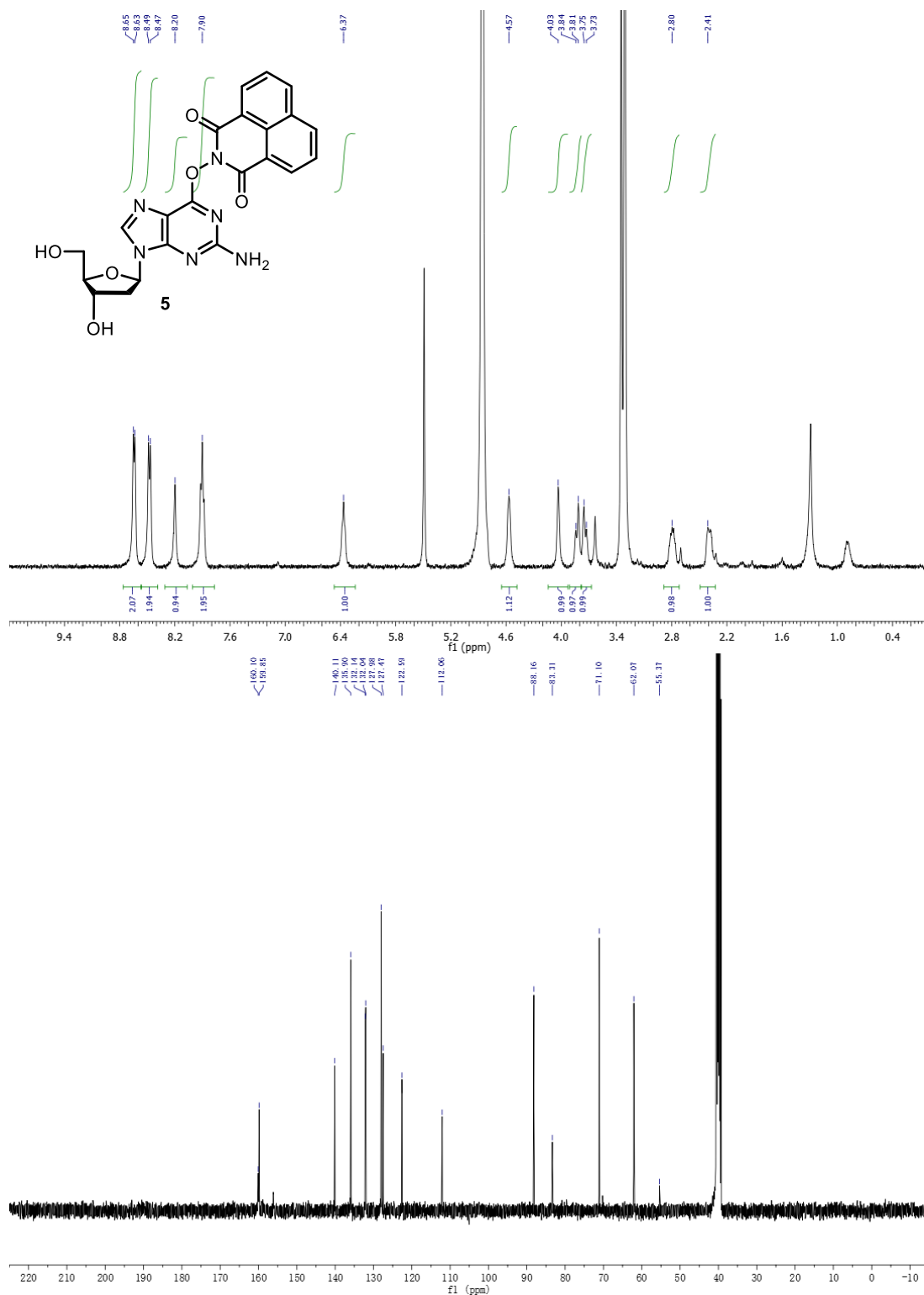
Appendix Figure 86. ^{1}H NMR and ^{13}C NMR spectra of **5**.
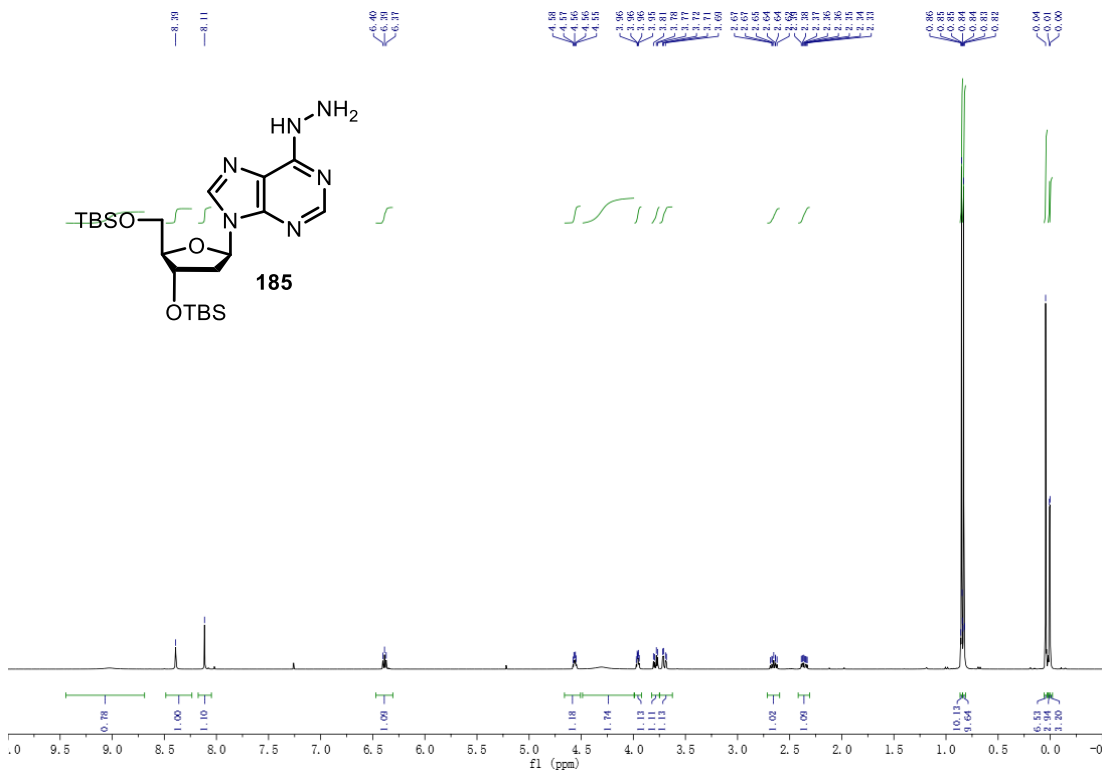
Appendix Figure 87. ^{1}H NMR spectrum of **185**.
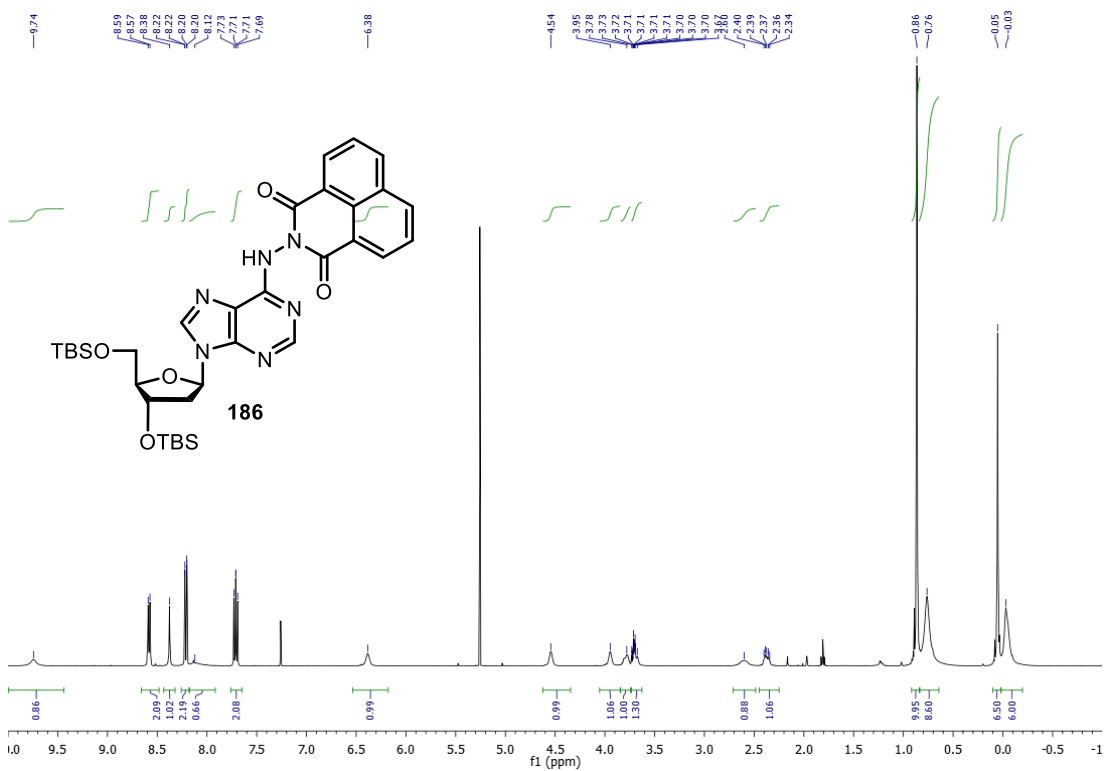
Appendix Figure 88. ^{1}H NMR spectrum of **186**.

301
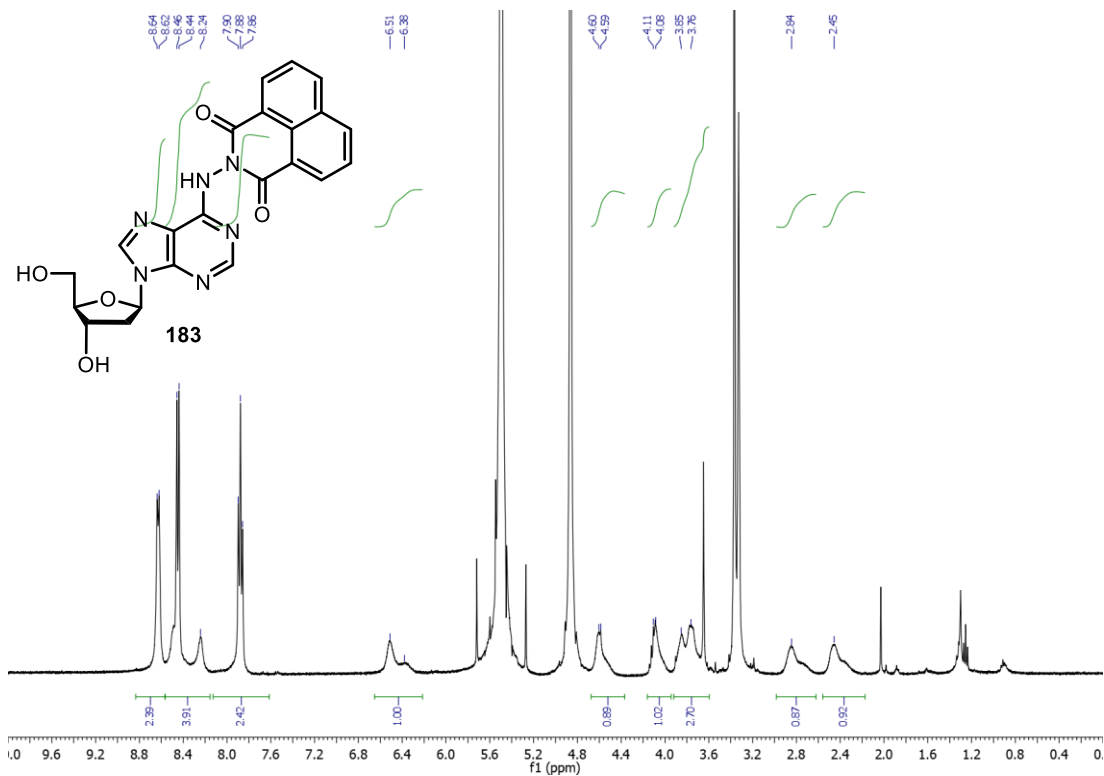
Appendix Figure 89. ^{1}H NMR spectrum of **183**.
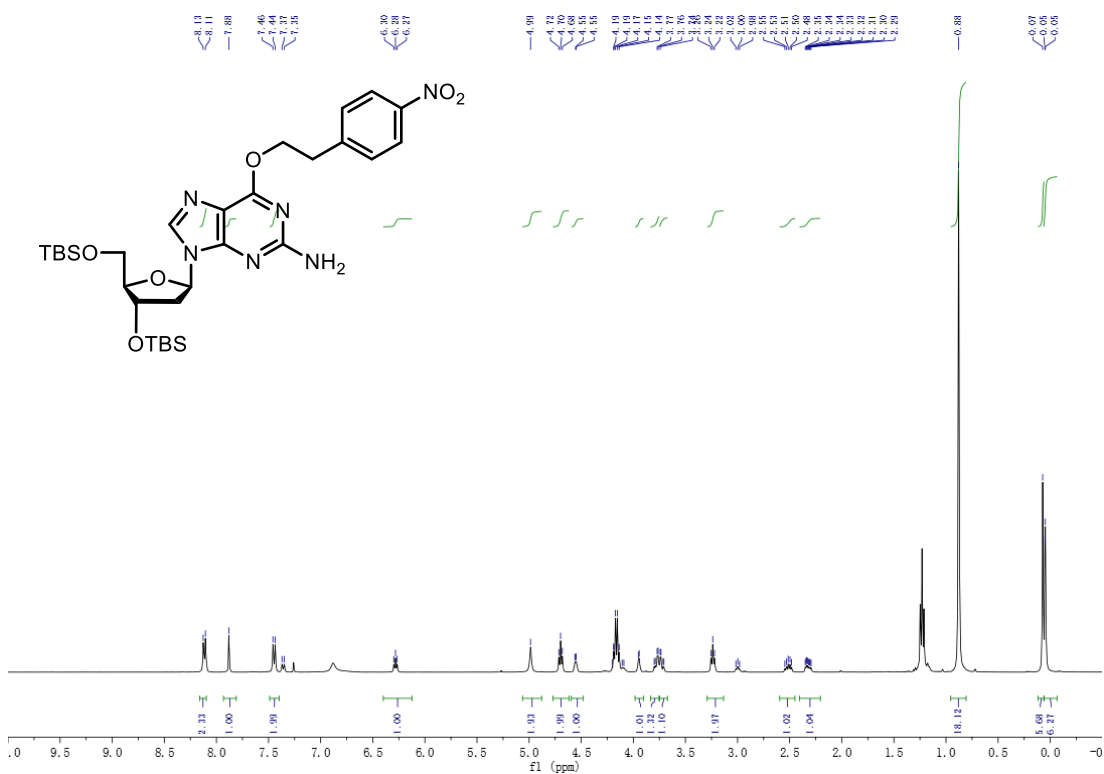
Appendix Figure 90. ^{1}H NMR spectrum of 3',5'-bis-O-TBDMS-O6-2-(*p*-nitrophenyl)ethyl 2'-deoxyguanosine.
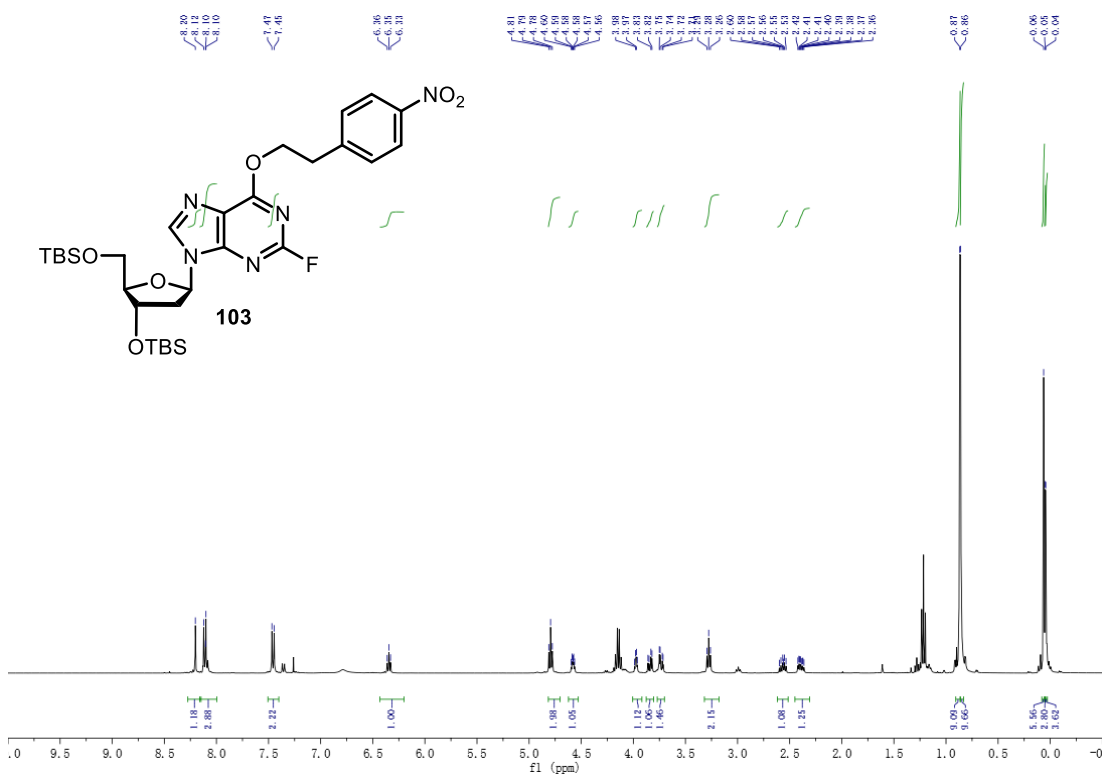
Appendix Figure 91. ^{1}H NMR spectrum of **103**.
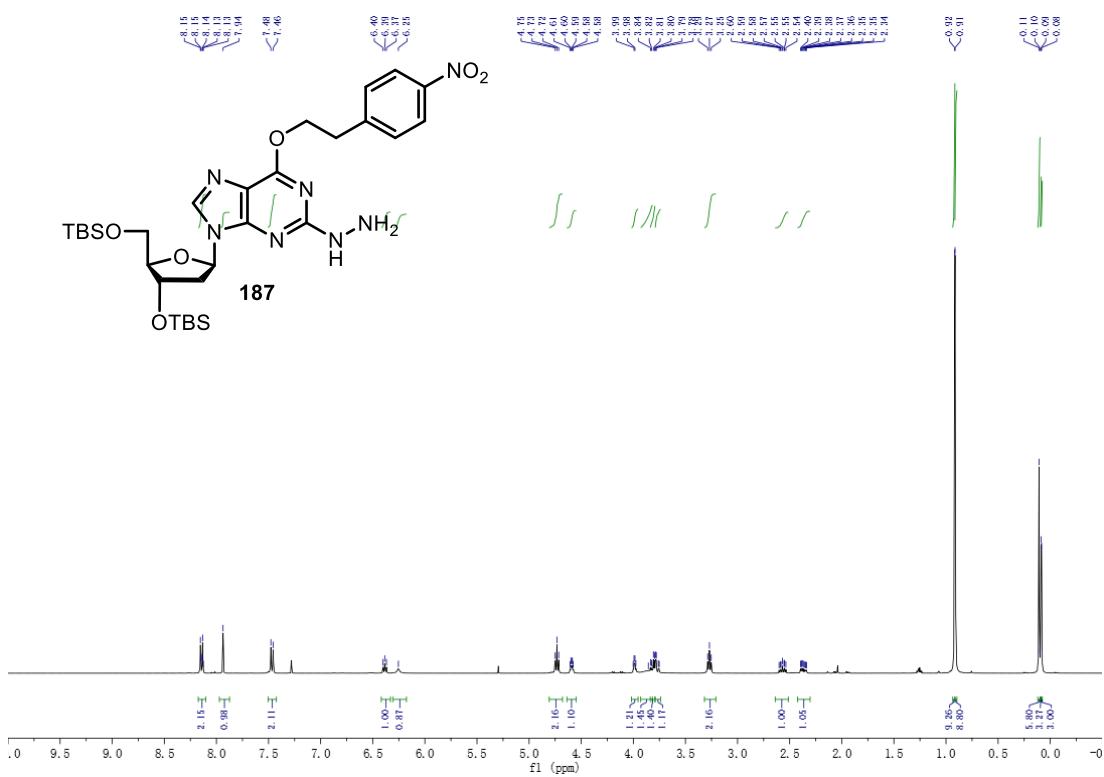
Appendix Figure 92. ^{1}H NMR spectrum of **187**.

303
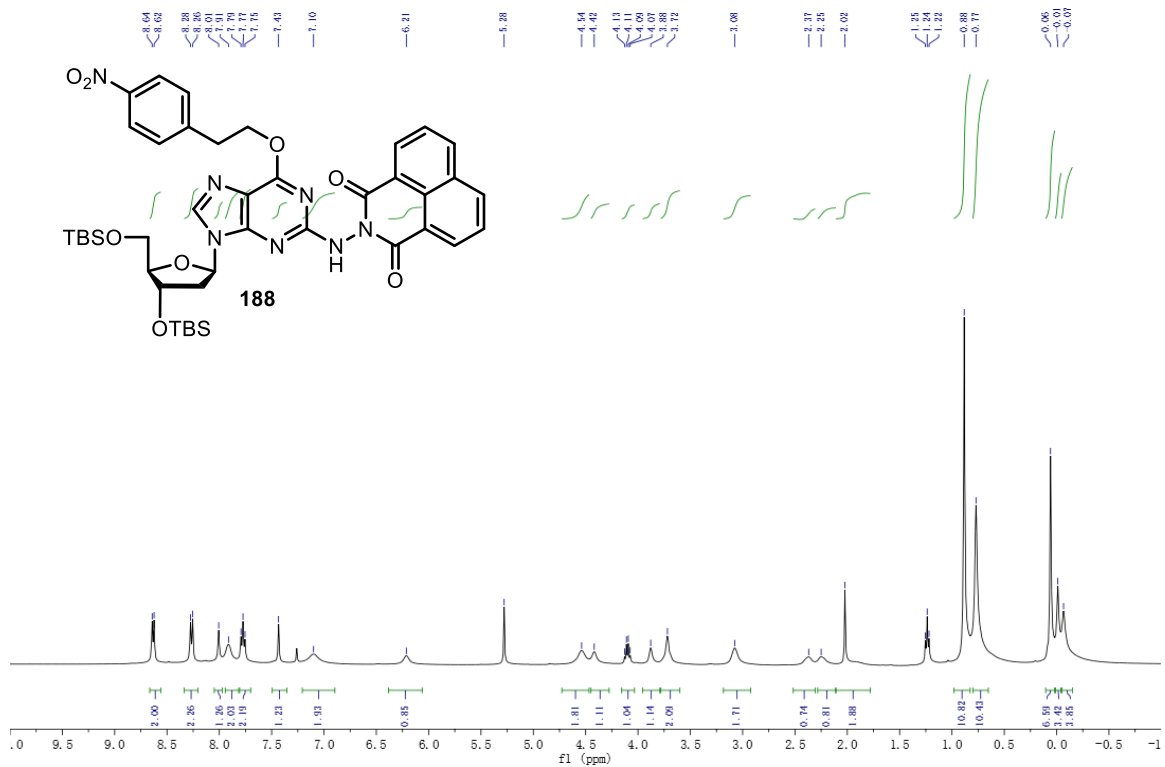
Appendix Figure 93. ^{1}H NMR spectrum of **188**.
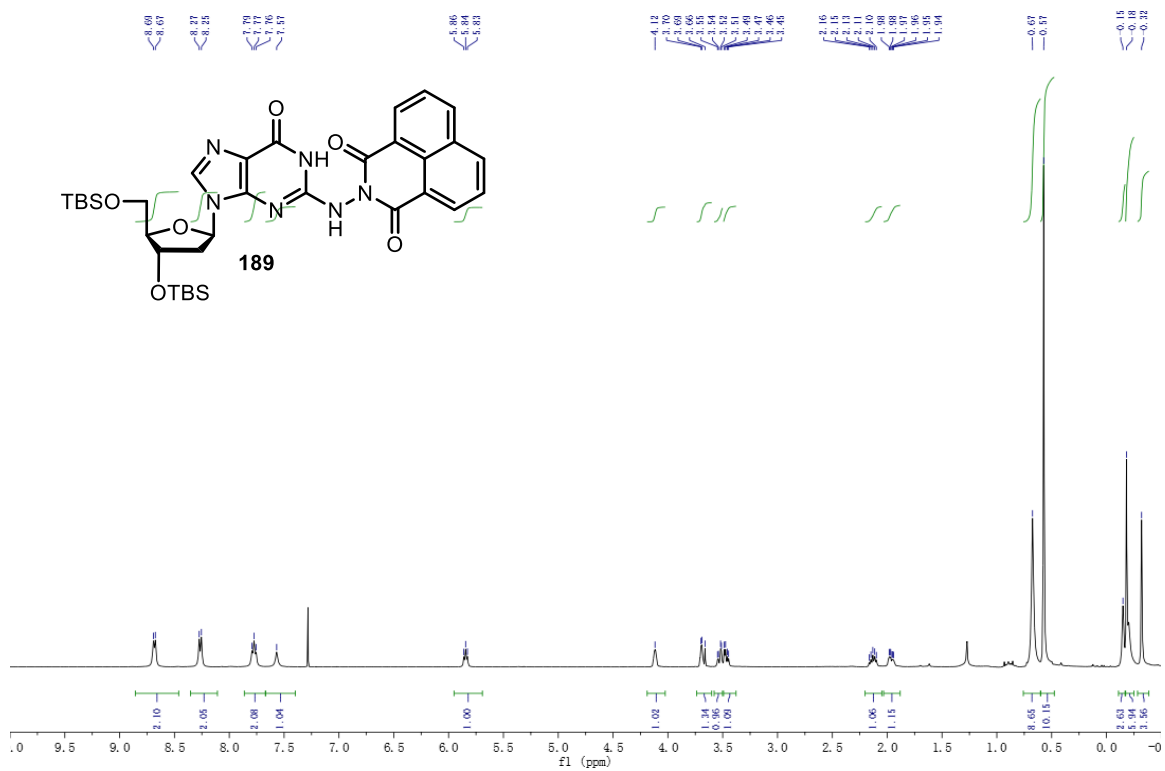
Appendix Figure 94. ^{1}H NMR spectrum of **189**.
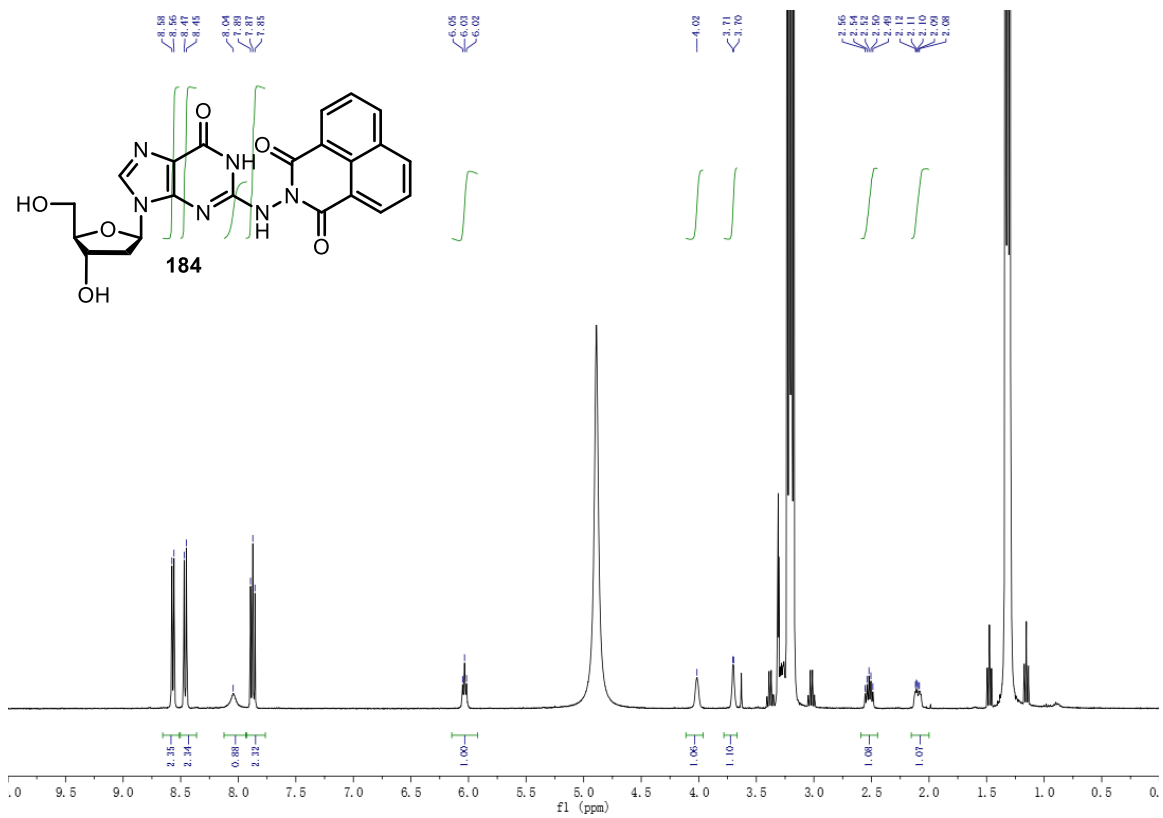
Appendix Figure 95. ^{1}H NMR spectrum of **184**.
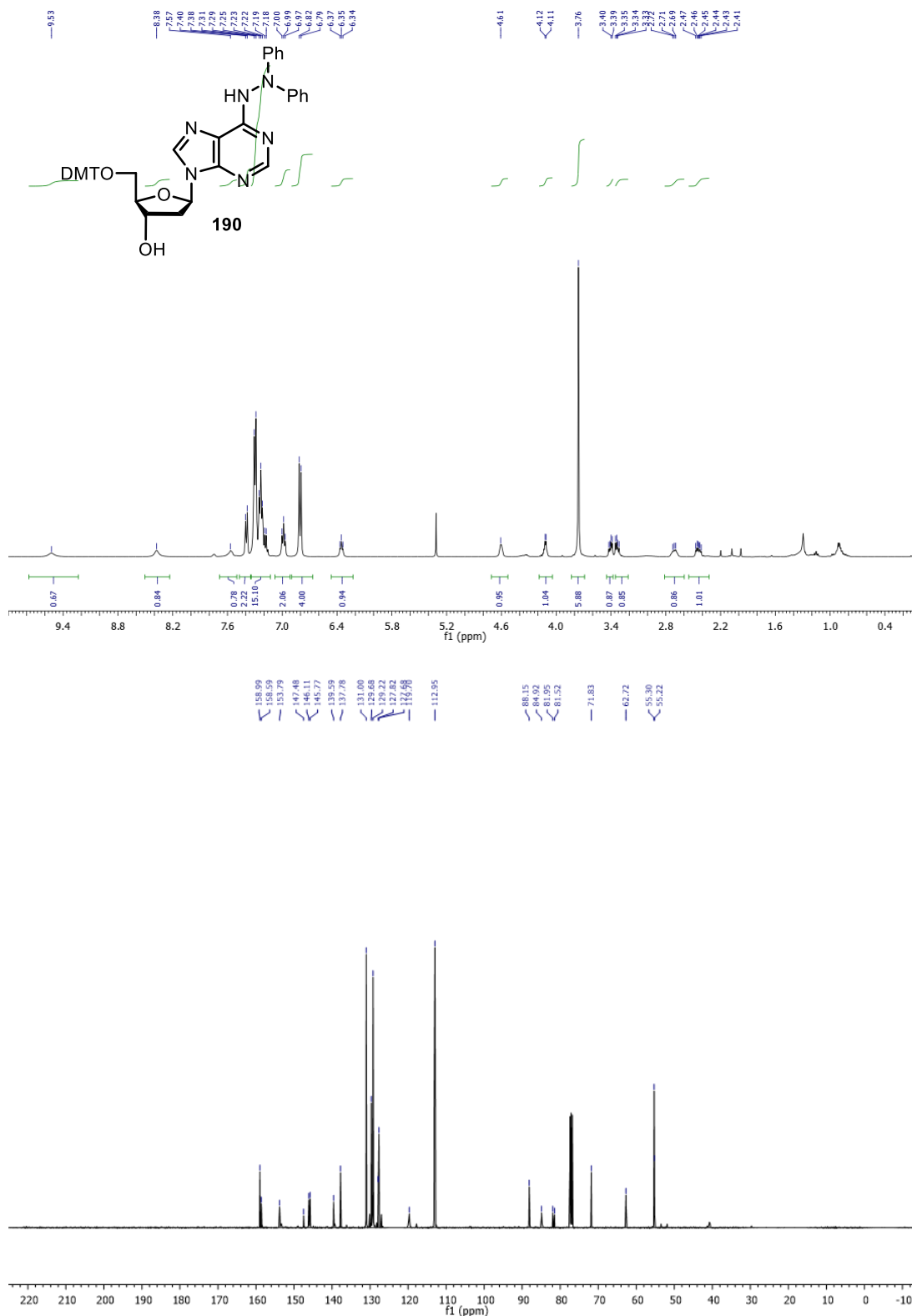
Appendix Figure 96. ^{1}H NMR and ^{13}C NMR spectra of **190**.
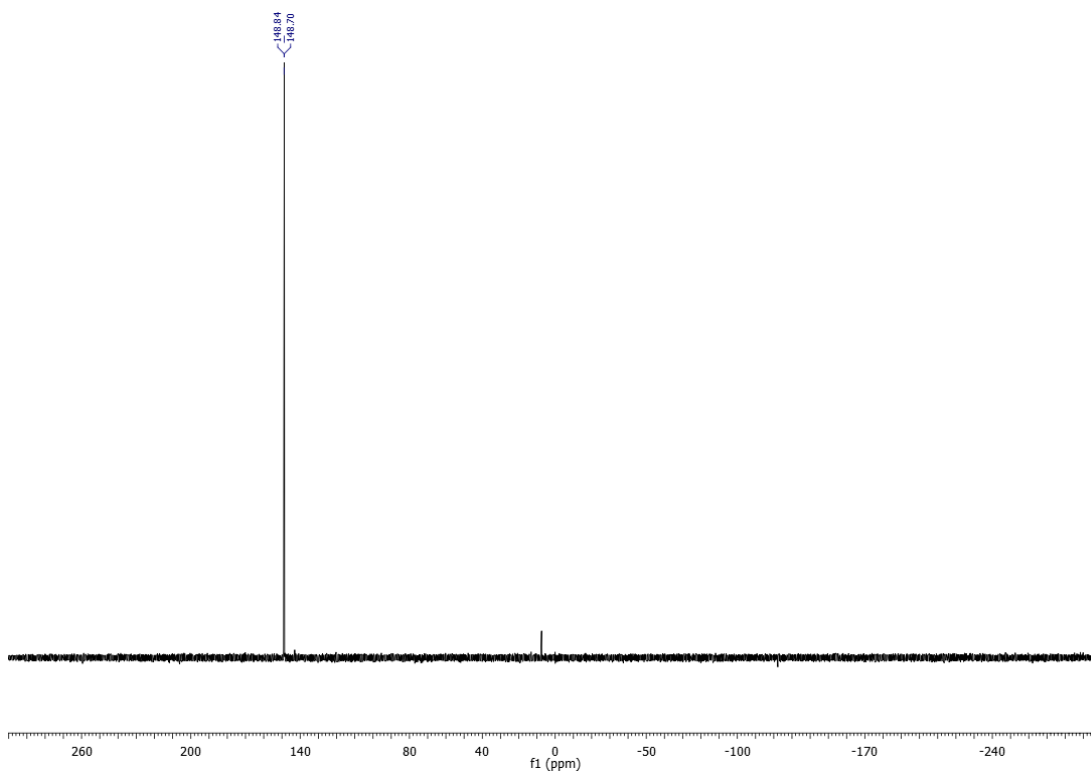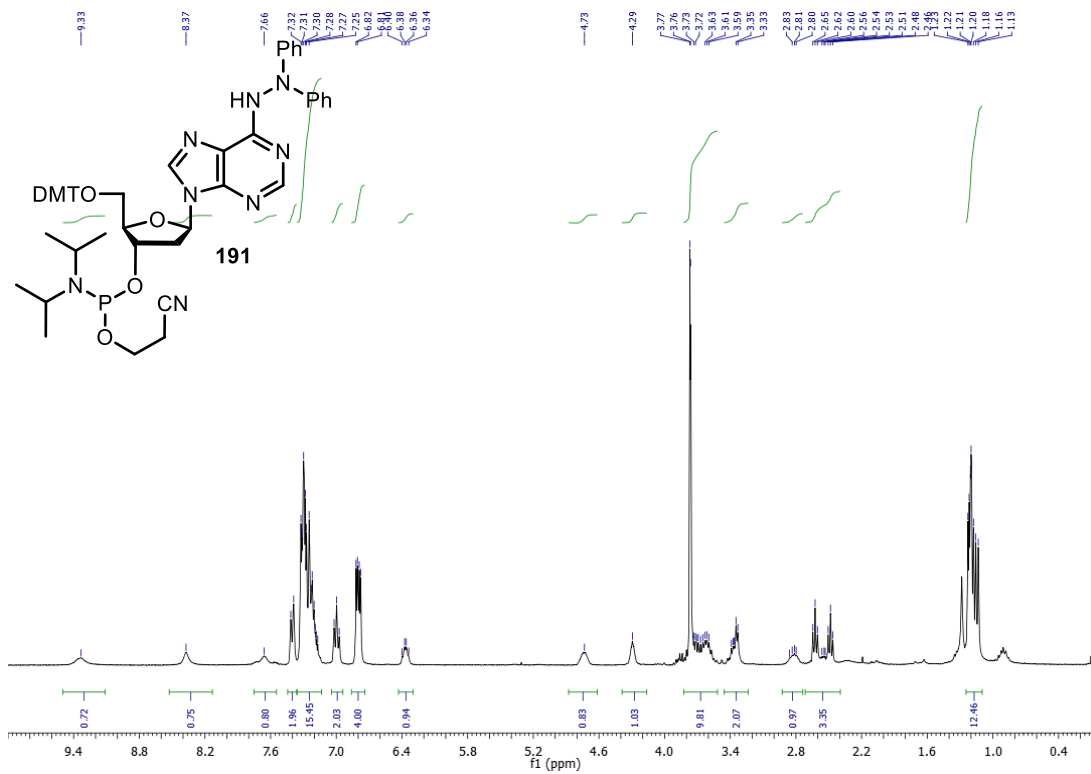
Appendix Figure 97. ^{1}H NMR and ^{31}P NMR spectra of **191**.
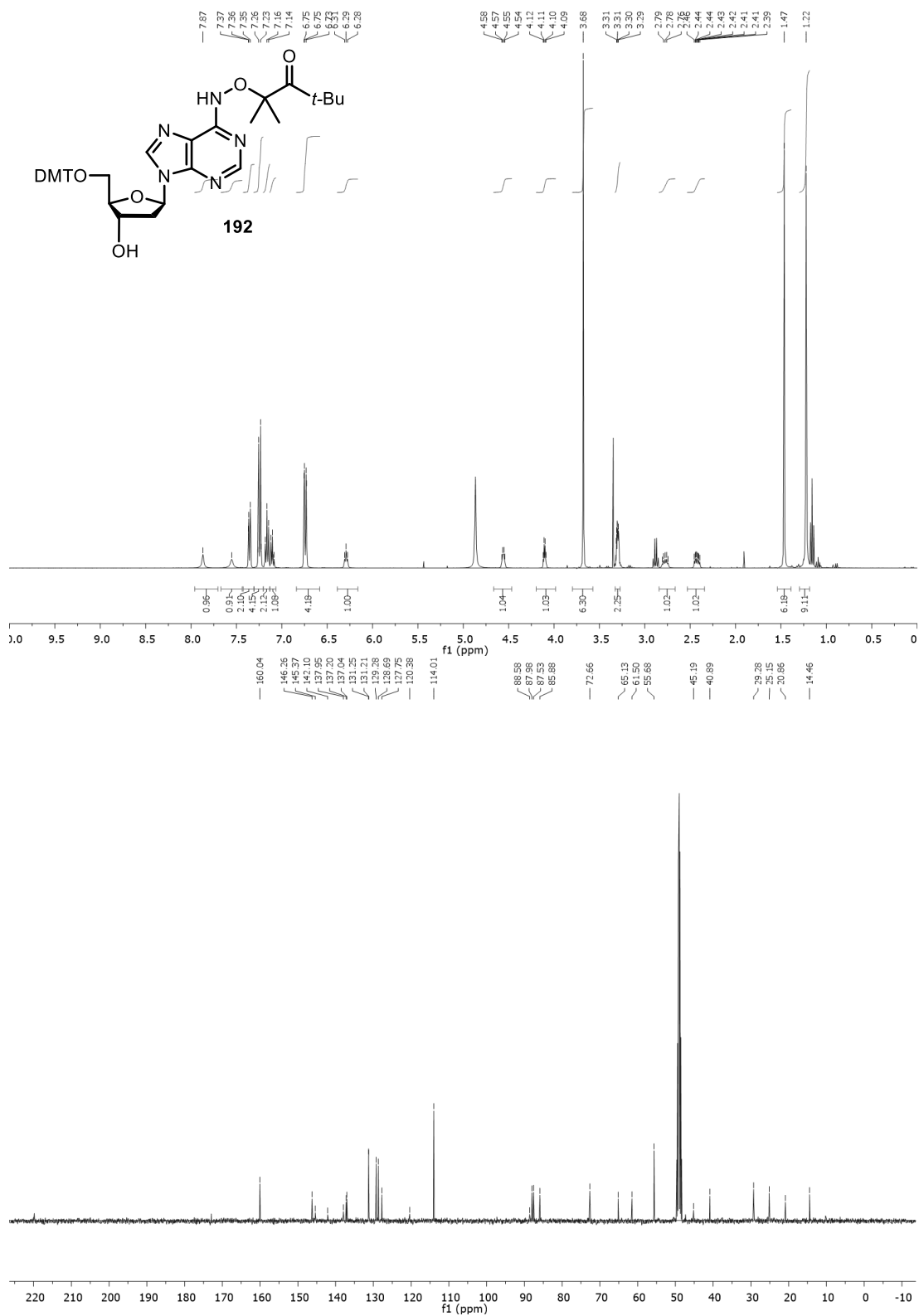
Appendix Figure 98. ^{1}H NMR and ^{13}C NMR spectra of **192**.
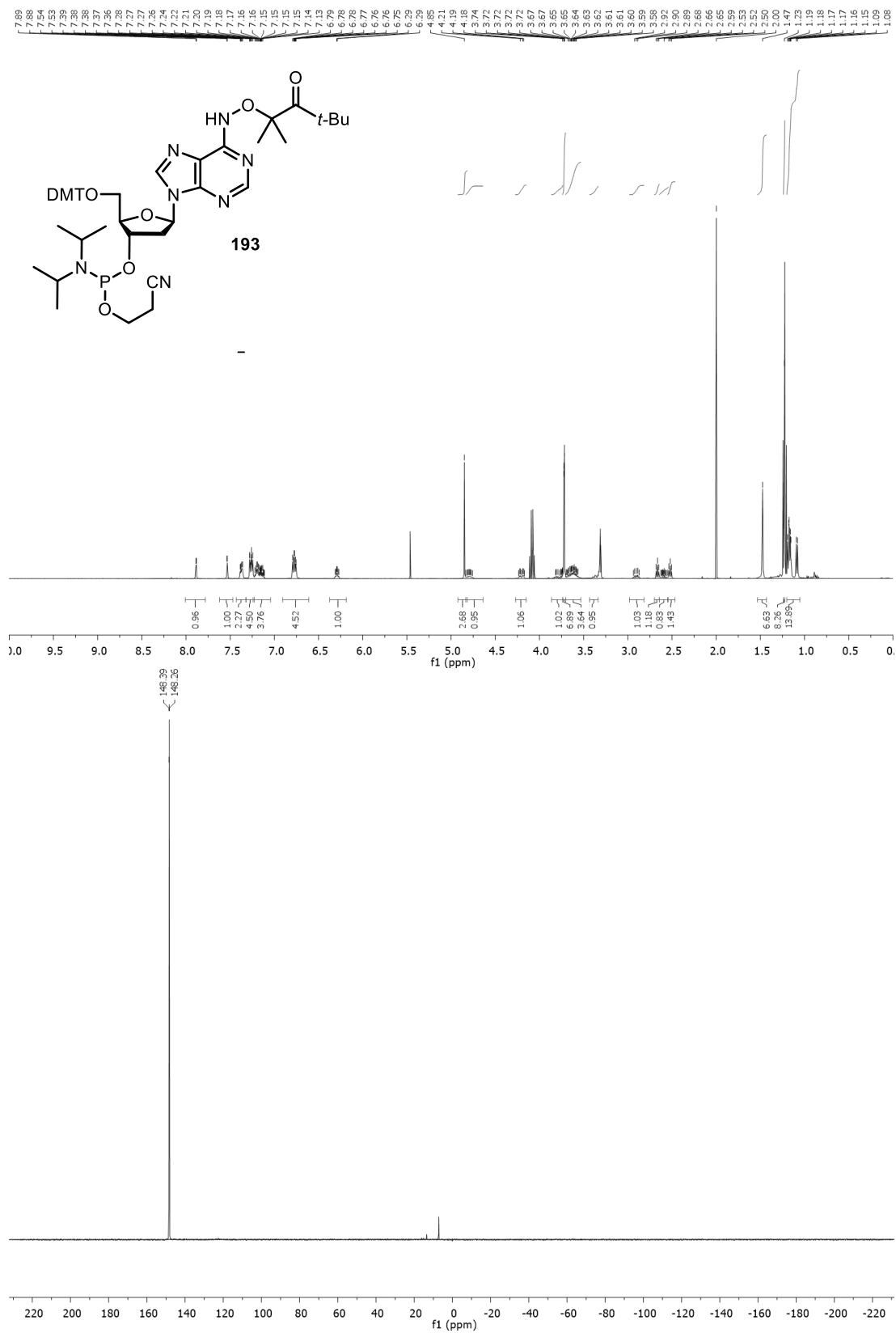
Appendix Figure 99. ^{1}H NMR and ^{31}P NMR spectra of **193**.

Appendix Figure 100. ¹H NMR spectrum of 5,6-dihydrothymidine.

Appendix Figure 101. ¹H NMR spectrum of 5'-O-dimethoxytrityl-5,6-dihydrothimidine.
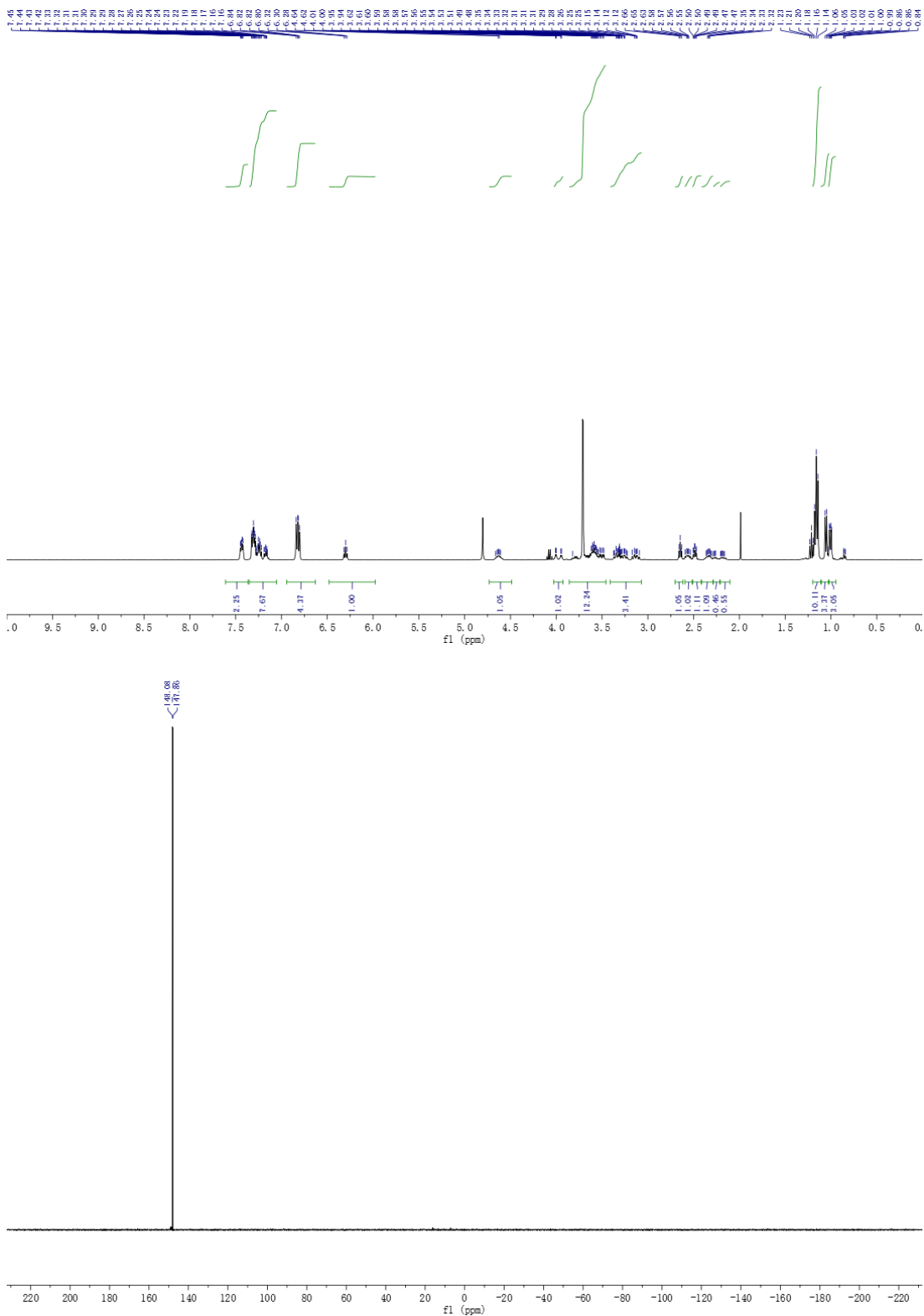
Appendix Figure 102. ^{1}H NMR and ^{31}P NMR spectra of 5,6-dihydrothimidine phosphoramidite.
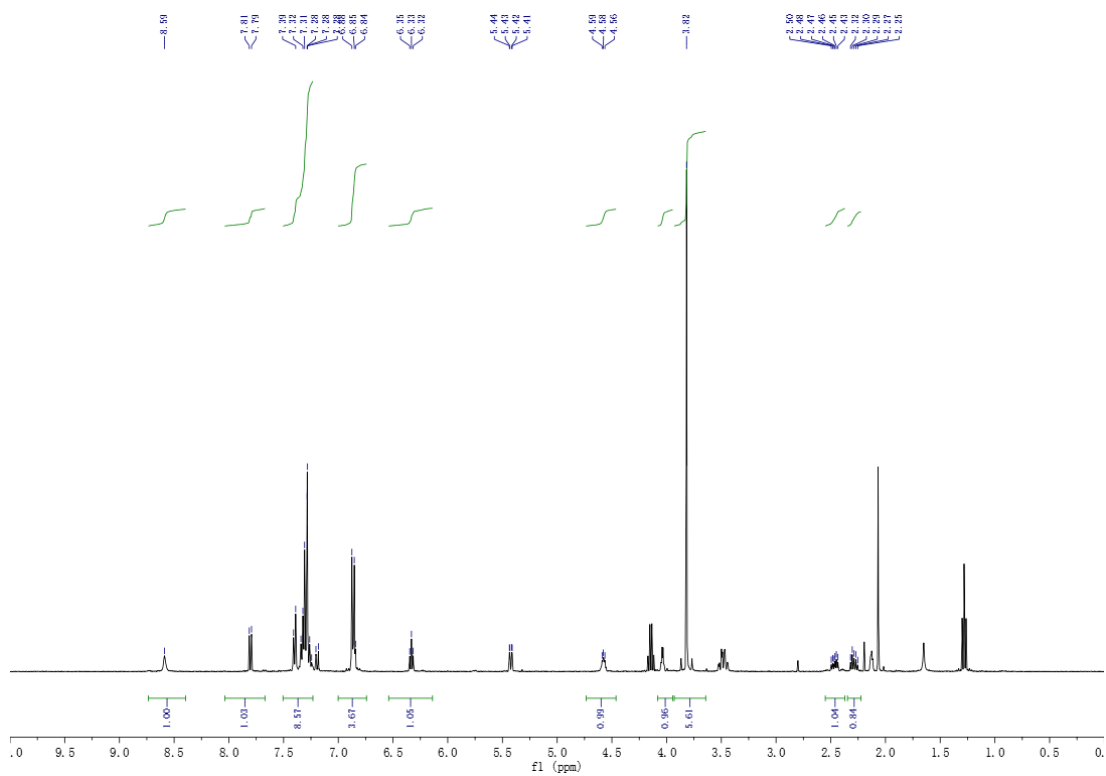
Appendix Figure 103. ^{1}H NMR spectrum of 5'-O-dimethoxytrityl-2'-deoxyuridine.
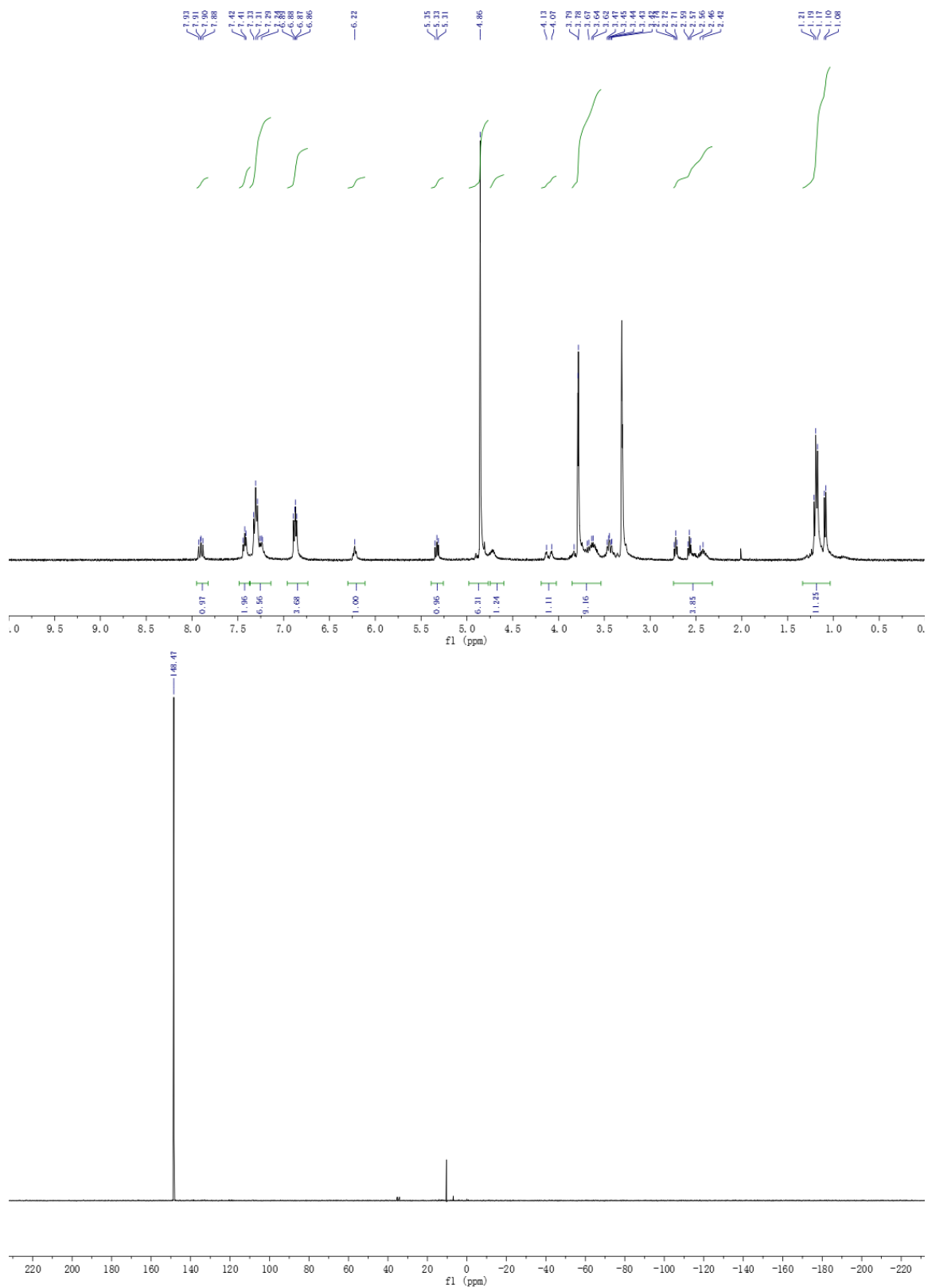
Appendix Figure 104. ^{1}H NMR and ^{31}P NMR spectra of 2'-deoxyuridine phosphoramidite.
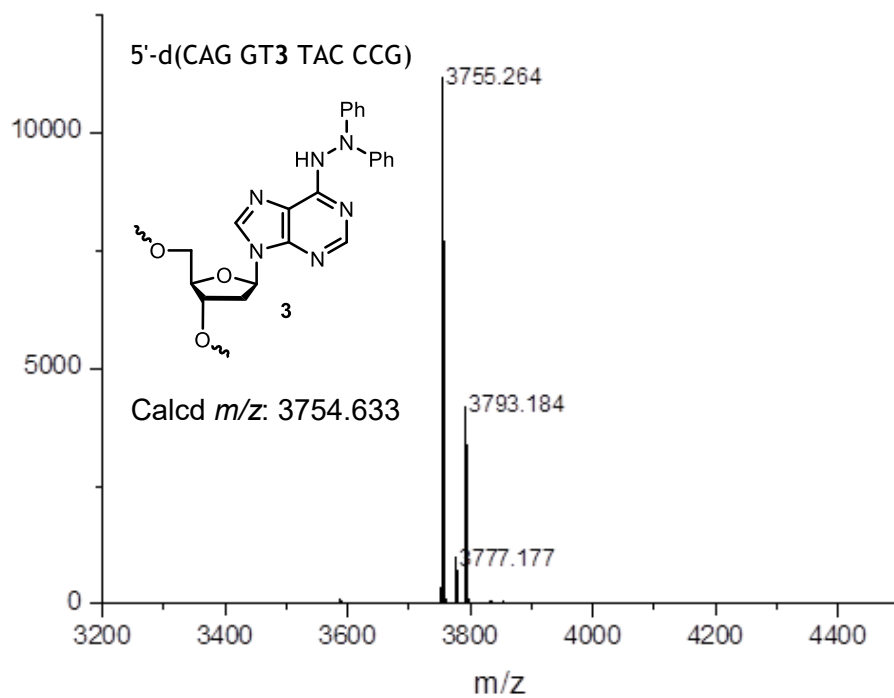
Appendix Figure 105. MALDI-TOF spectrum of **194a** containing **3**. Ions at *m/z* = 3777 and 3793 correspond to M + Na and M + K, respectively.
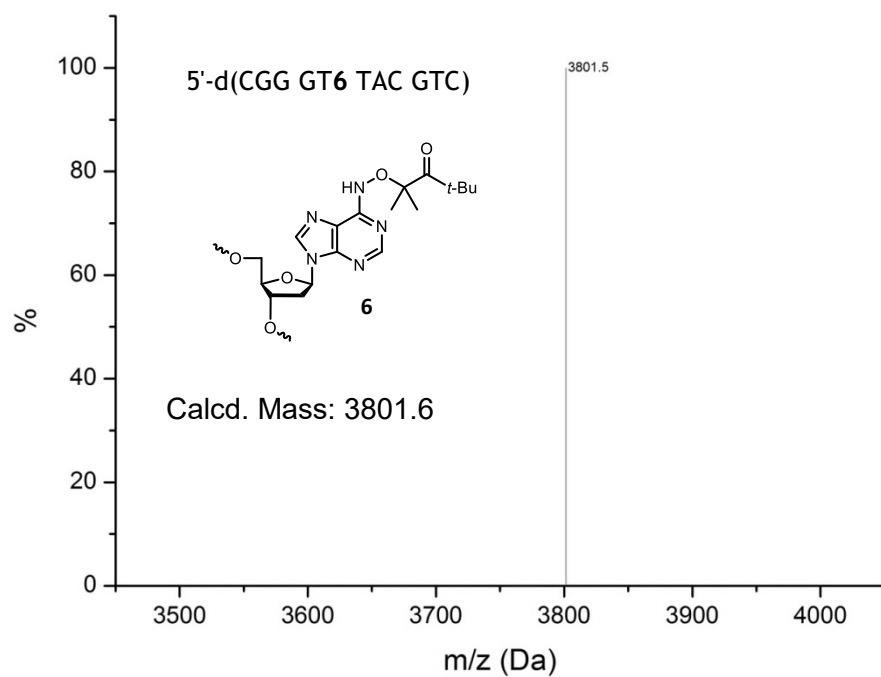
Appendix Figure 106. UPLC-MS of the strand of **195a** containing **6**.
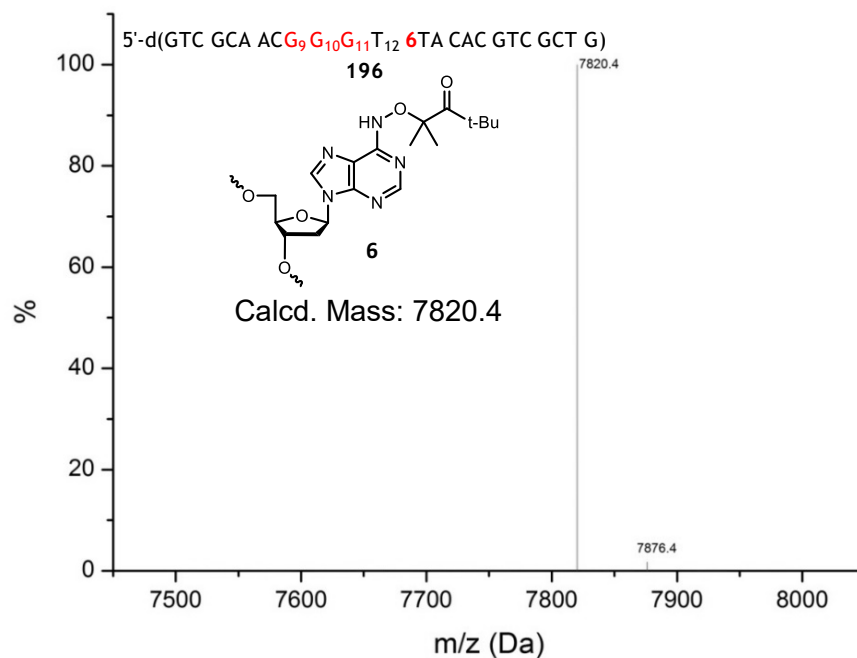
Appendix Figure 107. UPLC-MS of the strand of **196** containing **6**.
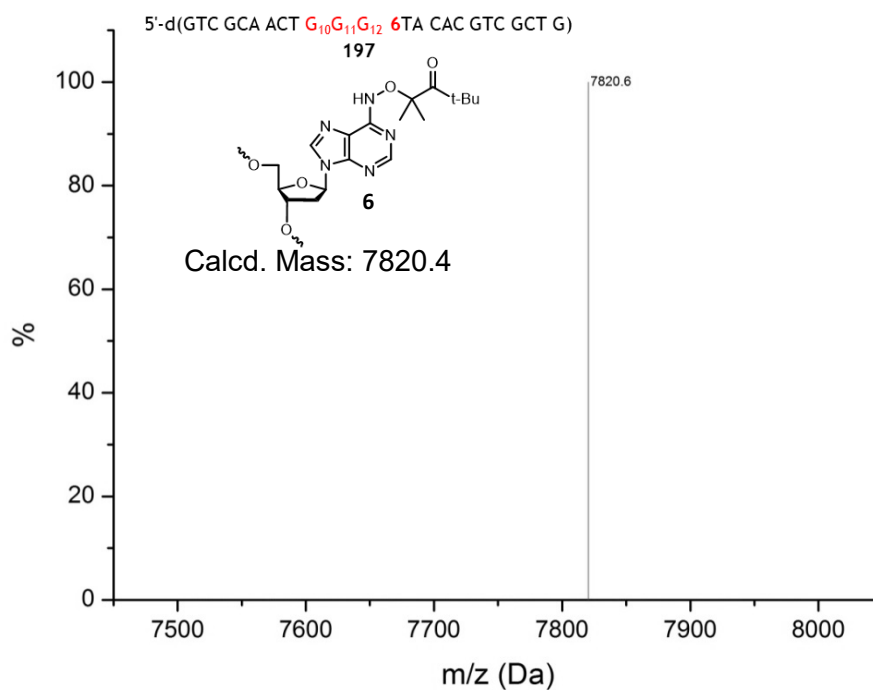
Appendix Figure 108. UPLC-MS/MS of the strand of **197** containing **6**.

5'-d(GTC GCA ACG GGT$_{12}$ **6**T$_{14}$G GGC GTC GCT G)
198

Calcd. MW: 7841.0
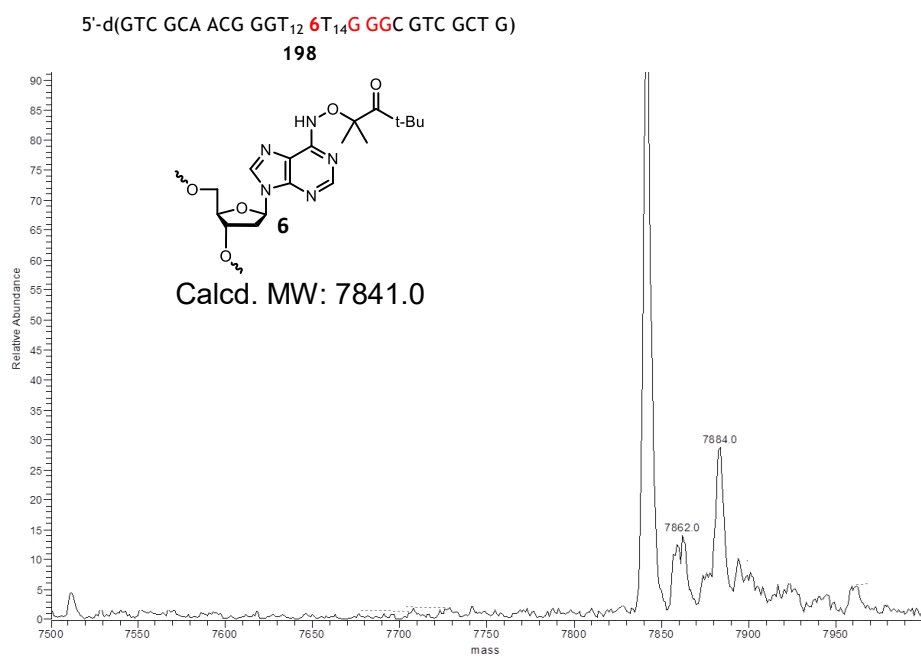
Appendix Figure 109. ESI-MS of the strand of **198** containing **6**.

5'-d(GTC GCA CG$_8$G$_9$ G$_{10}$T$_{11}$G$_{12}$ **6**TA CAC GTC GCT G)
199

Calcd. mass: 7845.4
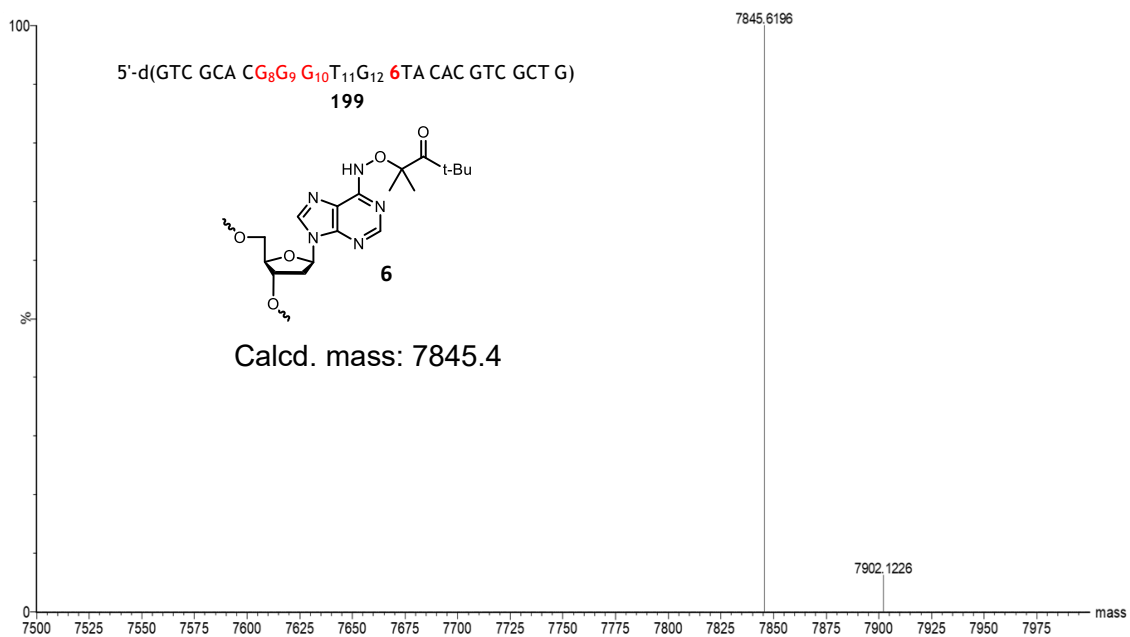
Appendix Figure 110. UPLC-MS/MS of the strand of **199** containing **6**.

316

5'-d(GTC GCA ACG CAT$_{12}$ **6**G$_{14}$G$_{15}$ G$_{16}$AC GTC GCT G)
200

6

Calcd. Mass: 7836.4
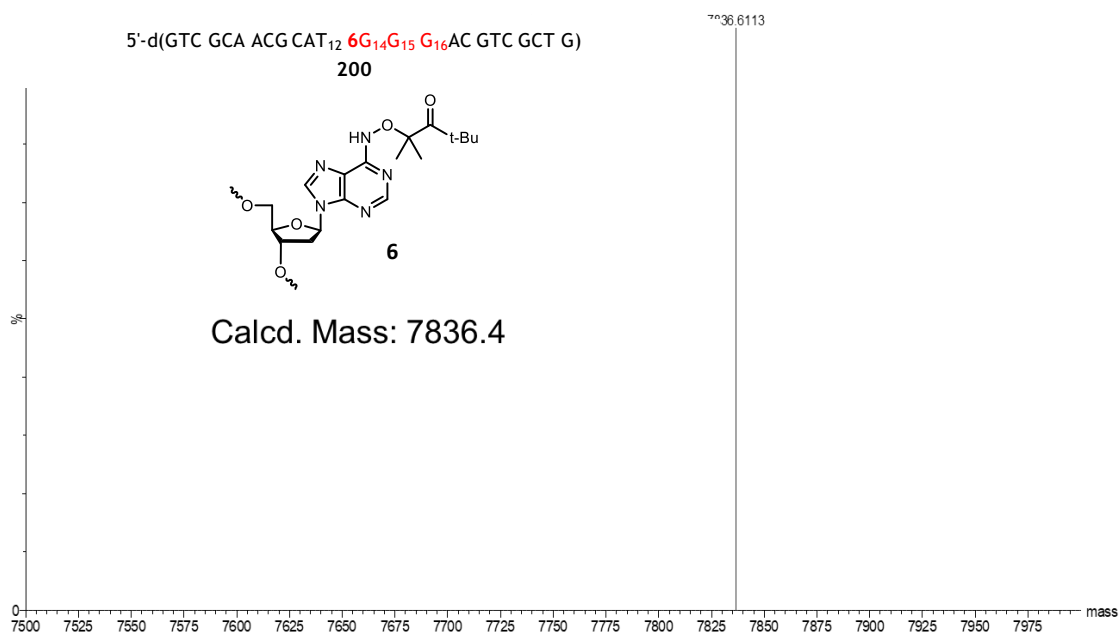
Appendix Figure 111. UPLC-MS/MS of the strand of **200** containing **6**.

5'-d(GTC GCA ACC$_9$ G$_{10}$G$_{11}$T$_{12}$ **6**TA CAC GTC GCT G)
201

6

Calcd. Mass: 7780.4
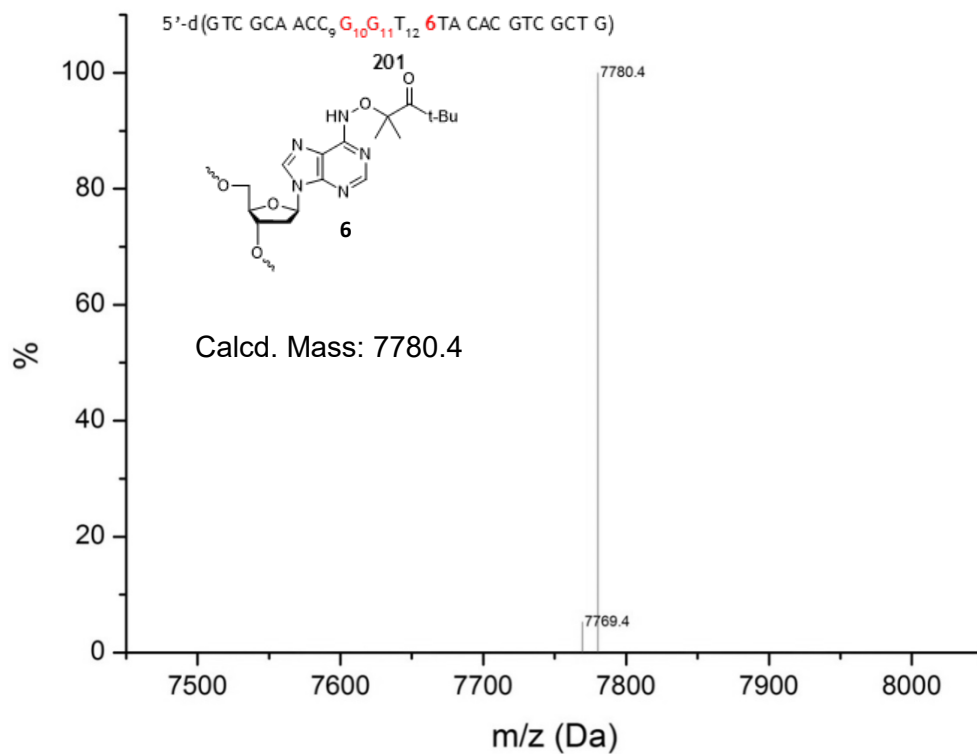
Appendix Figure 112. UPLC-MS/MS of the strand of **201** containing **6**.

317
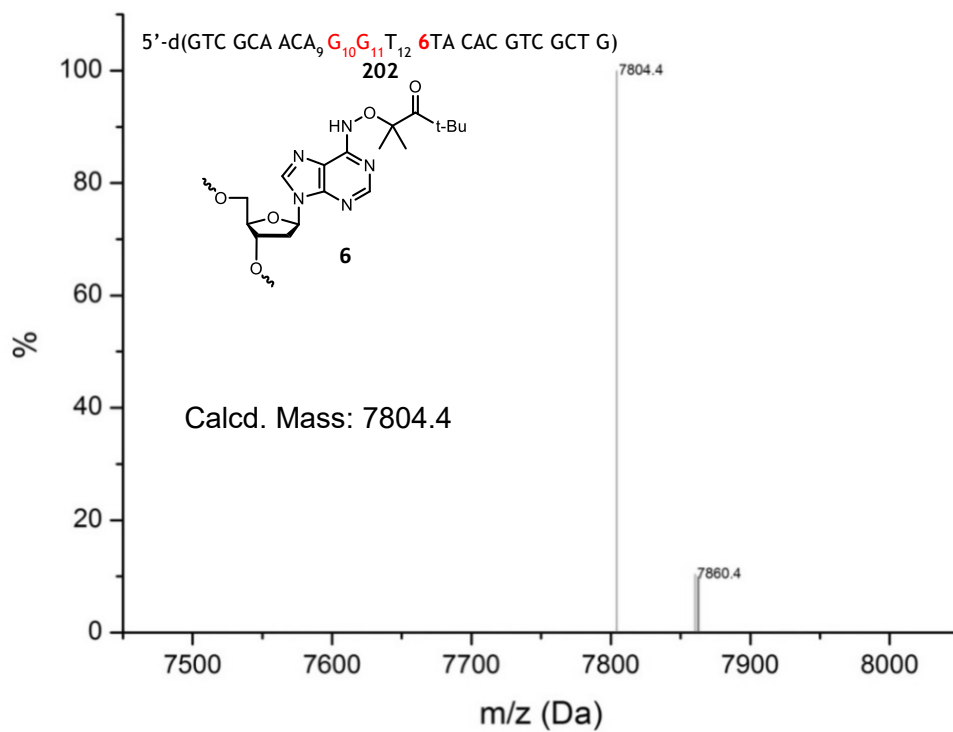
Appendix Figure 113. UPLC-MS/MS of the strand of **202** containing **6**.
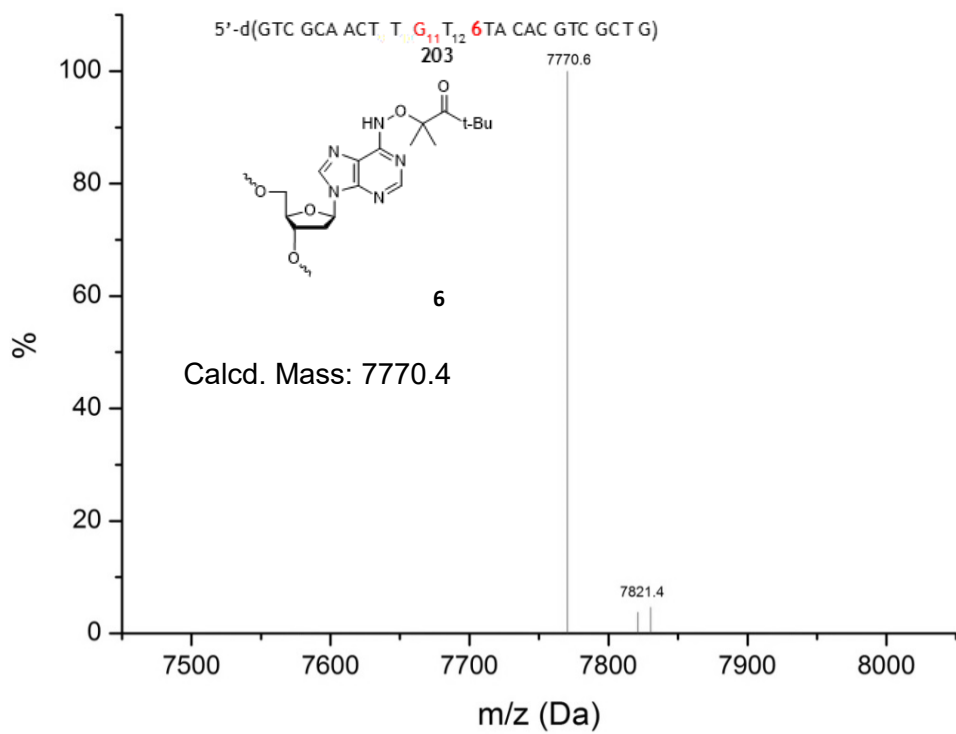
Appendix Figure 114. UPLC-MS/MS of the strand of **203** containing **6**.

318
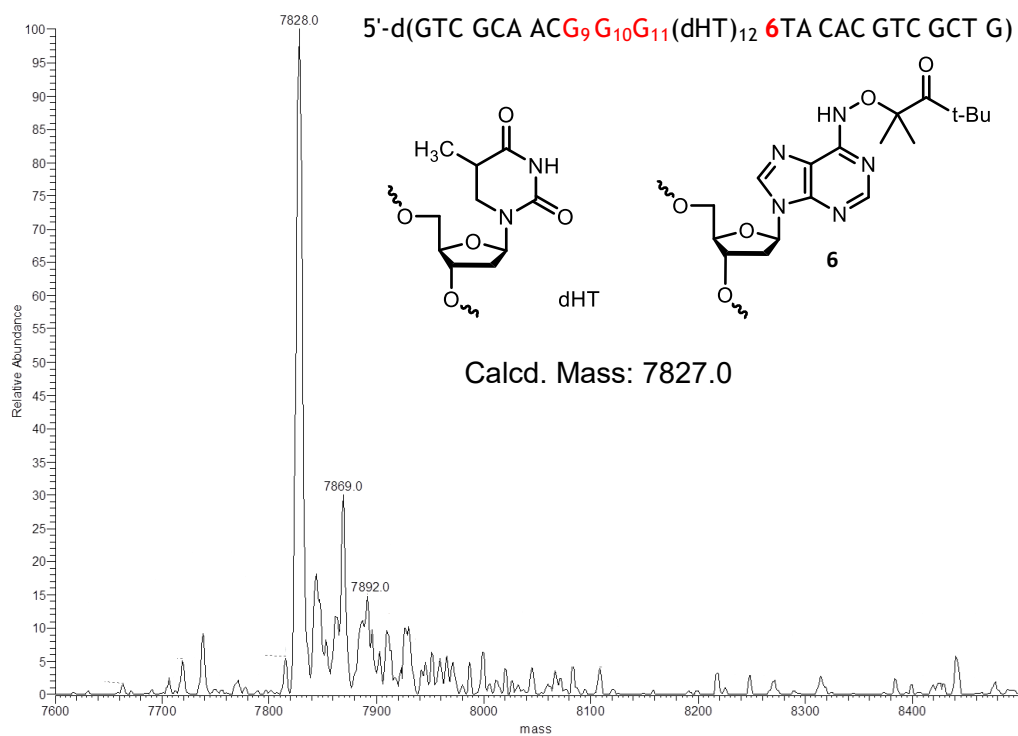
Appendix Figure 115. ESI-MS of the strand of **208** containing **6**.
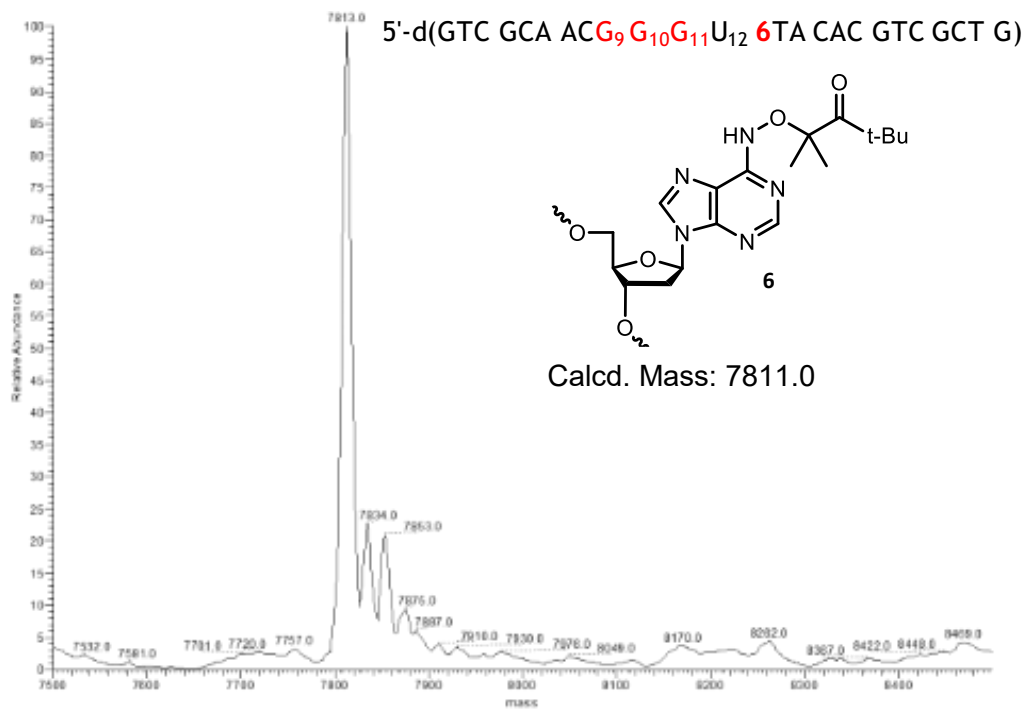
Appendix Figure 116. ESI-MS of the strand of **209** containing **6**.

319
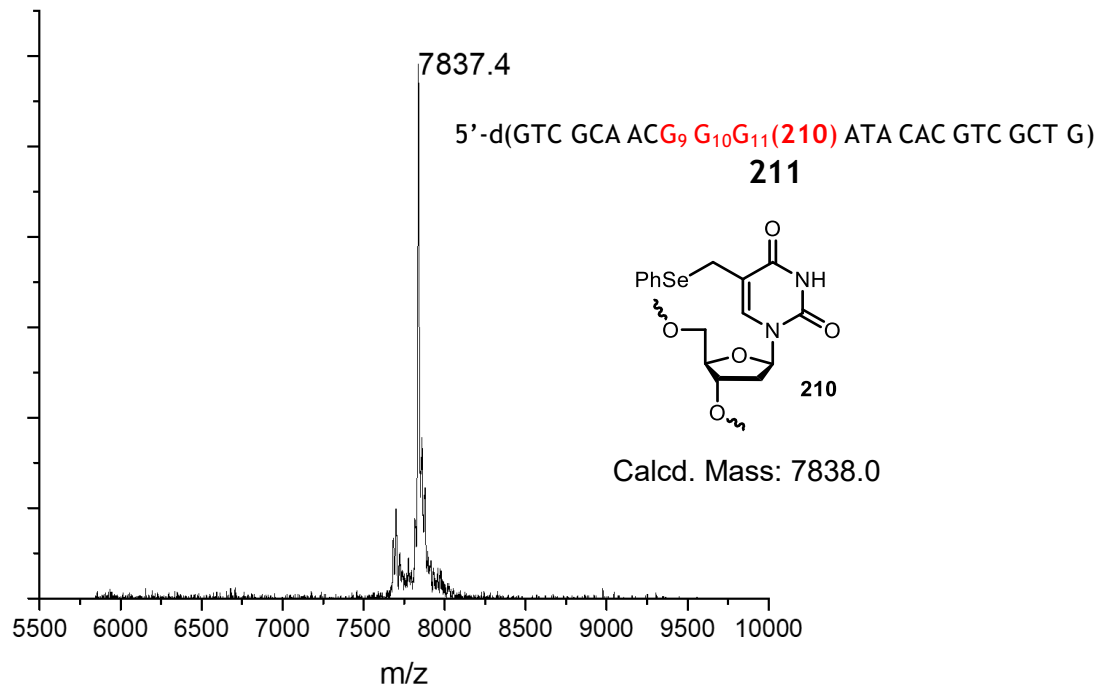
Appendix Figure 117. MALDI-TOF mass spectrum of the strand of **211** containing **210**.
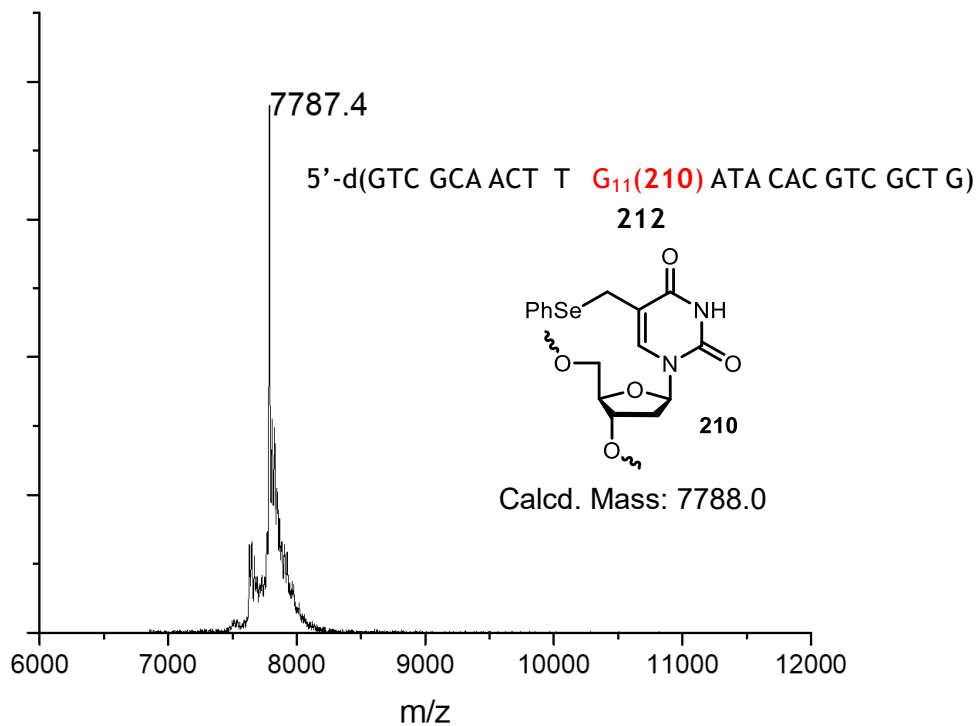
Appendix Figure 118. MALDI-TOF mass spectrum of the strand of **212** containing **210**.

5'-d(GTC CAT ATG$_9$G$_{10}$G$_{11}$T$_{12}$A6T ATA CGT GCA G)

6

Calcd. MW: 7863.0
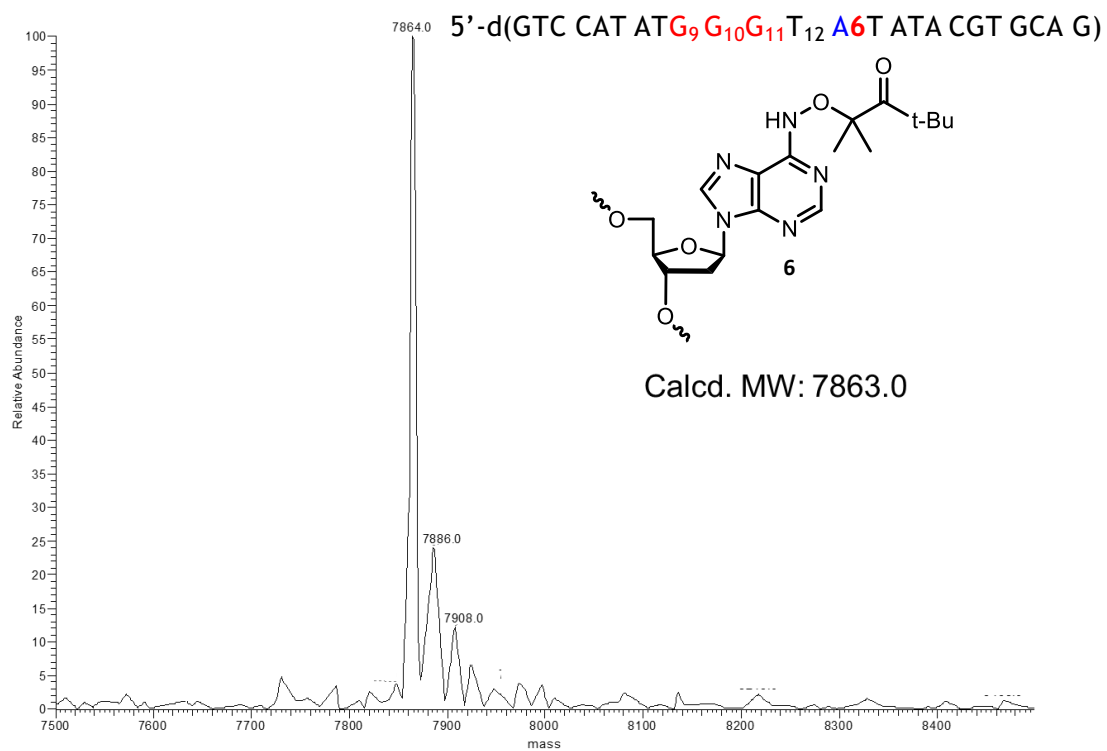
Appendix Figure 119. ESI-MS of the strand of **220** containing **6**.

5'-d(TCC ATA TG$_8$G$_9$ G$_{10}$TG$_{12}$ A6T ATA CGT GCA G)

221

6

Calcd. MW: 7863.0
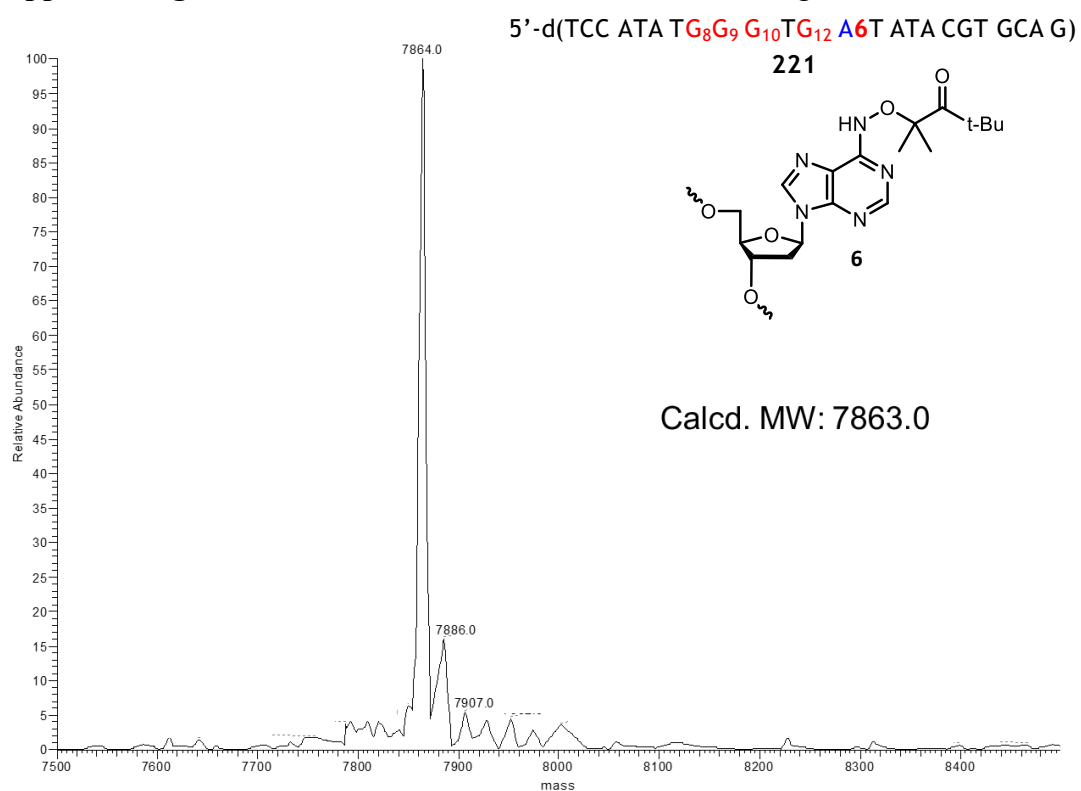
Appendix Figure 120. ESI-MS of the strand of **221** containing **6**.

5'-d(GTC GCG CTA TAT **6**AG₁₅ G₁₆G₁₇T ATA GCT G)

5'-d(GTC GCG CTA TAT **6**AG_{15} $G_{16}G_{17}$T ATA GCT G)

222

Calcd. MW: 7879.0
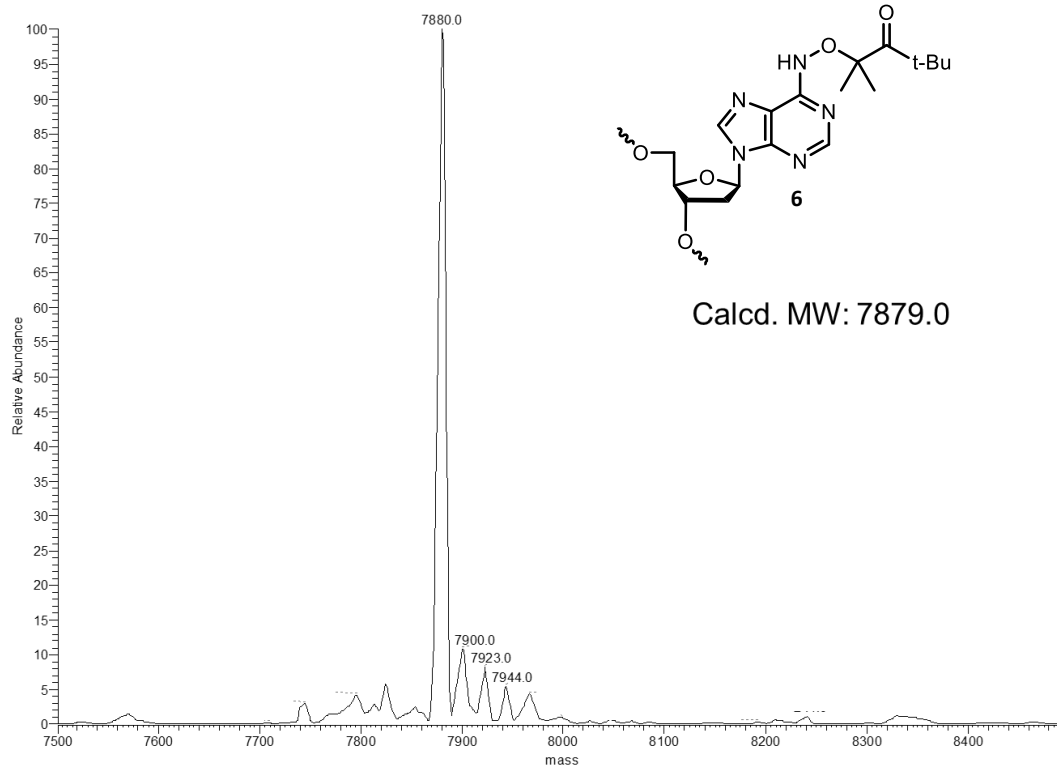
Appendix Figure 121. ESI-MS of the strand of **222** containing **6**.

5'-d(GTC GAT ATG_9 $G_{10}G_{11}$$T_{12}$ AAA **6**AT ATA GCT G)

223

Calcd. MW: 7911.0
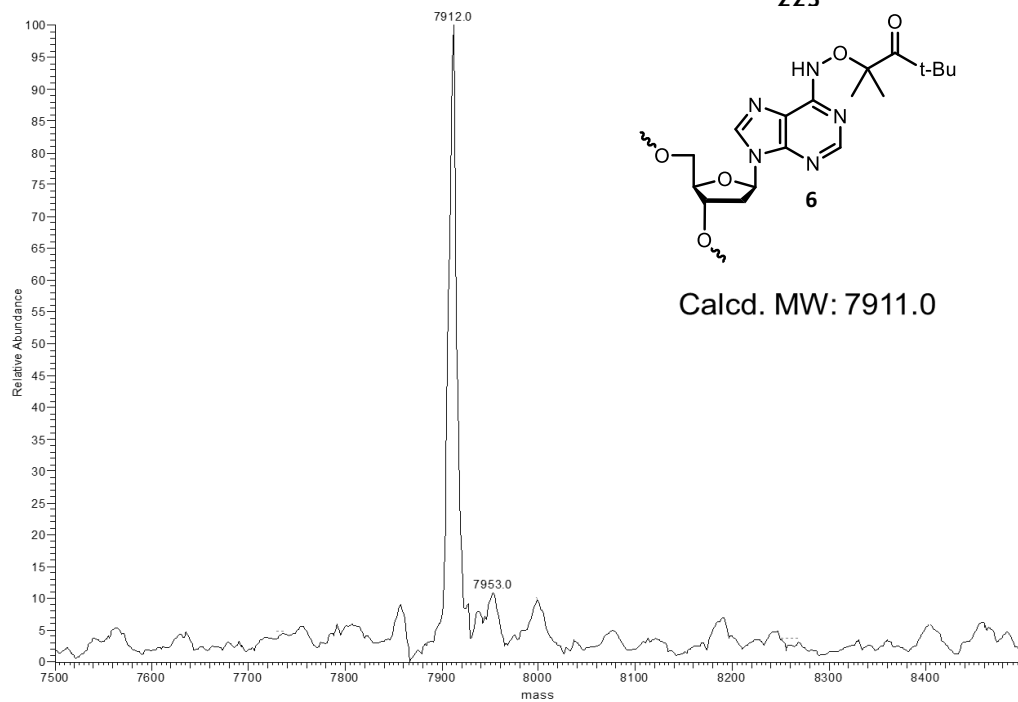
Appendix Figure 122. ESI-MS of the strand of **223** containing **6**.
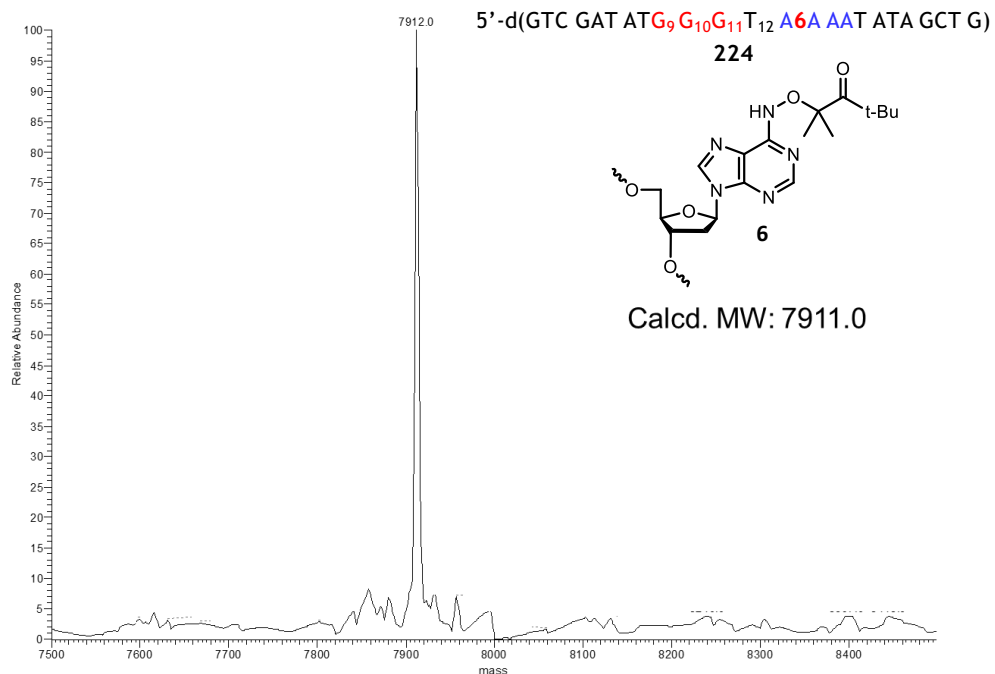
Appendix Figure 123. ESI-MS of the strand of **224** containing **6**.
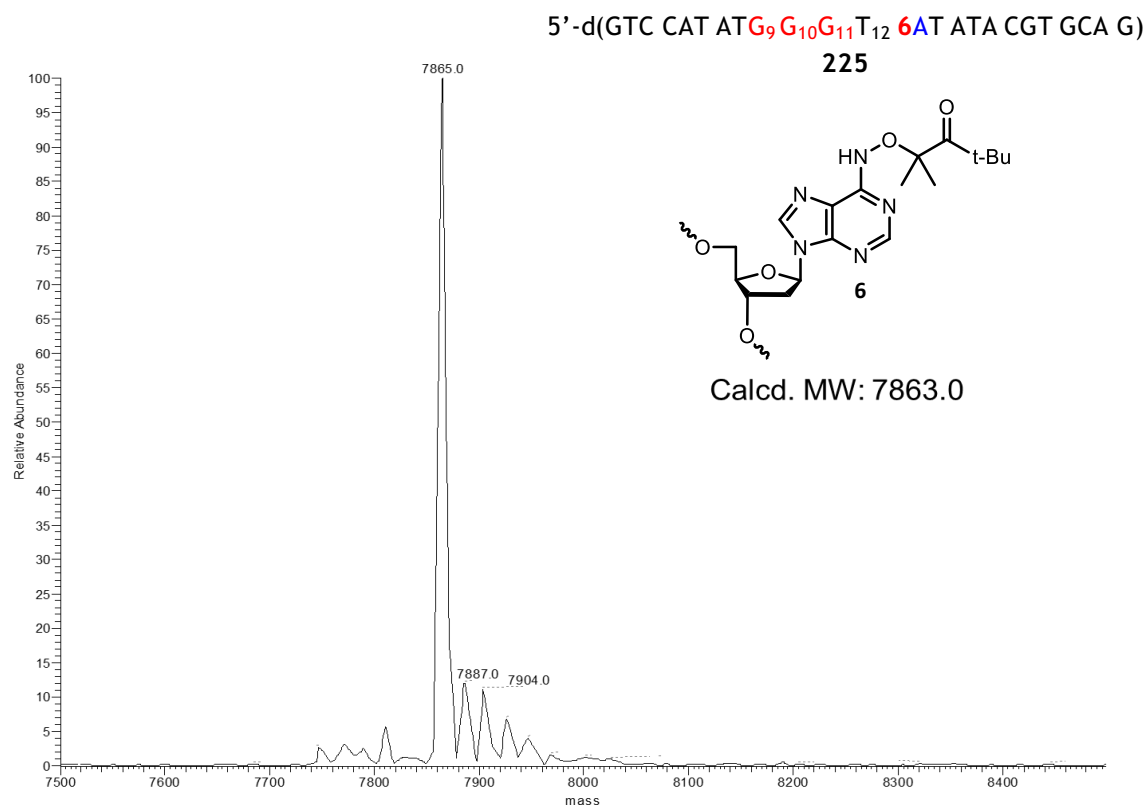
Appendix Figure 124. ESI-MS of the strand of **225** containing **6**.

5'-d(TTT TTT TTT ATA T$_{13}$T$_{14}$**6** TAT ATT TTT TTT TTT)
229

Calcd. m/z = 9251
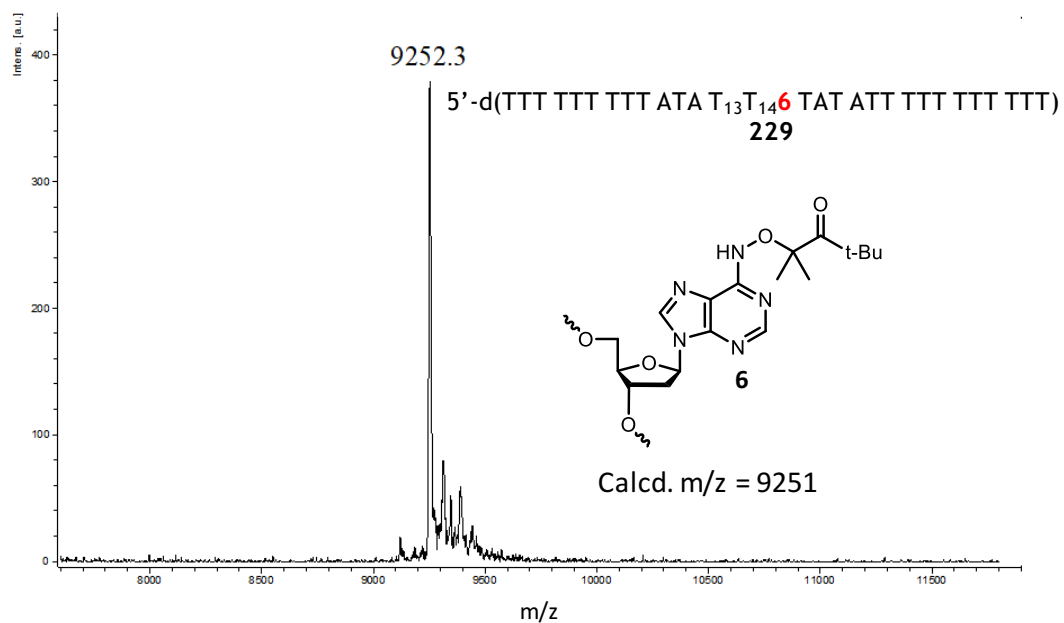
Appendix Figure 125. MALDI-TOF-MS spectrum of the strand of **229** containing **6**.

5'-d(TTT TTT TTT ATA T$_{13}$U$_{14}$**6** TAT ATT TTT TTT TTT)
230

Calcd. m/z = 9237
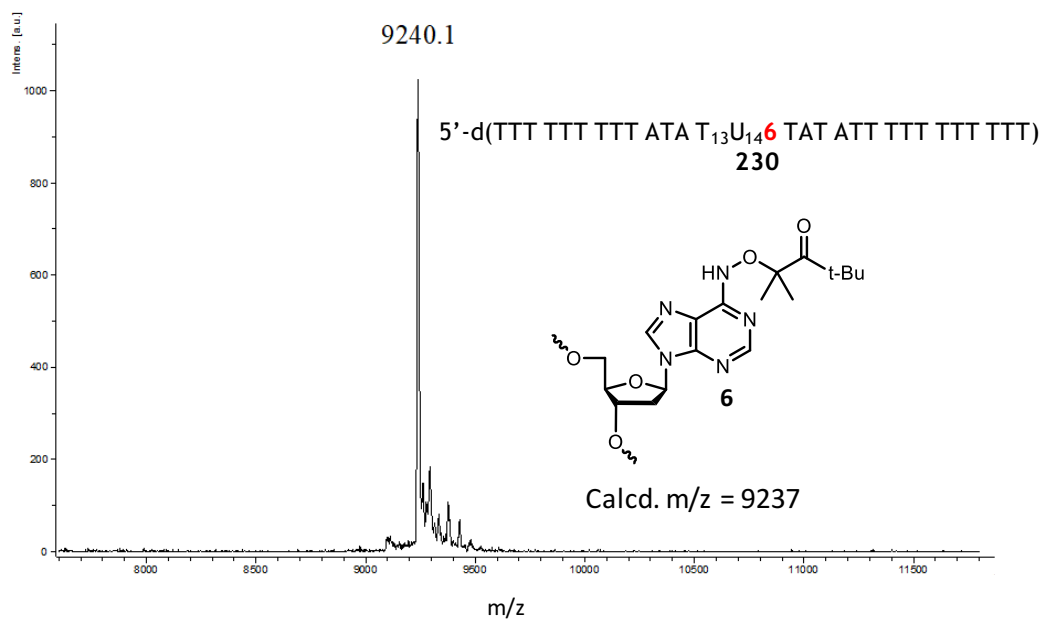
Appendix Figure 126. MALDI-TOF-MS spectrum of the strand of **230** containing **6**.
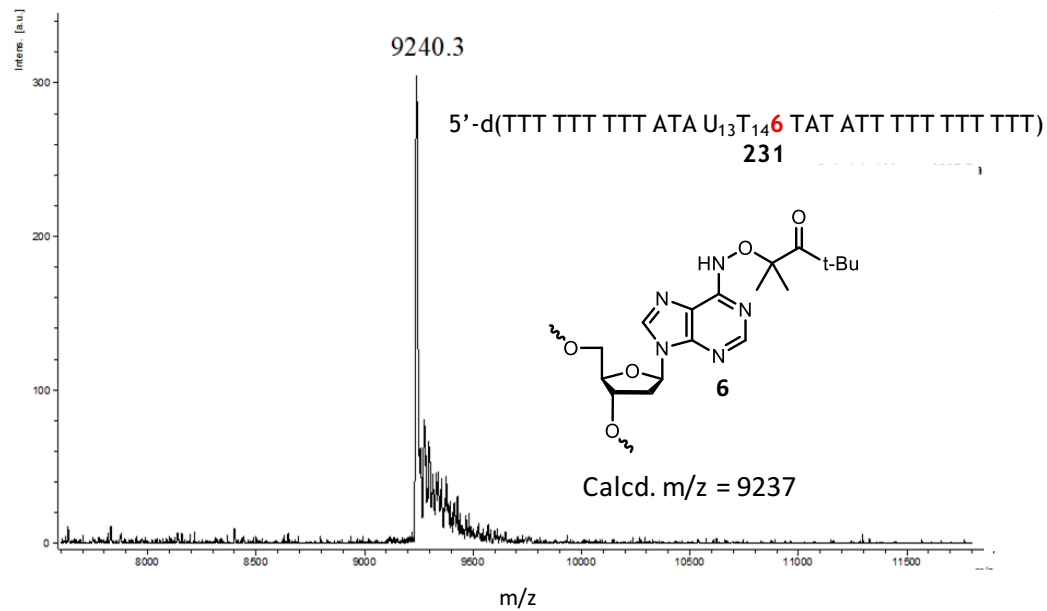
Appendix Figure 127. MALDI-TOF-MS spectrum of the strand of **231** containing **6**.
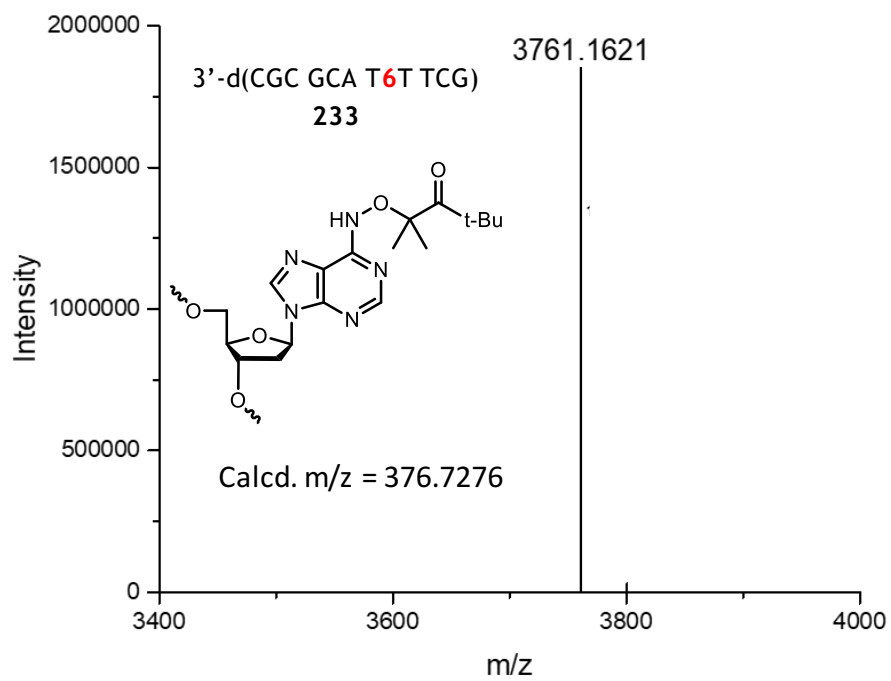
Appendix Figure 128. UPLC-MS spectrum of the strand of **233** containing **6**.
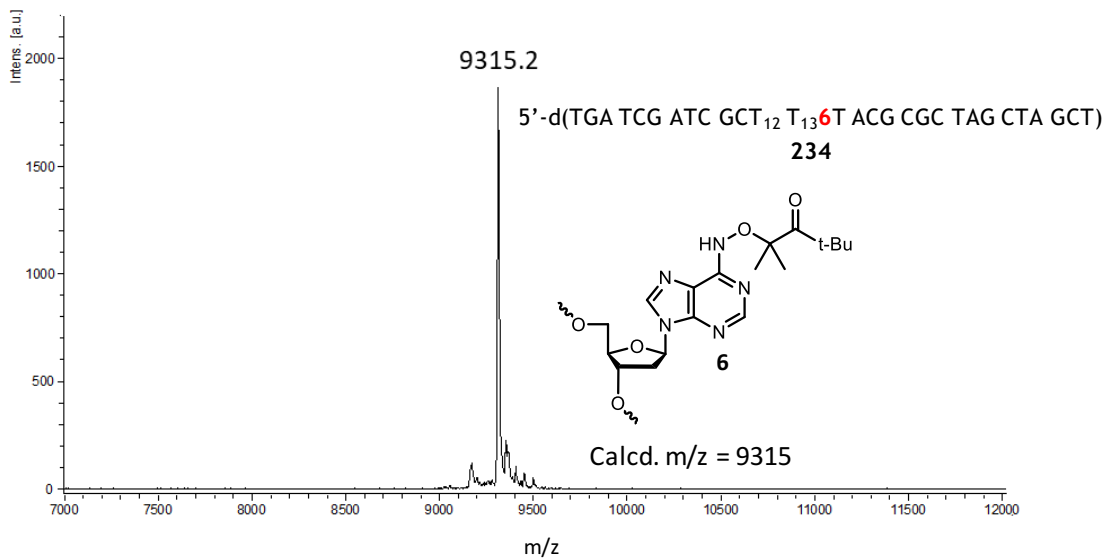
Appendix Figure 129. MALDI-TOF-MS spectrum of the strand of **234** containing **6**.
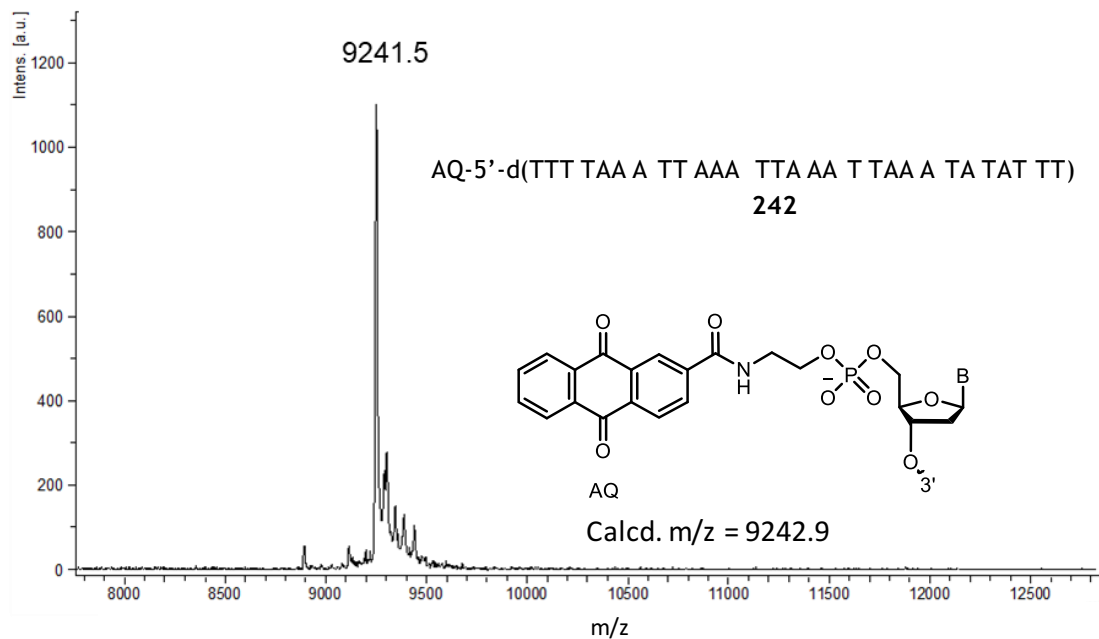
Appendix Figure 130. MALDI-TOF-MS spectrum of the strand of **242** containing **AQ**.
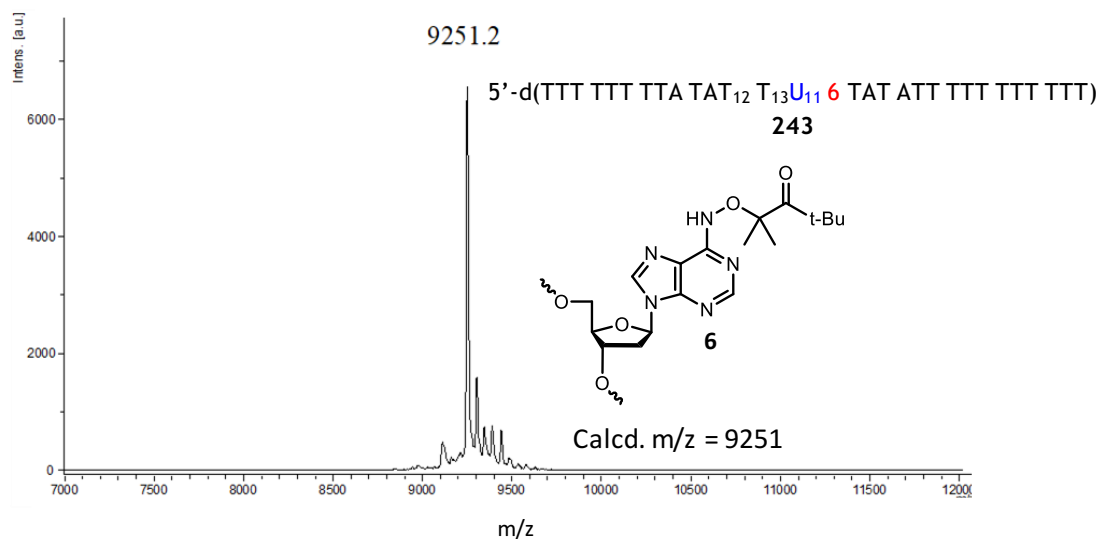
Appendix Figure 131. MALDI-TOF-MS spectrum of the strand of **243** containing **6**.
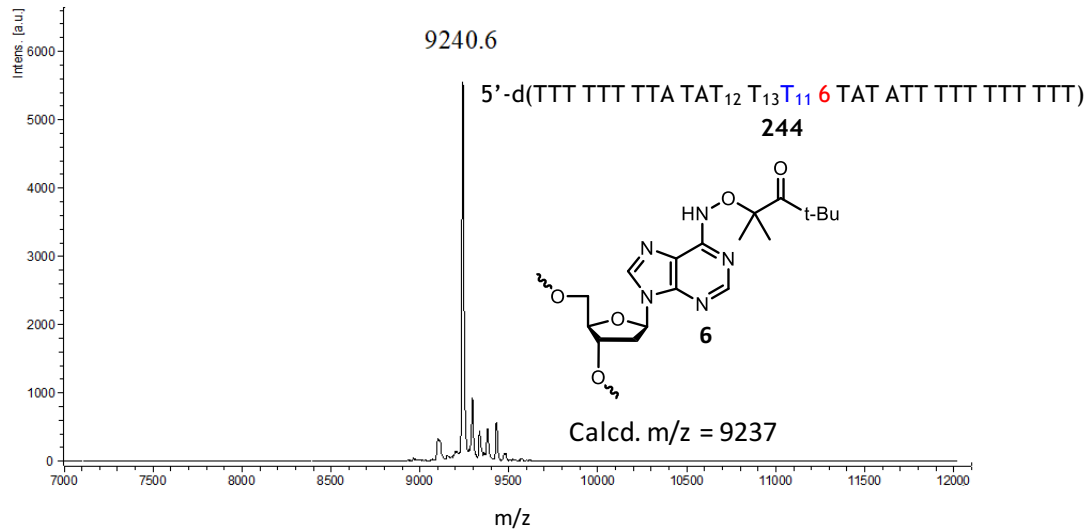
Appendix Figure 132. MALDI-TOF-MS spectrum of the strand of **244** containing **6**.

8.   References

1.   Tubbs, A.; Nussenzweig, A., Endogenous DNA Damage as a Source of Genomic Instability in Cancer. *Cell* **2017,** *168*, 644-656.

2.   von Sonntag, C., *Free-Radical-Induced DNA Damage and Its Repair*. Springer-Verlag: Berlin, 2006.

3.   Galm, U.; Hager, M. H.; Van Lanen, S. G.; Ju, J.; Thorson, J. S.; Shen, B., Antitumor Antibiotics: Bleomycin, Enediynes, and Mitomycin. *Chem. Rev.* **2005,** *105*, 739-758.

4.   Steenken, S.; Jovanovic, S. V., How Easily Oxidizable Is DNA? One-Electron Reduction Potentials of Adenosine and Guanosine Radicals in Aqueous Solution. *J. Am. Chem. Soc.* **1997,** *119*, 617-618.

5.   Steenken, S., Structure, Acid/Base Properties and Transformation Reactions of Purine Radicals. *Free Radic. Res. Commun.* **1989,** *6*, 117-120.

6.   Steenken, S., Purine Bases, Nucleosides, and Nucleotides: Aqueous Solution Redox Chemistry and Transformation Reactions of Their Radical Cations and e- and •OH Adducts. *Chem. Rev.* **1989,** *89*, 503-20.

7.   Candeias, L. P.; Steenken, S., Structure and Acid-Base Properties of One-Electron-Oxidized Deoxyguanosine, Guanosine, and 1-Methylguanosine. *J. Am. Chem. Soc.* **1989,** *111*, 1094-9.

8.   Close, D. M., Calculated pK_a's of the DNA Base Radical Ions. *J. Phys. Chem. A* **2013,** *117*, 473-480.

9.   Candeias, L. P.; Steenken, S., Reaction of Ho· with Guanine Derivatives in Aqueous Solution: Formation of Two Different Redox-Active •OH-Adduct Radicals and Their Unimolecular Transformation Reactions. Properties of G(-H)•. *Chem. - Eur. J.* **2000,** *6*, 475-484.

10.   Vieira, A. J. S. C.; Steenken, S., Pattern of Hydroxy Radical Reaction with Adenine and Its Nucleosides and Nucleotides. Characterization of Two Types of Isomeric Hydroxy Adduct and Their Unimolecular Transformation Reactions. *J. Am. Chem. Soc.* **1990,** *112*, 6986-94.

11.   Giese, B., Long Distance Charge Transport in DNA: The Hopping Mechanism. *Acc. Chem. Res.* **2000,** *33*, 631-636.

12.   Giese, B.; Amaudrut, J.; Kohler, A.-K.; Spormann, M.; Wessely, S., Direct Observation of Hole Transfer through DNA by Hopping between Adenine Bases and by Tunnelling. *Nature* **2001,** *412*, 318-320.

13.   Meggers, E.; Michel-Beyerle, M. E.; Giese, B., Sequence Dependent Long Range Hole Transport in DNA. *J. Am. Chem. Soc.* **1998,** *120*, 12950-12955.

14.   Saito, I.; Nakanura, T.; Nakatani, K.; Yoshioka, Y.; Yamaguchi, K.; Sugiyama, H., Mapping of the Hot Spots for DNA Damage by One-Electron Oxidation: Efficacy of Gg Doublets and Ggg Triplets as a Trap in Long-Range Hole Migration. *J. Am. Chem. Soc.* **1998,** *120*, 12686-12687.

15.   Hall, D. B.; Holmlin, R. E.; Barton, J. K., Oxidative DNA Damage through Long-Range Electron Transfer. *Nature* **1996,** *382*, 731-735.

16.   Genereux, J. C.; Barton, J. K., Mechanisms for DNA Charge Transport. *Chem. Rev.* **2010,** *110*, 1642-1662.

17.   Genereux, J. C.; Wuerth, S. M.; Barton, J. K., Single-Step Charge Transport through DNA over Long Distances. *J. Am. Chem. Soc.* **2011,** *133*, 3863-3868.

18.   Harris, M. A.; Mishra, A. K.; Young, R. M.; Brown, K. E.; Wasielewski, M. R.; Lewis, F. D., Direct Observation of the Hole Carriers in DNA Photoinduced Charge Transport. *J. Am. Chem. Soc.* **2016,** *138*, 5491-5494.

19.   Fujitsuka, M.; Majima, T., Charge Transfer Dynamics in DNA Revealed by Time-Resolved Spectroscopy. *Chem. Sci.* **2017,** *8*, 1752-1762.

20.   Steenken, S., Electron Transfer in DNA? Competition by Ultra-Fast Proton Transfer? *Biol. Chem.* **1997,** *378*, 1293-1297.

21.   Adhikary, A.; Kumar, A.; Khanduri, D.; Sevilla, M. D., Effect of Base Stacking on the Acid−Base Properties of the Adenine Cation Radical [A•+] in Solution: ESR and DFT Studies. *J. Am. Chem. Soc.* **2008,** *130*, 10282-10292.

22.   Kobayashi, K., Evidence of Formation of Adenine Dimer Cation Radical in DNA: The Importance of Adenine Base Stacking. *J. Phys. Chem. B* **2010,** *114*, 5600-5604.

23.   Banyasz, A.; Ketola, T.-M.; Muñoz-Losa, A.; Rishi, S.; Adhikary, A.; Sevilla, M. D.; Martinez-Fernandez, L.; Improta, R.; Markovitsi, D., UV-Induced Adenine Radicals Induced in DNA A-Tracts: Spectral and Dynamical Characterization. *J. Phys. Chem. Lett.* **2016,** *7*, 3949-3953.

24.   Joy, A.; Ghosh, A. K.; Schuster, G. B., One-Electron Oxidation of DNA Oligomers That Lack Guanine: Reaction and Strand Cleavage at Remote Thymines by Long-Distance Radical Cation Hopping. *J. Am. Chem. Soc.* **2006,** *128*, 5346-5347.

25.   Ghosh, A.; Joy, A.; Schuster, G. B.; Douki, T.; Cadet, J., Selective One-Electron Oxidation of Duplex DNA Oligomers: Reaction at Thymines. *Org. Biomol. Chem.* **2008,** *6*, 916-928.

26.   Joseph, J.; Schuster, G. B., One-Electron Oxidation of DNA: Reaction at Thymine. *Chem. Comm.* **2010,** *46*, 7872-7878.

27.   Barnett, R. N.; Joseph, J.; Landman, U.; Schuster, G. B., Oxidative Thymine Mutation in DNA: Water-Wire-Mediated Proton-Coupled Electron Transfer. *J. Am. Chem. Soc.* **2013,** *135*, 3904-3914.

28.   Kanvah, S.; Schuster, G. B., One-Electron Oxidation of DNA: Thymine Versus Guanine Reactivity. *Org. Biomol. Chem.* **2010,** *8*, 1340-1343.

29.   Joy, A.; Ghosh, A. K.; Schuster, G. B., One-Electron Oxidation of DNA Oligomers That Lack Guanine: Reaction and Strand Cleavage at Remote Thymines by Long-Distance Radical Cation Hopping. *J. Am. Chem. Soc.* **2006,** *128*, 5346-5347.

30.   Al-Sheikhly, M., The Reactivity of Adenyl and Guanyl Radicals Towards Oxygen. *Radiat. Phys. Chem.* **1994,** *44*, 297-301.

31.   Rokhlenko, Y.; Geacintov, N. E.; Shafirovich, V., Lifetimes and Reaction Pathways of Guanine Radical Cations and Neutral Guanine Radicals in an Oligonucleotide in Aqueous Solutions. *J. Am. Chem. Soc.* **2012,** *134*, 4955-4962.

32.   Candeias, L. P. S., S., Electron Transfer in Di(deoxy)nucleoside Phosphates in Aqueous Solution: Rapid Migration of Oxidative Damage (via A) to G. *J. Am. Chem. Soc.* **1993,** *115*, 2437-2440.

33.   Bamatraf, M. M. M.; O'Neill, P.; Rao, B. S. M., OH Radical-Induced Charge Migration in Oligodeoxynucleotides. *J. Phys. Chem. B* **2000,** *104*, 636-642.

34.   Kobayashi, K., Evidence of Formation of Adenine Dimer Cation Radical in DNA: The Importance of Adenine Base Stacking. *J. Phys. Chem. B* **2010,** *114*, 5600-5604.

35.	Chatgilialoglu, C.; D'Angelantonio, M.; Guerra, M.; Kaloudis, P.; Mulazzani, Q. G., A Reevaluation of the Ambident Reactivity of the Guanine Moiety Towards Hydroxyl Radicals. *Angew. Chem., Int. Ed.* **2009,** *48*, 2214-2217.

36.	Chatgilialoglu, C.; Caminal, C.; Guerra, M.; Mulazzani, Q. G., Tautomers of One-Electron-Oxidized Guanosine. *Angew. Chem., Int. Ed.* **2005,** *44*, 6030-6032.

37.	Chatgilialoglu, C.; Caminal, C.; Altieri, A.; Vougioukalakis, G. C.; Mulazzani, Q. G.; Gimisis, T.; Guerra, M., Tautomerism in the Guanyl Radical. *J. Am. Chem. Soc.* **2006,** *128*, 13796-13805.

38.	Rokhlenko, Y.; Cadet, J.; Geacintov, N. E.; Shafirovich, V., Mechanistic Aspects of Hydration of Guanine Radical Cations in DNA. *J. Am. Chem. Soc.* **2014,** *136*, 5956-5962.

39.	Kumar, A.; Pottiboyina, V.; Sevilla, M. D., Hydroxyl Radical (OH•) Reaction with Guanine in an Aqueous Environment: A Dft Study. *J. Phys. Chem. B* **2011,** *115*, 15129-15137.

40.	Anderson, R. F.; Shinde, S. S.; Maroz, A., Cytosine-Gated Hole Creation and Transfer in DNA in Aqueous Solution. *J. Am. Chem. Soc.* **2006,** *128*, 15966-15967.

41.	Zheng, L.; Lin, L.; Qu, K.; Adhikary, A.; Sevilla, M. D.; Greenberg, M. M., Independent Photochemical Generation and Reactivity of Nitrogen-Centered Purine Nucleoside Radicals from Hydrazines. *Org. Lett.* **2017,** *19*, 6444-6447.

42.	Zheng, L.; Griesser, M.; Pratt, D. A.; Greenberg, M. M., Aminyl Radical Generation Via Tandem Norrish Type I Photocleavage, β-Fragmentation: Independent

Generation and Reactivity of the 2′-Deoxyadenosin- N6-yl Radical. *J. Org. Chem.* **2017,** *82*, 3571-3580.

43.　　　　Zheng, L.; Greenberg, M. M., Traceless Tandem Lesion Formation in DNA from a Nitrogen-Centered Purine Radical. *J. Am. Chem. Soc.* **2018,** *140*, 6400-6407.

44.　　　　Zheng, L.; Greenberg, M. M., DNA Damage Emanating from a Neutral Purine Radical Reveals the Sequence Dependent Convergence of the Direct and Indirect Effects of γ-Radiolysis. *J. Am. Chem. Soc.* **2017,** *139*, 17751-17754.

45.　　　　Sun, H.; Zheng, L.; Greenberg, M. M., Independent Generation of Reactive Intermediates Leads to an Alternative Mechanism for Strand Damage Induced by Hole Transfer in Poly(dA–T) Sequences. *J. Am. Chem. Soc.* **2018,** *140*, 11308-11316.

46.　　　　Krisch, R. E.; Flick, M. B.; Trumbore, C. N., Radiation Chemical Mechanisms of Single- and Double-Strand Break Formation in Irradiated Sv40 DNA. *Radiat. Res.* **1991,** *126*, 251-259.

47.　　　　Bernhard, W. A.; Purkayastha, S.; Milligan, J. R., Which DNA Damage Is Likely to Be Relevant in Hormetic Responses? *Dose-Response* **2008,** *6*, 184-195.

48.　　　　Wu, L.; Liu, K.; Jie, J.; Song, D.; Su, H., Direct Observation of Guanine Radical Cation Deprotonation in G-Quadruplex DNA. *J. Am. Chem. Soc.* **2015,** *137*, 259-266.

49.　　　　Shafirovich, V.; Dourandin, A.; Huang, W.; Geacintov, N. E., The Carbonate Radical Is a Site-Selective Oxidizing Agent of Guanine in Double-Stranded Oligonucleotides. *J. Biol. Chem.* **2001,** *276*, 24621-24626.

50. Crean, C.; Geacintov, N. E.; Shafirovich, V., Oxidation of Guanine and 8-Oxo-7,8-dihydroguanine by Carbonate Radical Anions: Insight from Oxygen-18 Labeling Experiments. *Angew. Chem. Int. Ed.* **2005,** *44*, 5057-5060.

51. Joffe, A.; Geacintov, N. E.; Shafirovich, V., DNA Lesions Derived from the Site Selective Oxidation of Guanine by Carbonate Radical Anions. *Chem. Res. Toxicol.* **2003,** *16*, 1528-1538.

52. Candeias, L. P.; Steenken, S., Structure and Acid-Base Properties of One-Electron-Oxidized Deoxyguanosine, Guanosine, and 1-Methylguanosine. *J. Am. Chem. Soc.* **1989,** *111*, 1094-1099.

53. Wagner, J. R.; Cadet, J., Oxidation Reactions of Cytosine DNA Components by Hydroxyl Radical and One-Electron Oxidants in Aerated Aqueous Solutions. *Acc. Chem. Res.* **2010,** *43*, 564-571.

54. Decarroz, C.; Wagner, J. R.; Cadet, J., Specific Deprotonation Reactions of the Pyrimidine Radical Cation Resulting from the Menadione Mediated Photosensitization of 2′-Deoxycytidine. *Free Radic. Res. Commun.* **1987,** *2*, 295-301.

55. Decarroz, C.; Wagner, J. R.; Van Lier, J. E.; Krishna, C. M.; Riesz, P.; Cadet, J., Sensitized Photo-Oxidation of Thymidine by 2-Methyl-1,4-naphthoquinone. Characterization of the Stable Photoproducts. *Int. J. Radiat. Biol.* **1986,** *50*, 491-505.

56. Cuquerella, M. C.; Lhiaubet-Vallet, V.; Cadet, J.; Miranda, M. A., Benzophenone Photosensitized DNA Damage. *Acc. Chem. Res.* **2012,** *45*, 1558-1570.

57. Cadet, T. D. J., Modification of DNA Bases by Photosensitized One-Electron Oxidation. *Int. J. Radiat. Biol.* **1999,** *75*, 571-581.

58.   Imlay, J.; Chin, S.; Linn, S., Toxic DNA Damage by Hydrogen Peroxide through the Fenton Reaction in Vivo and in Vitro. *Science* **1988,** *240*, 640-642.

59.   Winterbourn, C. C., Reconciling the Chemistry and Biology of Reactive Oxygen Species. *Nat. Chem. Biol.* **2008,** *4*, 278.

60.   Wagner, J. R.; Van Lier, J. E.; Decarroz, C.; Berger, M.; Cadet, J., [52] Photodynarnic Methods for Oxy Radical-Induced DNA Damage. In *Methods Enzymol.*, Academic Press: 1990; Vol. 186, pp 502-511.

61.   Cooke, M. S.; Evans, M. D.; Dizdaroglu, M.; Lunec, J., Oxidative DNA Damage: Mechanisms, Mutation, and Disease. *FASEB J.* **2003,** *17*, 1195-1214.

62.   Cadet, J.; Delatour, T.; Douki, T.; Gasparutto, D.; Pouget, J.-P.; Ravanat, J.-L.; Sauvaigo, S., Hydroxyl Radicals and DNA Base Damage. *Mutat. Res.* **1999,** *424*, 9-21.

63.   Crespo-Hernández, C. E.; Close, D. M.; Gorb, L.; Leszczynski, J., Determination of Redox Potentials for the Watson−Crick Base Pairs, DNA Nucleosides, and Relevant Nucleoside Analogues. *J. Phys. Chem. B* **2007,** *111*, 5386-5395.

64.   Shinde, S. S.; Maroz, A.; Hay, M. P.; Anderson, R. F., One-Electron Reduction Potential of the Neutral Guanyl Radical in the GC Base Pair of Duplex DNA. *J. Am. Chem. Soc.* **2009,** *131*, 5203-5207.

65.   Lewis, F. D.; Liu, X.; Liu, J.; Hayes, R. T.; Wasielewski, M. R., Dynamics and Equilibria for Oxidation of G, GG, and GGG Sequences in DNA Hairpins. *J. Am. Chem. Soc.* **2000,** *122*, 12037-12038.

66.	Lewis, F. D.; Liu, X.; Liu, J.; Miller, S. E.; Hayes, R. T.; Wasielewski, M. R., Direct Measurement of Hole Transport Dynamics in DNA. *Nature* **2000,** *406*, 51.

67.	Steenken, S., Electron-Transfer-Induced Acidity/Basicity and Reactivity Changes of Purine and Pyrimidine Bases. Consequences of Redox Processes for DNA Base Pairs. *Free Radic. Res. Commun.* **1992,** *16*, 349-379.

68.	Adhikary, A.; Kumar, A.; Munafo, S. A.; Khanduri, D.; Sevilla, M. D., Prototropic Equilibria in DNA Containing One-Electron Oxidized GC: Intra-Duplex Vs. Duplex to Solvent Deprotonation. *Phys. Chem. Chem. Phys.* **2010,** *12*, 5353-5368.

69.	Adhikary, A.; Kumar, A.; Becker, D.; Sevilla, M. D., The Guanine Cation Radical: Investigation of Deprotonation States by ESR and DFT. *J. Phys. Chem. B* **2006,** *110*, 24171-24180.

70.	Adhikary, A.; Khanduri, D.; Sevilla, M. D., Direct Observation of the Hole Protonation State and Hole Localization Site in DNA-Oligomers. *J. Am. Chem. Soc.* **2009,** *131*, 8614-8619.

71.	Kumar, A.; Sevilla, M. D., Cytosine Iminyl Radical (CytN•) Formation Via Electron-Induced Debromination of 5-Bromocytosine: A DFT and Gaussian 4 Study. *J. Phys. Chem. A* **2017,** *121*, 4825-4829.

72.	Kumar, A.; Sevilla, M. D., SOMO–HOMO Level Inversion in Biologically Important Radicals. *J. Phys. Chem. B* **2018,** *122*, 98-105.

73.	Candeias, L. P.; Steenken, S., Reaction of HO• with Guanine Derivatives in Aqueous Solution: Formation of Two Different Redox-Active OH-Adduct Radicals and

Their Unimolecular Transformation Reactions. Properties of G(-H)•. *Chem. Eur. J.* **2000,** *6*, 475-84.

74.   Chatgilialoglu, C.; D'Angelantonio, M.; Kciuk, G.; Bobrowski, K., New Insights into the Reaction Paths of Hydroxyl Radicals with 2′-Deoxyguanosine. *Chem. Res. Toxicol.* **2011,** *24*, 2200-2206.

75.   Adhikary, A.; Kumar, A.; Bishop, C. T.; Wiegand, T. J.; Hindi, R. M.; Adhikary, A.; Sevilla, M. D., π-Radical to σ-Radical Tautomerization in One-Electron-Oxidized 1-Methylcytosine and Its Analogs. *J. Phys. Chem. B* **2015,** *119*, 11496-11505.

76.   Al-Sheikhly, M., The Reactivity of Adenyl and Guanyl Radicals Towards Oxygen. *Radiat. Phys. Chem.* **1994,** *44*, 297-301.

77.   Reynisson, J.; Steenken, S., DFT Calculations on the Electrophilic Reaction with Water of the Guanine and Adenine Radical Cations. A Model for the Situation in DNA. *Phys. Chem. Chem. Phys.* **2002,** *4*, 527-532.

78.   Steenken, S.; Telo, J. P.; Novais, H. M.; Candeias, L. P., One-Electron-Reduction Potentials of Pyrimidine Bases, Nucleosides, and Nucleotides in Aqueous Solution. Consequences for DNA Redox Chemistry. *J. Am. Chem. Soc.* **1992,** *114*, 4701-4709.

79.   Candeias, L. P.; Steenken, S., Electron Transfer in di(deoxy)Nucleoside Phosphates in Aqueous Solution: Rapid Migration of Oxidative Damage (via Adenine) to Guanine. *J. Am. Chem. Soc.* **1993,** *115*, 2437-2440.

80.   Kobayashi, K.; Tagawa, S., Direct Observation of Guanine Radical Cation Deprotonation in Duplex DNA Using Pulse Radiolysis. *J. Am. Chem. Soc.* **2003,** *125*, 10213-10218.

81.   Scheek, R. M.; Stob, S.; Schleich, T.; Alma, N. C. M.; Hilbers, C. W.; Kaptein, R., Photo-CIDNP Study of Adenosine 5'-Monophosphate. Pair-Substitution Effects Due to Cation Radical Deprotonation. *J. Am. Chem. Soc.* **1981,** *103*, 5930-5932.

82.   Kawai, K.; Majima, T., Hole Transfer Kinetics of DNA. *Acc. Chem. Res.* **2013,** *46*, 2616-2625.

83.   Harris, M. A.; Mishra, A. K.; Young, R. M.; Brown, K. E.; Wasielewski, M. R.; Lewis, F. D., Direct Observation of the Hole Carriers in DNA Photoinduced Charge Transport. *J. Am. Chem. Soc.* **2016,** *138*, 5491-5494.

84.   Conwell, E. M., Charge Transport in DNA in Solution: The Role of Polarons. *Proc. Natl. Acad. Sci. U. S. A.* **2005,** *102*, 8795-8799.

85.   Augustyn, K. E.; Genereux, J. C.; Barton, J. K., Distance-Independent DNA Charge Transport across an Adenine Tract. *Angew. Chem. Int. Ed.* **2007,** *46*, 5731-5733.

86.   Shao, F.; O'Neill, M. A.; Barton, J. K., Long-Range Oxidative Damage to Cytosines in Duplex DNA. *Proc. Natl. Acad. Sci. U. S. A.* **2004,** *101*, 17914-17919.

87.   Broom, A. D.; Schweizer, M. P.; Ts'o, P. O. P., Interaction and Association of Bases and Nucleosides in Aqueous Solutions. V. Studies of the Association of Purine Nucleosides by Vapor Pressure Osmometry and by Proton Magnetic Resonance. *J. Am. Chem. Soc.* **1967,** *89*, 3612-3622.

88.   Olsthoorn, C. S. M.; Bostelaar, L. J.; Rooij, J. F. M.; Boom, J. H.; Altona, C., Circular Dichroism Study of Stacking Properties of Oligodeoxyadenylates and Polydeoxyadenylate. *Eur. J. Biochem.* **1981,** *115*, 309-321.

89.   Itahara, T.; Imaizumi, K., Role of Nitrogen Atom in Aromatic Stacking. *J. Phys. Chem. B* **2007,** *111*, 2025-2032.

90.   Kumar, A.; Sevilla, M. D., Density Functional Theory Studies of the Extent of Hole Delocalization in One-Electron Oxidized Adenine and Guanine Base Stacks. *J. Phys. Chem. B* **2011,** *115*, 4990-5000.

91.   Raoul, S.; Bardet, M.; Cadet, J., .Gamma. Irradiation of 2'-Deoxyadenosine in Oxygen-Free Aqueous Solutions: Identification and Conformational Features of Formamidopyrimidine Nucleoside Derivatives. *Chem. Res. Toxicol.* **1995,** *8*, 924-933.

92.   Davies, R. J. H., Bioorganic Photochemistry. Volume 1: Photochemistry and the Nucleic Acids Edited by H. Morrison, John Wiley & Sons, Chichester, 1990. *J. Chem. Technol. Biotechnol.* **1991,** *52*, 587-587.

93.   Frelon, S.; Douki, T.; Cadet, J., Radical Oxidation of the Adenine Moiety of Nucleoside and DNA: 2-Hydroxy-2′-Deoxyadenosine Is a Minor Decomposition Product. *Free Radic. Res.* **2002,** *36*, 499-508.

94.   Bamatraf, M. M. M.; O'Neill, P.; Rao, B. S. M., OH Radical-Induced Charge Migration in Oligodeoxynucleotides. *J. Phys. Chem. B* **2000,** *104*, 636-642.

95.   Chatgilialoglu, C.; D'Angelantonio, M.; Kaloudis, P.; Mulazzani, Q. G.; Guerra, M., One-Electron Reduction of 8-Bromoisoguanosine and 8-Bromoxanthosine in

the Aqueous Phase: Sequential Versus Concerted Proton-Coupled Electron Routes. *J. Phys. Chem. Lett.* **2010,** *1*, 174-177.

96.   Kino, K.; Saito, I.; Sugiyama, H., Product Analysis of GG-Specific Photooxidation of DNA Via Electron Transfer: 2-Aminoimidazolone as a Major Guanine Oxidation Product. *J. Am. Chem. Soc.* **1998,** *120*, 7373-7374.

97.   Cadet, J.; Berger, M.; Buchko, G. W.; Joshi, P. C.; Raoul, S.; Ravanat, J.-L., 2,2-Diamino-4-[(3,5-di-O-acetyl-2-deoxy-β-d-erythro-pentofuranosyl)amino]-5-(2H)-oxazolone: A Novel and Predominant Radical Oxidation Product of 3',5'-Di-O-acetyl-2'-deoxyguanosine. *J. Am. Chem. Soc.* **1994,** *116*, 7403-7404.

98.   Raoul, S.; Berger, M.; Buchko, G. W.; Joshi, P. C.; Morin, B.; Weinfeld, M.; Cadet, J., ^{1}H, ^{13}C and [15]N Nuclear Magnetic Resonance Analysis and Chemical Features of the Two Main Radical Oxidation Products of 2′-Deoxyguanosine: Oxazolone and Imidazolone Nucleosides. *J. Chem. Soc., Perkin Trans. 2* **1996**, 371-381.

99.   Lim, K. S.; Cui, L.; Taghizadeh, K.; Wishnok, J. S.; Chan, W.; DeMott, M. S.; Babu, I. R.; Tannenbaum, S. R.; Dedon, P. C., In Situ Analysis of 8-Oxo-7,8-dihydro-2′-Deoxyguanosine Oxidation Reveals Sequence- and Agent-Specific Damage Spectra. *J. Am. Chem. Soc.* **2012,** *134*, 18053-18064.

100.   Gasparutto, D.; Ravanat, J.-L.; Gérot, O.; Cadet, J., Characterization and Chemical Stability of Photooxidized Oligonucleotides That Contain 2,2-Diamino-4-[(2-deoxy-β-D-erythro-pentofuranosyl)amino]-5(2H)-oxazolone. *J. Am. Chem. Soc.* **1998,** *120*, 10283-10286.

101. Fleming, A. M.; Alshykhly, O.; Zhu, J.; Muller, J. G.; Burrows, C. J., Rates of Chemical Cleavage of DNA and RNA Oligomers Containing Guanine Oxidation Products. *Chem. Res. Toxicol.* **2015,** *28*, 1292-1300.

102. Douki, T.; Spinelli, S.; Ravanat, J.-L.; Cadet, J., Hydroxyl Radical-Induced Degradation of 2′-Deoxyguanosine under Reducing Conditions. *J. Chem. Soc., Perkin Trans. 2* **1999**, 1875-1880.

103. Adam, W.; Kurz, A.; Saha-Möller, C. R., Peroxidase-Catalyzed Oxidative Damage of DNA and 2'-Deoxyguanosine by Model Compounds of Lipid Hydroperoxides: Involvement of Peroxyl Radicals. *Chem. Res. Toxicol.* **2000,** *13*, 1199-1207.

104. Kasai, H.; Yamaizumi, Z.; Berger, M.; Cadet, J., Photosensitized Formation of 7,8-Dihydro-8-oxo-2'-deoxyguanosine (8-Hydroxy-2'-deoxyguanosine) in DNA by Riboflavin: A Nonsinglet Oxygen-Mediated Reaction. *J. Am. Chem. Soc.* **1992,** *114*, 9692-9694.

105. Bernstein, R.; Prat, F.; Foote, C. S., On the Mechanism of DNA Cleavage by Fullerenes Investigated in Model Systems: Electron Transfer from Guanosine and 8-Oxo-Guanosine Derivatives to C60. *J. Am. Chem. Soc.* **1999,** *121*, 464-465.

106. Duarte, V.; Muller, J. G.; Burrows, C. J., Insertion of Dgmp and Damp During in Vitro DNA Synthesis Opposite an Oxidized Form of 7,8-Dihydro-8-oxoguanine. *Nucleic Acids Res.* **1999,** *27*, 496-502.

107. Luo, W.; Muller, J. G.; Rachlin, E. M.; Burrows, C. J., Characterization of Hydantoin Products from One-Electron Oxidation of 8-Oxo-7,8-dihydroguanosine in a Nucleoside Model. *Chem. Res. Toxicol.* **2001,** *14*, 927-938.

108.   Luo, W.; Muller, J. G.; Burrows, C. J., The pH-Dependent Role of Superoxide in Riboflavin-Catalyzed Photooxidation of 8-Oxo-7,8-dihydroguanosine. *Org. Lett.* **2001,** *3*, 2801-2804.

109.   Steenken, S.; Jovanovic, S. V.; Bietti, M.; Bernhard, K., The Trap Depth (in DNA) of 8-Oxo-7,8-dihydro-2'-deoxyguanosine as Derived from Electron-Transfer Equilibria in Aqueous Solution. *J. Am. Chem. Soc.* **2000,** *122*, 2373-2374.

110.   Luo, W.; Muller, J. G.; Rachlin, E. M.; Burrows, C. J., Characterization of Spiroiminodihydantoin as a Product of One-Electron Oxidation of 8-Oxo-7,8-dihydroguanosine. *Org. Lett.* **2000,** *2*, 613-616.

111.   Fleming, A. M.; Muller, J. G.; Dlouhy, A. C.; Burrows, C. J., Structural Context Effects in the Oxidation of 8-Oxo-7,8-dihydro-2′-deoxyguanosine to Hydantoin Products: Electrostatics, Base Stacking, and Base Pairing. *J. Am. Chem. Soc.* **2012,** *134*, 15091-15102.

112.   Ye, Y.; Muller, J. G.; Luo, W.; Mayne, C. L.; Shallop, A. J.; Jones, R. A.; Burrows, C. J., Formation of [13]C-, [15]N-, and ^{18}O-Labeled Guanidinohydantoin from Guanosine Oxidation with Singlet Oxygen. Implications for Structure and Mechanism. *J. Am. Chem. Soc.* **2003,** *125*, 13926-13927.

113.   Fleming, A. M.; Burrows, C. J., G-Quadruplex Folds of the Human Telomere Sequence Alter the Site Reactivity and Reaction Pathway of Guanine Oxidation Compared to Duplex DNA. *Chem. Res. Toxicol.* **2013,** *26*, 593-607.

114.   Eley, D. D.; Leslie, R. B., Conduction in Nucleic Acid Components. *Nature* **1963,** *197*, 898.

115. Murphy, C.; Arkin, M.; Jenkins, Y.; Ghatlia, N.; Bossmann, S.; Turro, N.; Barton, J., Long-Range Photoinduced Electron Transfer through a DNA Helix. *Science* **1993,** *262*, 1025-1029.

116. Giese, B., Long-Distance Electron Transfer through DNA. *Annu. Rev. Biochem.* **2002,** *71*, 51-70.

117. Schuster, G. B., *Long-Range Charge Transfer in DNA, I and Ii*. 2004; Vol. 236.

118. Arnold, Anna R.; Grodick, Michael A.; Barton, Jacqueline K., DNA Charge Transport: From Chemical Principles to the Cell. *Cell Chem. Biol.* **2016,** *23*, 183-197.

119. Kelley, S. O.; Barton, J. K.; Jackson, N. M.; Hill, M. G., Electrochemistry of Methylene Blue Bound to a DNA-Modified Electrode. *Bioconjugate Chem.* **1997,** *8*, 31-37.

120. Boal, A. K.; Barton, J. K., Electrochemical Detection of Lesions in DNA. *Bioconjugate Chem.* **2005,** *16*, 312-321.

121. Gorodetsky, A. A.; Ebrahim, A.; Barton, J. K., Electrical Detection of Tata Binding Protein at DNA-Modified Microelectrodes. *J. Am. Chem. Soc.* **2008,** *130*, 2924-2925.

122. Hall, D. B.; Barton, J. K., Sensitivity of DNA-Mediated Electron Transfer to the Intervening π-Stack: A Probe for the Integrity of the DNA Base Stack. *J. Am. Chem. Soc.* **1997,** *119*, 5045-5046.

123.	O'Brien, E.; Holt, M. E.; Thompson, M. K.; Salay, L. E.; Ehlinger, A. C.; Chazin, W. J.; Barton, J. K., The [4Fe4S] Cluster of Human DNA Primase Functions as a Redox Switch Using DNA Charge Transport. *Science* **2017,** *355*.

124.	Turro, N. J.; Barton, J. K., Paradigms, Supermolecules, Electron Transfer and Chemistry at a Distance. What's the Problem? The Science or the Paradigm? *J. Biol. Inorg. Chem.* **1998,** *3*, 201-209.

125.	Kelley, S. O.; Barton, J. K., Electron Transfer between Bases in Double Helical DNA. *Science* **1999,** *283*, 375-381.

126.	Meggers, E.; Kusch, D.; Spichty, M.; Wille, U.; Giese, B., Electron Transfer through DNA in the Course of Radical-Induced Strand Cleavage. *Angew. Chem. Int. Ed.* **1998,** *37*, 460-462.

127.	Fukui, K.; Tanaka, K., Distance Dependence of Photoinduced Electron Transfer in DNA. *Angew. Chem. Int. Ed.* **1998,** *37*, 158-161.

128.	Brun, A. M.; Harriman, A., Dynamics of Electron Transfer between Intercalated Polycyclic Molecules: Effect of Interspersed Bases. *J. Am. Chem. Soc.* **1992,** *114*, 3656-3660.

129.	Lewis, F. D.; Wu, T.; Zhang, Y.; Letsinger, R. L.; Greenfield, S. R.; Wasielewski, M. R., Distance-Dependent Electron Transfer in DNA Hairpins. *Science* **1997,** *277*, 673-676.

130.	Giese, B.; Spichty, M., Long Distance Charge Transport through DNA: Quantification and Extension of the Hopping Model. *ChemPhysChem* **2000,** *1*, 195-198.

131.		Ly, D.; Sanii, L.; Schuster, G. B., Mechanism of Charge Transport in DNA: Internally-Linked Anthraquinone Conjugates Support Phonon-Assisted Polaron Hopping. *J. Am. Chem. Soc.* **1999,** *121*, 9400-9410.

132.		Lewis, F. D.; Letsinger, R. L.; Wasielewski, M. R., Dynamics of Photoinduced Charge Transfer and Hole Transport in Synthetic DNA Hairpins. *Acc. Chem. Res.* **2001,** *34*, 159-170.

133.		Bixon, M.; Giese, B.; Wessely, S.; Langenbacher, T.; Michel-Beyerle, M. E.; Jortner, J., Long-Range Charge Hopping in DNA. *Proc. Natl. Acad. Sci. U. S. A.* **1999,** *96*, 11713-11716.

134.		Jortner, J.; Bixon, M.; Langenbacher, T.; Michel-Beyerle, M. E., Charge Transfer and Transport in DNA. *Proc. Natl. Acad. Sci. U. S. A.* **1998,** *95*, 12759-12765.

135.		Sartor, V.; Boone, E.; Schuster, G. B., Long-Distance Radical Cation Migration through A/T Base Pairs in DNA: An Experimental Test of Theory. *J. Phys. Chem. B* **2001,** *105*, 11057-11059.

136.		Yoo, J.; Delaney, S.; Stemp, E. D. A.; Barton, J. K., Rapid Radical Formation by DNA Charge Transport through Sequences Lacking Intervening Guanines. *J. Am. Chem. Soc.* **2003,** *125*, 6640-6641.

137.		Kendrick, T.; Giese, B., Charge Transfer through DNA Triggered by Site Selective Charge Injection into Adenine. *Chem. Commun.* **2002**, 2016-2017.

138.		Jortner, J.; Bixon, M.; Voityuk, A. A.; Rösch, N., Superexchange Mediated Charge Hopping in DNA. *J. Phys. Chem. A* **2002,** *106*, 7599-7606.

139.		Giese, B.; Wessely, S., The Influence of Mismatches on Long-Distance Charge Transport through DNA. *Angew. Chem. Int. Ed.* **2000,** *39*, 3490-3491.

140.		Bixon, M.; Jortner, J., Charge Transport in DNA Via Thermally Induced Hopping. *J. Am. Chem. Soc.* **2001,** *123*, 12556-12567.

141.		Conwell, E. M.; Park, J. H.; Choi, H. Y., Polarons in DNA: Transition from Guanine to Adenine Transport. *J. Phys. Chem. B* **2005,** *109*, 9760-9763.

142.		Yoshioka, Y.; Kitagawa, Y.; Takano, Y.; Yamaguchi, K.; Nakamura, T.; Saito, I., Experimental and Theoretical Studies on the Selectivity of GGG Triplets toward One-Electron Oxidation in B-Form DNA. *J. Am. Chem. Soc.* **1999,** *121*, 8712-8719.

143.		Hall, D. B.; Holmlin, R. E.; Barton, J. K., Oxidative DNA Damage through Long-Range Electron Transfer. *Nature* **1996,** *382*, 731.

144.		Gasper, S. M.; Schuster, G. B., Intramolecular Photoinduced Electron Transfer to Anthraquinones Linked to Duplex DNA: The Effect of Gaps and Traps on Long-Range Radical Cation Migration. *J. Am. Chem. Soc.* **1997,** *119*, 12762-12771.

145.		Hada, M.; Georgakilas, A. G., Formation of Clustered DNA Damage after High-LET Irradiation: A Review. *J. Radiat. Res.* **2008,** *49*, 203-210.

146.		Sage, E.; Harrison, L., Clustered DNA Lesion Repair in Eukaryotes: Relevance to Mutagenesis and Cell Survival. *Mutat. Res.* **2011,** *711*, 123-133.

147.		Dizdaroglu, M.; Jaruga, P., Mechanisms of Free Radical-Induced Damage to DNA. *Free Radic. Res.* **2012,** *46*, 382-419.

148.   Box, H. C.; Budzinski, E. E.; Freund, H. G.; Evans, M. S.; Patrzyc, H. B.; Wallace, J. C.; Maccubbin, A. E., Vicinal Lesions in X-Irradiated DNA? *Int. J. Radiat. Biol.* **1993,** *64*, 261-263.

149.   Douki, T.; Rivière, J.; Cadet, J., DNA Tandem Lesions Containing 8-Oxo-7,8-dihydroguanine and Formamido Residues Arise from Intramolecular Addition of Thymine Peroxyl Radical to Guanine. *Chem. Res. Toxicol.* **2002,** *15*, 445-454.

150.   Bourdat, A.-G.; Douki, T.; Frelon, S.; Gasparutto, D.; Cadet, J., Tandem Base Lesions Are Generated by Hydroxyl Radical within Isolated DNA in Aerated Aqueous Solution. *J. Am. Chem. Soc.* **2000,** *122*, 4549-4556.

151.   Yuan, B.; Jiang, Y.; Wang, Y.; Wang, Y., Efficient Formation of the Tandem Thymine Glycol/8-Oxo-7,8-dihydroguanine Lesion in Isolated DNA and the Mutagenic and Cytotoxic Properties of the Tandem Lesions in Escherichia Coli Cells. *Chem. Res. Toxicol.* **2010,** *23*, 11-19.

152.   Yun, B. H.; Geacintov, N. E.; Shafirovich, V., Generation of Guanine–Thymidine Cross-Links in DNA by Peroxynitrite/Carbon Dioxide. *Chem. Res. Toxicol.* **2011,** *24*, 1144-1152.

153.   Crean, C.; Uvaydov, Y.; Geacintov, N. E.; Shafirovich, V., Oxidation of Single-Stranded Oligonucleotides by Carbonate Radical Anions: Generating Intrastrand Cross-Links between Guanine and Thymine Bases Separated by Cytosines. *Nucleic Acids Res.* **2008,** *36*, 742-755.

154.   Madugundu, G. S.; Wagner, J. R.; Cadet, J.; Kropachev, K.; Yun, B. H.; Geacintov, N. E.; Shafirovich, V., Generation of Guanine–Thymine Cross-Links in Human Cells by One-Electron Oxidation Mechanisms. *Chem. Res. Toxicol.* **2013,** *26*, 1031-1033.

155.   Jiang, Y.; Hong, H.; Cao, H.; Wang, Y., In Vivo Formation and in Vitro Replication of a Guanine−Thymine Intrastrand Cross-Link Lesion. *Biochemistry* **2007,** *46*, 12757-12763.

156.   Bellon, S.; Ravanat, J.-L.; Gasparutto, D.; Cadet, J., Cross-Linked Thymine-Purine Base Tandem Lesions: Synthesis, Characterization, and Measurement in γ-Irradiated Isolated DNA. *Chem. Res. Toxicol.* **2002,** *15*, 598-606.

157.   Hong, H.; Cao, H.; Wang, Y.; Wang, Y., Identification and Quantification of a Guanine−Thymine Intrastrand Cross-Link Lesion Induced by Cu(II)/H_2O_2/Ascorbate. *Chem. Res. Toxicol.* **2006,** *19*, 614-621.

158.   Okonogi, T. M.; Alley, S. C.; Reese, A. W.; Hopkins, P. B.; Robinson, B. H., Sequence-Dependent Dynamics of Duplex DNA: The Applicability of a Dinucleotide Model. *Biophys. J.* **2002,** *83*, 3446-3459.

159.   Jones, M. J.; Moad, G.; Rizzardo, E.; Solomon, D. H., The Philicity of Tert-Butoxy Radicals. What Factors Are Important in Determining the Rate and Regiospecificity of Tert-Butoxy Radical Addition to Olefins? *J. Org. Chem.* **1989,** *54*, 1607-1611.

160.   Francisco, C. G.; Freire, R.; Herrera, A. J.; Peréz-Martín, I.; Suárez, E., Intramolecular 1,5- Versus 1,6-Hydrogen Abstraction Reaction Promoted by Alkoxy Radicals in Carbohydrate Models. *Org. Lett.* **2002,** *4*, 1959-1961.

161.   Beckwith, A. L. J.; Hay, B. P., Generation of Alkoxy Radicals from N-Alkoxypyridinethiones. *J. Am. Chem. Soc.* **1988,** *110*, 4415-4416.

162.   Hartung, J.; Kneuer, R.; Schwarz, M.; Svoboda, I.; Fueß, H., On the Selective O-Alkylation of Ambident Nucleophiles – the Synthesis of Thiohydroxamic Acid O-Esters by Phase-Transfer Reactions. *Eur. J. Org. Chem.* **1999,** *1999*, 97-106.

163.   Hartung, J.; Hiller, M.; Schmidt, P., Photoreactions of Phenyl-Substituted N-(Pent-4-enyl-1-oxy)pyridine-2(1H)-Thiones. *Chem. - Eur. J.* **1996,** *2*, 1014-1023.

164.   Aveline, B. M.; Kochevar, I. E.; Redmond, R. W., Photochemistry of N-Hydroxy-2(1H)-pyridone, a More Selective Source of Hydroxyl Radicals Than N-Hydroxypyridine-2(1H)-thione. *J. Am. Chem. Soc.* **1996,** *118*, 10124-10133.

165.   Gardner, J. N.; Katritzky, A. R., 875. N-Oxides and Related Compounds. Part V. The Tautomerism of 2- and 4-Amino- and -Hydroxy-pyridine 1-Oxide. *J. Chem. Soc.* **1957**, 4375-4385.

166.   Hartung, J.; Schwarz, M.; Svoboda, I.; Fuess, H.; Duarte, M. T., A New Generation of Alkoxyl Radical Precursors – Preparation and Properties of N-(Alkoxy)-4-arylthiazole-2(3H)-thiones. *Eur. J. Org. Chem.* **1999,** *1999*, 1275-1290.

167.   Adam, W.; Hartung, J.; Okamoto, H.; Saha-Möller, C. R.; Špehar, K., N-Hydroxy-4-(4-chlorophenyl)thiazole-2(3H)-thione as a Photochemical Hydroxyl-Radical Source: Photochemistry and Oxidative Damage of DNA (Strand Breaks) and 2′-Deoxyguanosine (8-Oxodg Formation)¶. *Photochem. Photobiol.* **2000,** *72*, 619-624.

168.   Adam, W.; Hartung, J.; Okamoto, H.; Marquardt, S.; Nau, W. M.; Pischel, U.; Saha-Möller, C. R.; Špehar, K., Photochemistry of N-Isopropoxy-substituted 2(1H)-

pyridone and 4-*p*-Tolylthiazole-2(3H)-thione: Alkoxyl-radical Release (Spin-Trapping, Epr, and Transient Spectroscopy) and Its Significance in the Photooxidative Induction of DNA Strand Breaks. *J. Org. Chem.* **2002,** *67*, 6041-6049.

169.	Lipczynska-Kochany, E., Photochemistry of Hydroxamic Acids and Derivatives. *Chem. Rev.* **1991,** *91*, 477-491.

170.	Pratsch, G.; Lackner, G. L.; Overman, L. E., Constructing Quaternary Carbons from N-(Acyloxy)phthalimide Precursors of Tertiary Radicals Using Visible-Light Photocatalysis. *J. Org. Chem.* **2015,** *80*, 6025-6036.

171.	Malval, J.-P.; Suzuki, S.; Morlet-Savary, F.; Allonas, X.; Fouassier, J.-P.; Takahara, S.; Yamaoka, T., Photochemistry of Naphthalimide Photoacid Generators. *J. Phys. Chem. A* **2008,** *112*, 3879-3885.

172.	Malval, J.-P.; Morlet-Savary, F.; Allonas, X.; Fouassier, J.-P.; Suzuki, S.; Takahara, S.; Yamaoka, T., On the Cleavage Process of the N-Trifluoromethylsulfonyloxy-1,8-naphthalimide Photoacid Generator. *Chem. Phys. Lett.* **2007,** *443*, 323-327.

173.	Choi, G. J.; Zhu, Q.; Miller, D. C.; Gu, C. J.; Knowles, R. R., Catalytic Alkylation of Remote C–H Bonds Enabled by Proton-Coupled Electron Transfer. *Nature* **2016,** *539*, 268.

174.	McBurney, R. T.; Walton, J. C., Dissociation or Cyclization: Options for a Triad of Radicals Released from Oxime Carbamates. *J. Am. Chem. Soc.* **2013,** *135*, 7349-7354.

175.   Walton, J. C., The Oxime Portmanteau Motif: Released Heteroradicals Undergo Incisive EPR Interrogation and Deliver Diverse Heterocycles. *Acc. Chem. Res.* **2014,** *47*, 1406-1416.

176.   Kärkäs, M. D., Photochemical Generation of Nitrogen-Centered Amidyl, Hydrazonyl, and Imidyl Radicals: Methodology Developments and Catalytic Applications. *ACS Catalysis* **2017,** *7*, 4999-5022.

177.   Zard, S. Z., Recent Progress in the Generation and Use of Nitrogen-centred Radicals. *Chem. Soc. Rev.* **2008,** *37*, 1603-1618.

178.   Newcomb, M.; Marquardt, D. J.; Deeb, T. M., N-Hydroxypyridine-2-thione Carbamates. V. Syntheses of Alkaloid Skeletons by Aminium Cation Radical Cyclizations. *Tetrahedron* **1990,** *46*, 2329-2344.

179.   Newcomb, M.; Musa, O. M.; Martinez, F. N.; Horner, J. H., Kinetics of 5-Exo Cyclizations of N-Alkyl-4-pentenaminyl Radicals and β-Fragmentations of β-(Dialkylamino)alkyl Radicals. *J. Am. Chem. Soc.* **1997,** *119*, 4569-4577.

180.   Boivin, J.; Fouquet, E.; Schiano, A.-M.; Zard, S. Z., Iminyl Radicals: Part III. Further Synthetically Useful Sources of Iminyl Radicals. *Tetrahedron* **1994,** *50*, 1769-1776.

181.   Wu, M.; Begley, T. P., B-Scission of the N-O Bond in Alkylhydroxamate Radicals: A Fast Radical Trap. *Org. Lett.* **2000,** *2*, 1345-1348.

182.   Siskos, M. G.; Zarkadis, A. K.; Steenken, S.; Karakostas, N.; Garas, S. K., Photodissociation of N-(Triphenylmethyl)anilines: A Laser Flash Photolysis, ESR, and Product Analysis Study. *J. Org. Chem.* **1998,** *63*, 3251-3259.

183.		Hirata, Y.; Ohta, M.; Okada, T.; Mataga, N., Direct Observation of Photodissociation of Tetraphenylhydrazine and Its Derivatives in the Solution Phase: Picosecond Study of Nitrogen-Nitrogen Bond Rupture in the Fluorescence State. *J. Phys. Chem* **1992,** *96*, 1517-1520.

184.		Giese, B.; Beyrich-Graf, X.; Erdmann, P.; Giraud, L.; Imwinkelried, P.; Mueller, S. N.; Schwitter, U., Cleavage of Single-stranded 4'-Oligonucleotide Radicals in the Presence of O_2. *J. Am. Chem. Soc.* **1995,** *117*, 6146-6147.

185.		Barvian, M. R.; Greenberg, M. M., Independent Generation of 5,6-Dihydrothymid-5-yl and Investigation of Its Ability to Effect Nucleic Acid Strand Scission Via Hydrogen Atom Abstraction. *J. Org. Chem.* **1995,** *60*, 1916-1917.

186.		Vollenweider, J.-K.; Paul, H., On the Rates of Decarbonylation of Hydroxyacetyl and Other Acyl Radicals. *Int. J. Chem. Kinet.* **1986,** *18*, 791-800.

187.		Giese, B., Hole Injection and Hole Transfer through DNA: The Hopping Mechanism. In *Long-Range Charge Transfer in DNA I*, Schuster, G. B., Ed. Springer Berlin Heidelberg: Berlin, Heidelberg, 2004; pp 27-44.

188.		Vrantza, D.; Kaloudis, P.; Leondiadis, L.; Gimisis, T.; Vougioukalakis, G. C.; Orfanopoulos, M.; Gasparutto, D.; Cadet, J.; Encinas, S.; Paris, C.; Miranda, M. A., Modification of Guanine with Photolabile N-Hydroxypyridine-2(1H)-thione: Monomer Synthesis, Oligonucleotide Elaboration, and Photochemical Studies. *Helv. Chim. Acta* **2006,** *89*, 2371-2386.

189.		Kaloudis, P.; Paris, C.; Vrantza, D.; Encinas, S.; Perez-Ruiz, R.; Miranda, M. A.; Gimisis, T., Photolabile N-Hydroxypyrid-2(1H)-one Derivatives of Guanine

Nucleosides: A New Method for Independent Guanine Radical Generation. *Org. Biomol. Chem.* **2009,** *7*, 4965-4972.

190.   Nakatani, K.; Dohno, C.; Saito, I., Design of a Hole-Trapping Nucleobase: Termination of DNA-Mediated Hole Transport at N2-Cyclopropyldeoxyguanosine. *J. Am. Chem. Soc.* **2001,** *123*, 9681-9682.

191.   Kuttappan-Nair, V.; Samson-Thibault, F.; Wagner, J. R., Generation of 2 '-Deoxyadenosine N(6)-Aminyl Radicals from the Photolysis of Phenylhydrazone Derivatives. *Chem. Res. Toxicol.* **2010,** *23*, 48-54.

192.   Raoul, S.; Bardet, M.; Cadet, J., Gamma-Irradiation of 2'-Deoxyadenosine in Oxygen-Free Aqueous-Solutionssidentification and

Conformational Features of Formamidopyrimidine Nucleoside Derivatives. *Chem. Res. Toxicol.* **1995,** *8*, 924-933.

193.   Siskos, M. G.; Zarkadis, A. K.; Steenken, S.; Karakostas, N., Photodissociation of N-Arylmethylanilines: A Laser Flash Photolysis, Fluorescence, and Product Analysis Study1. *J. Org. Chem.* **1999,** *64*, 1925-1931.

194.   Masajiro, K.; Kikuko, T.; Takayo, O.; Hiroyoshi, K., The Synthesis of C-Methyl Branched-chain Deoxy Sugar Nucleosides by the Deoxygenative Methylation of O-Tosylated Adenosines with Grignard Reagents. *Bull. Chem. Soc. Jpn.* **1988,** *61*, 2437-2442.

195.   Maggio, A.-F.; Lucas, M.; Barascut, J.-L.; Imbach, J.-L., Synthese Regiospecifique D'un Dinucleoside Ponte : (O6-Desoxyguanosinyl)-1 (N4-desoxycytidyl)-2 ethane. *Tetrahedron Lett.* **1984,** *25*, 3195-3198.

196.   Luo, Y.-R.; Luo, Y.-R., *Comprehensive Handbook of Chemical Bond Energies*. CRC Press: Boca Raton, 2007.

197.   Michl, J.; Bonacic-Koutecký, V., *Electronic Aspects of Organic Photochemistry*. Wiley: New York, 1990.

198.   Michl, J., Relationship of Bonding to Electronic Spectra. Comments. *Acc. Chem. Res.* **1990,** *23*, 127-128.

199.   Zheng, Y.; Zheng, W.; Wang, J.; Chang, H.; Zhu, D., Computational Study on N–N Homolytic Bond Dissociation Enthalpies of Hydrazine Derivatives. *J. Phys. Chem. A* **2018,** *122*, 2764-2780.

200.   Bae, S.; Lakshman, M. K., O6-(Benzotriazol-1-yl)inosine Derivatives: Easily Synthesized, Reactive Nucleosides. *J. Am. Chem. Soc.* **2007,** *129*, 782-789.

201.   Hirata, Y.; Niga, Y.; Ohta, M.; Takizawa, M.; Okada, T., Photodissociation and Geminate Dynamics in Solution Phase: Picosecond Transient Absorption Studies of Tetraphenylhydrazines and Diphenyl Disulfides. *Res. Chem. Intermed.* **1995,** *21*, 823-36.

202.   Lenderink, E.; Duppen, K.; Wiersma, D. A., Femtosecond Fragmentation of Tetraphenylhydrazine in Solution. *Chem. Phys. Lett.* **1992,** *194*, 403-9.

203.   Hyde, M. G.; Reid, G. D.; Beddard, G. S., Picosecond Photodissociation of Tetraphenylhydrazine. *Chem. Phys. Lett.* **1992,** *190*, 130-4.

204.   Neugebauer, F. A.; Bamberger, S., Aminyls. 7. Diarylaminyls. *Chem. Ber.* **1974,** *107*, 2362-82.

205.   Pratt, D. A.; DiLabio, G. A.; Valgimigli, L.; Pedulli, G. F.; Ingold, K. U., Substituent Effects on the Bond Dissociation Enthalpies of Aromatic Amines. *J. Am. Chem. Soc.* **2002,** *124*, 11085-11092.

206.   Ingold, K. U.; Pratt, D. A., Advances in Radical-Trapping Antioxidant Chemistry in the 21st Century: A Kinetics and Mechanisms Perspective. *Chem. Rev.* **2014,** *114*, 9022-9046.

207.   Kolarski, D.; Szymanski, W.; Feringa, B. L., Two-Step, One-Pot Synthesis of Visible-Light-Responsive 6-Azopurines. *Org. Lett.* **2017,** *19*, 5090-5093.

208.   Too, K.; Brown, D. M.; Bongard, E.; Yardley, V.; Vivas, L.; Loakes, D., Anti-Malarial Activity of N6-Modified Purine Analogues. *Bioorg. Med. Chem.* **2007,** *15*, 5551-5562.

209.   Nair, V.; Richardson, S. G., Utility of Purinyl Radicals in the Synthesis of Base-Modified Nucleosides and Alkylpurines: 6-Amino Group Replacement by Hydrogen, Chlorine, Bromine, and Iodine. *J. Org. Chem.* **1980,** *45*, 3969-3974.

210.   Veliz, E. A.; Beal, P. A., 6-Bromopurine Nucleosides as Reagents for Nucleoside Analogue Synthesis. *J. Org. Chem.* **2001,** *66*, 8592-8598.

211.   Lakshman, M. K.; Ngassa, F. N.; Keeler, J. C.; Dinh, Y. Q. V.; Hilmer, J. H.; Russon, L. M., Facile Synthesis of O6-Alkyl-, O6-Aryl-, and Diaminopurine Nucleosides from 2'-Deoxyguanosine. *Org. Lett.* **2000,** *2*, 927-930.

212.   Wolfe, J. P.; Wagaw, S.; Marcoux, J.-F.; Buchwald, S. L., Rational Development of Practical Catalysts for Aromatic Carbon−Nitrogen Bond Formation. *Acc. Chem. Res.* **1998,** *31*, 805-818.

213.　　　　Hartwig, J. F., Carbon−Heteroatom Bond-Forming Reductive Eliminations of Amines, Ethers, and Sulfides. *Acc. Chem. Res.* **1998,** *31*, 852-860.

214.　　　　Lakshman, M. K.; Hilmer, J. H.; Martin, J. Q.; Keeler, J. C.; Dinh, Y. Q. V.; Ngassa, F. N.; Russon, L. M., Palladium Catalysis for the Synthesis of Hydrophobic C-6 and C-2 Aryl 2'-Deoxynucleosides. Comparison of C-C Versus C-N Bond Formation as well as C-6 Versus C-2 Reactivity. *J. Am. Chem Soc.* **2001,** *123*, 7779-7787.

215.　　　　Lakshman, M. K.; Keeler, J. C.; Hilmer, J. H.; Martin, J. Q., Palladium-Catalyzed C-N Bond Formation: Facile and General Synthesis of N6-Aryl 2'-deoxyadenosine Analogues. *J. Am. Chem Soc.* **1999,** *121*, 6090-6091.

216.　　　　Zhang, Y.; Lavigne, G.; César, V., Buchwald–Hartwig Amination of (Hetero)Aryl Tosylates Using a Well-Defined N-Heterocyclic Carbene/Palladium(II) Precatalyst. *J. Org. Chem.* **2015,** *80*, 7666-7673.

217.　　　　DeAngelis, A.; Wang, D.-H.; Buchwald, S. L., Mild and Rapid Pd-Catalyzed Cross-Coupling with Hydrazine in Continuous Flow: Application to the Synthesis of Functionalized Heterocycles. *Angew. Chem. Int. Ed.* **2013,** *52*, 3434-3437.

218.　　　　Wolfe, J. P.; Buchwald, S. L., Scope and Limitations of the Pd/BINAP-Catalyzed Amination of Aryl Bromides. *J. Org. Chem.* **2000,** *65*, 1144-1157.

219.　　　　Fujita, K.-i.; Yamashita, M.; Puschmann, F.; Alvarez-Falcon, M. M.; Incarvito, C. D.; Hartwig, J. F., Organometallic Chemistry of Amidate Complexes. Accelerating Effect of Bidentate Ligands on the Reductive Elimination of N-Aryl Amidates from Palladium(II). *J. Am. Chem. Soc.* **2006,** *128*, 9044-9045.

220.	Harwood, E. A.; Hopkins, P. B.; Sigurdsson, S. T., Chemical Synthesis of Cross-Link Lesions Found in Nitrous Acid Treated DNA: A General Method for the Preparation of N2-Substituted 2'-Deoxyguanosines. *J. Org. Chem.* **2000,** *65*, 2959-2964.

221.	Szombati, Z.; Baerns, S.; Marx, A.; Meier, C., Synthesis of C8-Arylamine-Modified 2′-Deoxyadenosine Phosphoramidites and Their Site-Specific Incorporation into Oligonucleotides. *ChemBioChem* **2012,** *13*, 700–712.

222.	Huang, X.; Yu, P.; LeProust, E.; Gao, X., *Nucleic Acids Res.* **1997,** *25*, 4758-4763.

223.	Newcomb, M.; Park, S. U.; Kaplan, J.; Marquardt, D. J., Facile Generation of Dialkylaminyl Radicals from N-Hydroxypyridine-2-thione Carbamates. Application in Kinetic Studies of Small Ring Cycloalkylaminyl Radical Ring Openings. *Tetrahedron Lett.* **1985,** *26*, 5651-4.

224.	Maxwell, B. J.; Smith, B. J.; Tsanaktsidis, J., The Cyclization of N-Butylpent-4-enylaminyl Revisited: A Combined Theoretical and Experimental Study. *J. Chem. Soc. Perkin Trans. 2* **2000**, 425-431.

225.	Van Speybroeck, V.; De Kimpe, N.; Waroquier, M., N-Alkenyl-2-aziridinylmethyl Radicals and N-Alkenylaminyl Radicals in Cascade Cyclizations to Pyrrolizidines and Indolizidines. *J. Org. Chem.* **2005,** *70*, 3674-3681.

226.	Watanabe, N.; Sano, Y.; Suzuki, H.; Tanimura, M.; Ijuin, H. K.; Matsumoto, M., Synthesis of Thermally Stable Acylamino-Substituted Bicyclic Dioxetanes and Their Base-Induced Chemiluminescent Decomposition. *J. Org. Chem.* **2010,** *75*, 5920-5926.

227.   Foo, K.; Sella, E.; Thomé, I.; Eastgate, M. D.; Baran, P. S., A Mild, Ferrocene-Catalyzed C–H Imidation of (Hetero)Arenes. *J. Am. Chem. Soc.* **2014,** *136*, 5279-5282.

228.   McGilvray, K. L.; Decan, M. R.; Wang, D.; Scaiano, J. C., Facile Photochemical Synthesis of Unprotected Aqueous Gold Nanoparticles. *J Am Chem Soc* **2006,** *128*, 15980-15981.

229.   Khanna, S.; Verma, S., Crystallographic Signatures of N6-Methoxyadenine Imino Tautomer–Silver Complexes. *Cryst. Growth Des.* **2012,** *12*, 3025-3035.

230.   Chen, C., The Past, Present, and Future of the Yang Reaction. *Org. Biomol. Chem.* **2016,** *14*, 8641-8647.

231.   Yang, N. C.; Yang, D.-D. H., Photochemical Reactions of Ketones in Solution. *J. Am. Chem. Soc.* **1958,** *80*, 2913-2914.

232.   Iida, A.; Nakazawa, S.; Okabayashi, T.; Horii, A.; Misaki, T.; Tanabe, Y., Powerful Ti-Crossed Claisen Condensation between Ketene Silyl Acetals or Thioacetals and Acid Chlorides or Acids. *Org. Lett.* **2006,** *8*, 5215-5218.

233.   Stolarski, R.; Kierdaszuk, B.; Hagberg, C. E.; Shugar, D., Hydroxylamine and Methoxyamine Mutagenesis: Displacement of the Tautomeric Equilibrium of the Promutagen N6-Methoxyadenosine by Complementary Base Pairing. *Biochemistry* **1984,** *23*, 2906-2913.

234.   Ito, T.; Kuno, S.; Uchida, T.; Fujita, S.; Nishimoto, S., Properties and Reactivity of the Adenosine Radical Generated by Radiation-Induced Oxidation in Aqueous Solution. *J. Phys. Chem. B* **2009,** *113*, 389-394.

235.   Porter, G.; Dogra, S. K.; Loutfy, R. O.; Sugamori, S. E.; Yip, R. W., *J. Chem. Soc. Faraday Trans. 1* **1973,** *69*, 1462-1474.

236.   Bhattacharjee, S.; Deterding, L. J.; Chatterjee, S.; Jiang, J.; Ehrenshaft, M.; Lardinois, O.; Ramirez, D. C.; Tomer, K. B.; Mason, R. P., Site-Specific Radical Formation in DNA Induced by Cu(II)-H_2O_2 Oxidizing System, Using ESR, Immuno-Spin Trapping, LC-MS, and Ms/Ms. *Free Rad. Biol. & Med.* **2011,** *50*, 1536-1545.

237.   Rauk, A.; Yu, D.; Armstrong, D. A., Oxidative Damage to and by Cysteine in Proteins: An Ab Initio Study of the Radical Structures, C-H, S-H, and C-C Bond Dissociation Energies, and Transition Structures for H Abstraction by Thiyl Radicals. *J. Am. Chem. Soc.* **1998,** *120*, 8848-8855.

238.   Zierhut, M.; Roth, W.; Fischer, I., Dynamics of H-Atom Loss in Adenine. *Phys. Chem. Chem. Phys.* **2004,** *6*, 5178-5183.

239.   Lind, M. C.; Richardson, N. A.; Wheeler, S. E.; Schaefer III, H. F., Hydrogen-Abstracted Adenine-Thymine Radicals with Interesting Transferable Properties. *J. Phys. Chem. B* **2007,** *111*, 5525-5530.

240.   Musa, O. M.; Horner, J. H.; Shahin, H.; Newcomb, M., A Kinetic Scale for Dialkylaminyl Radical Reactions. *J. Am. Chem. Soc.* **1996,** *118*, 3862-3868.

241.   Horner, J. H.; Musa, O. M.; Bouvier, A.; Newcomb, M., Absolute Kinetics of Amidyl Radical Reactions. *J. Am. Chem. Soc.* **1998,** *120*, 7738-7748.

242.   Johnson, C. C.; Horner, J. H.; Tronche, C.; Newcomb, M., Absolute Kinetics Of α-Methoxy Radical Reactions. A Foundation for a Kinetic Scale For α-Alkoxy Radical Reactions. *J. Am. Chem. Soc.* **1995,** *117*, 1684-7.

243.   El-Agamey, A.; Fukuzumi, S.; Naqvi, K. R.; McGarvey, D. J., Kinetic Studies of Retinol Addition Radicals. *Org. Biomol. Chem.* **2011,** *9*, 1459-1465.

244.   Lamola, A. A., Lowest Π, Π* Triplet State of Acetophenone. *J. Chem. Phys.* **1967,** *47*, 4810-4816.

245.   Yang, N.-C.; McClure, D. S.; Murov, S.; Houser, J. J.; Dusenbery, R., Photoreduction of Acetophenone and Substituted Acetophenones. *J. Am. Chem. Soc.* **1967,** *89*, 5466-5468.

246.   Lamola, A. A.; Hammond, G. S., Mechanisms of Photochemical Reactions in Solution. XXXIII. Intersystem Crossing Efficiencies. *J. Chem. Phys.* **1965,** *43*, 2129-2135.

247.   Adam, W.; Arnold, M. A.; Nau, W. M.; Pischel, U.; Saha-Möller, C. R., Structure-Dependent Reactivity of Oxyfunctionalized Acetophenones in the Photooxidation of DNA: Base Oxidation and Strand Breaks through Photolytic Radical Formation (Spin Trapping, EPR Spectroscopy, Transient Kinetics) Versus Photosensitization (Electron Transfer, Hydrogen-Atom Abstraction). *Nucleic Acids Res.* **2001,** *29*, 4955-4962.

248.   Epe, B.; Henzl, H.; Adam, W.; Saha-Möller, C. R., Endonuclease-Sensitive DNA Modifications Induced by Acetone and Acetophenone as Photosensitizers. *Nucleic Acids Res.* **1993,** *21*, 863-869.

249.   Wagner, P. J.; Giri, B. P.; Frerking, H. W.; DeFrancesco, J., Spacer Independent Intramolecular Triplet Energy Transfer in Diketones. *J. Am. Chem. Soc.* **1992,** *114*, 8326-8327.

250.   McMahon, K.; Wagner, P. J., Intramolecular Photosensitization of the Pinene-Ocimene Rearrangement. *Can. J. Chem.* **2003,** *81*, 669-672.

251.   Takebayashi, S.; Dabral, N.; Miskolzie, M.; Bergens, S. H., Experimental Investigations of a Partial Ru–O Bond During the Metal–Ligand Bifunctional Addition in Noyori-Type Enantioselective Ketone Hydrogenation. *J. Am. Chem. Soc.* **2011,** *133*, 9666-9669.

252.   Arterburn, J. B.; Perry, M. C., Selective Rhenium-Catalyzed Oxidation of Secondary Alcohols with Methyl Sulfoxide in the Presence of Ethylene Glycol, a Convenient One-Pot Synthesis of Ketals. *Org. Lett.* **1999,** *1*, 769-771.

253.   Gowda, A. S. P.; Lee, M.; Spratt, T. E., N2-Substituted 2′-Deoxyguanosine Triphosphate Derivatives as Selective Substrates for Human DNA Polymerase K. *Angew. Chem. Int. Ed.* **2017,** *56*, 2628-2631.

254.   Xia, X.; Gao, X.; Xu, J.; Hu, C.; Peng, X., Selective Oxidation of Styrene Derivatives to Ketones over Palladium(0)/Carbon with Hydrogen Peroxide as the Sole Oxidant. *Synlett* **2017,** *28*, 607-610.

255.   Watson, A. A.; Nesnow, S. C.; Brown, G. B., Purine N-Oxides. XIVIII. 1-Hydroxyguanine. *J. Org. Chem.* **1973,** *38*, 3046-3048.

256.   Alshykhly, O. R.; Fleming, A. M.; Burrows, C. J., 5-Carboxamido-5-formamido-2-iminohydantoin, in Addition to 8-Oxo-7,8-dihydroguanine, Is the Major Product of the Iron-Fenton or X-Ray Radiation-Induced Oxidation of Guanine under Aerobic Reducing Conditions in Nucleoside and DNA Contexts. *J. Org. Chem.* **2015,** *80*, 6996-7007.

257. Aveline, B. M.; Matsugo, S.; Redmond, R. W., Photochemical Mechanisms Responsible for the Versatile Application of Naphthalimides and Naphthaldiimides in Biological Systems. *J. Am. Chem. Soc.* **1997,** *119*, 11785-11795.

258. Ravanat, J.-L.; Cadet, J., Reaction of Singlet Oxygen with 2'-Deoxyguanosine and DNA. Isolation and Characterization of the Main Oxidation Products. *Chem. Res. Toxicol.* **1995,** *8*, 379-388.

259. Banyasz, A.; Ketola, T.-M.; Muñoz-Losa, A.; Rishi, S.; Adhikary, A.; Sevilla, M. D.; Martinez-Fernandez, L.; Improta, R.; Markovitsi, D., UV-Induced Adenine Radicals Induced in DNA A-Tracts: Spectral and Dynamical Characterization. *J. Phys. Chem. Lett.* **2016,** *7*, 3949-3953.

260. Xu, X.; Yu, T.; Chen, S.-J., Understanding the Kinetic Mechanism of RNA Single Base Pair Formation. *Proc. Natl. Acad. Sci. U. S. A.* **2016,** *113*, 116-121.

261. Fleming, A. M.; Alshykhly, O.; Zhu, J.; Muller, J. G.; Burrows, C. J., Rates of Chemical Cleavage of DNA and RNA Oligomers Containing Guanine Oxidation Products. *Chem. Res. Toxicol.* **2015,** *28*, 1292-1300.

262. Muller, J. G.; Duarte, V.; Hickerson, R. P.; Burrows, C. J., Gel Electrophoretic Detection of 7,8-Dihydro-8-oxoguanine and 7,8-Dihydro-8-oxoadenine Via Oxidation by Ir(IV). *Nucleic Acids Res.* **1998,** *26*, 2247-2249.

263. Cullis, P. M.; Malone, M. E.; Merson-Davies, L. A., Guanine Radical Cations Are Precursors of 7,8-Dihydro-8-oxo-2'-deoxyguanosine but Are Not Precursors of Immediate Strand Breaks in DNA. *J. Am. Chem. Soc.* **1996,** *118*, 2775-81.

264.   D'Ham, C.; Romieu, A.; Jaquinod, M.; Gasparutto, D.; Cadet, J., Excision of 5,6-Dihydroxy-5,6-dihydrothymine, 5,6-Dihydrothymine, and 5-Hydroxycytosine from Defined Sequence Oligonucleotides by Escherichia Coli Endonuclease III and Fpg Proteins: Kinetic and Mechanistic Aspects. *Biochemistry* **1999,** *38*, 3335-3344.

265.   Dizdaroglu, M.; Coskun, E.; Jaruga, P., Repair of Oxidatively Induced DNA Damage by DNA Glycosylases: Mechanisms of Action, Substrate Specificities and Excision Kinetics. *Mutat. Rev. Res. Mutagen.* **2017,** *771*, 99-127.

266.   Tchou, J.; Bodepudi, V.; Shibutani, S.; Antoshechkin, I.; Miller, J.; Grollman, A. P.; Johnson, F., Substrate Specificity of Fpg Protein. Recognition and Cleavage of Oxidatively Damaged DNA. *J. Biol. Chem.* **1994,** *269*, 15318-24.

267.   Giese, B.; Wessely, S., The Significance of Proton Migration During Hole Hopping through DNA. *Chem. Commun.* **2001**, 2108-2109.

268.   Sugiyama, H.; Matsuda, S.; Kino, K.; Zhang, Q.-M.; Yonei, S.; Saito, I., New Synthetic Method of 5-Formyluracil-Containing Oligonucleotides and Their Melting Behavior. *Tetrahedron Lett.* **1996,** *37*, 9067-9070.

269.   Berney, M.; McGouran, J. F., Methods for Detection of Cytosine and Thymine Modifications in DNA. *Nature Reviews Chemistry* **2018**.

270.   Tretyakova, N.; Villalta, P. W.; Kotapati, S., Mass Spectrometry of Structurally Modified DNA. *Chem. Rev.* **2013,** *113*, 2395-2436.

271.   Cadet, J.; Douki, T.; Frelon, S.; Sauvaigo, S.; Pouget, J.-P.; Ravanat, J.-L., Assessment of Oxidative Base Damage to Isolated and Cellular DNA by HPLC-MS/MS Measurement. *Free Radical Biol. Med.* **2002,** *33*, 441-449.

272.   Chowdhury, G.; Guengerich, F. P., Direct Detection and Mapping of Sites of Base Modification in DNA Fragments by Tandem Mass Spectrometry. *Angew. Chem. Int. Ed.* **2008,** *47*, 381-384.

273.   Chowdhury, G.; Guengerich, F. P., Tandem Mass Spectrometry-based Detection of C4'-Oxidized Abasic Sites at Specific Positions in DNA Fragments. *Chem. Res. Toxicol.* **2009,** *22*, 1310-1319.

274.   Ni, J.; Pomerantz, S. C.; Rozenski, J.; Zhang, Y.; McCloskey, J. A., Interpretation of Oligonucleotide Mass Spectra for Determination of Sequence Using Electrospray Ionization and Tandem Mass Spectrometry. *Anal. Chem.* **1996,** *68*, 1989-1999.

275.   Huber, C. G.; Oefner, P. J.; Preuss, E.; Bonn, G. K., High-resolution Liquid Chromatography of DNA Fragments on Non-Porous Poly(Styrene-divinylbenzene) Particles. *Nucleic Acids Res.* **1993,** *21*, 1061-1066.

276.   Hong, H.; Wang, Y., Derivatization with Girard Reagent T Combined with LC−MS/MS for the Sensitive Detection of 5-Formyl-2'-deoxyuridine in Cellular DNA. *Anal. Chem.* **2007,** *79*, 322-326.

277.   Kumar, A.; Sevilla, M. D., π- Vs σ-Radical States of One-Electron-Oxidized DNA/RNA Bases: A Density Functional Theory Study. *J. Phys. Chem. B* **2013,** *117*, 11623-11632.

278.   Hong, I. S.; Greenberg, M. M., Mild Generation of 5-(2'-Deoxyuridinyl)methyl Radical from a Phenyl Selenide Precursor. *Org. Lett.* **2004,** *6*, 5011-5013.

279.   Hong, I. S.; Ding, H.; Greenberg, M. M., Oxygen Independent DNA Interstrand Cross-Link Formation by a Nucleotide Radical. *J. Am. Chem. Soc.* **2006,** *128*, 485-491.

280.   Weng, L.; Horvat, S. M.; Schiesser, C. H.; Greenberg, M. M., Deconvoluting the Reactivity of Two Intermediates Formed from Modified Pyrimidines. *Org. Lett.* **2013,** *15*, 3618-3621.

281.   Bergeron, F.; Auvré, F.; Radicella, J. P.; Ravanat, J.-L., HO• Radicals Induce an Unexpected High Proportion of Tandem Lesion Base Lesions Refractory to Repair by DNA Glycosylases. *Proc. Nat. Acad. Sci. USA* **2010,** *107*, 5528-5533.

282.   San Pedro, J. M. N.; Greenberg, M. M., 5,6-Dihydropyrimidine Peroxyl Radical Reactivity in DNA. *J. Am. Chem. Soc.* **2014,** *136*, 3928-3936.

283.   Joy, A.; Schuster, G. B., Long-Range Radical Cation Migration in DNA: Investigation of the Mechanism. *Chem. Comm.* **2005**, 2778-2784.

284.   Kupan, A.; Sauliere, A.; Broussy, S.; Seguy, C.; Pratviel, G.; Meunier, B., Guanine Oxidation by Electron Transfer: One- Versus Two-Electron Oxidation Mechanism. *ChemBioChem* **2006,** *7*, 125-133.

285.   Newcomb, M., Competition Methods and Scales for Alkyl Radical Reaction Kinetics. *Tetrahedron* **1993,** *49*, 1151-1176.

286.   Hildenbrand, K.; Schulte-Frohlinde, D., Time-Resolved EPR Studies on the Reaction Rates of Peroxyl Radicals of Poly(acrylic acid) and of Calf Thymus DNA with Glutathione. Re-Examination of a Rate Constant for DNA. *Int. J. Radiat. Biol.* **1997,** *71*, 377-385.

287.	Morita, Y.; Shibutani, T.; Nakanishi, N.; Nishikura, K.; Iwai, S.; Kuraoka, I., Human Endonuclease V Is a Ribonuclease Specific for Inosine-Containing Rna. *Nat. Commun.* **2013,** *4*, 2273.

288.	Capuano, F.; Mülleder, M.; Kok, R.; Blom, H. J.; Ralser, M., Cytosine DNA Methylation Is Found in Drosophila Melanogaster but Absent in Saccharomyces Cerevisiae, Schizosaccharomyces Pombe, and Other Yeast Species. *Anal. Chem.* **2014,** *86*, 3697-3702.

289.	Shafirovich, V.; Dourandin, A.; Huang, W.; Luneva, N. P.; Geacintov, N. E., Oxidation of Guanine at a Distance in Oligonucleotides Induced by Two-Photon Photoionization of 2-Aminopurine. *J. Phys. Chem. B* **1999,** *103*, 10924-10933.

290.	Fukui, K.; Tanaka, K.; Fujitsuka, M.; Watanabe, A.; Ito, O., Distance Dependence of Electron Transfer in Acridine-Intercalated DNA. *J. Photochem. Photobiol* **1999,** *50*, 18-27.

291.	Davis, W. B.; Naydenova, I.; Haselsberger, R.; Ogrodnik, A.; Giese, B.; Michel-Beyerle, M. E., Dynamics of Hole Trapping by G, Gg, and Ggg in DNA. *Angew. Chem.* **2000,** *112*, 3795-3798.

292.	Nakatani, K.; Dohno, C.; Saito, I., Modulation of DNA-Mediated Hole-Transport Efficiency by Changing Superexchange Electronic Interaction. *J. Am. Chem. Soc.* **2000,** *122*, 5893-5894.

293.	von Feilitzsch, T.; Tuma, J.; Neubauer, H.; Verdier, L.; Haselsberger, R.; Feick, R.; Gurzadyan, G.; Voityuk, A. A.; Griesinger, C.; Michel-Beyerle, M. E.,

Chromophore/DNA Interactions: Femto- to Nanosecond Spectroscopy, NMR Structure, and Electron Transfer Theory. *J. Phys. Chem. B* **2008,** *112*, 973-989.

294.   O'Neill, M. A.; Barton, J. K., Effects of Strand and Directional Asymmetry on Base–Base Coupling and Charge Transfer in Double-Helical DNA. *Proc. Natl. Acad. Sci. U. S. A.* **2002,** *99*, 16543-16550.

295.   Renaud, N.; Berlin, Y. A.; Lewis, F. D.; Ratner, M. A., Between Superexchange and Hopping: An Intermediate Charge-Transfer Mechanism in Poly(A)-poly(T) DNA Hairpins. *J. Am. Chem. Soc.* **2013,** *135*, 3953-3963.

296.   Kawai, K.; Takada, T.; Tojo, S.; Majima, T., *J. Am. Chem. Soc.* **2003,** *125*, 6842-6843.

297.   Curtin, D. Y., Stereochemical Control of Organic Reactions. Differences in Behavior of Diastereoisomers. I. Ethane Derivatives. The Cis Effect. *Rec. Chem. Progr.* **1954,** *15*, 111-28.

298.   Barnett, R. N.; Joseph, J.; Landman, U.; Schuster, G. B., Oxidative Thymine Mutation in DNA: Water-Wire-Mediated Proton-Coupled Electron Transfer. *J. Am. Chem. Soc.* **2013,** *135*, 3904-3914.

299.   Carter, K. N.; Greenberg, M. M., Tandem Lesions Are the Major Products Resulting from a Pyrimidine Nucleobase Radical. *J. Am. Chem. Soc.* **2003,** *125*, 13376-13378.

300.   Schuster, G. B., Long-Range Charge Transfer in DNA: Transient Structural Distortions Control the Distance Dependence. *Acc. Chem. Res.* **2000,** *33*, 253-260.

301.   Kanvah, S.; Joseph, J.; Schuster, G. B.; Barnett, R. N.; Cleveland, C. L.; Landman, U., Oxidation of DNA: Damage to Nucleobases. *Acc. Chem. Res.* **2010,** *43*, 280-287.

302.   Rogstad, D. K.; Heo, J.; Vaidehi, N.; Goddard, W. A.; Burdzy, A.; Sowers, L. C., 5-Formyluracil-Induced Perturbations of DNA Function. *Biochemistry* **2004,** *43*, 5688-5697.

303.   Ni, J.; Pomerantz, S. C.; Rozenski, J.; Zhang, Y.; McCloskey, J. A., Interpretation of Oligonucleotide Mass Spectra for Determination of Sequence Using Electrospray Ionization and Tandem Mass Spectrometry. *Anal. Chem.* **1996,** *68*, 1989-1999.

304.   Wang, Y., HPLC Isolation and Mass Spectrometric Characterization of Two Isomers of Thymine Glycols in Oligodeoxynucleotides. *Chem. Res. Toxicol.* **2002,** *15*, 671-676.

305.   Wagner, J. R.; van Lier, J. E.; Berger, M.; Cadet, J., Thymidine Hydroperoxides: Structural Assignment, Conformational Features, and Thermal Decomposition in Water. *J. Am. Chem. Soc.* **1994,** *116*, 2235-2242.

306.   Samson-Thibault, F.; Madugundu, G. S.; Gao, S.; Cadet, J.; Wagner, J. R., Profiling Cytosine Oxidation in DNA by LC-MS/MS. *Chem. Res. Toxicol.* **2012,** *25*, 1902-1911.

307.   Fujimoto, J.; Tran, L.; Sowers, L. C., Synthesis and Cleavage of Oligodeoxynucleotides Containing a 5-Hydroxyuracil Residue at a Defined Site. *Chem. Res. Toxicol.* **1997,** *10*, 1254-1258.

308.	Morningstar, M. L.; Kreutzer, D. A.; Essigmann, J. M., Synthesis of Oligonucleotides Containing Two Putatively Mutagenic DNA Lesions: 5-Hydroxy-2'-deoxyuridine and 5-Hydroxy-2'-deoxycytidine. *Chem. Res. Toxicol.* **1997,** *10*, 1345-1350.

309.	Cadet, J.; Douki, T.; Frelon, S.; Sauvaigo, S.; Pouget, J. P.; Ravanat, J. L., Assessment of Oxidative Base Damage to Isolated and Cellular DNA by HPLC-MS/MS Measurement. *Free Rad. Biol. Med.* **2002,** *33*, 441-449.

310.	Jones, G. D. D.; Boswell, T. V.; Lee, J.; Milligan, J. R.; Ward, J. F.; Weinfeld, M., A Comparison of DNA Damage Produced under Conditions of Direct and Indirect Action of Radiation. *Int. J. Radiat. Biol.* **1994,** *66*, 441-445.

311.	Sharma, K. K. K.; Swarts, S. G.; Bernhard, W. A., Mechanisms of Direct Radiation Damage to DNA: The Effect of Base Sequence on Base End Products. *J. Phys. Chem. B* **2011,** *115*, 4843-4855.

312.	Kumar, A.; Sevilla, M. D., Proton-Coupled Electron Transfer in DNA on Formation of Radiation-Produced Ion Radicals. *Chem. Rev.* **2010,** *110*, 7002-7023.

313.	Zheng, L.; Greenberg, M. M., Traceless Tandem Lesion Formation in DNA from a Nitrogen-Centered Purine Radical. *J. Am. Chem. Soc.* **2018,** *140*, 6400-6407.

314.	San Pedro, J. M. N.; Greenberg, M. M., 5,6-Dihydropyrimidine Peroxyl Radical Reactivity in DNA. *J. Am. Chem. Soc.* **2014,** *136*, 3928-3936.

315.	Taverna Porro, M. L.; Greenberg, M. M., DNA Double Strand Cleavage Via Interstrand Hydrogen Atom Abstraction. *J. Am. Chem. Soc.* **2013,** *135*, 16368-16371.

316.	Yun, B. H.; Geacintov, N. E.; Shafirovich, V., Generation of Guanine-thymidine Cross-Links in DNA by Peroxynitrite/Carbon Dioxide. *Chem. Res. Toxicol.* **2011,** *24*, 1144-1152.

317.	Li, X.; Sevilla, M. D.; Sanche, L., Hydrogen Atom Loss in Pyrimidine DNA Bases Induced by Low-Energy Electrons: Energetics Predicted by Theory. *J. Phys. Chem. B* **2004,** *108*, 19013-19019.

318.	Brown, D. M.; Hewlins, M. J. E.; Schell, P., The Tautomeric State of N(4)-Hydroxy- and of N(4)-Amino-cytosine Derivatives. *J. Chem. Soc. C* **1968**, 1925-1929.

319.	Scaiano, J. C.; Stamplecoskie, K. G.; Hallett-Tapley, G. L., Photochemical Norrish Type I Reaction as a Tool for Metal Nanoparticle Synthesis: Importance of Proton Coupled Electron Transfer. *Chem. Comm.* **2012,** *48*, 4798-4808.

320.	Schulhof, J. C.; Molko, D.; Teoule, R., Synthesis of DNA Fragments Containing 5,6-Dihydrothymine, a Major Product of Thymine Gamma Radiolysis. *Nucleic Acids Res.* **1988,** *16*, 319-326.

321.	Hong, I. S.; Greenberg, M. M., Efficient DNA Interstrand Cross-Link Formation from a Nucleotide Radical. *J. Am. Chem. Soc.* **2005,** *127*, 3692-3693.

322.	Peng, X.; Pigli, Y. Z.; Rice, P. A.; Greenberg, M. M., Protein Binding Has a Large Effect on Radical Mediated DNA Damage. *J. Am. Chem. Soc.* **2008,** *130*, 12890-12891.

323.	Warshaw, M. M.; Tinoco, I., Optical Properties of Sixteen Dinucleoside Phosphates. *J. Mol. Biol.* **1966,** *20*, 29-38.

324.	Véliz, E. A.; Beal, P. A., 6-Bromopurine Nucleosides as Reagents for Nucleoside Analogue Synthesis. *J. Org. Chem.* **2001,** *66*, 8592-8598.

325.	Szombati, Z.; Baerns, S.; Marx, A.; Meier, C., Synthesis of C8-Arylamine-modified 2′-Deoxyadenosine Phosphoramidites and Their Site-Specific Incorporation into Oligonucleotides. *ChemBioChem* **2012,** *13*, 700-712.

326.	Čapek, P.; Pohl, R.; Hocek, M., Cross-Coupling Reactions of Unprotected Halopurine Bases, Nucleosides, Nucleotides and Nucleoside Triphosphates with 4-Boronophenylalanine in Water. Synthesis of (Purin-8-yl)- and (Purin-6-yl)phenylalanines. *Org. Biomol. Chem.* **2006,** *4*, 2278-2284.

327.	Too, K.; Brown, D. M.; Bongard, E.; Yardley, V.; Vivas, L.; Loakes, D., Anti-Malarial Activity of N6-Modified Purine Analogues. *Bioorg. Med. Chem.* **2007,** *15*, 5551-5562.

9. Curriculum Vitae

LIWEI ZHENG

Education

2013 – 2018   **Johns Hopkins University**, Baltimore, MD. Doctor of Philosophy in Chemistry

Advisor: Professor Marc M. Greenberg.

2009 – 2013   **Wuhan University**, Wuhan, Hubei, China. Bachelor of Science in Chemistry.

Advisor: Professor Aiwen Lei.

Awards

Glen E. Meyer '39 Fellowship, Johns Hopkins University, 2017

Travel Assistance Awards, The Division of Chemical Toxicology, 2017

Emmet and Elsie Buhle Fellowship Award, Johns Hopkins University, 2015

The National Scholarship, Ministry of Education of China, 2010

The National Scholarship, Ministry of Education of China, 2009

Publications

Chao Liu, Shan Tang, Dong Liu, Jiwen Yuan, **Liwei Zheng**, Lingkui Meng, and Aiwen Lei, Nickel-Catalyzed Heck-Type Alkenylation of Secondary and Tertiary α-Carbonyl Alkyl Bromides. *Angew. Chem. Int. Ed.*, **2012**, *51*, 3638–3641. DOI:10.1002/anie.201108350

Chao Liu, Shan Tang, **Liwei Zheng**, Dong Liu, Heng Zhang, and Aiwen Lei, Covalently Bound Benzyl Ligand Promotes Selective Palladium-Catalyzed Oxidative Esterification of Aldehydes with Alcohols. *Angew. Chem. Int. Ed.*, **2012**, *51*, 5662–5666. DOI:10.1002/anie.201201960

Liwei Zheng, Markus Griesser, Derek A. Pratt, and Marc M. Greenberg. Aminyl Radical Generation via Tandem Norrish Type I Photocleavage, β-Fragmentation: Independent Generation and Reactivity of the 2′-Deoxyadenosin-*N6*-yl Radical. *J. Org. Chem.* **2017**, *82*, 3571-3580. DOI: 10.1021/acs.joc.7b00093

Liwei Zheng, Lu Lin, Ke Qu, Amitava Adhikary, Michael D. Sevilla, and Marc M. Greenberg. Independent Photochemical Generation and Reactivity of Nitrogen-Centered Purine Nucleoside Radicals from Hydrazines. *Org. Lett.* **2017**, *19*, 6444-6447. DOI: 10.1021/acs.orglett.7b03368

Liwei Zheng and Marc M. Greenberg. DNA Damage Emanating From a Neutral Purine Radical Reveals the Sequence Dependent Convergence of the Direct and Indirect Effects of γ-Radiolysis. *J. Am. Chem. Soc.*, **2017**, *139*, 17751-17754. DOI: 10.1021/jacs.7b10942

Liwei Zheng and Marc M. Greenberg. Traceless Tandem Lesion Formation in DNA From a Neutral Purine Radical. *J. Am. Chem. Soc.*, **2018**, *140*, 6400-6407. DOI: 10.1021/jacs.8b02828

Huabing Sun, **Liwei Zheng (co-first authors),** and Marc M. Greenberg. Independent Generation of Reactive Intermediates Lead to an Alternative Mechanism for Product Formation in Poly(dA-T) via Hole Migration. *J. Am. Chem. Soc.* **2018,** *140* (36), 11308-11316. DOI: 10.1021/jacs.8b05484.

Presentations

1. **Zheng, L.**; Greenberg, M. M. Independent Generation of Neutral Purine Radicals Involved in DNA Damage. 254th ACS National Meeting 2017, Division of Chemical Toxicology, Washington, DC. (Poster)

2. **Zheng, L.**; Griesser, M.; Pratt, D. A.; Greenberg, M. M. Independent Generation of 2'-Deoxyadenosine-N6-yl Radical and Its Reactivity in DNA. 254th ACS National Meeting 2017, Division of Chemical Toxicology, Washington, DC. (Oral and Poster, selected for Sci-Mix)